I. Author's Declaration

This thesis is submitted in fulfilment of the requirements of the PhD Project, and except where duly acknowledged or referenced it is entirely my own work. It has not been submitted, either in whole or in part, for any other award at University of the West of England (UWE) or elsewhere.

Signed..... Date.../..../…

II. Abstract

Breast cancer is a deadly disease that accounts for a third of all female cancer-related deaths globally. Although recent advances in early diagnosis and targeted therapy using prognostic markers have reduced deaths, more than 50% of newly diagnosed cases have already developed metastatic disease at diagnosis. Furthermore, the remaining cases still have a high risk of secondary disease and relapse. Breast cancer metastasis is the leading cause of breast cancer related mortality, it is incurable and current treatments aim to prolong life alongside pain management. Thus, there is a need for treatment for this disease.

The epithelial-mesenchymal transition (EMT) is one of the processes by which cancer cells acquire the ability to invade and eventually metastasise. Therefore, understanding the regulation of breast cancer cell metastasis is essential for identifying methods for management of metastatic disease either by prevention or treatment. The first aim of this study was to develop an *in vitro* tissue culture model that can be used to assess breast cancer cell lines, that belong to several molecular subtypes, to undergo an EMT-like transition.

Results showed that there were EMT-like changes seen in breast cancer cell lines and that the activation of these pathways is not restricted to, nor governed by, molecular subtypes of breast cancer. Also, an intermediate phenotype, where the cells showed mixed epithelial and mesenchymal morphology was observed in the basal-like breast cancer cells lines. This phenotype is observed for the first time in a tissue culture model of breast cancer cell lines and further identification of the criteria of these intermediate phenotype cells is required to draw further conclusions. These cells could represent the hybrid epithelial/mesenchymal cells that have increased metastatic ability. Thus, this model was utilised to study the role of Hedgehog (Hh) signalling pathway in the regulation of EMT in breast cancers.

Data from a breast cancer cohort of patients samples showed that there was increased expression of Hh proteins (Gli1, Gli2 and Gli3) at the invasive front. This is the first study to assess subcellular localisation of the Gli proteins in breast cancer human patient samples. Also, the data suggested that breast cancer cells gain the ability to activate Hh signalling by autocrine rather than by paracrine signalling. These findings encouraged further investigation to understand the effect of inhibiting the Hh signalling using cyclopamine or LDE225 *in vitro*.

Inhibition with cyclopamine or LDE225 resulted in a reduction of cell yield and viability with increased cellular apoptosis. There was an observed alteration of Hh pathway proteins expression and subcellular localisation. Also, assessment of the catenin-related transcription, the outputs of canonical Wnt signalling, showed that inhibiting Hh signalling using cyclopamine and LDE225 resulted in reduction of Wnt signalling activity in MCF7 and MDA-MB-231 cell lines. Also, there was a reduction in E-cadherin expression in a dose dependent manner with a reduction in cell motility and invasion.

Findings showed that Hh signalling was involved in the regulation of EMT in breast cancer cell lines and also showed that there was crosstalk between Hh and Wnt in breast cancer cells. Assessment of the co-expression of Hh pathway proteins in breast cancer samples provides potential prognostic markers for identifying breast cancer patients who could benefit from Hh-targeted therapy.

III. Acknowledgement

My study has been a long and tedious journey. Here I would like to state few lines of gratitude to so many wonderful people that were essential in helping me through this time.

I owe a great deal of gratitude to my country, the late King Abdullah Bin Abdul Aziz (may Allah bless his soul), my King Salman Bin Abdul Aziz and his son the crown prince of Saudi Arabia Mohammad bin Salman Bin Abdul Aziz. Their devotion to the people of Saudi and continues effort for Saudi Arabia and citizens development is and continue to be inspiring. I owe my success to them and I hope that upon returning to my country, I will help them serve my country and raise value of sciences.

To several institutions in my country, for the endless support. To the Ministry of Education of Saudi Arabia, Umm Al Qura University, His Royal Highness Prince Mohammed bin Nawaf Al Saud (the ambassador of Saudi Arabia in the UK) and the cultural bureau for sponsoring my study and endless support.

To this country, the United Kingdom, for all the friendships and family gained during my time here. I will be forever thankful for this country that provided me with a second home.

To my supervisor and my friend Dr. David Qualtrough. You have been an amazing mentor, a teacher and a great friend. Thank you for your kind words, your advice, endless patience and comforting in time of need. Thank you for your kind understanding and all your time. I will be forever in debt for all the things you taught me.

To Saeed Kabrah, my best friend and valued partner in life. Thank you for your tolerance, love and support. Thank you for giving me faith when I had none. For trusting me and your endless patience. I only hope that one day you will be proud of me and that I can give back some of all your efforts.

To my family and loved ones back at home, for my mom, dad and my brother and sister. Their support and understanding made this journey easier. I thank them all for the tolerance and endless love and support. I only hope I made you all proud.

This journey was long, it took me six years to complete. I had the chance to meet great people and make strong connections. To every one of my friends that took part and made this trip a nice one. For all the memories, good and bad, and all the love. Thank you all. Special thanks to my best friend Mike Devey. For all the good times, support and comfort.

To all my PhD colleagues; Layla Al Hijab, Sultan Al Malki, Mai Shafie, Marian Manso, Bertrand Monnier, Marcela Usmari, Samantha Jume, Tareg Belali, and Grace Okoro and technical staff; David Corry, Jeff Davey, Paul Kendrick and all others. For the team work and kindness. For advice, support and help in time of need.

For all my students who were part of my PhD experience, thank you for your help.

To Dr Tim Craig for his support and kindly allowing us to use the Li-Cor Odyssey® FC imaging system, also for the advice and support. Thank you so much. To Dr Ruth Morse my second supervisor, thank you for your support and kind words.

Table of content

IV. List of Figures

V. List of Tables

VI. Abbreviation

ABC	Avidin/Biotin complex
ANOVA	Analysis of variance
AO	Acridine orange
APC	Adenomatosis polyposis coli
AR	Androgen receptor
BCA	Bicinchoninic acid
BD	Becton, Dickinson
CMF	Cyclophosphamide-Methotrexate-5-Fluorouracil
CMV	Cytomegalovirus
CRT	Catenin-related transcription
DAB	3,3' Diaminobenzidine
DAPI	4',6-diamidino-2-phenylindole
DCIS	Ductal Carcinoma *In situ*
DMEM	Dulbecco's Modified Eagle Medium
DMSO	Dimethyl sulfoxide
DPX	Distyrene, Plasticizer and Xylene
ECACC	European Collection of Authenticated Cell Cultures
ECL	Enhanced Chemiluminescence
EDTA	Ethylenediaminetetraacetic acid
EGF	Epidermal growth factor
EGFR	Epidermal growth factor receptor
EMT	Epithelial-mesenchymal transition
ER	Oestrogen receptor
FBS	Foetal bovine serum
FDA	Food and Drug Administration
FGF	Fibroblast growth factor
FISH	Fluorescence *in situ* hybridisation
FITC	Fluorescein-5-isothiocyanate
GIT	Gastrointestinal tract
H&E	Haematoxylin and Eosin
HGF	Hepatocyte growth factor
HMEC	Homo sapiens dermal endothelium
ICF	Immunocytofluorescence

IHC	Immunohistochemistry
IRS	Immune reactive scoring
LB	Luria-Broth
LRP	Lipoprotein receptor-related protein
LumA	Luminal A
MET	Mesenchymal-epithelial transition
MFI	Median fluorescence intensity
NCCN	National Comprehensive Cancer Network
NCCP	National Cancer Control Program
NPI	Nottingham prognostic index
NICD	National Institute for Communicable Diseases
PBS	Phosphate buffered saline
PCR	Polymerase chain reaction
PFA	Paraformaldehyde
PI	Propidium Iodide
PLB	Passive Lysis Buffer
PLL	Poly-L-Lysine
PR	Progesterone receptor
PTCH	Patched
PVDF	Polyvinylidene fluoride
RIPA	Radioimmunoprecipitation assay buffer
RNA	Ribonucleic acid
SDS	Sodium Dodecyl Sulphate
SEM	Scanning Electron Microscope
SMAD	Homologues of the drosophila protein mothers against decapentaplegic (MAD) and the *Caenorhabditis elegans* protein Sma
SUFU	Suppressor of fused homolog
TAC	Docetaxel, Doxorubicin and Cyclophosphamide
TB	Trypan blue
TCF	T-cell Factor
TE	Tris-EDTA
TEMED	Tetraacetylethylenediamine
TGF	Transforming growth factor
TN	Triple Negative
TNBC	Triple-negative breast cancer

TNF	Tumour Necrosis Factor
TNM	Tumour, Node and Metastasis
VEGF	Vascular endothelial growth factor

General Introduction

1.1 Mammary gland development is a multistage process that involves epithelial and mesenchymal interaction

The mammary gland is characterised by dynamic cellular plasticity that is responsible for hormonal responsive tissue remodelling in puberty (Javed and Lteif, 2013). This remodelling is continuous throughout life and involves complex interactions between epithelial and mesenchymal tissue, which makes the mammary gland tissue prone to carcinogenesis (Kratochwil, 1986; Robinson *et al.*, 1999; Gusterson and Stein, 2012; Javed and Lteif, 2013). Moreover, it was found that the process of epithelial-mesenchymal transition (EMT) is essential for the morphogenesis of mammary gland (Watson and Khaled, 2008; Chakrabarti *et al.*, 2012). Understanding the anatomy and histology during stages of the mammary gland development, and the molecular pathways that regulate them provides insight into the deregulated processes during carcinogenesis (Hassiotou and Geddes, 2013).

Significant remodelling of both the parenchyma and the stroma of the mammary gland occurs at the various phases of the postnatal stage, and several studies indicated that these changes correlate to the breast cancer subtypes and patient prognosis (Patsialou *et al.*, 2009; McCready *et al.*, 2010).

1.1.1 The phases of mammary gland development require interactions and between epithelial and mesenchymal components

The human mammary gland is an apocrine gland consisting of parenchymal (ductal, lobular epithelial and myoepithelial) and stromal elements (adipocytes, fibroblasts, blood vessels, and immune cells) (Van Keymeulen *et al.*, 2011; Javed and Lteif, 2013). The ductal epithelial tissue is composed of two types of cells, inner luminal epithelial cells separated from basement membrane by myoepithelial cells (Figure 0-1-G) (Deugnier *et al.*, 1995; Howard and Gusterson, 2000). Some of the luminal epithelial cells are in contact with basement membrane in the area of acini between the processes of myoepithelial cells (Figure 0-1-H) (Hamperl, 1970; Howard and Gusterson, 2000).

Luminal cells that form the alveoli produce nutrients and secrete water while myoepithelial cells contract to guide the milk out of the breast ducts (Deugnier *et al.*, 2002; Van Keymeulen *et al.*, 2011; Van Keymeulen *et al.*, 2017). The ductal elements

are embedded in fibrous stromal tissue (Figure 0-1-E) (Hassiotou and Geddes, 2013). The mesenchymal cues control branching patterns of mammary gland regardless of epithelial origin (Sternlicht, 2006).

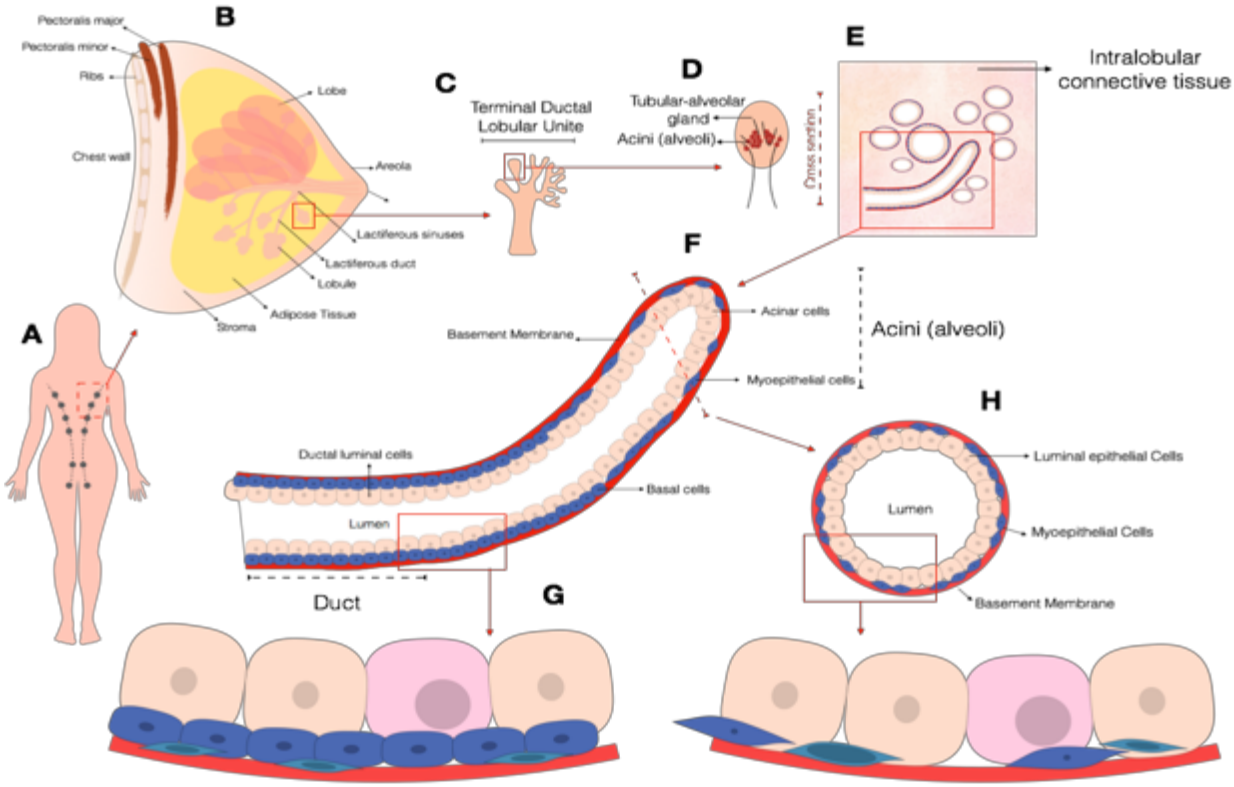

Figure 0-1, The structure of mammary gland.
Summary of mammary gland structure. (A) The mammary gland is a localised pectoral region between the second and sixth ribs (Vorherr, 1974; Geddes, 2007). (B) The nipple is infiltrated by nipple ducts (Cooper, 1840; Hassiotou and Geddes, 2013). The ductal system is composed of small ductules draining alveoli and combine into main ducts that dilate slightly to form the lactiferous sinus. The glandular structure at puberty is composed of lobes. The lobules are separated from each other by interlobular stroma consisting of dense fibrous tissue embedded in adipose tissue (Cooper, 1840; Hassiotou and Geddes, 2013). (C) Acini develop at the end of terminal branches (D) the terminal duct lobular unit, the functional unit of mammary gland (Sternlicht, 2006; Javed and Lteif, 2013). (D) The smaller lobules in terminal ductal lobular unit contain 10-100 alveoli (Cooper, 1840; Hassiotou and Geddes, 2013). (G) The myoepithelial cells on basement membrane of ducts are cuboidal whereas (H) myoepithelial cells in acini showed flattened morphology (Deugnier *et al.*, 1995; Howard and Gusterson, 2000). The figure was drawn by the author from the mentioned references.

Myoepithelial cells have a crucial role in the establishment of the polarised mammary epithelial bilayer and control the level of stromal invasion (Deugnier *et al.*, 2002; Gudjonsson *et al.*, 2002). A significant function of myoepithelial cells is the production of basement membrane (Warburton *et al.*, 1981; Kedeshian *et al.*, 1998; Gudjonsson *et al.*, 2002). Studies found that the interaction between luminal epithelial cells and extracellular matrix is mediated by myoepithelial cells (Deugnier *et al.*, 2002).

Barsky and Karlin (2006) found that myoepithelial cells have anti-angiogenic properties and an anti-invasive function.

1.2 Breast cancer

1.2.1 Epidemiology and aetiology of breast cancer

1.2.1.1 Breast cancer statistics show that it is an international burden

According to the World Health Organisation WHO (2008), breast cancer is the most common type of cancer in females in both developed and the less developed countries. Incidence rate is increasing with a low survival rate of breast cancer particularly in less developed countries, due to diagnosis at late stages (Coleman *et al.*, 2008). In the UK, breast cancer remains the most common cancer in the UK since 1997 with a 2% increase expected between 2014 and 2035 according to CRUK (2017). The ten year survival rate for breast cancer in the UK is 78%, which was doubled over the last 40 years (CRUK, 2017).

1.2.1.2 Age is the most significant risk factor for breast cancer

One of the most well-documented risk factors for breast cancer and many other cancers is age (Singletary, 2003). The risk of breast cancer increases in females significantly after the age of 30 until it reaches a plateau at 80 years old (Schlange *et al.*, 2007).

Lifestyle factors that cause an increased risk of breast cancer include alcohol consumption (Harvey *et al.*, 1987; Schatzkin *et al.*, 1987) and increased body weight (Tretli, 1989; Singletary, 2003). Duration of use of hormone replacement therapy (Colditz *et al.*, 1990; Steinberg *et al.*, 1991; Lancet, 1997), exposure to radiation (Land *et al.*, 1980; Boice *et al.*, 1991), early onset of the menstrual cycle (Brinton *et al.*, 1988), and smoking (Conway *et al.*, 2002) have also been implicated. Furthermore, late full-term pregnancy and lactation (after the age of 30) (Brinton *et al.*, 1983a; Brinton *et al.*, 1983b), and a prior history of breast cancer (Hankey *et al.*, 1983; Rosen *et al.*, 1989a) increase disease risk. Moreover, 5% of breast cancer cases are due to germline mutation (Easton *et al.*, 1995).

1.2.2 Challenges in identifying patients with poor prognosis via clinical diagnosis, histological classification and molecular classification

The National Cancer Control Program (NCCP (2002) recommend the early diagnosis of the high-risk group (females over the age of 50); they concluded that use of

mammography is the most effective diagnostic method for early detection (NCCP, 2002; Bevers *et al.*, 2009).

Symptoms of breast cancer include increased breast pain and tenderness (Barton *et al.*, 1999; Millet and Dirbas, 2002), palpable mass detection (Pruthi, 2001), and nipple discharge (Meisner *et al.*, 2008). Clinical breast examination recommended by the NCCN guidelines (Gradishar *et al.*, 2017) includes inspection of breast positioning and examination of the breast parameters (van Dam *et al.*, 1988; Pruthi, 2001). This is then followed by ultrasound, and fine needle aspiration and clinical confirmation procedures by core needle biopsy (Pruthi, 2001; Gradishar *et al.*, 2017). Sections of fixed total tumour resection is the diagnostic procedure for confirmation of suspected malignancy by pathological examination (Meisner *et al.*, 2008).

The standard staging system for breast cancer following the guidelines of the American Joint Committee on Cancer (Edge and Compton, 2010) is based on the evaluation of the primary tumour size (T), lymph node involvement (N), and detected metastasis (M). Breast cancer is also categorised into five stages (I-V) depending on the TNM criteria and types (Woodward *et al.*, 2003; Edge and Compton, 2010).

Following the staging of the breast cancer, histological examination of the excised tumour is needed for evaluation of the subtype of breast cancer to determine the appropriate treatment (Gradishar *et al.*, 2017).

1.2.2.1 Histological classification of breast cancer was limited to the skill of the pathologist and was not successful in determining prognosis

Breast cancer is a heterogeneous disease that has several distinctive histological and biological subtypes (Malhotra *et al.*, 2010; Weigelt *et al.*, 2010). Histologically, breast cancer is categorised into ductal and lobular types which are further divided into *in situ* and invasive carcinomas that were first described by Wellings and Jensen (1973); Wellings *et al.* (1975) and reviewed by Malhotra *et al.* (2010); Weigelt *et al.* (2010); Kaufman *et al.* (1984).

Ductal carcinoma *in situ* is further categorised into Comedo, Cribriform, Micropapillary, Papillary and Solid-based on the architectural features of the tumours (Malhotra *et al.*, 2010). The invasive tumours also include infiltrating ductal, invasive lobular, mixed ductal/lobular, mucinous (colloid), tubular, medullary and papillary carcinomas (Malhotra *et al.*, 2010).

The ductal and lobular classification of breast cancer does not reflect their origin, but they are designated according to morphology, architecture, and

immunohistochemical properties (Malhotra *et al.*, 2010; Weigelt *et al.*, 2010). Invasive ductal carcinoma is the most common type (80%), and lobular is least frequent (8-24.7%) of all the invasive adenocarcinomas of the breast (Martinez and Azzopardi, 1979; Dixon *et al.*, 1982; Dixon *et al.*, 1991).

There were limitations to the histological classification and staging of breast cancer depending on the skill of the pathologist, and subclassifying rare and poorly-differentiated cases can be difficult. Therefore, several methods were conducted to find new approaches for subclassifying this heterogeneous disease and identify cases that require additional intervention. Breast cancers are extremely diverse both morphologically and genetically which results in differing responses to treatment (Perou *et al.*, 2000), however, histological classification of breast cancer subtypes alone was not successful in identifying patients with the worst prognosis (Sims *et al.*, 2007).

1.2.2.2 Molecular classification of breast cancer from the discovery of the importance of hormone receptors to the development of targeted therapies

Molecular classification of breast cancer commenced with the utilisation of receptors status, including oestrogen receptor (ER), progesterone receptor (PR) and the overexpression/amplification of human epidermal growth factor receptor two (HER2) as recommended by the World Health Organisation (WHO, 2008). Additionally, the cell proliferation marker (Ki67) is used to determine the prognosis of breast cancer patients (Sims *et al.*, 2007).

Determination of the status of these receptors identified patients likely to respond to targeted therapies (Rakha *et al.*, 2010b). For example, tamoxifen and aromatase inhibitors (for ER or PR) (Cole *et al.*, 1971; Giudici *et al.*, 1988) or trastuzumab or lapatinib (for HER2) (Slamon *et al.*, 1987; Press *et al.*, 2008). However, the use of molecular profiling alone was not successful in predicting responses without the clinicopathological diagnosis (Rouzier *et al.*, 2005).

The molecular expression profiles were used to classify breast cancer according to poor prognosis (van 't Veer *et al.*, 2002), relapse predictors (Paik *et al.*, 2004), and genes associated with an increased risk of metastasis (Wang *et al.*, 2005). The molecular classes provided unbiased hierarchical groups that displayed a significant difference in prediction of patient's overall survival (Malhotra *et al.*, 2010). Perou *et al.* (2000) identified several clusters of molecular classes of breast cancer including; basal-like, $HER2^{+ve}$, normal-like, luminal A and luminal B (Table 0-1) (Sorlie *et al.*, 2001;

Sorlie *et al.*, 2003). Rouzier *et al.* (2005) later found that breast cancer cases that belong to these clusters responded differently to chemotherapy treatment.

Genetic profiling studies were able to identify molecular subtypes with poor prognosis including triple-negative (TNBC) (subtypes that are negative for the three prognostic receptors) and basal-like breast cancers (BLBC) comprise around 15% of all breast cancer cases with 90% of these cases showing poor differentiation at diagnosis, and 70% expressing basal markers (Rakha *et al.*, 2009; Rakha and Chan, 2011). The basal-like breast cancers are also characterised by high-grade, increased mitotic activity and high nuclear atypia with pushing boundaries and spindle-shaped cells (Chao *et al.*, 2010; Seal and Chia, 2010).

TNBC and BLBC subtypes have peak recurrence in the first three years after diagnosis that drops significantly after that, with decreased survival rate after detection of metastasis (Rakha *et al.*, 2008; Rakha *et al.*, 2009; Badve *et al.*, 2011). Therefore, there is a pressing need for the identification of new prognostic markers, and their utilisation for the development of novel targeted therapies, see Table 0-1 (Sorlie *et al.*, 2001; de Ruijter *et al.*, 2011; Arnedos *et al.*, 2012).

Table 0-1: Molecular classification of breast cancer, percentage prevalence, hormone receptor expression, HER2 status, cytokeratin expression and genetic characteristics.

The table shows the subclassification of breast cancer according to the molecular clusters. The table also lists the markers associated with these subtypes (Perou *et al.*, 2000; Sorlie *et al.*, 2001; Sorlie *et al.*, 2003; Herschkowitz *et al.*, 2007; Prat *et al.*, 2010; Rakha *et al.*, 2010a).

Molecular subclassification	% prevalence	Hormone receptors		HER2	Cytokeratin	Genetic characteristics
		ER	PR			
Normal-like	Unknown	-	-	-	-	Adipose tissue gene signature
Luminal A	19-39%	+	+/-	-	CKs 8/18	-
Luminal B	10-23%	+	+/-	+	CKs 8/18	Proliferation markers
HER2+	4-10%	-	+/-	+	CKs 8/18	-
Basal-like	16-37%	-	-	-	CKs 5/6, CK14, and CK17	EGFR
Claudin-low	12-14%	-	+/-	-	-	Claudin3/4/7 low. Vimentin, E-cadherin low, Zeb1

Additional breast cancer molecular subtypes were discovered including the apocrine tumours, identified by Farmer *et al.* (2005), which are $HER2^{+ve}$ and androgen receptor (AR) positive. This subtype comprises the majority of the $HER2^{+ve}$ tumours and form the third major group after luminal and basal subtypes (Farmer *et al.*, 2005;

Sims *et al.*, 2007). The claudin-low subtype was identified based on the intrinsic genetic expression profile and low patient survival (Table 0-1) (Herschkowitz *et al.*, 2007; Prat *et al.*, 2010).

1.2.3 Treatment options for breast cancer

Three types of treatment are available for breast cancer, the selection of treatment depends on the histological, clinicopathological features, and molecular type. The choices for treatment include surgical resection, radiation and systemic therapies used singly or in combination. Systemic therapy includes the use of targeted therapies (e.g. endocrine treatments) and chemotherapies.

1.2.3.1 Surgery

The first option for breast cancer treatment was the Halsted radical mastectomy that includes complete resection of the mammary gland, skin, breast tissue, underlying pectoralis major and minor muscles with the axillary lymph nodes (Halsted, 1907). This approach resulted in the reduction of local recurrence that ranged from 6% to 80%, however, with side effects of: sensory abnormalities, deformity, and lymphedema (Halsted, 1907). Fisher *et al.* (1989) developed a less radical surgical approach with preservation of most of the necessary breast tissue. This approach was developed further to the surgical approach used currently involving resection of primary tumour and the involved lymph nodes (Akram and Siddiqui, 2012).

Neoadjuvant chemotherapy was utilised as the first approach to reduce the bulk of the tumour for locally invading tumours, followed by resection or total breast mastectomy depending on the clinical situation (Akram and Siddiqui, 2012). Still, surgery alone was not successful in treating breast cancer, nor in reducing recurrence and increasing survival.

1.2.3.2 Radiotherapy

Pfahler (1932) was the first to record the use of radiation therapy for the treatment of breast cancer. This technique increased the survival rate of early stage breast cancer patients by 80% (Pfahler, 1932). Radiation therapy showed the same efficacy as radical breast surgery (Atkins *et al.*, 1972; Fisher *et al.*, 1985; Fisher *et al.*, 1989). Later, studies found that the use of adjuvant radiation therapy resulted in the reduction, but not eradication, of local and regional metastasis and improved overall survival (Overgaard *et al.*, 1997; Ragaz *et al.*, 1997; Overgaard, 1999), thus, supporting the use of radiation therapy as a standard treatment in breast cancer.

1.2.3.3 Systemic therapy

The initial chemotherapy treatment was using a single agent such as cyclophosphamide, and later combination of chemotherapeutic agents was tested with a varied response rate (Bonadonna *et al.*, 1976; Brambilla *et al.*, 1976). In the 1970s, Cyclophosphamide-Methotrexate-5-Fluorouracil (CMF) regimen was the gold standard for treating breast cancer cases as well as other solid cancers (Bonadonna *et al.*, 1976).

In the 1990s, CMF became the primary treatment regimen used as adjuvant chemotherapy for early breast cancers (Akram and Siddiqui, 2012). It was later found that it reduced breast cancer mortality by 20% (Early Breast Cancer Trialists' Collaborative, 2005). Other regimens were developed and tested including Docetaxel, Doxorubicin and Cyclophosphamide (TAC) and 5-Fluorouracil, Doxorubicin and Cyclophosphamide and found to be beneficial for early-stage breast cancer (Martin *et al.*, 2005).

Currently, chemotherapeutics are used as neoadjuvant, adjuvant and in metastatic breast cancer treatment (Akram and Siddiqui, 2012). The use of chemotherapy is not preferred because of the cytotoxic and genotoxic side effects (Evrard *et al.*, 1999; Sodergren *et al.*, 2016). Therefore, there has been a massive effort in the medical community to develop more advanced treatments with fewer side-effects.

Targeted therapy consists of blockers (e.g. Tamoxifen) and small molecules (aromatase inhibitors) (Malhotra *et al.*, 2010; Rakha *et al.*, 2010b; Liedtke and Kiesel, 2012), which block peripheral synthesis of oestrogen (Giudici *et al.*, 1988). The most recent targeted therapy is against the oncogene *HER2* with either targeted antibodies (Trastuzumab) or small molecule inhibitors (lapatinib) (Slamon *et al.*, 2001).

1.2.4 Relapse, metastasis, and lack of targeted therapy persist in treating breast cancer

Even with the advances in targeted treatments, there are three difficulties to overcome for the effective treatment of breast cancer. A significant number of patients with luminal/hormone-positive breast cancer and HER2-overexpressing breast cancers develop resistance to targeted therapy, followed by relapse and metastasis (Early Breast Cancer Trialists' Collaborative, 2005; Coates *et al.*, 2007; Group *et al.*, 2009; Cuzick *et al.*, 2010). Another challenge is the management of disease already metastatic at presentation (Akram and Siddiqui, 2012).

Also, according to the recommended regimen of chemotherapy more than 80% breast cancer patients receive adjuvant chemotherapy (Eifel *et al.*, 2001; NCCP, 2002). It is estimated that only 40% of those cases develop relapse and die eventually. Thus, indicating that more than half of those patients were over-treated with chemotherapy that has toxic side-effects (Eifel *et al.*, 2001; O'Shaughnessy, 2005; Weigelt *et al.*, 2005).

Another problem is the lack of targeted therapy for triple-negative breast cancers (hormone and HER2 receptor negative) (Rakha *et al.*, 2009; Peddi *et al.*, 2012). Moreover, triple-negative breast cancer has a high risk of distal recurrence, with increased cancer-related deaths after relapse, compared to the other subtypes of breast cancer (Dent *et al.*, 2007; Tang *et al.*, 2016).

1.2.5 Breast cancer metastasis

Almost 90% of all breast cancer-related deaths are caused by metastasis (Wang and Zhou, 2013). Detection of cancer metastasis is the worst prognostic factor and correlates with a poor survival rate (Rosen *et al.*, 1989a; Kowalski *et al.*, 2003; Weigelt *et al.*, 2005). It is estimated that around 15% of breast cancer cases develop metastasis within five years of initial diagnosis (Weigelt *et al.*, 2005; WHO, 2008; CRUK, 2017).

Cancer metastasis commences with the invasion of tumour cells into the surrounding stroma followed by migration in the lymphatic system or bloodstream (Clark and Vignjevic, 2015), which is one of the hallmarks of cancer (Hanahan and Weinberg, 2011). Cancer cells achieve this through changing their cellular structure and alteration of their interaction with surrounding cells and extracellular matrix (Hanahan and Weinberg, 2011).

1.2.5.1 Challenges associated with the management and treatment of breast cancer metastasis

Breast cancer metastasis has a heterogeneous nature, making it difficult to identify risk factors and to develop effective treatments for this condition (Weigelt *et al.*, 2005). The established prognostic indications that are currently used in clinical diagnosis are histological and clinicopathological factors used in the staging and grading of breast cancer (lymph node involvement, primary tumour size and loss of differentiation) (Koscielny *et al.*, 1984; Carter *et al.*, 1989; Elston and Ellis, 1991).

Rosen *et al.* (1989b) found that about third of breast cancer cases that did not show signs of lymph node involvement went on to developed metastases. In addition, a third of breast cancer cases that did showed lymph node involvement also went on to

develop metastasise. They found that a third of breast cancer cases showing lymph node involvement did not develop metastasis in ten years following local therapy (Rosen *et al.*, 1989b; McGuire and Clark, 1992). Similarly, Weiss *et al.* (1983) argued that there was no relationship between the tumour size and the metastatic potential of a tumour.

Gene expression studies assisted in isolating signatures for metastatic traits and helped in identifying new therapeutic targets (Weigelt *et al.*, 2005). Several studies identified molecular signatures that were associated with metastasis and poor survival (van 't Veer *et al.*, 2002; van de Vijver *et al.*, 2002; Ramaswamy *et al.*, 2003). However, it was hypothesised that a rare subpopulation of cells acquires metastatic potential, which makes the genetic detection of such a rare population difficult (Fidler and Kripke, 1977).

According to Weigelt *et al.* (2005), the challenges of managing breast cancer metastasis includes a lack of prognostic markers to identify patients with the worst prognosis, improving targeted treatments, and availability of model systems to study the process of breast cancer metastasis. Therefore, it is important to find new molecular markers that can be exploited in either the early identification of cases with a poor prognosis, or in the development of targeted therapy.

The modes and the dynamics of cancer cell migration were previously described by Clark and Vignjevic (2015). Human cancer cells migrate in one of three ways; either as single-cells, multicellular streaming, or in collective migration (Clark and Vignjevic, 2015). In all modes of metastasis, cells lose cell-cell contact and display a more mesenchymal phenotype (Clark and Vignjevic, 2015). It was observed that in epithelial tumours, including breast cancer, cancer cells metastasised collectively (Caussinus *et al.*, 2008). Cancer cells formed strands and cords of tumour cells that invaded the adjacent stroma at the invasive front of a tumour (Caussinus *et al.*, 2008; Clark and Vignjevic, 2015).

As mentioned previously, the morphology of the cells at the invasive front of primary breast tumours have a spindle-shaped morphology (Chao *et al.*, 2010; Seal and Chia, 2010). The process of EMT is linked prominently to the cellular alterations that take place to facilitate metastasis (Klymkowsky and Savagner, 2009; Thiery *et al.*, 2009).

1.3 EMT is essential for mammary gland development, and disturbance of EMT is an essential event in breast cancer progression and metastasis

EMT is the phenotypic switching in shapes of cells that provides a flexibility of cellular function that is essential during normal embryogenesis and in other physiological stresses such as wound healing (Micalizzi *et al.*, 2010).

EMT involves a series of events that commence with loss of epithelial cell polarity with the disassembly of tight junctions (Micalizzi *et al.*, 2010), followed by the loss of cell-cell contact and degradation of the basement membrane (Peinado *et al.*, 2004; Micalizzi *et al.*, 2010). Epithelial membrane proteins such as E-cadherin and integrins are replaced by other types of cadherins and integrins with transient adhesive properties (Peinado *et al.*, 2004). Also, vast changes in the arrangement of the cytoskeletal proteins take place, such as the replacement of the actin cytokeratin with stress fibres and, replacement of intermediate filaments with vimentin. Together, these cellular changes result in a phenotypic conversion of cuboidal epithelial cells to spindle/mesenchymal-like cells (Micalizzi *et al.*, 2010).

Kalluri and Weinberg (2009) classified EMT into three types, depending on clear functional consequence, but the molecular regulation of each subtype is not fully understood. EMT types I and II are involved in normal physiological processes including; embryogenesis and organogenesis (type I) and in the process of wound healing, tissue regeneration, inflammation and fibrosis (type II), (Kalluri and Weinberg, 2009; Zeisberg and Neilson, 2009; Wang and Zhou, 2011). On the other hand, type III is involved in cancer metastasis and include misappropriation of the EMT signalling pathways (Kalluri and Weinberg, 2009; Zeisberg and Neilson, 2009; Wang and Zhou, 2011).

Complete EMT occurs during single cell migration, which is the mechanism that immune cells use to migrate to the site of inflammation (Halin *et al.*, 2005). Complete EMT is not the only method by which epithelial cells gain the ability to migrate during development. Partial EMT results in collective movement in sheets of cells (Rorth, 2009). This form of cellular migration is also essential in human development as it helps in maintaining the cellular structure of the tissue while remodelling. It also allows immobile cells to be moved with the mobile cells, ensuring appropriate cellular distribution (Rorth, 2009).

Collective cell movement is seen during normal tissue remodelling such as in intestinal turnover (Batlle *et al.*, 2002; Barker *et al.*, 2008) and in mammary gland

remodelling (Pearson and Hunter, 2007; Ewald *et al.*, 2008). In collective migration, the cells display cellular alterations associated with EMT such as loss of polarity, modification of the extracellular matrix, and acquisition of mesenchymal phenotype while, at the same time, the cells maintain cell-cell junctions (Rorth, 2009). Therefore, due to the similarities between collective cellular migration and EMT, it was suggested that the epithelial and mesenchymal phenotypic conversion does not reflect an absolute status but rather a spectrum of epithelial and mesenchymal properties (Rorth, 2009; Micalizzi *et al.*, 2010). There is evidence that the process of EMT is involved in the regulation of mammary gland development. In fact, EMT is involved in the regulation of the development of all the human body organs and this process is type I EMT (Wang and Zhou, 2011). Expansion of tissue occurs with infiltration of epithelial tissue through the mesenchyme to form the primary ducts (Tobon and Salazar, 1974; Sakakura *et al.*, 1987; Hens and Wysolmerski, 2005).

1.3.1 The EMT process is regulated by several signalling pathways that implies the possibility of crosstalk and is triggered by cellular status and stimulation from the microenvironment

Several pathways are involved in the regulation of EMT in human tissue including Hedgehog, TGF-β, Notch, Wnt/β-catenin, TNF-α, integrins and receptor tyrosine kinase pathways (Garg, 2013) (Figure 0-2). Upon activation of the receptors with ligands, a signalling cascade is triggered inside the cells and initiates the process of EMT.

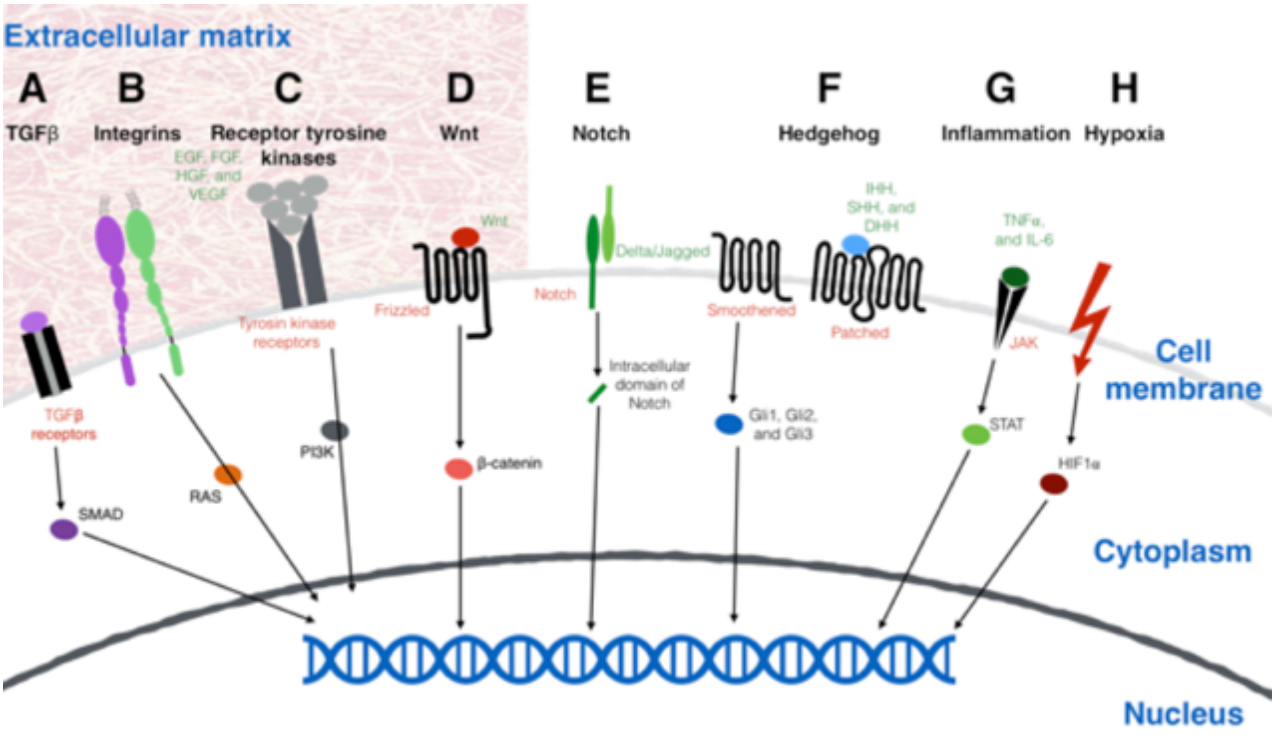

Figure 0-2, Pathways involved in the regulation of the process of EMT.
The signalling pathways involved in regulating EMT. (A) Transforming growth factor β (TGFβ) signalling is induced by binding of ligands to receptor. TGFβ receptor activation by phosphorylation results in recruitment of SMAD transcription factors that translocate to nucleus and binds to DNA (Xu *et al.*, 2000; Gonzalez and Medici, 2014). (B) Integrins are heterodimeric transmembrane proteins. Integrin interact with TGFβ and activate the pathway (Mamuya and Duncan, 2012) also, integrins interacts with components of extracellular matrix (Yen *et al.*, 2014). (C) Receptor tyrosine kinases (RTKs) are activated by binding to growth factors including epidermal growth factor (EGF), fibroblast growth factor (FGF), hepatocyte growth factor (HGF), and vascular endothelial growth factor (VEGF). The binding results in dimerisation of receptors and eventually activation of signalling cascade (Lemmon and Schlessinger, 2010; Gonzalez and Medici, 2014). (D) Wnt signalling is transduced by Wnt binding to Frizzled receptor or low-density lipoprotein receptor-related protein (LRP) receptors. Wnt activation releases β-catenin which translocates to nucleus and binds to T-cell factor/lymphoid enhancer binding factor-1 (TCF/LEF-1) (Gonzalez and Medici, 2014; Nusse and Clevers, 2017). (E) Notch receptor is composed of extracellular and intracellular domain. Upon binding γ-secretase cleaves intracellular domain of Notch (NICD) that translocates to nucleus (Kopan, 2002; Miele *et al.*, 2006; Gonzalez and Medici, 2014). (F) Ligands of Hedgehog signalling pathway include Sonic hedgehog (Shh), Indian hedgehog (Ihh), and Desert hedgehog (Dhh) that bind to patched homolog 1 (Ptch1) and Ptch2, which release inhibition on Smoothened (Smo) (Gallet and Therond, 2005; Gonzalez and Medici, 2014). (G) The inflammatory stimuli activate TNFα and IL-6 which activate transcription factor signal transducer and activator of transcription 3 (STAT3), that activates Snail expression. (H) Hypoxia influence EMT by activation of Twist expression after activation of hypoxia-inducible factor 1α (HIF1α) (Yang *et al.*, 2008a). The figure was drawn by the author from the mentioned references.

Several layers of crosstalk between the EMT pathways have been identified. This crosstalk is due to the diverse range of processes involving EMT (Gonzalez and Medici, 2014). The context of cross-interaction between these signalling cascades also depends on interactions with the surrounding microenvironment and the cell state (Gonzalez and Medici, 2014).

The cellular statuses that result in triggering the EMT process include hypoxia (Lundgren *et al.*, 2009; Daly *et al.*, 2017); activation TGFβ and other growth factors (Daniel *et al.*, 1996; Cheng *et al.*, 2012); autocrine feedback loops (Schlange *et al.*, 2007); and extracellular matrix remodelling (Silberstein *et al.*, 1992; Gonzalez and Medici, 2014).

Zeisberg and Neilson (2009) categorised the biomarkers that identify the various types of EMT into five groups; cell surface markers (E-cadherin), cytoskeletal markers (vimentin), extracellular matrix proteins (collagen and fibronectin), transcription factors (Snail, Slug, and Twist), and micro-RNAs (Figure 0-3).

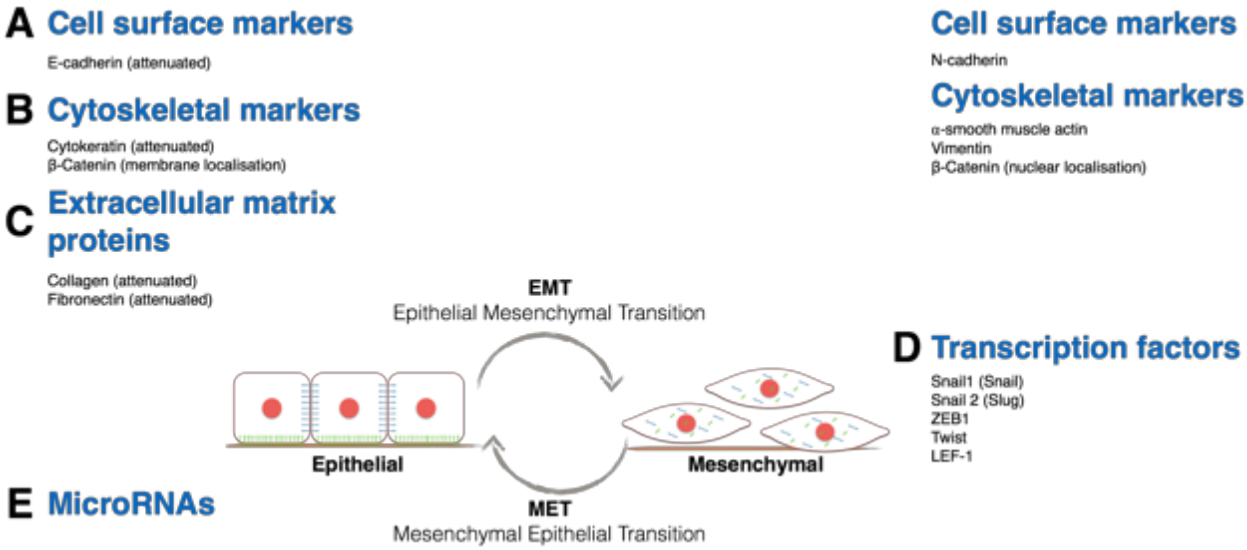

Figure 0-3, Markers of EMT.
The types of markers that are affected by EMT with few examples. (A) Changes in cell surface markers including attenuated expression of E-cadherin and change of N-cadherin level. (B) Changes in cytoskeletal markers such as attenuated expression of cytokeratin; changes in localisation of β-catenin; changes of mesenchymal markers level such as vimentin and α-smooth muscle actin. (C) Changes of extracellular matrix proteins such as collagen and fibronectin. (D) Changes of EMT transcription factors expression such as; Snail 1 (Snail), Snail 2 (Slug), ZEB 1, Twist and LEF-1. (E) Changes of microRNAs expression. The figure was drawn by the author and details adapted from (Zeisberg and Neilson, 2009; Wang and Zhou, 2013).

The most important hallmark of EMT commences with the loss of E-cadherin which directly affects the Wnt/β-catenin pathway. Also, increased expression of the mesenchymal markers (such as vimentin), with changes in the level and localisation of E-cadherin, status of Wnt/β-catenin signalling provides further confirmation of the mesenchymal change.

1.3.1.1 Constant E-cadherin expression and localisation to the cell membrane are the principal determinant of the epithelial status of cells

Cell-cell contact organises the structure of mammary epithelial cells which is mediated by E-cadherin and other membrane proteins (Claudin and Occludin) (Morrow *et al.*, 2010; Chen *et al.*, 2014). E-cadherin facilitates several cellular functionalities including cell-cell contact, cellular polarity, differentiation, stem cell properties, cell motility, migration, proliferation and survival. These functions are mediated through interaction with β-catenin and cytoskeletal protein (Figure 0-4-B) (Nagafuchi and Takeichi, 1989; Nieman *et al.*, 1999; Junxia *et al.*, 2010; Chen *et al.*, 2014).

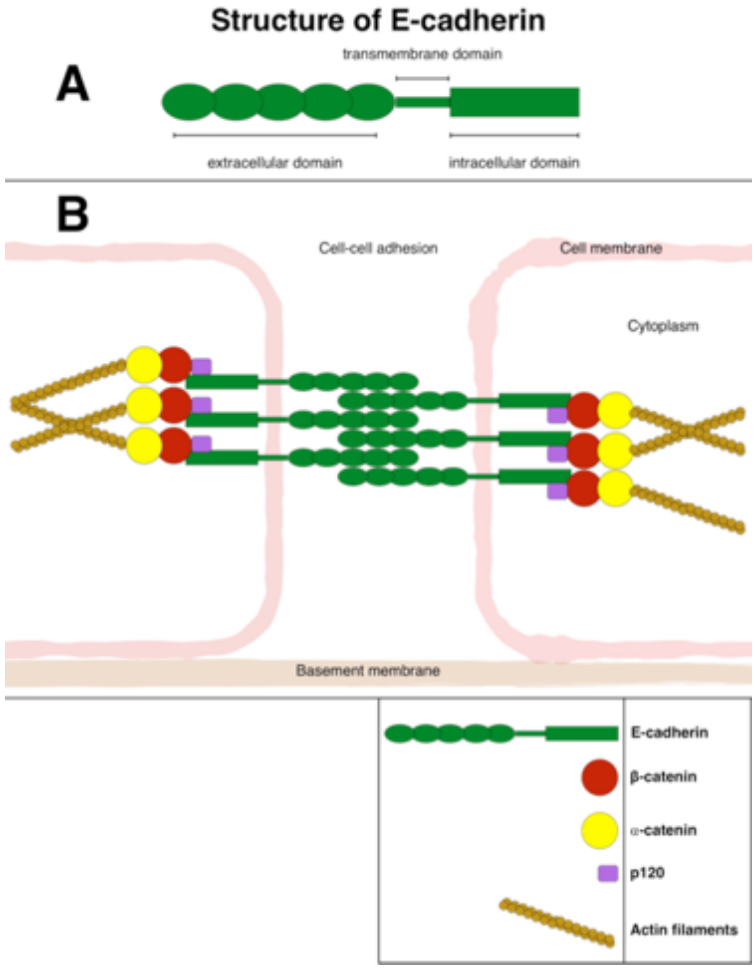

Figure 0-4, E-cadherin structure and the cell-cell adhesion structure formed by E-cadherin.
The figure shows the structure of E-cadherin protein and the cell-cell adhesion that is formed by E-cadherin protein. A- E-cadherin multidomain glycoprotein structure (van Roy and Berx, 2008). B- The cell-cell calcium-dependent adhesions formed by E-cadherin assembly to the actin cytoskeleton through catenin proteins. It is linked to the cytoskeletal filaments via interaction with cytoplasmic proteins including (α-catenin and β-catenin) (Yoshida and Takeichi, 1982; Peyrieras *et al.*, 1983). The key below explains the different components of the cell-cell adhesion. The figure was drawn by the author from the mentioned references.

E-cadherin is known as the caretaker of the epithelial phenotype (Thiery, 2002; Oloumi *et al.*, 2004). E-cadherin functions to maintain the epithelial morphology via interaction of extracellular domains, and by intracellular domain binding to catenins (Takeichi, 1991; Tian *et al.*, 2011). Of the components that interact with the intracellular domain of the of E-cadherin, β-catenin is also a crucial regulator of the Wnt signalling pathway (Clevers and Nusse, 2012). Cell contact is a critical determinant of the EMT status of cells, as loss of E-cadherin eventually leads to increasing the free β-catenin pool and, therefore, activation of the EMT process (Hay and Zuk, 1995). Therefore, the loss of cell-cell contact that is mediated by E-cadherin/β-catenin triggers EMT in normal physiological processes as well as in diseases such as cancer (Tian *et al.*, 2011).

In epithelial cells, E-cadherin clusters to the cell membrane and interacts with the E-cadherin of neighbouring cells (Adams and Nelson, 1998; Thiery, 2002). This localisation of the protein to the cell membrane is critical for the maintenance of stable adherens junctions, and disturbance of E-cadherin is known to induce a mesenchymal change (Imhof *et al.*, 1983; Thiery, 2002). In addition, there is a direct correlation between the increase in mesenchymal phenotype and reduction in E-cadherin production (Behrens *et al.*, 1989; Thiery, 2002).

E-cadherin expression in normal mammary gland tissue is strong and localised at the cell boundaries of epithelial cells, forming a cobblestone appearance of epithelial tissue (Wheelock *et al.*, 2001; Kowalski *et al.*, 2003). All non-epithelial tissue in the mammary gland does not express E-cadherin (Kowalski *et al.*, 2003).

Loss of E-cadherin protein or its function as result of mutation is a very rare event in breast cancer (Graff *et al.*, 2000). It was reported previously that the *CDH1* (E-cadherin gene) tumour suppressor was lost in ductal carcinoma (Li and Mattingly, 2008; Chen *et al.*, 2014). Graff *et al.* (2000) concluded that E-cadherin epigenetically silenced was transient and heterogeneous depending on cancer cells microenvironment. They also concluded that loss of E-cadherin expression by methylation in primary breast tumours is an early event (Graff *et al.*, 2000).

E-cadherin is involved in several essential pathways necessary for breast cancer progression. Vutskits *et al.* (2006) found that E-cadherin has a role in controlling the molecular pathway that regulates the cell cycle. Moreover, disturbance of cell-cell contacts and the cytoplasmic localisation of cadherins stimulate anoikis resistance in

breast cancer cells (Ribeiro *et al.*, 2013). Therefore, loss of E-cadherin is considered as one of the most critical hallmarks of cancer metastasis.

The loss of E-cadherin protein is a hallmark for EMT activation in embryogenesis and cancer progression (Hazan *et al.*, 2000; Huber *et al.*, 2005; Yang and Weinberg, 2008; Polyak and Weinberg, 2009; Thiery *et al.*, 2009; Yuki *et al.*, 2014). Onder *et al.* (2008) found that complete loss of E-cadherin was essential for cancer progression and induction of EMT in breast cancer. Derksen *et al.* (2006) confirmed that E-cadherin loss was responsible for anoikis-resistance and increased angiogenesis associated with metastasis in breast cancer, therefore suggested that E-cadherin is essential for tumour initiation and progression. Onder *et al.* (2008) also found that a truncated form of E-cadherin, lacking external domain of the protein, was sufficient to induce EMT in mammary epithelial cells. These findings were similar to Liu *et al.* (2006b), in which they noticed two distinct regulatory functions of E-cadherin; mediating an increase in proliferation at low density and inhibiting proliferation at higher densities.

In breast cancer, partial or total loss of E-cadherin is linked to increased invasiveness (Siitonen *et al.*, 1996), metastasis (Oka *et al.*, 1993; Hunt *et al.*, 1997) and poor prognosis (Heimann *et al.*, 2000). Qureshi *et al.* (2006) found that loss of E-cadherin expression correlated with prognosis and inversely with increased risk of metastasis in invasive ductal carcinoma. Rakha *et al.* (2005) suggested that loss of E-cadherin in non-lobular breast cancers assists in identifying patients with the worst prognosis. Similarly, Mahler-Araujo *et al.* (2008) found that poor prognosis non-lobular breast carcinomas that have triple-negative and metaplastic characteristics were associated with reduced E-cadherin expression.

Emerging evidence in the literature suggests that E-cadherin expression is essential in subsequent steps in EMT and cancer metastasis, but E-cadherin loss alone was not sufficient to start the invasion cascade in breast cancer cells (Onder *et al.*, 2008). Knocking down the expression of E-cadherin in normal-like breast cancer cell line MCF10A was insufficient to activate EMT nor increased the aggressiveness of this cell line (Chen *et al.*, 2014). Likewise, restoring E-cadherin expression in the E-cadherin knocked down cells did not restore the full epithelial morphology of MCF10A showing that E-cadherin expression alone was not enough to reverse mesenchymal transition (Li and Mattingly, 2008). Thus, loss of E-cadherin alone does not initiate invasion, even if it resulted in mesenchymal phenotypic change. Similarly, the

restoration of E-cadherin alone did not reverse the mesenchymal morphology of cells. Therefore, suggesting that the loss of E-cadherin is transient and can be reversed.

Re-expression of E-cadherin is essential and parenchyma-tumour cell-cell contact is necessary to induce MET to establish metastases in distant site. Thus, the loss of E-cadherin is transient, and re-expression of the protein occurs by mesenchymal-epithelial transition (MET) after establishing metastasis. Increased E-cadherin expression in metastatic ovarian cancer and high-grade glioma was associated with an increase in tumour invasiveness and poorer prognosis (Sundfeldt, 2003; Reddy *et al.*, 2005; Lewis-Tuffin *et al.*, 2010). Furthermore, Chao *et al.* (2010) found that E-cadherin expression increased at the metastatic site in 60% of cases of breast cancer compared to the original tumour. Also, the MDA-MB-231 (TN and basal-like) breast cancer cell line re-expresses E-cadherin when co-cultured with liver cells and when injected into mouse tail. Therefore, they concluded that E-cadherin expression was essential to complete tumour metastasis and that loss of E-cadherin in tumour cells is reversible (Chao *et al.*, 2010). Normal parenchymal cells from normal breast tissue was able to restore E-cadherin in the MDA-MB-231 cell line, however, culturing the same cells in the normal extracellular matrix or normal parenchyma-conditioned medium was not sufficient to change the mesenchymal phenotype to an epithelial one (Chao *et al.*, 2010).

In conclusion, loss of E-cadherin is the first step of EMT, yet this loss was not permanent, and re-expression was essential to promote secondary tumour establishment in breast cancer. Furthermore, acquisition of additional invasive properties is necessary for breast cancer progression in addition to the loss of E-cadherin (Onder *et al.*, 2008; Kumar *et al.*, 2011). It was suggested that breast cancer cell metastasis requires a reduction of E-cadherin and increased expression of other EMT-associated proteins (Nieman *et al.*, 1999; Hazan *et al.*, 2000). Therefore, assessing the expression of E-cadherin alone does not reflect the status of EMT or invasiveness of breast cancer because the loss or changes in expression is not a permanent situation. So, it is essential to include additional markers in the confirmation of the EMT status in the assessment of the changes of this process in breast cancer.

1.3.1.2 Increased expression of mesenchymal markers is associated with metastasis and increased cellular motility

Vimentin is a type III intermediate filament that is expressed in normal cells of mesenchymal origin (Gilles *et al.*, 2003; Herrmann and Aebi, 2004; Liu *et al.*, 2015). It is an essential filament during the developmental stages of the mammary gland and for

maintenance of tissue integrity (Liu *et al.*, 2015). It is highly organised and is involved in dynamic cellular processes. It is also associated with intracellular organelles and cell adhesion molecules (Kokkinos *et al.*, 2007). Thus, vimentin protein maintains cellular structure and function (Kokkinos *et al.*, 2007). Increased expression of this marker has been documented in several physiological processes including migration of epithelial cells in embryogenesis and organogenesis, and also during wound healing (Gilles *et al.*, 2003; Kokkinos *et al.*, 2007; Lundgren *et al.*, 2009).

In the human breast, myoepithelial cells express vimentin (Qu *et al.*, 2015). It is also expressed in fibroblasts, stromal cells, leukocytes, and it is low in epithelial cells (Kokkinos *et al.*, 2007). The vimentin promoter is targeted by the β-catenin/TCF transcription factor in mammary cells (Gilles *et al.*, 2003). Thus, the activation of EMT by the Wnt/β-catenin pathway results in increased mammary epithelial cell migration, caused by physiological and pathological processes (Gilles *et al.*, 2003; Kokkinos *et al.*, 2007).

Derksen *et al.* (2006) found that most adenocarcinomas and solid carcinomas that express an epithelial phenotype lacked expression of vimentin. Meanwhile carcinomas of metaplastic and biphasic histology express a high level of vimentin and lack expression of E-cadherin.

Increased expression of vimentin was associated with increased EMT and linked to increased metastatic potential in breast cancer. Cell lines that show increased vimentin expression had increased fibroblastic morphology, with increased motility and migration through a Matrigel® matrix; whereas cells that have low expression of vimentin, had more epithelial-like morphology and decreased motility (Sommers *et al.*, 1991). Loss of epithelial cytokeratin alongside an increase in vimentin expression was associated with lymph node metastasis, high tumour grade, poor prognosis and reduced disease-free survival (Chen *et al.*, 2008; Vora *et al.*, 2009). Hemalatha *et al.* (2013) found that increased expression of vimentin was associated with higher breast cancer tumour grade and with increased proliferative marker expression.

Association of this marker with the different subtypes of breast cancer has been reported. Increased expression of vimentin is associated with high-grade ductal carcinomas, but not with lobular carcinoma (Hemalatha *et al.*, 2013; Liu *et al.*, 2015). The expression of vimentin was also associated with low ER and PR breast cancers, as well as with increased invasiveness of the basement membrane (Kokkinos *et al.*, 2007; Sarrio *et al.*, 2008; Hemalatha *et al.*, 2013; Liu *et al.*, 2015). Moreover, it was reported

that vimentin overexpression is associated with TNBC and BLBC (Sarrio *et al.*, 2008; Kasper *et al.*, 2009; Ricardo *et al.*, 2011). Studies also concluded that increased vimentin expression is associated with HER2 positivity, metastasis and advanced disease stage (Ribeiro *et al.*, 2013; Tanaka *et al.*, 2016). (Hemalatha *et al.*, 2013). Furthermore, it was reported in several studies that loss of E-cadherin expression in highly invasive breast cancer cell lines is associated with increased expression of vimentin (Gilles *et al.*, 2003; Chen *et al.*, 2008).

Increased vimentin expression was seen at the invasive front of breast cancer along with increased β-catenin expression in the cytoplasm and nucleus and the loss of E-cadherin localisation at cell-cell adhesions (Gilles *et al.*, 2003; Sarrio *et al.*, 2008). Several studies reported that β-catenin functions in EMT by regulating the expression level of vimentin (Mestdagt *et al.*, 2006; Wang *et al.*, 2015). Liu *et al.* (2015) found that vimentin increases the aggressiveness of cancer cells by increasing their tolerance to extracellular stress by maintaining mechanical homeostasis and reorganising the cellular cytoskeleton.

High expression of vimentin has been seen in circulating tumour cells of patients with breast cancer, indicating that it was associated with increased early metastasis (Kallergi *et al.*, 2011). Dwedar *et al.* (2016) found that hypomethylation of the *vimentin* gene was frequently associated with TN breast cancer. Yamashita *et al.* (2013) also found that vimentin expression was associated with poorer prognosis in TN breast cancer cases and suggested its use as a prognostic marker.

However, no association was found between vimentin expression and tumour size, lymph node involvement and patient survival (Hemalatha *et al.*, 2013). One of the reasons for this apparent contradiction in reporting is vimentin expression within the stem cells of the breast. It was concluded that the expression of vimentin in breast tissue is associated with cells that have bilinear origin or differentiation potential (epithelial and myoepithelial) and that it was not associated with the process of EMT (Hemalatha *et al.*, 2013). Many studies indicated that vimentin expression is associated with stem cell-like properties in breast cancer cells (Manuel Iglesias *et al.*, 2013; Liu *et al.*, 2014; Qu *et al.*, 2015).

In conclusion, the assessment of more than one marker is essential for the estimation of the epithelial/mesenchymal status of breast cancer cells. Furthermore, expression scoring, and subcellular localisation of the markers must also be considered.

In addition to the decrease in E-cadherin and increase of the free pool of β-catenin, increased vimentin expression is indicative for active EMT in human cancer (Gilles *et al.*, 2003; Sarrio *et al.*, 2008). Increased expression of vimentin was associated with several pathological conditions including human tumours (Conacci-Sorrell *et al.*, 2003; Ha *et al.*, 2013).

1.4 The critical role of Wnt/β-catenin pathway in the regulation of EMT during mammary gland development and breast cancer metastasis

β-catenin protein is the intermediate protein that facilitates the interaction between α-catenin and E-cadherin, and it is typically localised to the cell membrane (Nagafuchi and Takeichi, 1989). At multiple stages during human development, β-catenin is found in the cytoplasm and can facilitate the Wnt pathway. Upon activation of the pathway, β-catenin translocates to the nucleus and associates with the T-cell factor/lymphoid enhancer (TCF/LEF) transcription factors (Figure 0-4) (Korinek *et al.*, 1997; Morin *et al.*, 1997; Porfiri *et al.*, 1997).

Expression of β-catenin in normal breast tissue, or normal-adjacent tissue, was seen localised at inter-cellular borders of epithelial cells with no localisation at the basal or luminal surface of the epithelial cells (Karayiannakis *et al.*, 2001; Jiang *et al.*, 2009). Weak punctate staining was observed in the cytoplasm of myoepithelial cells, with no localisation at the basal surface and no staining found in parenchymal cells of mammary gland (Karayiannakis *et al.*, 2001).

1.4.1 The Wnt/β-catenin pathway is essential for the regulation of EMT

The localisation of β-catenin to areas of the cell-cell contact area is facilitated by binding to the E-cadherin intracellular domain and interaction with the actin cytoskeletal proteins essential for maintaining the epithelial phenotype (Chen *et al.*, 1999; Jeanes *et al.*, 2008). Without activation of Wnt signalling (Figure 0-5-1), the cytoplasmic level of the β-catenin protein pool is controlled by adenomatous polyposis coli (APC). The APC protein targets the β-catenin protein for phosphorylation, resulting in ubiquitination and rapidly targeting for proteasomal degradation (Aberle *et al.*, 1997; Bienz, 1999; Nusse and Clevers, 2017).

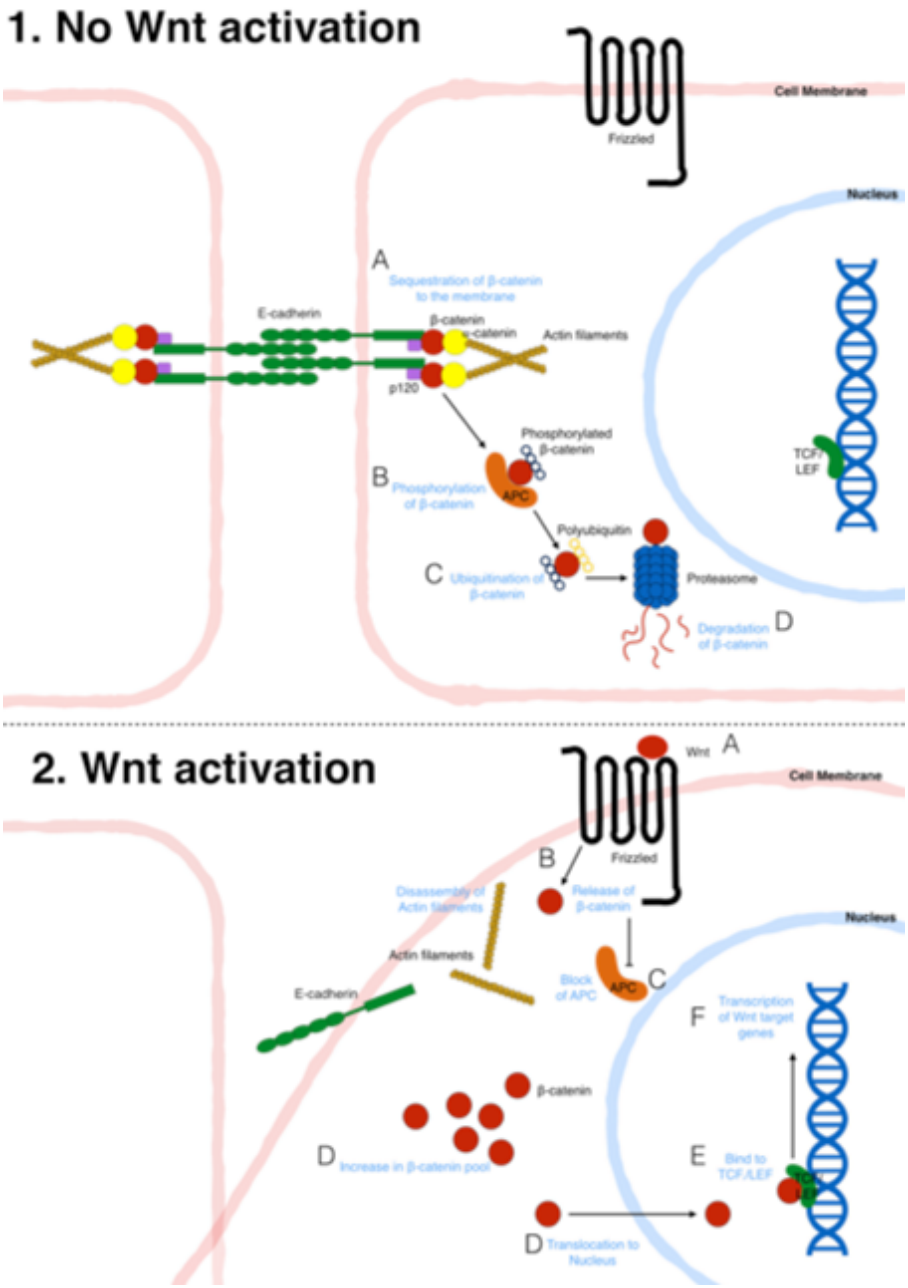

Figure 0-5, the Wnt signalling activation.

The Wnt pathway. 1- Deactivated or resting Wnt signalling pathway. (A) β-catenin protein in normal cells is sequestered to cell membrane (Nagafuchi and Takeichi, 1989; Nusse and Clevers, 2017). (B) Free β-catenin is rapidly targeted by the tumour suppressor adenomatous polyposis coli (APC) complex that phosphorylates β-catenin (Pronobis *et al.*, 2015; Nusse and Clevers, 2017). (C) Phosphorylated β-catenin is ubiquitinated. (D) Phosphorylated β-catenin rapid degradation by the proteasome (Aberle *et al.*, 1997; Clevers and Nusse, 2012). 2- Wnt signalling activation. (A) Wnt signalling is activated by binding of ligand (Wnt) to Frizzled receptor (Janda *et al.*, 2012; Nusse and Clevers, 2017). (B) Activation of Wnt releases of β-catenin protein from E-cadherin/β-catenin complex (Hulsken *et al.*, 1994; Tian *et al.*, 2011; Nusse and Clevers, 2017). (C) Active Wnt signalling inhibits of APC complex and disassembly of actin filaments from the E-cadherin/β-catenin complex (Hulsken *et al.*, 1994; Bienz, 1999). (D) Increase β-catenin free pool in cytoplasm as a result of Wnt activation. D- Free β-catenin protein translocates to nucleus (Bienz, 1999; Nusse and Clevers, 2017). (E) In nucleus, β-catenin binds to TCF/LEF and (F) and activates transcription of targeted genes (Korinek *et al.*, 1998; Bienz, 1999; Clevers and Nusse, 2012). The figure was drawn by the author from the mentioned references.

Loss of E-cadherin alone does not result in nuclear localisation of β-catenin due to constant activation of the APC degradation pathway (Hulsken *et al.*, 1994; Bienz, 1999). Activated Wnt signalling inhibits APC and results in reduced β-catenin degradation and accumulation of the protein in the cytoplasm (Aberle *et al.*, 1997; Clevers and Nusse, 2012). Free β-catenin then translocates to the nucleus and functions as a transcriptional co-regulator with a TCF/LEF transcription factor (Korinek *et al.*, 1998; Nusse and Clevers, 2017). The Wnt/β-catenin pathway is essential in embryonic development and implicated in many other physiological processes (Korinek *et al.*, 1998; Chu *et al.*, 2004; Nusse and Clevers, 2017).

1.4.2 The Wnt/β-catenin signalling is essential during the development of the mammary gland

The Wnt/β-catenin pathway is involved in several aspects of mammary gland development (both prenatal and postnatal) and is also crucial for mammary stem cell maintenance (van Amerongen *et al.*, 2012). Also, it has been found that Wnt/β-catenin is involved in determining the fate of mammary gland stem and progenitor cells (van Amerongen *et al.*, 2012).

There is an agreement in the literature that the lymphoid enhancer binding factor 1 gene (*Lef1*) is involved early in mammary gland development (van Genderen *et al.*, 1994; Hennighausen and Robinson, 2001). Members of the Wnt family (*Wnt6, Wnt3 and Wnt10B*) are involved in the initiation, primitive bud formation and branching of the mammary gland (Mailleux *et al.*, 2002; Chu *et al.*, 2004; Eblaghie *et al.*, 2004; Veltmaat *et al.*, 2004). Additionally, the Tcf1 and Tcf4 transcription factors are also active in the mammary epithelial cells during early mammary gland development (Wodarz and Nusse, 1998; Roose *et al.*, 1999).

Another essential mediator in prenatal mammary gland development is Slug, which is a member of the Snail family of zinc-finger transcriptional repressors (Phillips *et al.*, 2014). It is also implicated in many cellular and developmental processes including EMT, cellular migration and differentiation (Guo *et al.*, 2012; Phillips and Kuperwasser, 2014). Proia *et al.* (2011) found that Slug controls luminal epithelial cell differentiation.

During the postnatal stage of mammary gland development, the branching of the ducts is controlled by sex hormones (oestrogen and progesterone) (Brisken *et al.*, 2000). In particular, Brisken *et al.* (2000) found that sex hormones caused side-branching by

influencing Wnt4 during early pregnancy. They also found that *Wnt4* expression was localised in the luminal cells of the ductal epithelium and that it is controlled by progesterone (Brisken *et al.*, 2000).

1.4.3 The involvement of Wnt/β-catenin pathway in the activation of EMT process in breast cancer metastasis

EMT is activated stably or transiently during cancer invasion and metastasis (Hanahan and Weinberg, 2011). Several studies linked the EMT process to the metastasis of human cancers including colon cancer (Conacci-Sorrell *et al.*, 2003), cervical cancer (Ha *et al.*, 2013), prostate cancer (Tsai and Yang, 2013), and breast cancer (Sarrio *et al.*, 2008).

Wnt activation drives tumour-associated gene expression in colorectal and other cancers (Korinek *et al.*, 1997; Nusse and Clevers, 2017). The release of β-catenin from E-cadherin results in nuclear accumulation and activation of Wnt-related transcription via binding to the TCF/Lef complex and that lead to the onset of tumour-promoting activity (Figure 0-5) (Rijsewijk *et al.*, 1987; Khramtsov *et al.*, 2010; Nusse and Clevers, 2017). Continuous activation of this pathway is associated with many human cancers (Conacci-Sorrell *et al.*, 2003; Rosa *et al.*, 2015; Wang *et al.*, 2015). In colon cancer, there is a cumulative effect that starts with the loss of E-cadherin and release of β-catenin which localises to the nucleus and activates *slug*, which further represses E-cadherin production (Conacci-Sorrell *et al.*, 2003). Dey *et al.* (2013) found that increased activity of Wnt/β-catenin signalling associated with high-grade breast tumours, poor prognosis and metastasis to lung and brain, but not to bone marrow.

The same signalling pathways involved in regulating EMT during mammary gland development have been implicated in breast cancer metastasis (Wang and Zhou, 2011). It was also concluded that EMT provides the breast cancer cells with the ability to tolerate physiological stress and could provide an opportunity to develop novel treatments (Trimboli *et al.*, 2008).

Several studies considered abnormalities in β-catenin protein expression in breast cancer as a predictive marker of poor prognosis, including nuclear accumulation and loss of membrane localisation (Lin *et al.*, 2000; Geyer *et al.*, 2011; He *et al.*, 2014; Wang *et al.*, 2015). In breast cancer, altered availability of β-catenin was reported to result from the suppression or loss of E-cadherin expression (Onder *et al.*, 2008). Bukholm *et al.* (1998) found that disrupting components of adherens junctions,

including E-cadherin, α-catenin and γ-catenin, resulted in an increased availability of β-catenin, and thereby, increasing the risk of metastasis in breast cancer patients.

The free pool of β-catenin can translocate to the nucleus and regulate transcription of EMT-related proteins (Figure 0-5). The transcriptional targets of β-catenin (with TCF/Lef) are known regulators of EMT (Figure 0-5). Onder *et al.* (2008) concluded that CRT (catenin related transcription) was responsible for regulating a number of target genes known to induce and facilitate changes associated with EMT. β-catenin, on its own, was not sufficient to induce EMT.

1.4.3.1 Dysfunction of Wnt/β-catenin is associated with breast cancer

Many studies have indicated that there were dysfunctions of the Wnt/β-catenin pathway in breast cancers (Geyer *et al.*, 2011; Li and Zhou, 2011). In fact, this pathway was reported to be active at the earliest stages of tumour development in both ductal carcinoma *in situ* (DCIS) and lobular carcinoma *in situ* (LCIS), (Karayiannakis *et al.*, 2001; Geyer *et al.*, 2011; He *et al.*, 2014). The dysfunction of Wnt/β-catenin signalling was also reported in advanced stage breast cancer (Bukholm *et al.*, 1998; Geyer *et al.*, 2011). Dey *et al.* (2013) found that there was increased Wnt/β-catenin pathway activation in TNBC, and that this increase correlated with tumour grade, poor prognosis and development of metastasis.

1.4.3.2 Mutation of β-catenin gene is not common in breast cancers

No genetic mutations have been detected in β-catenin in breast cancer, and it is thought that the changes in the function of this protein are due to post-transcriptional modifications, such as phosphorylation (Karayiannakis *et al.*, 2001; Nakopoulou *et al.*, 2006; He *et al.*, 2014). Schlosshauer *et al.* (2000) conducted a genetic analysis of β-catenin protein and concluded that there were no mutations of β-catenin found in the most common breast cancer cell lines including MCF7, MDA-MB-361, BT20, MDA-MB-231, and MDA-MB-453.

Similarly, mutations in *APC* were rare in breast cancer (Lin *et al.*, 2000; Nakopoulou *et al.*, 2006; Rosa *et al.*, 2015). Also, Schlosshauer *et al.* (2000) found that only one in 27 breast cancers had a truncating mutation in the APC gene, therefore, concluding that APC mutations are rare in breast cancer.

1.4.3.3 Abnormalities of β-catenin expression is associated with breast cancer

Several studies have reported that abnormalities in β-catenin expression are seen in all stages of breast cancer. Overexpression of β-catenin correlates with tumour size, grade, lymph node involvement and metastasis in breast cancer (Bukholm *et al.*, 1998; Geyer *et al.*, 2011). There is also a significant correlation between increased β-catenin expression and lack or loss of E-cadherin expression in grade three lobular and non-lobular breast carcinomas (Geyer *et al.*, 2011). Also, loss of β-catenin expression was reported by Jiang *et al.* (2009) in TNBC infiltrating ductal carcinoma of high-grade.

In contrast, Karayiannakis *et al.* (2001) concluded that there was no association between β-catenin staining pattern and tumour grade. They also reported that there was no significant correlation between β-catenin expression and features including tumour size, lymph node involvement, metastasis-free survival and hormonal status (Karayiannakis *et al.*, 2001). The variation in the findings of these studies could be due to variation in sample size, antibody clone, used scoring criteria, variation in the method of statistical analysis.

Geyer *et al.* (2011) attributed the contradiction in the literature around β-catenin expression in breast cancer subtypes to variations in the interpretation of histological localisation of the protein in human samples. Rosa *et al.* (2015) also mentioned that the assessment and analysis of β-catenin protein in human samples could be challenging, and that confirmation of β-catenin activation should be assessed by more than one method of analysis. Moreover, Rosa *et al.* (2015) related this issue to β-catenin antibody cross-reactivity with other catenin types that was not addressed and confirmed in published research.

Assessing the localisation of β-catenin protein is equally important. Several studies recorded the pattern of distribution in breast cancer samples. Paredes *et al.* (2008), reported that there were alterations in the localisation and level of expression of all catenins in breast cancer samples.

β-catenin in particular showed a reduction in localisation at cell-cell contact sites and increased cytoplasmic localisation in 70% of cases in that study (Paredes *et al.*, 2008). Membranous localisation of β-catenin require E-cadherin (Li and Mattingly, 2008; Paredes *et al.*, 2008; Wang *et al.*, 2015). Karayiannakis *et al.* (2001) found that there was heterogeneous β-catenin staining in around 60% and loss of expression of β-catenin in around 50% of lobular breast carcinomas compared to heterogeneous staining

of β-catenin in 80% and cytoplasmic or nuclear staining in less than 15% of lobular carcinomas.

Jiang *et al.* (2009) found that in benign breast tumours β-catenin was localised in the nucleus of myoepithelial and luminal epithelial cells with moderate cytoplasmic staining in non-tumorous ducts. In addition, either complete loss or increase of nuclear localisation was associated with TNBC, BLBC and poor clinical outcomes (Geyer *et al.*, 2011; Rosa *et al.*, 2015). Cytoplasmic localisation of β-catenin significantly correlated with increased tumour size, and therefore associated with increased breast cancer stage (Paredes *et al.*, 2008).

The reports of alteration in β-catenin patterns associated with increased tumour stage in breast cancer samples led the researchers to conclude that this pathway could be utilised to develop a targeted therapy. Wu *et al.* (2012) found in their study that resistance to targeted therapy in $HER2^{+ve}$ cancers was associated with partial EMT as a result of activation of Wnt/β-catenin pathway. They also attributed the resistance to targeted therapy itself to the activation of Wnt/β-catenin pathway (Wu *et al.*, 2012). Conversely, Zhu *et al.* (2010) found that Herceptin treatment resulted in a reduction of the β-catenin pool by increasing phosphorylation of the protein. Therefore, many studies suggested the use of Wnt/β-catenin pathway as a therapeutic target in breast cancer for prevention of therapy resistance and treatment of breast cancer metastasis (Lin *et al.*, 2000; Geyer *et al.*, 2011).

1.5 A vital role for Hedgehog (Hh) signalling pathway in the regulation of EMT during mammary gland development and breast cancer metastasis

The Hedgehog signalling (Hh) pathway was discovered in 1980 in a study aimed to understand the segmentation of the body (Nusslein-Volhard and Wieschaus, 1980) and mediates epithelial-mesenchymal interaction during human embryonic development and organogenesis (Ingham and McMahon, 2001; McMahon *et al.*, 2003). This pathway can be activated by interaction between the Hh receptor and its ligand (canonical) and also via an alternate pathway through interaction with other signalling cascades (non-canonical) (Jenkins, 2009; Brennan *et al.*, 2012; Flemban and Qualtrough, 2015).

1.5.1 Components of the Hedgehog signalling pathway

The components of the Hh signalling pathway include the secreted glycoproteins; Sonic (Shh), Desert (Dhh) and Indian (Ihh) (Ingham and McMahon, 2001; Pasca di Magliano and Hebrok, 2003). These ligands bind to one of the receptors including; Hedgehog-interacting protein 1 (Hip1), Patched1 (Ptch1) and Patched2 (Ptch2) (Marigo *et al.*, 1996; Chuang and McMahon, 1999). The receptors then release the blocking effect on another transmembrane protein called Smoothened, Smo (Figure 0-6-B, and Figure 0-7-C)(Pasca di Magliano and Hebrok, 2003; Flemban and Qualtrough, 2015). As a consequence of this, Smo activates intracellular signalling via the Glioma-associated oncogene (Gli1, Gli2, and Gli3) transcription factors (Figure 0-7-D) (Ruiz i Altaba *et al.*, 2002; Pasca di Magliano and Hebrok, 2003). These transcription factors are sequestered in the cytoplasm through connection to the cellular cytoskeleton by interaction with multiprotein complex Fused (Fu) and suppressor of Fused (SuFu) (Figure 0-6-D) (Murone *et al.*, 2000; Pasca di Magliano and Hebrok, 2003).

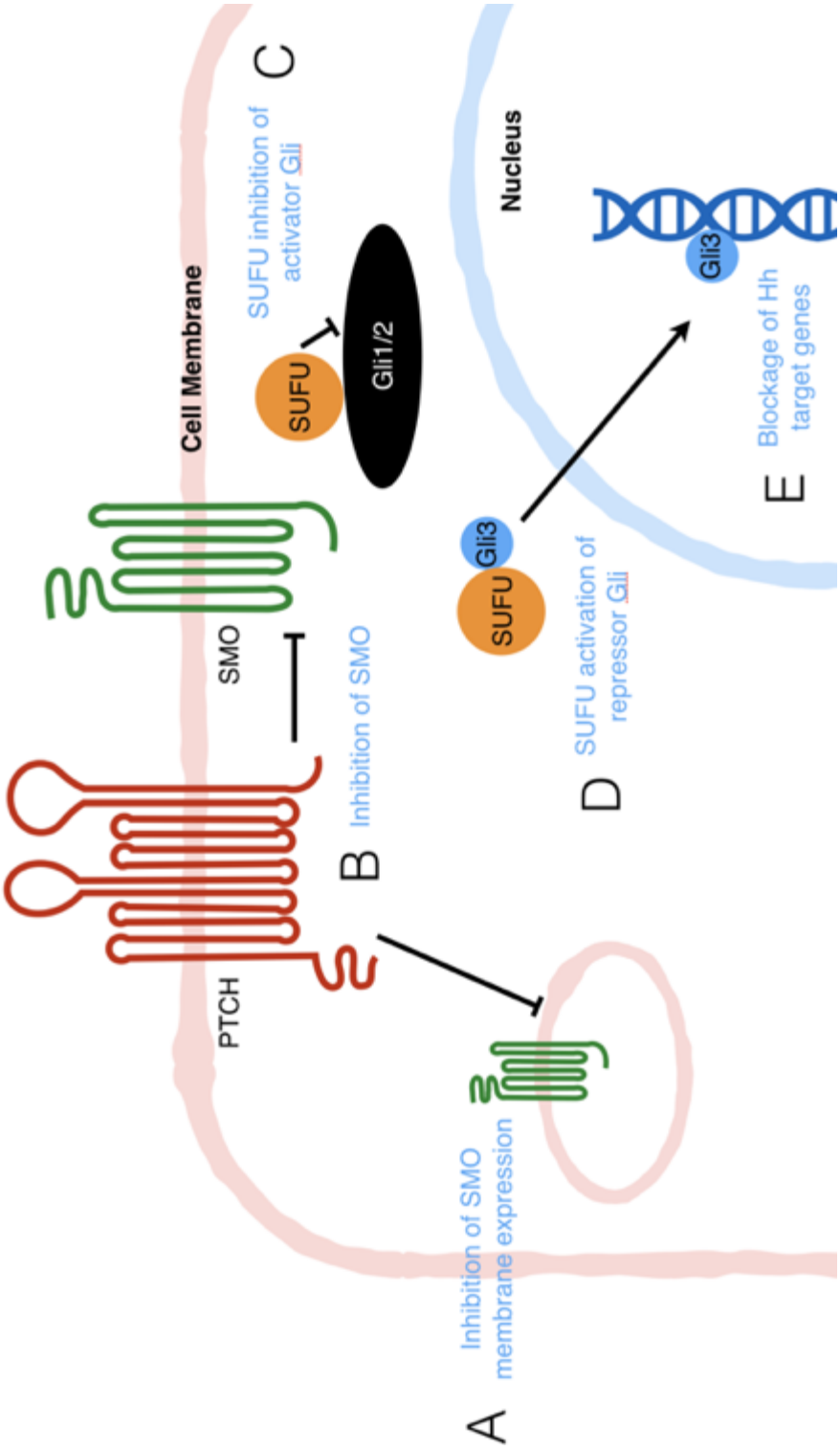

Figure 0-6, The resting status of the Hh signalling pathway.
The resting (inactivated) hedgehog (Hh) signalling pathway. (A) In the absence of Hh ligand, Patched (Ptch) protein form an inactive complex with downstream receptor Smoothened (Smo) (Corbit *et al.*, 2005). It works as inhibitor of Smo protein expression (Denef *et al.*, 2000) and a suppressor of Smo (B) (Ding and Wang, 2017). (C) Several Hh pathway components transduce the signal intracellularly including suppressor of Fused (SUFU) protein that function to inhibit the Gli transcription factors by sequestering them to cytoplasm in absence of Hh signalling (Nozawa *et al.*, 2013). Thus, blocking Hh target genes by localisation of repressor form of Gli (Gli3) in nucleus of inactive cells (Rubin and de Sauvage, 2006). The figure was drawn by the author from the mentioned references.

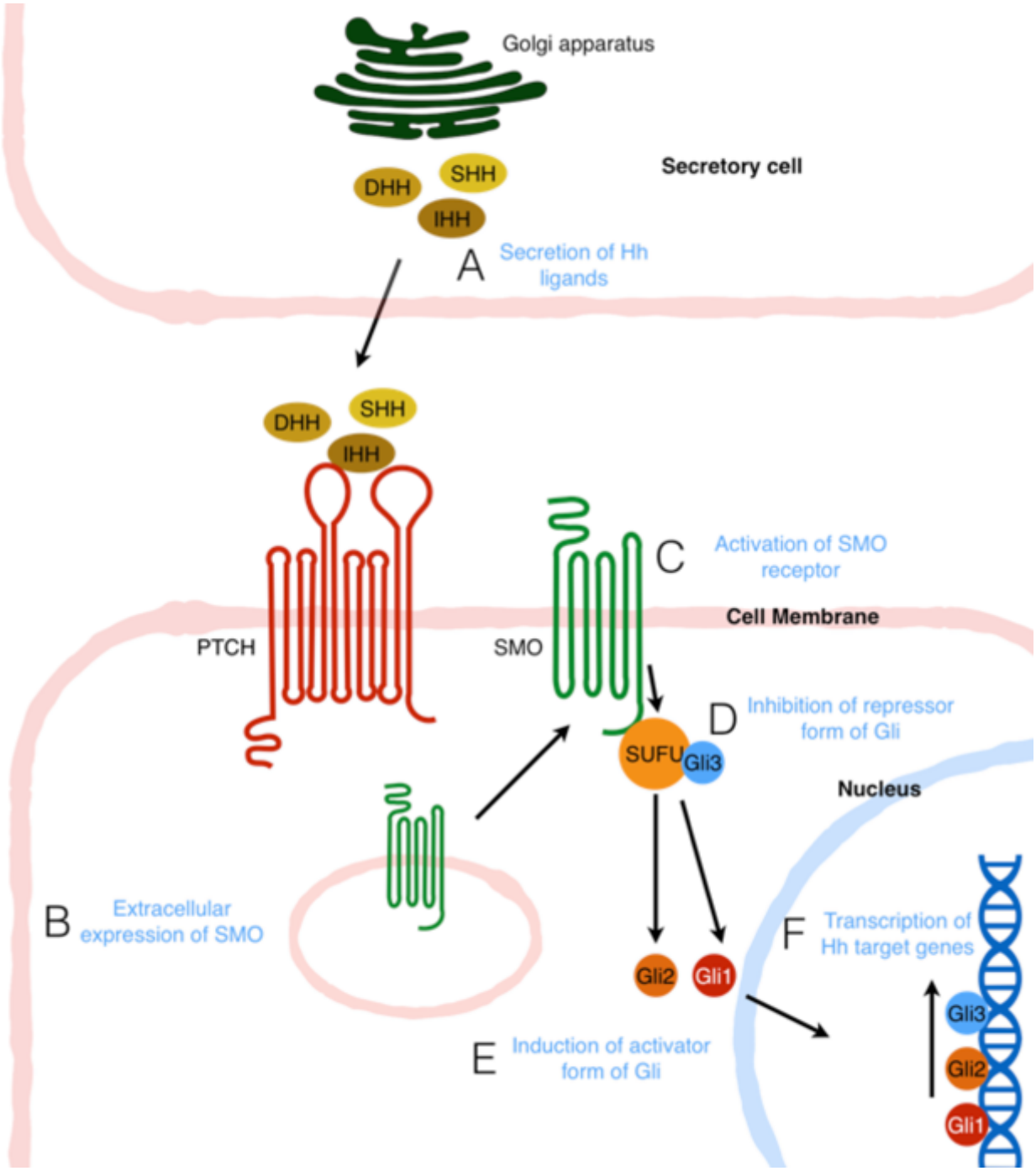

Figure 0-7, The active status of the Hh signalling pathway.
The active status of Hedgehog (Hh) signalling. (A) Hh ligands are synthesised as precursor proteins in the Golgi apparatus (Huangfu *et al.*, 2003; Ramsbottom and Pownall, 2016) that is cleaved in endoplasmic reticulum before secretion (Ramsbottom and Pownall, 2016). The ligand presence and binding to Ptch receptor results in release of inhibiting function of Ptch on the expression (B) and function of Smo receptor (C) (Ramsbottom and Pownall, 2016), which leads to the activation of pathway (D). This result in induction of activated form of Gli that translocate to nucleus and act as a transcription factor and result in transcription of Hh target genes (F) (Rubin and de Sauvage, 2006; Ramsbottom and Pownall, 2016). The figure was drawn by the author from the mentioned references.

The Gli proteins are large zinc-finger transcription factors that are composed of more than a thousand amino acids (Ruiz i Altaba *et al.*, 2002; Ruiz i Altaba *et al.*, 2007). There are three Gli proteins in humans, and they have a context-dependent transcriptional regulation function (Stecca and Ruiz, 2010). These Gli proteins have both activator and repressor forms (Figure 0-8) which is referred to as the Gli code (Ruiz i Altaba *et al.*, 2007; Aberger and Ruiz, 2014).

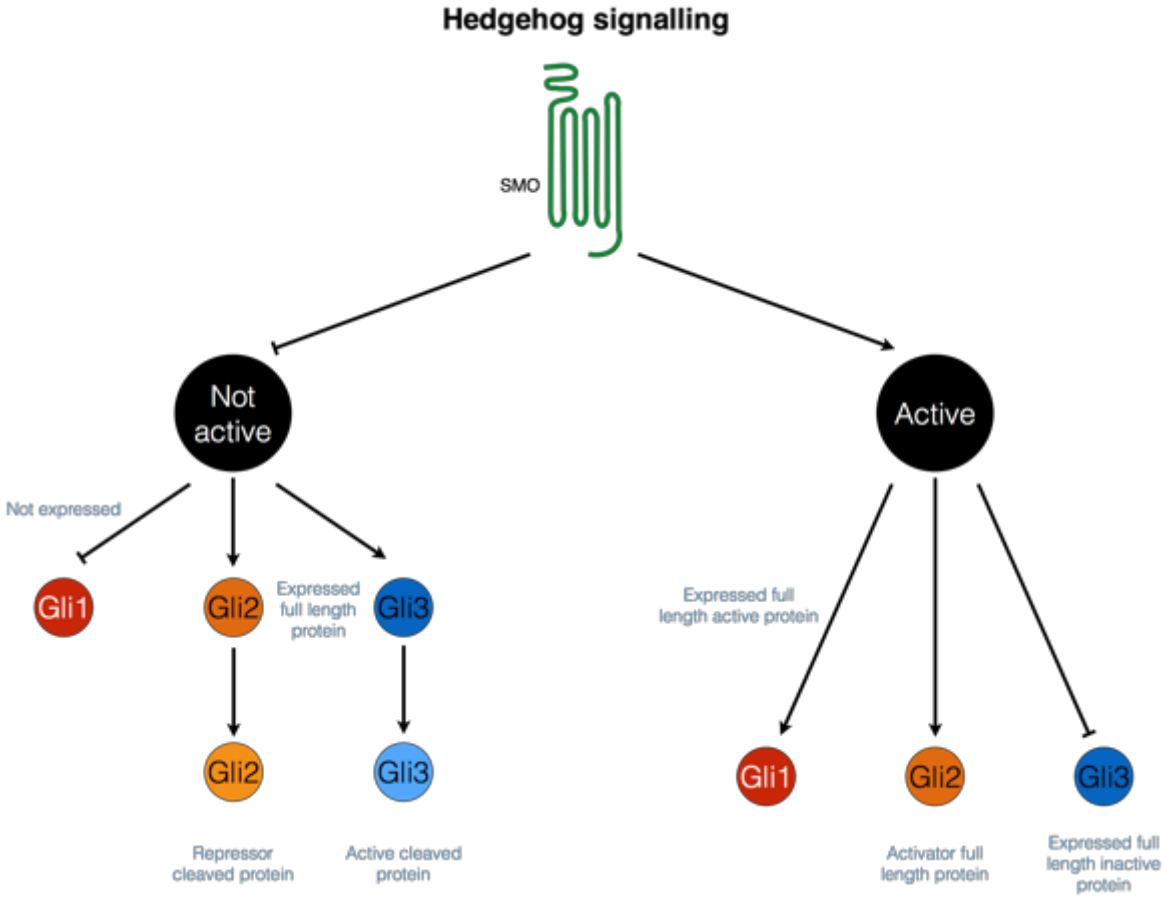

Figure 0-8, The gli code.
The repressor and activator forms of Gli proteins. During resting status of Hh signalling, Gli1 protein is not expressed while Gli2 and Gli3 are expressed in full-length form that is cleaved into repressor forms (Ruiz i Altaba, 1998; Stamataki *et al.*, 2005). With activation of Hh signalling, Gli1 is transcribed as an active form (full-length) while cleavage of both Gli2 and Gli3 halts. Thus, Gli2 remain in full-length activator form, and Gli3 is no longer active (full-length) (Stamataki *et al.*, 2005; Ruiz i Altaba *et al.*, 2007). The figure was drawn by the author from the mentioned references.

The nuclear localisation of these Gli transcription factors is essential for protein function (Ruiz i Altaba *et al.*, 2007). Negative modulators of the Hh signalling pathway (including Ptch) sequester Gli1 in cytoplasm of cells (Ruiz i Altaba *et al.*, 2007). Thus, studying of localisation of Gli transcription factors is essential for the determination of the activation status of the pathway.

Other factors can activate Hh signalling in a non-canonical way including dysregulation of the signalling pathway and activation by other signalling cascades such as Wnt signalling. Several mechanisms were indicated to dysregulate Hh signalling including both ligand-independent and ligand-dependent mechanisms (Hui *et al.*, 2013). The ligand-dependent mechanisms are a result of increased expression of *SMO* and *Gli1* or inactivation of *PTCH* (Hui *et al.*, 2013).

1.5.1.1 Crosstalk between the hedgehog signalling and Wnt signalling pathways

One of the pathways that can activate the Hh signalling pathway non-canonically is the Wnt pathway (Figure 0-9 and Figure 0-10) (Ding and Wang, 2017). In fact, interaction between the Wnt and Hh signalling pathway is seen during embryogenesis and cellular differentiation (Price, 2006; Moussaif and Sze, 2009; Ding and Wang, 2017).

Several studies showed that there was cross reaction between the two signalling pathways. The integration between Hh and Wnt signalling was revealed by pharmacological studies using inhibitory drugs. Singh *et al.* (2012) found that the Hh signalling inhibits the activation of Wnt signalling during embryogenesis (Figure 0-9-A). Additionally, Wnt activation rescues the suppression of the Hh signalling. Kim *et al.* (2010a) found that increased Gli1 expression resulted in a decreased level of nuclear β-catenin localisation (Figure 0-9-B). The Wnt/β-catenin signalling inhibits Hh activity via transcriptional regulation of Gli3 (Figure 0-10-A) (Alvarez-Medina *et al.*, 2008). Gli3 expression was directly regulated by the β-catenin/TCF/LEF complex (Figure 0-10-B) (Alvarez-Medina *et al.*, 2008).

The overlap between these signalling pathways is not well understood, but the regulation of both signalling pathways is disturbed in human cancer. Co-activation of both Wnt and Hh pathways has been observed in several types of human cancers (Yang *et al.*, 2008b). Qualtrough *et al.* (2015) found that inhibition of Hh signalling using cyclopamine resulted in a reduction in β-catenin-related transcription (CRT) in colorectal cancer cell lines that was rescued by addition of Shh protein. Furthermore, a significant association between the nuclear expression of Gli1 and nuclear expression of β-catenin was observed in human breast cancer samples (Arnold *et al.*, 2017). Thus, indicating that the crosstalk between the Hh and Wnt signalling pathways in breast cancer is context-dependent and requires further study.

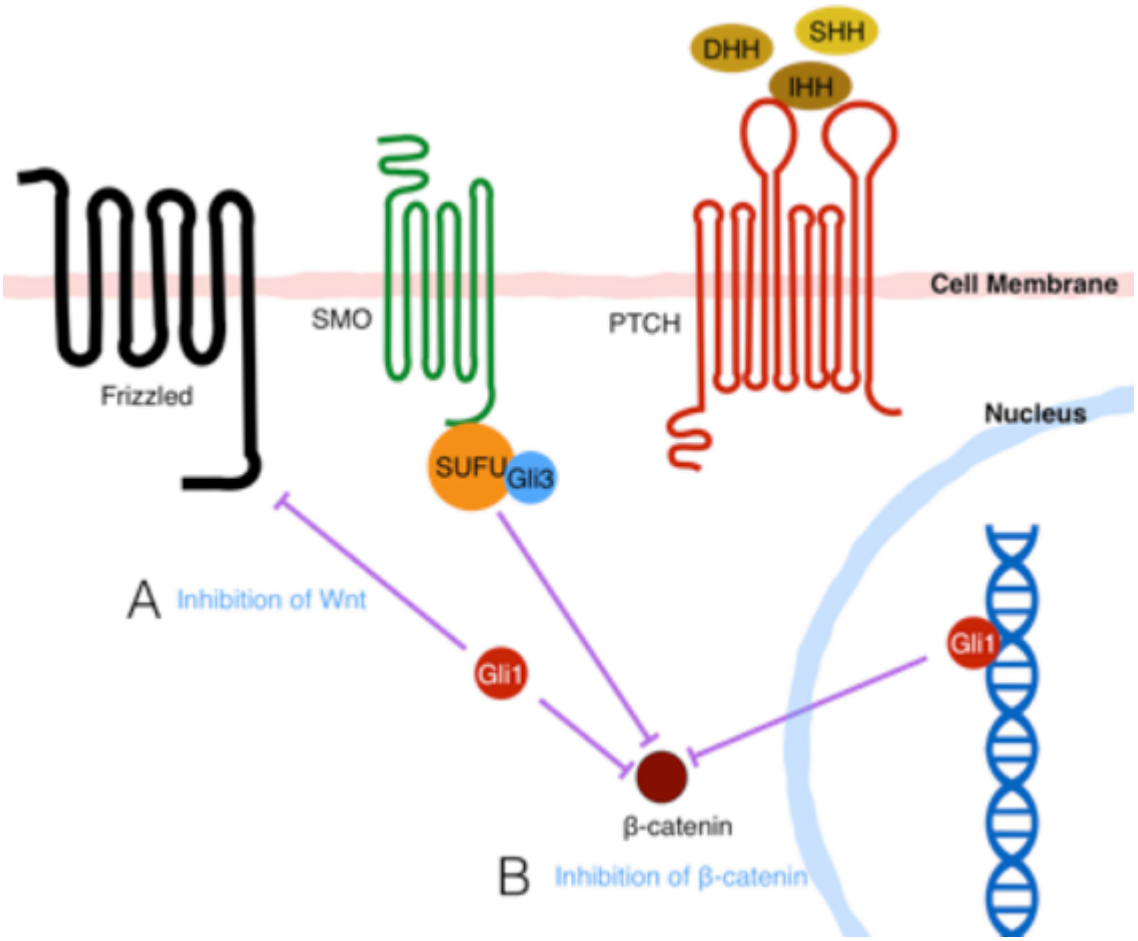

Figure 0-9, Hh signalling mediated inhibition of the Wnt signalling pathway.
The inhibitory effect of Hh signalling on the Wnt signalling pathway. (A) Active Gli1 expression directly inhibit Wnt receptor Frizzled. (B) Gli1 protein directly inhibits localisation of β-catenin in nucleus of cells. The figure was drawn by the author from the mentioned references (Ding and Wang, 2017).

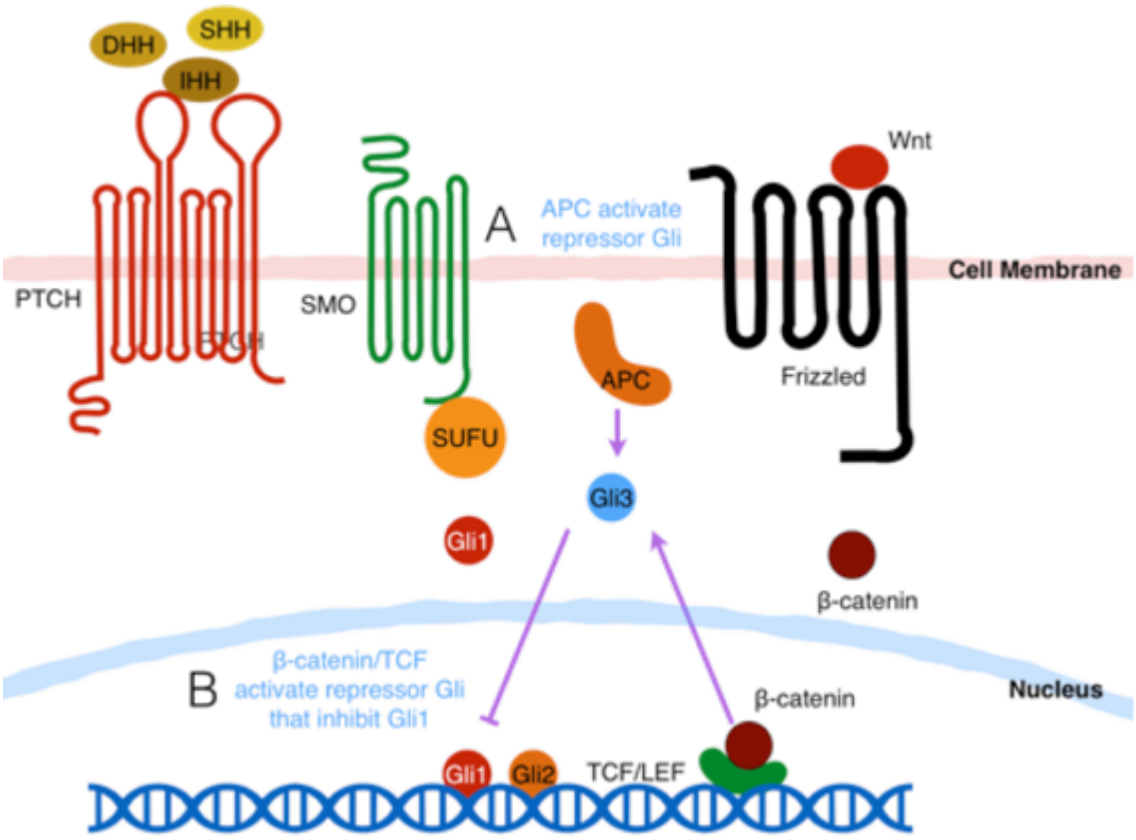

Figure 0-10, Wnt signalling mediated inhibition on the Hh signalling pathway.
The inhibitory effect of the Wnt pathway on Hh signalling. (A) APC protein directly regulates expression of Gli3 protein. B- β-catenin/TCF/LEF complex control expression of Gli3 protein which inhibit Gli1. The figure was drawn by the author from (Ding and Wang, 2017).

1.5.2 The Hedgehog signalling pathway is essential for mammary gland development and breast cancer progression and metastasis

The activation of the Hh signalling pathway during the development of the mammary gland first occurs during early embryogenesis (Michno *et al.*, 2003; Lee *et al.*, 2013). Lewis (2001) reported involvement of hedgehog signalling in mouse mammary gland development. Hh signalling was active in the terminal end bud during early adulthood and was continuously activated in the stromal components around the ducts in all phases of postnatal development except for the early stage of involution after weaning (Lewis, 2001). Hh signalling activation was seen in ducts and alveoli of the mammary gland during early and late pregnancy, and lactation (Lewis, 2001)

All members of the Hh signalling pathway are found expressed in the components of the mammary gland during different stages of its development (prenatal and postnatal). They are also thought to have a function in the differentiation and maintenance of the normal structure of the mammary gland (Flemban and Qualtrough,

2015). Epithelial expression of the ligands Shh and Ihh was found to be essential in early mammary bud formation (Hens and Wysolmerski, 2005). Lewis *et al.* (1999) found that *Ihh* expression increased during pregnancy and lactation.

The expression of *Ptch1* was also shown to be essential in both the epithelial and mesenchymal compartments during prenatal mammary gland development (Lewis *et al.*, 1999). Later, during postnatal phase a lack of *Ptch1* in mice resulted in both hyperplasia and dysplasia in the ductal compartment during puberty and adulthood (Lewis *et al.*, 1999; Flemban and Qualtrough, 2015).

Michno *et al.* (2003) found that mesenchymal *Gli2* was essential for mammary gland development during embryogenesis. Hatsell and Cowin (2006) found that Gli3 had an essential role in repressing Hh signalling during embryogenesis and both Gli3 and Gli2 were expressed in the prenatal phase of mammary gland development. In the postnatal stages, *Gli3* was expressed in the luminal cells and both *Gli2* and *Gli3* were expressed in the stromal and myoepithelial cells (Hatsell and Cowin, 2006). It was found that Gli2 protein was expressed in the mesenchymal cells during puberty near the terminal buds and the expression increased in the alveolar epithelial cells during the later phases of pregnancy (Michno *et al.*, 2003; Flemban and Qualtrough, 2015).

1.5.3 The Hedgehog signalling pathway is involved in cancer progression and metastasis

Inappropriate activation of Hh signalling is apparent in 25% of all tumours, therefore, highlighting the importance of dysregulation of this pathway in human tumour progression (Briscoe and Therond, 2005; Flemban and Qualtrough, 2015). Loss of balance of Hh signalling was implicated in many human tumours including; sporadic basal-cell carcinoma (Xie *et al.*, 1998), tumours of the central nervous system (Reifenberger *et al.*, 1998), lung cancer (Watkins *et al.*, 2003), tumours of the gastrointestinal tract (Berman *et al.*, 2003), pancreatic cancer (Thayer *et al.*, 2003), and prostate cancer (Karhadkar *et al.*, 2004). Other studies showed that the inhibition of Hh signalling resulted in similar effects in other human cancers as summarised Table 0-2.

The first inhibitor of the Hh signalling pathway to be discovered was the plant alkaloid cyclopamine (Bryden *et al.*, 1971). The mechanism of action was discovered later, and it was found that this inhibitor binds to and inactivates Smo (Cooper *et al.*, 1998). Several other small molecule inhibitors such as LDE225 have since been synthesised and found to have a more potent effect when compared with cyclopamine (Gupta *et al.*, 2010).

Table 0-2: Inhibition of Hh signalling in human cancers has been investigated.
This table provide examples of the studies that investigated the effect of inhibiting the Hh signalling in human cancers and their main findings.

Cancer type	Inhibitor	Finding	Reference
Medulloblastoma	Cyclopamine	Growth inhibition.	(Berman *et al.*, 2002)
Small cell lung carcinoma	Cyclopamine	Inhibit the Shh-dependent growth.	(Watkins *et al.*, 2003)
Prostate cancer	Cyclopamine	Inhibition of proliferation and evidence of autocrine signalling.	(Sanchez *et al.*, 2004)
Colon cancer	Cyclopamine	Induced apoptosis.	(Qualtrough *et al.*, 2004)
Colon cancer	GANT61	Cell death caused by increased DNA damage.	(Mazumdar *et al.*, 2011)
Colon cancer	GANT61	DNA damage followed by cell death.	(Agyeman *et al.*, 2012)
Colon cancer	Cyclopamine and GANT61	Hh signalling controls tissue inflammation and antagonise apoptosis.	(Yoshimoto *et al.*, 2012)
Colon cancer	GANT61	Inhibition of Gli1 DNA interaction and reduction of transcription of Hh signalling output genes.	(Agyeman *et al.*, 2014)
Lung squamous cell carcinoma	Vismodegib	Suppressed migration and up-regulated E-cadherin.	(Yue *et al.*, 2014)
Renal cell carcinoma	LDE225	Reduction of tumour growth and metastatic spread.	(D'Amato *et al.*, 2014)
Colon cancer	Cyclopamine	Reduction of expression of EMT transcription factors and reduction in invasiveness.	(Qualtrough *et al.*, 2015)
Gastric carcinoma	Cyclopamine	Reduction of viability in concentration dependent manner and decrease invasion and metastasis.	(Gao *et al.*, 2015)

1.5.3.1 The Hedgehog signalling is involved in the regulation of EMT in breast cancer

Mutations of Hh signalling are rare events in breast cancer (Wicking *et al.*, 1998; Hui *et al.*, 2013). Other epigenetic and post-transcriptional events were found to cause improper activation of Hh signalling in mammary tumours. These include dysregulation of alternative splicing that causes inappropriate expression of the active Gli isoforms (Cao *et al.*, 2012) and methylation of the *PTCH* promoter (Wolf *et al.*, 2007). These studies led to the notion that Hh signalling activation is context-dependent and affected by cellular contact, polarity and other factors that can manipulate post-transcriptional modification of the Gli proteins (Aberger and Ruiz, 2014; Gonnissen *et al.*, 2015).

Moraes *et al.* (2007) reported that Ptch1 expression was reduced in about half of the cases of DCIS and invasive breast cancer. They also found that Smo was ectopically expressed in 70% of DCIS and 30% of invasive breast cancers (Moraes *et al.*, 2007). They concluded that altered Hh signalling causes increased proliferation of cells that were capable of anchorage-independent growth (Moraes *et al.*, 2007). Cui *et al.* (2010) observed that there was significant upregulation of Shh in breast carcinoma and concluded that this was an essential event for breast carcinogenesis.

Several studies inhibited this pathway in breast cancer cell lines *in vitro* and found that the inhibition of Hh signalling with cyclopamine resulted in a decrease in TNBC cell line proliferation and reduced invasive ability (Kameda *et al.*, 2009). Also, Che *et al.* (2013) found that cyclopamine treatment resulted in reduced cell proliferation in the ER^{+ve} cell line MCF7 and suggested the utilisation of this pathway as a therapeutic target for breast cancer. Nonetheless, the correlation between reduction in the migration, proliferation and the changes in the expression of key EMT markers was not the focus of many of previous studies. Similarly, the expression of the hedgehog signalling components and changes in localisation of the Gli proteins or β-catenin following inhibition of the Hh signalling was not conducted in previous studies.

Changes in the Gli proteins expression was studied in clinical breast tissue sections in several studies and intensity and proportion of expression correlated with the clinicopathological criteria only. Overexpression of the Gli1 transcription factor in breast tumours was associated with unfavourable overall survival, high tumour stage, and increased lymph node metastasis (ten Haaf *et al.*, 2009). Jeng *et al.* (2013) suggested that high expression of *Shh*, *PTCH1*, *GLI1*, and *Smo* correlated with increased breast cancer invasiveness. Also, few of the previous studies focused on assessing subcellular localisation of the Gli proteins. One study reported that the nuclear translocation of Gli1 was involved in micro-invasion and suggested that this pathway is involved in the progression of a non-invasive phenotype towards invasive behaviour (Souzaki *et al.*, 2010). Kubo *et al.* (2004) found that high intensity of Gli1 was associated with malignancy and that nuclear expression of this marker was associated with ER expression. Co-activation of the Hh and Wnt signalling was not explored in detail in breast cancer. In fact, a single study explored both pathways in breast cancer clinical samples and it was concluded that co-activation of Wnt and Hh signalling in TNBC and is associated with an increased risk of disease recurrence and decreased overall survival (Arnold *et al.*, 2017).

1.6 Challenges in studying EMT in human cancer particularly in breast cancer

1.6.1 Lack of direct clinical evidence of EMT in breast cancer and partial EMT theory

The involvement of the EMT process in breast cancer progression and metastasis is not ascertained due to a lack of direct clinical evidence (Tarin *et al.*, 2005; Savagner, 2010). Also, dedifferentiated carcinomas with a poor prognosis are described clinically as "EMT-like morphology" rather than in terms of an EMT transition and full transition is a rare event and occur only in high grade carcinomas. In addition, both EMT and differentiation processes are controlled by mutual pathways (Klymkowsky and Savagner, 2009; Savagner, 2010). The only direct clinical evidence for EMT in breast cancer cases is seen in metaplastic carcinomas, which is very rare subclass of breast cancers. In this type, the epithelial cancer cells undergo complete mesenchymal transition and the only way to distinguish the epithelial and mesenchymal compartments is by staining for cytokeratins and vimentin (Zhuang *et al.*, 1997; Saegusa *et al.*, 2009; Savagner, 2010).

It was suggested previously by Savagner (2010) that the involvement of EMT in breast cancer varied due to tumour heterogeneity and variations in molecular signatures, however, no further investigation was carried to explore this hypothesis. Several studies reported evidence of EMT activation in basal-like breast cancers (Sarrio *et al.*, 2008; Chen *et al.*, 2014). One aspect that remains missing in previous studies is the comparison of the expression and activation of EMT in various breast cancer cell lines that belong to various molecular subclassification of breast cancer. Exploring this hypothesis could show if the status of EMT differ according to the molecular subclass and could lead to exploring the causes of this variation.

Aleskandarany *et al.* (2014) reported that lack of E-cadherin, a hallmark for EMT, was associated with lobular breast cancers. Other studies found that the lack of E-cadherin in lobular breast cancers is due to genetic or epigenetic silencing mechanisms (Moll *et al.*, 1993; Berx *et al.*, 1996). Lack of E-cadherin expression in these subtypes did not result in full EMT. In fact, several studies proposed the "term partial EMT" to describe the ability of cells to detach and undertake a mode of invasion similar to the ameboid described previously by Clark and Vignjevic (2015) and Yang *et al.* (2004).

Hase *et al.* (1993) described partial EMT in cells at the invasive front of colorectal cancer. These cells had disorganised structure and showed a uniformed phenotype irrespective of the differentiation status of the original tumours (Hase *et al.*, 1993). In breast cancer, co-expression of both epithelial and mesenchymal markers occurs in those single detached cells in multiple breast cancer cell lines (Grosse-Wilde *et al.*, 2015; Hong *et al.*, 2015). Tran *et al.* (2014) found that the same EMT inducing transcription factors can increase tumour-initiating (stem-cell-like) potential in the "partial EMT" cells that was identified in breast cancer metastasis by Sarrio *et al.* (2008). Pastushenko *et al.* (2018) was able to identify multiple subpopulations of cells within a tumour associated with different stages of EMT. These cells showed differences in plasticity, invasiveness and metastatic potential that regulate the EMT transcription states (Pastushenko *et al.*, 2018).

Previous studies showed that EMT is not an absolute state, but rather a spectrum of changes regulated by intracellular and extracellular components. The identification of EMT in clinical breast cancer samples is elusive and we hypothesis that the mesenchymal status of breast cancer cells could be transient and perhaps not synchronised across the whole tumour cell population *in vitro* which contribute to challenges in identifying EMT in clinical samples. Also, our study hypothesised that breast cancer luminal and basal subtypes present various states in the spectrum of EMT with molecular subtypes that present the end of the epithelial and mesenchymal spectrum. Comparison of the changes in expression and activation of EMT proteins would provide additional understanding of breast cancer metastasis through EMT regulation and status variation according to molecular subclass of breast cancer.

1.6.2 Lack of *in vitro* cell line model for the investigation of EMT in breast cancer

One of the challenges in studying EMT in breast cancer is the lack of a well-defined *in vitro* model to investigate this process. Researchers in the field have taken a variety of approaches for studying EMT. These include using mouse xenograft models (Han *et al.*, 2015), 3D cultures in Matrigel® or mammospheres (Manuel Iglesias *et al.*, 2013; Liu *et al.*, 2014; Qu *et al.*, 2015). There are drawbacks to using these models including the expense of growing the mouse models. The 3D models using mammospheres or Matrigel® are known to enrich the cancer stem cell population in the cell lines (Manuel Iglesias *et al.*, 2013; Liu *et al.*, 2014; Qu *et al.*, 2015) therefore, adding variables and further complexity. These models can be successfully utilised for

understanding how cancer stem cells could initiate the mesenchymal transition leading to cancer invasion. Currently, most of the *in vitro* work using breast cancer cell lines on the topic of EMT focuses on the expression of the adhesion molecules, metastasis, and invasion markers at a single density (Chekhun *et al.*, 2013; Manuel Iglesias *et al.*, 2013; Liu *et al.*, 2014).

Some studies used varying seeding densities approach to study changes in morphology and cell-cell contact in breast cancer. Using this seeding density model, Zhang *et al.* (2006) found that the expression and function of anchorage-dependent proteins reduced with decreasing density of breast cancer cells (Zhang *et al.*, 2006). In Liu *et al.* (2006b) study, they also used a serial dilution of densities and their objective was to determine cellular spreading and the effect of cell-cell adhesion on proliferation. Although changes in seeding density of cells caused changes in cellular functions, this approach of *in vitro* investigation was not utilised with the focus on studying EMT using breast cancer cell lines.

Changing specifications of *in vitro* tissue culture are known to influence changes in cell lines including changes in cellular contact, cellular spreading, morphology, proliferation, and differentiation. Watt (1988) noted that chondrocytes showed decreased cellular spreading and differentiation when seeded at low density. Also, by culturing chondrocytes at a higher density and enhanced differentiation. Recently, Yassin *et al.* (2015) found that seeding density was one of the essential factors for differentiation of bone and that optimisation of the seeding density was critical for new bone formation. Colon cancer cell line CaCo-2 differentiated in a density-dependent manner (Behrens *et al.*, 2004).

Beside differentiation effects, other studies found that the density of tissue culture affected the proliferation of cell lines. A study of hepatic cancer and smooth muscle cell lines showed that low-density culture reduced proliferation by transient gene silencing (Selli *et al.*, 2016). The same cell lines showed phenotypic switching in association with the proliferative changes (Selli *et al.*, 2016). It was also noted that prostate cancer cell lines showed reduced cellular proliferation due to lack of cell-cell contact when seeded at very low density (Liberio *et al.*, 2014). The proliferative changes associated with changes in seeding density was also noted in many other cell lines derived from a range of tissue types (Haverty *et al.*, 2016). Several studies used density alteration to evoke epithelial-mesenchymal transition-like (EMT-like) change in

cancer cells (Conacci-Sorrell *et al.*, 2003; Nelson *et al.*, 2008; Sarrio *et al.*, 2008; Benton *et al.*, 2009; Chen *et al.*, 2014; Cichon *et al.*, 2015).

The seeding density model was adapted by Conacci-Sorrell *et al.* (2003) to study the effect of density on colon cancer cells. They found that by culturing two colon cancer cell lines at high density, the cells regained the phenotype of epithelial cells and that in sparse culture the same cells switched to fibroblastic morphology similar to cells seen at the tumour invasive front (Conacci-Sorrell *et al.*, 2003). This study concluded that this phenotypic switch in cellular morphology was the result of high β-catenin expression in these colon cancer cells. At higher density, the β-catenin localises with E-cadherin protein to form the adherens junction. As density decreased, adherens junctions decrease resulting in translocation of the highly expressed β-catenin protein to the nucleus, where it forms the β-catenin-TCF complex and initiates the EMT pathway (Conacci-Sorrell *et al.*, 2003).

Sarrio *et al.* (2008) used the seeding density approach to assess EMT in basal-like breast cancer. They found that MCF10A cells (a normal-like and basal-like type B breast cancer cell lines) display EMT-like change in low density and reorganisation of cytoskeletal proteins. This study concluded that this phenotypic switch was associated with breast tumours that have a basal phenotype genetic context and that this subtype of breast cancer can undergo EMT under specific environmental conditions that were present with sparse density (Sarrio *et al.*, 2008). However, they have not compared this with any other cell line that belongs to a different molecular subclassification. They compared epithelial and mesenchymal markers later in a human tissue cohort of several subclassification. Sarrio *et al.* (2008) proposed that the basal-like breast cancers have some of the mesenchymal criteria that made them vulnerable to change from epithelial to mesenchymal. This finding enforces the hypothesis that the basal molecular signature could make breast cancer belonging to this subtype more susceptible to EMT, which was not explored in detail in previous studies.

Later Kim *et al.* (2011) used the seeding density approach and found that by simple manipulation of cell-cell adhesion they discovered a regulatory function of E-cadherin protein that controls cellular proliferation in normal-like breast cell line MCF10A. They also found that by restoring E-cadherin in the MDA-MB-231 cell line (basal-like and triple-negative subtype) they were able to restore this cell-cell adhesion regulatory function (Kim *et al.*, 2011). Cichon *et al.* (2015) found that upon reducing cellular contact of mouse breast cancer cells by decreasing seeding density, epithelial

differentiation-associated genes were reduced, and concluded that loss of cell contact is essential in the earliest stages of cancer development.

1.7 Aims

1.7.1 Aims to

The aim of the current study is to investigate the ability of breast cancer cell lines to undergo EMT-like change and to assess if this is affected by the molecular subtype of breast cancer. Also, this study aims to compare the potential role of Hedgehog signalling to regulate EMT-like change in the various subtypes of breast cancer. These investigations will include the potential crosstalk between Hh and Wnt signalling to drive the metastatic process and evaluate the therapeutic potential of Hh inhibitors in treating patients with advanced disease.

1.7.2 Objectives

- To develop an *in vitro* cell density-based model of EMT using breast cancer cell lines, allowing comparison of the different subtypes of breast cancer. Also, to compare changes in the expression (level and localisation) of three EMT markers (E-cadherin, β-catenin, and vimentin) in response to changes induced in response to varied levels of cell-cell contact using the seeding density model.
- To assess the expression of several markers of EMT (E-cadherin, and β-catenin) and the hedgehog pathway (Gli1, Gli2 and Gli3) in a cohort of breast cancer samples and to correlate the expression of these markers with breast cancer subtypes and clinicopathological features. The expression of the Gli effector proteins will also be measures in a panel of cell lines representing the various molecular subtypes of breast cancers. Also, to assess the effect of inhibiting the Hh signalling pathway in breast cancer cell lines on several cellular parameters (viability, cell yield, cell death, motility and invasion). Also, to assess the effect of Hh signalling inhibition on the outputs of the Wnt/β-catenin and EMT process.

2. Materials and Methods

All materials were obtained from SIGMA-ALDRICH (*Dorset, UK*) unless otherwise stated.

2.1 Tissue culture

2.1.1 Experimental cell lines

A number of established breast cell lines were used to define the seeding density model characteristics (2.1.5) and in the rest of the experiments. Also, a number of other immortalised cell lines were used as positive controls in several experiments (Table 2-9 and Table 2-11). Cell lines were obtained from the Health Protection Agency (*ECACC, Salisbury, UK)* unless otherwise stated.

2.1.1.1 Breast cancer cell lines

A number of human breast cancer cell lines were cultured *in vitro* in this study including one normal-like breast cancer cell line (Table 2-1).

Table 2-1: The breast cancer cell lines selected for investigation.
The breast cancer cell lines used in this study and a summary of breast cancer subtype they were originally from. The source of cell lines is also summarised with hormone receptors status. Intra-Ductal Carcinoma (IDC), Adenocarcinoma (AC), Fibrocystic disease (FD), Plural Effusion (PE), Primary breast (P.Br), Oestrogen Receptor (ER), Progesterone (PR), Human EGF Receptor 2 (HER2), and Receptor tyrosine-protein kinase erbB-2 gene (ERBB2).

Cell line	Breast cancer subtype	Origin	Source	ER	PR	HER2		Reference
						Amplification of *ERBB2*	Overexpression of HER2	
MCF7	**Luminal A**	IDC	PE	+	+	–	–	(Soule *et al.*, 1973)
MDA-MB-361	**Luminal B**	AC	P. Br	+	+	+	+	(Cailleau *et al.*, 1974)
MDA-MB-453	**Unclassified**	AC	PE	–	–	+	–	(Cailleau *et al.*, 1978)
BT20	**Basal A**	IDC	P. Br	–	–	–	–	(Lasfargues and Ozzello, 1958)
MDA-MB-231	**Basal B**	AC	PE	–	–	–	–	(Cailleau *et al.*, 1978)
MCF10A	**Basal B**	FD	P. Br	–	–	–	–	(Soule *et al.*, 1990)

2.1.1.2 Non-breast cancer cell lines

A number of established human cancer cell lines were cultured *in vitro* in this study to be used during initial screens and antibody validation experiments as established positive controls (Table 2-9 and Table 2-11). These were used for many of

the EMT process experiments and analysis of Hedgehog (Hh) pathway components (Table 2-2).

Table 2-2: Control cell lines used for verification.
A number of established non-breast cancer cell lines were used during initial screens and antibody validation experiments as established positive controls for many of the EMT process and Hedgehog pathway components.

Cell line	Origin	Reference
HT29	Human colorectal adenocarcinoma	(Fogh *et al.*, 1977)
SW480	Human colorectal adenocarcinoma	(Leibovitz *et al.*, 1976)
Hela	Human cervical cancer	(Scherer *et al.*, 1953)
SKOV3	Human ovarian cancer	(Fogh *et al.*, 1977)
HepG2	Human hepatocellular carcinoma	(Aden *et al.*, 1979)
K562	Human chronic myelogenous leukaemia (CML)	(Lozzio and Lozzio, 1975)
Jurkat	Human acute T cell leukaemia	(Schneider *et al.*, 1977)
DU145	Human prostate cancer	(Mickey *et al.*, 1977)
PC3	Human prostate cancer	(Kaighn *et al.*, 1979)
U251	Human glioma cell line	(Westermark *et al.*, 1973)

The immortalised glioma cell line U251, MCF10A, DU145 and MDA-MB-231 were obtained from The American Type Tissue Culture Collection (*ATCC, USA*).

2.1.2 Standard tissue culture procedure

For consistency and unless otherwise stated, all cell lines were cultured in Dulbecco's Modified Eagle Medium (DMEM) supplemented with 10% heat inactivated foetal bovine serum (FBS) (*Life Technologies, UK*) and 2mM L-glutamine (complete medium).

MCF10A cells (Table 2-1) were cultured in 1:1 mixture of DMEM/Ham's F12 medium with 15mM HEPES supplemented with 5% heat inactivated horse serum, 2mM L-glutamine, and 0.5mg/ml hydrocortisone, 10µg/ml Insulin-Transferrin (*Life Technologies, UK*), 100ng/ml Cholera toxin and 20ng/ml EGF. After 24hours, the MCF10A full medium was replaced with a medium that does not contain EGF and incubated for additional 24hours before further analysis to reduce the effect of EGF on EMT.

Suspension cell line (K562 and Jurkat) (Table 2-2) was maintained by collection and centrifugation at 350xg for 10minutes. Cells were then resuspended in fresh culture medium.

All other cell lines were cultured as adherent monolayers (Table 2-1 and Table 2-2) in 75cm^2 (T75) or 25cm^2 (T25) tissue culture flasks (*Corning Costar, UK*) and maintained at 37ºC and 5% CO_2 in a humidified atmosphere. The growth media was changed twice weekly and cells were passaged at 80–90% confluency.

2.1.3 Sub-culturing of cells

For passaging, cells were washed with phosphate buffered saline (PBS) before incubation at 37ºC in PBS containing 1000unit/ml trypsin and 0.5mM ethylenediaminetetraacetic acid (EDTA). Trypsinised cells were removed in normal growth medium, collected by centrifugation at 1000xg for 3minutes, resuspended in fresh growth medium and re-seeded accordingly.

2.1.4 Seeding for experimental procedures

For experiments, sub-confluent cells were trypsinised (2.1.3) and resuspended in a known volume of normal growth medium (2.1.2). Cell number was determined using of a Neubauer counting chamber (*BDH, UK*) and cells were centrifuged at 1000xg for 3minutes, then resuspended in an appropriate volume of fresh growth medium. For routine tissue culture maintenance, cells were seeded at density equivalent to 4x10^4 cells/cm^2, unless otherwise stated, into tissue culture flasks (T25 or T75) (*Corning Costar, UK*). Control cell lines (Table 2-2), cells were seeded at a density equivalent to 4x10^4 cells/cm^2 (1x10^6 cells per T25 flask).

2.1.5 Seeding density experiment

Breast cancer cell lines were cultured as previously described. The seeding density method used by Conacci-Sorrell (2003) (based on colon cancer cell lines) and was adapted to be used for studying EMT in breast cancer cell lines. The initial procedure used is summarised in (Table 2-3).

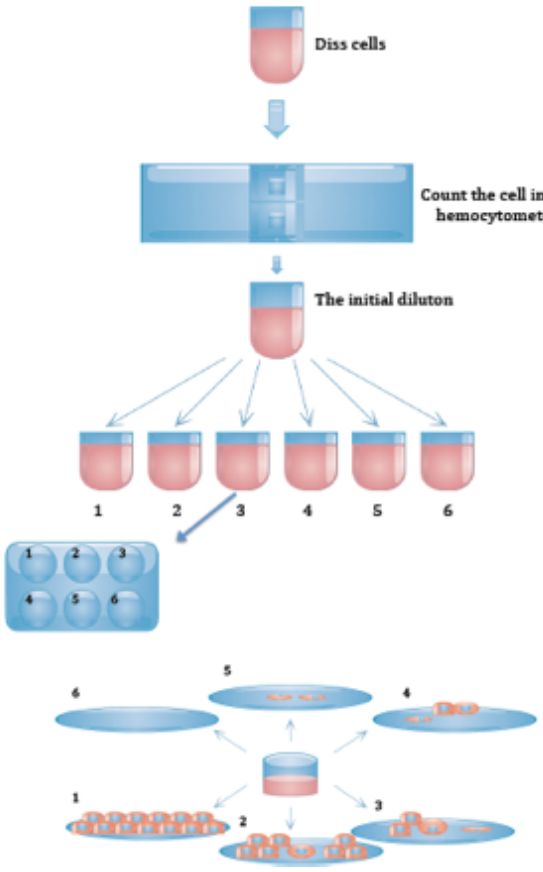

Figure 2-1, Initial step in seeding density experiment.
The figure illustrates the method used for determining the seeding densities used in the seeding density model. After the maximum seeding densities were determined, the cells were cultured at serial of dilution of cells in six well plate. The shape and morphology of the cells were then observed under the phase contrast microscope for selecting the seeding densities used in the model.

2.1.5.1 Determining Seeding Densities used in the model

Breast cancer cell lines were seeded in T75 flasks and maintained as described earlier (2.1.2). Subsequently, cells were detached from the flask using trypsin and cell number was determined using a haemocytometer and divided by 75 to estimate the number of cells that grow in 1 cm^2 (Figure 2-1). This number was used to determine the total cells number that form a confluent layer in well of 6-well plate. The density of the confluent culture was seeded into the first well of a 24 well plate and then diluted in the following wells and cultured for 24hours in humidified condition at 37°C in 5% carbon dioxide. Afterward, cell morphology was observed under the light microscope at three densities (high, medium, and low) for further study.

Table 2-3: The number of cells required to produce 95% confluent tissue culture in 24 hours.

Table list a summary of the numbers of cells seeded per cm^2 to form 95 % confluent culture after 24 hours

Cell line	Cells per cm^2
MCF7	$2x10^4$
MDA-MB-361	$4.8x10^4$
MDA-MB-453	$2.8x10^4$
BT20	$1x10^4$
MDA-MB-231	$1.2x10^4$
MCF10A	$1x10^4$

2.1.6 Cryopreservation of cells

To ensure consistency between experiments, cell use was confined within a narrow range of passage numbers (less than 8) and replenished from stocks maintained in liquid nitrogen. For freezing, confluent cells were trypsinised, resuspended in growth medium and centrifuged at 1000xg for 3minutes. Cells were then resuspended in growth medium containing 10% (v/v) DMSO cryoprotectant and 20% FBS in complete culture medium (2.1.2). The cell suspension was dispensed as 1ml aliquots into cryovials. Cells were frozen slowly in a cryopreserving chamber (Mr. Frosty) containing fresh isopropanol and placed at -80ºC for 24hours before being transferred to liquid nitrogen. Cells were recovered by thawing at 37ºC and the DMSO/medium was removed by centrifugation and washing in complete medium. Cells were resuspended and seeded in normal growth medium and were allowed to recover for at least one passage before experimental use.

2.1.7 Cell counts and viability

Cell numbers were assessed manually using a haemocytometer, and automated using Luna-FL™ Automated Fluorescence Cell Counters (*Labtech International Ltd, East Sussex, UK*). Automated cell counts were compared to manual counts by measuring the number of cells from different cultures to minimise counting errors and ensure accurate live/dead cell counting.

The viability of the cells was determined using trypan blue (TB), which is a cell membrane impermeable dye, with x2 dilution factor (10µl sample and 10µl stain). It is an exclusion assay based on the principle that live cells possess intact cell membranes

that exclude certain dyes (such as TB) whereas dead cells do not (Strober, 2001). In addition, acridine orange/propidium iodide (AO/PI) (*Labtech, Sussex, UK*) was used to measure cell viability with 1:10 dilution factor as recommended by the manufacturer (2µl sample and 18µl stains). AO/PI are nucleic acid binding dyes, where AO is cell permeable and stains nucleated cells generating a green fluorescence, while PI (~668Daltons) only enters cells with compromised membranes and therefore dying, dead, and necrotic nucleated cells stain with PI and generate a red fluorescence. When cells are stained with both AO and PI, live nucleated cells only fluoresce green and dead nucleated cells only fluoresce red. The AO/PI viability assay is a functionally linear rapid assay that is superior to conventional viability measurement by TB exclusion (Mascotti *et al.*, 2000).

2.1.8 Tissue culture treatment

Treatments were prepared in reduced serum medium, 1:1 mixture of DMEM/Ham's F12 medium with 15mM HEPES supplemented with 2% FBS, 2mM L-Glutamine, 0.5mg/ml hydrocortisone, and 10µg/ml insulin/transferrin. Two inhibitors were selected (cyclopamine and LDE225) were used at three concentrations (1µM, 5µM, and 10µM). The selected concentrations did not exceed 10µM to avoid non-specific cytotoxicity and off-target effects. Also, vehicle controls were prepared by the addition of 0.1% (v/v) of 95% ethanol. The cells were incubated for 48hours in 37°C in humid atmosphere that contain 5% CO_2 tissue culture incubator.

Two cell lines were selected for assessing the effect of inhibiting Hh signalling in breast cancer (MCF7 and MDA-MB-231). MCF7 is a luminal cell line was shown to have low metastatic ability and MDA-MB-231 a triple-negative and basal-like cell line that have high metastatic ability (Rizwan *et al.*, 2015).

2.1.8.1 Cyclopamine

Cyclopamine is a steroidal alkaloid isolated from the plant *Veratrum californicum* in the late 1960s and was identified for its teratogenic properties (Cooper *et al.*, 1998). It was later discovered that it has strong potential to bind to the transmembrane domain of Smo and act as a potent inhibitor of the Hh signalling pathway (Binns *et al.*, 1959; Keeler and Binns, 1964; Cooper *et al.*, 1998; Ma *et al.*, 2013; Lee *et al.*, 2014; Rimkus *et al.*, 2016).

Cyclopamine (obtained from *Selleckchem, UK*) was prepared as a 10mM stock solution in 95% Ethanol (v/v) and stored at -80º C. Cells were treated for 48 hours with

different concentrations of cyclopamine (1µM, 5µM and 10µM) or an equivalent volume of 95% ethanol (vehicle control) in serum reduced medium.

2.1.8.2 Sonidegib (Erismodegib, NVP-LDE225)

LDE225 is a Smo antagonist that belongs to the biphenyl carboxamides family and was first marketed by Novartis as Odomzo approved by the FDA in 2015 for treating basal-cell carcinoma. This drug interacts with the binding site of Smo and prevents the downstream activation of the hedgehog signalling pathway (Pan *et al.*, 2010; Skvara *et al.*, 2011; Fu *et al.*, 2013; D'Amato *et al.*, 2014; Kish and Corry, 2016; Jain *et al.*, 2017).

LDE225 (obtained from *Selleckchem, UK*) was prepared as a 10mM stock solution in 95% Ethanol (v/v) and stored at -80ºC. cells were treated for 48hours with different concentrations of LDE225 (1µM, 5µM and 10µM) or an equivalent volume of 95% ethanol (vehicle control) in reduced serum medium.

2.1.9 Plasmid preparation

A range of expression and reporter plasmids were used as described previously (Qualtrough *et al.*, 2015) and contain the coding sequences or promoter regions of a number of different components (Table 2-4).

2.1.9.1 Reporters used

pTOPFLASH (experimental reporter used to detect the activity of β-CRT) and pFOPFLASH (containing mutated TCF binding sites as a negative control) were obtained from Upstate Biotechnology (*NY*) (Figure 2-2-A and B). *pCMV-Renilla* control plasmid that is intended for use as an internal control reporter and may be used in combination with any experimental reporter vector to co-transfect mammalian cells was obtained from Promega (*Madison, WI, USA*) (Figure 2-2-C).

Table 2-4: Promotor reporter constructs.

Construct	Function	Reference
pCMV-Renilla	*Renilla* control	Promega
pTOPFLASH	*LEF/TCF responsive reporter*	(Korinek *et al.*, 1997)
pFOPFLASH	*TOPFLASH control reporter*	(Korinek *et al.*, 1997)

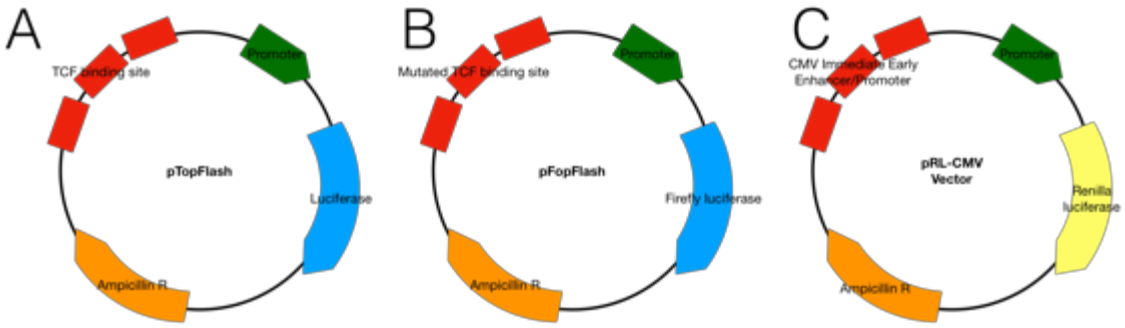

Figure 2-2, The maps for the reporter plasmid constructs.
The maps for reporter plasmid constructs used. All plasmids consist of promoter, Luciferase and amplification sites. (A) pTOPFLASH reporter consisting of several TCF binding sites. (B) pFOPFLASH reporter consisting of mutated TCF binding site. (C) *pCMV-Renilla* contains the Cytomegalovirus (CMV) enhancer and immediate/early promoter elements to provide high-level expression of *Renilla* luciferase in co-transfected mammalian cells. This figure was drawn by the author.

The activity of the *pCMV-Renilla* reporter provides an internal control that serves as the baseline response in transfected cells. Normalising the activity of the experimental reporter to the activity of the internal control minimises experimental variability caused by differences in cell viability or transfection efficiency. Other sources of variability, such as differences in pipetting volumes, cell lysis efficiency and assay efficiency, can be effectively eliminated.

2.1.9.2 Plasmid preparation

E.coli recipient strain *DH5α* was kindly provided by Dr. Tim Craig (UWE) and was used to make competent bacteria for transformation and plasmid production. *DH5α* were grown to log phase in 500ml of Maitland Lysogeny broth (LB) broth and used to produce glycerol stocks of Chemocompetent bacteria. These were maintained at -70°C until required for transformation. Chemocompetent *E.coli* were transformed by resting on ice for 30minutes in the presence of 5µl of plasmid DNA, then heat shocking for 90seconds at 42°C and returning to ice for a further 15minutes. *E.coli* were plated out on nutrient agar plates (*Maitland, UK*) containing 20µg/ml^{-1} Ampicillin and incubated at 37°C overnight. A single colony was used to inoculate 10ml of LB broth containing 50µg/ml^{-1} of Ampicillin and incubated with shaking at 37°C overnight. 5ml of the resultant inoculum was then spun down at 6000xg for 15minutes and plasmid purified using Qiagen miniprep kit (*Qiagen, Germany*).

1ml of inoculum was used to inoculate 500ml of LB broth, which was incubated overnight at 37°C with shaking. The plasmids were extracted using Qiagen maxiprep kit (*Qiagen, Germany*) and resuspended in Tris-EDTA (TE) buffer (10mM Tris Base,

1mM EDTA solution, 1% Tween 20 (v/v), pH9.0). The final concentration and purity were determined by dsDNA analysis were determined in triplicate samples using the Nanodrop 1000 spectrophotometer (*Thermo Scientific*), where 2µl of dsDNA extract was measured. Purified plasmids in TE buffer were stored at 4°C.

2.1.10 Transfection procedure

2.1.10.1 Cell seeding

For analysis of promotor activity, the various promotor reporter constructs (Table2-3) were transiently transfected into cells. In general, this was performed on cells grown in 24 well plates (*Corning Costar, UK*) at $8x10^4$ cells/well (equivalent to $1x10^6$ cells in a T25 tissue culture flask). Cells were grown under standard growth conditions for 48hours in reduced serum medium or treatment medium (5.2.1). Experimental design is shown in Table 2-4 using two breast cancer cell lines (MCF7 and MDA-MB-231). Transfection of the SW480 colorectal cancer cell line was carried out as a positive control for the transfection procedure (Qualtrough *et al.*, 2015).

Table 2-5: Transfection procedure for determining the effect of Hh inhibition by cyclopamine and LDE225 on CRT.
This table is a layout for the experimental design followed to determine effect of Hh inhibition on the CRT. This experiment was conducted in triplicate with (n=3) for each cell line.

Vehicle control (0.1% (v/v) of 95% ethanol	Vehicle control pTOPFLASH *pCMV-Renilla*	Vehicle control pFOPFLASH *pCMV-Renilla*
1µM cyclopamine	1µM cyclopamine pTOPFLASH *pCMV-Renilla*	1µM cyclopamine pFOPFLASH *pCMV-Renilla*
1µM LDE225	1µM LDE225 pTOPFLASH *pCMV-Renilla*	1µM LDE225 pFOPFLASH *pCMV-Renilla*

2.1.10.2 Lipofectamine reagent protocol

For reporter and expression construct co-transfection experiments (per triplicate wells), 0.72µg of each reporter constructs was mixed with 0.08µg *Renilla* construct in 150µl of Optimem mix (*Life Technologies, UK*) (0.8µg DNA in total). 6µl of Lipofectamine 2000 reagent (*Life Technologies, UK*) was mixed in a separate 150µl of Optimem and incubated at room temperature for 5minutes. The two reaction mixtures were combined with 1200µl of Optimem and incubated for a further 20minutes. Cells

were washed with PBS, which was thoroughly removed to avoid dilution effects, and 500µl of the reaction mixture was added to each well. After 6hours, the transfection mix was replaced with serum reduced-medium or treatment medium (according to the experiment) and the cells were maintained under standard conditions until harvested after 48 hours.

2.1.10.3 Passive cell lysis and luminescent analysis

After transfection, cells were lysed in 100µl/well of 1x Passive Lysis Buffer (PLB) (*Promega, USA*). After 15minutes, lysates were transferred to an Eppendorf tube for analysis and stored at -70°C. Cell lysates were assayed using Promega Dual Luciferase Reporter Assay System (*Promega, USA*) in 96 wells white plates (*Corning Costar, UK*) on a FluoStar luminometer. Samples were corrected for background emission against the average of five readings from an untransfected control. Firefly luciferase activity was determined from three separate experiments performed in triplicate.

2.2 Western Blotting analysis

2.2.1 Sample preparation from trypsinised cells

In experiments where cells were harvested by trypsinisation and counted, aliquots were retained for analysis by Western blotting. Counted cells were transferred into 1.5ml Eppendorf tubes. Cells pellets were obtained by centrifugation at 1000xg for 3minutes at 4°C and the PBS was aspirated. Cell pellets were lysed in 100µl of Radioimmunoprecipitation (RIPA) lysis buffer with protease inhibitor cocktail (prepared according to manufacturer's instruction; *Roche*) for 30minutes on ice, by vortexing with 5minutes intervals for 30seconds. The lysate was then centrifuged for 30minutes at maximum speed (17949.49xg) at 4°C. The supernatants were transferred to fresh 1.5ml Eppendorf tubes and the protein concentrations of supernatants determined with a Pierce Bicinchoninic acid assay (BCA) protein assay kit (Thermo Scientific) as instructed by the manufacturer.

2.2.2 Whole cell protein extraction

To avoid significant cleavage of cellular protein, cell samples were prepared by lysing the cells *in situ* using RIPA lysis buffer with protease inhibitor cocktail (prepared according to manufacturer's instruction; *Roche*). The medium was aspirated, and cells were washed twice in ice cold PBS prior to an appropriate amount of lysis buffer being

added. Cells were incubated on ice for 15minutes before scraping and then transferred to a 1.5ml Eppendorf tube. Lysates were centrifuged for 30minutes at maximum speed (17949.49xg) at 4°C. The supernatants were transferred to fresh 1.5ml Eppendorf tubes and the protein concentrations of supernatants were determined with a Pierce BCA protein assay kit (Thermo Scientific) as explained by the manufacturer.

2.2.3 Quantification of extracted protein

Briefly, 25µl of each sample was incubated for 30minutes at 37°C with 200µl of working solution in a 96-well plate (*Corning Costar, UK*), in triplicate. Subsequently, the absorbance was measured by a FluoStar spectrophotometer at 562nm. Protein concentrations were calculated by using a standard curve of known albumin standards ranging from 0 to 1500µg/ml. Protein samples were stored at -70°C until analysed.

2.2.4 SDS-PAGE technique

2.2.4.1 Acrylamide gel preparation

The components for the solutions used in the Sodium Dodecyl Sulphate Polyacrylamide Gel Electrophoresis (SDS-PAGE) technique are listed in (Table 2-6). Proteins from cell lysates were separated by protein size using SDS-PAGE. The mini-Protean 3 electrophoresis system (*Bio-Rad, USA*) was used to cast 8-12% acrylamide resolving gels (1.5mm thick). In this study, different concentrations of acrylamide gels were prepared depending on the size of the protein investigated, 10% for E-cadherin and β-catenin, and 12% for smaller sized proteins (

Table 2-7). Gels were allowed to set for at least 30minutes before loading and running. Then a stacking gel was made on top of the resolving gel at 5% concentration (Table2-7).

Table 2-6: Western blotting buffers used in this study.
Buffers used in western blotting and their components and concentrations.

Solution components	
10% SDS	**10xElectrode buffer**
10g Sodium Dodecyl Sulphate (SDS)	30.3g Tris base
100ml H_2O	144g Glycine
1.5M Tris-HCl/ SDS pH8.8	1L H_2O
45.41g Tris	**Running buffer**
0.4% SDS (10ml of the 10% stock)	0.1% SDS (10ml of 10% stock)
200ml H_2O	1xTris Glycine (100ml of 10xelectrode buffer)
pH to 8.8 with 1M HCl	Make up to 1L with H_2O
Make to 250ml with H_2O	**Transfer Buffer**
1M Tris-HCl/SDS pH6.8	100ml Methanol
6.06g Tris	1XTris Glycine (50ml of 10xelectrode buffer)
0.4% SDS (4ml of 10% stock)	Make up to 500ml with H_2O
90ml H_2O	**0.1% Ponceau S Red**
pH to 6.8 with 1M HCl	0.1mg
Make to 100ml	1L 1% Acetic acid

Table 2-7: A list of the concentration of resolving SDS/PAGE gels used in this study.
Component volumes (mL) per gel mould volume of 10ml.

Solution components	**Components volumes (ml) per gel volume of 15ml**		
Gel concentration	**8%**	**10%**	**12%**
H_2O	6.9	5.9	4.9
30% Acrylamide mix	4	5	6
1.5M Tris (pH8.8)	3.8	3.8	3.8
10% SDS (*SLS, UK*)	0.15	0.15	0.15
10% ammonium persulfate	0.15	0.15	0.15

TEMED	0.018	0.016	0.012

Table 2-8: List of the solutions used in the preparation of 5% stacking SDS/PAGE. Components of solution used to prepare 5% stacking gel. Components volumes (ml) per gel mould volume of 4mL.

Solution components	Components volumes (ml) per gel mould volume of 4ml
H_2O	2.7
30% Acrylamide mix	0.67
1.5M Tris (pH6.8)	0.5
10% SDS (*SLS, UK*)	0.04
10% ammonium persulfate	0.04
TEMED	0.008

100µg of protein (unless otherwise stated) was loaded into each lane. 10µl of Amersham ECL Plex Fluorescent Rainbow Marker (*GE Healthcare Life Sciences, USA*) was loaded into a spare well and sample was electrophoresed until stain front remained visible.

2.2.4.2 Sample preparation

Equal amounts of protein were loaded from each lysate that were diluted in 1x NuPAGE LDS sample buffer (*Novex, Life Technologies, USA*) or Laemmli sample buffer (*Bio-Rad, USA*) containing 5% Beta-Mercaptoethanol. Samples were then heated in a preheated heat block at 100°C for 5minutes. The samples are cooled briefly in ice prior to loading into the gel.

2.2.4.3 Gel electrophoresis conditions

Gels were run at constant voltage (125v) for 90minutes in room temperature in 1x running buffer (Table 2-6).

2.2.4.4 Protein transfer

The proteins were then transferred onto polyvinylidene difluoride (PVDF) membrane (*GE Healthcare Life Sciences, USA*) using the Mini Trans-Blot Electrophoretic Transfer Cell (*Bio-Rad, USA*). PVDF membrane is activated by incubation in 100% methanol for 15minutes. Then proteins were transferred from gel to

PVDF in methanol containing transfer buffer (Table 2-6) at constant voltage (25V) for 90minutes. To confirm successful protein transfer, both the gel and the membrane were stained by a reversible stain with 0.1% Ponceau S (w/v) in 1% acetic acid (v/v), subsequently removed by washing with distilled water, without affecting the proteins in the blots.

2.2.5 Probing for proteins of interest

2.2.5.1 Blocking, washing and antibody preparation

Membranes were blocked in 5% low fat milk prepared in PBS containing 0.1% Tween 20 (PBS/T) overnight at -4°C with continuous agitation. Membranes were washed in PBS/T three times for 3minutes between incubations. Antibody dilutions (Table 2-9) were prepared in blocking buffer. Loading accuracy was subsequently assessed by analysis using a primary antibody raised against α-Tubulin.

Table 2-9: List of primary antibodies used for probing the membranes.
The primary antibodies used in this study and their origin. Also, dilations and incubation period used in this study.

Antibody	Clone	Isotype	Company	Concentration	Band size	Control
E-cadherin	34/E-cadherin	Mouse monoclonal IgG2b	Becton, Dickinson (BD) Transduction laboratories™	1:100	120kDa	HT29, and MCF7
β-catenin	14/Beta-catenin	Mouse monoclonal IgG1	BD Transduction laboratories™	1:150	92kDa	SW480, and HT29
Vimentin	RV202	Mouse monoclonal IgG1	BD Transduction laboratories™	1:50	57kDa	MDA-MB-231, and Hela
Gli1	H-300	Rabbit poly clonal IgG	Santa Cruz Biotechnology	1:100	114-173kDa	K562, and PC3
Gli2	C-10	Mouse monoclonal IgG_1	Santa Cruz Biotechnology	1:100	86-168kDa	K562, and PC3
Gli3	B-4	Mouse monoclonal IgG2b kappa light chain	Santa Cruz Biotechnology	1:100	190kDa	K562, and Jurkat
Smoothened	E-5	Mouse monoclonal IgG2a kappa light chain	Santa Cruz Biotechnology	1:100	85kDa	K562, and Hela
Patched	3B3	Mouse monoclonal IgG2a kappa light chain	Santa Cruz Biotechnology	1:100	140kDa	PC3
Sonic Hedgehog (Shh)	E-1	Mouse monoclonal IgG1 kappa light chain	Santa Cruz Biotechnology	1:100	19-45kDa	Hela
Indian Hedgehog (Ihh)	H-12	Mouse monoclonal IgG1 kappa light chain	Santa Cruz Biotechnology	1:100	45kDa	Hela, and HepG2
α-Tubulin	DM1A	Mouse monoclonal IgG1	SIGMA-ALDRICH	1:1000	50kDa	-

Table 2-10: List of secondary antibodies used for visualisation of blot and their origin.
Table include a summary of dilation and incubation periods of antibodies.

Antibody	Host	Reactivity	Company	Concentration
IRDye® 800CW anti-Mouse IgG (H+L)	Donkey	Mouse	Li-Cor®	1:15000
IRDye® 680RD anti-Rabbit IgG (H+L)	Donkey	Rabbit	Li-Cor®	1:15000

2.2.5.2 Visualisation and imaging of proteins bands

Protein bands were detected using the Enhanced Chemiluminescence (ECL) method by adding 2mL of the chemiluminescent substrate to the membrane (Millipore Forte) for 2minutes in continuous rotation, followed by developing the ECL film (Amersham, GE Healthcare, USA) in the dark room after 30second, 1minute and 3minutes exposure. The Li-Cor Odyssey® FC system was used for detection of secondary antibodies labelled by the near-infrared fluorescence. Images were captured at appropriate exposure time using the appropriate detector filter using the Image Studio™ software.

2.2.5.3 Densitometric analysis

In order to quantify differences in protein expression observed by Western blotting analysis, the films were scanned (600dpi) using Photoshop software (*Adobe*) and densitometric analysis was performed using ImageJ software (*NIH, USA*). All densitometric analysis was normalised to a common band on each film and for protein screening experiments, averages are representative of data from three separate experiments.

2.3 Immunocytochemistry

2.3.1 Seeding cells on coverslips

Cells were cultured on 19-22mm diameter rounded glass coverslips (*VWR, International*) pre-coated with Poly-L-Lysine (PLL) according to manufacturer's instructions. In brief, coverslips were sterilised in 100 % ethanol for 30minutes then coated with 0.01% PLL (v/v) for 5minutes, drained and air dried. Coverslips were stored in sterile plates until needed.

2.3.2 Sample preparation

Cells were seeded onto sterile coated 19-22mm glass coverslips (*VWR, international*) at the appropriate density/well in 12 well plates (*Corning Costar, UK*). For treatment IC, cells were seeded at medium density (Table 3-1). Cells were grown under standard growth conditions for 24hours prior to changing to treatment medium.

2.3.3 Cell fixation and permeabilisation

Cells on coverslips were washed once with sterile PBS before being fixed and permeabilised by 4% (w/v) paraformaldehyde (PFA) containing 0.1% (v/v) Triton X-100 (*BDH, UK*) for 15minutes at room temperature inside the tissue culture hood. Subsequently, they were washed three time with sterile PBS and stored in PBS at -2°C until further analysis.

2.3.4 Immunocytochemistry procedure

Cells were washed once with PBS and then blocked for 60minutes in PBS containing 2% (w/v) Bovine Serum Albumin (BSA), 5% FBS (v/v) (*Life Technologies, UK*), and 0.1% Gelatine from cold fish skin. Coverslips were then incubated for 1hour in primary antibody prepared in the blocking buffer at the appropriate concentration at room temperature (Table 2-11). After this, coverslips were washed three times for 5minutes each in PBS, cells were then incubated in the dark with the appropriate secondary antibody at the recommended concentration, at room temperature (Table 2-11). Following antibody adhesion, cells were washed a further three times and then incubated for 5minutes in (1:10,000) 4',6-Diamidino-2-phenylindole (DAPI) nuclear counterstain. Cells were then washed with PBS a further three times for 5minutes and then the coverslips were mounted in aqueous mounting medium containing DAPI (*Vector Labs, UK*). Cells were visualised using the fluorescence microscope (*Leica, Germany*) or using the inverted Leica UltraView spinning disc confocal laser scanning microscopy and images acquired/compiled using Leica Confocal Software (*Leica, Germany*).

Controls were prepared for each set of experiments, including control cell lines positive for the protein of interest (Table 2-11). A negative control of each cell line was also included by incubating the cells in blocking buffer instead of primary antibody step. This step was necessary to ensure proper quality control measures in all experiments.

Table 2-11: List of the primary antibodies used for IC.
These were the primary antibodies used in this study and their origin. Also, listed are the dilutions and the incubation period used in this study.

Antibody	Clone	Isotype	Company	Concentration	Control
E-cadherin	34/E-cadherin	Mouse monoclonal IgG2b	BD Transduction laboratories™	1:100	HT29, and MCF7
β-catenin	14/Beta-catenin	Mouse monoclonal IgG1	BD Transduction laboratories™	1:150	SW480, and HT29
Vimentin	RV202	Mouse monoclonal IgG1	BD Transduction laboratories™	1:50	MDA-MB-231, and Hela
Gli1	H-300	Rabbit poly clonal IgG	Santa Cruz Biotechnology	1:50	K562
Gli2	C-10	Mouse monoclonal IgG_1	Santa Cruz Biotechnology	1:50	K562
Gli3	B-4	Mouse monoclonal IgG2b kappa light chain	Santa Cruz Biotechnology	1:50	K562

Table 2-12: List of the secondary antibodies used for visualisation of IC.
Table include a summary of the dilutions and the incubation period.

Antibody	Host	Reactivity	Company	Concentration
Anti-Mouse IgG (H+L) Secondary Antibody, Alexa Fluor® 488	Chicken	Mouse	Life Technologies	1:100
Anti-Rabbit IgG (H+L) Secondary Antibody, Alexa Fluor® 488	Chicken	Rabbit	Life Technologies	1:100
Anti-Mouse IgG (H+L) Secondary Antibody, Alexa Fluor® 594	Chicken	Mouse	Life Technologies	1:100
Anti-Rabbit IgG (H+L) Secondary Antibody, Alexa Fluor® 594	Chicken	Rabbit	Life Technologies	1:100

2.4 Flow cytometry

Flow assisted cell cytometry was used to analyse protein expression following various treatments.

2.4.1 Cell preparation and fixation

Following appropriate treatment, cells were trypsinised and counted before centrifugation at 1000xg for 3minutes. Cells were treated by fixation buffer (*BD Biosciences, UK*) for 15minutes at room temperature and then washed in 5ml PBS with 0.1% (v/v) Triton X-100 (PBS/Triton). Cells were suspended at $1x10^6$ cells/ml in blocking buffer and gently mixed, and then incubated at room temperature for 1hour.

2.4.2 Immunofluorescent staining

Cells were then allowed to pellet at room temperature and then the supernatant were carefully collected and discarded. Cells were then incubated with primary antibody solution (made in blocking buffer) for 1hour at room temperature (Table 2-11). Cells were allowed to pellet, and supernatant was collected and discarded followed by washing three times in PBS/Triton for 5minutes each time. Cells were then incubated in secondary antibody solution, made in blocking buffer, for 1hour at room temperature (Table 2-11). This was followed by washing three times in PBS/Triton for 5minutes each time and resuspending the cells in PBS/Triton.

Controls were prepared for each set of experiments, including control cell lines that are positive for the protein of interest (Table 2-11). A negative control for each antibody was also included, by incubating the cells in blocking buffer instead of primary antibody. This step was necessary to ensure proper quality control measure in all experiments.

2.4.3 Apoptosis assay

FITC Annexin V apoptosis detection kit I (*BD Biosciences, UK*) was used for identification of the different stages of apoptosis in the cells following treatment (Casciola-Rosen *et al.*, 1996). FITC Annexin V is a sensitive probe for identifying apoptotic cells and, when used in conjunction with a vital dye such as PI (Propidium Iodide), allows the identification of early apoptotic cells (PI negative, FITC Annexin V positive). Viable cells with intact membranes exclude PI, whereas the membranes of dead and damaged cells are permeable to PI.

The cells were prepared according to manufacturer's instructions. In brief, cells were washed twice with cold PBS and suspended in 1X Binding buffer at a concentration of $1x10^6$ cells/ml. 100µl of that solution ($1x10^5$ cells) was transferred to an Eppendorf tube and stained with 5µl of FITC Annexin V and 5µl PI (provided in the kit), gently mixed and then incubated for 15minutes in the dark. Following this, 400µl of 1X Binding buffer was added to each sample and sample analysed by flow cytometry within 1hour.

Apoptosis percentage in cells were determined using FITC Annexin V apoptosis detection kit I (*BD Biosciences, UK*) (2.4.3). Several appropriate controls were added to ensure proper analysis and for quality control measures. Unstained control for each cell line was included for each experiment. Two positive controls for each cell line were also included by incubating cells in heat block for 10 seconds at 60°C, one was stained

with FITC Annexin V and one stained with PI. One untreated control was added for each cell line used to determine the baseline of normal apoptosis in cells and to ensure that the cells were not subjected to damage during experimental setting.

Samples and controls were analysed using BD Accuri™ C6 (*BD Biosciences, UK*) and data was analysed using BD Accuri™ C6 Plus software (*BD Biosciences, UK*). Gating was conducted on unstained control (Figure 2-3-A). Compensation for FITC/PI signal overlap is conducted using positive FITC control, positive PI control and mixed control (positive FITC: positive PI) (Figure 2-3-B).

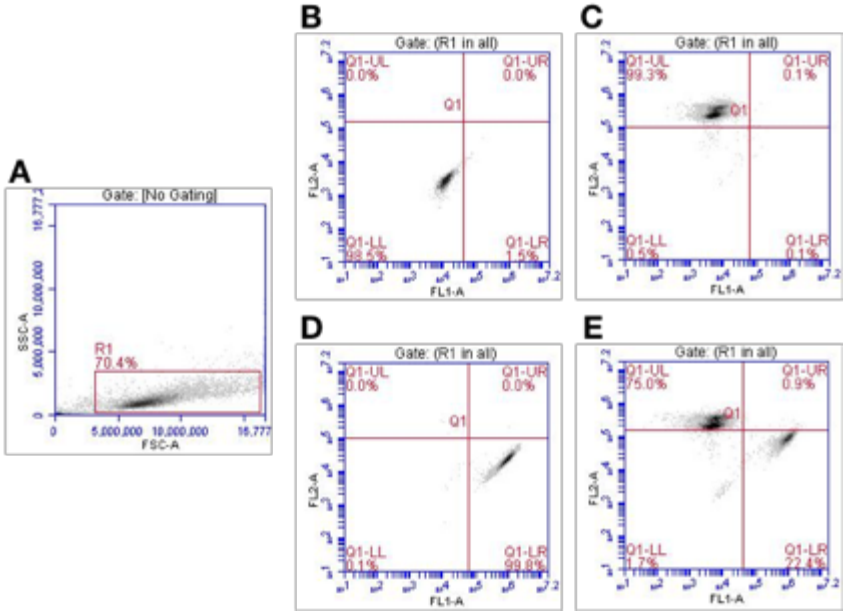

Figure 2-3, Example of gating strategy used for measuring breast cancer cell lines integrity and compensation technique used to measure positive cells in each flow cytometry channel.

This figure shows gating strategy used for breast cancer cell line to exclude dead cells, debris and cellular doubling, using gated region shown in the first plot, using 10,000 events analysed each time. (A) Shows unstained breast cancer cells in forward and side scatter; also, it shows the gate of live cells. (B) Shows unstained cells in FL1 and FL2 detectors. This histogram was used to set threshold for positive cells after negative histogram. (C) The positive cells stained with propidium iodide detected in FL2. (D) The positive cells stained with primary Annexin V-FITC conjugated fluorescence antibody detected in FL1. (E) Compensation control (combination of cells stained with Annexin V-FITC conjugated fluorescence antibody only and cells stained with PI only) was used to set the compensation level for differentiating the FL1 and FL2 signal.

2.4.4 Flow cytometric technique

All flow cytometry analysis was performed using a BD Accuri™ C6 (*BD Biosciences, UK*) and data was analysed using the BD Accuri™ C6 Plus software (*BD Biosciences, UK*). A single cell population was gated based on appropriate size on the basis of forward scatter (FCS-A) versus side scatter (SSC-A). A total of 10,000 events

for each sample was measured, and all experiments were repeated a minimum of three times. Increased fluorescence was compared to unstained controls for all proteins investigated. Computational analysis was performed using the BD Accuri™ C6 Plus software.

Cells were gated to exclude debris and cellular doubling, and analysis was based on collecting 10,000 events through the gate as shown in (Figure 3-3). Flow cytometry was used as well to measure the percentage of positive cells as well as the median fluorescence intensity (MFI), which provided an indication of the overall level of protein in cells. All comparisons were done by one-way analysis of variance (ANOVA) test prepared using SPSS and GraphPad Prism software for data analysis. Negative control (secondary only), positive controls (Table 2-2), and unstained cell control was included in the experiments.

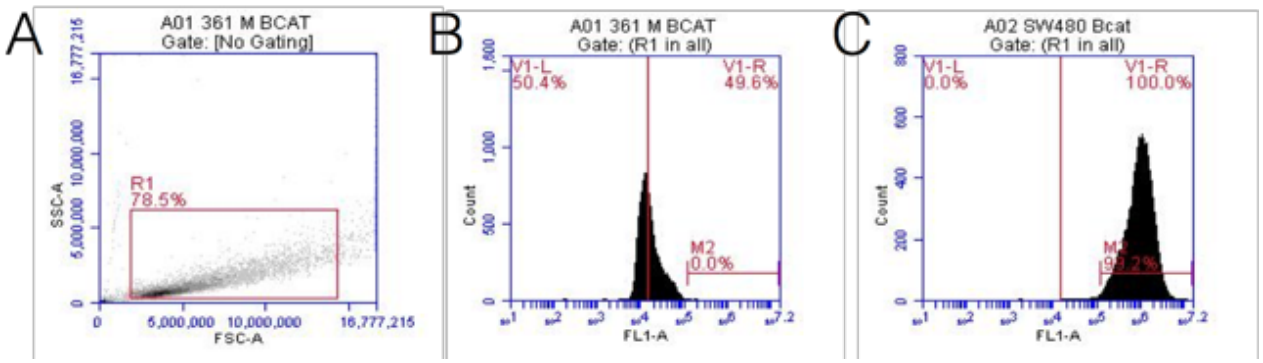

Figure 2-4, Example of the gating strategy used for measuring breast cancer cell lines integrity and compensation technique used to measure the positive cells in each flow cytometry channel.
This figure shows the gating strategy used for breast cancer cell line to exclude cellular doubling, using the gated region shown in the first plot, using 10,000 events analysed each time. (A) Shows the unstained breast cancer cells in forward and side scatter, also, it shows the gate of the live cells. (B) Shows the unstained cells in FL1 detector. This histogram was used to set the threshold for the positive cells after the negative histogram. (C) The positive cells stained with the primary and secondary conjugate fluorescence antibody detected in FL1.

2.5 Migration and in vitro invasion assays

2.5.1 Transwell filter assay

Cell migration assays were carried out using a Transwell filter migration assay as previously described (Efstathiou *et al.*, 1999; Qualtrough *et al.*, 2007). In brief, insert filters of 8µm pore size (*Merc Millipore, UK*), were coated with 500µl of 10µg/ml VitroCol® human collagen type I solution (*Cell Systems, USA*). Cell invasion assays

were carried out using 8 μm pore size Corning BioCoat™ Matrigel® Invasion Chambers with BD Matrigel® Matrix (*Fisher Scientific, UK*) as described previously (Qualtrough *et al.*, 2007; Qualtrough *et al.*, 2015). 24hours prior to assay, cells were lifted using trypsin, counted and resuspended to a final concentration of $1x10^5$ cells/ml in calcium-free-DMEM with 2% FBS (with or without treatment). The lower chamber was filled with calcium-free-DMEM with 5%FBS, to act as an attractant, and 2ml of cell solution ($2x10^5$ cells) was added to each filter. Following 24hours of incubation at 37°C, cells attached to the filter were fixed for 10minutes in 100% methanol and stained using Mayer's haematoxylin (*BDH, UK*). Cells were removed from the upper filter surface with a cotton swab, while those on the lower filter surface were considered migratory and counted in ten separate fields at 200 times magnifications. Three independent experiments were carried out in triplicate, and the data are expressed as mean ±SDM. Statistical analysis of this data performed using the Student's t-test. Differences were considered significant when the *p*-value was <0.05.

2.6 *Statistical analysis*

All value quoted represent mean ± Standard Deviation of the mean (S.D.) of the sample unless otherwise stated. While some data has been normalised to aid graphical display, all statistical analyses were performed on raw data. Graphical representation and basic data manipulation were conducted in GraphPad Prism 6 for Mac. The majority of statistical analysis was performed using SPSS version 17 used.

Where samples were found to be normally distributed a paired T-test, or two-sample T-test was utilised for statistical analysis, with each sample compared with relevant controls. A *p*-value of 0.05 or below was considered to be significant. Non-normal distributions were analysed using the Mann-Whitney test for unpaired samples; in the case of comparing more than two groups, a Kruskal-Wallis test was performed. If significant differences were indicated, Mann-Whitney analysis was subsequently performed between groups with Bonferroni correction to identify where the significant differences can be found.

2.7 *Immunohistochemical analysis*

2.7.1 Human tissues and ethical approval

Surgically resected human tissue (formalin-fixed paraffin-embedded) was selected and anonymised by a qualified histopathologist from the tissue archives at the Department of Histopathology, Bristol Royal Infirmary. All tissue was obtained under

approval from the NHS Health Research Authority (Ref: 11/SW/0127) and UWE ethics committee. All methods were performed in accordance with the NHS Health Research Authority guidelines and regulations.

2.7.2 Tissue sectioning and rehydration

Paraffin blocks containing embedded human breast tissue were sectioned at 4µm using a microtome (*Leica RM2235*) (*Leica, Germany*) and mounted on superfrost Plus glass slides (*Thermo-Fisher, UK*). Sections were allowed to adhere for at least 30minutes in an oven at 60°C followed by deparaffinisation in two changes of Histoclear (*National Diagnostics, USA*) for 5minutes. Slides used in this study were serial sections probed with antibodies against the markers while one section was stained with H&E (Haematoxylin and Eosin) to show details of tissue structure. Sections were then deparaffinised with Histoclear (*National Diagnostics*) and rehydrated using a series of ethanol concentrations and dH_2O. Sections were rehydrated gradually in descending concentrations of ethanol and in dH_2O. Antigen unmasking was performed by heating in 0.01M/L citrate buffer (pH6.0) using a 95-100°C water bath for 30minutes then allowing the sections to cool to room temperature in the buffer. Slides were then moved to running tap water.

2.7.3 Immunohistochemistry staining procedure

Endogenous peroxidases were quenched with 3% (v/v) H_2O_2 for 5minutes (*BDH, UK*). Slides were incubated in blocking serum (Goat or horse serum (*Vector Labs, UK*) diluted in PBS for 30minutes at room temperature, then incubated in primary antibody overnight at 4°C. Antibodies used were anti-human (Table 2-13).

Table 2-13: List of the primary antibodies used for Immunohistochemistry (IHC).
These were the primary antibodies used in this study and their origin. Also, listed are the dilutions and the incubation period used in this study.

Antibody	Clone	Isotype	Company	Concentration
E-cadherin	4A2C7	Mouse monoclonal IgG_1-kappa	Invitrogen™, Life Technologies	1:100
β-catenin	14/Beta-catenin	Mouse monoclonal IgG1	BD Transduction laboratories™	1:100
Gli1	H-300	Rabbit poly clonal IgG	Santa Cruz Biotechnology	1:100
Gli2	C-10	Mouse monoclonal IgG_1	Santa Cruz Biotechnology	1:200
Gli3	B-4	Mouse monoclonal IgG2b kappa light chain	Santa Cruz Biotechnology	1:150
Smoothened	E-5	Mouse monoclonal IgG2a kappa light chain	Santa Cruz Biotechnology	1:100
Progesterone	PgR636	Mouse monoclonal IgG_1-kappa	Dakocytomation, Agilent Technologies	1:200
ER α	1D5	Mouse monoclonal IgG	Dakocytomation, Agilent Technologies	1:200
HER2		Rabbit monoclonal IgG	Fisher Scientific	1:400
Ki67/MK167	SP6	Rabbit monoclonal IgG	Fisher Scientific	

The next day, slides were washed in PBS and then incubated with suitable biotinylated secondary antibodies for 1hour at room temperature (Table 2-14). The secondary antibody was prepared from the Universal Elite Kit (*Vector Labs, UK*). Following the secondary antibody incubation, the Avidin-biotin complex (ABC) reagent from the Vectastain® Elite kit was prepared in PBS according to the manufacturer's instructions. The slides were washed three times in PBS and then incubated in the ABC reagent for 30minutes. Slides were washed three times for 5minutes with PBS. The slides were then incubated in Diaminobenzidine tetrahydrochloride (DAB) to produce the chromogen (*Dakocytomation, Cambridge, UK*). Tissue was then counterstained by Meyer's haematoxylin (*BDH, UK*) for 3minutes and washed in running tap water for 5minutes. Slides were dehydrated in a series of increasing concentrations of alcohol and cleared in two changes in Histoclear for 5minutes in each, followed by mounting in DPX (Distyrene, a plasticizer, and xylene) (*BDH, UK*). Secondary only controls were included in each batch to ensure specificity of immunoreactivity.

Table 2-14: List of the secondary antibodies used for visualisation of IHC.
Table include a summary of the dilation and the incubation period.

Antibody	Clone	Host	Reactivity	Company	Concentration
Anti-Rabbit IgG	BA-1100	Horse	Rabbit	Vectorlabs	1:50
Anti-Mouse IgG	BA-2000	Horse	Mouse	Vectorlabs	1:50

2.7.4 Scoring and analysis

Stained tissue was scored by semi-quantitative analysis under the light microscope according to immune reactive scoring (IRS) (Remmele and Stegner, 1987; Kaemmerer et al., 2012) (Table 2-15). 10 fields were selected in each sample and scored using the IRS criteria (Table 2-15). The IRS score includes evaluation of the reaction intensity and the relative percentage of positive tumour cells. 5 fields were selected from the tumour centre and five at the invasive front of the tumour (if available). The invasive front is defined here as an area of three-to six layers of cells at the border of the tumour mass or the scatter of tumour cells between the edge of the tumour and the surrounding stroma (Eiro *et al.*, 2012; Gong *et al.*, 2013). Additionally, nuclear staining in the ten fields was scored according to the scheme used by Volante et al. (2007) for Gli1, Gli2, Gli3 and β-catenin (Table 2-15).

The scores were compared between the invasive front and the tumour centre. The nuclear scores for the tumour centre were also compared to the nuclear score of the invasive front.

Representative images of the immune reaction were obtained using a GT slide scanner (*GT Vision, UK*) and photomicrographs of stained tissue were acquired using Leica microscope (*Leica, Germany*).

Table 2-15: IRS and IRS classification and scoring system.

Table include a summary of the scoring method used.

Percentage of positive cells		**Staining intensity**	
Proportion of stained cells (%)	**Score**	**Intensity of staining**	**Score**
0	0	No colour reaction	0
< 10	1	Mild reaction	1
10 - 50	2	Moderate reaction	2
51 - 80	3	Intense reaction	3
> 80	4	**IRS classification**	
IRS Score = Percentage x Staining intensity			
Points (0 - 12)	**Description**		
0 - 1	Negative	0 =	Negative
2 - 3	Mild	1 =	Positive, weak expression
4 - 8	Moderate	2 =	Positive, mild expression
9 - 12	Strongly positive	3 =	Positive, strong reaction

Table 2-16: Nuclear scoring system.

Table include a summary of the nuclear scoring method used.

Nuclear staining score	**Score**
< 10 % of cells in tumour have nuclear staining	1
10 % - 50 % of cells in tumour have nuclear staining	2
≥ 51 % of cells in tumour have nuclear staining	3

2.7.5 Tissue imaging

All stained tissue was imaged using the GT Vision scanner (*GT Vision, UK*). Also, photomicrographs of stained tissue presented here were acquired using the Nikon camera under the Leica microscope (*Leica, Germany*).

2.7.6 Statistical analysis of IHC scores

All statistical analysis was performed using the SPSS software version 24 (*SPSS GmbH Software, Germany*). p-value<0.05 were considered to be statistically significant. Kendall's Tau B test was used for determination of correlations between the expression of proteins and clinicopathological characteristics. One-way ANOVAs analysis was used for comparison of difference in expression levels.

The correlation analysis was conducted between the pathology report criteria (age, size, stage, grade, histological subtype, molecular subgroup, hormone receptor positivity, lymph node involvement) with (percentage positivity, intensity of immune reaction, IRS class and nuclear score) of (Gli1, Gli2 and Gli3) in tumour centre and at invasive front. All correlations were conducted, and the data presented were results that showed high correlations.

2.7.7 Confirmation of subtype of breast cancer samples showed that all selected cases followed the classification specified in the pathology report

First, H&E staining of all tumour samples in this cohort verified that there was tumour present in sections (Figure 11-4). All sections were assigned codes before staining and scoring to avoid bias during analysis, and all scores were assessed by at least three researchers with any mismatches were assessed in joint consultation and a score agreed upon. Antibodies were verified using both negative and positive controls.

Breast tumour tissue sections were immunohistochemically stained using antibodies raised against ER, PR and HER2, to verify their classification according to prognostic marker expression profile. Detection of these markers was carried out in accordance with the methodology of Dean and Rhodes (2014). Immunoreactivity was assessed using standardised methods (Leake *et al.*, 2000; Rakha *et al.*, 2015).

Table 2-17 summarises the numbers of sections stained with each antibody investigated. Table 11-1 summarises the clinicopathological parameters from the pathology report for the samples in this cohort. The numbers of cases in each stain was not the same due to variations during section preparation, antibody optimisation and duration of experimentation. Table 11-2 shows the numbers of cases and the corresponding histological subtype according to the pathology reports. Lymph node (Table 11-3-A) and metastasis (Table 11-3-B) status of the cases that represent the sections investigated by antibody staining (β-catenin, E-cadherin, Gli1, Gli2 and Gli3). Correlations to metastasis was not conducted because of low numbers of confirmed metastatic cases in the cohort used (Table 11-3-B).

The correlation between the expression of proteins (Gli1, Gli2, Gli3, β-catenin and E-cadherin) in tumour centre and at invasive front as well as correlation of nuclear localisation were conducted on all parameters. Data shown in the result section were the data that had high correlation with statistical significance the rest of the data were shown in Table 11-12-Table 11-20

Table 2-17: Numbers of sections stained by each antibody in this study
Total number of sections stained by each antibody by IHC. Antibodies investigated in this study were (β-catenin, E-cadherin, Gli1, Gli2 and Gli3).

Stain	β-catenin	E-cadherin	Gli1	Gli2	Gli3
Total	37	23	48	29	23

3. Chapter Three: Defining an EMT Model for Breast Cancer

3.1 Introduction

Breast cancer is the second most common cause of cancer death for females in the UK. Cancer metastasis is responsible for 90% of all cancer-related deaths. Invasion and metastasis are one of the hallmarks of cancer, and the dysregulation of epithelial-mesenchymal transition is one of the key mechanisms by which metastasis is accomplished (Tsai and Yang, 2013; Wang and Zhou, 2013). To assess for the ability of breast cancer cells to undergo EMT an *in vitro* model most be utilised to stimulate EMT-like changes in breast cancer cell lines. Having such model is essential for the understanding of the regulation of this process and for varying if the EMT process is varied depending on the molecular subclassification of breast cancer.

Sarrio *et al.* (2008), found that the normal-like breast cancer cell line (MCF10A) was more susceptible to EMT-like change when subjected to stress caused by decreased cell-cell contact. They suggested that this was due to the basal-like molecular signature, therefore, suggesting that basal-like breast cancer could be further down the EMT spectrum (Sarrio *et al.*, 2008). However, since that study the susceptibility of basal-like breast cancer cells to EMT compared to other subtypes. The seeding density approach as proposed and facilitated by Conacci-Sorrell *et al.* (2003) study and in Sarrio *et al.* (2008) could produce an interesting tool to study EMT-like in breast cancer cell lines. Using this approach could be promising in giving indications of the EMT status in each sub-classification of breast cancer which has not been reported using this approach before. So, the hypothesis of this study is that all breast cancer cell lines have EMT capabilities depending on the subtype to which they belong. Also, it is hypothesised that some of the breast cancer cell lines, basal in particular, could be further down in the EMT pathway (Figure 3-1).

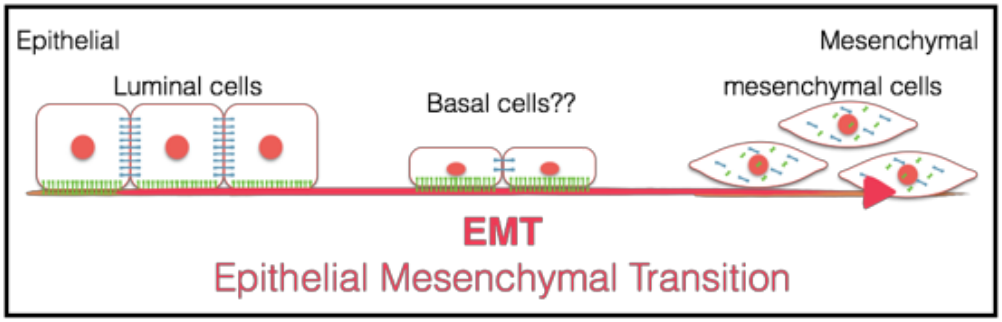

Figure 3-1, Hypothesis of the position of cells within the EMT spectrum depending on the molecular classification of breast cancer cell lines in the pathway.
The pathway of EMT in cancer involves the loss of epithelial criteria and acquisition of mesenchymal markers that allow the dissociation of the cells from the tumour mass and subsequent invasion. The hypothesis is that the breast cancer cell lines are arranged in the EMT line with some subtypes further down the pathway closer to the mesenchymal phenotype.

3.1.1 Aim

To develop an *in vitro* cell density-based model of EMT in breast cancer cell lines, allowing comparison of the different subtypes of breast cancer.

3.1.2 Objectives

- To culture breast cancer cell lines at a gradual decrease of seeding density and observe the morphological changes (cellular contact, spreading, and spindle formation).
- To select the densities at which there were significant morphological changes.
- To assess the expression of E-cadherin, β-catenin and vimentin at the selected densities, and thereby to evaluate the status of EMT in breast cancer cell lines with changing in density.

3.2 Results

3.2.1 Changes in breast cancer cell lines morphology were observed with different seeding densities

Observations were made under phase contrast microscope to assess for morphological changes in response to altered cellular density in order to determine the confluency of the culture and to select the densities for further analysis. After 24hours of incubation, cells were observed under phase contrast and images were captured. The highest density selected was based on the confluency level, cell-cell contact and the degree of cellular stacking up (stratification). Other densities were selected according to apparent morphological transformations including cellular spreading, or an increase in rounded and spindle shaped cells.

Several morphological changes were observed and recorded during the seeding density experiments. These include changes in the degree of cell-cell contact, cellular spreading and spindle cell formation. Other criteria were considered unfavourable changes because they were associated with increased in morphological signs of apoptosis and were therefore avoided. These include the formation of stratification (stacking up of cells leading to decreased cellular viability and poor culture conditions) and very low densities (increased in cell death due to anoikis and very low proliferation) (Figure 3-2 to Figure 3-4).

3.2.1.1 Selecting the number of cells in the high density

The maximum density was determined by seeding the cells at different densities and counting the number of cells that can cover 95% of the culture vessel after 24 hours incubation (**Error! Reference source not found.**). Stratification, or stacking up of cells, results in poor viability as a result of hypoxia and limitation of medium/waste exchange. Thus, the density selected was with minimal stratification.

The MDA-MB-361 cell line required the highest numbers of cells per cm^2 ($4.8x10^4$), even though, the selected density showed less than 95% confluency. MDA-MB-453, MCF7 and MDA-MB-231 required ($2.8x10^4$, $2x10^4$ and $1.3x10^4$ cells per cm^2 respectively). The cell lines that required the least number of cells as a monolayer were BT20 and MCF10A ($1x10^4$ cells per cm^2) (**Error! Reference source not found.**). In addition, it was observed that cell lines from the same molecular subtype had different degrees of cellular spreading and cell-cell adherence (Figure 3-6).

All breast cancer cell lines formed stratification at high density. It was observed that luminal breast cancer cell lines (MCF7 and MDA-MB-361) and basal-cell lines

(MCF10A and BT20) needed additional mixing to ensure proper dissociation of cells and longer incubation in trypsin. The cell lines (MDA-MB-361, MDA-MB-453, BT20, and MDA-MB-231) showed an ability to form stratification at all densities (Figure 3-2). The highest density of the MDA-MB-361 cell line was selected that covered less than 95% of the tissue culture surface, because this cell line formed condensed colonies with an increased tendency to form stratifications of cells. At the selected highest density of MDA-MB-361, the cells showed the least stratification and highest cell-cell contact as seen in Figure 3-2, Figure 3-3 and Figure 3-6.

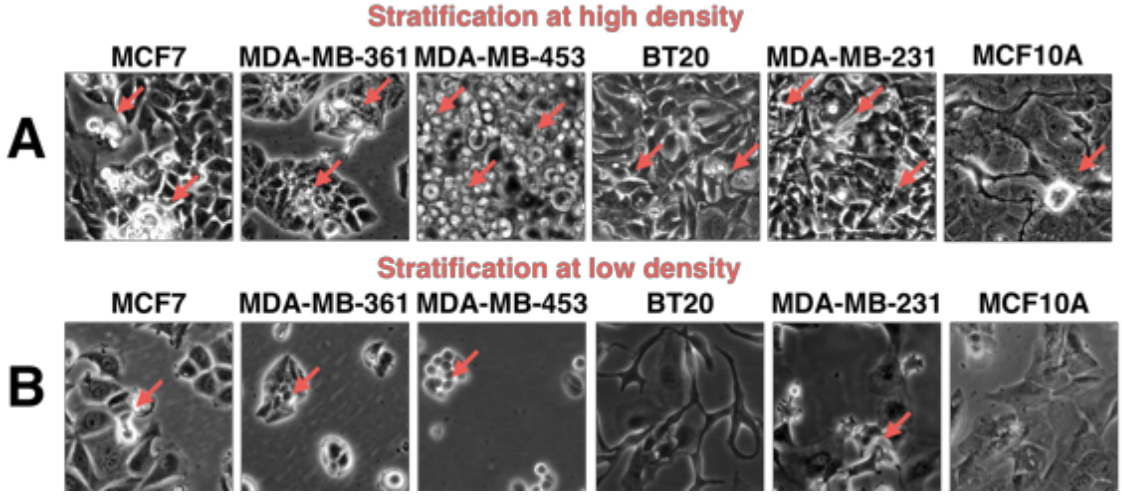

Figure 3-2, Phase contrast microscopic images showing stratification of breast cancer cells in cultures at high and low densities

Stratification changes associated with reduction in seeding density of breast cancer cell lines (MCF7, MDA-MB-361, MDA-MB-453, BT20, MDA-MB-231 and MCF10A) were highlighted in this figure. (A) cellular stratification at high densities, (Red) arrows point to areas of stratification. (B) cellular stratification at low densities, red arrows point to areas of stratification. All images were taken at 200 times magnification power using the Leica phase contrast microscope. This figure is representative of three biological repeats with similar observation.

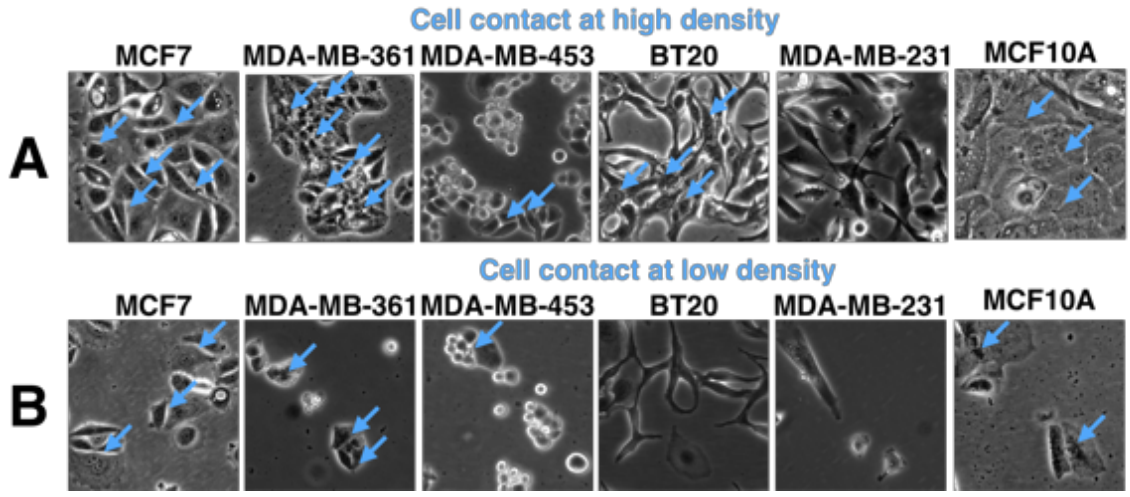

Figure 3-3, Phase contrast microscopic images comparing degree of cell-cell contact seen between cells in cultures at high and low densities
Cell-cell contact changes associated with different seeding densities of breast cancer cell lines (MCF7, MDA-MB-361, MDA-MB-453, BT20, MDA-MB-231, BT20, and MCF10A) were highlighted in this figure. (A) cell-cell contact at high density; (Blue) arrows point to areas of cell-cell contact. (B) cell-cell contact at low density; blue arrows point to areas of cell-cell contact. All images were taken at 200 times magnification power using the Leica phase contrast microscope. This figure is representative of three biological repeats with similar observation.

3.2.1.2 Selection of the densities that showed the most potent morphological changes in cell-cell contact, spindle cells, rounded cells and cellular spreading

Luminal (MCF7, and MDA-MB-361) and normal-like breast cancer cell line (MCF10A) had a more differentiated morphology of epithelial cobblestone morphology with tight cell-cell contact (Figure 3-3). There was an increase in rounded cells as the density of the culture decreases (Figure 3-4). Also, there was an increase in cellular spreading towards the edges of the colonies at low densities (Figure 3-5). MCF7, MDA-MB-361 and MCF10A showed increased fibroblastic morphology in the isolated cells with less cell-cell contact and at the borders of colonies (Figure 3-3).

The TNBC cell line MDA-MB-453 had rounded grape-like morphology with a lesser degree of cellular spreading (Figure 3-5). This cell line showed poor cell-cell contact as well as weak cellular attachment to the culture surface (Figure 3-3).

BT20 and MDA-MB-231 (triple-negative and basal-like) breast cancer cell line had obvious fibroblastic morphology (Figure 3-4) with a high degree of cellular spreading (Figure 3-5). BT20 shows an ability to form cell-cell contacts at all densities that increase inversely to seeding density (Figure 3-3-A). MDA-MB-231 showed a fibroblastic morphology that did not change in the rest of the densities (Figure 3-4).

BT20 and MDA-MB-231 cells showed increased cellular spreading and formation of flat cells at the medium density, which is a pattern not seen in the other cell lines (Figure 3-3-B). Thus, the medium density was selected for further analysis for all the cell lines to cover all observed morphological changes.

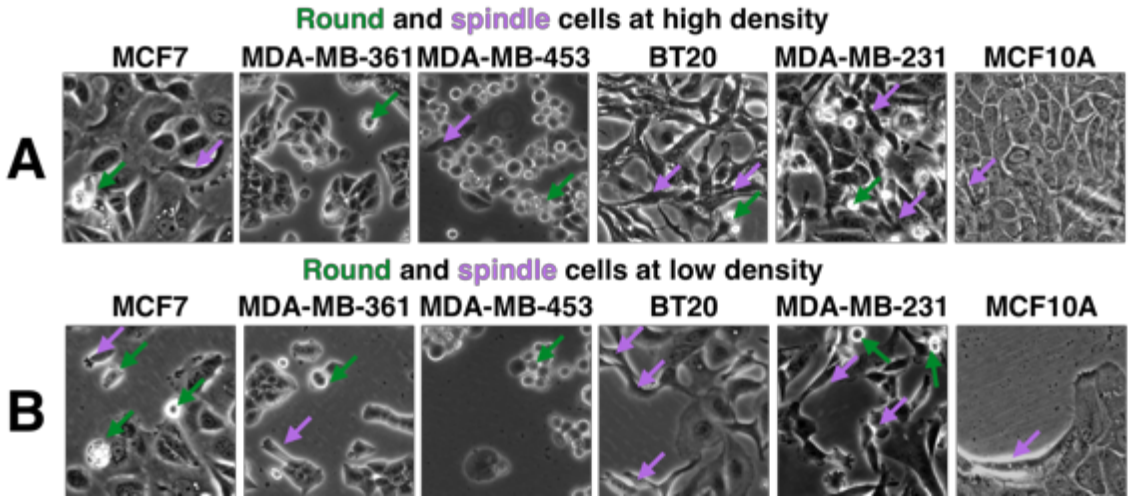

Figure 3-4, Phase contrast microscopic images highlighting formation of round cells and spindle-shaped cells seen in breast cancer cell line cultures at high and low density

Changes in rounded cells and spindle-shaped cells with decrease in seeding density were highlighted in this figure. (A) formation of round cells (Green arrows) and spindle-shaped cells (Purple arrows) at high density. (B) and at low density. All images were taken in 200 times magnification power using the phase contrast microscope. This figure is a representative of three biological repeats with similar observation.

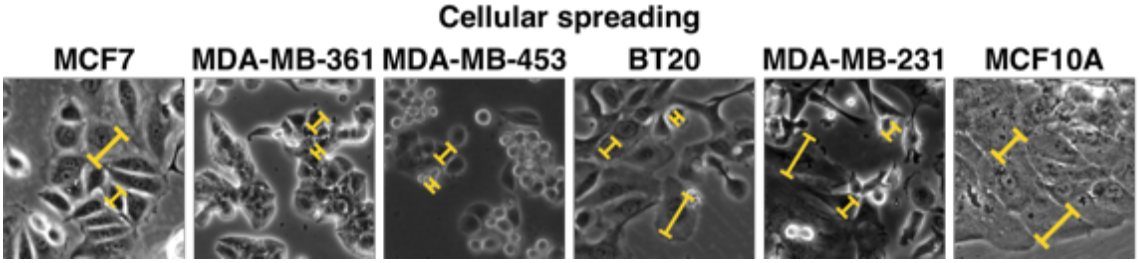

Figure 3-5, Phase contrast microscopic images highlighting cellular spreading seen in breast cancer cell line cultures compared inside and at border of cell line colonies

Changes in cellular spreading associated with decrease of seeding density were highlighted in this figure. Cellular spreading increases at the borders of the cell lines colonies. Bars added to compare cellular spread inside and at border of colonies. All images were taken in 200 times magnification power using the phase contrast microscope. This figure is a representative of three biological repeats with similar observation.

3.2.1.3 Three densities showed potent morphological changes seen by phase contrast microscopy and therefore selected for markers analysis

By observing morphological criteria including; the degree of stratification, cell spreading, cell-cell contact and presence of spindle and rounded shaped cells, three seeding densities were selected for further analysis (Figure 3-6). The high seeding density was selected where cells formed a lesser degree of stratification while covering as much as possible of the tissue culture surface. The lowest was the density in which the cells had less cell-cell contact with minimal morphological signs of apoptosis and cellular death. A medium density was also selected for each cell line, in this density cellular morphology was mixed especially in BT20 and MDA-MB-231. The number of cells per cm^2 is listed in Table 3-1.

Table 3-1: The seeding densities of breast cancer cell lines per $1cm^2$ of culture surface area.
This table lists the numbers of cells seeded at each seeding density per cm^2. The breast cancer cell lines are arranged according to their molecular subclassification.

Cell lines	Molecular classification	Cell number/cm^2		
		High	Medium	Low
MCF7	Luminal A	$2x10^4$	$6.6x10^3$	$2.2x10^2$
MDA-MB-361	Luminal B HER2 overexpressing	$4.8x10^4$	$1.6x10^4$	$5.3x10^3$
MDA-MB-453	Triple-negative Unclassified	$2.8x10^4$	$9.3x10^3$	$3.1x10^3$
BT20	Triple-negative and Basal A	$1x10^4$	$3.3x10^3$	$1.1x10^3$
MDA-MB-231	Triple-negative and Basal B	$1.2x10^4$	$4.2x10^3$	$1.4x10^3$
MCF10A	Triple-negative and Basal B/ Normal-Like	$1x10^4$	$3.3x10^3$	$1.1x10^3$

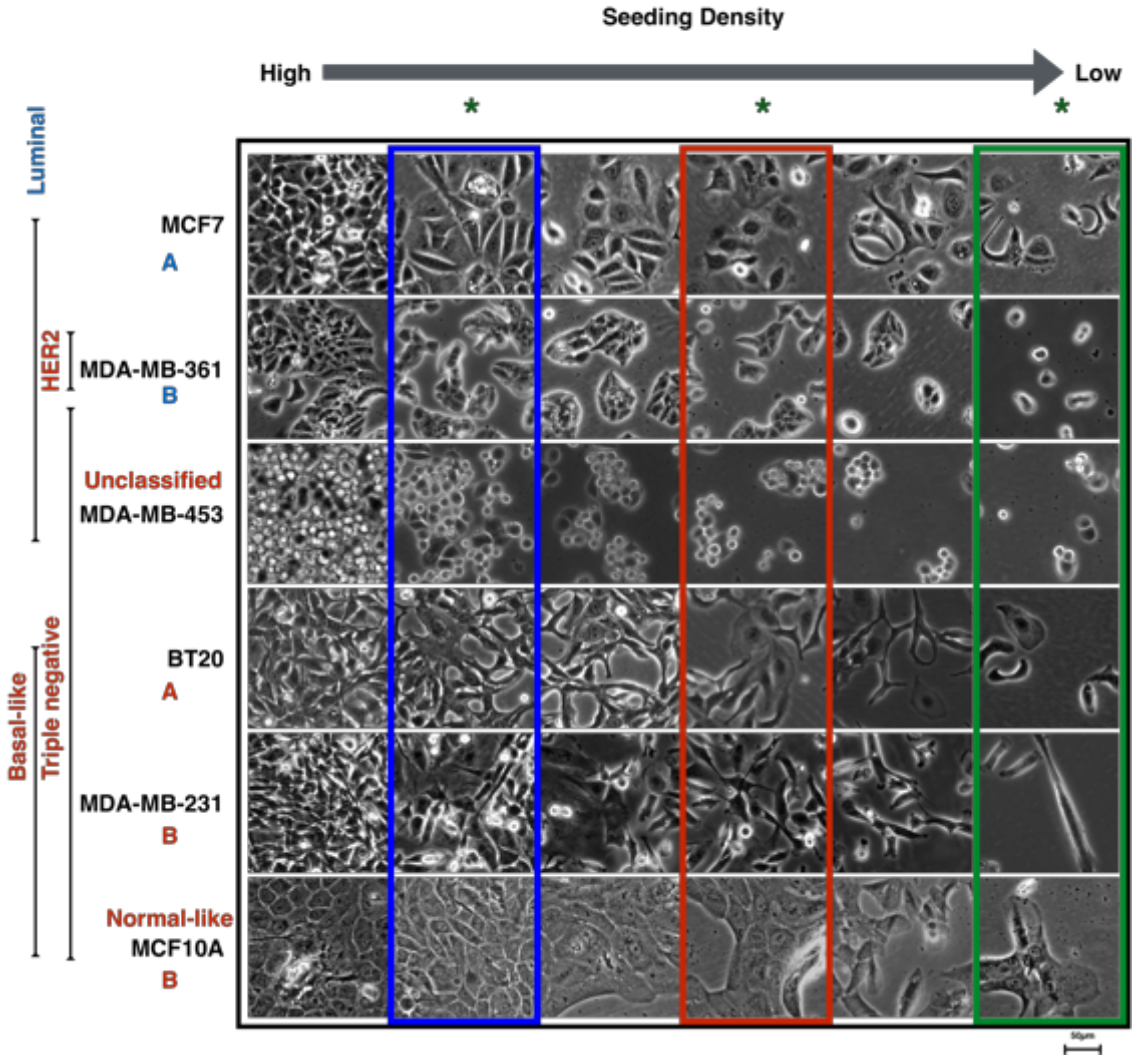

Figure 3-6, Phase contrast microscope images of breast cancer cell lines at various seeding densities (changing in cellular morphology observed with reduction of density)

Summary of morphological changes associated with reduction of densities of breast cancer cell lines (MCF7, MDA-MB-361, MDA-MB-453, BT20, MDA-MB-231 and MCF10A). The classifications of breast cancer cell lines are highlighted at the far left with the names of cell lines. Selected densities were highlighted with a star on top. Blue rectangular highlight (high), red rectangular highlight (medium) and green rectangular highlight the (low) densities. The scale bar at the bottom right represents 50µm. All pictures were taken at 200 times magnification power using the Leica phase contrast microscope. This figure is a representative of three biological repeats with similar observation.

3.2.1.4 Summary of the morphological changes associated with decreasing seeding densities

Epithelial cells have several morphological characteristics including an ability to form tight cell-cell contact illustrated as the cobblestone morphology. Also, epithelial cells show less cellular spreading because of this tight cell-cell contact. On the other hand, the mesenchymal cells display increased cellular spreading with a loss of cell-cell

contact and increased spindle-shaped cell formation. The changes were scored qualitatively as seen in the summary table below (Table 3-2). This summary provided a helpful tool in capturing the most significant morphological changes and detecting the patterns associated with a decrease in density.

Table 3-2: Summary of the morphological changes associated with high, medium and low density for the breast cancer cell lines.
This table summarises the morphological changes in high, medium and low densities. These changes are represented as a qualitative score (0 to 3) based on the morphological observation.

Breast cancer cell lines	Molecular classification	Morphological change								
		High			Medium			Low		
		Spreading	Contact	Spindles	Spreading	Contact	Spindles	Spreading	Contact	Spindles
MCF7	Luminal A	0	3	1	1	1	1	2	1	3
MDA-MB-361	Luminal B HER2 overexpressing	0	3	1	1	2	1	2	1	2
MDA-MB-453	Triple-negative Unclassified	0	2	0	1	2	0	1	2	0
BT20	Triple-negative and Basal A	1	2	2	2	3	1	2	0	2
MDA-MB-231	Triple-negative and Basal B	1	1	2	3	2	1	3	0	3
MCF10A	Triple-negative and Basal B/ Normal-Like	0	3	1	1	2	1	3	1	2

Taken together, it can be seen that all the cell lines showed an increase in mesenchymal morphological features with decreasing seeding density. All cell lines showed an increase in spindle morphology and cellular spreading with decreasing cell-cell contact, which are all morphological features of mesenchymal morphological change. The luminal cell lines (MCF7 and MDA-MB-361) and the TNBC cell line (MDA-MB-453) showed less significant morphological mesenchymal changes compared to those observed in all of the basal breast cancer cell lines (BT20, MDA-MB-231 and MCF10A).

3.2.2 Expression of the epithelial marker E-cadherin, β-catenin and the mesenchymal marker vimentin in the breast cancer cell lines in response to reduction of density

3.2.2.1 The luminal cell lines MCF7 and MDA-MB-361 and normal-like/basal-like cell line MCF10A show reduced E-cadherin expression with decreased density

MCF7, MDA-MB-361 and MCF10A cells were seeded at the three selected densities and expression of the proteins (E-cadherin, β-catenin and vimentin) were compared using either western blotting (see section 2.2) or flow cytometry (see section 2.4 and changes in the localisation of these proteins were observed using ICF (see section 2.3).

E-cadherin localisation in MCF7, MDA-MB-361 and MCF10A was observed at areas of cell-cell contact (Figure 3-12-A, Figure3-13-A, and Figure 3-14-A). Visible cytoplasmic deposits of E-cadherin were more frequent in MCF10A and MDA-MB-361 at all densities (Figure 3-12-A and Figure 3-14-A). These three cell lines retained the honeycomb E-cadherin pattern at the medium and low densities with less uniform localisation in cells at the border of colonies.

The percentage of positively expressing cells in the three cell lines (MCF10A, MCF7 and MDA-MB-361) was reduced gradually with reducing seeding density (Figure 3-12-B, Figure 3-13-B, and Figure 3-14-B). In the MDA-MB-361 cell line (luminal), the decrease in percentage of positive cells was significant between medium and low densities (p-value<0.05) (Figure 3-14-B). In the normal-like breast cancer cell line MCF10A, the MFI increased significantly from high to medium density (p-value<0.01) (Figure 3-12-B). MFI of positive MDA-MB-361 cells showed highly significant decrease between the high, medium and low density (p-value<0.0001) (Figure 3-14-B). Also, median fluorescence intensity (MFI) of cells in the medium seeding density was significantly less than that of the lower density (p-value<0.01) (Figure 3-14-B).

MDA-MB-361 showed two populations of E-cadherin positive expressing cells as seen using flow cytometry. One of these subpopulations had a higher percentage and level expression of E-cadherin compared to the other (Figure 3-13-B).

Among the three cell lines, MDA-MB-361 had the highest expression of E-cadherin. The expression of E-cadherin protein decreased with decreasing density in MCF10A, MCF7 and MDA-MB-361 (Figure 3-12-C, Figure 3-13-C, and Figure 3-14-

C). There were significant differences between high and low density in MCF10A (*p-value*<0.01) (Figure 3-12-C) and a significant difference between high and medium densities (*p*-value<0.01). There was also a highly significant difference between high and low densities (*p*-value<0.0001) in MDA-MB-361 (Figure3-14-C).

Overall, it can be concluded that the expression level of E-cadherin decreased in both level and cell-cell contact localisation with reducing of cell density in the three cell lines (MCF7, MDA-MB-361 (luminal) and MCF10 (normal-like and basal-like)). The decrease in E-cadherin expression is can cause activation of EMT, however, analysis of other markers is essential to draw a frim conclusion.

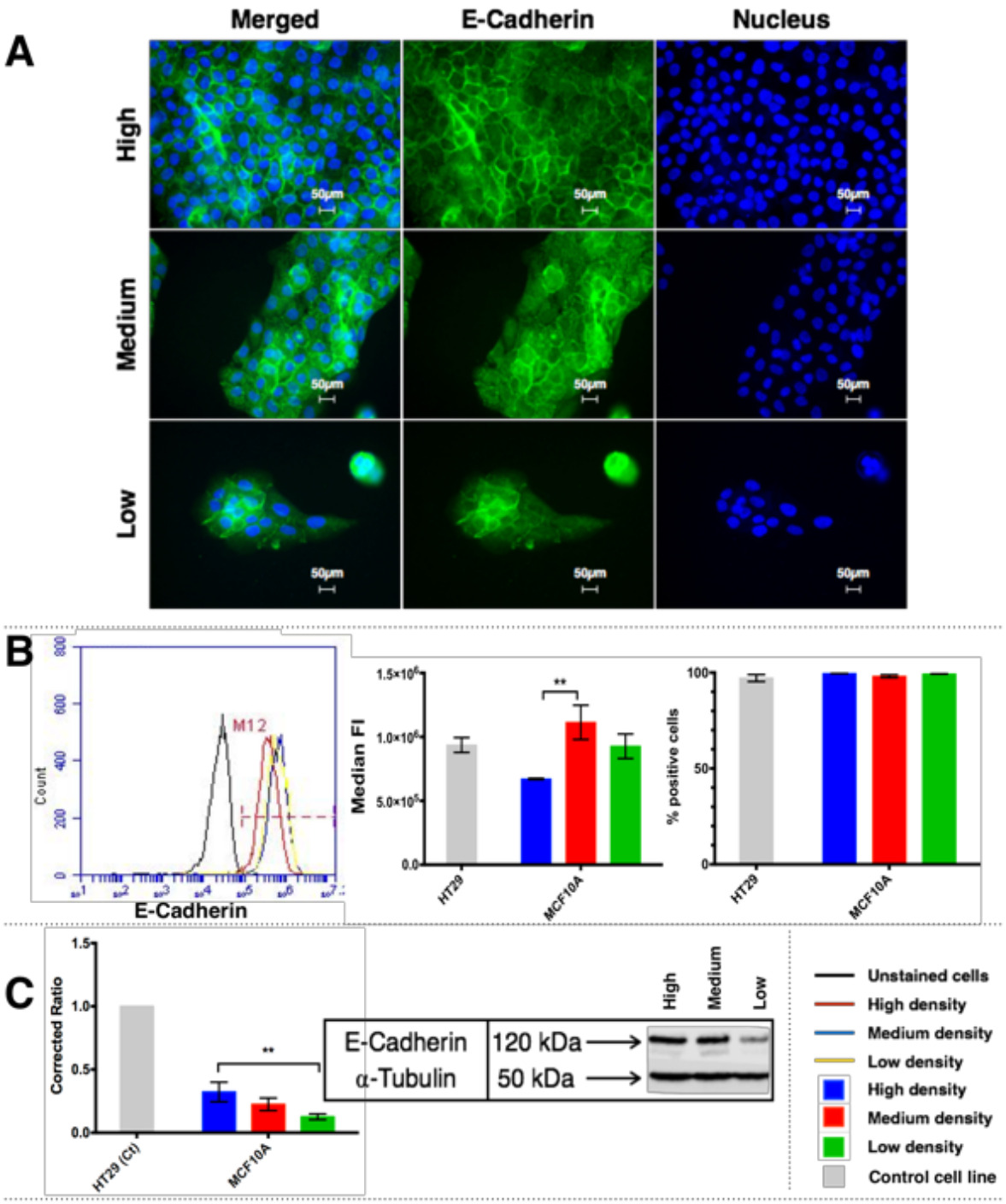

Figure 3-7, E-Cadherin expression in normal-like breast cancer cell line MCF10A
(A) immunofluorescence representative images of E-cadherin expression in MCF10A cell line seeded at three seeding densities (high, medium, and low) labelled with Alexa Fluor® (488 or 594) secondary antibodies (Green) and the nuclei were stained with DAPI (Blue). Images were obtained using Leica fluorescence microscope under 400 times magnification. (B) Flow cytometry results of E-cadherin expression levels in MCF10A cells. Overlay histogram on the left is for unstained cells and three densities expression. The bar charts on the right show comparison of percentage of E-cadherin expressing cells as well as MFI of E-cadherin in three densities. (C) The level of E-cadherin in MCF10A lysates corrected against α-Tubulin internal loading control. Results displayed as bars of mean ±S.D. This figure is representative of n=3 experiments in triplicate. Statistical analysis was conducted and significant differences between samples were indicated by * p-value<0.05, *** p-value<0.01 and **** p-value<0.0001.

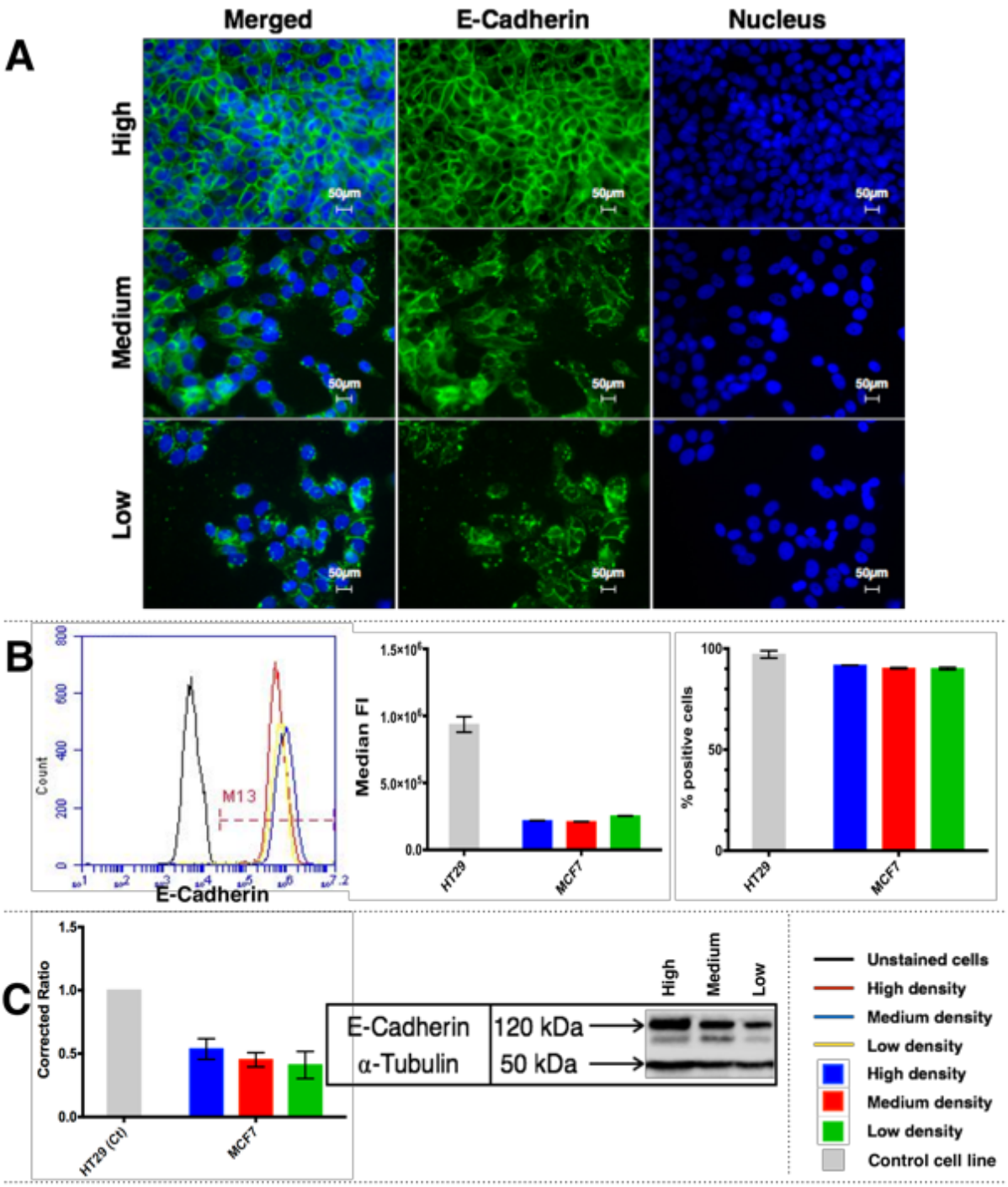

Figure 3-8, E-Cadherin expression in luminal breast cancer cell line MCF7

(A) immunofluorescence representative images of E-cadherin expression in MCF7 cell line seeded at three seeding densities (high, medium, and low) labelled with Alexa Fluor® (488 or 594) secondary antibodies (Green) and the nuclei were stained with DAPI (Blue). Images were obtained using Leica fluorescence microscope under 400 times magnification. (B) Flow cytometry results of E-cadherin expression levels in MCF7 cells. Overlay histogram on the left is for unstained cells and three densities expression. The bar charts on the right show comparison of percentage of E-cadherin expressing cells as well as MFI of E-cadherin in three densities. (C) The level of E-cadherin in MCF7 lysates corrected against α-Tubulin internal loading control. Results displayed as bars of mean ±S.D. This figure is representative of n=3 experiments in triplicate. Statistical analysis was conducted and significant differences between samples were indicated by * p-value<0.05, *** p-value<0.01 and **** p-value<0.0001.

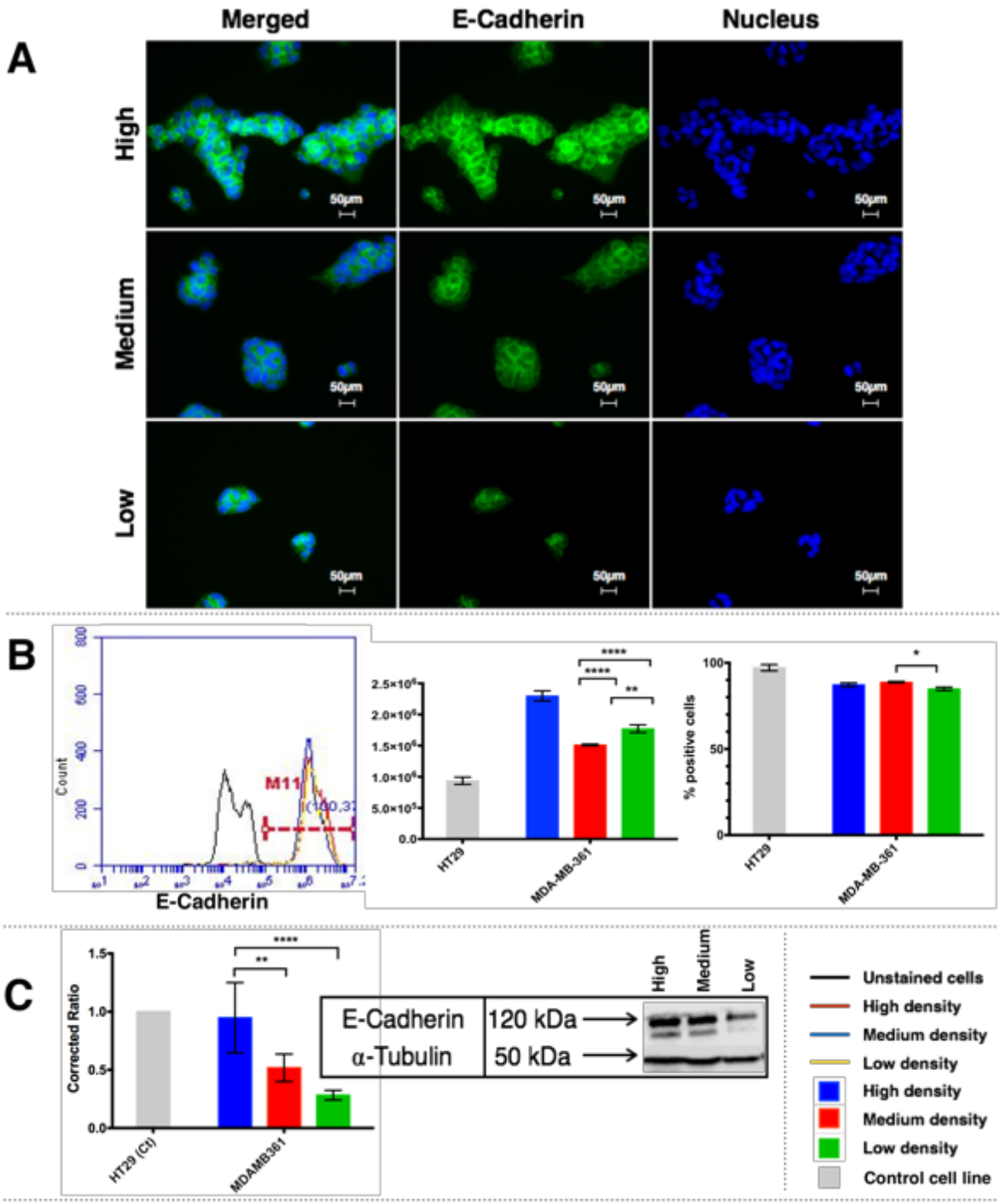

Figure 3-9, E-Cadherin expression in luminal breast cancer cell line MDA-MB-361
(A) immunofluorescence representative images of E-cadherin expression in MDA-MB-361 cell line seeded at three seeding densities (high, medium, and low) labelled with Alexa Fluor® (488 or 594) secondary antibodies (Green) and the nuclei were stained with DAPI (Blue). Images were obtained using Leica fluorescence microscope under 400 times magnification. Scale bars added at the bottom right corner of images. (B) Flow cytometry results of E-cadherin expression levels in MDA-MB-361 cells. Overlay histogram on the left is for unstained cells and three densities expression. The bar charts on the right show comparison of percentage of E-cadherin expressing cells as well as MFI of E-cadherin in three densities. (C) The level of E-cadherin in MDA-MB-361 lysates corrected against α-Tubulin internal loading control. Results displayed as bars of mean ±S.D. This figure is representative of n=3 experiments in triplicate. Statistical analysis was conducted and significant differences between samples were indicated by * p-value<0.05, *** p-value<0.01 and **** p-value<0.0001.

The localisation of β-catenin at all densities of the three cell lines (MCF10A, MCF7 and MDA-MB-361) was found to be high at cell-cell borders as seen by ICF (Figure 3-10-A, Figure 3-11-A and Figure 3-12-A). The cytoplasmic localisation of β-catenin protein became less pronounced with reduction in density in all three cell lines. Nuclear localisation was observed in MCF10A and MCF7 cell lines at the medium and low density.

The percentage of β-catenin positive expressing cells was reduced with seeding density in MCF10A, MCF7 and MDA-MB-361 with the highest expression of β-catenin in MCF10A, which is a basal-like cell line. The difference in positive expressing cells was highly significant in all comparisons in MCF10A (p-value<0.0001) (Figure 3-10-B). In MCF7 (luminal), the percentage of positively expressing cells declined with a significant difference seen only between medium and low density (p-value<0.05) (Figure 3-11-B). MDA-MB-361 showed a slight increase in percentage of positive cells between medium and low density with a significant difference (p-value<0.0001) (Figure 3-12-B). The percentage decreased from medium to low density with a significant difference seen in all comparisons in the same cell line (p-value<0.0001) (Figure 3-12-B). Mostly, the MFI of positive β-catenin cells decreased with density in the three cell lines. In MCF10A the difference in MFI was significant between all comparisons (p-value<0.0001) (Figure 3-10-B). In MDA-MB-361, the difference in MFI was significant between high and medium as well as between high and low density (p-value<0.0001) (Figure 3-12-B). Similar to E-cadherin subpopulations seen in MDA-MB-361, subpopulation of MDA-MB-361 had a slightly higher expression of β-catenin in the highest density, which was then decreased in percentage in medium and low density (Figure 3-12-B).

The relative expression level of β-catenin protein was reduced with decreasing in density in the three cell lines. In MCF10A, the difference in expression of β-catenin showed high significance between high and medium as well as between high and low density (p-value<0.001) (Figure 3-10-C).

In conclusion, the expression of β-catenin in MCF10A, MCF7 and MDA-MB-361 decreased with reduction in seeding density. The localisation of β-catenin at the cell-cell contact area also decreased with reducing density.

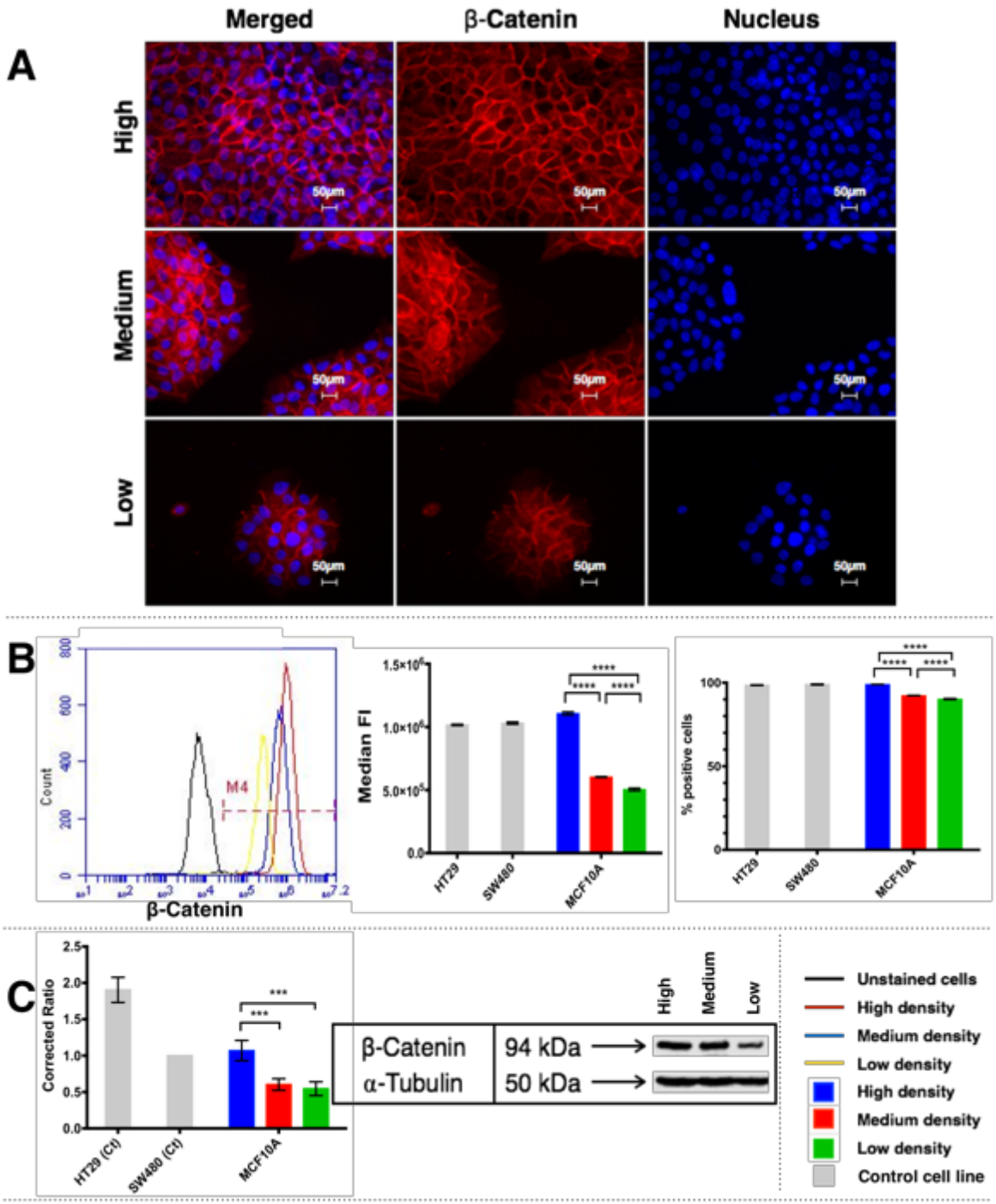

Figure 3-10, β-catenin expression in normal-like breast cancer cell line MCF10A

(A) immunofluorescence representative images of β-catenin expression in MCF10A cell line seeded at three seeding densities (high, medium, and low) labelled with Alexa Fluor® (488 or 594) secondary antibodies (Red) and the nuclei were stained with DAPI (Blue). Images were obtained using Leica fluorescence microscope at 400 times magnification. Scale bars added at the bottom right corner of images. (B) Flow cytometry results of β-catenin expression levels in MCF10A cells. Overlay histogram on the left is for unstained cells and three densities expression. The bar charts on the right show comparison of percentage of β-catenin expressing cells as well as MFI of β-catenin in three densities. (C) The level of β-catenin in MCF10A lysates corrected against α-Tubulin internal loading control. Results displayed as bars of mean ±S.D. This figure is representative of n=3 experiments in triplicate. Statistical analysis was conducted and significant differences between samples were indicated by * p-value<0.05, *** p-value<0.01 and **** p-value<0.0001.

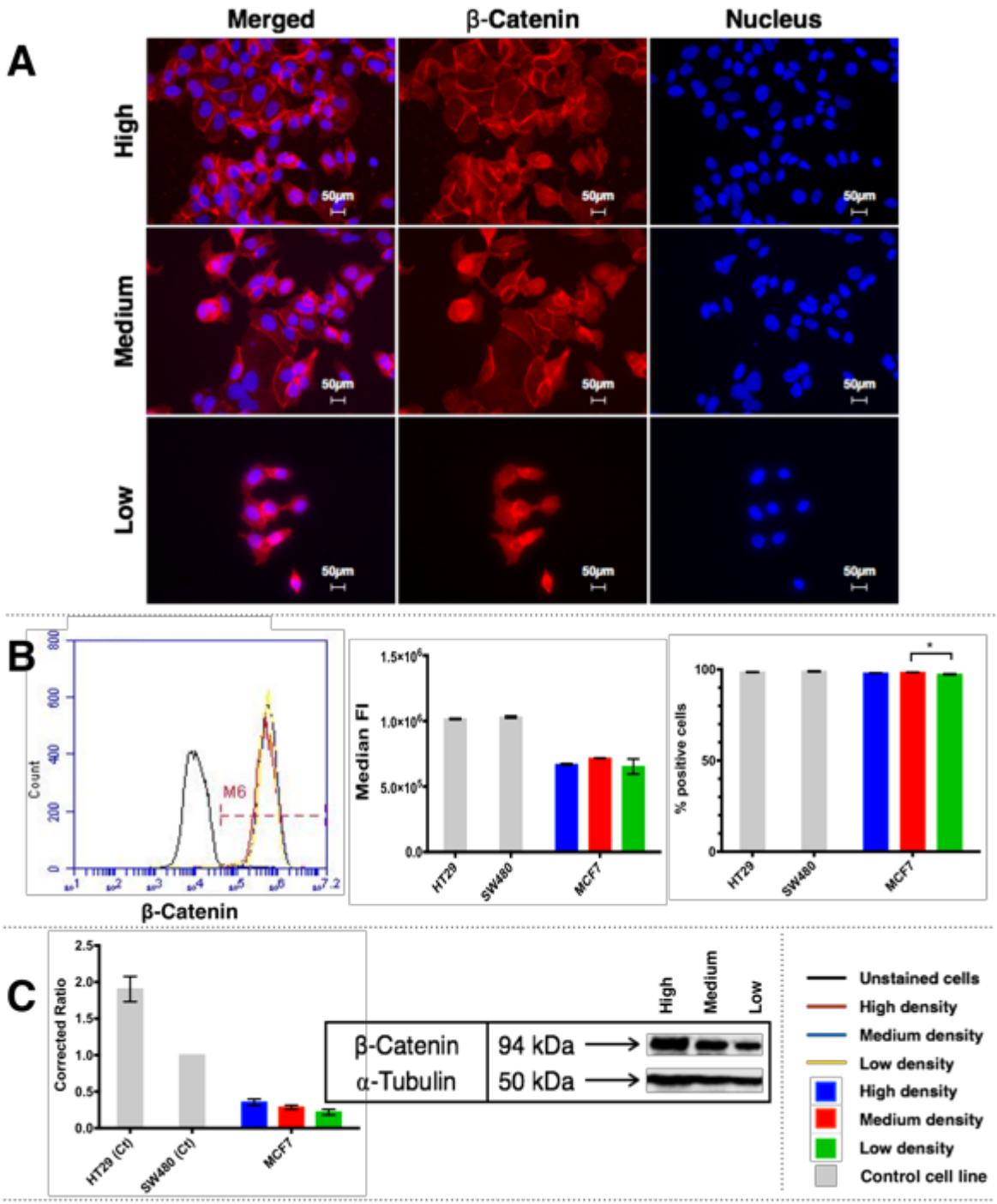

Figure 3-11, β-catenin expression in luminal breast cancer cell line MCF7

(A) immunofluorescence representative images of β-catenin expression in MCF7 cell line seeded at three seeding densities (high, medium, and low) labelled with Alexa Fluor® (488 or 594) secondary antibodies (Red) and the nuclei were stained with DAPI (Blue). Images were obtained using Leica fluorescence microscope at 400 times magnification. Scale bars added at the bottom right corner of images. (B) Flow cytometry results of β-catenin expression levels in MCF7 cells. Overlay histogram on the left is for unstained cells and three densities expression. The bar charts on the right show comparison of percentage of β-catenin expressing cells as well as MFI of β-catenin in three densities. (C) The level of β-catenin in MCF7 lysates corrected against α-Tubulin internal loading control. Results displayed as bars of mean ±S.D. This figure is representative of n=3 experiments in triplicate. Statistical analysis was conducted and significant differences between samples were indicated by * p-value<0.05, *** p-value<0.01 and **** p-value<0.0001.

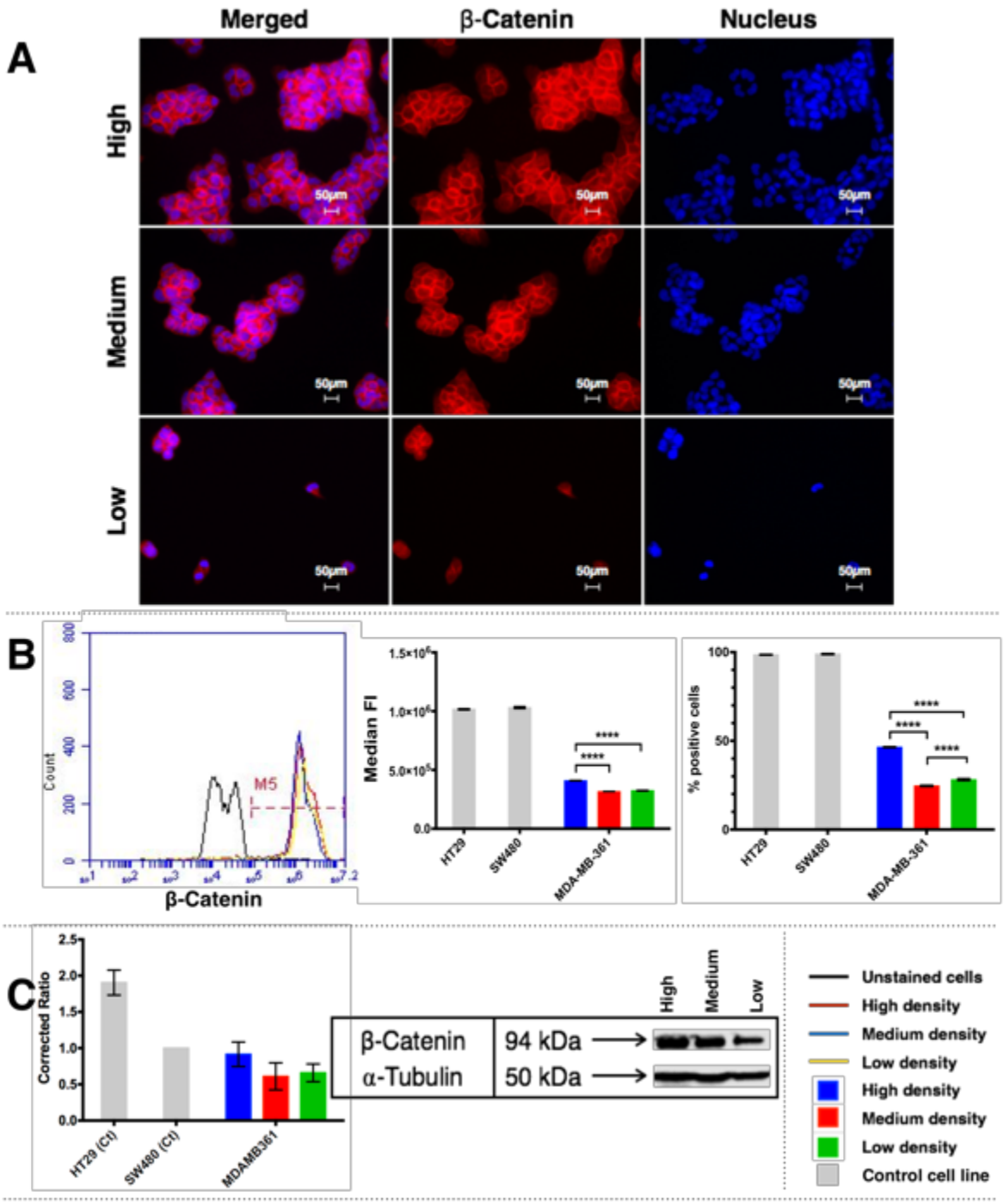

Figure 3-12, β-catenin expression in luminal breast cancer cell line MDA-MB-361

(A) immunofluorescence representative images of β-catenin expression in MDA-MB-361 cell line seeded at three seeding densities (high, medium, and low) labelled with Alexa Fluor® (488 or 594) secondary antibodies (Red) and the nuclei were stained with DAPI (Blue). Images were obtained using Leica fluorescence microscope at 400 times magnification. Scale bars added at the bottom right corner of images. (B) Flow cytometry results of β-catenin expression levels in MDA-MB-361 cells. Overlay histogram on the left is for unstained cells and three densities expression. The bar charts on the right show comparison of percentage of β-catenin expressing cells as well as MFI of β-catenin in three densities. (C) The level of β-catenin in MDA-MB-361 lysates corrected against α-Tubulin internal loading control. Results displayed as bars of mean ±S.D. This figure is representative of n=3 experiments in triplicate. Statistical analysis was conducted and significant differences between samples were indicated by * p-value<0.05, *** p-value<0.01 and **** p-value<0.0001.

Vimentin is a mesenchymal marker that is increased in epithelial cells undergoing EMT, see section 1.3.1.2. Vimentin protein expression was observable in the cytoplasm at all densities of MCF10A, MCF7 and MDA-MB-361. A notable increase was observed in the expression of the protein in the detaching cells at the border of colonies of MCF10A at medium density which increased further at the low density (Figure 3-13-A). There was an increase in nuclear localisation of vimentin in MCF7 and MCF10A at low density compared to other densities (Figure 3-14-B and Figure 3-15-A).

The percentage of vimentin expressing cells was increased with reducing density in MCF10A and MDA-MB-361 but not in MCF7. The difference was highly significant between all comparisons in MCF10A and MDA-MB-361 ($p < 0.0001$) (Figure 3-13-B and Figure 3-15-B). The MFI showed a similar trend with increased vimentin expression in MCF10A and MDA-MB-361 cells with decreased density (Figure 3-13-B and Figure 3-15-B). Conversely, MCF7 showed decrease in vimentin with reduction in density (Figure 3-14-B). In the MCF10A cell line, the MFI showed strong statistical difference in all comparisons (p-value<0.0001) (Figure 3-13-B). In the luminal cell line MCF7, the MFI difference was highly significant in all comparisons (p-value<0.0001) (Figure 3-14-B) with a drop in the medium and an increase at low density. A subpopulation of MCF10A cells showed greater expression of vimentin, the percentage of these cells increased in the low density compared to high and medium as observed in the overlapped histogram (Figure 3-13-B). In MDA-MB-361 cells, there was a small proportion of cells displaying a lack of vimentin expression which increased in the medium density as seen in the overlay histogram (Figure 3-15-B).

The relative expression of vimentin protein increased with decreasing density in the MCF10A and MDA-MB-361 cell lines (Figure 3-13-C and Figure 3-15-C). In MCF10A, there was a significant difference between high and low as well as between medium and low density (p-value<0.0001) (Figure 3-13-C). The relative level of expression was decreased with density in MCF7 (Figure 3-14-C). In conclusion, the vimentin protein increased strongly in MCF10A at the low density but did not change significantly in MCF7 and MDA-MB-361.

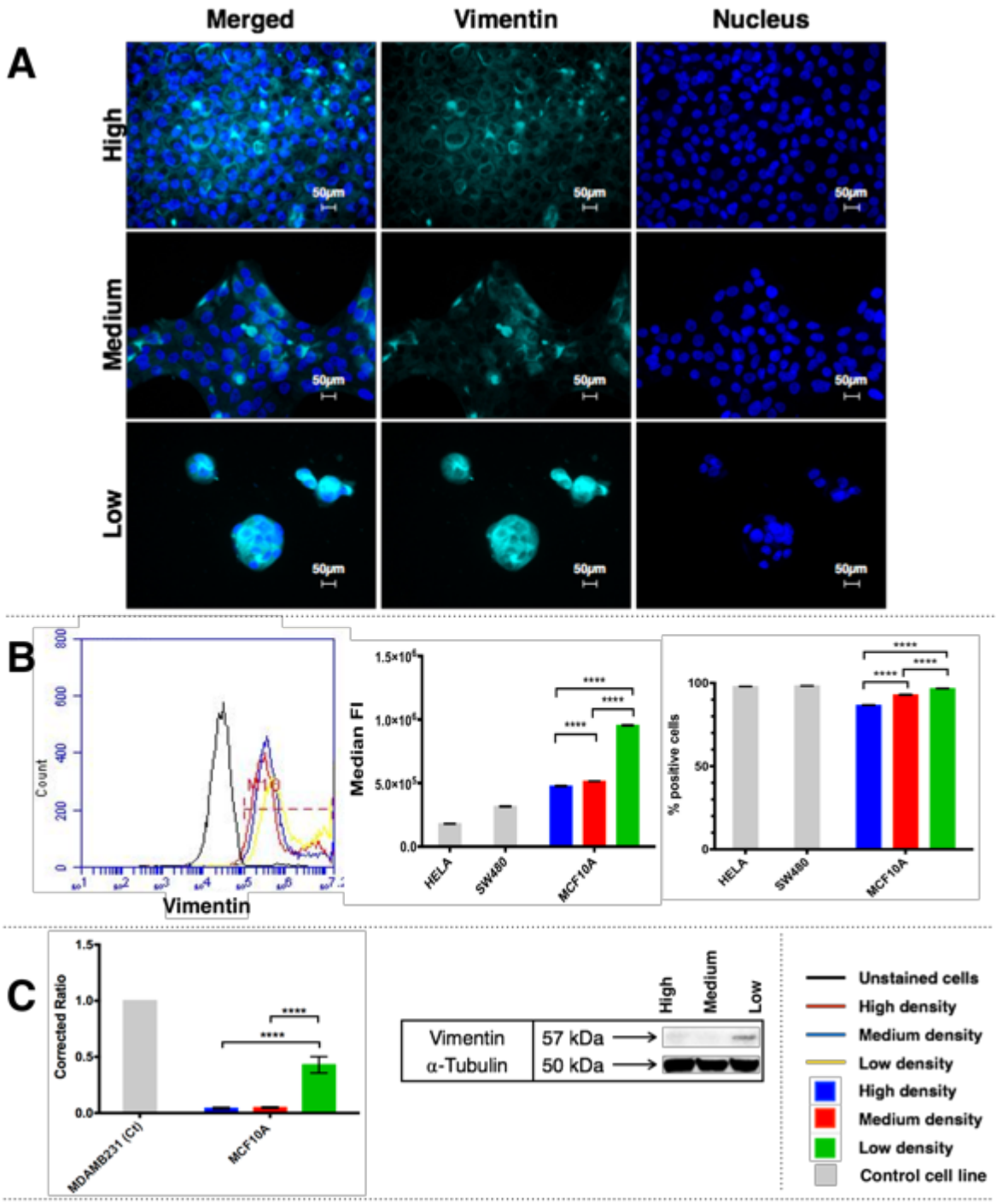

Figure 3-13, Vimentin expression in normal-like breast cancer cell line MCF10A
(A) immunofluorescence representative images of vimentin expression in MCF10A cell line seeded at three seeding densities (high, medium, and low) labelled with Alexa Fluor® (488 or 594) secondary antibodies (light teal) and the nuclei were stained with DAPI (Blue). Images were obtained using Leica fluorescence microscope under 400 times magnification. Scale bars added at the bottom right corner of images. (B) Flow cytometry results of vimentin expression levels in MCF10A cells. Overlay histogram on the left is for unstained cells and three densities expression. The bar charts on the right show comparison of percentage of vimentin expressing cells as well as MFI of vimentin in three densities. (C) The level of vimentin in MCF10A lysates corrected against α-Tubulin internal loading control. Results displayed as bars of mean ±S.D. This figure is representative of n=3 experiments in triplicate. Statistical analysis was conducted and significant differences between samples were indicated by * p-value<0.05, *** p-value<0.01 and **** p-value<0.0001.

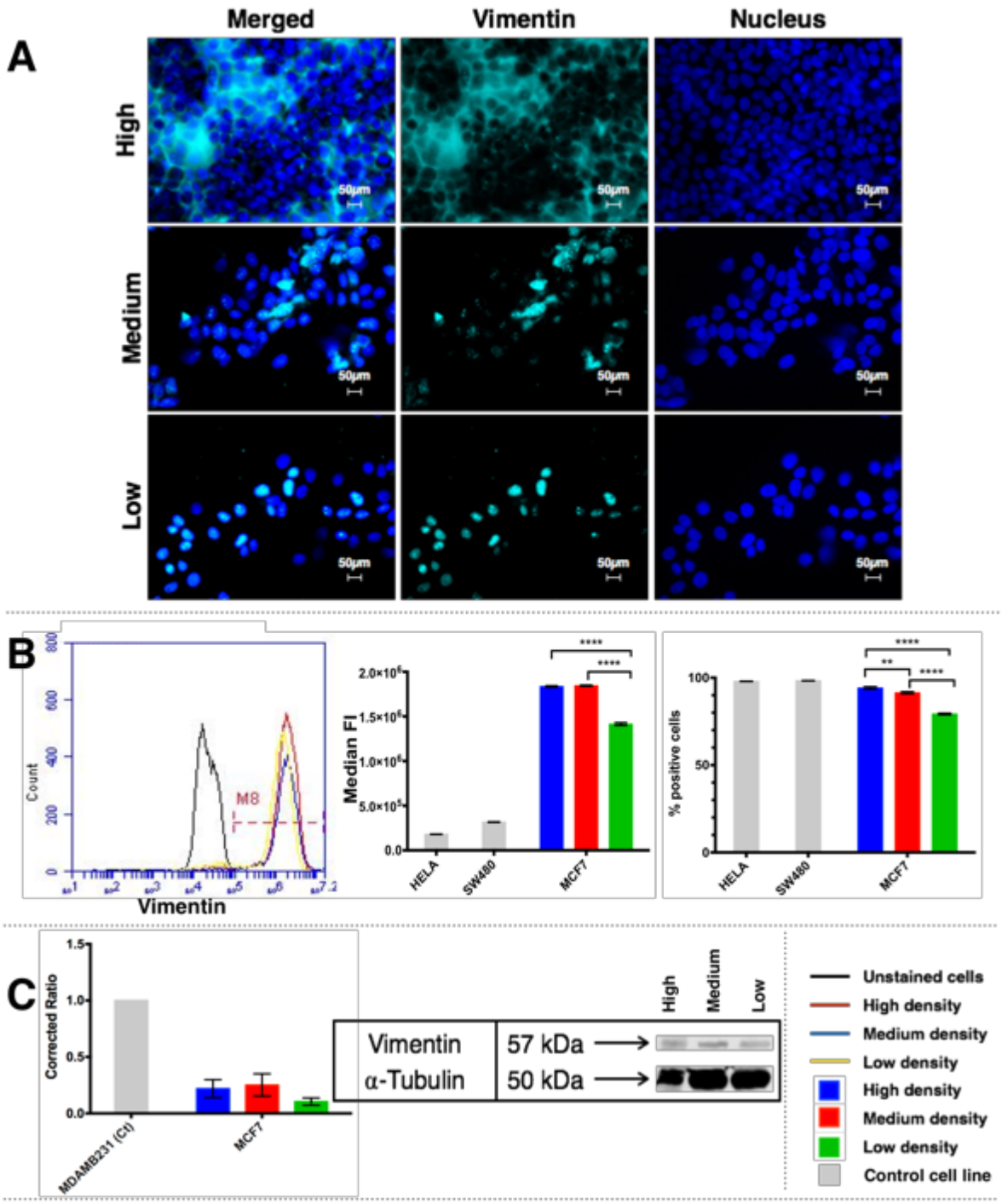

Figure 3-14, Vimentin expression in luminal breast cancer cell line MCF7

(A) immunofluorescence representative images of vimentin expression in MCF7 cell line seeded at three seeding densities (high, medium, and low) labelled with Alexa Fluor® (488 or 594) secondary antibodies (light teal) and the nuclei were stained with DAPI (Blue). Images were obtained using Leica fluorescence microscope under 400 times magnification. Scale bars added at the bottom right corner of images. (B) Flow cytometry results of vimentin expression levels in MCF7 cells. Overlay histogram on the left is for unstained cells and three densities expression. The bar charts on the right show comparison of percentage of vimentin expressing cells as well as MFI of vimentin in three densities. (C) The level of vimentin in MCF7 lysates corrected against α-Tubulin internal loading control. Results displayed as bars of mean ±S.D. This figure is representative of n=3 experiments in triplicate. Statistical analysis was conducted and significant differences between samples were indicated by * p-value<0.05, *** p-value<0.01 and **** p-value<0.0001.

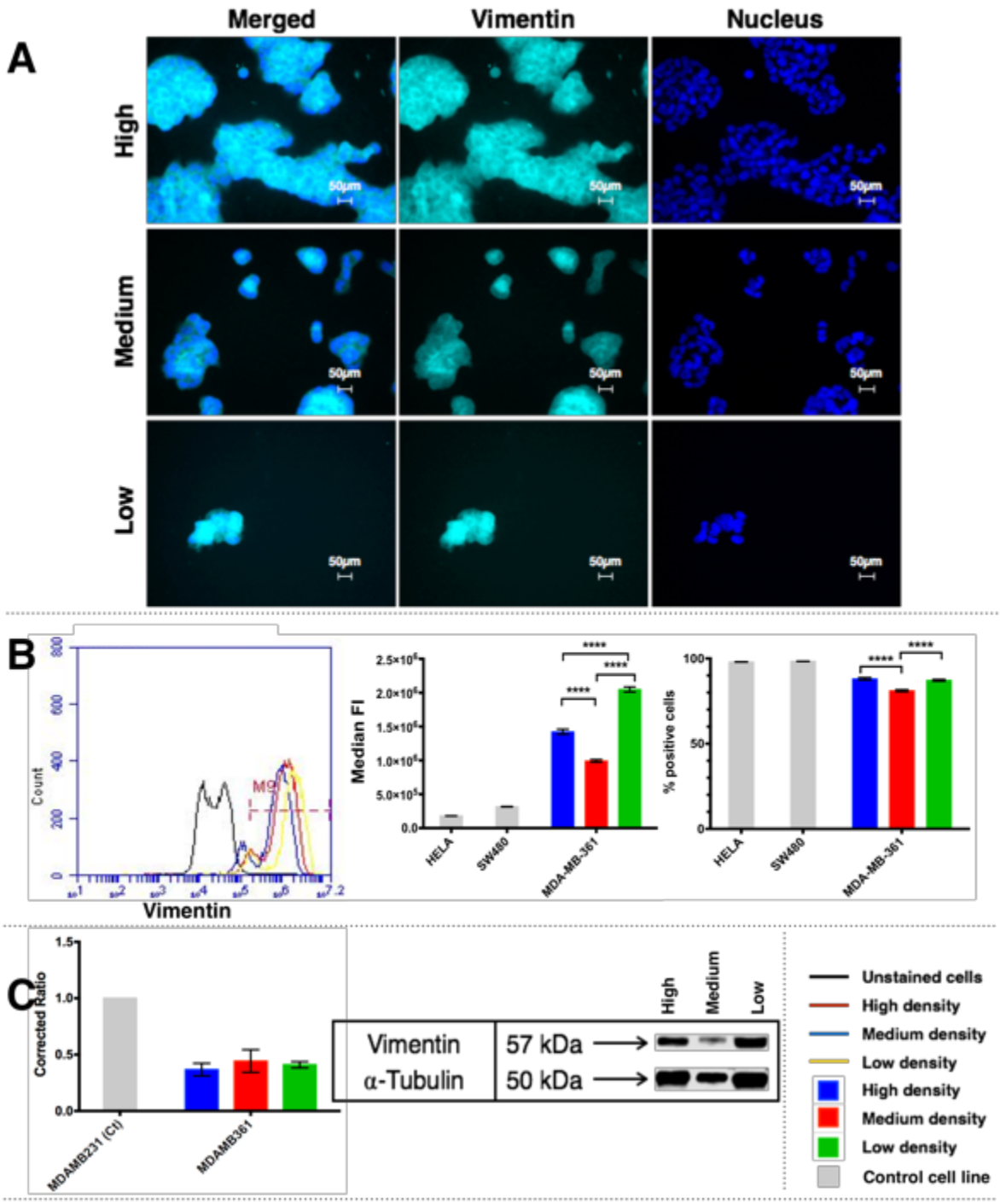

Figure 3-15, Vimentin expression luminal breast cancer cell line MDA-MB-361
(A) immunofluorescence representative images of vimentin expression in MDA-MB-361 cell line seeded at three seeding densities (high, medium, and low) labelled with Alexa Fluor® (488 or 594) secondary antibodies (light teal) and the nucleus were stained with DAPI (Blue). Images were obtained using Leica fluorescence microscope under 400 times magnification. Scale bars added at the bottom right corner of images. (B) Flow cytometry results of vimentin expression levels in MDA-MB-361 cells. Overlay histogram on the left is for unstained cells and three densities expression. The bar charts on the right show comparison of percentage of vimentin expressing cells as well as MFI of vimentin in three densities. (C) The level of vimentin in MDA-MB-361 lysates corrected against α-Tubulin internal loading control. Results displayed as bars of mean ±S.D. This figure is representative of n=3 experiments in triplicate. Statistical analysis was conducted and significant differences between samples were indicated by * p-value<0.05, *** p-value<0.01 and **** p-value<0.0001.

In comparing the expression pattern and level of the three markers (E-cadherin, β-catenin and vimentin) in the three cell lines (MCF10A, MCF7 and MDA-MB-361) we can conclude that there was a reduction in the localisation of both E-cadherin and β-catenin at the cell-cell borders. At the same time, the level of both E-cadherin and β-catenin decreased with seeding density. Only MCF10A showed a strong increase in vimentin with decreasing in density, suggesting increased EMT in the basal cell line MCF10A compared to the luminal breast cancer cell lines MCF7 and MDA-MB-361. Further analysis and expression of other EMT markers is, however, needed to confirm this finding.

3.2.2.2 The triple-negative cell line MDA-MB-453 showed increased of epithelial marker expression with decrease in density

The triple negative breast cancer cell line MDA-MB-453 was seeded at the three selected densities and expression of the proteins (E-cadherin, β-catenin and vimentin) were compared using either western blotting (see section 2.2) or flow cytometry (see section 2.4 and changes in the localisation of these proteins were observed using ICF (see section 2.3).

E-cadherin localisation in the triple-negative cell line (MDA-MB-453) was entirely cytoplasmic and decreased with density (Figure 3-16-A).

The percentage of positive cells and MFI of E-cadherin expressing MDA-MB-453 cells showed an increase with reduction in density by flow cytometry. In the MDA-MB-453 cell line, the percentage of E-cadherin positive cells showed high statistical significance when comparing the high and medium or the high and low densities (p-value<0.0001), and there was a significant difference between the medium and low density (p-value<0.01) (Figure 3-16-B). Also, the MFI of MDA-MB-453 positive cells showed a significant increase at medium density (p-value<0.0001) and then a significant decrease at lower density (p-value<0.0001) (Figure 3-17-B). E-cadherin expression increased with decreasing density.

The expression of E-cadherin in MDA-MB-453 was significant between high and low density (p-value<0.05) (Figure 3-17-C). Altogether, the epithelial marker (E-cadherin) expression was low in the MDA-MB-453 cell line and the level of expression showed inverse correlation to density with cytoplasmic localisation.

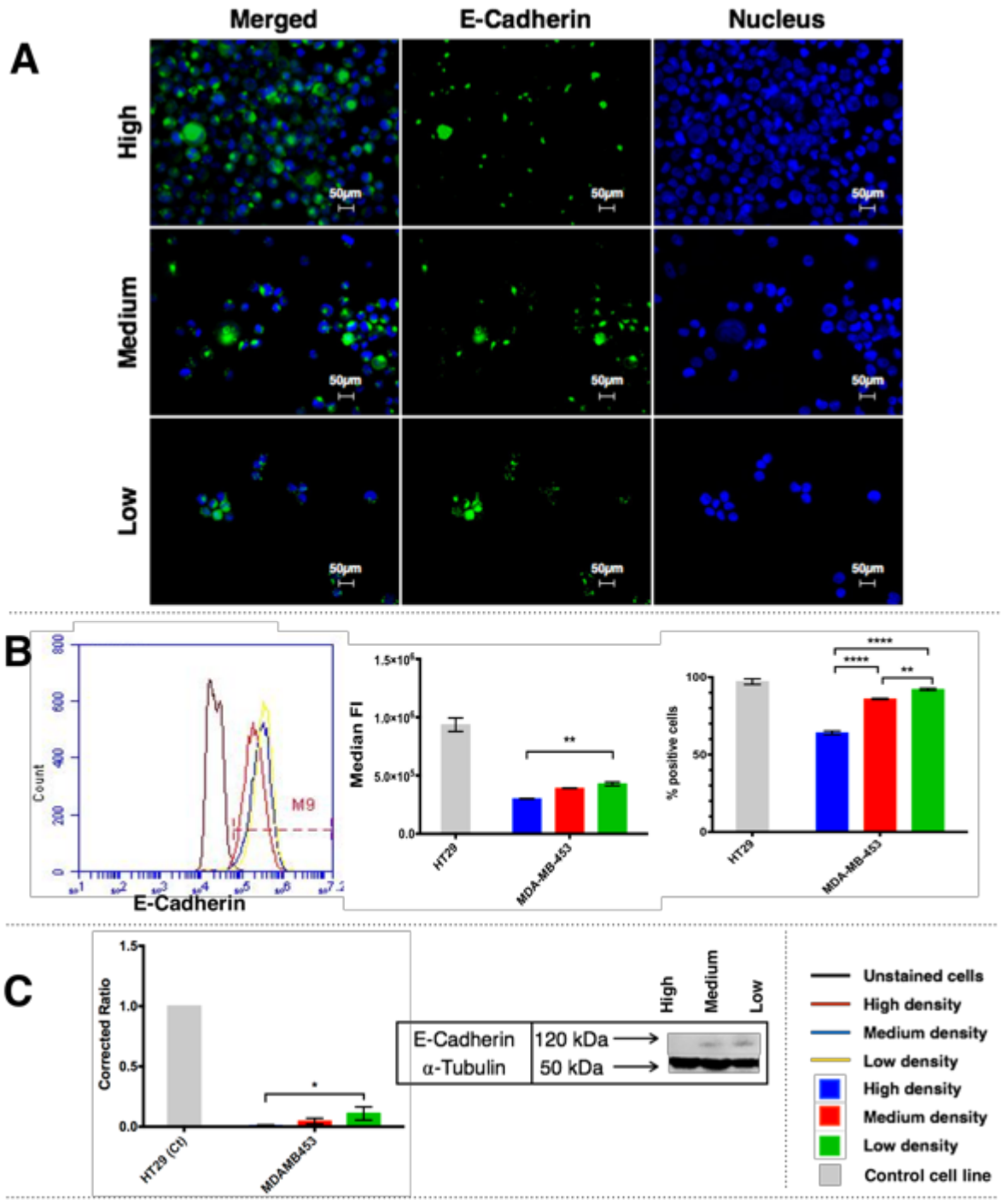

Figure 3-16, E-Cadherin expression in TNBC cell line MDA-MB-453

(A) immunofluorescence representative images of E-cadherin expression in MDA-MB-453 cell line seeded at three seeding densities (high, medium, and low) labelled with Alexa Fluor® (488 or 594) secondary antibodies (Green) and the nuclei were stained with DAPI (Blue). Images were obtained using Leica fluorescence microscope under 400 times magnification. Scale bars added at the bottom right corner of images. (B) Flow cytometry results of E-cadherin expression levels in MDA-MB-453 cells. Overlay histogram on the left is for unstained cells and three densities expression. The bar charts on the right show comparison of percentage of E-cadherin expressing cells as well as MFI of E-cadherin in three densities. (C) The level of E-cadherin in MDA-MB-453 lysates corrected against α-Tubulin internal loading control. Results displayed as bars of mean ±S.D. This figure is representative of n=3 experiments in triplicate. Statistical analysis was conducted and significant differences between samples were indicated by * p-value<0.05, *** p-value<0.01 and **** p-value<0.0001.

The expression of β-catenin protein in MDA-MB-453 cells was cytoplasmic. The expression of β-catenin protein was very low and was observed to be mostly in cytoplasmic and cell-cell location (Figure 3-17-A). The increase in β-catenin protein expression with decreasing in density in MDA-MB-453 was also associated with cytoplasmic localisation of the protein. The expression of vimentin was cytoplasmic in MDA-MB-453 cells and there was no change in the localisation of the protein with changes in density (Figure 3-18-A).

The percentage of β-catenin positive expressing cells and MFI in MDA-MB-453 increased with decreased density. In the MDA-MB-453 cell line, the percentage of positive β-catenin cells showed a highly significant difference between high and medium and high and low density (p-value<0.0001) (Figure 3-17-B). The percentage of vimentin expressing cells and the MFI in MDA-MB-453 cells showed an inverse correlation with cellular density. There was a significant difference seen in all comparisons of percentage of expressing cells and the MFI against seeding density in MDA-MB-453 cells (p-value<0.0001) (Figure 3-18-B).

The relative expression of β-catenin protein in the MDA-MB-453 cell line was very low in high density and increased with decreasing density (Figure 3-17-C). The difference in expression of the protein was significant between high and low density of MDA-MB-453 cells (p-value<0.01) (Figure 3-18-C). Though significant, this increase in expression was not substantial. Taken together, MDA-MB-453 had a relatively low expression level of E-cadherin, β-catenin and vimentin.

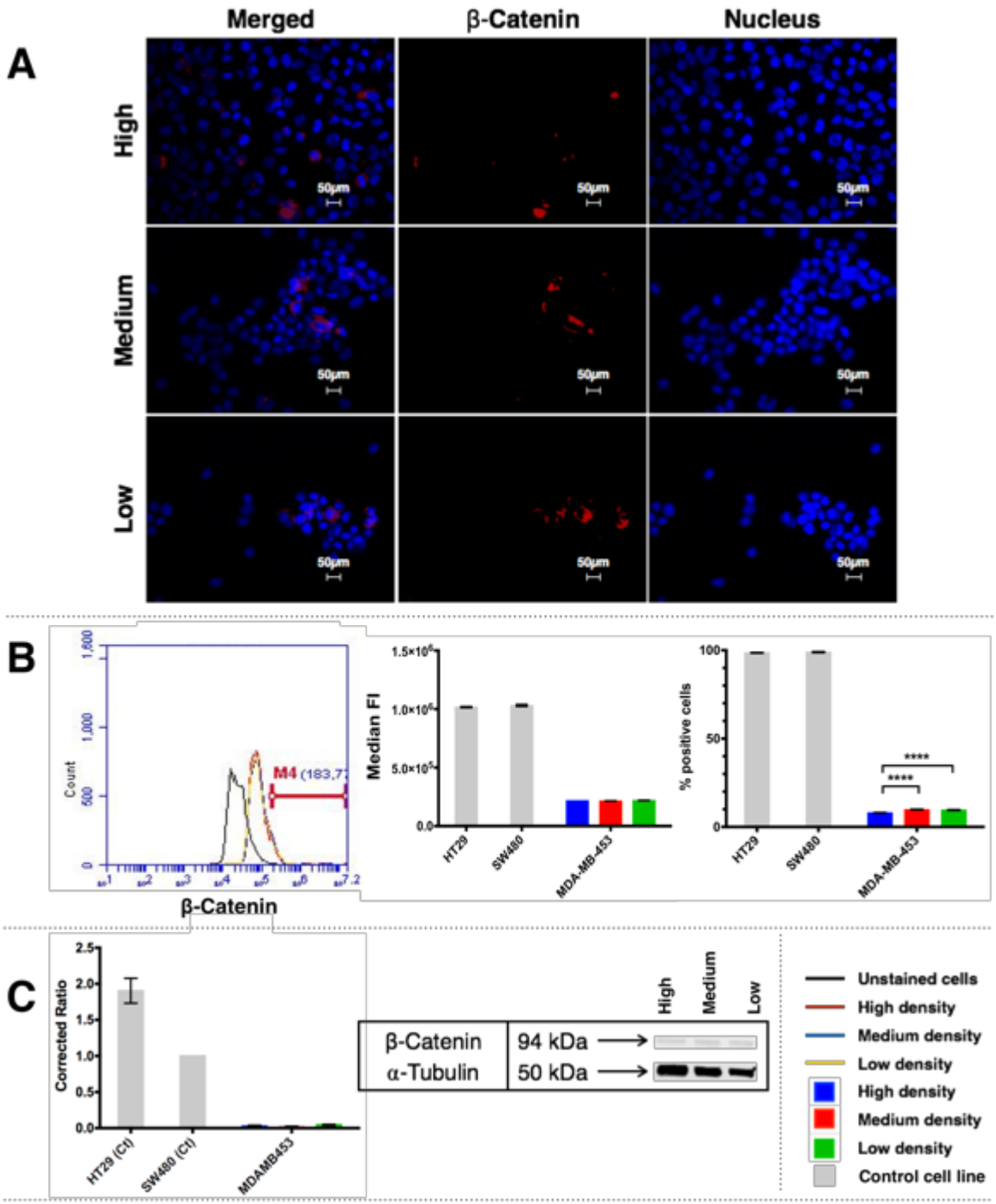

Figure 3-17, β-catenin expression in TNBC cell line MDA-MB-453

(A) immunofluorescence representative images of β-catenin expression in MDA-MB-453 cell line seeded at three seeding densities (high, medium, and low) labelled with Alexa Fluor® (488 or 594) secondary antibodies (Red) and the nuclei were stained with DAPI (Blue). Images were obtained using Leica fluorescence microscope under 400 times magnification. Scale bars added at the bottom right corner of images. (B) Flow cytometry results of β-catenin expression levels in MDA-MB-453 cells. Overlay histogram on the left is for unstained cells and three densities expression. The bar charts on the right show comparison of percentage of β-catenin expressing cells as well as MFI of β-catenin in three densities. (C) The level of β-catenin in MDA-MB-453 lysates corrected against α-Tubulin internal loading control Results displayed as bars of mean ±S.D. This figure is representative of n=3 experiments in triplicate. Statistical analysis was conducted and significant differences between samples were indicated by * p-value<0.05, *** p-value<0.01 and **** p-value<0.0001.

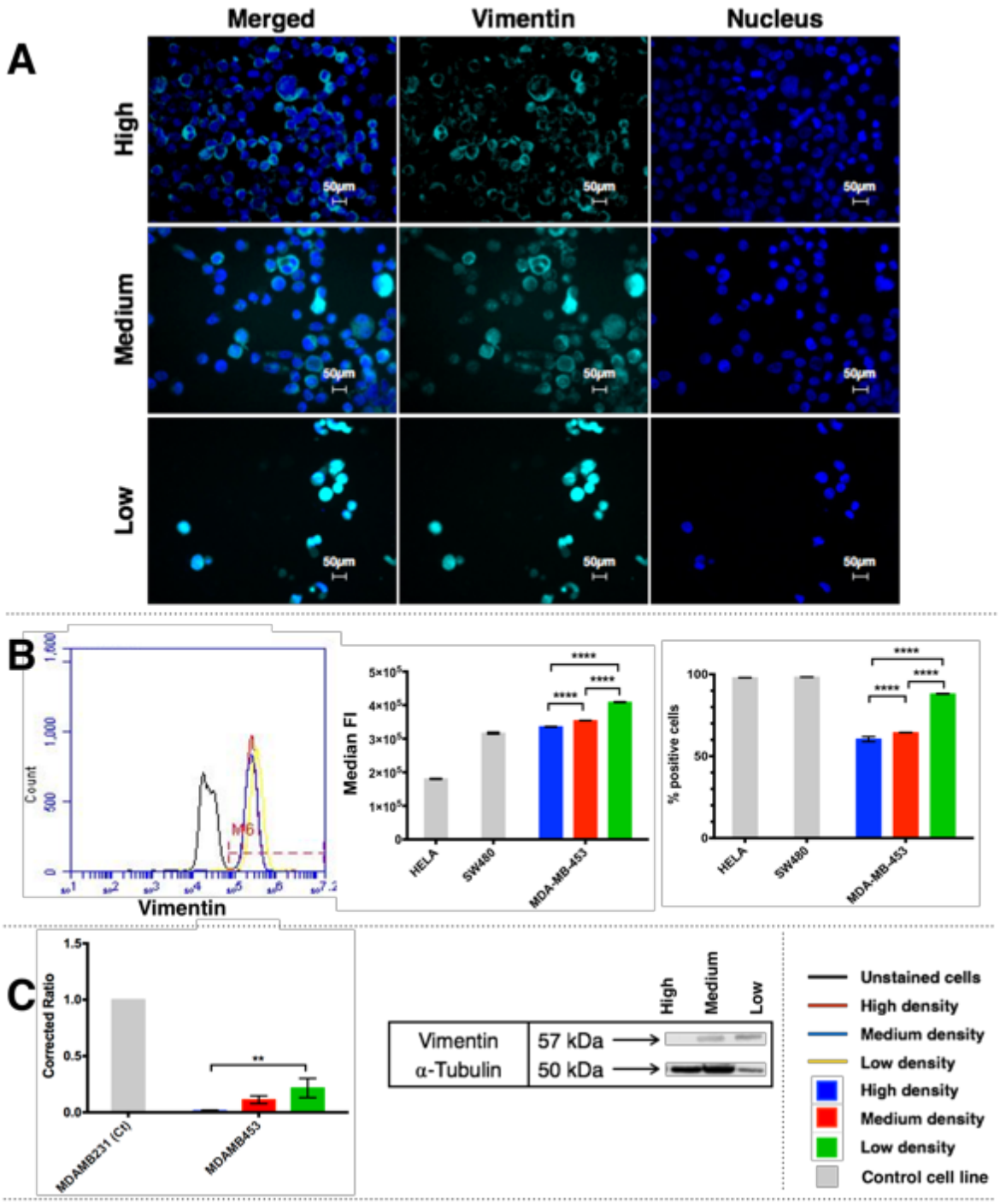

Figure 3-18, Vimentin expression in TNBC cell line MDA-MB-453

(A) immunofluorescence representative images of vimentin expression in MDA-MB-453 cell line seeded at three seeding densities (high, medium, and low) labelled with Alexa Fluor® (488 or 594) secondary antibodies (light teal) and the nuclei were stained with DAPI (Blue). Images were obtained using Leica fluorescence microscope under 400 times magnification. Scale bars added at the bottom right corner of images. (B) Flow cytometry results of vimentin expression levels in MDA-MB-453 cells. Overlay histogram on the left is for unstained cells and three densities expression. The bar charts on the right show comparison of percentage of vimentin expressing cells as well as MFI of vimentin in three densities. (C) The level of vimentin in MDA-MB-453 lysates corrected against α-Tubulin internal loading control. Results displayed as bars of mean ±S.D. This figure is representative of n=3 experiments in triplicate. Statistical analysis was conducted and significant differences between samples were indicated by * p-value<0.05, *** p-value<0.01 and **** p-value<0.0001.

3.2.2.3 The basal-cell lines BT20 and MDA-MB-231 showed an increase in epithelial marker E-cadherin at the medium density

The triple negative and basal-like breast cancer cell lines BT20 and MDA-MB-231 were seeded at the three selected densities and expression of the proteins (E-cadherin, β-catenin and vimentin) were compared using either western blotting (see section 2.2) or flow cytometry (see section 2.4 and changes in the localisation of these proteins were observed using ICF (see section 2.3).

Cytoplasmic localisation of E-cadherin was seen in the ICF images of the triple-negative and basal-like breast cancer cell lines (BT20 and MDA-MB-231). The BT20 cell line showed β-catenin localisation at cell-cell borders. The cytoplasmic localisation increased with decreasing density in both cell lines (Figure 3-19-A and Figure 3-20-A).

The percentage positive and MFI of E-cadherin-expressing cells did not change significantly in the BT20 cell line (Figure 3-19-B). In the MDA-MB-231 cell line, the percentage of positively expressing cells and MFI increased in the medium density followed by sharp decrease at the low density. There was a significant difference between high and medium, high and low, and medium and low of MDA-MB-231 cell line (p-value<0.0001) (Figure 3-20-B). Also, the MFI of MDA-MB-231 showed a significant increase at the medium density (p-value<0.0001) and then a significant decrease at lower density (p-value<0.0001) (Figure 3-20-B). In MDA-MB-231 at medium density, there were two populations with different levels of E-cadherin expression as seen in the overlay histogram (Figure 3-20-B).

The relative expression of E-cadherin protein dropped from the medium to low density with significant difference in BT20 cells (p-value<0.05) and in MDA-MB-231 cell (p-value<0.001) (Figure 3-19-C and Figure 3-20-C).

In summary, MDA-MB-453 cells showed the same trend of increasing expression in the medium density with drop in the low density. The E-cadherin expression was cytoplasmic in MDA-MB-231 and there was an increase in cytoplasmic E-cadherin in BT20. The localisation of E-cadherin in the cell-cell contact area of BT20 can indicate stronger cell-cell contact and suggesting increase in epithelial morphological change in the medium density of BT20 cell line. In MDA-MB-231, the increase in E-cadherin expression was not associated with increase in localisation in the cell-cell border, therefore, there was no increase in epithelial phenotype.

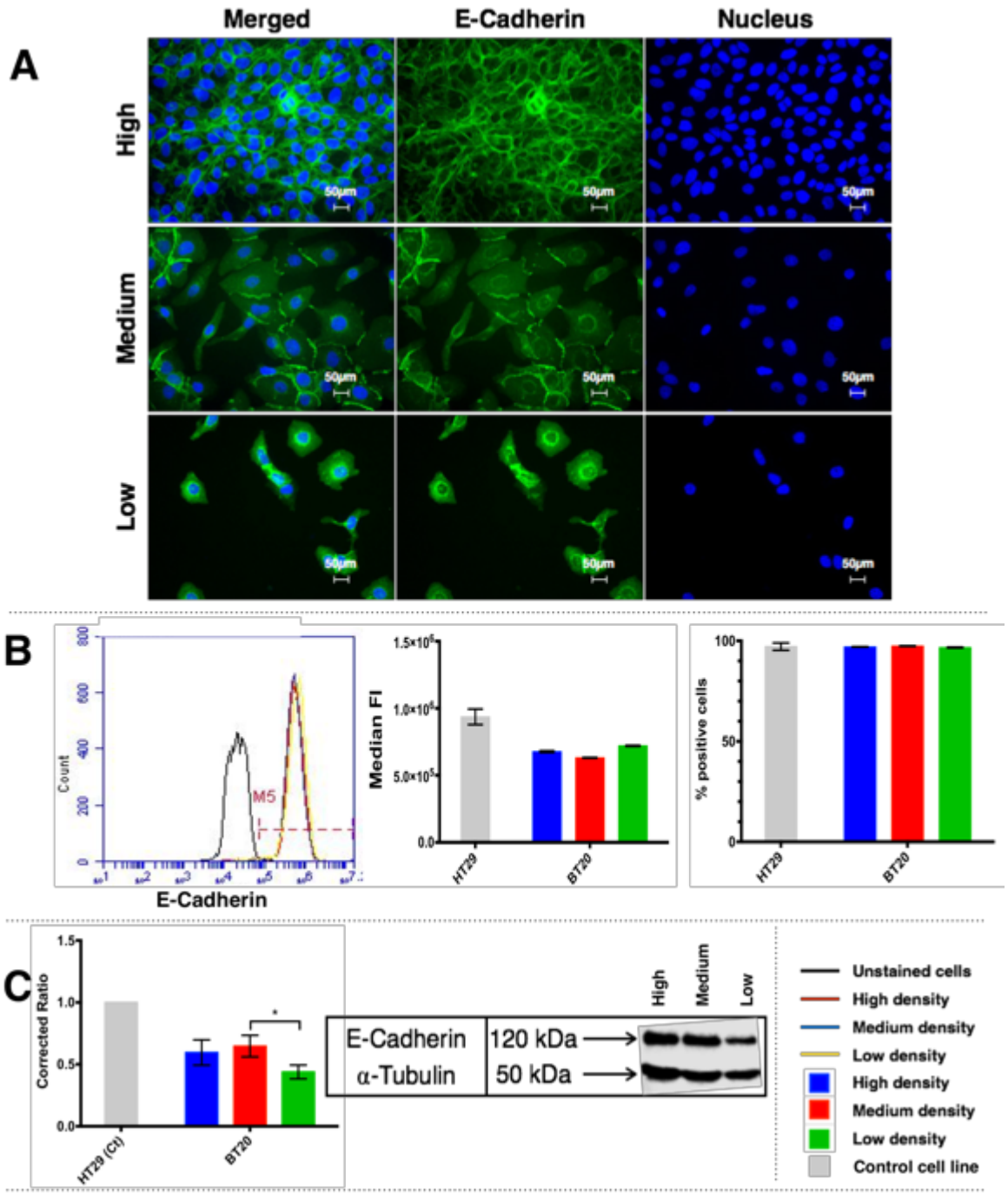

Figure 3-19, E-Cadherin expression in triple-negative and basal-like breast cancer cell line BT20

(A) immunofluorescence representative images of E-cadherin expression in BT20 cell line seeded at three seeding densities (high, medium, and low) labelled with Alexa Fluor® (488 or 594) secondary antibodies (Green) and the nuclei were stained with DAPI (Blue). Images were obtained using Leica fluorescence microscope under 400 times magnification. Scale bars added at the bottom right corner of images. (B) Flow cytometry results of E-cadherin expression levels in BT20 cells. Overlay histogram on the left is for unstained cells and three densities expression. The bar charts on the right show comparison of percentage of E-cadherin expressing cells as well as MFI of E-cadherin in three densities. (C) The level of E-cadherin in BT20 lysates corrected against α-Tubulin internal loading control. Results displayed as bars of mean ±S.D. This figure is representative of n=3 experiments in triplicate. Statistical analysis was conducted and significant differences between samples were indicated by * p-value<0.05, *** p-value<0.01 and **** p-value<0.0001.

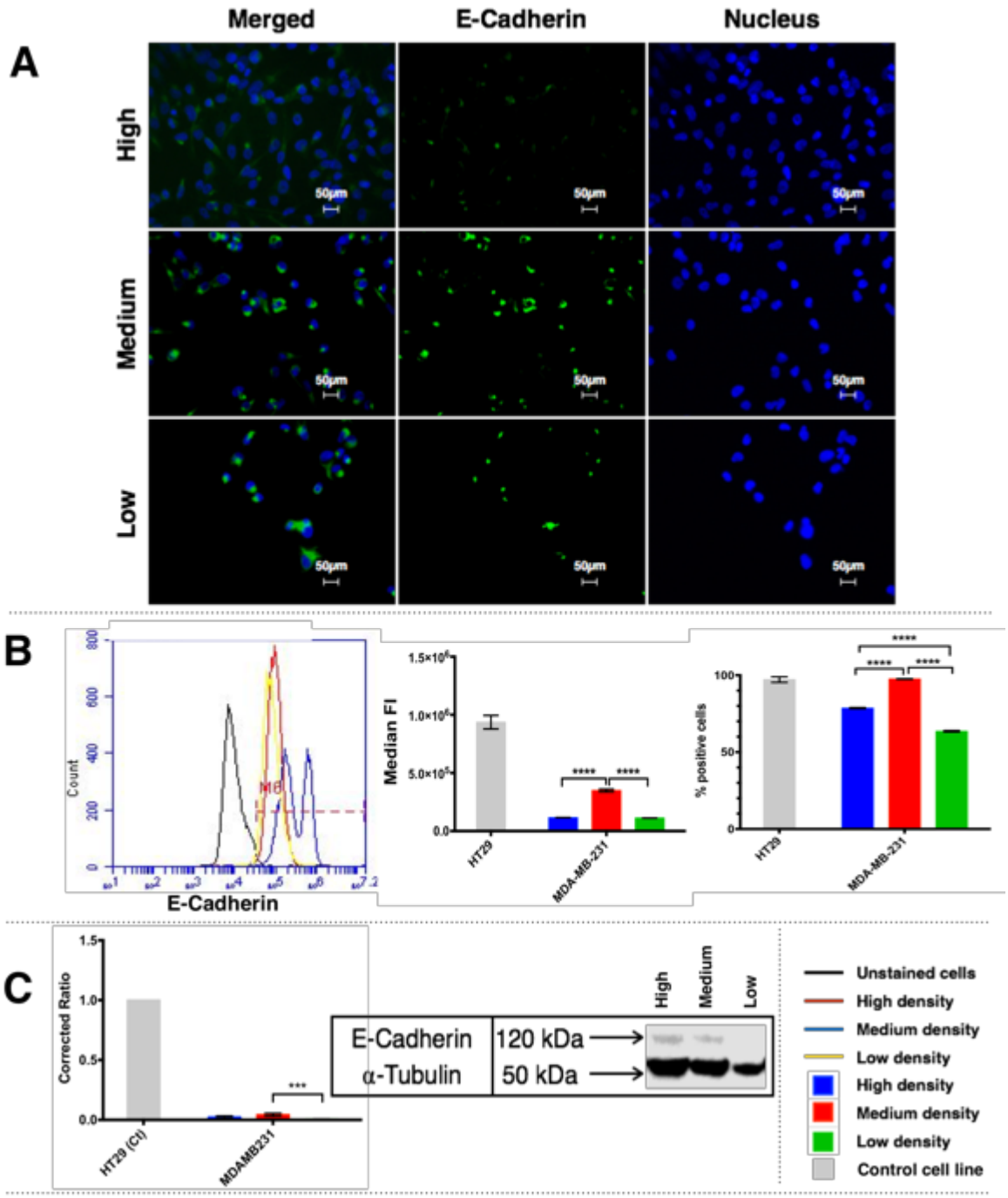

Figure 3-20, E-Cadherin expression in triple-negative and basal-like cell line MDA-MB-231

(A) immunofluorescence representative images of E-cadherin expression in MDA-MB-231 cell line seeded at three seeding densities (high, medium, and low) labelled with Alexa Fluor® (488 or 594) secondary antibodies (Green) and the nuclei were stained with DAPI (Blue). Images were obtained using Leica fluorescence microscope under 400 times magnification. Scale bars added at the bottom right corner of images. (B) Flow cytometry results of E-cadherin expression levels in MDA-MB-231 cells. Overlay histogram on the left is for unstained cells and three densities expression. The bar charts on the right show comparison of percentage of E-cadherin expressing cells as well as MFI of E-cadherin in three densities. (C) The level of E-cadherin in MDA-MB-231 lysates corrected against α-Tubulin internal loading control. Results displayed as bars of mean ±S.D. This figure is representative of n=3 experiments in triplicate. Statistical analysis was conducted and significant differences between samples were indicated by * p-value<0.05, *** p-value<0.01 and **** p-value<0.0001.

The localisation of β-catenin protein was strong in the area of cell-cell contact of the BT20 cell line especially at the medium density (Figure 3-21-A). The expression of β-catenin in MDA-MB-231 cells was nuclear and cytoplasmic in both high and medium density with increase at cell-cell contacts in the low density (Figure 3-22-A).

The percentage of positive β-catenin cells was reduced with decreasing density in both BT20 and MDA-MB-231. There was a highly significant difference between high and medium, high and low, and medium and low densities of BT20 (p-value<0.0001) (Figure 3-21-B). Similarly, β-catenin expression showed significant difference between the high and low and medium and low densities of the MDA-MB-231 cell line (Figure 3-22-B). In BT20, the MFI also reduced with the decrease in density, showing a significant difference between high and medium (p-value<0.001) and also between high and low densities (p-value<0.0001) (Figure 3-21-B). MFI of β-catenin in the MDA-MB-231 cell line was significantly increased from high to medium density (p-value<0.01) and then declined with reduced density, showing a significant difference (p-value<0.001) (Figure 3-22-B). A small proportion of BT20 and MDA-MB-231 cells were negative for β-catenin. The percentage of these cells decreased from the highest to the lowest density as seen in the overlay histogram (Figure 3-21-B and Figure 3-22-B).

In BT20, the relative expression of β-catenin protein was significantly increased between high and medium density (p-value<0.01) and between high and low density (p-value<0.05) (Figure 3-21-C). In MDA-MB-231 cells, the relative expression of β-catenin protein was very weak and declined with decreasing density. There was no significant difference between all comparisons in the MDA-MB-231 cell line (Figure 3-22-C).

In summary, the expression of β-catenin protein in the BT20 cell line increased with density reduction. In ICF images of BT20 cells, the localisation of the protein was strong in the cell-cell contact area. In MDA-MB-231, the expression of β-catenin protein decreased with reducing density without any statistical significance. Strong cytoplasmic and nuclear localisation of the protein was observed in both cell lines in the medium and low densities.

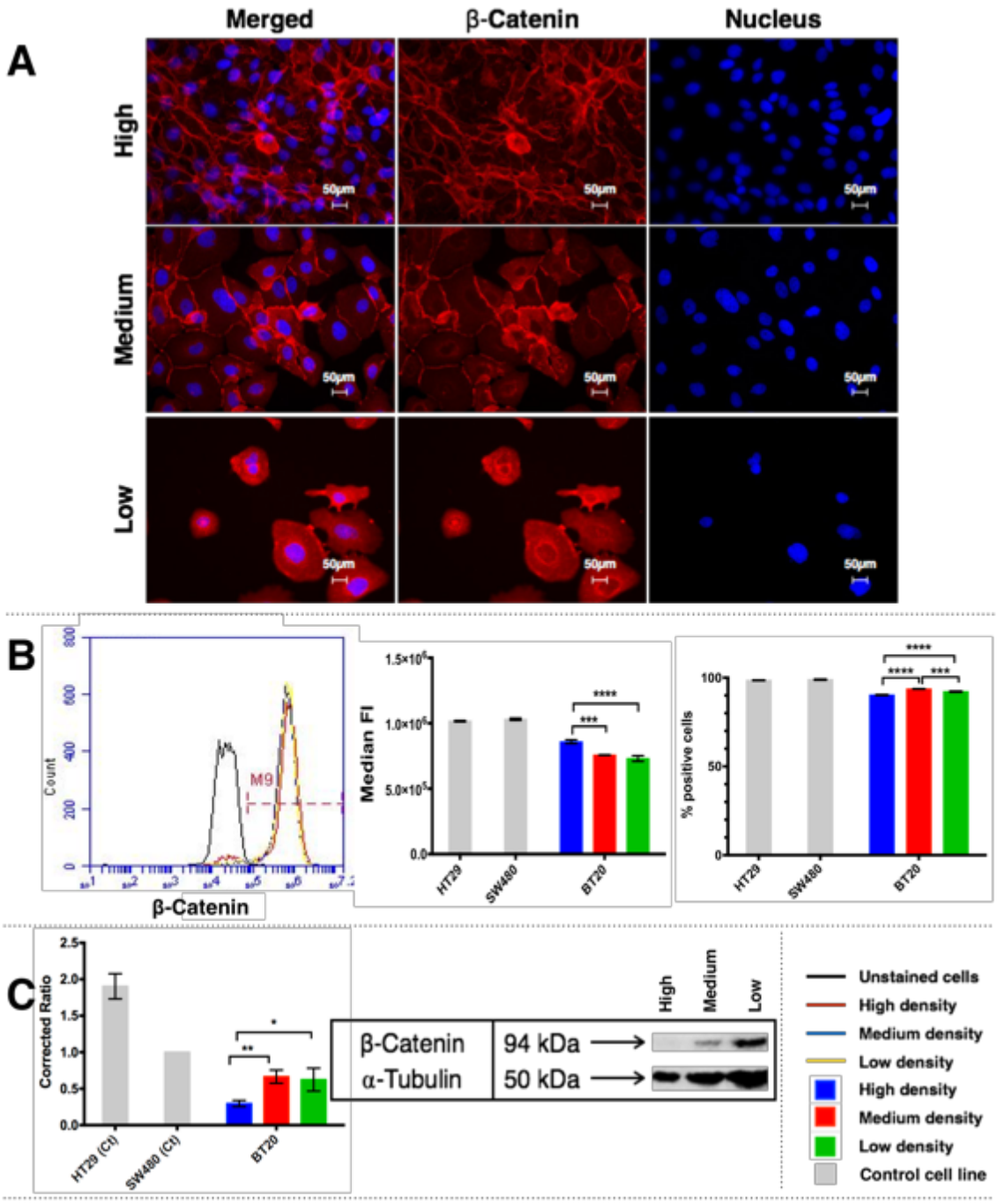

Figure 3-21, β-catenin expression in triple-negative and basal-like breast cancer cell line BT20

(A) immunofluorescence representative images of β-catenin expression in BT20 cell line seeded at three seeding densities (high, medium, and low) labelled with Alexa Fluor® (488 or 594) secondary antibodies (Red) and the nuclei were stained with DAPI (Blue). Images were obtained using Leica fluorescence microscope under 400 times magnification. Scale bars added at the bottom right corner of images. (B) Flow cytometry results of β-catenin expression levels in BT20 cells. Overlay histogram on the left is for unstained cells and three densities expression. The bar charts on the right show comparison of percentage of β-catenin expressing cells as well as MFI of β-catenin in three densities. (C) The level of β-catenin in BT20 lysates corrected against α-Tubulin internal loading control. Results displayed as bars of mean ±S.D. This figure is representative of n=3 experiments in triplicate. Statistical analysis was conducted and significant differences between samples were indicated by * p-value<0.05, *** p-value<0.01 and **** p<0.0001.

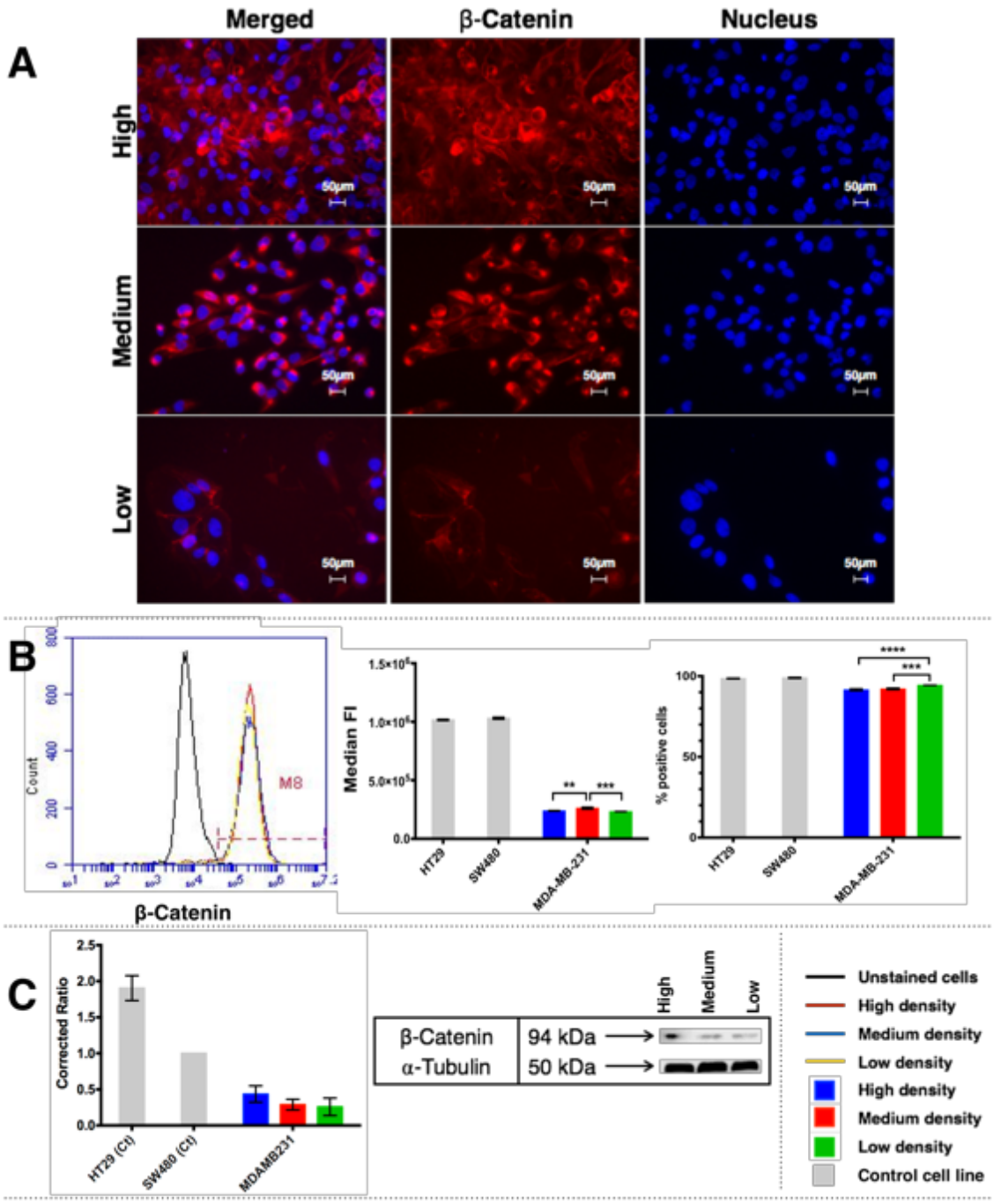

Figure 3-22, β-catenin expression in triple-negative and basal-like cell line MDA-MB-231

(A) immunofluorescence representative images of β-catenin expression in MDA-MB-231 cell line seeded at three seeding densities (high, medium, and low) labelled with Alexa Fluor® (488 or 594) secondary antibodies (Red) and the nuclei were stained with DAPI (Blue). Images were obtained using Leica fluorescence microscope under 400 times magnification. Scale bars added at the bottom right corner of images. (B) Flow cytometry results of β-catenin expression levels in MDA-MB-231 cells. Overlay histogram on the left is for unstained cells and three densities expression. The bar charts on the right show comparison of percentage of β-catenin expressing cells as well as MFI of β-catenin in three densities. (C) The level of β-catenin in MDA-MB-231 lysates corrected against α-Tubulin internal loading control. Results displayed as bars of mean S.D. This figure is representative of n=3 experiments in triplicate. Statistical analysis was conducted and significant differences between samples were indicated by * *p*-value<0.05, *** *p*-value0.01 and **** *p*-value<0.0001.

The expression of vimentin was very strong in ICF images of the basal-like and triple-negative cell lines BT20 and MDA-MB-231 (Figure 3-23-A and Figure 3-24-A). The MDA-MB-231 cells showed the highest expression of vimentin among all the breast cancer cell lines used, and it was therefore utilised as positive control.

Both the percentage of positive cells and the MFI of vimentin expressing cells increased as density reduced with the exception of the MFI for MDA-MB-231 at low density, that showed drop in expression of the protein. In BT20 cells, there was a highly significant difference of both the percentage and MFI compared to density seen between high and medium, high and low, and medium and low (p-value<0.0001) (Figure 3-23-B). In MDA-MB-231, the difference in the percentage of vimentin expressing cells was significant between high and medium (p-value<0.01) and also between high and low (p-value<0.001) (Figure 3-24-B). Also, MFI showed a significant difference between high and medium, high and low, and medium and low (p-value<0.0001) (Figure 3-24-B).

The relative expression of vimentin also increased as density decreased, with the exception of the low density of MDA-MB-231, at which they showed a decreased expression. In BT20 cells, the difference was significant between high and low, and medium and low densities (Figure 3-23-C). In MDA-MB-231 cells, the difference was also significant between high and low (p-value<0.01) and medium and low density (p-value<0.0001) (Figure 3-24-C).

Taking the expression of E-cadherin, β-catenin and vimentin expression in BT20 and MDA-MB-231 cell into account, it can be suggested that these cells maintained in an intermediate phase of EMT.

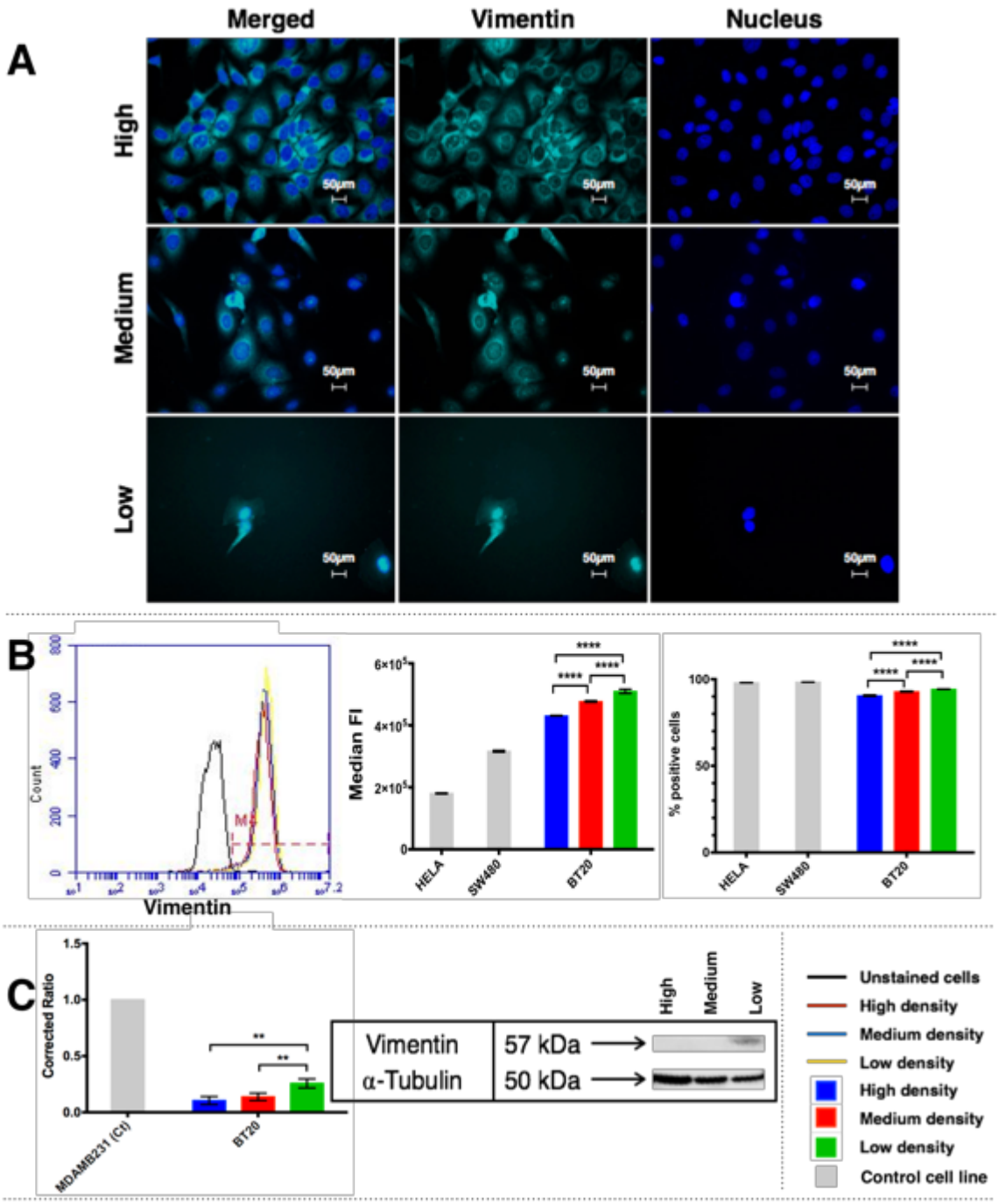

Figure 3-23, Vimentin expression in triple-negative and basal-like breast cancer cell line BT20

(A) immunofluorescence representative images of vimentin expression in BT20 cell line seeded at three seeding densities (high, medium, and low) labelled with Alexa Fluor® (488 or 594) secondary antibodies (light teal) and the nuclei were stained with DAPI (Blue). Images were obtained using Leica fluorescence microscope under 400 times magnification. Scale bars added at the bottom right corner of images. (B) Flow cytometry results of vimentin expression levels in BT20 cells. Overlay histogram on the left is for unstained cells and three densities expression. The bar charts on the right show comparison of percentage of vimentin expressing cells as well as MFI of vimentin in three densities. (C) The level of vimentin in BT20 lysates corrected against α-Tubulin internal loading control. Results displayed as bars of mean ±S.D. This figure is representative of n=3 experiments in triplicate. Statistical analysis was conducted and significant differences between samples were indicated by * *p*-value<0.05, *** *p*-value<0.01 and **** *p*-value<0.0001.

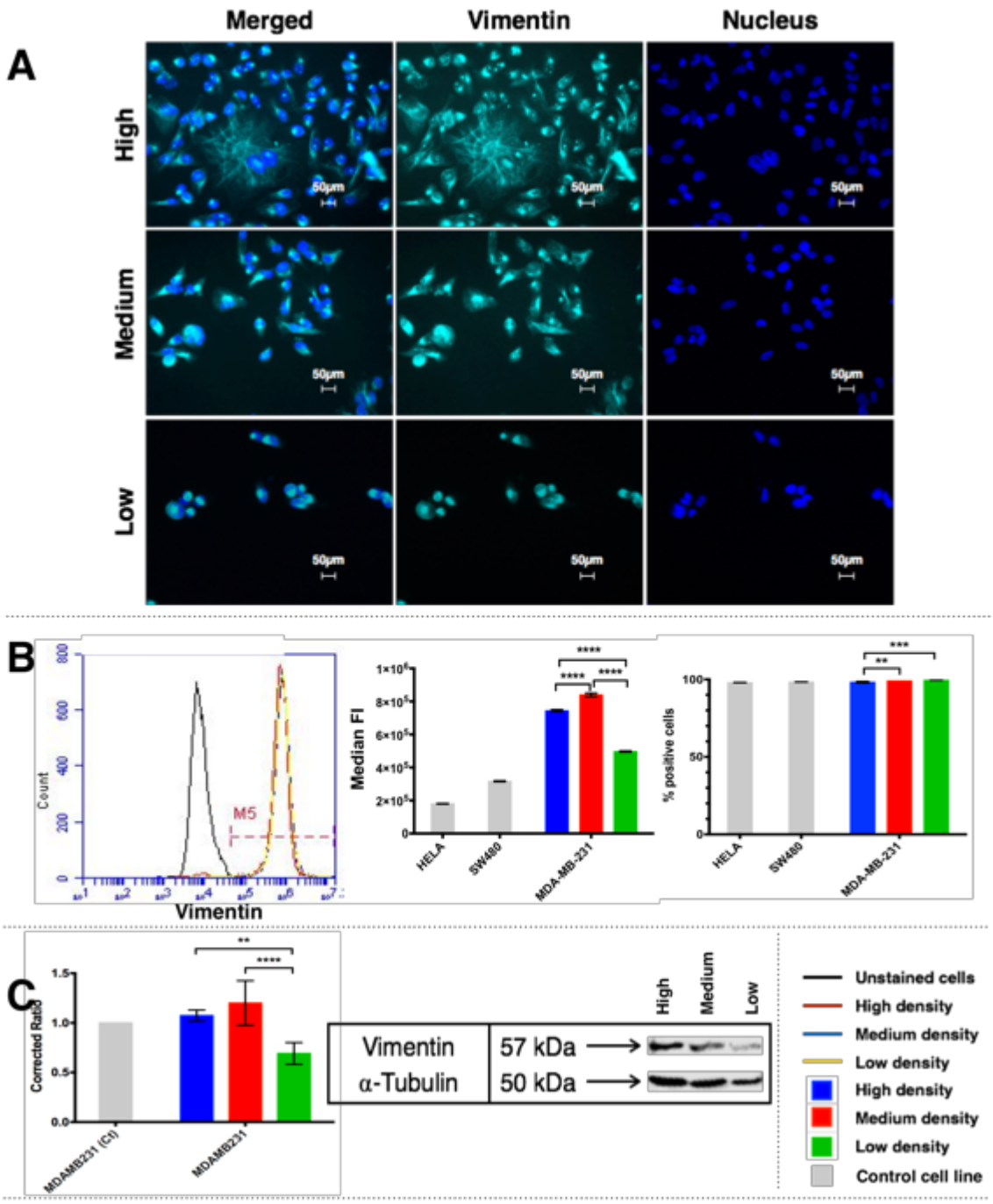

Figure 3-24, Vimentin expression in triple-negative and basal-like cell line MDA-MB-231

(A) immunofluorescence representative images of vimentin expression in MDA-MB-231 cell line seeded at three seeding densities (high, medium, and low) labelled with Alexa Fluor® (488 or 594) secondary antibodies (light teal) and the nuclei were stained with DAPI (Blue). Images were obtained using Leica fluorescence microscope under 400 times magnification. Scale bars added at the bottom right corner of images. (B) Flow cytometry results of vimentin expression levels in MDA-MB-231 cells. Overlay histogram on the left is for unstained cells and three densities expression. The bar charts on the right show comparison of percentage of vimentin expressing cells as well as MFI of vimentin in three densities. (C) The level of vimentin in MDA-MB-231 lysates corrected against α-Tubulin internal loading control. Results displayed as bars of mean ±S.D. This figure is representative of n=3 experiments in triplicate. Statistical analysis was conducted and significant differences between samples were indicated by * p-value<0.05, *** p-value<0.01 and **** p-value<0.0001.

3.2.2.4 Summary of the status of the expression and localisation of EMT markers in breast cancer cell lines

The table below (Table 3-3) summarises the changes in E-cadherin, β-catenin and vimentin in response a reduction in seeding density. Of all the cell lines MDA-MB-361, BT20, MCF7 and MCF10A cell lines had the strongest expression of E-cadherin. It can be concluded in general that both the expression of E-cadherin and the change in the expression in response to reduction of the seeding density did not depend on the subclassification of the breast cancer cell lines.

As seen in the summary of the E-cadherin expression levels in the cell lines, three patterns of protein level changes can be seen. The three cell lines (MCF10A, MCF7, and MDA-MB-361) have high expression of E-cadherin and showed a similar pattern of reduction of the protein as seeding density reduced. MDA-MB-453 had very low expression of E-cadherin that increased with density reduction. Lastly, in the two basal-like and TNBC cell lines (BT20 and MDA-MB-231) E-cadherin protein expression increased slightly at the medium density and then reduced in the low density.

The expression of β-catenin protein was higher in MCF10A, MDA-MB-361, BT20, MDA-MB-231 and MCF7 cell lines compared to the rest of the cell lines. The TNBC cell line (MDA-MB-453) had the lowest expression of β-catenin. The expression of β-catenin protein decreased with density reduction in MCF7, MDA-MB-361, MDA-MB-231, and MCF10A. On the other hand, the expression level increased with seeding density in MDA-MB-453, and BT20 cell lines (Table 3-3).

The basal-like and triple-negative cell line (MDA-MB-231) had the strongest expression level of vimentin compared to all other cell lines. This protein increases in cells that undergo EMT, therefore, the increase of this marker can be suggestive of a more mesenchymal phenotype. The cell lines that showed an increase in this protein with reduction in density were MCF10A, BT20 (basal-like and triple-negative) and MDA-MB-453 (triple-negative). The expression of vimentin increased in the medium density of MDA-MB-231 and then decreased in the low density. This pattern was similar to the expression of vimentin seen in MCF7 and MDA-MB-361.

From all the data analysed previously and the summary in the table below (Table 3-3) it can be suggested that three basal-like and TNBC cell lines (BT20, MDA-MB-231 and MCF10A) increased mesenchymal morphology with decreases in density. This was because they showed a decrease in the epithelial marker E-cadherin and an

increase in vimentin expression at the lowest density. Also, both BT20 and MDA-MB-231 show an intermediate phenotype, seen as maintaining high expression of vimentin and E-cadherin in all densities (Table 3-2). The luminal cell lines also showed a decrease in the epithelial marker (E-cadherin) and an increase in vimentin with reduction in density (Table 3-2). MDA-MB-453 cells showed an increase in the epithelial marker (E-cadherin) in response to decreasing density. This corresponded to the morphological decrease in spindle-shaped cells and in cellular spreading (Table 3-2).

Table 3-3: Summary of the changes in the marker's expression levels with seeding density of the breast cancer cell lines.

This table summarise the markers (E-cadherin, β-catenin, and vimentin) changes (expression level and localisation) in high, medium and low density. These changes are represented as a qualitative score (0 to 3) based on the western blotting and ICF observation. The localisation of the protein was indicated as (N = Nuclear, C = Cytoplasmic, and M = membrane).

Breast cancer cell lines	E-cadherin						Beta-catenin						Vimentin		
	High		Medium		Low		High		Medium		Low		High	Medium	Low
	Expression	Localisation	Expression	Localisation	Expression	Localisation	Expression	Localisation	Expression	Localisation	Expression	Localisation	Expression	Expression	Expression
MCF7	3	M/C	2	M/1C	2	M/2C	2	M	2	1C/N	2	2C/N	2	2	1
MDA-MB-361	3	M/C	2	M/0C	2	M/1C	3	M/C	2	M/C	2	M/C	2	2	2
MDA-MB-453	0	C	1	C	2	C	0	C/N	0	C/N	1	C/N	1	2	0
BT20	3	M	3	M/C	2	M/C	1	M/C/N	3	1C/1N	3	1C/1N	1	1	3
MDA-MB-231	0	C	1	1C	0	2C	2	2C/N	1	1C/1N	1	C/N	3	3	2
MCF10A	2	M/C	2	M/1C	1	M/2C	3	M/C	2	M/1C/1N	2	M/1C	0	0	2

3.3 Discussion

3.3.1 Cell line morphology follows the subclass of breast cancer and changes in response to reducing cell density

The morphology of the breast cancer cell lines showed several changes with alteration in the seeding density depending on the cell line (Figure 3-6). The highest seeding density depends on several factors including size, spreading, stratification, degree of cell-cell contacts and cellular attachment to the culture surface as observed by phase contrast microscopy.

The cell lines with the smallest degree of cellular spreading and highest degree of cellular stratification, such as MDA-MB-361, had the highest seeding density compared to other cell lines (Figure 3-5). Also, strong cell-cell contacts observed in luminal cells (MCF7, and MDA-MB-361) that visually increased with increasing density (Figure 3-3). The three basal breast cancer cell lines (MCF10A, BT20 and MDA-MB-231) required the fewest cells for the high density (Table 3-1).

The luminal breast cancer cell lines (MCF7 and MDA-MB-361) and the normal-like and basal-like breast cancer cell line (MCF10A) had a classical cobblestone epithelial phenotype with tight cell-cell junctions (Figure 3-6) which was described by Neve *et al.* (2006) and by Kenny *et al.* (2007b). The triple negative cell line MDA-MB-453 had a grape-like morphology with fewer cell-cell contact and showed increased cell-cell adhesions with decreasing density (Figure 3-6) which is similar to the morphology observed in 3D culture by Kenny *et al.* (2007b).

Basal breast cancer cell line morphology showed more prominent changes as seeding density decreased. The epithelial morphology of MCF10A was transformed slowly to a fibroblastic type , especially at the lowest density, and was associated with a reduction in cell adhesion with more gaps formed between cell clusters, especially at colony borders (Figure 3-6). This morphological transformation of MCF10A has also been reported previously (Sarrio *et al.*, 2008; Chen *et al.*, 2014; Qu *et al.*, 2015). MCF10A cells retained a largely epithelial morphology at all densities used in the current study with visibly increased of fibroblastic morphology at the lowest density. This can be explained by the fact that EGF was removed from the culture medium after 24 hours of incubation to reduce the effect of EGF on EMT. The EGF growth factor is a well-known mediator of EMT in breast cancer (Antonyak *et al.*, 2004; Lo *et al.*, 2007; Drasin *et al.*, 2011; Wang *et al.*, 2012; Zanetti *et al.*, 2015) and also other cancer types including ovarian (Cheng *et al.*, 2012), cervical (Ha *et al.*, 2013), hepatocellular

carcinoma (Ogunwobi *et al.*, 2012), and colorectal cancer (Sakuma *et al.*, 2012). The period of incubation of cells without EGF was 24 hours because the average half-life of EGF in cells ranges from 8-24 hours (Sorkin and Duex, 2010).

The BT20 cell line (basal type A) showed fibroblastic morphology with spindle-shaped cells at the highest density while maintaining cell-cell adhesion. In the medium density BT20 cells had mixed morphology, with an increase in epithelial flat cells and more cell-cell adhesions (Figure 3-6). A similar observation was reported by Neve *et al.* (2006) where they found that basal cells of type A have a mixed phenotype including well differentiated epithelial type seen in luminal cells, as well as displaying a mesenchymal or fibroblastic morphology. This mixed morphology was lost at the lowest density with predominated mesenchymal phenotype that have increased spindle shape and less cell-cell adhesion. The MDA-MB-231 cell line (basal type B) demonstrated a strong mesenchymal morphology with spindle-shaped cells with few to no cell-cell adhesions (Figure 3-6). Neve *et al.* (2006) also noted that the basal type B cells showed a less differentiated-phenotype with a fibroblastic morphology. It should be noted that in all previous studies basal cells were cultured at a single seeding density.

The low seeding density used for MCF10A (normal-like/basal-like) was $1.3x10^3$ cells/cm^2 and similar to a "sparse" density selected by Liu *et al.* (2006b). However, the "dense" culture for MCF10A used by Liu *et al.* (2006b) was $2x10^5$ / cm^2, which exceeded the highest density used here ($1x10^4/cm^2$ (Table 3-1)), because in this study cellular stacking was eliminated.

These three densities reflected the growth pattern of normal breast cells. First at sparse density, loss of cell-cell contacts results in decreased of cell proliferation with cellular resistance to anoikis (Liu *et al.*, 2006b; Onder *et al.*, 2008; Kumar *et al.*, 2011). The MCF7 cell line was also reported to show a similar reduction in cell growth when seeded at low density in 3D culture (Manuel Iglesias *et al.*, 2013). At high density, MCF10A cells reduce proliferation due to cell-cell contact inhibition (Liu *et al.*, 2006b). The MCF10A showed increased proliferation at the intermediate degree of cell-cell contact (medium density) (Liu *et al.*, 2006b). This increase in growth was previously reported in MCF7 cells at an intermediate density, which then decreased in dense cultures (Manuel Iglesias *et al.*, 2013). Therefore, there is an intermediate density between dense and sparse culture that was reported to show a significant change in the proliferation of cells (Liu *et al.*, 2006b; Manuel Iglesias *et al.*, 2013).

3.3.2 Luminal (MCF7 and MDA-MB-361) and normal-like breast cancer (MCF10A) cell lines showed increased fibroblastic morphology and reduced E-cadherin at low density

The three cell lines (MCF7, MDA-MB-361 and MCF10A) showed an increase in spindle morphology, decreasing cell-cell contact, and increasing cellular spreading with reduction in seeding density (Table 3-2). The expression of E-cadherin and β-catenin proteins was reduced and their localisation at sites of cell-cell contact visually reduced as density decreased (Figure 3-7, Figure 3-10, Figure 3-8, Figure 3-11, Figure 3-9 and Figure 3-12). The expression of vimentin increased as density decreased in MDA-MB-361 and MCF10A, suggesting an increased mesenchymal transition. However, additional analysis and expression of other markers, including EMT transcription factors including Slug, Snail and Twist, is recommended in order to confirm this conclusion.

In MCF7, vimentin expression decreased with density reduction. Previous studies have reported that the MCF7 cells were less aggressive due to low expression of vimentin as seen by Western blotting (Cai *et al.*, 2013; Shan *et al.*, 2015). Zhang *et al.* (2006) examined the effect of changing the confluency of MCF7 cells on gene expression, including genes that controlled EMT, but no further analysis were conducted under the effect of confluency (Zhang *et al.*, 2006).

MCF10A is a normal-like cell line with a basal-like molecular signature that made these cells more susceptible to mesenchymal morphological change (Jonsson *et al.*, 2007). The expression of E-cadherin protein was shown previously to be lower in MCF10A compared to the luminal cell lines (MCF7 and MDA-MB-361) (Chen *et al.*, 2014). Lombaerts *et al.* (2006) found that E-cadherin expression was lower due to promoter methylation in MCF10A cell line, which may explain why the protein was less abundant in this cell line compared with MCF7 and MDA-MB-361.

The localisation of β-catenin protein in MCF7 and MDA-MB-361 cells showed the honeycomb pattern that was retained at all densities (Figure 3-11 and Figure 3-12). Both cell lines also showed increased cytoplasmic β-catenin localisation with reduction in cellular density. A similar pattern was reported previously in MCF7 at a density similar to the highest used here (Cai *et al.*, 2013; Ding *et al.*, 2016). Suzuki and Takahashi (2006) found that β-catenin protein co-precipitated with E-cadherin in MCF7 cells, hence, indicating proper interaction between both proteins to form adherens junctions. Benhaj *et al.* (2006) also investigated β-catenin protein localisation in MCF7

and found that it depended on the expression of E-cadherin with cells expressing E-cadherin showing less nuclear localisation of β-catenin, as confirmed by confocal microscopy.

Most studies showed that E-cadherin expression was localised in the membrane in high density MCF10A (Sarrio *et al.*, 2008; Sun *et al.*, 2014a; Qu *et al.*, 2015). MCF10A showed membrane localised expression of β-catenin as seen in several reports, however they all used a single seeding density (Fournier *et al.*, 2008; Zhang *et al.*, 2011; Listerman *et al.*, 2014). Fournier *et al.* (2008) found that β-catenin co-localises with E-cadherin, seen under fluorescence microscopy in MCF10A at a single density. MCF10A also was reported to express β-catenin using Western blotting (Fournier *et al.*, 2008; Sun *et al.*, 2014a). Whereas, Sarrio *et al.* (2008) found that seeding MCF10A cells at a sparse density resulted in a reduction of E-cadherin protein expression and increased cytoplasmic and nuclear localisation of β-catenin protein compared to increased membrane localisation at the confluent density.

Similar to the findings in the current study, Shan *et al.* (2015) found that MCF7 showed weak vimentin expression, which contributed to their low motility. Yan *et al.* (2012) also attempted to assess the expression level of vimentin in MCF7 and found that it was not detectable.

The mesenchymal morphological change of MCF10A at sparse densities was reported previously in several studies (Maeda *et al.*, 2005; Liu *et al.*, 2006b; Sarrio *et al.*, 2008; Kim *et al.*, 2011; Marro *et al.*, 2014). The basal signature of this cell line caused increased expression of vimentin protein, which increases the susceptibility of the cells to mesenchymal morphological change (Qu *et al.*, 2015). Qu *et al.* (2015) suggested that MCF10A cells have a basal-like phenotype while expressing luminal features, or that they are luminal cells that are undergoing EMT. Reorganisation of vimentin filaments was noticed when these cells were seeded at sparse density, but the difference in the levels of vimentin expression between confluence and sparse culture was not assessed (Sarrio *et al.*, 2008). The expression of additional markers, such as Slug, Snail and Twist, is needed to verify that there was an increase in EMT at lower seeding densities in MCF10A.

3.3.3 The MDA-MB-453 cell line showed an increased epithelial phenotype with decreasing seeding density

The effect of reducing cellular density was not previously reported for the MDA-MB-453 cell line. The expression levels of EMT markers was studied in a single

density of this cell line that was selected usually around the medium or high density used here (Blick *et al.*, 2008; Zhang *et al.*, 2008).

E-cadherin protein was not detectable in MDA-MB-453 cell line using Western blotting or PCR (Nieman *et al.*, 1999; Lombaerts *et al.*, 2006). However, we showed that MDA-MB-453 had an innately low expression of E-cadherin compared to the other breast cancer cell lines (Figure 3-16) which concurs with other reports (Junxia *et al.*, 2010; Yang *et al.*, 2014). The discrepancies in the reports of E-cadherin expression in these studies could be explained by the variation in the densities in which these cells were cultured. Low levels of E-cadherin in MDA-MB-453 cell line has been shown due to hypermethylation of the *CDH1* promoter (Mariner *et al.*, 2004; Junxia *et al.*, 2010; Yang *et al.*, 2014). Thus, reinforcing the importance of determining and reporting the seeding densities in researches and their effect on the expression of EMT related proteins.

MDA-MB-453 expressed very low levels of β-catenin protein compared to the other breast cancer cell lines tested (Figure 3-17) which had also been reported in previous studies on this cell line (Nieman *et al.*, 1999; Schlosshauer *et al.*, 2000; Kenny *et al.*, 2007b; Sun *et al.*, 2014a). This is the first study to report the difference in this protein expression in several seeding densities of MDA-MB-453. Schlosshauer *et al.* (2000) concluded that there were no mutations in β-catenin in MDA-MB-453. The same study concluded that abnormalities in the function of β-catenin protein in this cell lines was not due to genetic mutations (Schlosshauer *et al.*, 2000; Jiang *et al.*, 2009). The expression of vimentin in MDA-MB-453 was low similar to previous reports (Lombaerts *et al.*, 2006; Tanaka *et al.*, 2016).

The estimation of expression levels of these proteins (E-cadherin, β-catenin and vimentin) were affected by the threshold of detection of the technique used. Also, according to the findings of the current research, the density at which the cells are cultured may cause variation in the level of protein.

Two cell lines that had amplification of the ErbB2 gene (MDA-MB-361 and MDA-MB-453) and one that overexpresses of the protein (MDA-MB-361). MDA-MB-453 showed an increased epithelial morphology and increase in E-cadherin with reduction of density. Benhaj *et al.* (2006) examined the nuclear expression of β-catenin and found that there was no nuclear expression in MDA-MB-453. Similarly, Kim *et al.* (2010b) found that very week nuclear β-catenin was found in MDA-MB-453. This is

similar to the observation of the location of β-catenin in this study, which conclude that there was no cross talk between ErbB2 and Wnt/β-catenin pathway in this cell line.

3.3.4 The triple-negative and basal-like breast cancer cell lines BT20 and MDA-MB-231 showed an intermediate phenotype on the EMT spectrum

The triple-negative and basal-like breast cancer cell lines (BT20 and MDA-MB-231) showed fibroblastic morphology at all densities used (Figure 3-6). There was a noticeable morphological switching at the medium density of these cell lines. Both cell lines showed increased cell-cell contact with decreased spindle morphology (Figure 11-2 and Figure 11-3). The epithelial marker E-cadherin was also increased at the medium density in both cell lines (Figure 3-19 and Figure 3-20) with strong membranous localisation observed in BT20 (Figure 3-19).

Memmi *et al.* (2015), reported that the molecular subtype of breast cancer indicated the capacity of cells to undergo invasion through EMT activation. The MDA-MB-231 cell line (basal type B) is hypothesised here to be further down the EMT pathway which was also suggested previously by Xie *et al.* (2014). Additionally, it was found in the same study that MCF10A cells (also basal type B) were able to undergo EMT but were not able to initiate tumour formation (Xie *et al.*, 2014). This was also confirmed by microarray and gene expression profiling. It was also reported that the mesenchymal and basal breast cancer cell lines expressed significantly more vimentin compared to the luminal cell lines (Charafe-Jauffret *et al.*, 2006; Neve *et al.*, 2006; Kumar *et al.*, 2011). Together with the findings here, it can be concluded that the basal-like breast cancer cell lines showed signs of EMT with reduction in seeding density.

The expression level of E-cadherin in BT20 has been previously studied using a only single seeding density (around that of the "medium density" used in this study) and found it to be highly expressed (Nieman *et al.*, 1999; von Schlippe *et al.*, 2000; Hajra *et al.*, 2002; Johnson *et al.*, 2004; Sultan *et al.*, 2005; Shirure *et al.*, 2015). E-cadherin in BT20 localised at cellular adhesion sites as seen by ICF (Figure 3-19) which was also reported to show a similar pattern in other studies (Shirure *et al.*, 2015).

A low expression level of E-cadherin was reported in the MDA-MB-231 cell line and was found to be cytoplasmic by ICF (Lombaerts *et al.*, 2006; Zhang *et al.*, 2008; Yang *et al.*, 2014). Benton *et al.* (2009) found that the expression of E-cadherin in MDA-MB-231 cells was undetectable when they were grown on a plastic tissue culture surface. E-cadherin was also not detected by Western blotting or PCR in other studies (Nieman *et al.*, 1999; Graff *et al.*, 2000; Mariner *et al.*, 2004; Sun *et al.*, 2014a;

Zhao *et al.*, 2016). Low expression of E-cadherin explains the aggressive nature of this cell line in xenograft studies (Iorns *et al.*, 2012; Kil *et al.*, 2014).

The promoter of *CDH1* (E-cadherin) in MDA-MB-231 has been shown to be methylated, explaining the low expression (Benton *et al.*, 2009). Shirure *et al.* (2015) showed a functional link between the low expression of E-cadherin and high expression of Slug (an E-cadherin repressor) in MDA-MB-231 cell line compared to BT20 cells that has high E-cadherin expression. This was also concluded by Hajra *et al.* (2002), who they found that the inhibition of E-cadherin in MDA-MB-231 was caused by increased expression of Slug. However, transcription factors of EMT were not assessed in the current study and assessing the changes in expression of such proteins in effect of seeding density changes will aid in making stronger conclusions in future studies.

Lombaerts *et al.* (2006) found that MDA-MB-231 had a partially methylated E-cadherin promoter, and flow cytometry analysis showed two subpopulations of E-cadherin expressing cells, one of these two subpopulations showed low expression of E-cadherin (Lombaerts *et al.*, 2006). Thus, they concluded that the methylation of the *CDH-1* promoter in this cell line could be partial and reversible (Lombaerts *et al.*, 2006). The two populations seen in Lombaerts *et al.* (2006) was similar to the finding in the medium density flow cytometry in this study (Figure 3-20). The small population of cells that had lower expression of E-cadherin could represent a population of cells that have increased stem cell characteristics, which gave them additional aggressive characteristic. Also, it could show the ability to segregate these cells using the seeding density model and to identify them in the medium density. However, further analysis and experimentation to assess the expression of stem cell markers and other EMT transcription factors to make further conclusions.

β-catenin expression increased with reduction in density in BT20 cells, with localisation of the protein increasing at regions of cell-cell contact at the medium density (Figure 3-21). Nieman *et al.* (1999) and Schlosshauer *et al.* (2000) also found that BT20 and MDA-MB-231 cells expressed β-catenin. They concluded that the loss of E-cadherin in MDA-MB-231 cells resulted in reduced in expression of several catenin types, including β-catenin (Suzuki and Takahashi, 2006).

Benhaj *et al.* (2006) examined β-catenin in BT20 and found that they have weak nuclear β-catenin expression. Gilles *et al.* (2003) reported that BT20 express β-catenin and E-cadherin but not vimentin. β-catenin was localised to the membranes, forming the epithelial phenotypes of the cells. Furthermore, the localisation of β-catenin protein

in MDA-MB-231 was variable across many studies. It was found that the expression of β-catenin in MDA-MB-231 was both cytoplasmic and nuclear (Gilles *et al.*, 2003). On the other hand, Ravindranath *et al.* (2011) reported that β-catenin expression was both membranous and nuclear in MDA-MB-231. Yan *et al.* (2012) also measured β-catenin protein in MDA-MB-231 and found that most of the protein was in the cytoplasmic and membranous fraction compared to a low amount in the nuclear fraction. This variation in reports on the localisation and level of β-catenin expression in these cell lines may have been due to discrepancies in the seeding densities used and tissue culture method.

The expression of vimentin increased significantly in BT20 at lower density compared to higher density (Figure 3-21). The MDA-MB-231 cell line expressed high levels of vimentin protein (as seen in Figure 3-24) and this is consistent with previous findings. Sommers *et al.* (1991) assessed the expression of vimentin in breast cancer cell lines using Northern blotting and found the MDA-MB-231 had strong vimentin expression. High vimentin expression in MDA-MB-231 was also confirmed by Western blotting (Cai *et al.*, 2014). Tanaka *et al.* (2016) found that changes in vimentin expression was significantly correlated with changes in β-catenin expression in MDA-MB-231. The high expression of vimentin in MDA-MB-231 cells was maintained in both the high and medium densities (Figure 3-24). Yuki *et al.* (2014), concluded that the expression of vimentin correlated with the mesenchymal or basal phenotype of MDA-MB-231 and MCF10A cells.

The intermediate status of MDA-MB-231 and BT20 was noted previously in several studies and was referred to as partial EMT in previous studies (Grigore *et al.*, 2016; Saitoh, 2018), hybrid EMT (Jolly *et al.*, 2015; Jolly *et al.*, 2016; Vergara *et al.*, 2016) and transition states (Pastushenko *et al.*, 2018). The intermediate status of basal-like breast cancer cell lines (BT20 and MDA-MB-231) is a status termed because the MDA-MB-231 and BT20 showed increased in epithelial characteristic when were seeded in the medium density. Thus, these cells were able to maintain epithelial and mesenchymal phenotype. In medium density, the cells showed increase in the expression of E-cadherin with reduction in vimentin and β-catenin. In high and low density, MDA-MB-231 and BT20 cells had mesenchymal phenotype with reduction in E-cadherin and β-catenin compared to the medium density. The observation of the partial EMT in the medium density in BT20 and MDA-MB-231 cell lines has not been observed *in vitro*, until the time of submitting this work. Further confirmation and verification of this status is recommended before drawing further conclusions. The cell

density model developed here can be utilised for further understanding of the scope and regulation of the intermediate status in those cell lines in breast cancer and other epithelial cancers.

3.3.5 The molecular subtype of breast cancer cell lines did not dictate the response to stimuli introduced in the cell density *in vitro* model

According to the results and analysis of the expression of E-cadherin and vimentin proteins at the three densities, it can be seen that the breast cancer cell lines changed both in morphology and in the expression of these markers. The strength of the response to lowering the cellular density varied between the cell lines. Further experimental verification by analysis of expression level of EMT transcription factors Snail, Slug and Twist is required to draw stronger conclusions. The response noticed with reducing density can be divided into three types; a classical increase in mesenchymal morphology with reduction in E-cadherin and increased vimentin, an inverted response characterised by an increase in epithelial morphology with a reduction in vimentin and increased E-cadherin, and an intermediate status showed mixed response to reduction in density.

MCF7, MDA-MB-361, MDA-MB-453 are luminal cell lines, yet, MDA-MB-453 did not follow the pattern of response as the two other luminal cell lines. Similarly, MDA-MB-361 and MDA-MB-453 are HER2 amplified cell lines, yet MDA-MB-361 did not show an inverse EMT like that seen when MDA-MB-453 were subjected to lower density. Additionally, MCF10A, BT20 and MDA-MB-231 are basal-like breast cancer cell lines and only BT20 and MDA-MB-231 showed the intermediate phenotype when cultured in the seeding density experiment. Thus, these findings indicate that the molecular subtype of breast cancer cell lines did not predict their response to reduction of density, and therefore did not affect EMT associated markers and EMT-related morphological changes.

3.4 Conclusion

Reduction of cell density was applied in previous breast cancer studies and was sufficient to induce phenotypical switch and variation in cellular functions including changes in proliferation, marker expression and pathway activation. The seeding density model used in this study successfully induced EMT-like response in all of the breast cancer cell lines used provides a useful tool to investigate how cell-cell interaction can promote EMT-related changes. Furthermore, identifying the medium density anomaly was useful in capturing intermediate phenotypical switches that were previously only identified in clinical observation. Additionally, the investigation of several cell lines that belong a range of different breast cancer subtypes provides an insight into how the subclassification of breast cancer may predict a tumour's ability to undergo EMT due to changes in cell-cell interaction, which has not been attempted previously using this approach *in vitro*. It is also concluded from the use of the cell density model that the type of response could not be predicted by the subtype of breast cancer cell line.

The morphological changes associated with reduced in density were paralleled to changes in epithelial and mesenchymal marker expression (E-cadherin and vimentin). Three types of response to reducing density noted using this model. A subset of breast cancer cell lines showed mesenchymal-like morphological changes with decrease in density. Another group of breast cancer cell lines showed increase in epithelial-like phenotype with reduction in cellular density. Lastly, a group of cell lines showed intermediate state, where the cells showed mixed morphology in the medium density.

This model allowed us to identify the cell lines that can undergo an EMT-like response. Thus, this model provides a tool to study the regulation of EMT, especially by identifying the cell lines that showed the intermediate status in the medium density. MCF10A, BT20 and MDA-MB-231 cells were able to undergo stronger EMT-associated changes due to the mesenchymal molecular signature as seen in previous studies.

These findings confirm the hypothesis that the EMT is, in fact, a spectrum of changes, rather than an absolute status transition. However, the initial hypothesis that propensity to undergo EMT depends on, or can be predicted by, the subclass of breast cancer was incorrect. Although prognosis varies between tumour subtypes, they are all capable of generating life-threatening metastasis through this invasive adaption of cell phenotype.

4. Chapter four: The Expression of the Hedgehog Signalling Pathway in Breast Cancer

4.1 Introduction

Despite advances in screening, diagnosis and treatment of breast cancer, it remains the most common cause of cancer death in Europe for females and the third most common cause of cancer death overall (CRUK, 2017). In the UK the five-year survival rate of breast cancer at diagnosis drops from 99% at stage I to 15% at stage IV (CRUK, 2017). Nearly 30% of females initially diagnosed with early-stage breast cancer go on to develop metastatic disease, months or even years after initial diagnosis (Redig and McAllister, 2013).

The current clinical systems for grading, and staging, along with prognostic markers used to stratify breast cancer and predict prognosis, fall short in identifying patients with a high-risk of recurrence (Redig and McAllister, 2013). The current treatment and management strategies for advanced breast cancers include systemic chemotherapy, radiation and surgery with a goal to stabilise the disease especially in a metastatic setting (Orlando *et al.*, 2007). Thus, there is a clinical need to find reliable prognostic markers that could also be utilised for identifying either metastatic or high-risk cases. These markers could also be utilised as therapeutic targets that aid in treatment, or limit cancer invasion and subsequent metastasis.

Alteration in the components of Hh signalling are detected in 25% of human cancers (Moraes *et al.*, 2007). Overexpression of the Hh pathway signalling components *in vivo* and evidence of activation of Hh signalling in breast cancer were documented previously in *in vitro* models (Kubo *et al.*, 2004; O'Toole *et al.*, 2011). In studies conducted on clinical samples, overexpression of crucial components of the Hh pathway (including Gli1, Ptch1, and Shh) were more highly expressed in invasive carcinoma compared to normal breast tissue (Kubo *et al.*, 2004; O'Toole *et al.*, 2011). Several studies correlated the overexpression of Hh ligands with poor clinical outcomes, increased invasiveness and high-grade tumours in basal-like breast cancer (O'Toole *et al.*, 2011; Li *et al.*, 2012; Han *et al.*, 2015). Hh pathway activation associated with several clinicopathological parameters including high proliferation index, tumour size, invasion, lymph node metastasis, hormone receptor negativity and poor overall survival (Xuan and Lin, 2009; O'Toole *et al.*, 2011; Souzaki *et al.*, 2011). Im *et al.* (2013) assessed Gli1, Gli2 and Gli3 in breast cancer by tissue microarray and found they correlated with several clinicopathological parameters. Gli2, in particular,

was correlated with the worst overall survival (Im *et al.*, 2013). Concurrent activation of Hh signalling within specific molecular subtypes of breast cancer and the prognostic consequence is not fully understood and was not studied previously. More investigation is required to link changes in expression and localisation of Hh signalling proteins (Gli1, Gli2, and Gli3) to the molecular subtypes of breast cancer.

E-cadherin and β-catenin separately (or combined) are used as markers of EMT in breast cancers (Onder *et al.*, 2008; Sarrio *et al.*, 2008; Cheng *et al.*, 2012; Liu *et al.*, 2015). Localisation and distribution of both proteins changed in response to EMT stimuli (either changes in densities, or by treatment) in breast cancer cells *in vitro* (Gilles *et al.*, 2003; Sarrio *et al.*, 2008; Yan *et al.*, 2012; Shan *et al.*, 2015). Results from the previous section (3.3) showed that there was a difference in EMT regulation as a result of variation of density *in vitro*. Loss of E-cadherin, and loss or changes in the localisation of β-catenin, were reported previously in invasive breast cancer (Lin *et al.*, 2000; King *et al.*, 2012).

Most previous work investigating EMT in breast cancer assessed the expression of E-cadherin and β-catenin in human tissue sections. This was achieved through estimation of expression in the sample and correlating this with the clinicopathological criteria. Scientists have suggested that the invasive front of tumours is more suitable to investigate EMT (Bryne *et al.*, 1998; Christofori, 2006; Busch *et al.*, 2014). Therefore, several studies looked at proteins involved in EMT and compared their expression between the tumour centre and the invasive front. For example, E-cadherin and β-catenin changed in expression and intensity at the invasive front in colorectal (Zlobec and Lugli, 2009), parathyroid (Fendrich *et al.*, 2009), and oral carcinoma (Wang *et al.*, 2009). This approach of comparing E-cadherin and β-catenin expression in different regions of the tumour has not been previously reported in breast cancer, although this approach has shown promising data in other tumour types.

Concurrent activation of Wnt and Hedgehog (Hh) signalling has been reported in several human cancers including colon (Qualtrough *et al.*, 2015), ovarian (Schmid *et al.*, 2011), and basal-cell carcinoma (Yang *et al.*, 2008b; Skvara *et al.*, 2011). Arnold *et al.* (2017) found evidence that linked co-activation of Wnt and Hh signalling to poor prognosis in TNBC and decreased overall survival. Arnold *et al.* (2017) assessed nuclear localisation of Gli1 and β-catenin in human breast cancer samples. Combined analysis of the localisation of β-catenin, as well as Gli1, Gli2, and Gli3 (members of

active Wnt and Hh signalling respectively), has not been reported in previous work on mammary tumours.

Assessing E-cadherin expression in parallel with the comparative distribution and localisation of β-catenin, Gli1, Gli2, and Gli3 is vital for understanding how crosstalk between both Hh and Wnt could influence EMT in breast cancer. Also, assessment of expression and localisation of these proteins in the tumour centre compared with the invasive front could uncover correlations between changes in localisation, intensity and expression with clinicopathological criteria, tumour subtypes, lymph node invasion and metastasis. Investigating the variation in subcellular localisation and expression of β-catenin and the tissue distribution in tumour centre and at invasive front gives an indication of EMT activity. The changes in EMT at the invasive front compared to the tumour centre mimic the observed disruption in breast cancer cell lines after stimulation of EMT by reduction of density. Moreover, estimating the level of E-cadherin expression and comparing its expression in the tumour centre and at the invasive front and correlating it with the expression of β-catenin protein provides additional insight into the regulation of EMT in breast cancer. This approach of investigation has not been reported previously and could aid in the identification of invasion and/or metastatic properties during breast cancer progression.

4.2 Aim

- Investigate the expression of hedgehog signalling components in tumour centres and at invasive fronts to estimate if this pathway is involved in breast cancer progression through metastasis regulation.

4.2.1 Objectives

- To investigate and quantify the expression hedgehog signalling components (Gli1, Gli2 and Gli3) and EMT-associated proteins (E-cadherin, and β-catenin) in cohort of breast cancer samples and correlate this with the clinicopathological features and tumour subtypes.
- To assess the expression of Hh signalling components (Sonic hedgehog, Indian hedgehog, Patched, Smoothened, Gli1, Gli2, and Gli3) in a panel of breast cancer cell lines and to confirm if breast cancer cell lines can be used to further understand the regulation of EMT by Hh signalling in breast cancer.

4.3 Results

4.3.1 Validation of Gli1, Gli2, Gli3, β-catenin and E-cadherin antibodies

To assess if Hedgehog signalling proteins were expressed in breast cancer clinical samples, using serial sections of archival breast cancer tissues were sectioned and stained with either Gli1, Gli2, Gli3, β-catenin or E-cadherin antibodies (Figure 4-1). Secondary-only controls were added to confirm minimal background staining (Figure 4-1-B). Adjacent skin tissue in sections was used as positive control for Gli1, Gli2 and Gli3 staining (Figure 4-2-C, -D, and -E) (Green *et al.*, 1998; Regl *et al.*, 2002). It was also used as positive control for β-catenin and E-cadherin antibodies (Figure 4-2-B and -C). As seen in Figure 4-2-A, the level of background did not reach the level of staining intensity.

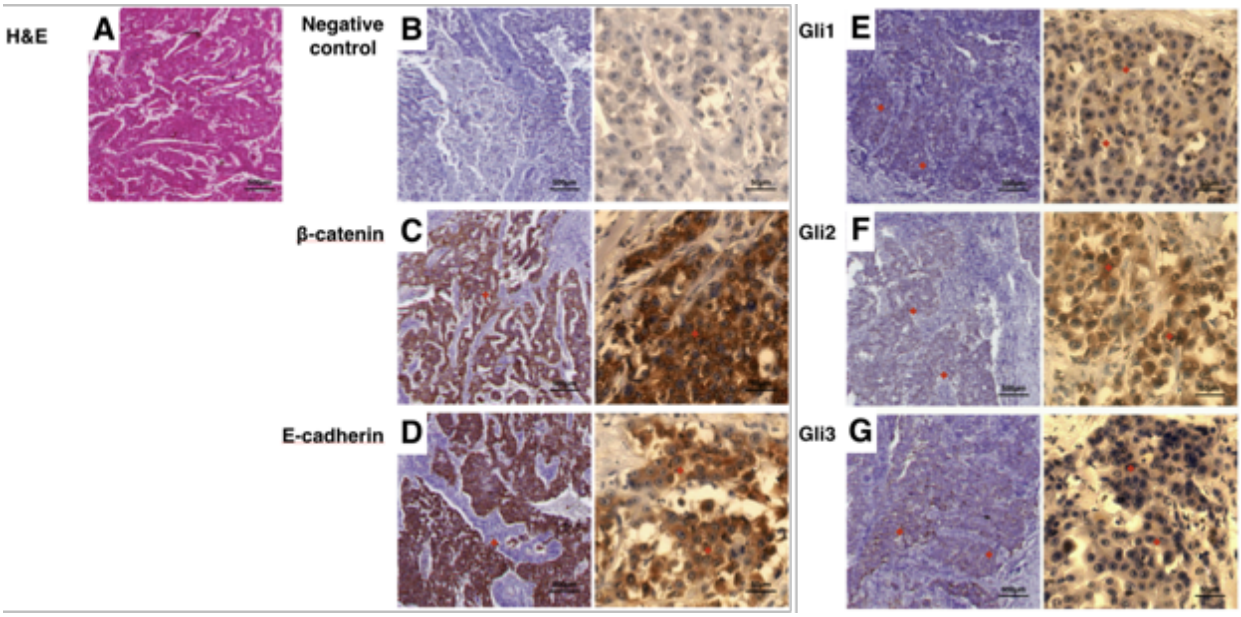

Figure 4-1, Representative IHC images of serial sections stained with the antibodies used in the study compared to the negative control.
Representative images of serial sections from the same case were stained for β-catenin (C), E-cadherin (D), Gli1 (E), Gli2 (F) and Gli3 (G) compared against the negative control (B). (♦) used in 100x images to point to the location of immune reaction and (●) used to indicate the location of immune reaction in 400x images. Images captured by Leica microscope the images (B, C, D, E, F and G) to the left were captured at 100X magnification. The images (B, C, D, E, F and G) to the right were captured at 400X magnification. Scale bars were added to the bottom right corner of images.

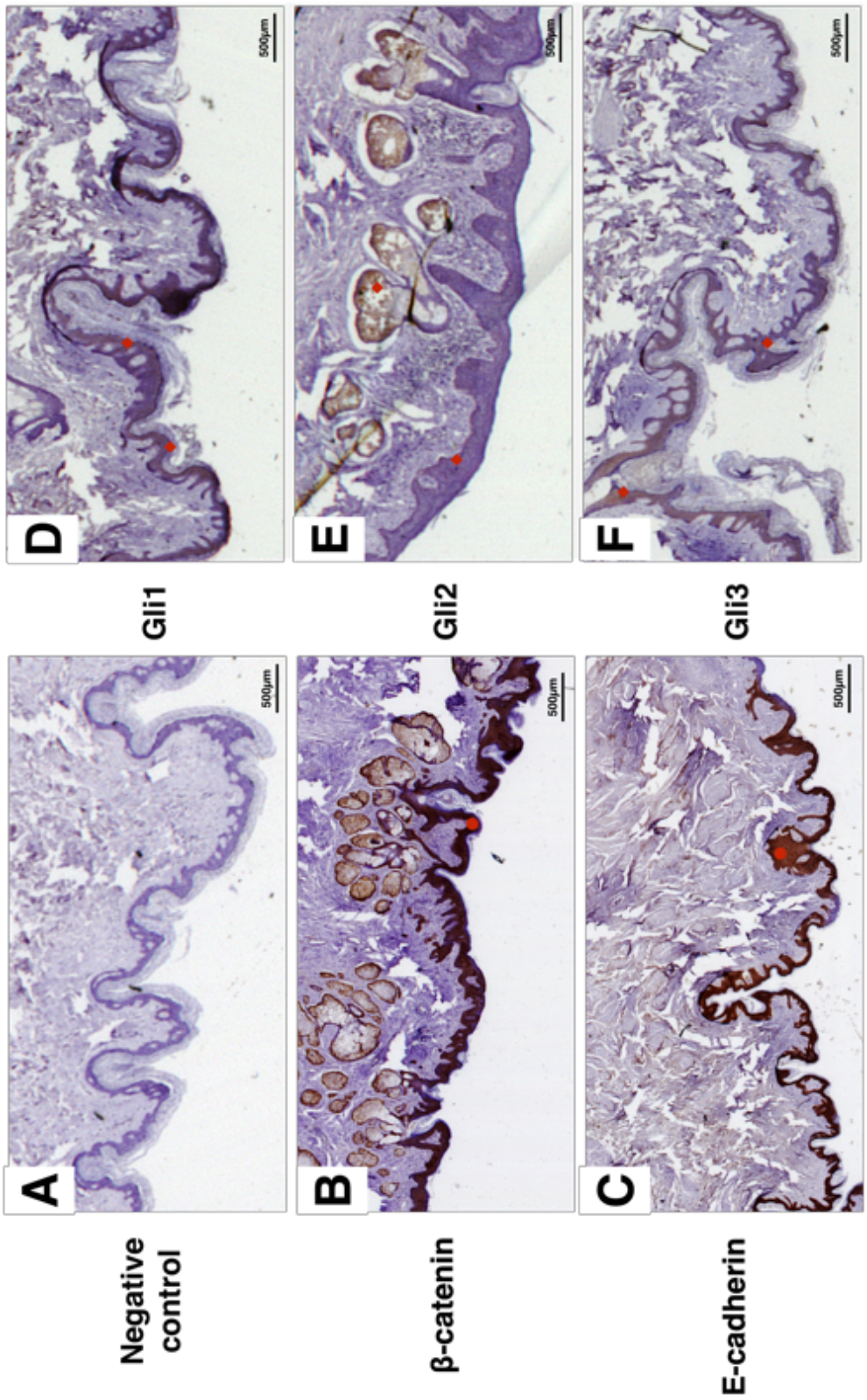

Figure 4-2, Adjacent skin tissue was used as a positive control for antibodies

Adjacent skin tissue in patient samples was used as a positive control for β-catenin (B), E-cadherin (C), Gli1 (D), Gli2 (E) and Gli3 (F). Negative control (A) showed no background staining. Images were captured by Leica microscope at 100X magnification. (♦ and •) used to indicate location of immune reaction. Scale bars were added at the bottom right corner of images.

4.3.2 Gli1, Gli2 and Gli3 were expressed in breast cancer with both nuclear and cytoplasmic distribution

Scoring of protein expression in sections was conducted following the percentage of positive tumour cells and intensity scores as seen in Figure 4-3 for Gli1, Figure 4-4 for Gli2 and Figure 4-5 for Gli3. 44 out of 48 cases (91%) were positive for Gli1, and all cases were positive for Gli2 and Gli3 (100%) as seen in Figure 4-6.

Gli1 was positive in more than half of the tumour cells in 23 out of 48 cases (48%) (Figure 4-7). 18 out of 29 cases (62%) showed more than 50% positivity for Gli2 (Figure 4-7). 22 out of 23 cases (95%) cases showed more than 50% positive tumour cells for Gli3 (Figure 4-7).

The score of Gli1 staining intensity showed that about 45%, 31% and 14% of cases had intense, moderate and mild staining respectively (Figure 4-8). Gli2 staining intensity analysis showed that almost 58%, 17% and 20% of cases had intense, moderate and mild staining respectively (Figure 4-8). The intensity of Gli3 staining showed that approximately 13%, 43% and 43% of cases had intense, moderate and mild staining intensity respectively (Figure 4-8).

The IRS class of Gli1 staining showed that 39 out of 48 cases (81%) were positive with mild to strong expression (Figure 4-9). Gli2 IRS class showed that 26 out of 29 cases (89%) were positive with either mild or strong expression (Figure 4-9). The IRS class of Gli3 showed that 20 out of 23 cases (87%) were positive with mild or strong expression (Figure 4-9).

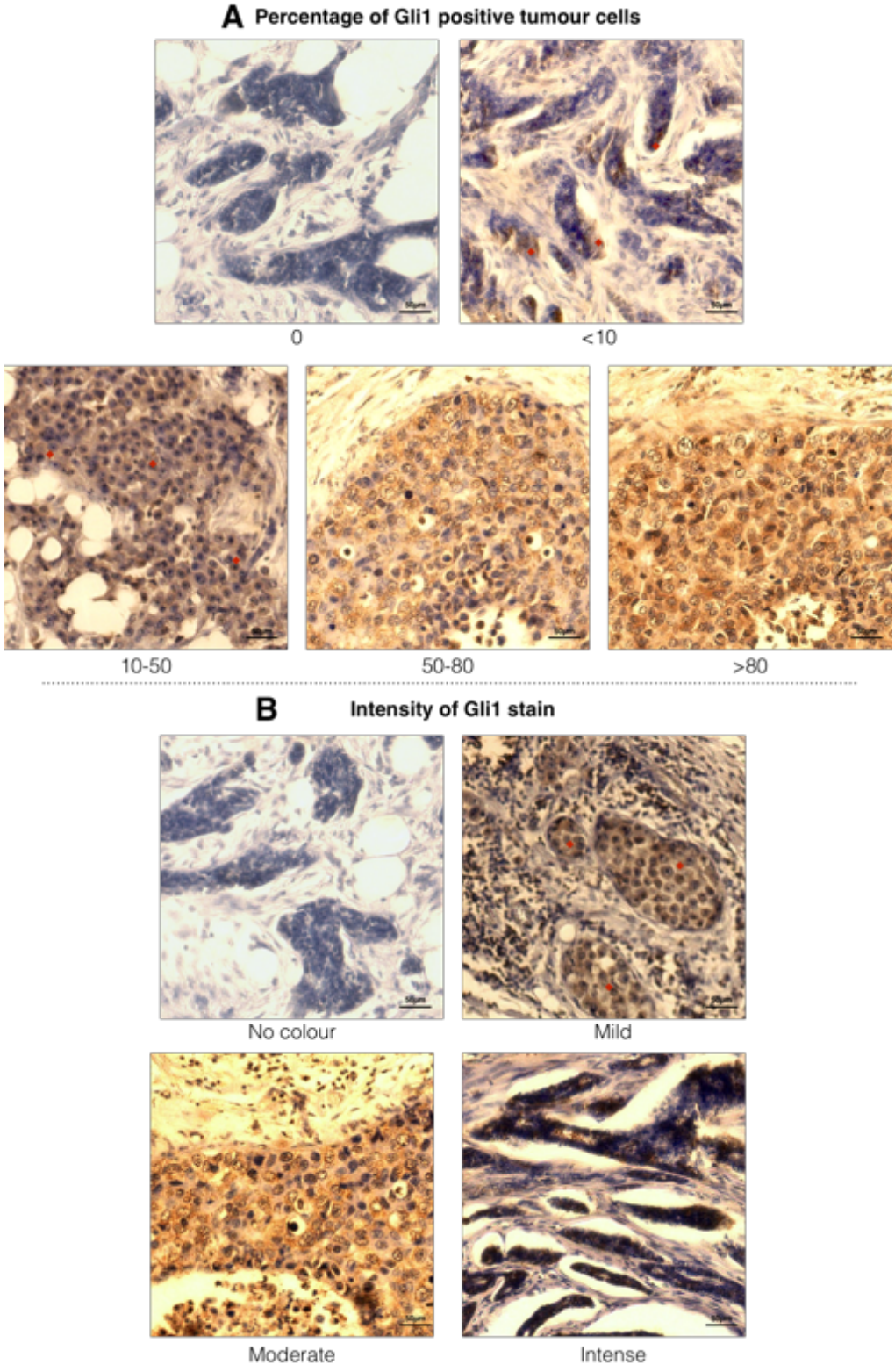

Figure 4-3, Representation of percentage of Gli1 positive tumour cells and the intensity of immune reaction in breast cancer sections

Representative sections stained for Gli1 by IHC. Images were captured by Leica microscope in 400x magnification. (A) the percentage of Gli1 positive tumour cells. (B) the intensity of the staining. Scale bars were added to the bottom right corner of each image. (♦) was used to indicate the area of positivity in images.

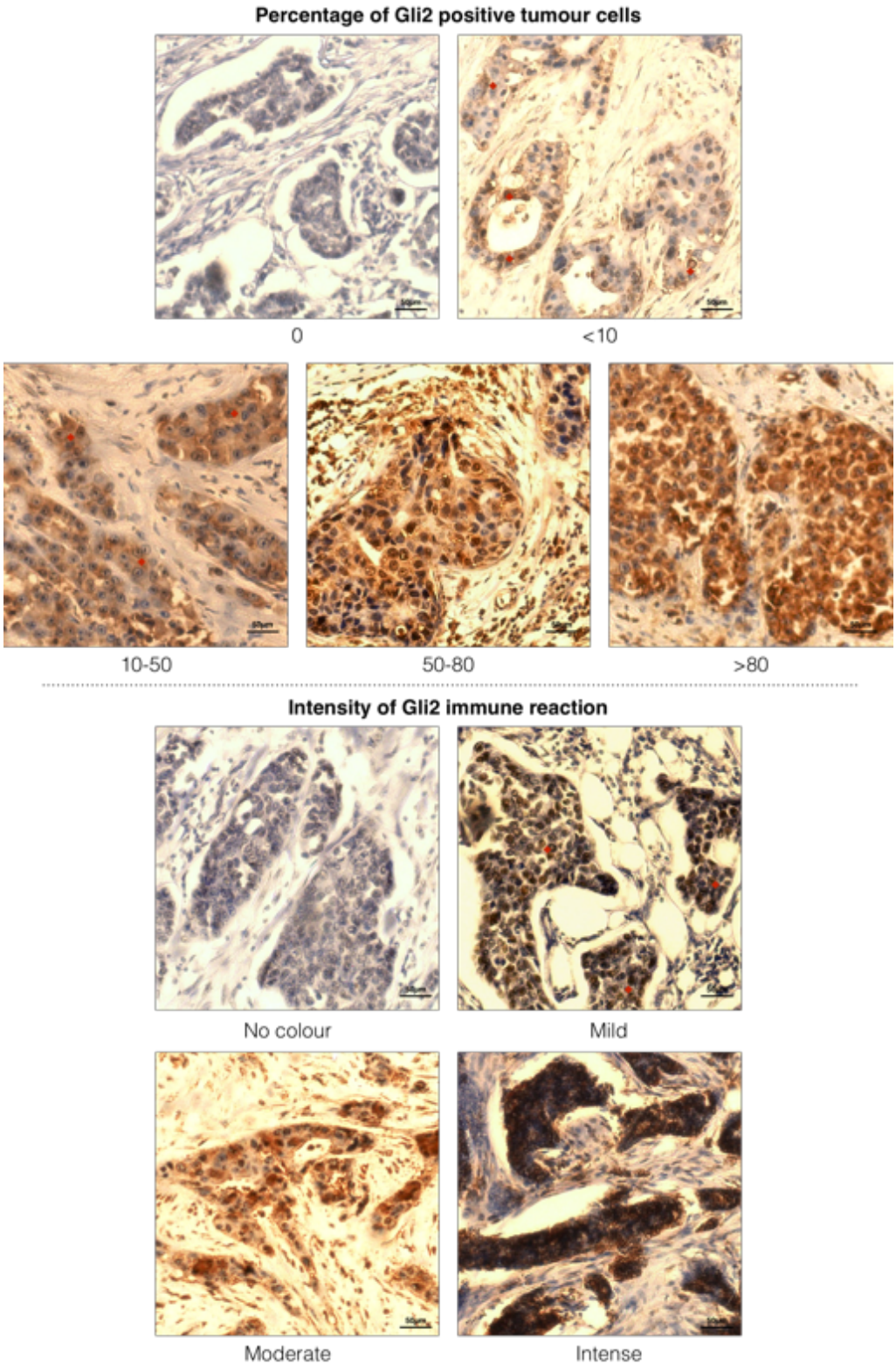

Figure 4-4, Representation of percentage of Gli2 positive tumour cells and the intensity of immune reaction in breast cancer sections

Representative sections stained for Gli2 by IHC. Images were captured by Leica microscope in 400x magnification. (A) the percentage of Gli2 positive tumour cells. (B) the intensity of the staining. Scale bars were added to the bottom right corner of each image. (♦) was used to indicate area of positivity in images.

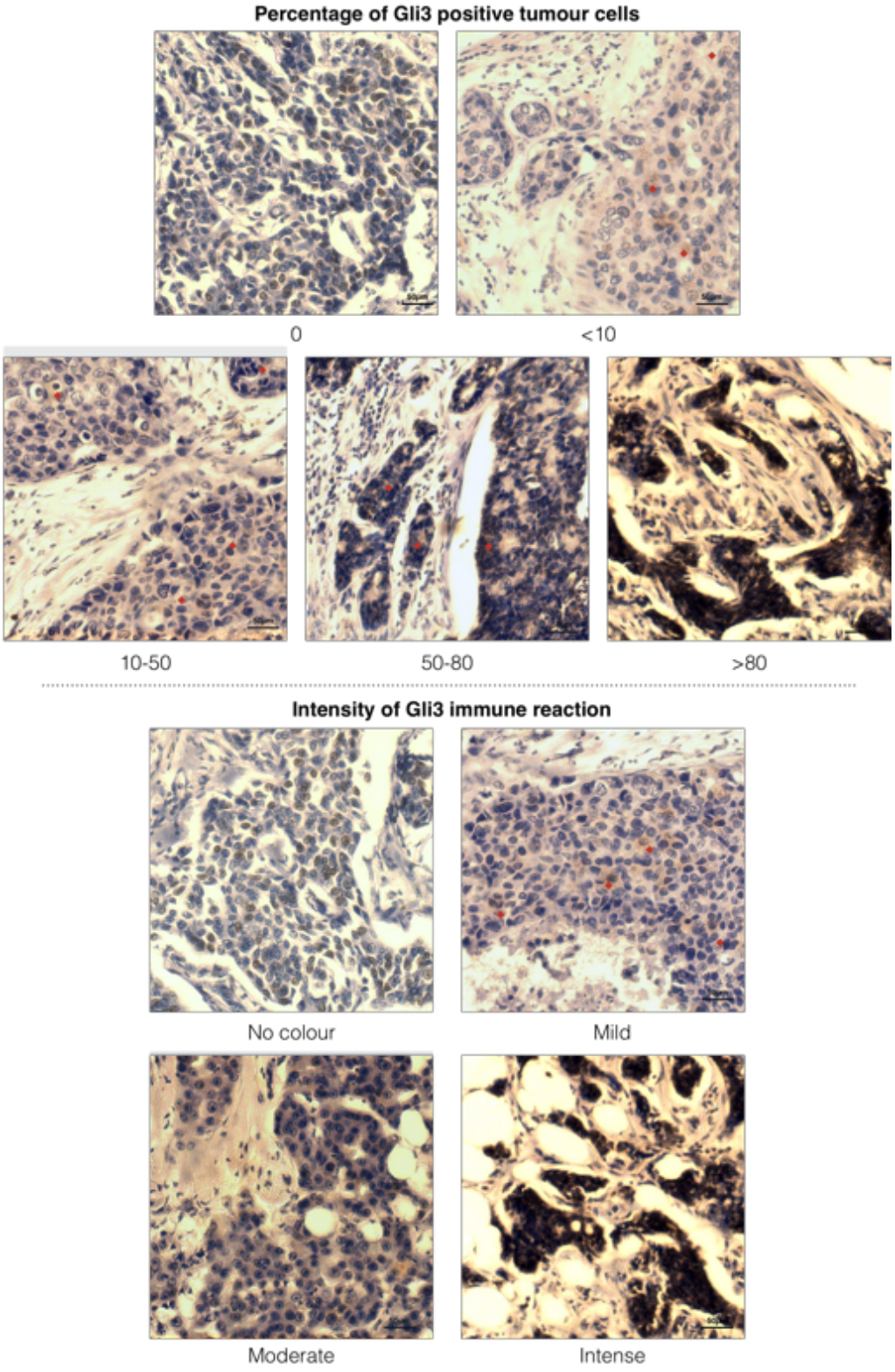

Figure 4-5, Representation of percentage of Gli3 positive tumour cells and the intensity of immune reaction in breast cancer sections

Representative sections stained for Gli3 by IHC. Images were captured by Leica microscope in 400x magnification. (A) the percentage of Gli3 positive tumour cells. (B) the intensity of the staining. Scale bars were added to the bottom right corner of each image. (♦) was used to indicate area of positivity in images.

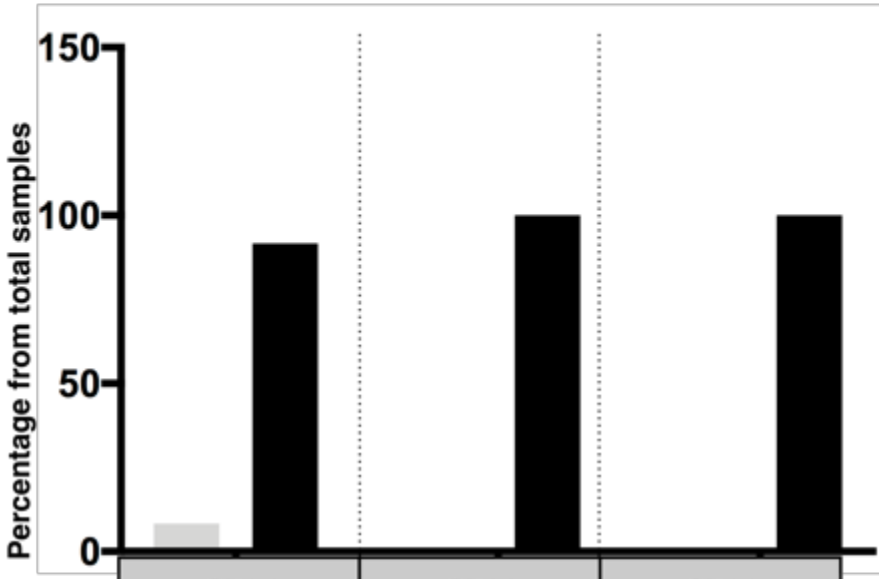

	Gli1		Gli2		Gli3	
	Number of samples	%	Number of samples	%	Number of samples	%
Negative	4	8.3	0	0	0	0
Positive	44	91.7	29	100	23	100
Total	48	100	29	100	23	100

Figure 4-6, Gli1, Gli2 and Gli3 are expressed in breast cancer samples
Bar chart presenting the percentage of (positive or negative) breast cancer samples from total cases. The table below presents the numbers of (positive or negative) samples and the corresponding percentage of expression from total cases.

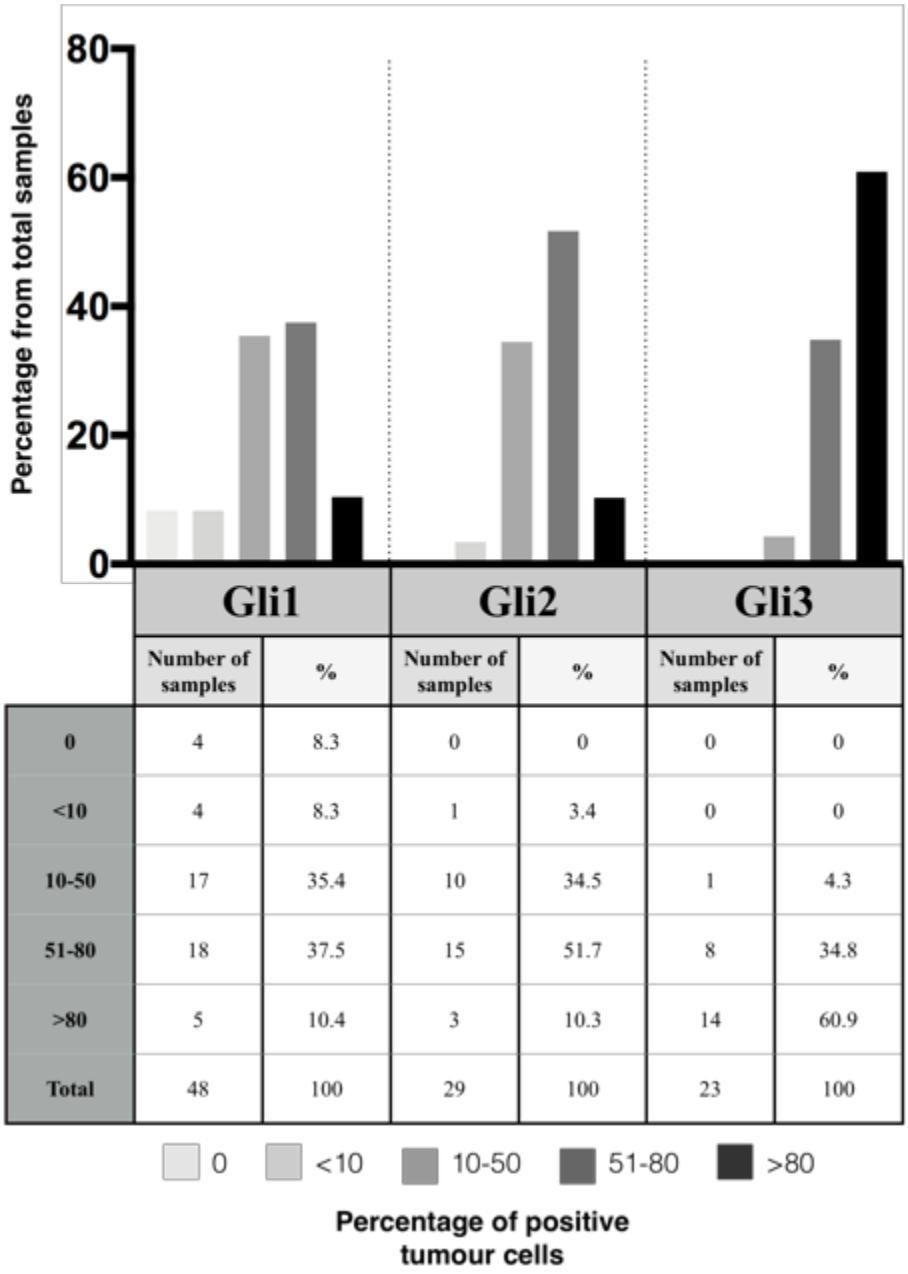

	Gli1		Gli2		Gli3	
	Number of samples	%	Number of samples	%	Number of samples	%
0	4	8.3	0	0	0	0
<10	4	8.3	1	3.4	0	0
10-50	17	35.4	10	34.5	1	4.3
51-80	18	37.5	15	51.7	8	34.8
>80	5	10.4	3	10.3	14	60.9
Total	48	100	29	100	23	100

Figure 4-7, Percentage of Gli1, Gli2 and Gli3 positive expressing cells in breast cancer samples

Bar chart presenting the percentage of (0, <10, 10-50, 51-80 and >80) breast cancer samples from total cases. The table below presents the numbers of (0. <10, 10-50, 51-80 and >80) samples and the corresponding percentage of expression from total cases.

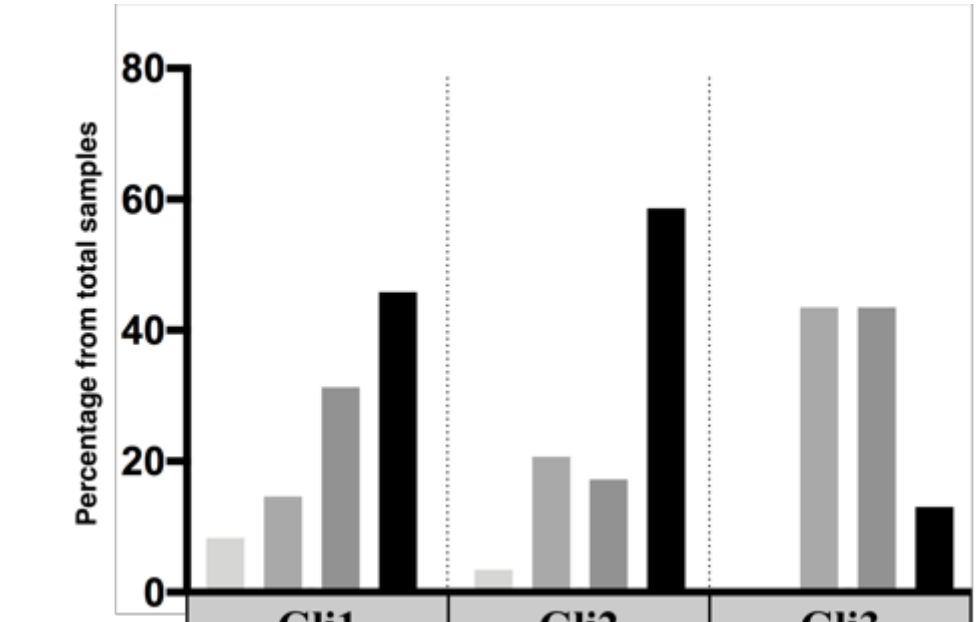

	Gli1		Gli2		Gli3	
	Number of samples	%	Number of samples	%	Number of samples	%
No staining	4	8.3	1	3.4	0	0
Mild	7	14.6	6	20.7	10	43.5
Moderate	15	31.3	5	17.2	10	43.5
Intense	22	45.8	17	58.6	3	13
Total	48	100	29	100	23	100

Figure 4-8, The intensity of Gli1, Gli2 and Gli3 staining in breast cancer samples
Bars chart of presenting the percentage of cases which show is showing (no staining, mild, moderate, and intense) of Gli1, Gli2 and Gli3 from total breast cancer samples. Table below shows the numbers of (positive or negative) breast cancer samples and the corresponding percentage from total cases.

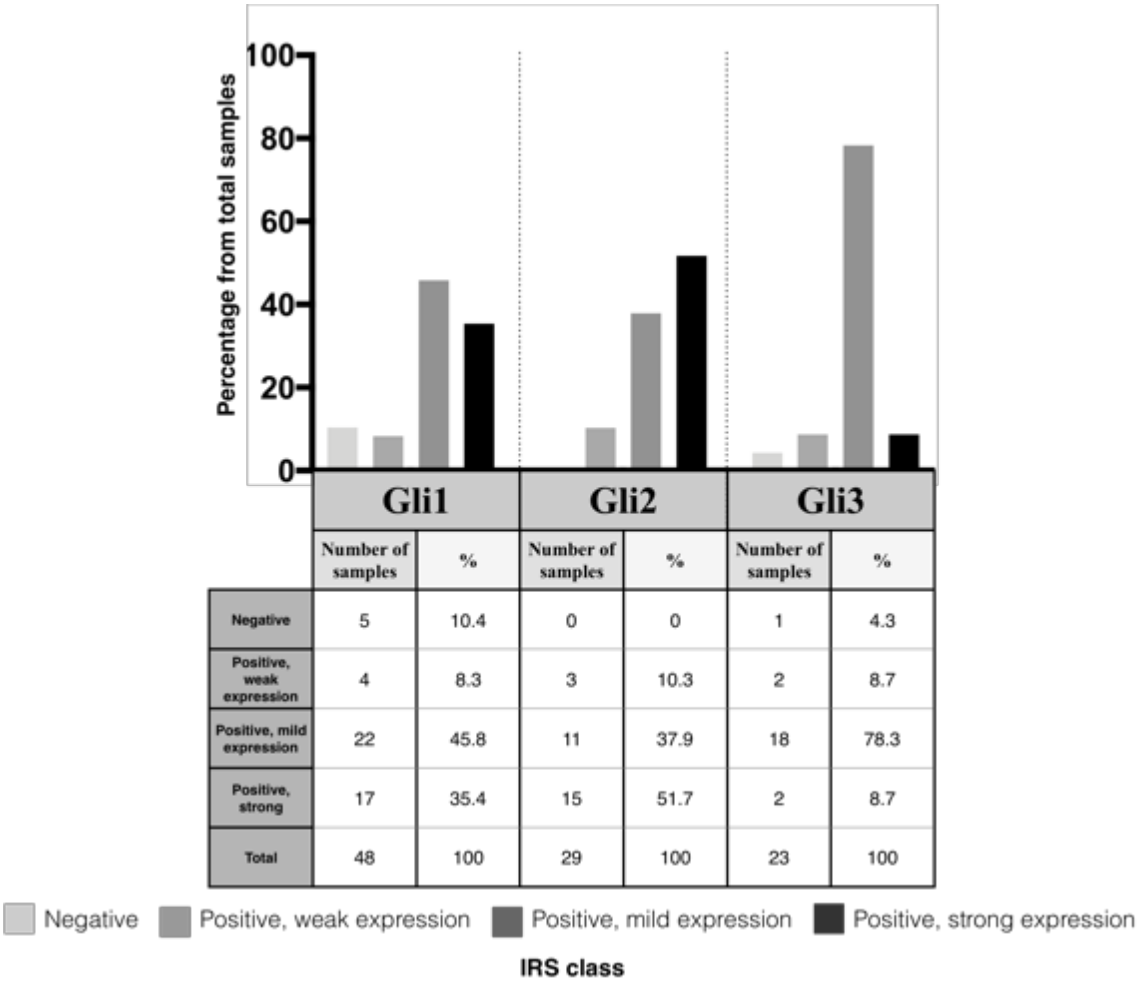

	Gli1		Gli2		Gli3	
	Number of samples	%	Number of samples	%	Number of samples	%
Negative	5	10.4	0	0	1	4.3
Positive, weak expression	4	8.3	3	10.3	2	8.7
Positive, mild expression	22	45.8	11	37.9	18	78.3
Positive, strong	17	35.4	15	51.7	2	8.7
Total	48	100	29	100	23	100

Figure 4-9, IRS classes of Gli1, Gli2 and Gli3 staining in breast cancer samples
Bars chart of presenting the percentage of cases which show (negative, positive with weak expression, positive with mild expression and positive with strong expression) of Gli1, Gli2 and Gli3 from total breast cancer samples. Table below shows the numbers of (negative, positive with weak expression, positive with mild expression and positive with strong expression) breast cancer samples and the corresponding percentage from total cases.

A mixture of both cytoplasmic only, nuclear only or both cytoplasmic and nuclear staining was detected for Gli1, Gli2 and Gli3 in the breast cancer tissue (Figure 4-10). The immunoreactivity was often diffuse and sometimes showed low intensity especially in the case of Gli3. Final sample number of cases assessed for Gli1, Gli2 and Gli3 were 48, 29 and 23, respectively. The clinicopathological criteria of the cases are summarised in Table 11-1.

31 out of 48 (64.6%) cases showed nuclear localisation of Gli1, 29 cases (100%) showed nuclear localisation of Gli2 and 20 out of 23 cases (87%) showed nuclear localisation of Gli3 (Figure 4-11).

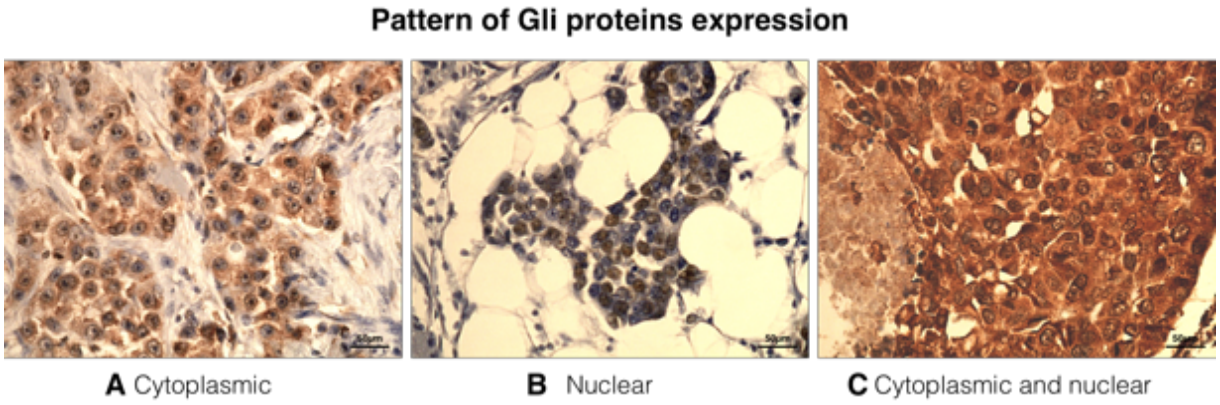

Figure 4-10, Cellular distribution of Gli proteins in representative sections containing breast cancer tissue

Representative sections stained for either Gli2, Gli2 or Gli3. Sections were selected to highlight the distribution pattern of Gli proteins in breast tissue. (A) section showing cytoplasmic distribution, (B) section showing nuclear distribution and (C) section showing both nuclear and cytoplasmic distribution. All images were captured by Leica microscope at 600x

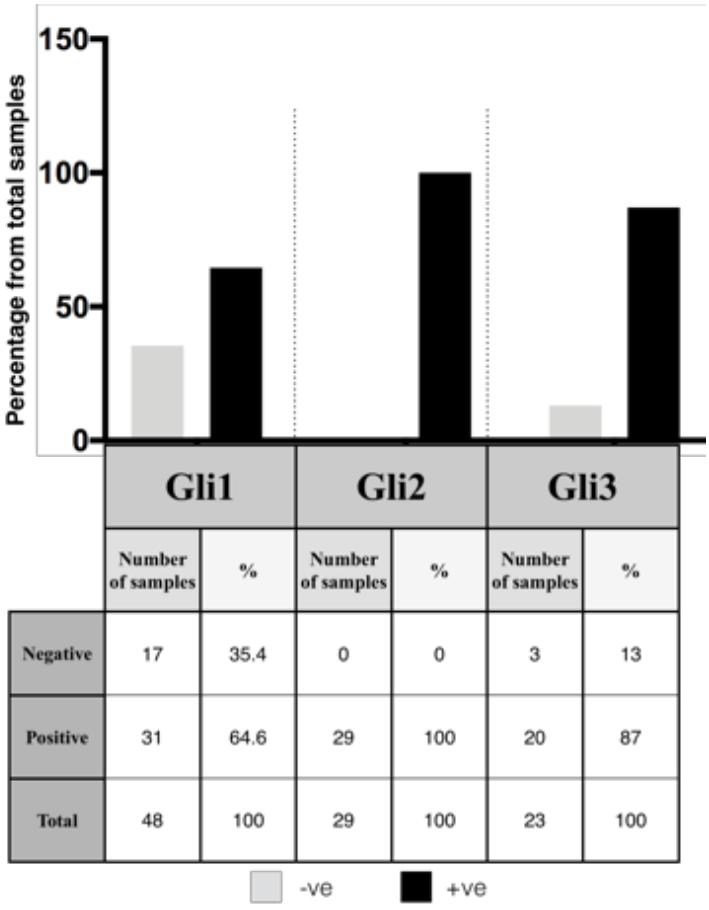

	Gli1		Gli2		Gli3	
	Number of samples	%	Number of samples	%	Number of samples	%
Negative	17	35.4	0	0	3	13
Positive	31	64.6	29	100	20	87
Total	48	100	29	100	23	100

Figure 4-11, Nuclear localisation of Gli1, Gli2 and Gli3 in breast cancer samples

Bars chart of presenting the percentage of cases which shows (positive or negative) localisation of Gli1, Gli2 and Gli3 from total breast cancer samples. Table below shows the numbers of (positive or negative) breast cancer samples and the corresponding percentage from total cases.

4.3.3 Increased Gli expression was observed at the invasive front of breast cancer samples

To evaluate the correlation between hedgehog signalling and breast cancer metastasis, the expression of Gli1, Gli2 and Gli3 were assessed both within the tumour centres and also at the invasive fronts. Pearson chi-square statistical analysis were conducted to compare the difference in percentage, intensity or IRS class staining of Gli1, Gli2 and Gli3 in tumour centre and at invasive front. Kendell's tau B test was used to assess for correlation between the Gli1, Gli2 and Gli3 percentage, intensity or IRS class of staining in tumour centre and at invasive front.

The percentage of positive tumour cells for Gli1 and Gli2 was significantly higher at the invasive front compared to the tumour centre (*p*-value= 0.0001 and *p*-value= 0.0001, respectively) (Table 4-1-A and

Table 4-2-A). Intensity and IRS scores of Gli1 and Gli2 staining were both higher at the invasive front compared with the tumour centre (*p*-value= 0.0001 and *p*-value= 0.0001, respectively) (Table 4-1-B and C,

Table 4-2-B and D). There was no significant difference between the percentage, intensity and IRS class of Gli3 in the tumour centre and at the invasive front (Table 4-3-A, -B and -C).

There was significant correlation between the percentages, intensities and IRS classes of Gli1, Gli2 and Gli3 in tumour centres and invasive fronts. this indicate that as the percentage, intensity or IRS class of Gli1, Gli2 and Gli3 increases in the tumour centre, it correspondingly increases at the invasive front of the same case. The percentage, intensity and IRS class of Gli1 in tumour centre were significantly correlated (*p-value*=0.0001 in all) with those at invasive front (Table 4-1-A, -B and -C, Figure 4-12-A, and -B, and Figure 4-13-A, -B and -C) with the highest correlation seen

between the IRS class followed by the intensity. The percentage, intensity and IRS class of Gli2 staining in tumour centre were significantly correlated (*p-value*=0.0001 in all) with that at invasive front. Similar to Gli1, Gli2 the IRS class had the highest correlation followed by intensity (0.683 and 0.656 respectively) (Table 4-2-A, -B and -C, Figure 4-14-A and -B, and Figure 4-15-A, -B and -C). Gli3 staining percentage, intensity and IRS class in tumour centre and invasive front were significantly correlated (*p-value*=0.034, *p-value*=0.007 and *p-value*=0.036 respectively). The highest correlation of Gli3 was seen in comparing intensity and IRS class (0.603 and 0.481 correlation coefficient respectively) in tumour centre and at invasive front.

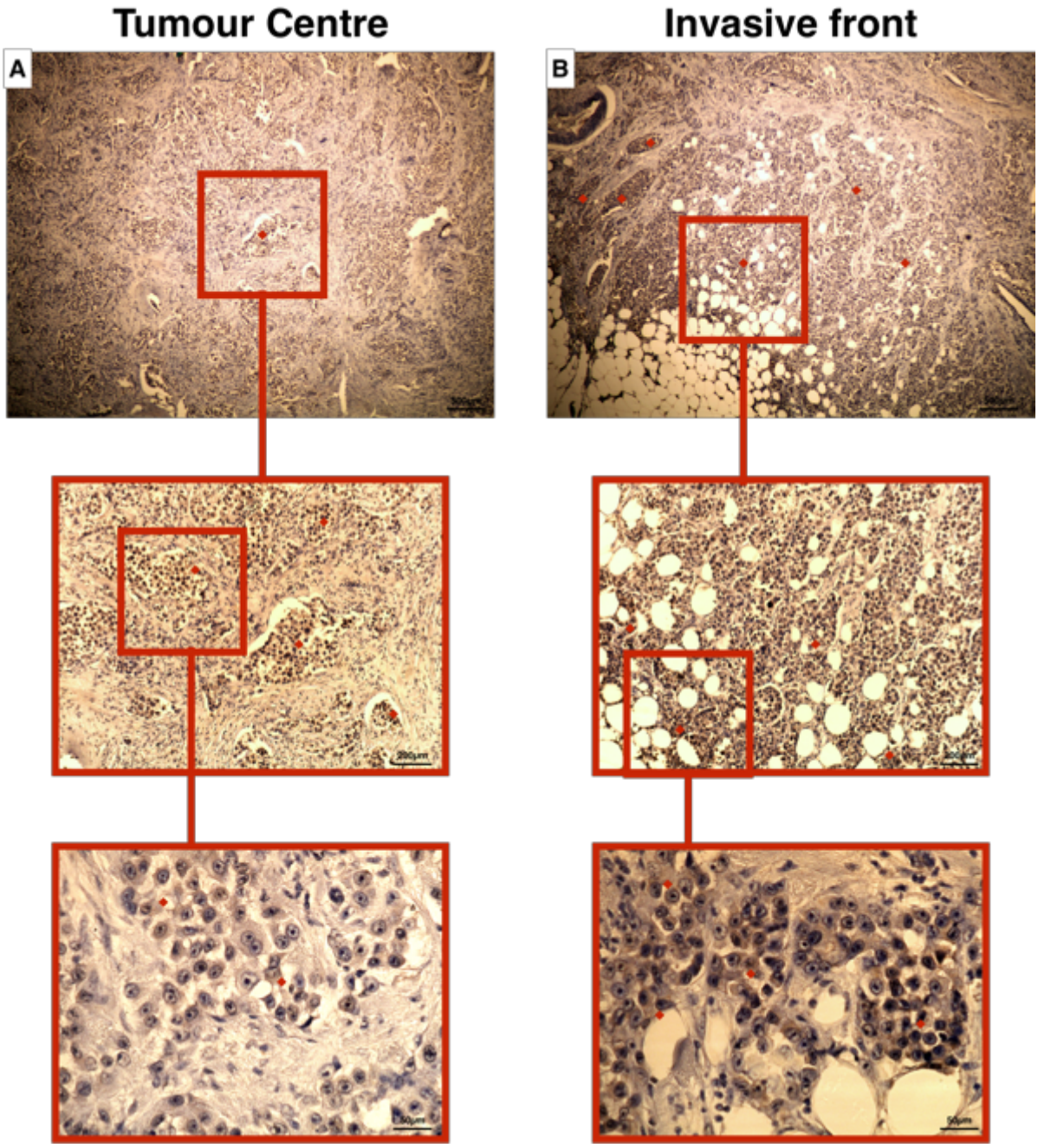

Figure 4-12, Gli1 expression was higher in invasive fronts of breast cancer samples
Representative IHC images of the same breast cancer sample showing higher Gli1 levels in the invasive front (B) compared to the tumour centre (A). Images were captured using three different magnifications (100X, 200X and 400X) by the Leica microscope. (♦) was used to indicate area of positivity in images.

Table 4-1: Percentage of positive tumour cells, staining intensity and IRS class of Gli1 showed significant difference between tumour centre and invasive front
Tumour centre and invasive front frequency tables (A) for percentage of positive tumour cells, (B) intensity of staining, and (C) IRS class. Pearson Chi-square test was used to estimate the difference between tumour centre and invasive front. The Kendall's Tau B correlation coefficient (between -1 and +1) was used to assess for degree of correlation between tumour centre and invasive front. The statistical significance of the correlation is indicated as follows: *P= <0.05, **P= <0.01.

A		Tumour centre	Invasive front
		No. (%)	No. (%)
Percentage of positive tumour cells	0	2 (4.2)	2 (5.4)
	<10	4 (8.3)	1 (2.7)
	10-50	11 (22.9)	4 (10.8)
	51-80	22 (45.8)	19 (51.4)
	>80	9 (18.8)	11 (29.7)
	Total	48 (100)	37 (100)
	Missing	0	11 (22.9)
	Total	48 (100)	48 (100)
Pearson Chi-Square		0.0001***	
p-value		0.0001	
Tau B		0.458**	

B		Tumour Centre	Invasive front
		No. (%)	No. (%)
Intensity of staining	No colour	8 (16.7)	5 (13.5)
	Mild	9 (18.8)	2 (5.4)
	Moderate	12 (25)	10 (27)
	Intense	19 (39.6)	20 (54.1)
	Total	48 (100)	37 (100)
	Missing	0	11 (22.9)
	Total	48 (100)	48 (100)
Pearson Chi-Square		0.0001***	
p-value		0.0001	
Tau B		0.687**	

C		Tumour Centre	Invasive front
		No. (%)	No. (%)
IRS class	Negative	9 (18.8)	5 (13.5)
	Positive, weak expression	8 (16.7)	3 (8.1)
	Positive, mild expression	17 (35.4)	12 (32.4)
	Positive, strong expression	14 (29.2)	17 (45.9)
	Total	48 (100)	37 (100)
	System	0	11 (22.9)
	Total	48 (100)	48 (100)
Pearson Chi-Square		0.0001***	
p-value		0.0001	
Tau B		0.771**	

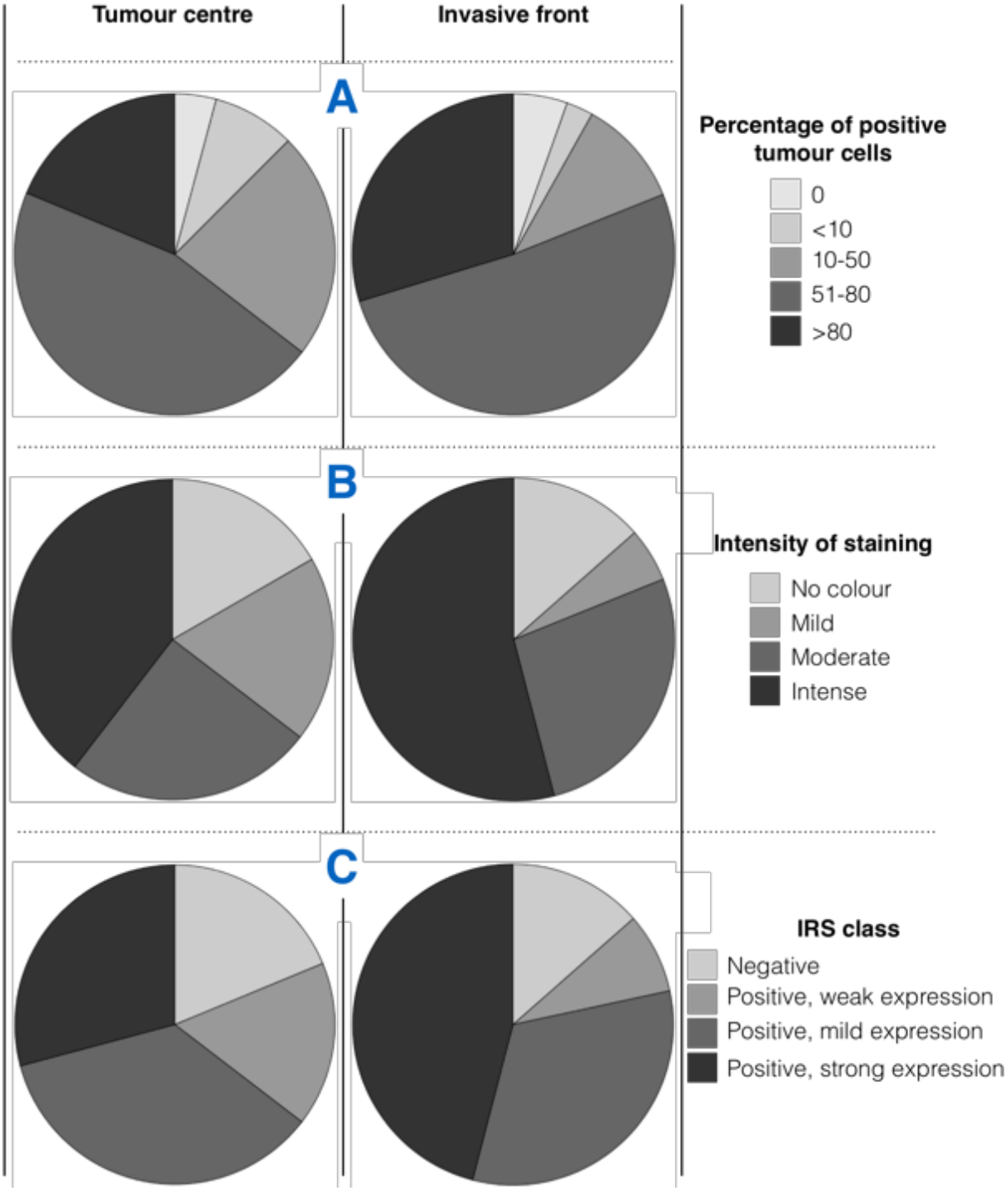

Figure 4-13, Gli1 expression was higher at invasive fronts in breast cancer cohort
Figure showing comparison of Gli1 levels in tumour centres (to the left) compared to the invasive front (to the right). (A) comparison of percentage of positive cells. (B) comparison of intensity of staining. (C) comparison of IRS class.

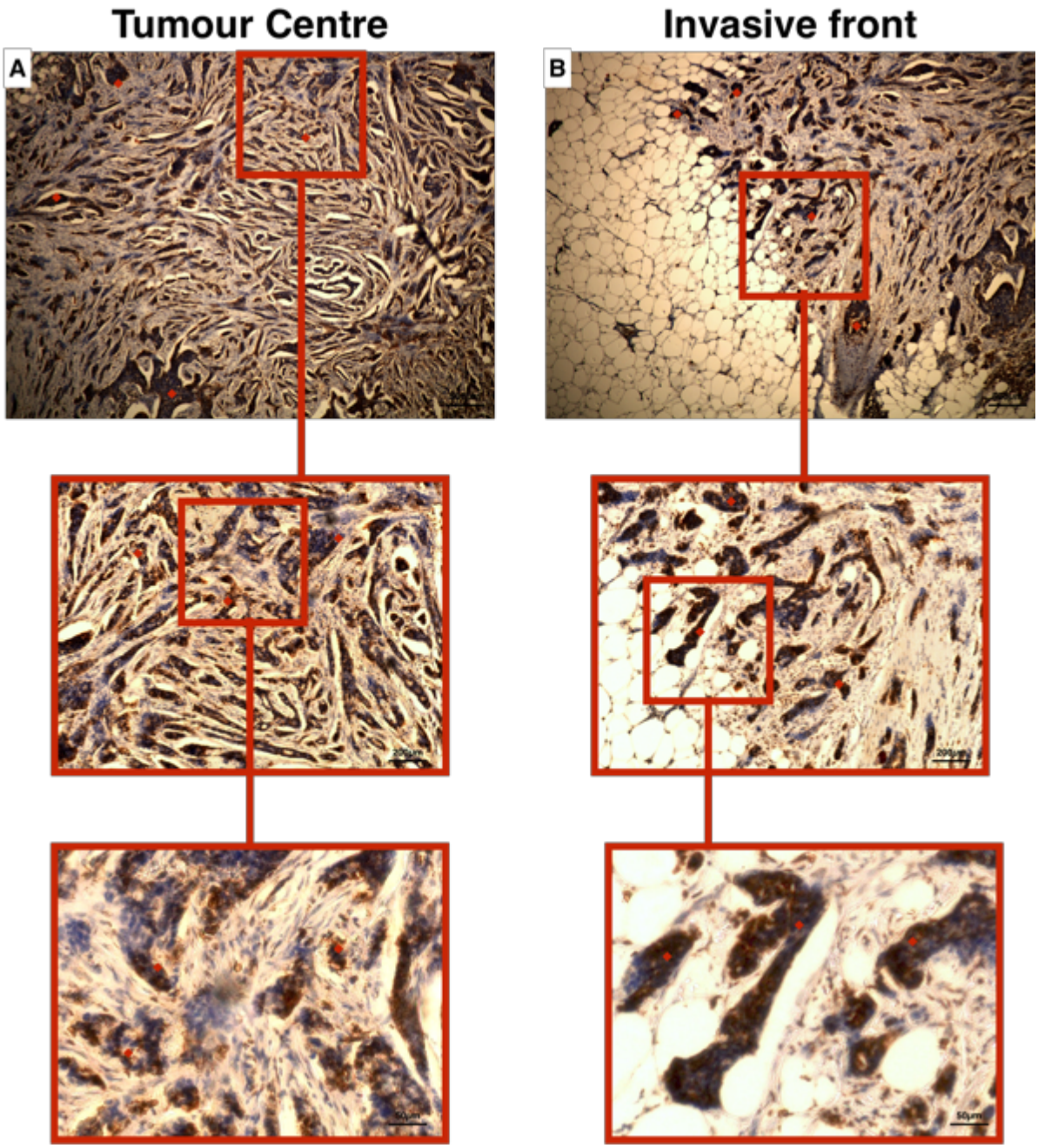

Figure 4-14, Gli2 expression was higher in invasive fronts of breast cancer samples
Representative IHC images of the same breast cancer sample showing higher Gli2 levels in the invasive front (B) compared to the tumour centre (A). Images were captured using three different magnifications (100X, 200X and 400X) by the Leica microscope. (♦) was used to indicate area of positivity in images.

Table 4-2: Percentage of positive tumour cells, staining intensity and IRS class of Gli2 showed significant difference between tumour centre and invasive front

Tumour centre and invasive front frequency tables (A) for percentage of positive tumour cells, (B) intensity of staining, and (C) IRS class. Pearson Chi-square test was used to estimate the difference between tumour centre and invasive front. The Kendall's Tau B correlation coefficient (between -1 and +1) was used to assess for degree of correlation between tumour centre and invasive front. The statistical significance of the correlation is indicated as follows: *P= <0.05, **P= <0.01.

Percentage of positive tumour cells	A	Tumour centre	Invasive front
		No. (%)	No. (%)
	0	0	0
	<10	2 (6.9)	2 (6.9)
	10-50	9 (31)	1 (3.4)
	51-80	4 (13.8)	7 (24.1)
	>80	14 (48.3)	19 (65.5)
	Total	29 (100)	29 (100)
Pearson Chi-Square		0.0001***	
p-value		0.0001	
Tau B		0.661**	

Intensity of staining	B	Tumour centre	Invasive front
		No. (%)	No. (%)
	No colour	1 (3.4)	0
	Mild	6 (20.7)	4 (13.8)
	Moderate	11 (37.9)	8 (27.6)
	Intense	11 (37.9)	17 (58.6)
	Total	29 (100)	29 (100)
Pearson Chi-Square		0.0001***	
p-value		0.0001	
Tau B		0.656**	

IRS class	C	Tumour centre	Invasive front
		No. (%)	No. (%)
	Negative	2 (6.9)	2 (6.9)
	Positive, weak expression	3 (10.3)	1 (3.4)
	Positive, mild expression	13 (44.8)	9 (31)
	Positive, strong expression	11 (37.9)	17 (58.6)
	Total	29 (100)	29 (100)
Pearson Chi-Square		0.0001***	
p-value		0.0001	
Tau B		0.683**	

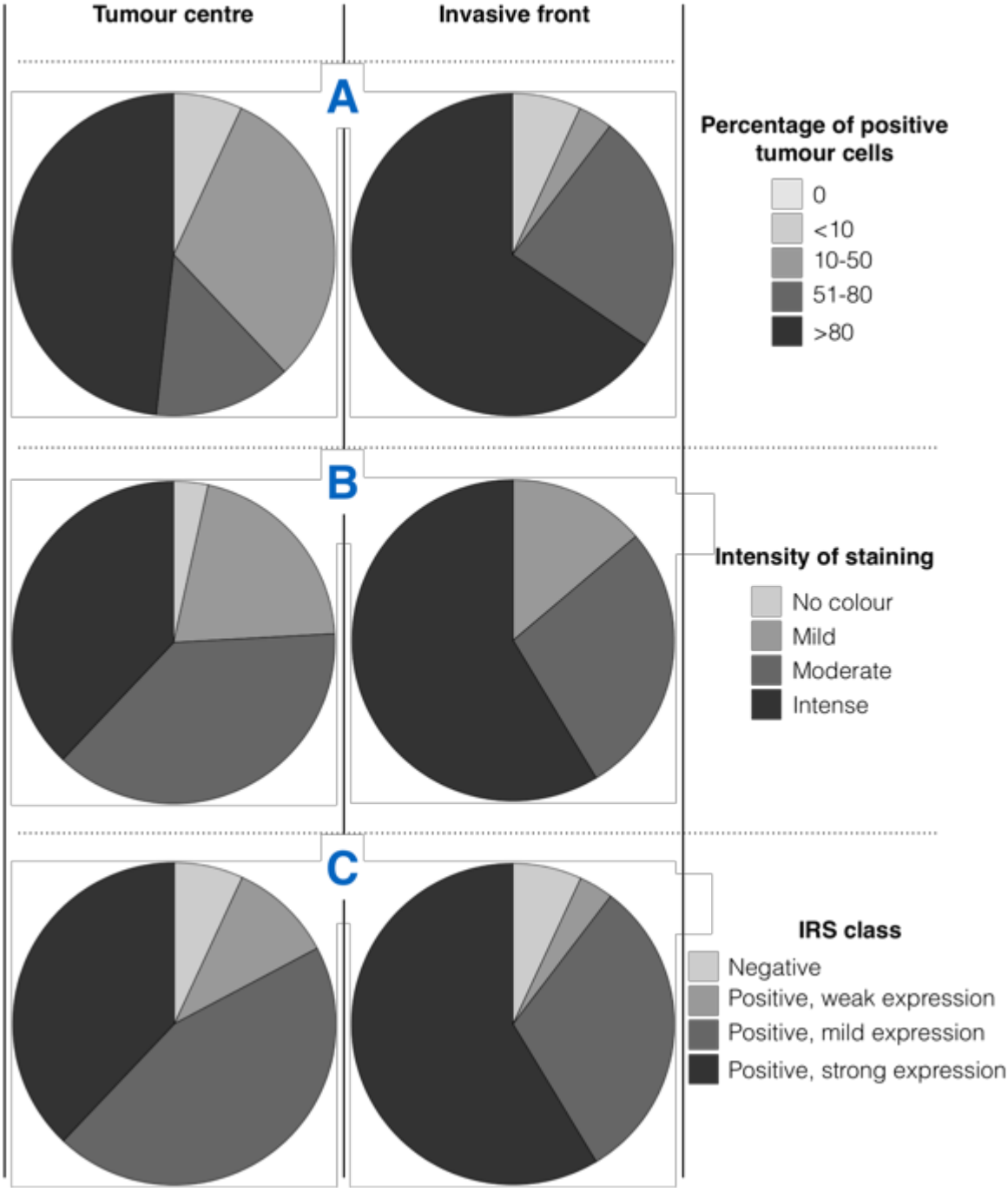

Figure 4-15, Gli2 expression was higher at invasive fronts in breast cancer cohort
Figure showing comparison of Gli2 in tumour centres (to the left) compared to the invasive front (to the right). (A) comparison of percentage of positive cells. (B) comparison of intensity of staining. (C) comparison of IRS class.

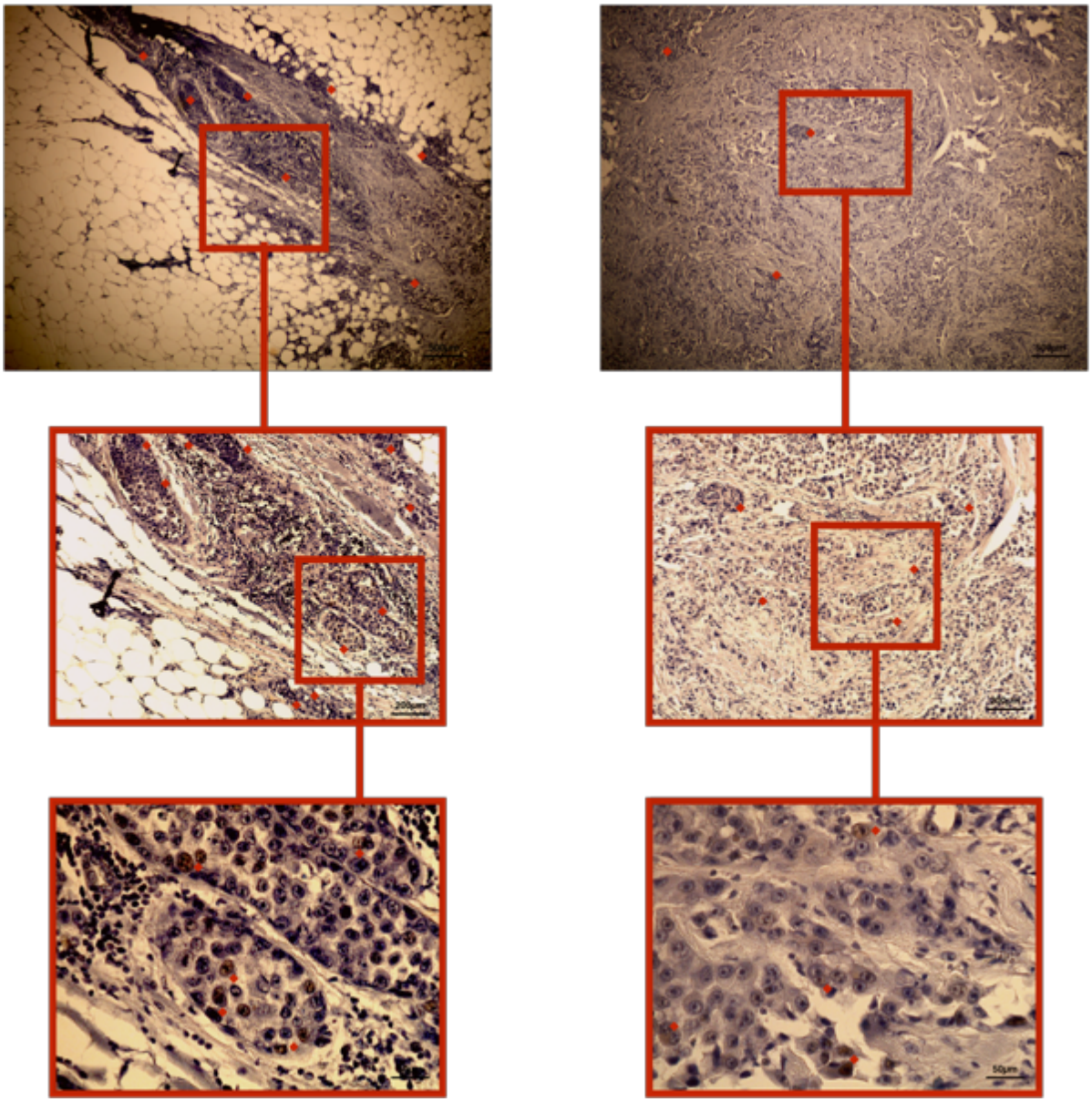

Figure 4-16, Gli3 expression was higher in invasive fronts of breast cancer samples
Representative IHC images of the same breast cancer sample showing higher Gli2 in the invasive front (B) compared to the tumour centre (A). Images were captured using three different magnifications (100X, 200X and 400X) by the Leica microscope. (♦) was used to indicate area of positivity in images.

Table 4-3: Correlation between Gli3 staining percentage, intensity and IRS class in tumour centres and that at invasive front

Tumour centre and invasive front frequency tables (A) for percentage of positive tumour cells, (B) intensity of staining, and (C) IRS class. Pearson Chi-square test was used to estimate the difference between tumour centre and invasive front. The Kendall's Tau B correlation coefficient (between -1 and +1) was used to assess for degree of correlation between tumour centre and invasive front. The statistical significance of the correlation is indicated as follows: *P= <0.05, **P= <0.01.

	A	Tumour centre	Invasive front
		No. (%)	No. (%)
Percentage of positive tumour cells	0	0	0
	<10	1 (4.3)	0
	10-50	7 (30.4)	0
	51-80	7 (30.4)	6 (33.3)
	>80	8 (34.8)	12 (66.7)
	Total	23 (100)	18 (100)
	Missing	0	5 (21.7)
	Total	23 (100)	23 (100)
Pearson Chi-Square		0.154	
p-value		0.034	
Tau B		0.477*	

	B	Tumour centre	Invasive front
		No. (%)	No. (%)
Intensity of staining	No colour	0	0
	Mild	11 (47.8)	2 (11.1)
	Moderate	8 (34.8)	10 (55.6)
	Intense	4 (17.4)	6 (33.3)
	Total	23 (100)	18 (100)
	Missing	0	5 (21.7)
	Total	23 (100)	23 (100)
Pearson Chi-Square		0.079	
p-value		0.007	
Tau B		0.602**	

	C	Tumour centre	Invasive front
		No. (%)	No. (%)
IRS class	Negative	1 (4.3)	0
	Positive, weak expression	8 (34.8)	0
	Positive, mild expression	11 (47.8)	12 (66.7)
	Positive, strong expression	3 (13)	6 (33.3)
	Total	23 (100)	18 (100)
	Missing	0	5 (21.7)
	Total	23 (100)	23 (100)
Pearson Chi-Square		0.124	
p-value		0.036	
Tau B		0.481*	

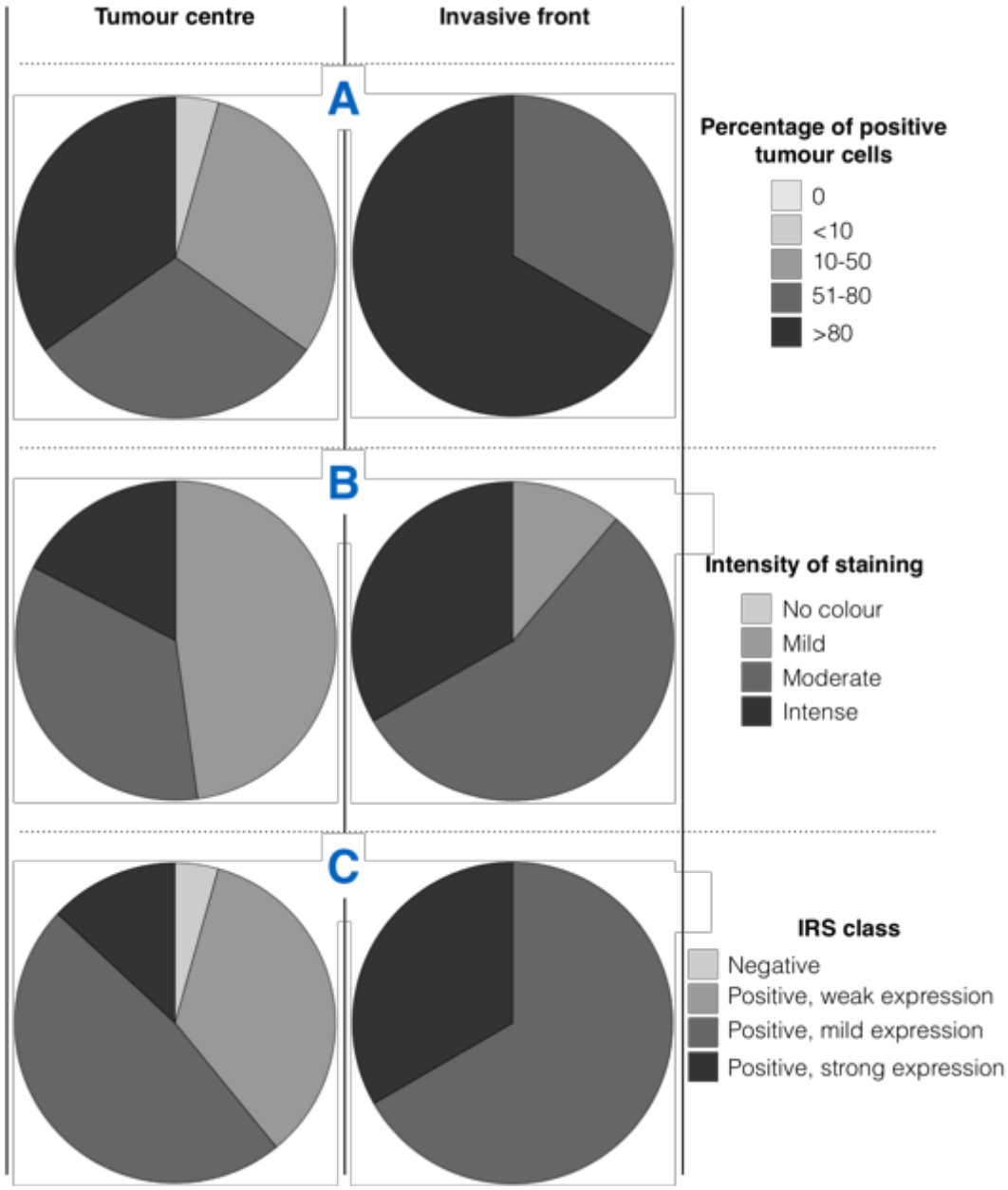

Figure 4-17, Gli3 expression was higher at invasive fronts in breast cancer cohort
Figure showing comparison of Gli2 in tumour centres (to the left) compared to the invasive front (to the right). (A) comparison of percentage of positive cells. (B) comparison of intensity of staining. (C) comparison of IRS class.

4.3.4 Increased nuclear localisation of Gli proteins observed at the invasive front of breast cancer samples

The nuclear localisation of Gli1, Gli2 and Gli3 was higher at invasive front compared to that in tumour centres as seen in representative images (Figure 4-18, Figure 4-19 and Figure 4-20). Pearson Chi-square analysis was used to assess if the difference between the nuclear localisation of Gli1, Gli2 and Gli3 in tumour centre and at invasive fronts were significant (summarised in Table 4-4-A, -B and -C). Also, Kendall's Tau B test was used to assess for the correlation between the nuclear localisation in tumour centres and invasive fronts of Gli1, Gli2 and Gli3 staining (summarised in Table 4-4-A, -B and -C).

The invasive front was identified in 37 out of 48 cases analysed for Gli1. Gli1 was observed in 31 out of 48 cases (65%) in tumour centres and 27 out of 37 cases at invasive fronts (73%) was observed (Table 4-4-A). the invasive front was identified in all the cases analysed for Gli2. All cases were positive for nuclear Gli2 (29 cases) in the tumour centre and at the invasive front (Table 4-4-B and Figure 4-21-B). The invasive front was identified in 16 out of 23 cases analysed for Gli3. Of 23 cases, 97 (87%) tumour centres and 16 (96%) invasive fronts were negative for Gli3 (Table 4-4-C and Figure 4-21-C).

Nuclear localisation was more evident in the invasive front compared to the tumour centres for Gli1 (Figure 4-18), Gli2 (Figure 4-19) and Gli3 (Figure 4-20) (*p*-value= 0.0001, *p*-value=0.002 and *p*-value=0.002, respectively) (Table 4-4-A, Figure 4-21-A, Table 4-4-B, Figure 4-21-B, Table 4-4-C and Figure 4-21-C). The nuclear localisation of Gli1, Gli2 and Gli3 at the invasive front had a significantly positive correlation with that in the tumour centre (*p-value*=0.0001, *p-value*=0.001 and *p-value*=0.002) (Table 4-4-A, Table 4-4-B and Table 4-4-C).

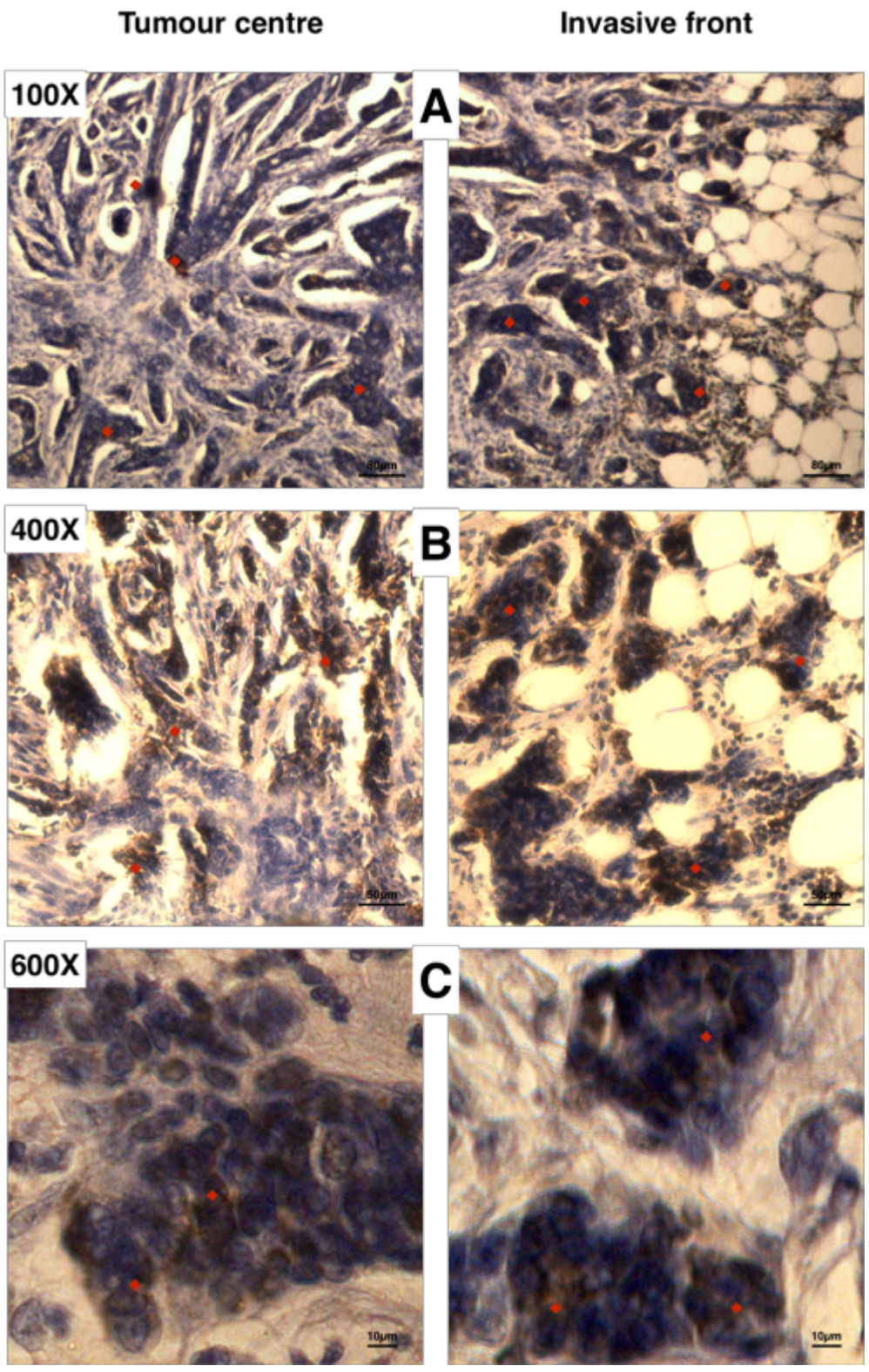

Figure 4-18, Nuclear expression of Gli1 in tumour cells is higher in invasive front of breast cancer

Representative IHC images of the same breast cancer sample showing increased nuclear localisation of Gli1 in tumour cells in the invasive front (to right) compared to the tumour centre (to left). Images were captured using three different magnifications (100X, 400X and 600X) by the Leica microscope. (♦) was used to indicate area of positivity in images.

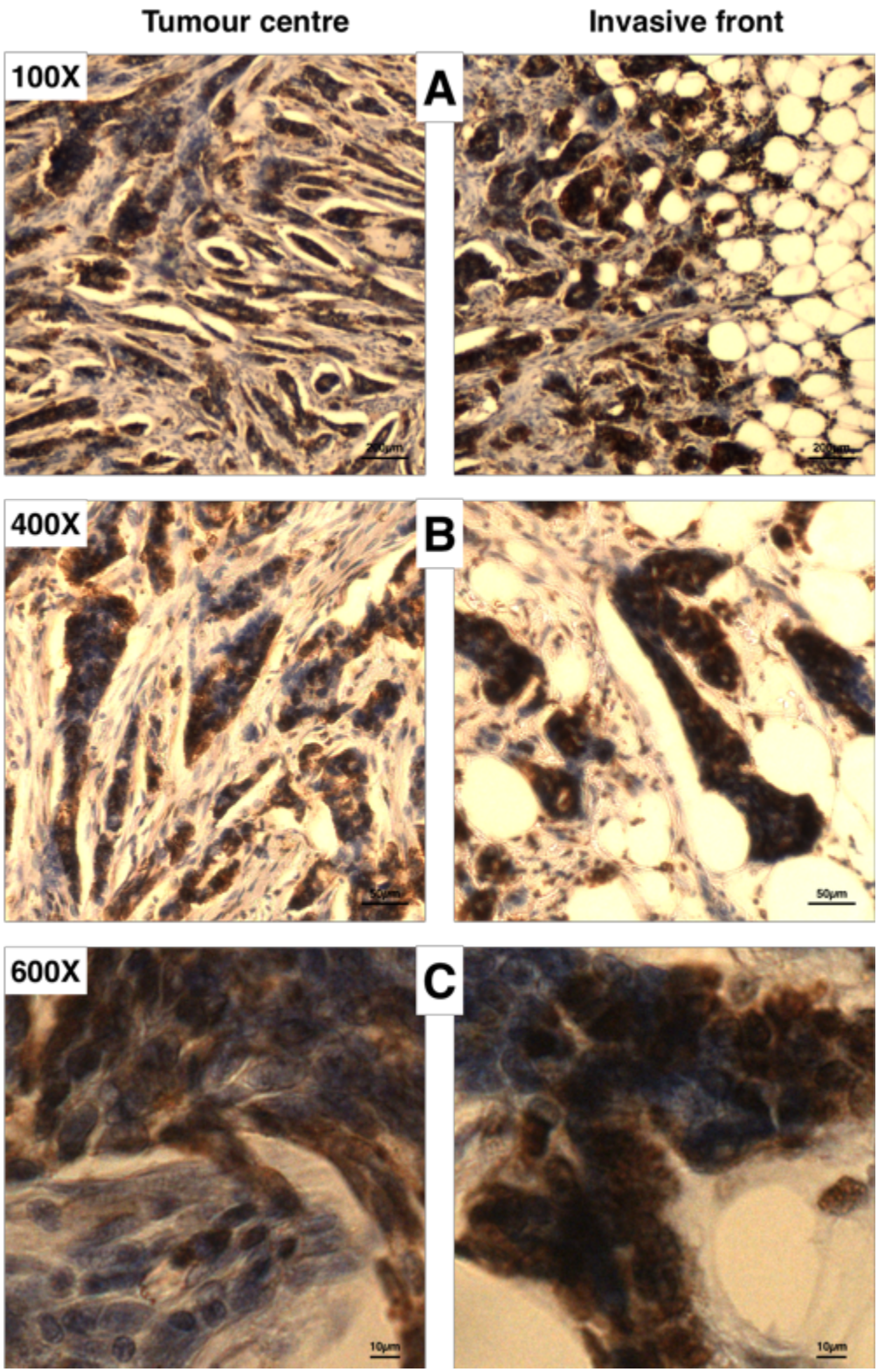

Figure 4-19, Nuclear expression of Gli2 in tumour cells is higher in invasive front of breast cancer

Representative IHC images of the same breast cancer sample showing increased nuclear localisation of Gli2 in tumour cells in the invasive front (to right) compared to the tumour centre (to left). Images were captured using three different magnifications (100X, 400X and 600X) by the Leica microscope. (♦) was used to indicate area of positivity in images.

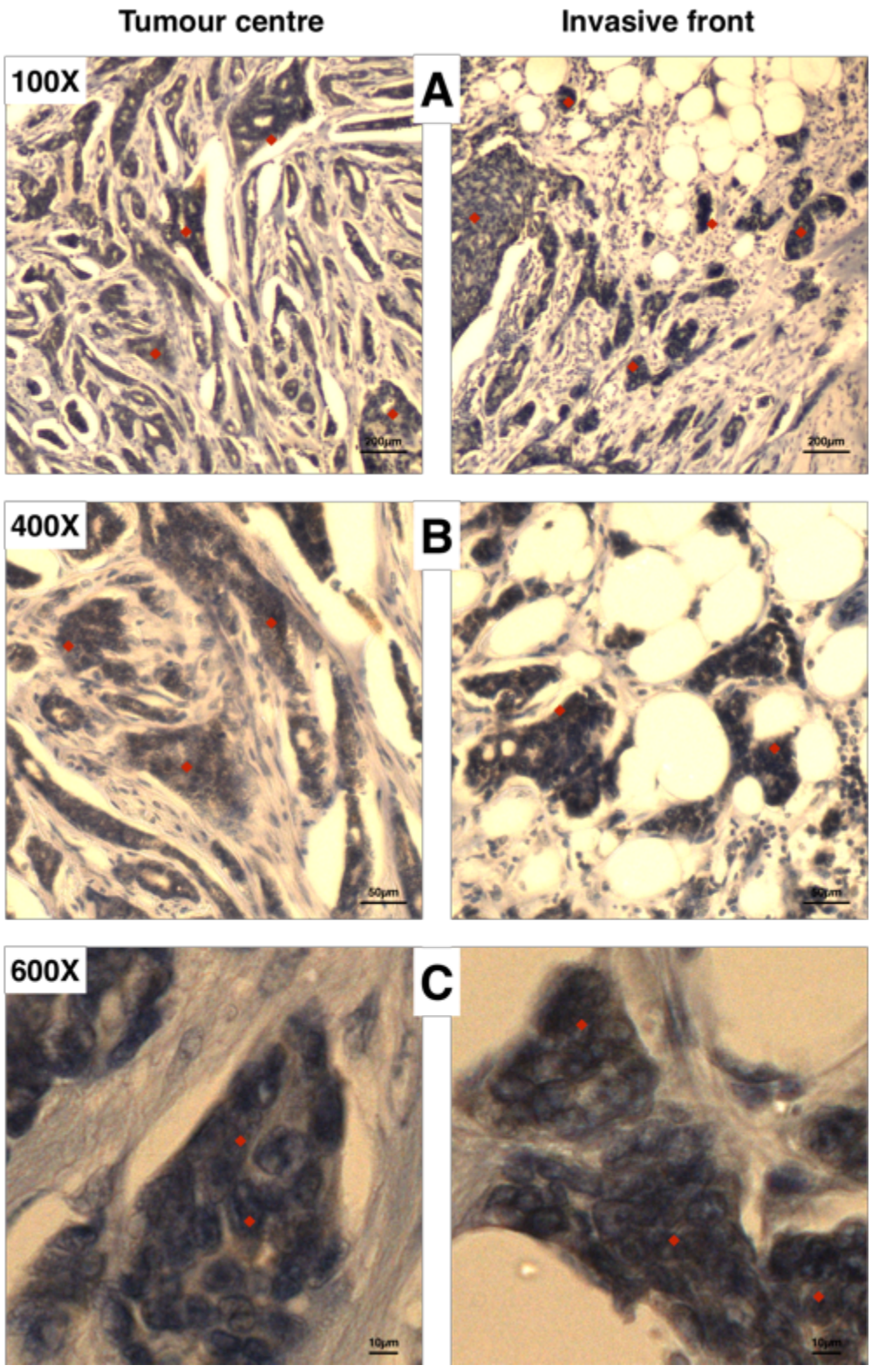

Figure 4-20, Nuclear expression of Gli3 in tumour cells is higher in invasive front of breast cancer

Representative IHC images of the same breast cancer sample showing increased nuclear localisation of Gli3 in tumour cells in the invasive front (to right) compared to the tumour centre (to left). Images were captured using three different magnifications (100X, 400X and 600X) by the Leica microscope. (♦) was used to indicate area of positivity in images.

Table 4-4: Nuclear expression of Gli1, Gli2 and Gli3 increased at invasive front compared to tumour centre

Tables showing nuclear expression of Gli1 (A), Gli2 (B) and Gli3 (C) in cells in tumour centre and invasive front. Pearson Chi-square test was used to estimate the difference between nuclear expression in tumour centres and invasive fronts. The Kendall's Tau B correlation coefficient (between -1 and +1) was used to assess for degree of correlation between tumour centre and invasive front. The statistical significance of the correlation is indicated as follows: *P= <0.05, **P= <0.01.

A	Nuclear expression of Gli1	
	Tumour Centre	Invasive Front
	No. (%)	No. (%)
No nuclear expression	17 (35.4)	10 (27)
<10% of tumour cells	8 (16.7)	3 (8.1)
10% - 50% of tumour cells	14 (29.2)	9 (24.3)
≥51% of tumour cells	9 (18.8)	15 (40.5)
Total included	48 (100)	37 (100)
Missing	0	11 (22.0)
Total	48 (100)	48 (100)
Pearson Chi-Square	0.0001***	
p-value	0.0001	
TauB	0.642**	

B	Nuclear expression of Gli2	
	Tumour Centre	Invasive Front
	No. (%)	No. (%)
No nuclear expression	0	0
<10% of tumour cells	7 (24.1)	3 (10.3)
10% - 50% of tumour cells	12 (41.4)	7 (24.1)
≥51% of tumour cells	10 (34.5)	19 (65.5)
Total included	29 (100)	29 (100)
Pearson Chi-Square	0.002**	
p-value	0.001	
TauB	0.582**	

C	Nuclear expression of Gli3	
	Tumour Centre	Invasive Front
	No. (%)	No. (%)
No nuclear expression	3 (13)	1 (4.3)
<10% of tumour cells	11 (47.8)	3 (13)
10% - 50% of tumour cells	5 (21.7)	7 (30.4)
≥51% of tumour cells	4 (17.4)	5 (21.7)
Total included	23 (100)	16 (69.6)
Missing	0	7 (30.4)
Total	23 (100)	23 (100)
Pearson Chi-Square	0.002**	
p-value	0.002	
TauB	0.710**	

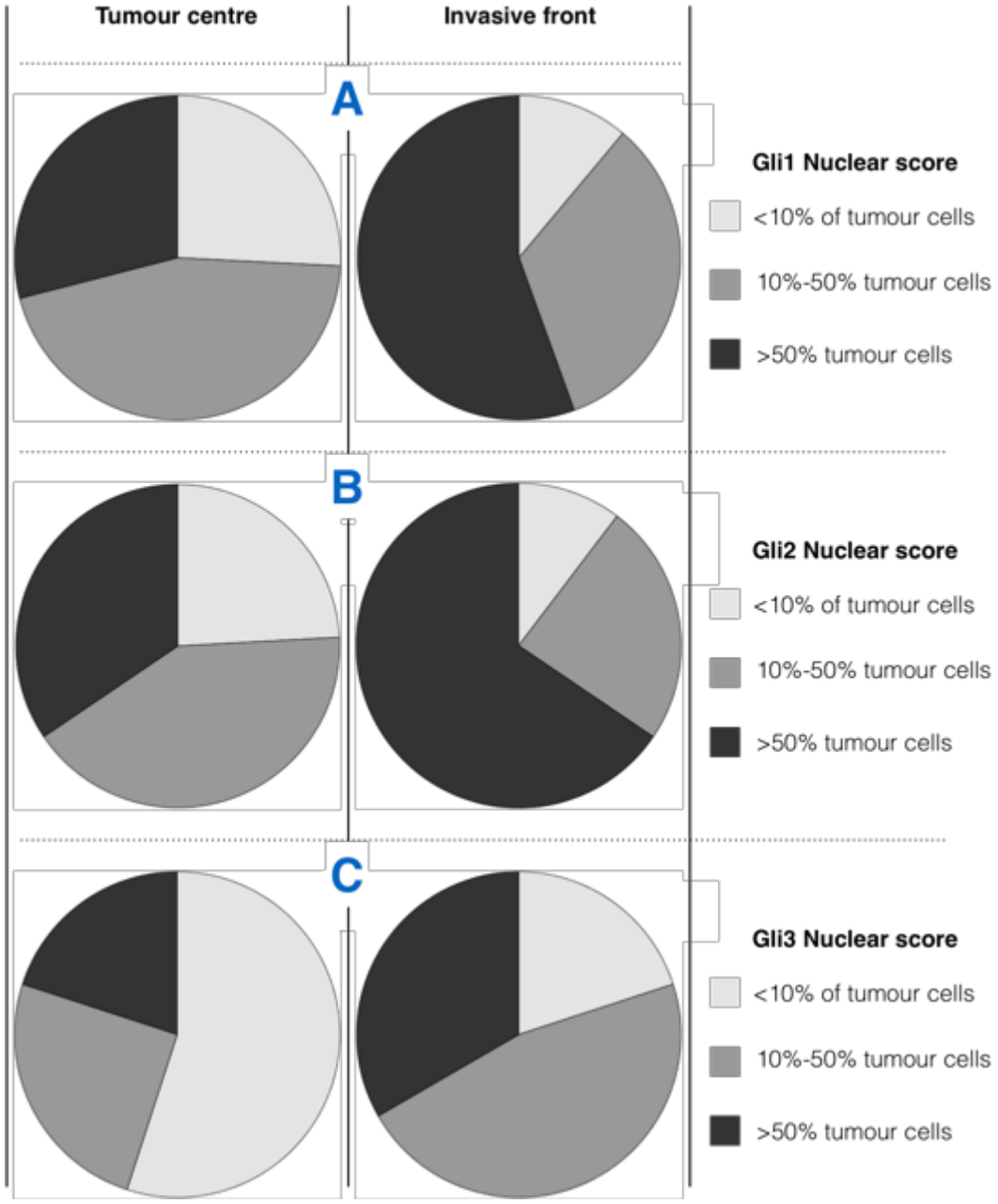

Figure 4-21, Gli nuclear expression was higher at invasive fronts in breast cancer
Figure showing comparison of Gli1 (A) Gli2 (B) and Gli3 (C) nuclear localisation in tumour centres (to the left) compared to the invasive front (to the right).

4.3.5 Gli1 expression correlates with size and the nuclear localisation correlated with tumour stage at invasive front

The percentage of Gli1 positive tumour cells increased with an increase in the size of the tumour. Gli1 IRS class significantly increased with tumour size with a high correlation coefficient (0.311, *p*-value= 0.046) (Figure 4-22).

IRS Class	Tumour size	
	2cm >	2cm <
	No. (%)	No. (%)
negative	4 (10.8)	1 (2.7)
positive, weak expression	2 (5.4)	1 (2.7)
positive, mild expression	5 (13.5)	7 (18.9)
positive, strong expression	5 (13.5)	12 (32.4)
Tau B	0.311*	
p-value	0.046	
Total	37	

Figure 4-22, IRS class of Gli1 staining increased in correlation with tumour size
Figure showed correlation between IRS class of Gli1 and increased tumour size. Comparison between the IRS class of Gli1 in 2cm ≥ tumours and 2cm < tumour sizes. Table showing the numbers of cases at two tumour sizes (2cm ≥ or 2cm<) and the corresponding IRS class (negative, positive with weak expression, positive with mild expression and positive with strong expression). The correlation was calculated using the Kendall's Tau B test.

The increase in Gli1 nuclear localisation in the tumour centre (Figure 4-23-A) had a positive correlation with tumour size. A positive correlation between Gli1 nuclear localisation and tumour size was also observed at the invasive front (Figure 4-23-B). A stronger correlation was observed at invasive front (0.367, *p*-value = 0.018) compared to that seen in the tumour centre (0.295, *p*-value =0.027). Therefore, the increase of nuclear localisation of Gli1 (with increasing tumour size) was higher at the invasive front compared to the tumour centre. Nuclear localisation of Gli1 at the invasive front showed correlation with increasing clinical tumour stage (0.317, *p*-value = 0.043 (Figure 4-24)).

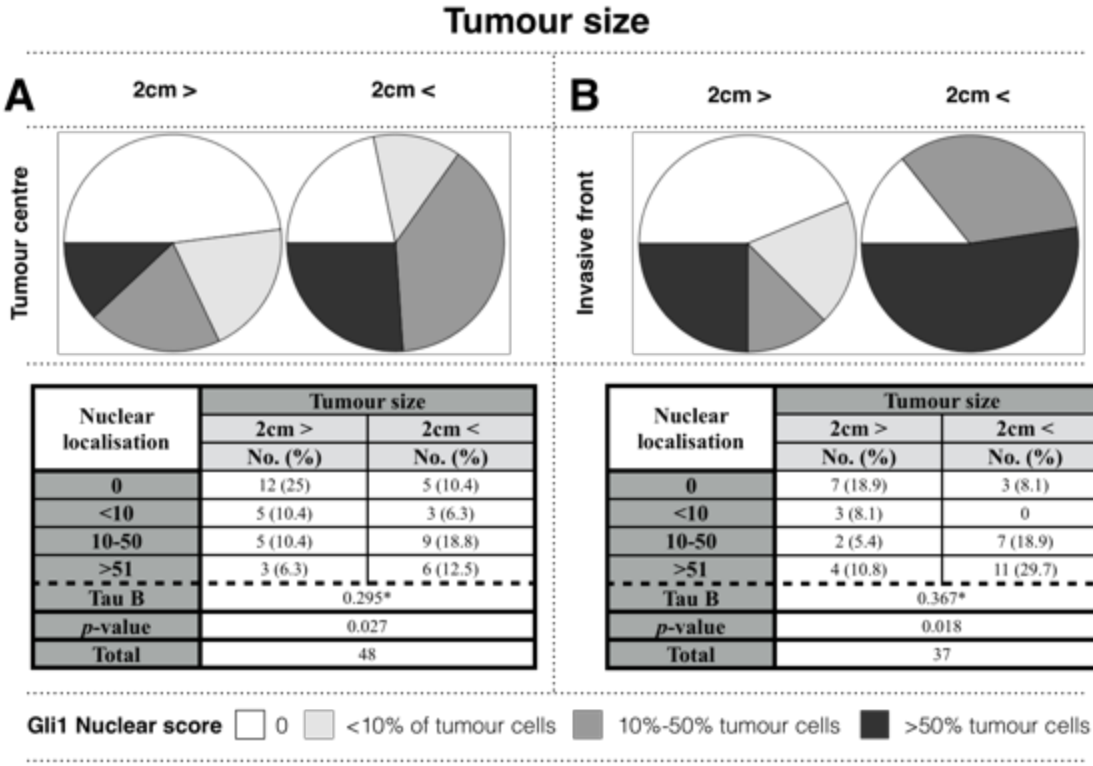

Nuclear localisation	Tumour size	
	2cm >	2cm <
	No. (%)	No. (%)
0	12 (25)	5 (10.4)
<10	5 (10.4)	3 (6.3)
10-50	5 (10.4)	9 (18.8)
>51	3 (6.3)	6 (12.5)
Tau B	0.295*	
p-value	0.027	
Total	48	

Nuclear localisation	Tumour size	
	2cm >	2cm <
	No. (%)	No. (%)
0	7 (18.9)	3 (8.1)
<10	3 (8.1)	0
10-50	2 (5.4)	7 (18.9)
>51	4 (10.8)	11 (29.7)
Tau B	0.367*	
p-value	0.018	
Total	37	

Figure 4-23, Increasing Gli1 nuclear localisation correlates with tumour size in tumour centre and at the invasive front

Figure showing comparison of nuclear localisation of Gli1 (0, <10%, 10-50% and >50%) in two tumour sizes (2cm≥ or 2cm<) in tumour centre (A) and at invasive front (B). Table showing the numbers of cases that have 2cm ≥ or 2cm < and the nuclear localisation of Gli1 (presented as 0, <10, 10-50 and >51) in these cases. The correlation was calculated using the Kendall's Tau B test.

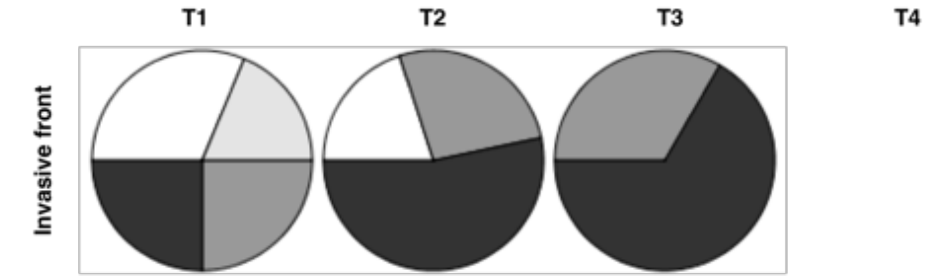

Nuclear localisation	Stage			
	T1	T2	T3	T4
	No. (%)	No. (%)	No. (%)	No. (%)
0	5 (14.7)	3 (8.8)	0	0
<10	3 (8.8)	0	0	0
10-50	4 (11.8)	4 (11.8)	1 (2.9)	0
>51	4 (11.8)	8 (23.5)	2 (5.9)	0
Tau B	0.317*			
p-value	0.043			
Total	34			

Figure 4-24, Increased of nuclear localisation of Gli1 at the invasive front correlated with tumour stage
Figure showing correlation between increased Gli1 nuclear localisation and increased tumour stage in tumour centre and at invasive front. Table below the figures shows the numbers of cases, the corresponding tumour stage (T1, T2, T3 and T4) and the nuclear localisation of Gli1 presented.

4.3.6 Gli2 expression inversely correlates with smaller tumour size, but positively with lower stage and grade and less lymph node involvement

The proportion of Gli2 expression in the tumour centre negatively correlated with tumour size (-0.348, *p*-value = 0.05) (Figure 4-25) as well as with tumour stage (-0.480, *p*-value = 0.009) (Figure 4-26). Tumours of smaller size (<2cm) had increased expression of Gli2 compared to tumours with sizes more than 2cm (Figure 4-25) and an increase in the proportion of Gli2 positive cells in the tumour centre was observed in tumours at an earlier stage (Figure 4-26). However, due to lack of cases with stages 3 and 4, no further conclusion can be drawn.

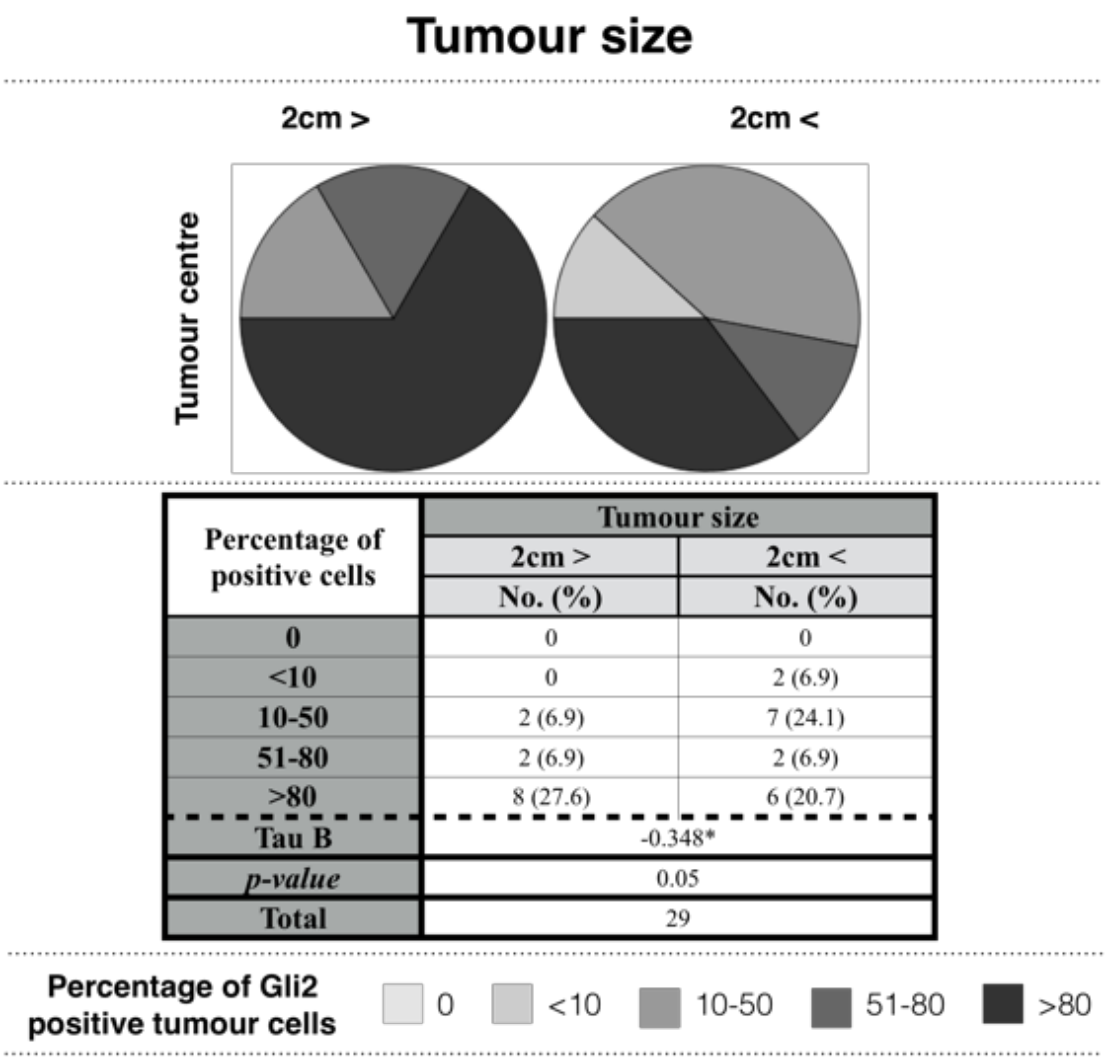

Percentage of positive cells	Tumour size	
	2cm >	2cm <
	No. (%)	No. (%)
0	0	0
<10	0	2 (6.9)
10-50	2 (6.9)	7 (24.1)
51-80	2 (6.9)	2 (6.9)
>80	8 (27.6)	6 (20.7)
Tau B	-0.348*	
p-value	0.05	
Total	29	

Figure 4-25, The percentage of Gli2 positive tumour cells in the tumour centre correlated with smaller tumour size

Figure showing increase of percentage of Gli1 positive tumour cells correlated with smaller tumour size in tumour centre. Table below the pie chart shows numbers of cases, tumour size (2cm ≥ or 2cm <) and the percentage of Gli2 positive tumour cells (presented as 0, <10, 10-50, 51-80 and >80). The correlation was calculated using the Kendall's Tau B test.

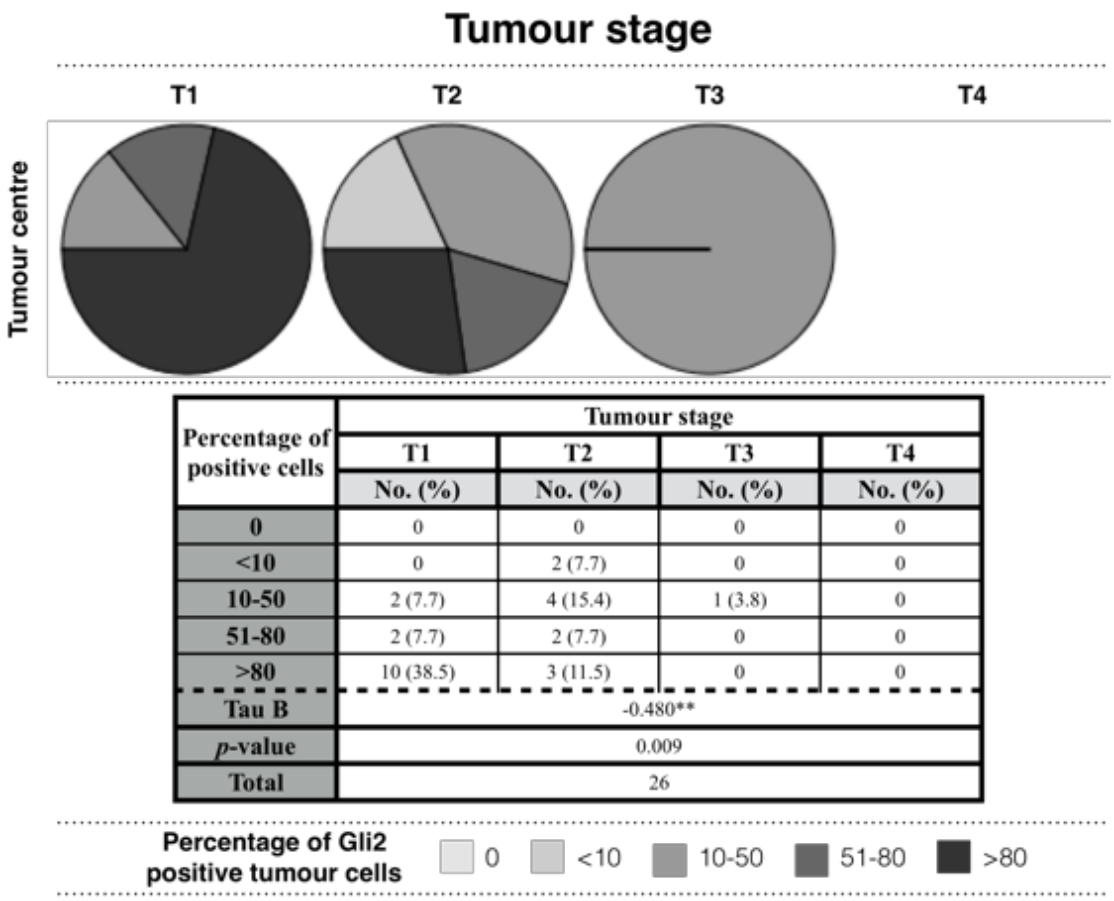

Percentage of positive cells	Tumour stage			
	T1	T2	T3	T4
	No. (%)	No. (%)	No. (%)	No. (%)
0	0	0	0	0
<10	0	2 (7.7)	0	0
10-50	2 (7.7)	4 (15.4)	1 (3.8)	0
51-80	2 (7.7)	2 (7.7)	0	0
>80	10 (38.5)	3 (11.5)	0	0
Tau B	-0.480**			
p-value	0.009			
Total	26			

Figure 4-26, Increased percentage of Gli2 positive tumour cells in the tumour centre correlated with lower tumour stage
Figure showing increase of percentage of Gli2 positive tumour cells correlated with lower tumour stage in tumour centre. The table below the pie chart presents the numbers of cases, tumour stage (T1, T2, T3, and T4) and percentage of Gli2 positive tumour cells (presented as 0, <10, 10-50, 51-80 and >80). The correlation was calculated using the Kendall's Tau B test.

Higher percentage of Gli2 expression in the tumour centre was correlated with lower lymph node involvement (-0.419, *p*-value = 0.003) (Figure 4-27). Cases with higher IRS class of Gli2 in the tumour centre showed had lower lymph node involvement (-0.321, *p*-value = 0.03) (Figure 4-28).

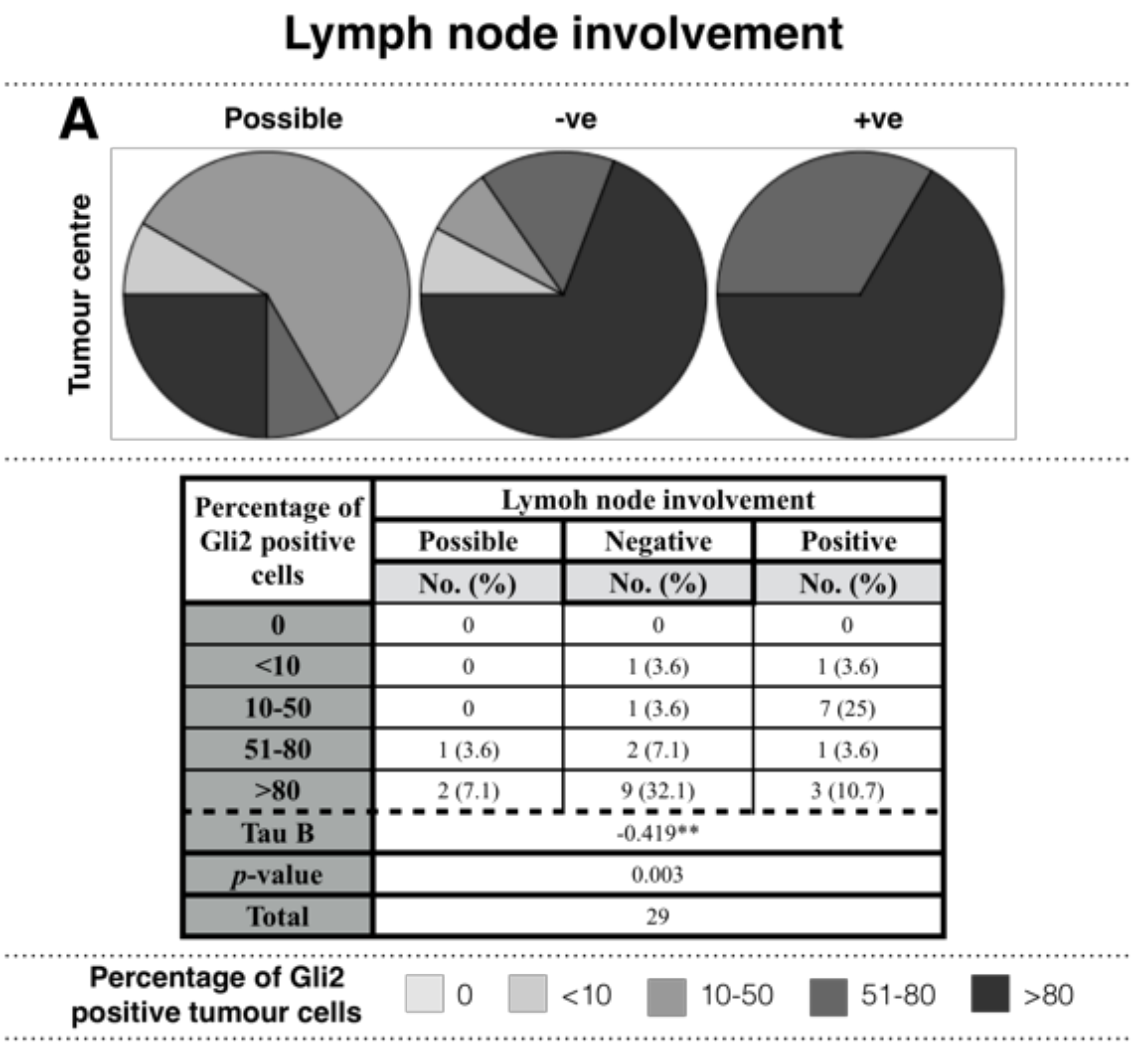

Percentage of Gli2 positive cells	Lymoh node involvement		
	Possible	Negative	Positive
	No. (%)	No. (%)	No. (%)
0	0	0	0
<10	0	1 (3.6)	1 (3.6)
10-50	0	1 (3.6)	7 (25)
51-80	1 (3.6)	2 (7.1)	1 (3.6)
>80	2 (7.1)	9 (32.1)	3 (10.7)
Tau B	-0.419**		
p-value	0.003		
Total	29		

Figure 4-27, The percentage of Gli2 positive tumour cells in the tumour centre correlated with low lymph node involvement

Figure showing increase of percentage of Gli2 positive tumour cells in tumour centre correlated with negative lymph node. Table below shows the numbers of cases, lymph node involvement (possible, negative or positive) and the percentage of Gli2 positive tumour cells in tumour centre. The correlation was calculated using the Kendall's Tau B test.

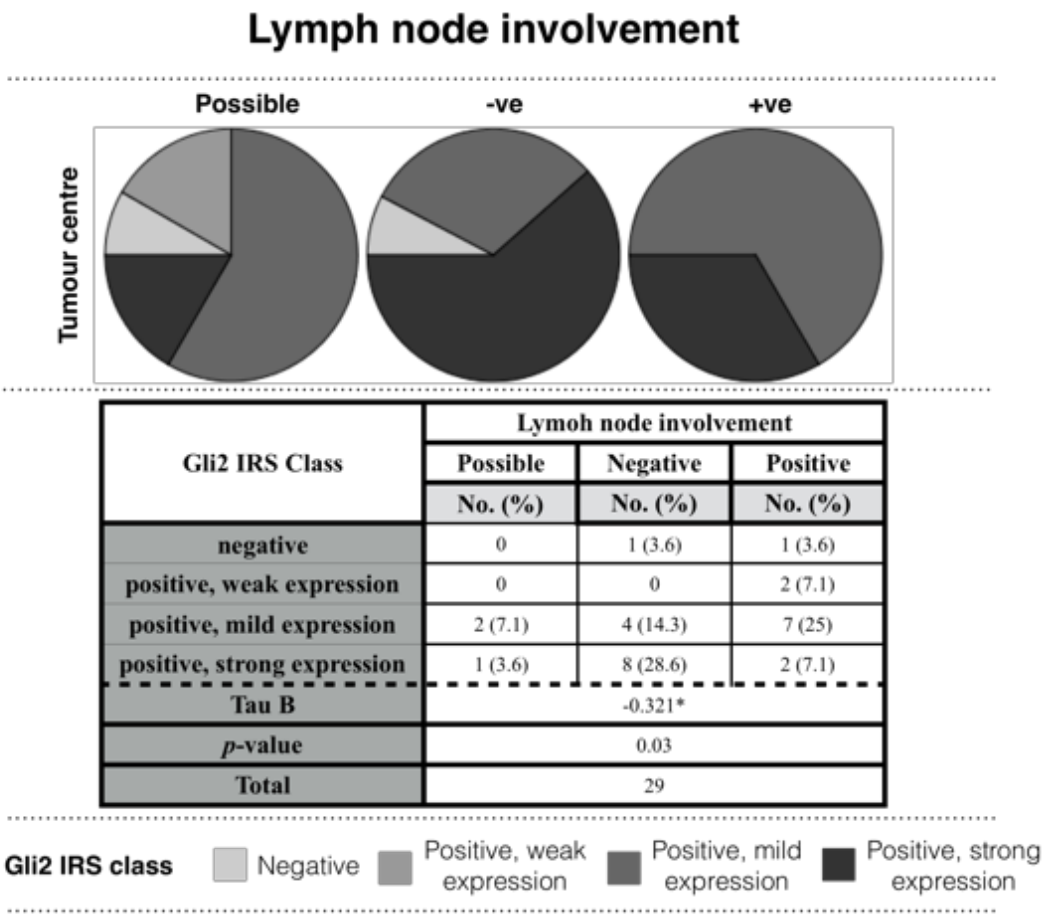

Gli2 IRS Class	Lymoh node involvement		
	Possible	Negative	Positive
	No. (%)	No. (%)	No. (%)
negative	0	1 (3.6)	1 (3.6)
positive, weak expression	0	0	2 (7.1)
positive, mild expression	2 (7.1)	4 (14.3)	7 (25)
positive, strong expression	1 (3.6)	8 (28.6)	2 (7.1)
Tau B	-0.321*		
p-value	0.03		
Total	29		

Figure 4-28, Higher Gli2 IRS class in the tumour centre correlated with low lymph node involvement
Figure showing higher Gli2 IRS class in tumour centre correlated with negative lymph node involvement. Table shows the numbers of cases, lymph node involvement (possible, negative and positive) and Gli2 IRS class (negative, positive with weak expression, positive with mild expression and positive with strong expression) in tumour centre. The correlation was calculated using the Kendall's Tau B test.

4.3.7 Increased Gli3 correlated with younger mean age at diagnosis and hormone receptor-positive breast cancer

The percentage of Gli3 expression at the invasive front correlated with a lower age at diagnosis (-0.495, *p*-value = 0.015). Increased percentage of Gli3 was observed with ER positive (0.402, *p*-value = 0.014) (Figure 4-29) and PR positive tumours (0.468, *p*-value = 0.006) (Figure 4-30).

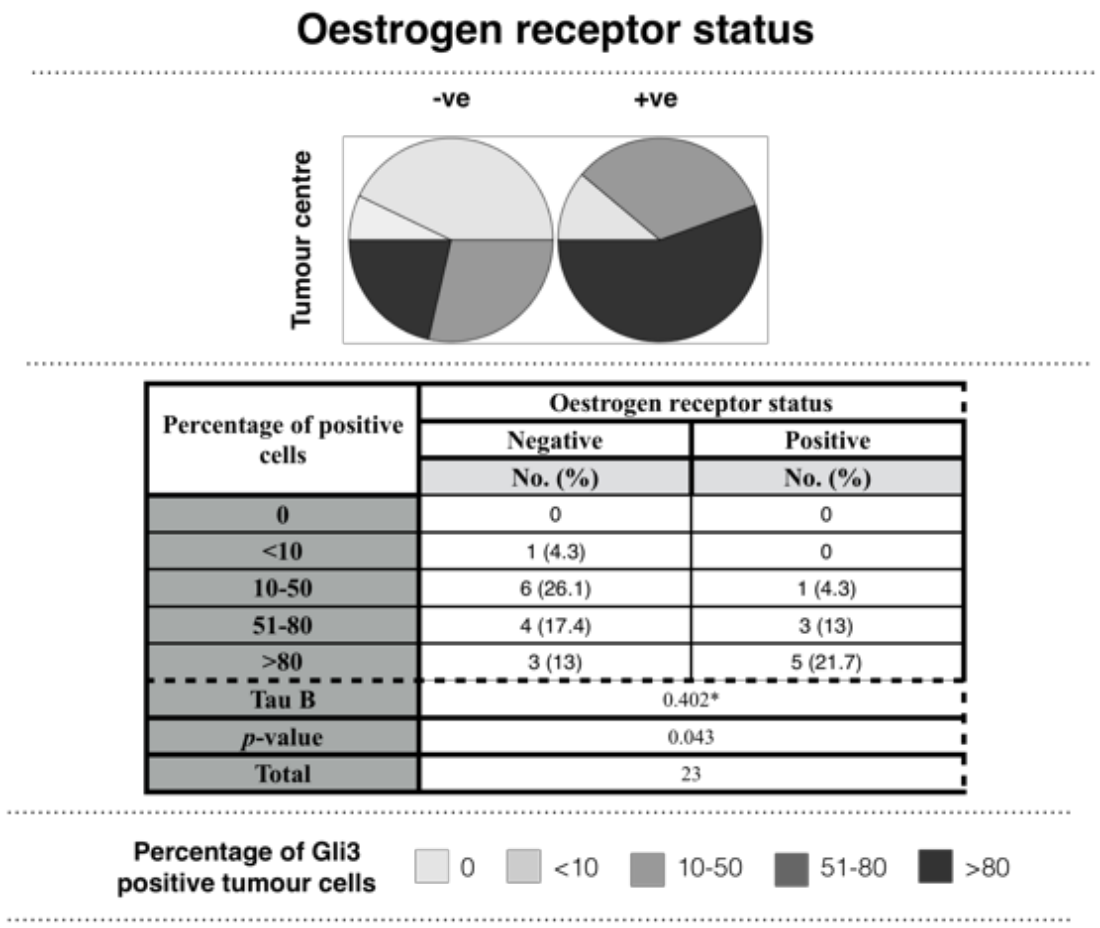

Percentage of positive cells	Oestrogen receptor status	
	Negative	Positive
	No. (%)	No. (%)
0	0	0
<10	1 (4.3)	0
10-50	6 (26.1)	1 (4.3)
51-80	4 (17.4)	3 (13)
>80	3 (13)	5 (21.7)
Tau B	0.402*	
p-value	0.043	
Total	23	

Figure 4-29, The percentage of Gli3 positive tumour cells in tumour centre correlated with Oestrogen hormone-positive breast cancer

Figure showing an increase in the percentage of Gli3 positive tumour cells in correlation with oestrogen hormone-positive breast cancer. Table shows the numbers of cases, oestrogen receptor status (negative and positive) and the percentage of Gli3 positive tumour cells (presented as 0, <10, 10-50, 51-80, and >80). The correlation was calculated using the Kendall's Tau B test.

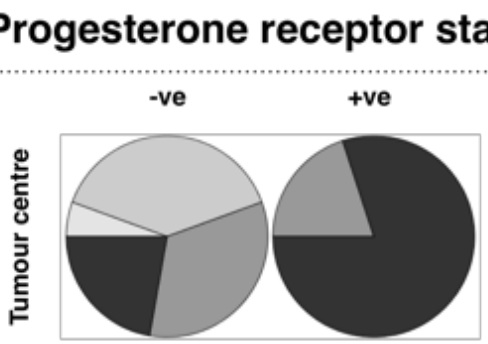

Percentage of positive cells	Progesterone receptor status	
	Negative	Positive
	No. (%)	No. (%)
0	0	0
<10	1 (4.3)	0
10-50	7 (30.4)	0
51-80	6 (26.1)	1 (4.3)
>80	4 (17.4)	4 (17.4)
Tau B	0.468*	
p-value	0.019	
Total	23	

Figure 4-30, The percentage of Gli3 positive tumour cells in tumour centre correlated with progesterone hormone-positive breast cancer
Figure showing an increase in the percentage of Gli3 positive tumour cells in correlation with hormone-positive breast cancer. Table shows the numbers of cases, progesterone hormone status (negative and positive) and the percentage of Gli3 positive tumour cells (presented as 0, <10, 10-50, 51-80, and >80). The correlation was calculated using the Kendall's Tau B test.

4.3.8 Gli1 and Gli2 were co-expressed in breast cancer samples

Gli1 and Gli2 were co-expressed in breast cancer samples. Gli1 intensity at the invasive front correlated with that of Gli2 at the invasive front (1, *p*-value = 0) (Figure 4-31).

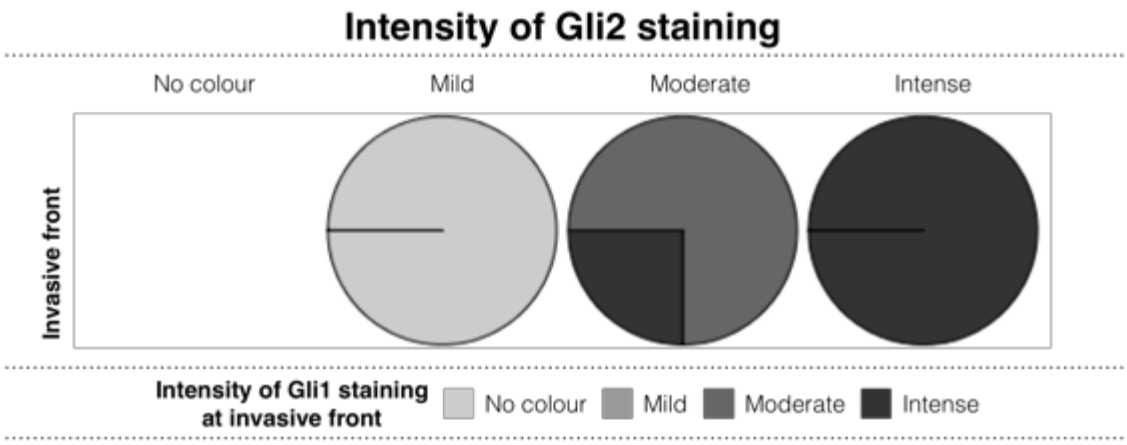

Figure 4-31, Correlation between Gli1 and Gli2 staining intensity at the invasive front

Figure showing correlation between Gli1 and Gli2 staining intensity at invasive front. This correlation confirms a mutual increase of Gli1 and Gli2 intensity at the invasive front and in the tumour centre.

Observation of increased Gli1 nuclear localisation at the invasive front was concomitant with an increase in both the proportion and intensity of Gli2 staining in the tumour centre (1, *p*-value = 0 and 1, *p*-value = 0) (Figure 4-32). This showed that the increase in nuclear localisation of Gli1 at the invasive front was co-expressed with increased Gli2 expression (percentage, staining intensity and IRS) and nuclear localisation at the invasive front.

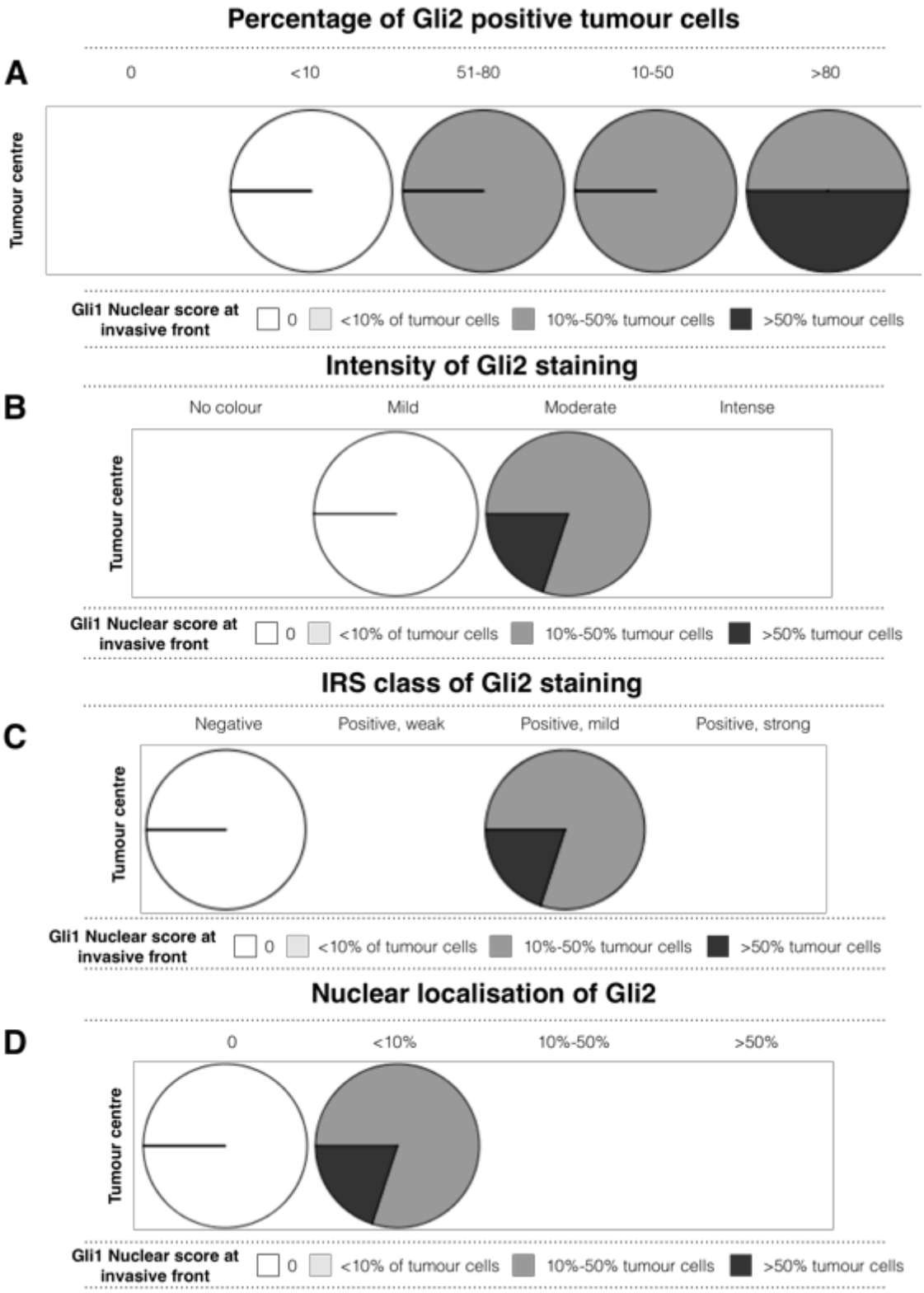

Figure 4-32, Nuclear localisation of Gli1 at the invasive front is correlated with Gli2 staining

Figure showing an increase in Gli1 nuclear localisation in correlation with an increase of Gli2 staining in the tumour centre. (A) shows correlation between the percentage of Gli2 positive tumour cells (B) Gli2 staining intensity (C) IRS class of Gli2 (D) increased nuclear localisation of Gli2 with increased localisation of Gli1 at the invasive front.

4.3.9 Inverse correlation between Gli1 and Gli3 staining in breast cancer and concurrent expression of Gli2 and Gli3 in tumour centre

Co-expression analysis was conducted on serial sections stained for all proteins. The increase of Gli1 staining at the invasive front correlated with a decrease of Gli3 staining intensity in the tumour centre (0.905, *p*-value = 0.034) (Figure 4-33).

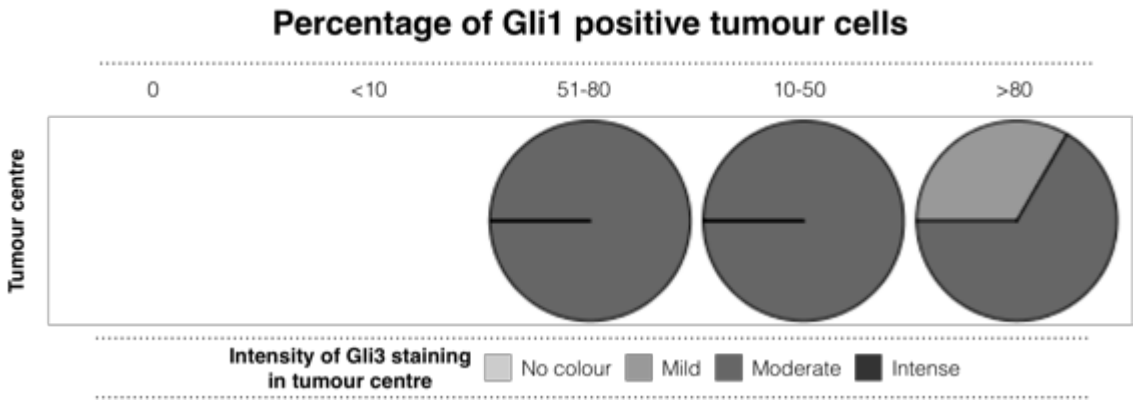

Figure 4-33, Increased percentage of Gli1 positive tumour cells in tumour centre is correlated with decrease Gli3 intensity in tumour centre
Figure showing that an increase of the percentage of Gli1 positive expressing cells in tumour centre correlated with decreased staining intensity of Gli3 in tumour centre.

4.3.10 Gli proteins expression correlated with E-cadherin alteration in tumour centre and at invasive front of breast cancer samples

Gli1 and Gli3 expression correlated negatively with E-cadherin expression in the tumour centre and Gli2 correlated positively with E-cadherin in breast cancer. Samples that had high IRS class of E-cadherin in the tumour centre concurrently has less nuclear localisation of Gli1 in the tumour centre (-0.700, *p*-value=0.044) (Figure 4-34). Thus, suggesting a negative correlation between E-cadherin expression and the activation of Hh signalling, measured by the nuclear localisation of Gli1.

Samples with high Gli2 intensity at the invasive front had high proportion of E-cadherin positivity in tumour centre (0.728, *p*-value = 0.046) (Figure 4-35-A) and at the invasive front (0.918, *p*-value = 0.011) (Figure 4-35-C). Also, samples that had high intensity of Gli2 staining at the invasive front concomitantly had high IRS class of E-cadherin staining in the tumour centre (0.775, *p*-value = 0.04) (Figure 4-35-B). Samples with more evident nuclear localisation of Gli2 in the tumour centre showed high IRS class for E-cadherin staining in tumour centre (0.745, *p*-value = 0.049) (Figure 4-36). It is difficult to interpret this finding at Gli2 has dual action, activation and suppression

(Figure 0-8). So, there were positive correlation between Gli2 staining at the invasive front and E-cadherin staining in tumour centre and at invasive front. These findings showed that high Gli2 at the invasive front could be a sign of less tumour invasive, as E-cadherin expression is higher in those tumours.

Similar to Gli2 finding Breast cancer samples that had higher intensity of Gli3 staining at the invasive front had higher IRS class of E-cadherin staining in the tumour centre (-1, *p*-value = 0.000) (Figure 4-37). Correlation between higher expression of E-cadherin in the tumour centre and increased Gli2 and Gli3 staining at the invasive front suggest that both proteins could indicate reduction of invasion. However, more investigation of the function of the Gli proteins in tumour cells is needed to confirm these findings.

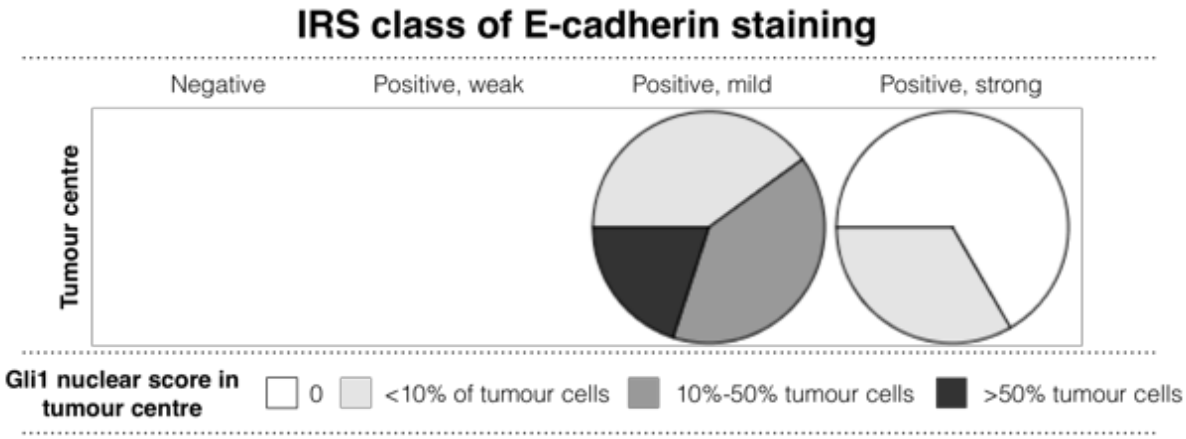

Figure 4-34, Reduction of nuclear localisation of Gli1 in tumour centre associated with high E-cadherin in tumour centre
Figure showing that Gli1 nuclear localisation in the tumour centre decreased in association with an increase of E-cadherin IRS class at the invasive front.

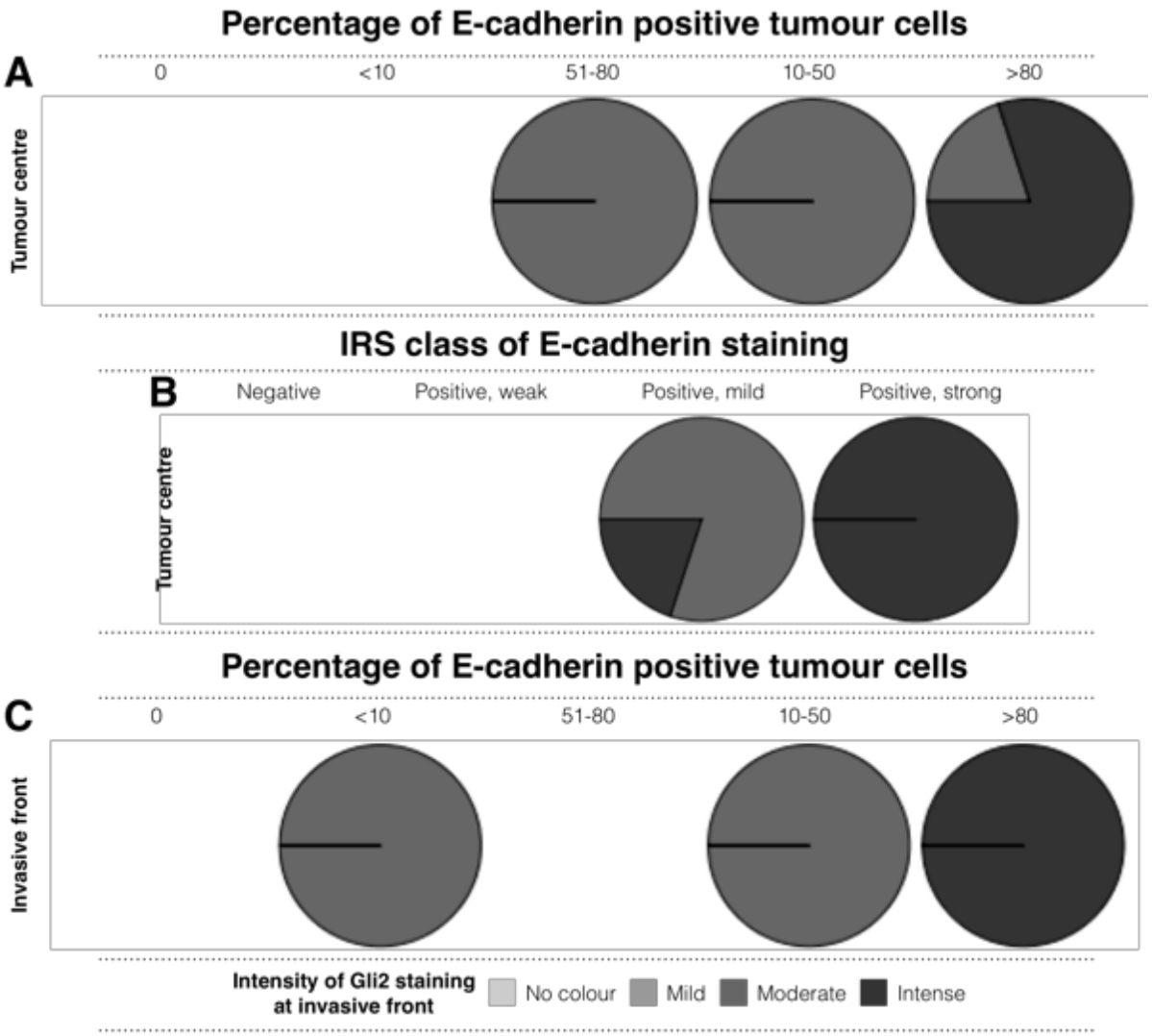

Figure 4-35, Increased of Gli2 staining intensity at the invasive front correlated with E-cadherin expression in the tumour centre and at the invasive front

Figure showing that the percentage of E-cadherin positivity (A) and IRS class (B) in the tumour centre correlated with an increase Gli2 intensity at the invasive front. Gli2 staining intensity at invasive front also correlated with increased percentage of E-cadherin in the invasive front (C).

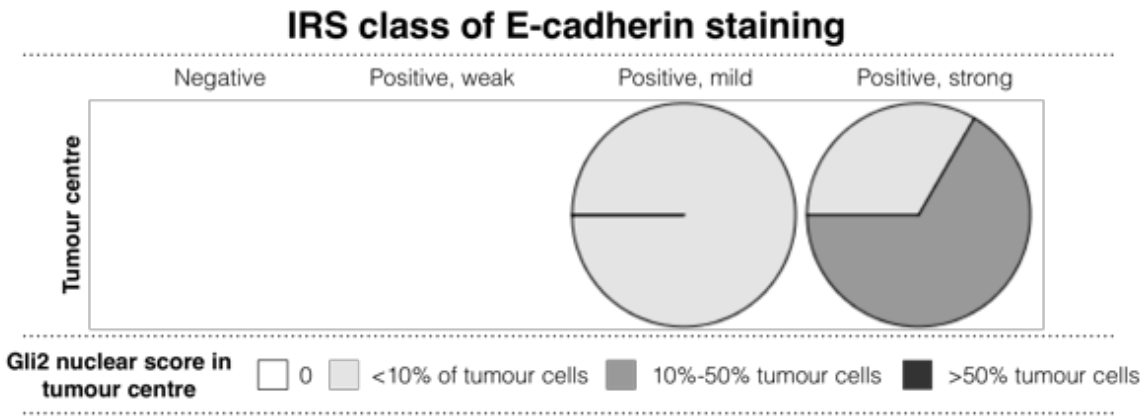

Figure 4-36, Increased nuclear localisation of Gli2 in the tumour centre associated with increased E-cadherin IRS class in the tumour centre
Figure showing that nuclear Gli2 localisation increased with an increased in IRS class of E-cadherin in the tumour centre.

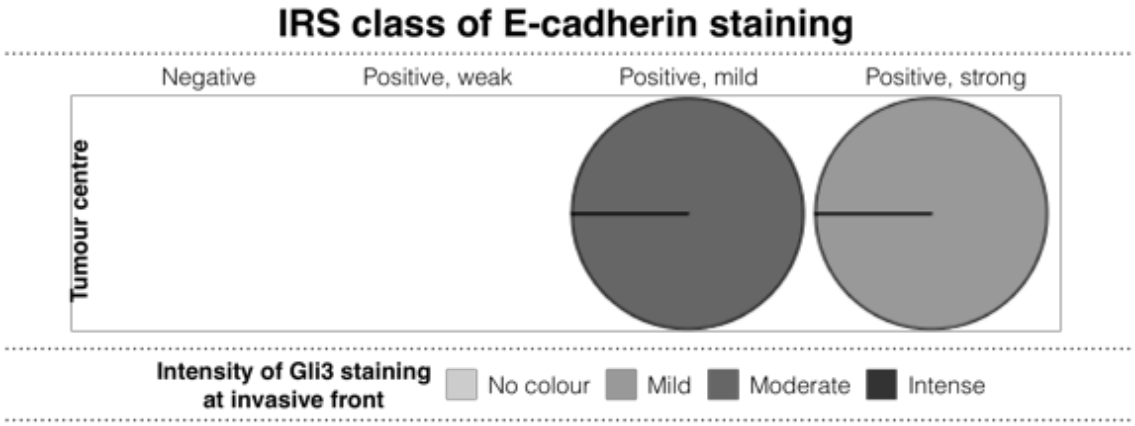

Figure 4-37, Intensity of Gli3 staining at the invasive front negatively correlated with IRS class of E-cadherin staining in the tumour centre
Figure showing that increased E-cadherin staining in the tumour centre correlated with a decrease in Gli3 staining at the invasive front.

4.3.11 The Hedgehog signalling (Hh) pathway components were expressed in breast cancer cell lines

The expression of Hh signalling components, Sonic Hedgehog (Shh), Indian Hedgehog (Ihh), Patched, Smoothened (Smo), Gli1, Gli2 and Gli3 were evaluated in breast cancer cell lines using Western blotting analysis (Figure 4-38-A). As seen in Figure 4-38-B the results Smoothened was detected in breast cancer cell lines (MCF7, MDA-MB-361, MDA-MB-453 and MDA-MB-231) but was not detected in BT20 and MCF10A. Patched was detected in MDA-MB-361and BT20, and was low in MDA-MB-453 (Figure 4-38-C). The ligands Shh and Ihh were detected in all cell lines

(Figure 4-38-D and Figure 4-38-E). Gli1 and Gli3 were also detected in all cell lines (Figure 4-38-F and Figure 4-38-H). Gli2 was detected in MCF7, MDA-MB-453, BT20 and MDA-MB-231 (Figure 4-38-G).

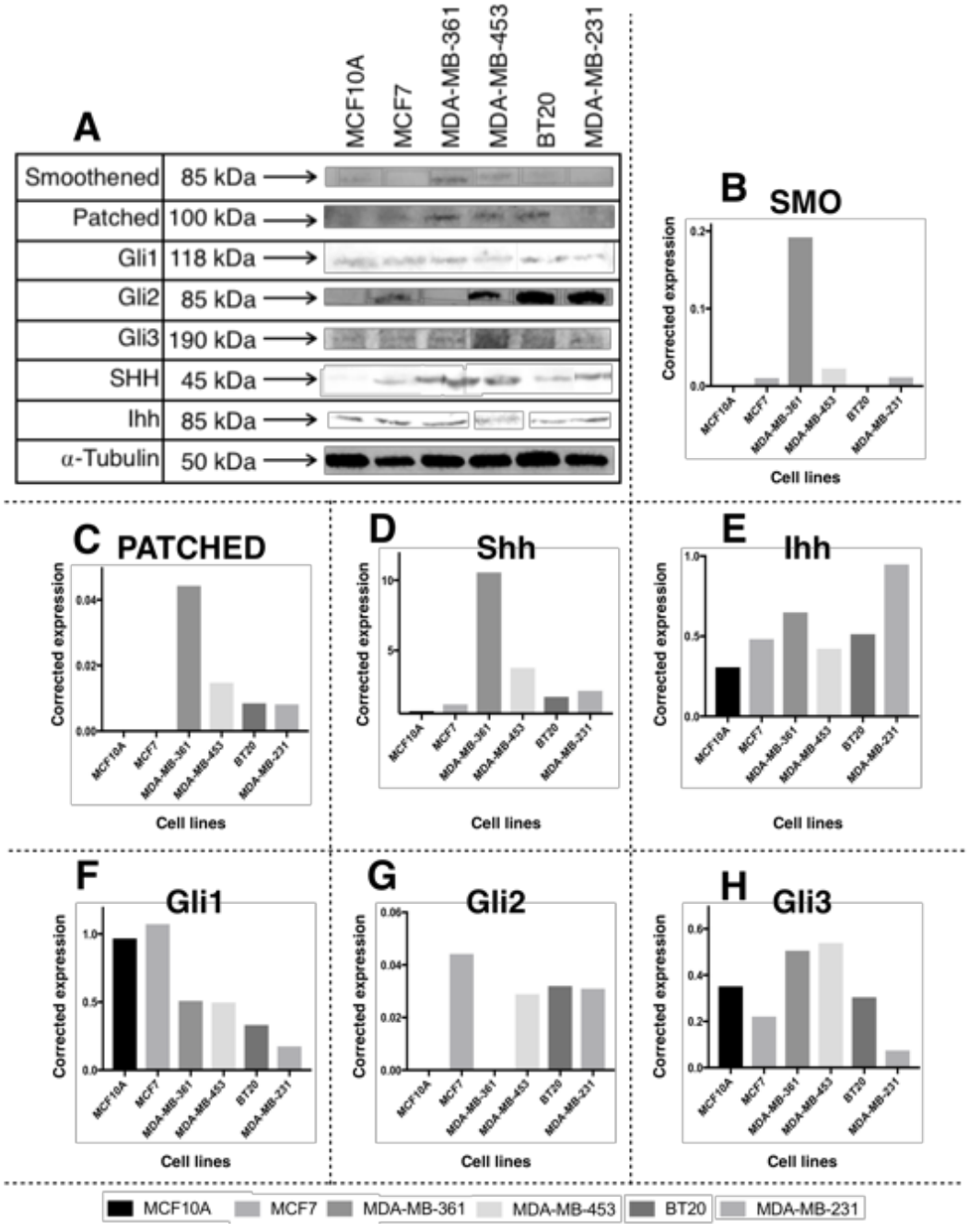

Figure 4-38, Hedgehog signalling components were expressed in breast cancer cell lines

Figure showing that the Hedgehog (Hh) signalling components (Smo, Patched, Shh, Ihh, Gli1, Gli2 and Gli3) were expressed in breast cancer cell lines (MCF10A, MCF7, MDA-MB-361, MDA-MB-453, BT20 and MDA-MB-231) as seen in Western blotting (A). The corrected ratio of Smoothened (Smo) (B), Patched (C), Sonic Hedgehog (Shh) (D), Indian Hedgehog (Ihh) (E), Gli1 (F), Gli2 (G) and Gli3 (F).

4.4 Discussion

Despite advances in the detection and treatment of breast cancer, development of metastatic disease remains fatal. In the UK, it is estimated that 20-70% of breast cancer cases diagnosed will have secondary or metastatic disease at diagnosis (Dewis and Gribbin, 2009). Furthermore, it was reported that the remaining cases have a 35% chance of developing metastases within 10 years after initial diagnosis (Dewis and Gribbin, 2009). Researchers are looking for new approaches to treat metastatic disease due to the failure of current treatment regimens. These current approaches comprise of systemic chemotherapy in combination with surgery or radiation, which aim to prolong survival rather than prevent metastatic disease. Identifying signalling pathways active during breast cancer metastasis is essential for the development of targeted therapy and to identify cases that could benefit from targeting these pathways.

Invasion and metastasis are one of the hallmarks of cancer and the process of EMT is involved in the regulation of invasion and metastasis and is also involved in normal physiological processes. In the previous section (3.3), data showed that breast cancer cell lines exhibited signs of EMT when exposed to external stress by changing the degree of cell-cell contact. The ability of breast cancer cells ability to undergo EMT was not limited to a specific subtype of breast cancer, but rather depended on other factors that are involved in the regulation of this process. Evidence showed that β-catenin protein, which is involved in the canonical Wnt/β-catenin signalling, has ability to crosstalk with other signalling pathways including the Hedgehog (Hh) signalling pathway (Garg, 2013). It has also been reported that Hh signalling can act on its own to regulate EMT in human cancers (Gonzalez and Medici, 2014).

To determine the involvement of Hh signalling in breast cancer, Gli1, Gli2 and Gli3 were assessed in serial sections from a breast cancer sample cohort using immunohistochemistry (IHC). The intensity of staining and percentage of positive cells were evaluated in both the tumour centre and invasive front of each sample. The expression of E-cadherin was also assessed in serial sections as loss of this protein in breast cancer is an indication for poor prognosis. Nuclear localisation of Gli1, Gli2, Gli3 and β-catenin was also evaluated.

The IRS scoring system was selected for estimating the levels of expression in breast cancer (Table 2-15). This scoring system was utilised previously for estimating the levels of Gli1 in breast cancer (ten Haaf *et al.*, 2009). Kaemmerer *et al.* (2012) reported that the IRS scoring system provided a reliable and uniformed score that was

suitable for routine diagnosis. Nuclear localisation was assessed using the scoring system suggested by Volante *et al.* (2007) and used for HER2 scoring in combination with IRS scoring by Kaemmerer *et al.* (2012) in Table 2-16. Adjacent normal tissue was present in some samples, but the infrequency of this observation meant that comparison of level of expression between normal and breast cancer was possible (data not included).

Analysis of prognostic markers (ER, PR and HER2) status and correlation with the clinical criteria of samples tested, showed that ER and PR receptor positivity correlated with smaller tumour size, stage and grade (Table 11-5). This concurs with previous work that found similar findings using IHC (reviewed by Rakha *et al.* (2010b)), gene-microarray analysis and expression analysis (Sorlie *et al.*, 2001; Sotiriou and Pusztai, 2009).

4.4.1 Gli proteins were expressed in breast cancer with nuclear and cytoplasmic distribution

Lewis and Veltmaat (2004) found that components of the Hh signalling pathway were expressed in normal breast tissue. They also found that Gli1, Gli2 and Gli3 were expressed in invasive ductal carcinoma at a higher level than that in normal breast tissue (Lewis and Veltmaat, 2004). All breast cancer samples used in this study expressed Gli2 and Gli3 and 92% of cases were positive for Gli1 (Figure 4-6).

Previous studies used a binary scoring outcome and included only 100 tumour cells from each section in the analysis (Kubo *et al.*, 2004). Souzaki *et al.* (2011) scored five fields and counted 300 tumour cells and considered >50% Gli1 expression as a positive result. The combined scoring utilised by IRS method that was introduced by Kaemmerer *et al.* (2012), provided a robust method for assessing the tissue distribution of the Gli proteins. This method was used for scoring hormone receptor status in breast cancer (Kaemmerer *et al.*, 2012). IRS scoring also uses a scale of positivity that can be used separately as percentage of positive tumour cells and intensity (Xu *et al.*, 2010), or in combination as IRS classes (ten Haaf *et al.*, 2009).

The percentage of positivity of tumour cells was highest for Gli3 and Gli2 respectively and lowest in Gli1 (Figure 4-7) yet the staining intensity of Gli2 and Gli1 were higher than that for Gli3 (Figure 4-8). Gli2 showed the highest IRS score followed by Gli1 then Gli3 (Figure 4-9). In agreement with the current findings, Im *et al.* (2013) showed that Gli2 was the highest expressed Gli member in breast cancer followed by Gli1 and Gli3. Gli3 is the repressor form of Gli and loss of *Gli3* induces *Gli1*

overexpression and loss of Hh repression. This is essential for normal mammary gland development (Hatsell and Cowin, 2006). Therefore, reduced Gli3 expression is expected in breast cancer (Figure 4-9). However, no comparison with normal tissue was conducted in the current study and confirmation of Gli3 loss in breast cancer samples compared to normal breast tissue can be recommended for future work. Similar to findings in a previous study reported by Im *et al.* (2013) nuclear and cytoplasmic localisation of Gli proteins was observed in the breast tumours (Figure 4-10).

4.4.2 Increased Gli1 and Gli2 are found at the invasive front of breast tumours

The invasive front is defined as the area where tumour cells interact with host tissue or organ, it is an area of three to six layers of tumour cells at the front edge (Gao *et al.*, 2010; Gong *et al.*, 2013). The expression of Gli1, Gli2 and Gli3 was compared in tumour centres and invasive fronts of the samples. This approach of IHC analysis was chosen following the notion that the invasive front was the location where EMT is observed in cancer (Bryne *et al.*, 1998; Christofori, 2006; Busch *et al.*, 2014).

Our findings were the first to provide detailed analysis by studying the tissue distribution and subcellular localisation of all three Gli proteins. These findings provide a better understanding of Hh signalling and its involvement in breast cancer invasion. It was observed that the percentage of positive cells, staining intensity and IRS score of Gli1 and Gli2 increased significantly at invasive fronts (Table 4-1 and

Table 4-2). Increased expression of Gli1 at the invasive front of breast cancer was previously reported by ten Haaf *et al.* (2009). The increase of Gli proteins at the invasive front of tumours provides a strong indication that the Hh signalling is active at the invasive front where many studies suggested as active site for EMT in cancer (Bryne *et al.*, 1998; Christofori, 2006; Busch *et al.*, 2014).

The estimation of nuclear localisation of Gli proteins is essential for determining their function, as indicated previously. Active Hh signalling require nuclear localisation of Gli proteins (Figure 0-7). Nuclear localisation of Gli1, Gli2 and Gli3 were increased at the invasive front compared to the tumour centre with statistical significance (Figure

4-23). 70% of breast cancer samples showed positive Gli1 nuclear localisation (Table 4-4-A). All samples showed positivity for Gli2 nuclear localisation (Table 4-4-B) and 90% cases showed positivity for Gli3 nuclear localisation (Table 4-4-C). This indicate that Gli proteins were active in most of breast cancer samples. Therefore, further analysis of correlation with clinical criteria is encouraged.

4.4.3 Gli1 overexpression correlated with higher stage, grade and size breast tumours

Assessment of the subcellular localisation of Gli proteins is essential for determining the status of Hh signalling (Ruiz i Altaba *et al.*, 2002). Nuclear localisation of Gli1 correlated with poor outcome of colon cancer (Ding *et al.*, 2012) medulloblastoma (Pizem *et al.*, 2011) and gastric cancer (Kim *et al.*, 2012). Research to date alluded to a role of Gli1 in the malignant progression of breast cancer with varied expression reported in breast cancer samples using IHC (Kubo *et al.*, 2004; ten Haaf *et al.*, 2009). Several studies found that increased Gli1 correlated with poor breast cancer prognosis (Kameda *et al.*, 2009; Kwon *et al.*, 2011; Xu *et al.*, 2015). Increased immunoreactivity for Gli1 in breast cancer samples has been correlated with high tumour stage in several studies Tao *et al.* (2011), ten Haaf *et al.* (2009) and Souzaki *et al.* (2011).

The nuclear localisation of Gli1 is associated with tumour size, and shorter recurrence-free and overall survival (Arnold *et al.*, 2017). In agreement with this finding, the nuclear localisation of Gli1 was correlated with tumour size in the tumour centre and at the invasive front with stronger nuclear localisation at the invasive front (Figure 4-23). We also showed that increased nuclear localisation of Gli1 was correlated with higher tumour stage with increased nuclear localisation at the invasive front of tumours with higher stage (Figure 4-24). Consistent with this, Li *et al.* (2012) found that nuclear localisation of Gli1 was significantly correlated with decreased life expectancy.

Kubo *et al.* (2004), Kameda *et al.* (2009), Xu *et al.* (2010), Souzaki *et al.* (2011) and Kwon *et al.* (2011) all reported high expression of Gli1 in TNBC in association with a poor prognosis and survival. The association of Gli1 expression and HER2 expression was also reported previously by Jeng *et al.* (2013). No association with molecular subtypes were found after analysing the expression of Gli1 tissue distribution and subcellular localisation in this study. This could be because the number of cases included in this study were less than that in previous studies. Bigger sample size is

required in order to find if there were correlation between Gli1 expression and molecular subtypes of breast cancer.

4.4.4 Gli2 and Gli3 expression correlate with favourable clinical criteria

Gli2 is a bi-functional protein that has two functional domains, an activator and a repressor, whereby proteolytic processing is required to determine function (Pan *et al.*, 2006). The oncogenic property of Gli2 overexpression was reported in basal-cell carcinoma (Tojo *et al.*, 2003) hepatocellular carcinoma (Zhang *et al.*, 2014) and prostate cancer (Thiyagarajan *et al.*, 2007). Gli3 is expressed as a full-length inactive protein that requires cleavage for translocation to the nucleus where it functions as a Hh signalling repressor (Ruiz i Altaba *et al.*, 2002). Several studies reported that there was an activator form for Gli3, however it is not clear if this was context-dependent or indeed if it was tissue-specific (Wang *et al.*, 2011a; Lee *et al.*, 2013).

Several studies assessed the expression Gli2 and Gli3 in human breast cancer samples. To date very few studies used combined assessment of all three parameters (expression, tissue distribution and subcellular localisation) of Gli2 and Gli3 in breast cancer. Lewis (2001) found that disruption of Gli2 function resulted in mammary ductal hyperplasia. Im *et al.* (2013) assessed the expression of Gli1, Gli2 and Gli3 and reported that Gli3 expression correlated with tumour stage and increased tumour size. They also reported that Gli2 correlated with ER status while Gli3 correlated with HER2 positive status (Im *et al.*, 2013). Contradictory to the previous finding, Gli2 expression correlated with smaller tumour size (Figure 4-25) whereas increased expression of Gli2 correlated with lower tumour stage (Figure 4-26) and grade (**Error! Reference source not found.**). The percentage of and IRS class of Gli2 expression in tumour centre was inversely associated with lymph node involvement (Figure 4-27 and Figure 4-28). Thiyagarajan *et al.* (2007) also reported that Gli2 overexpression accelerated the growth of prostate tumours. Yet, loss of Gli2 was seen in high-grade and larger breast tumours as seen here.

Gli3 expression correlated significantly with younger mean age at diagnosis and hormone-positive breast cancer (Figure 4-29) which contradicts the findings of previous studies (Im *et al.*, 2013). The cause of difference between the correlation between Gli3 expression and the molecular subtypes of breast cancer could be due to the difference in the method of assessment of IHC. In previous studies, Gli proteins expressions were assessed in all the tissue section without taking into account the importance of assessment of tissue distribution.

4.4.5 Gli1 and Gli2 were co-expressed in breast cancer samples while Gli1 increase was associated with reduction of Gli3

Gli1 and Gli2 were co-expressed in breast cancer samples in the tumour centre and at the invasive front (Figure 4-31). As seen in Figure 4-32, increased Gli2 expression was associated with increased nuclear localisation of Gli1 in the tumour centre and at the invasive front. Therefore, suggesting that these Gli proteins may have similar functions. This finding is novel and encourages further investigation of the co-expression and/or knockdown of Gli1 and Gli2 in cell lines. Schnidar *et al.* (2009) demonstrated that the synergistic effect of Gli1/ Gli2 and EGFR signalling promotes oncogenic modification of the Gli target genes, thus promoting cancer. Similar investigative approach is encouraged based on these findings using breast cancer cell lines.

Gli3 in breast tissue was reported to have an antagonistic effect to Gli1; in fact, co-expression of Gli1 and Gli3 led to mutual antagonism of Hh signalling in mice (Bai and Joyner, 2001). Here, we found that increased Gli1 expression corresponded to decreased Gli3 expression (Figure 4-33). This finding confirms that increased activation of Hh signalling was associated with loss of Gli3 expression and increased Gli1. This is the first study to report co-expression analysis of both Gli1 and Gli3, but no further conclusion can be made until analysis of Gli1 and Gli3 expression were done on larger sample size.

4.4.6 Correlation between Hh and Wnt/β-catenin in breast cancer samples

Several studies confirmed increased nuclear localisation of β-catenin at the invasive front compared to the tumour centre is indicative of EMT-like change in colon (Zlobec and Lugli, 2009), parathyroid (Fendrich *et al.*, 2009), and oral carcinomas (Wang *et al.*, 2009). To confirm the relationship between Hh activation and increased EMT, Gli1, Gli2 and Gli2 expression data was correlated with that for β-catenin and E-cadherin. Changes in β-catenin expression were found to be associated with EMT in colon cancer (Batlle *et al.*, 2002) and in breast cancer (Gong *et al.*, 2013). Tissue distribution of β-catenin was investigated by Wang *et al.* (2011b) and they reported that increased expression levels and nuclear localisation were observed at the invasive front of colon tumours. Detailed analysis of tissue distribution in combination with subcellular localisation of β-catenin in breast cancer was not investigated at this level of detail previously.

In the current study, no correlation was found between the expression of Gli proteins and β-catenin. Nuclear localisation of Gli2 was associated with increased E-cadherin expression in the tumour centre (Figure 4-36). This finding is in disagreement with previous finding. Alexaki *et al.* (2010) found increased expression of Gli2 was observed at the invasive front of melanoma and was associated with a loss of E-cadherin. Thus, indicating that there is a link between the Gli2 protein tissue distribution and cancer invasion by regulating E-cadherin expression in that type of cancer. This finding was different to the current data, which could either suggest that the regulation of Hh in breast tumours or that further analysis of tissue distribution and subcellular localisation is required. Additionally, the restriction of the small sample size in this study limit the ability to draw further conclusions.

Arnold *et al.* (2017) was the first study to report co-expression of Gli1 and β-catenin in breast cancer. They concluded that co-activation of Hh signalling and Wnt signalling occurs in breast cancer as they observed increased nuclear expression of Gli1 and β-catenin (Arnold *et al.*, 2017). However, their analysis did not include assessment of tissue distribution. Further analysis is required in the current cohort, and a larger sample size is needed to confirm the finding, crosstalk was also associated with loss of E-cadherin.

4.4.7 The Hedgehog (Hh) signalling pathway components were expressed in breast cancer cell lines

Theunissen and de Sauvage (2009) suggested that breast cancer invasion may be mediated through both autocrine and paracrine Hh signalling, which is also consistent with other studies (Habib and O'Shaughnessy, 2016; Hanna and Shevde, 2016). However, the difference in the roles of autocrine and paracrine Hh signalling in breast cancer has not been investigated. The study by Varnat *et al.* (2010) used human colon cancer cell lines and reported that expression of Shh, PTCH and Gli1 was detected in the epithelium,. Szczepny *et al.* (2017) used a mouse model of small cell lung cancer and found that autocrine, ligand-dependent signalling has increased tumour progression.

In order to investigate the potentially autocrine activity of Hh signalling, and possible crosstalk with Wnt signalling, *in vitro* investigation using breast cancer cell lines can be performed. Several studies have investigated the expression of these proteins in breast cancer cell lines. Previous researchers found that all components of Hh signalling including; *Smo*, *Ptch1*, *Ptch2*, *Shh*, *Ihh*, *Dhh*, *Gli1*, *Gli2*, and *Gli3* were expressed in breast cancer cell lines (Kubo *et al.*, 2004; Mukherjee *et al.*, 2006;

Kameda *et al.*, 2009; Thomas *et al.*, 2011; Diao *et al.*, 2016; Song *et al.*, 2016). Here, same finding is confirmed in those cell lines in order to use them for functional and mechanistic analysis (Figure 4-38).

Breast cancer cell lines can be utilised to investigate the Hh signalling and assess for crosstalk with Wnt. MCF7 (luminal) and MDA-MB-231 (basal and triple negative) were used for further *in vitro* analysis (see chapter 5). Han *et al.* (2015) found that MDA-MB-231 cells expressed low levels of Gli1 and high Gli2 levels and Gli3 using Western blotting similar to that observed in the current findings (Figure 4-38). Fu *et al.* (2016) and Di Mauro *et al.* (2017) found that MCF7 expressed Gli1 and Gli2 proteins at a slightly higher level than that seen in MDA-MB-231, which is similar to our data (Figure 4-38). Mukherjee *et al.* (2006) found that MCF7 and MDA-MB-231 cells expressed high levels of *Gli1* compared to normal breast cells which was even higher in MDA-MB-231. Taken together, both cell lines (MCF7 and MDA-MB-231) were selected for functional and mechanistic investigation as both cell lines show expression of most of the Hh signalling proteins. Also, these cell lines are representative of both luminal, triple negative and basal-like breast cancers.

4.5 Conclusion

There were signs of EMT-like in breast cancer cell lines according to the alteration of E-cadherin and β-catenin expression seen after culturing the cell lines in the density model *in vitro* (chapter 3). Upon reviewing the literature (Flemban and Qualtrough, 2015), Hh signalling was a promising target for investigation because of its involvement in the early developmental stages of mammary gland development.

Here, we showed that Hh signalling was involved in breast cancer invasive front, the site of active EMT (Bryne *et al.*, 1998; Christofori, 2006; Busch *et al.*, 2014), by assessing expression of Gli1, Gli2 and Gli3 in a cohort of breast cancer patient samples.

To determine whether Hh signalling may play a role in breast cancer invasion and metastasis, estimation of Gli1, Gli2 and Gli3 expression in both the tumour centre and at the invasive front was conducted. It was shown that all three Gli proteins were expressed in breast cancer with variation of tissue distribution and subcellular localisation. Gli1 and Gli2 were found higher at the invasive front of tumours with increased nuclear localisation for Gli1, Gli2 and Gli3. Therefore, indicating an active role in the regulation of breast cancer invasion. This confirmed the hypothesis that Hh signalling may indeed effect breast cancer prognosis and present as a potential therapeutic target. At the time of submitting the work, this research was the first to assess tissue distribution of Gli1, Gli2 and Gli3 with estimation of subcellular localisation at two tissue locations.

To confirm the involvement of Hh signalling in the regulation of EMT in breast cancer, the expression of E-cadherin and β-catenin was analysed for association with Gli1, Gli2 and Gli3 expression in the tumour centre and at the invasive front. Bigger sample size and further analysis is required to assess the relationship between the Hh signalling pathway and β-catenin. This is because as analysis of the current number of samples did not show any significant correlation. Increased expression of Gli1 was correlated with loss of E-cadherin. However, increased Gli2 staining and nuclear localisation was correlated with increased E-cadherin, therefore, suggesting a different role of Gli2 in breast cancer. All these data encourage further investigation of the role of Hh signalling in the regulation of EMT in breast cancer using cell lines.

5. Chapter Five: The Effect of Inhibiting the Hedgehog Signalling Pathway in Breast Cancer Cell Lines

5.1 Introduction

In animal models, dysregulation of Hh signalling results in an increased chance of developing breast cancer (Zhang *et al.*, 2009). Several studies found a constant activation of Hh signalling in breast cancer cell lines, reinforcing the importance of autocrine signalling in this model as discussed in 4.4.7 (Kubo *et al.*, 2004; Mukherjee *et al.*, 2006; Kameda *et al.*, 2009; Thomas *et al.*, 2011; Diao *et al.*, 2016; Song *et al.*, 2016). This sustained activation of the Hh pathway increased proliferation of breast cancer cells (Moraes *et al.*, 2007). Thus, several studies suggested targeting Hh for breast cancer treatment.

Researchers studied inhibiting Hh signalling in breast cancer cell lines and *in vivo* using a range of inhibitors, and also by gene silencing, and measured the effect of this inhibition on cancer cell proliferation, cell death and invasion. These studies are collected and summarised in Table 5-1. Breast cancer cell lines were treated with cyclopamine, a naturally-occurring inhibitor of the Hh signalling pathway, which caused inhibition of proliferation in a dose-dependent manner (Kubo *et al.*, 2004; Mukherjee *et al.*, 2006; Kameda *et al.*, 2009). Zhang *et al.* (2009) also showed that inhibiting Hh signalling in both oestrogen receptor-positive and -negative breast cancer reduced cell growth. Several studies found that Hh inhibition in breast cancer cell lines resulted in the inhibition of motility and invasion (Kameda *et al.*, 2009; Kwon *et al.*, 2011; Souzaki *et al.*, 2011; Thomas *et al.*, 2011).

As summarised in Table 5-1 the vast majority of *in vitro* studies that showed that Hh inhibition caused decreased cell proliferation, yield and increased cell death. The *in vivo* studies showed similar outcomes and suggested that inhibition of Hh signalling showed promising anti-tumour effects in a therapeutic setting. The measurement of the effect of Hh inhibition on the level of Gli protein expression and localisation, which provide a direct indicator of the functional status of the pathway, were not explored in previous work.

Table 5-1: The inhibition of Hh signalling in breast cancer has been a topic of intense investigation.
This table summarises some of the breast cancer studies that have inhibited the Hh signalling pathway and includes the type of model, inhibitor used, and general effect resulted from this inhibition.

Study	Inhibitor	In vitro	In vivo	Proliferation / growth	Cell cycle	Motility / invasion	Cell death	Proteins expression
(Kubo *et al.*, 2004)	Cyclopamine	Panel of breast cancer cell lines	-	↓	-	-	-	-
(Mukherjee *et al.*, 2006)	Cyclopamine		-	-	-	-	↑	-
(Wolf *et al.*, 2007)	Cyclopamine		-	↓	↓	-	-	Ptch ↑ following inhibition
(Zhang *et al.*, 2009)	Cyclopamine		-	↓	-	-	-	-
(Tanaka *et al.*, 2009)	Cyclopamine		-	↓	-	-	-	-
(Souzaki *et al.*, 2011)	Cyclopamine		-	-	-	↓	-	-
(Thomas *et al.*, 2011)	Small interfering RNA for Gli1		-	↓	-	↓	↑	↓ following inhibition
(Matevossian and Resh, 2015)	RU-SKI43 and LDE225		-	↓	-	-	-	-
(Song *et al.*, 2016)	Cyclopamine		-	-	-	-	↓	↓ Slug and ↑E-cadherin
(Bao *et al.*, 2016)	Vismodegib		-	-	-	↓	-	↓ in MMPs, ↓ Smo, ↓ Gli1 nuclear localisation
(Kameda *et al.*, 2009)	Cyclopamine	TN	-	↓	-	↓	-	-
(Diao *et al.*, 2016)	GANT61	tamoxifen resistant	-	↓	-	-	↓	-
(Liu *et al.*, 2006a)	Cyclopamine	Primary mammary cells	-	-	-	-	-	↓ stem cell markers expression cells
(Che *et al.*, 2013)	Cyclopamine	MCF7 and MDA-MB-231	-	↓	↓	-	-	↓ cyclin D expression
(Diao *et al.*, 2016)	GANT61	tamoxifen resistant	-	↓		-	↓	-
(Das *et al.*, 2011)	Cyclopamine	TN and HER2^{+ve}	Animal xenographt	-	-	↓	-	↓ ligand secretion
(Chai *et al.*, 2013)	Cyclopamine	TN		↓	-	-	↑	-
(Zhuang *et al.*, 2013)	Cyclopamine	Panel of breast cancer cell lines		-	-	-	↑	-
(Han *et al.*, 2015)	Vismodegib, GANT61 and LDE225	Panel of breast cancer cell lines		↓	-	-	↑	-
(Benvenuto *et al.*, 2016)	GDC-0449 and GANT61	Panel of breast cancer cell lines		↓	-	-	↑	-
(Di Mauro *et al.*, 2017)	LDE225	primary breast cancer and cell lines		↓	-	-	-	-
(Heller *et al.*, 2012)	Cyclopamine and LDE225	-		↓	-	-	↓	-
(Ramaswamy *et al.*, 2012)	Vismodegib	-		↓	-	-	-	-

The effect of the inhibition of Hh signalling on other EMT regulatory pathways including Wnt/β-catenin signalling (described in Figure 0-9 and Figure 0-10) was not reported previously. In fact, crosstalk between Hh and Wnt pathways in breast cancer is poorly understood, even though it has been proven to be co-affected in epithelial

tumours such as colon cancer (Qualtrough *et al.*, 2015). Additionally, Arnold *et al.* (2017) recently concluded that there is combined activation of Hh and Wnt signalling in TNBC cases showing increased risk of recurrence. We confirmed in the previous section (Figure 4-38) that there was a correlation between Hh signalling protein expression and changes in the level of β-catenin expression and nuclear localisation. Qualtrough *et al.* (2015) found that inhibition of Hh signalling induced expression of E-cadherin and reduced invasion in colon cancer cell lines whilst reducing catenin related proteins.

Due to the promising data from previous cell line and *in vivo* work, clinical trials commenced to using Hh signalling inhibitors in several types of solid tumours including advanced breast cancer, as summarised in Table 5-2. A Phase I clinical trial was completed that included advanced TN, hormone receptor-positive and metastatic breast cancers. Two more Phase II clinical trials are currently recruiting including one that specifically recruits breast cancer patients (NCT02694224); no results have been yet been published for these trials (Martin *et al.*, 2015).

Table 5-2: Clinical trials of Hh inhibitors that involved breast cancer patients
This table summarises the clinical trials conducted or active that involved treating breast cancer cases with Hh inhibitors.

Clinical trails	Conditions	Phase/Aims	Drug	Status
NCT01576666	Advanced solid tumours including triple-negative, (ER^{+ve}, ER^{-ve}, $HER2^{-ve}$) metastatic breast cancer	Phase Ib	Oral LDE225 in combination with BKM120	Completed
NCT02465060	Solid tumours or lymphomas including breast cancers (metastatic)	Phase II	Several	Recruiting
NCT02027376	Triple-negative advanced breast cancer	Phase Ib	LDE225 in combination with docetaxel	Active, not recruiting (estimated end in May 2017)
NCT02694224	Breast cancer	Phase II	Vismodegib in combination with neoadjuvant chemotherapy	Recruiting (estimated end in December 2018)
NCT01071564	Metastatic breast cancers that cannot be removed by surgery	Phase I	Vismodegib or other drugs (Notch inhibitor)	Terminated
NCT01757327	Stage II-III ER^{+ve} and $HER2^{-ve}$ breast cancer	Phase II	LDE225	Withdrawn (Poor accrual)

The NCT01071564 and NCT01757327 clinical trials recruited TNBC and advanced metastatic breast cancers specifically. However, the NCT01071564 trial was terminated, and NCT01757327 was withdrawn before completion due to poor accrual. The preliminary data published showed that there is a lack of therapeutic efficacy as

seen in these two trials that were terminated (Habib and O'Shaughnessy, 2016). In the absence of results from other trials, it is difficult to determine the cause of failure of the treatment regimens used (Habib and O'Shaughnessy, 2016). Also, the efficacy of Hh inhibition on breast cancer might not be specific to a particular subtype of breast cancer. Increased activation of Hh signalling was not restricted to advanced TNBC, it was also shown in advanced hormone-positive tumours (Sun *et al.*, 2014b; Diao *et al.*, 2016). It would seem prudent therefore, to assess the level of expression and activity of Hh signalling in breast cancer patient samples prior to administration of treatment to ensure proper selection of patients that would benefit.

Alteration of the expression levels of the Hh pathway components in breast cancer is not well-defined. Thus, understanding the functional consequences of the activation of Hh signalling in the breast cancer cells requires analysis and studies at the cellular level in a tractable model. The relationship between both the expression and the localisation of Gli proteins within the cellular compartments of breast cancer cells, and the functional consequence of this, remains poorly understood. Additionally, the potential crosstalk between Hh and Wnt signalling has not been elucidated in breast cancer. Further investigation of these pathways in breast cancer could lead to the identification of novel therapeutic targets particularly for advanced and metastatic disease which is currently incurable and has a poor prognosis.

5.1.1 Aims

- To study the effect of inhibiting hedgehog signalling (Hh) on breast cancer cells *in vitro*.
- To investigate the potential crosstalk between the Hh pathway and Wnt signalling in the regulation of EMT in breast cancer.

5.1.2 Objectives

- To inhibit Hh signalling in breast cancer cell lines using cyclopamine or LDE225 at three concentrations (1, 5 and 10μM) then:
    - To assess the effect of Hh inhibition on cell yield, viability and cell death in a panel of cell lines representing the different molecular subtypes of breast cancer.
    - To analyse the expression level and subcellular localisation of E-cadherin, β-catenin, Gli1, Gli2, and Gli3 in the breast cancer cell lines in response to Hh inhibition.
    - Evaluate the effect of Hh inhibition on cellular motility and invasion of breast cancer cell lines.
    - To assess the effect of these treatments on output of canonical Wnt signalling activity.

5.2 Results

5.2.1 Hedgehog inhibition with cyclopamine or LDE225 reduces cell yield in breast cancer cell lines

To understand the effect of Hh inhibition on growth, viability and cell death of breast cancer cells, two breast cancer cell lines were treated for 48hours with either cyclopamine or LDE225 (1, 5 or 10μM), and cell yield, viability, and cell death were assessed. Cells were harvested following 48hours of treatment and the number of live and dead cells were counted using viability staining (acridine orange and propidium iodide (AO/PI)). Viability and cell death are presented as mean viable and dead cells as a percentage of the total.

Treatment with cyclopamine or LDE225 caused a reduction in both cell yield and the viability of MCF7 cells (luminal A), shown in Figure 5-1. The viability of MCF7 decreased by 4% following 5μM and 10μM cyclopamine treatment (p-value<0.001 and p-value<0.001, respectively) as seen in Figure 5-1-B. MCF7 cell death doubled following 5μM and 10μM cyclopamine treatment (p-value<0.01 and p-value<0.001, respectively) shown in Figure 5-1-C. MCF7 cell yield showed a 20% and 46% reduction following 5μM (p-value<0.001) and 10μM (p-value<0.0001) LDE225 treatment, respectively compared to the vehicle control as summarised in Figure 5-1-D. Viability of MCF7 showed a 3% and 5% reduction following 5μM (p-value<0.0001) and 10μM (p-value<0.0001) LDE225 treatment, respectively, as seen in Figure 5-1-E. MCF7 cell death doubled following 5μM and 10μM LDE225 treatment (p-value<0.0001 and p-value<0.0001, respectively) as shown in Figure 5-1-F.

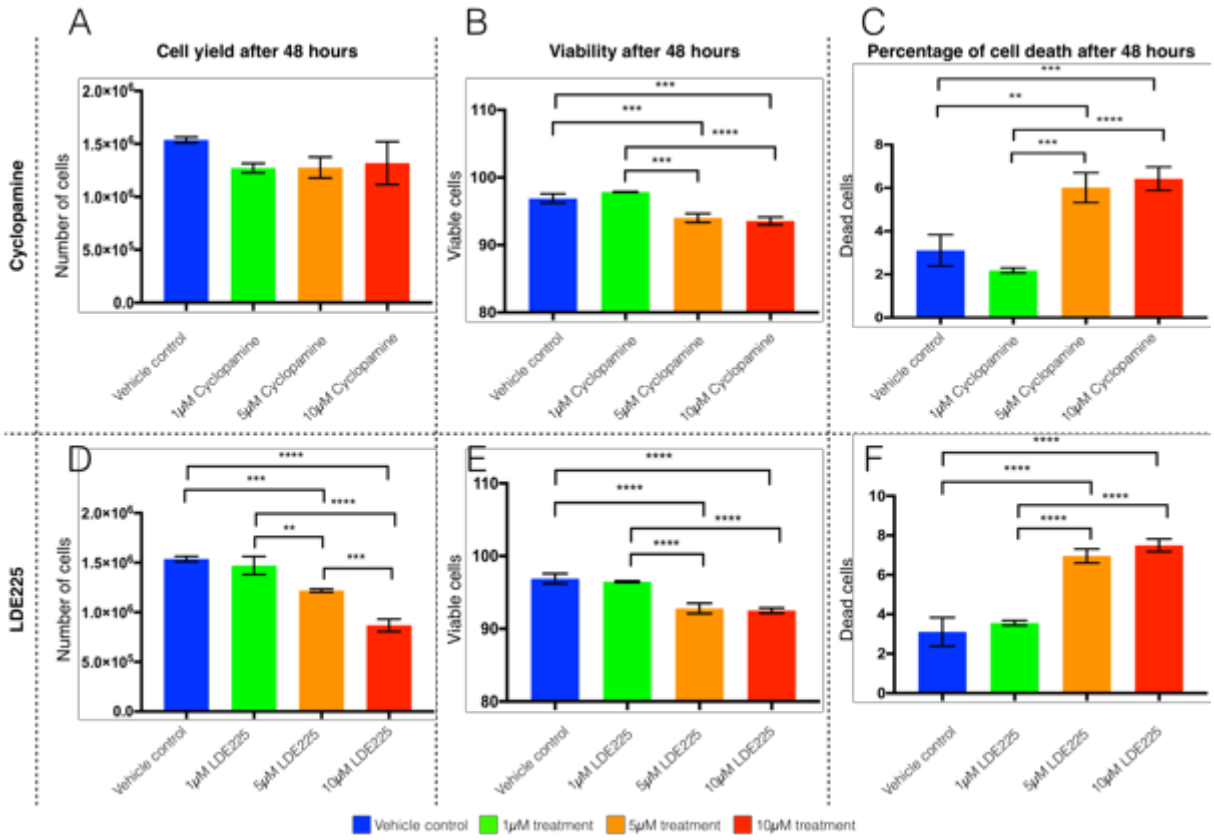

Figure 5-1, Reduction of cell yield and viability of MCF7 cell line following treatment with either cyclopamine or LDE225.
Comparison of the cell yields (A and D), viability (B and E) and percentage of dead (C and F) MCF7 cells following 48 hours of treatment with two Hh inhibitors (cyclopamine or LDE225) at three concentrations (1μM, 5μM and 10μM) compared to vehicle control. Change in yield following inhibition with cyclopamine (A) or LDE225 (D) treatment. Results displayed as bars of means of numbers of cells ± S.D. Changes in the viability of MCF7 cells following inhibition by cyclopamine (B) and LDE225 (E). Change in percentage of dead MCF7 cells following inhibition with cyclopamine (C) and LDE225 (F). Results displayed as bars of mean percentages of cells ± S.D. This figure is representative of n=3 experiments in triplicate. Statistical analysis was conducted, and significant differences between samples were indicated by *=*p*-value<0.05, **=*p*-value<0.01, ***=*p*-value<0.001 and ****=*p*-value<0.0001.

Treatment with cyclopamine or LDE225 caused a reduction in MDA-MB-231 (triple-negative and basal-like) cell yield and viability in a dose-dependent manner as summarised in Figure 5-2. Following cyclopamine treatment MDA-MB-231 cell yield showed a 6% decrease at 5μM (*p*-value<0.05) and 20% decrease at 10μM (*p*-value<0.0001) seen in Figure 5-2-A. The viability of MDA-MB-231 cells reduced in a dose-dependent manner following 1μM, 5μM and 10μM cyclopamine treatment (*p*-value<0.01, *p*-value<0.0001 and *p*-value 0.0001) seen in Figure 5-2-B. Cell death showed a 2% (*p*-value<0.01), 2.5% (*p*-value<0.0001) and 4% (*p*-value<0.0001) increase following 1μM, 5μM and 10μM treatment with cyclopamine, respectively, as seen in Figure 5-2-C. Following treatment with LDE225 cell yield decreased by 24% at

1μM (p-value<0.05), 19% at 5μM and 43% 10μM (p-value<0.01) as seen in Figure 5-2-D. The viability of MDA-MB-231 decreased in a dose-dependent manner following LDE225 treatment, however, the change was not statistically significant (Figure 5-2-E). The percentage of dead cells increased accordingly following LDE225 treatment without significant difference (Figure 5-2-F).

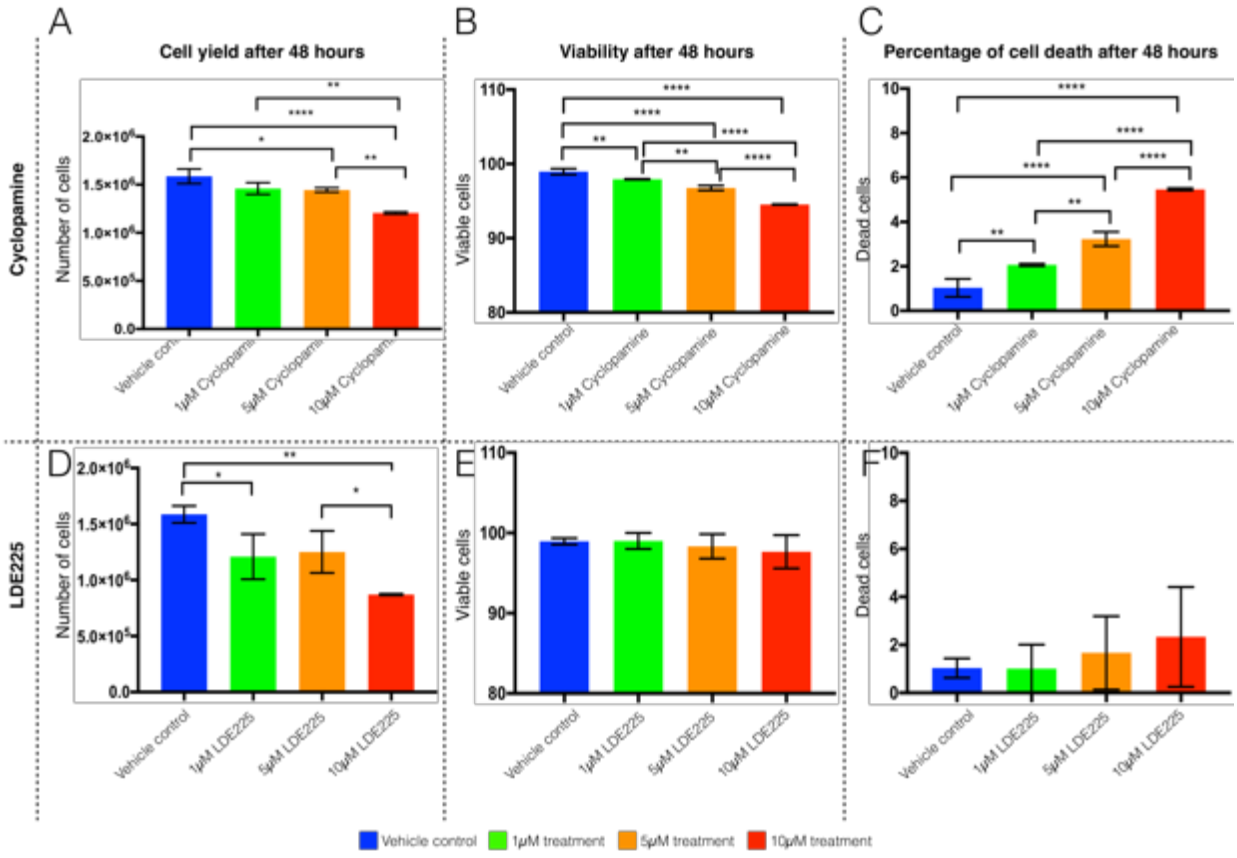

Figure 5-2, Reduction of cell yield and viability of MDA-MB-231 cell line following treatment with either cyclopamine or LDE225.
Comparison of the cell yields (A and D), viability (B and E) and percentage of dead (C and F) MDA-MB-231 cells following 48 hours of treatment with two Hh inhibitors (cyclopamine or LDE225) at three concentrations (1μM, 5μM and 10μM) compared to vehicle control. Change in yield following inhibition with cyclopamine (A) or LDE225 (D) treatment. Results displayed as bars of means of numbers of cells ± S.D. Changes in the viability of MDA-MB-231 cells following inhibition with cyclopamine (B) and LDE225 (E). Change in percentage of dead MDA-MB-231 cells following inhibition with cyclopamine (C) and LDE225 (F). Results displayed as bars of means percentages of cells ±S.D. This figure is representative of n=3 experiments in triplicate. Statistical analysis was conducted, and significant differences between samples were indicated by *=p-value<0.05, **=p-value<0.01, ***=p-value<0.001 and ****=p-value<0.0001.

5.2.2 Higher apoptosis in MCF7 than MDA-MB-231 following inhibition of Hh signalling

An apoptosis assay (Casciola-Rosen *et al.*, 1996) was utilised to see if the reduction in cell yield was caused by increased cell death of breast cancer cell lines after treatment with either cyclopamine or LDE225. FITC Annexin V detection was used to identify levels of apoptosis in MCF7 and MDA-MB-231 cells following 48hours of treatment. Probing the cells with Annexin V in combination with PI allowed distinction between early and late apoptotic cells, or dead cells (final stages of apoptotic death or might have undergone necrosis) in samples by means of flow cytometry.

In MCF7 cells, 1, 5 and 10μM of cyclopamine orLDE225 caused an increase in the percentage of dead cells (10%, 20% and 20% respectively) compared to the vehicle control (Figure 5-5-A and B). The percentage of dead cells following treatment showed a highly significant difference when compared with the vehicle control (*p*-value<0.0001) (Figure 5-5-A and B).

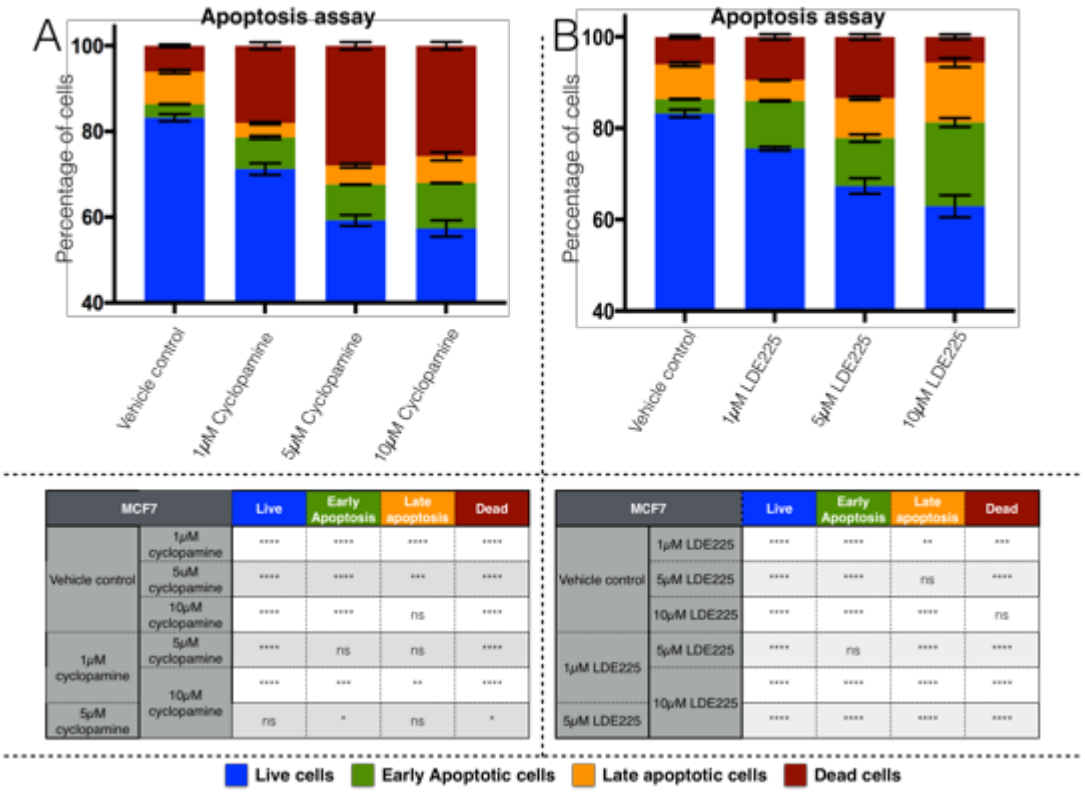

MCF7		Live	Early Apoptosis	Late apoptosis	Dead
Vehicle control	1μM cyclopamine	****	****	****	****
	5uM cyclopamine	****	****	***	****
	10μM cyclopamine	****	****	ns	****
1μM cyclopamine	5μM cyclopamine	****	ns	ns	****
	10μM cyclopamine	****	***	**	****
5μM cyclopamine		ns	*	ns	*

MCF7		Live	Early Apoptosis	Late apoptosis	Dead
Vehicle control	1μM LDE225	****	****	**	***
	5μM LDE225	****	****	ns	****
	10μM LDE225	****	****	****	ns
1μM LDE225	5μM LDE225	****	ns	****	****
	10μM LDE225	****	****	****	****
5μM LDE225		****	****	****	****

Figure 5-3, Increase in MCF7 cells (luminal A) apoptosis following cyclopamine or LDE225 treatment.

Comparison of the mean percentages of live (Blue), early apoptotic (Green), late apoptotic (Orange) and dead (Red) MCF7 cells following 48 hours of treatment with cyclopamine or LDE225 at 1μM, 5μM and 10μM. Stacked bars of apoptosis assay results of percentages of live, early and late apoptosis and dead cells following cyclopamine (A) or LDE225 treatment (B). Below are tables that summarise the statistical comparisons between all variables. Results displayed as stacked columns of means percentage of cells ± S.D. This figure is representative of n=3 experiments in triplicate. Statistical analysis was conducted, and significant differences between samples were indicated by *p-value<0.05, **p-value<0.01, ***p-value< 0.001 and ****p-value<0.0001

The triple-negative and basal-like breast cancer cell line MDA-MB-231 (Figure 5-4) showed less cell death following treatment compared to MCF7 (Figure 5-3). The percentage of cell death increased in a dose-dependent manner following treatment of MDA-MB-231 with cyclopamine or LDE225 for 48hours (Figure 5-4-A and B). Treatment of MDA-MB-231 cells with cyclopamine showed an increased in cell death to 2% at the highest concentration with statistical significance (Figure 5-4-A). The percentage of cell death following 48hours of LDE225 treatment (Figure 5-4-B) was higher than that seen following cyclopamine treatment (Figure 5-4-A). The increase in apoptosis following 5 and 10μM LDE225 treatment was twice as much as that seen in the vehicle control which was statistically significant (Figure 5-4-B). It should be noted that MCF7 cell line showed increased early apoptosis compared to increased late apoptosis percentage in MDA-MB-231 cell lines.

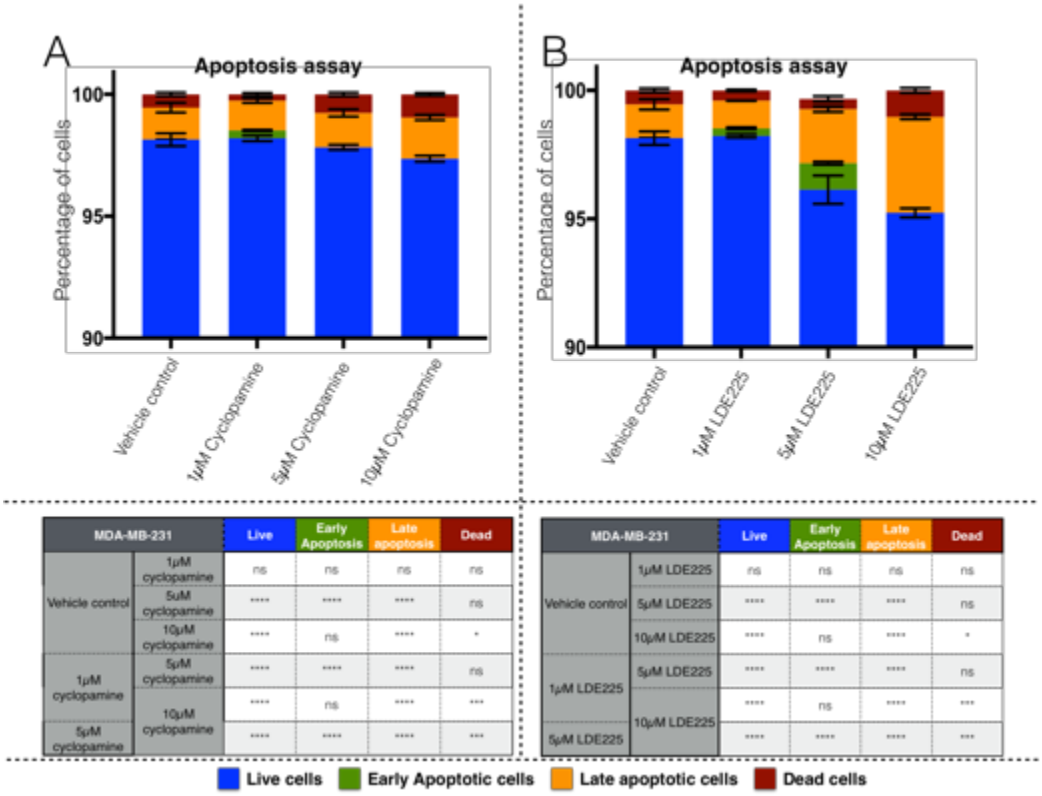

MDA-MB-231		Live	Early Apoptosis	Late apoptosis	Dead
Vehicle control	1μM cyclopamine	ns	ns	ns	ns
	5uM cyclopamine	****	****	****	ns
	10μM cyclopamine	****	ns	****	*
1μM cyclopamine	5μM cyclopamine	****	****	****	ns
	10μM cyclopamine	****	ns	****	***
5μM cyclopamine		****	****	****	***

MDA-MB-231		Live	Early Apoptosis	Late apoptosis	Dead
Vehicle control	1μM LDE225	ns	ns	ns	ns
	5μM LDE225	****	****	****	ns
	10μM LDE225	****	ns	****	*
1μM LDE225	5μM LDE225	****	****	****	ns
	10μM LDE225	****	ns	****	***
5μM LDE225		****	****	****	***

Figure 5-4, Increase MDA-MB-231 (triple-negative and basal) apoptosis following cyclopamine or LDE225 treatment.
Comparison of the mean percentages of live (Blue), early apoptotic (Green), late apoptotic (Orange) and dead (Red) MDA-MB-231 cells following 48 hours of treatment with cyclopamine or LDE225 at 1μM, 5μM and 10μM. Stacked bars of apoptosis assay results of percentages of live, early and late apoptosis and dead cells following cyclopamine (A) or LDE225 treatment (B). Below are tables that summarise the statistical comparisons between all variables. Results displayed as stacked columns of means percentage of cells ± S.D. This figure is representative of n=3 experiments in triplicate. Statistical analysis was conducted, and significant differences between samples were indicated by *p-value<0.05, **p-value<0.01, ***p-value< 0.001 and ****p-value<0.0001.

5.2.3 Localisation and level of Gli1 in breast cancer cell lines (MCF7 and MDA-MB-231)

Gli1, Gli2 and Gli3 were expressed in MCF7 and MDA-MB-231 cell lines in the vehicle control as seen in Figure 5-5. Gli1 showed cytoplasmic and nuclear localisation in MCF7 and MDA-MB-231 as shown in Figure 5-5-A and Figure 5-5-B. Gli2 showed relatively high cytoplasmic and low nuclear localisation in MCF7 cells as seen in Figure 5-5-B and showed high nuclear and low cytoplasmic localisation in MDA-MB-231 cells as seen in Figure 5-5-E. Gli3 was mainly nuclear in both cell lines with low cytoplasmic levels as seen in Figure 5-5-C and Figure 5-5-F.

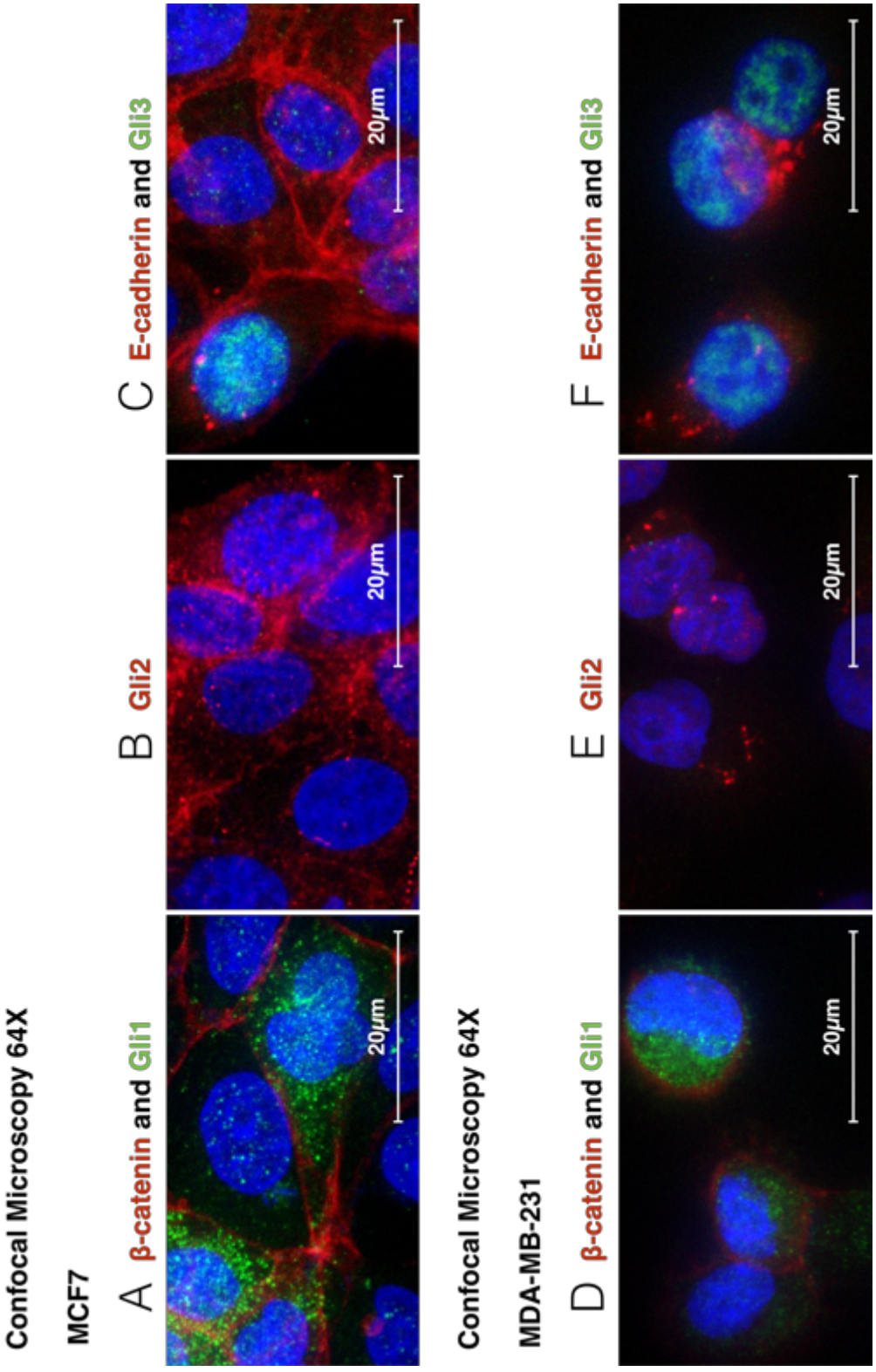

Figure 5-5, Expression of Gli1, Gli2, and Gli3 in MCF7 and MDA-MB-231.
Immunofluorescence Z stacked images of MCF7 and MDA-MB-231 cells captured under confocal microscope at 630x magnifications. MCF7 and MDA-MB-231 cells were double stained by β-catenin (Red) and Gli1 (green) antibodies (A and D). MCF7 and MDA-MB-231 cells were stained by Gli2 (Red) (B and E). MCF7 and MDA-MB-231 cells were double stained with E-cadherin (Red) and Gli3 (Green) (C and F). Cells were visualised by fluorescence labelled secondary antibodies Alexa Fluor® (488 and 594). DAPI stain was used to stain nuclei of cells (Blue).

5.2.4 Decreased Gli1 expression and nuclear localisation is concomitant with increased nuclear localisation of Gli2 and Gli3 in breast cancer cell lines following treatment with cyclopamine or LDE225

The expression of the Gli proteins following treatment were assessed for changes in level of expression using flow cytometry and for changes in localisation of proteins using Immunocytofluorescence (ICF). As seen in the histograms and bar charts that represent flow cytometry data, Gli1 expression increased following treatment with cyclopamine or LDE225 in MCF7 (Figure 5-6) and MDA-MB-231 (Figure 5-7). A notable decrease in Gli1 expression was observed following 5μM and 10μM LDE225 treatment in both cell lines compared to the alteration observed following cyclopamine treatment (Figure 5-6). ICF images of MCF7 (Figure 5-6) and MDA-MB-231 (Figure 5-7) apparently contradicted the flow cytometry expression results and showed that the overall protein level was decreased following treatment with either cyclopamine or LDE225 (Figure 5-6 and Figure 5-7).

Increased Gli1 expression in MCF7 (Figure 5-6-A, B and Figure 5-7-A, B) and MDA-MB-231 cells (Figure 5-8-A, B, and Figure 5-9-A and B) showed by flow cytometry analysis could be a result of cytoplasmic accumulation of Gli1 due to inhibition of Hh signalling by cyclopamine (Figure 5-6-E and F and Figure 5-7-E and F) or 1μM LDE225 (Figure 5-8-A and B, Figure 5-9-A and B). The increase in cytoplasmic protein shown in flow cytometry as an increase in expression level and then decreased in cells treated with more than 5μM of cyclopamine or LDE225. There was increased punctate Gli1 in the cytoplasm of MCF7 and MDA-MB-231 cells following treatment as seen in ICF images of Figure 5-6 and Figure 5-7.

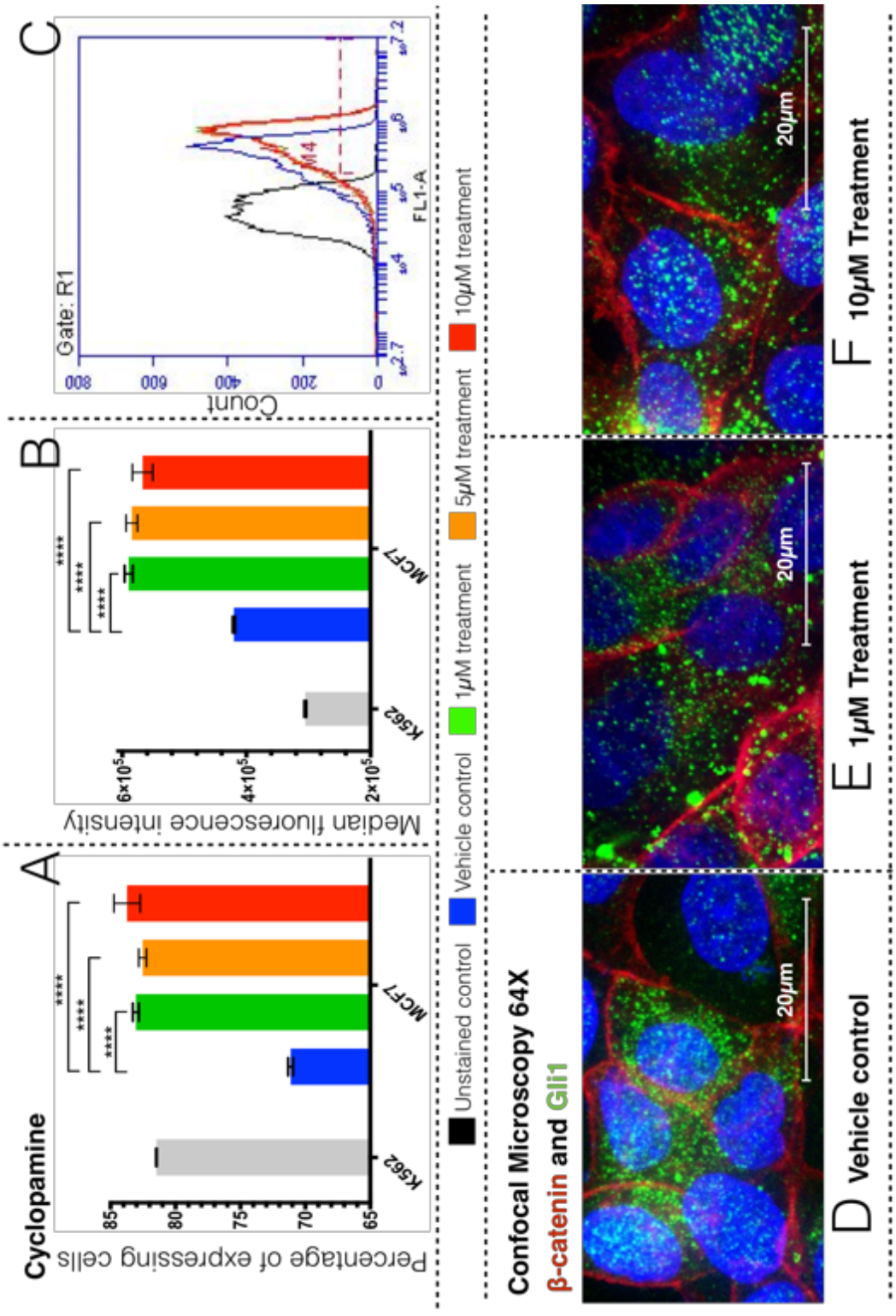

Figure 5-6, Alteration of Gli1 protein localisation and expression level in MCF7 following cyclopamine treatment.

Flow cytometry analysis of expression of Gli1 protein in MCF7 cells (A) percentage expression (B) MFI and (C) overlay histogram chart. Immunofluorescence Z stacked images of MCF7 cells captured using confocal microscope at 630x magnifications. MCF7 cells were double stained with β-catenin (Red) and Gli1 (green) antibodies. Vehicle control (D) MCF7 cells following 1μM and 10μM (F) treatment with cyclopamine for 48hours. Cells were visualised with fluorescence labelled secondary antibodies Alexa Fluor® (488 and 594). DAPI stain was used to stain cell nuclei (Blue).

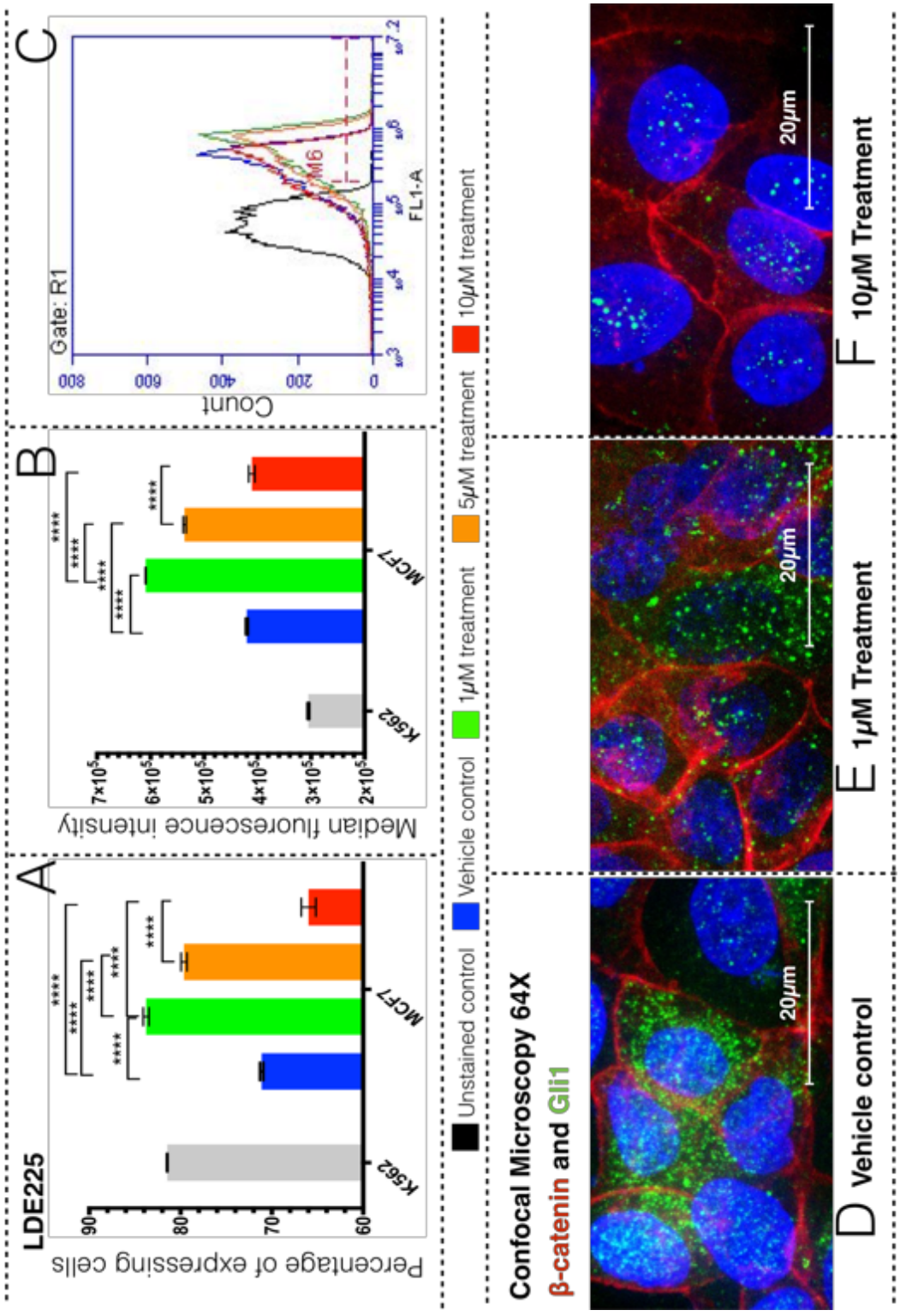

Figure 5-7, Alteration of Gli1 localisation and expression MCF7 following treatment with LDE225.

Flow cytometry analysis of expression of Gli1 protein in MCF7 cells (A) percentage expression (B) MFI and (C) overlay histogram chart. Immunofluorescence Z stacked images of MCF7 cells captured using confocal microscope at 630x magnifications. MCF7 cells were double stained with β-catenin (Red) and Gli1 (green) antibodies. Vehicle control (D) MCF7 cells following 1μM and 10μM (F) treatment with LDE225 for 48hours. Cells were visualised with fluorescence labelled secondary antibodies Alexa Fluor® (488 and 594). DAPI stain was used to stain cell nuclei (Blue).

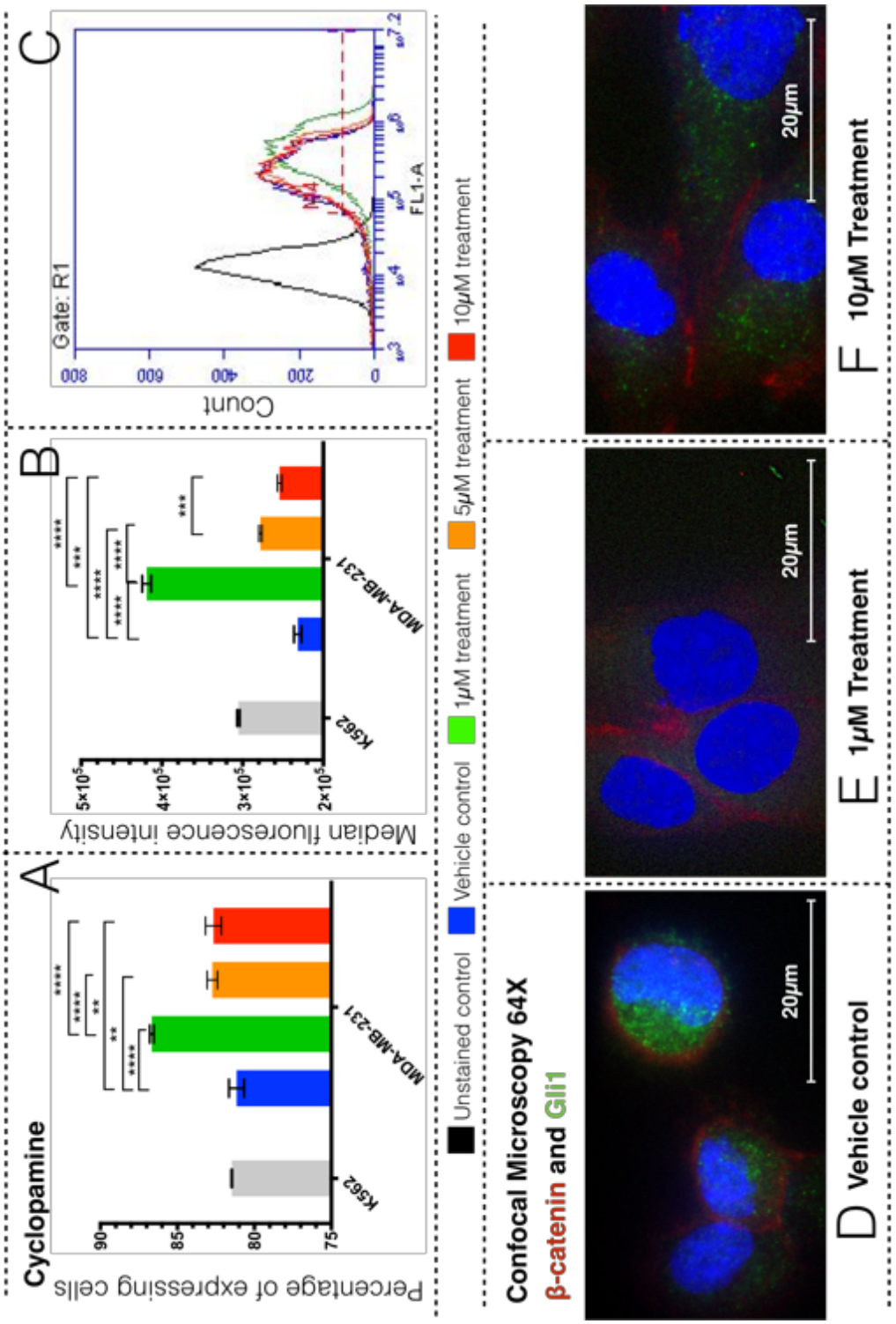

Figure 5-8, Alteration of Gli1 protein expression and localisation in MDA-MB-231 following cyclopamine treatment.

Flow cytometry analysis of expression of Gli1 protein in MDA-MB-231 cells (A) percentage expression (B) MFI and (C) overlay histogram chart. Immunofluorescence Z stacked images of MDA-MB-231 cells captured using confocal microscope at 630x magnifications. MDA-MB-231 cells were double stained with β-catenin (Red) and Gli1 (green) antibodies. Vehicle control (D) MDA-MB-231 cells following 1μM and 10μM (F) treatment with cyclopamine for 48hours. Cells were visualised with fluorescence labelled secondary antibodies Alexa Fluor® (488 and 594). DAPI stain was used to stain cell nuclei (Blue).

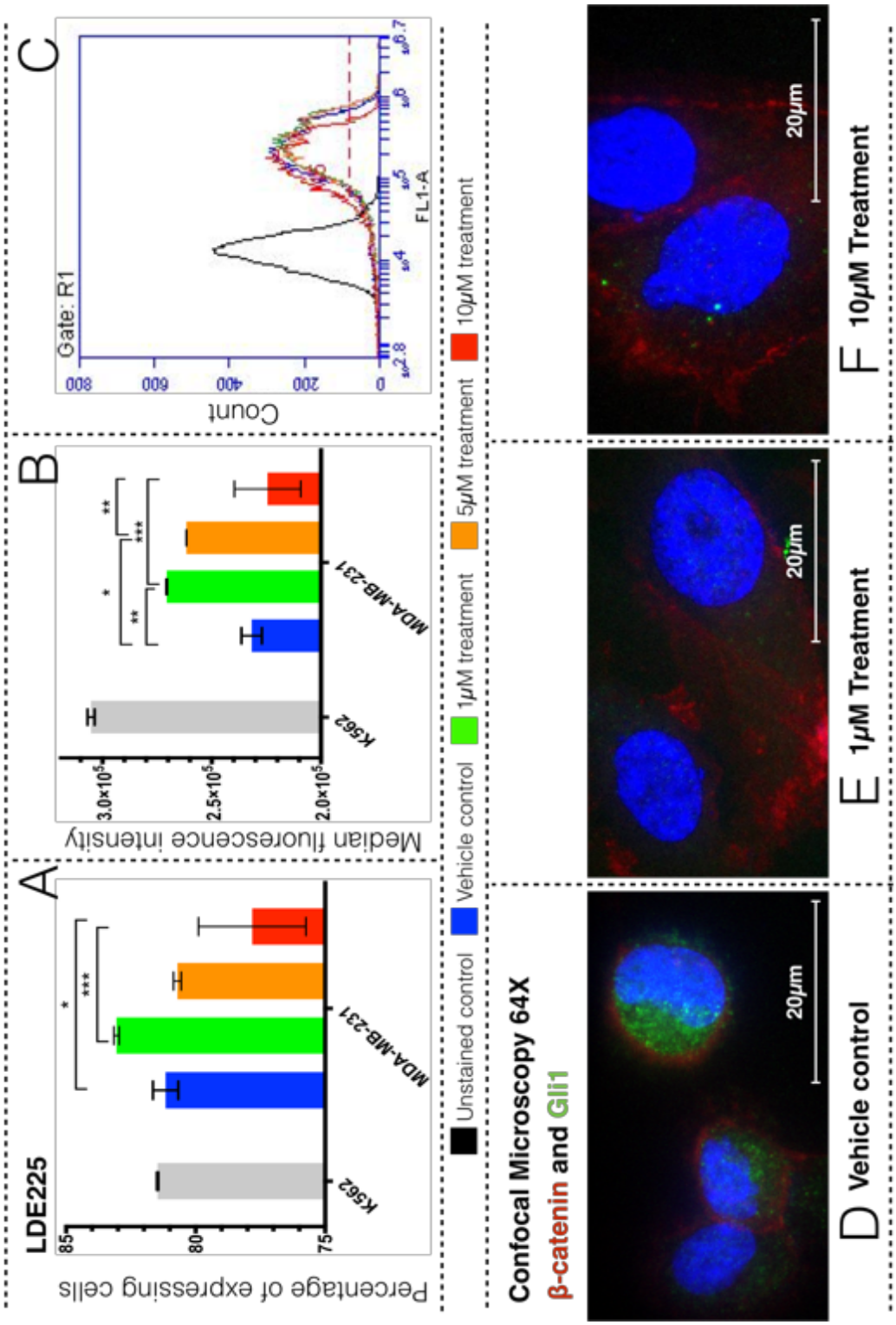

Figure 5-9, Alteration in Gli1 expression and localisation in MDA-MB-231 following treatment with LDE225.

Flow cytometry analysis of expression of Gli1 protein in MDA-MB-231 cells (A) percentage expression (B) MFI and (C) overlay histogram chart. Immunofluorescence Z stacked images of MDA-MB-231 cells captured using confocal microscope at 630x magnifications. MDA-MB-231 cells were double stained with β-catenin (Red) and Gli1 (green) antibodies. Vehicle control (D) MDA-MB-231 cells following 1μM and 10μM (F) treatment with LDE225 for 48hours. Cells were visualised by fluorescence labelled secondary antibodies Alexa Fluor® (488 and 594). DAPI stain was used to stain nucleus of cells (Blue).

Gli2 level decreased in MCF7 cells following treatment with either cyclopamine or LDE225 as seen in, Figure 5-10-A and B, and Figure 5-11-A and B. Nuclear localisation of Gli2 increased in MCF7 cells without observable alteration of cytoplasmic levels following cyclopamine treatment (Figure 5-10-E and F), while showing notable reduction in cytoplasmic levels following LDE225 treatment (Figure 5-11-E and F). In MCF7, the inhibition by LDE225 increased nuclear localisation of Gli2 (Figure 5-11-E and F) which was reflected as a reduction in expression seen by flow cytometry (Figure 5-11-A and B).

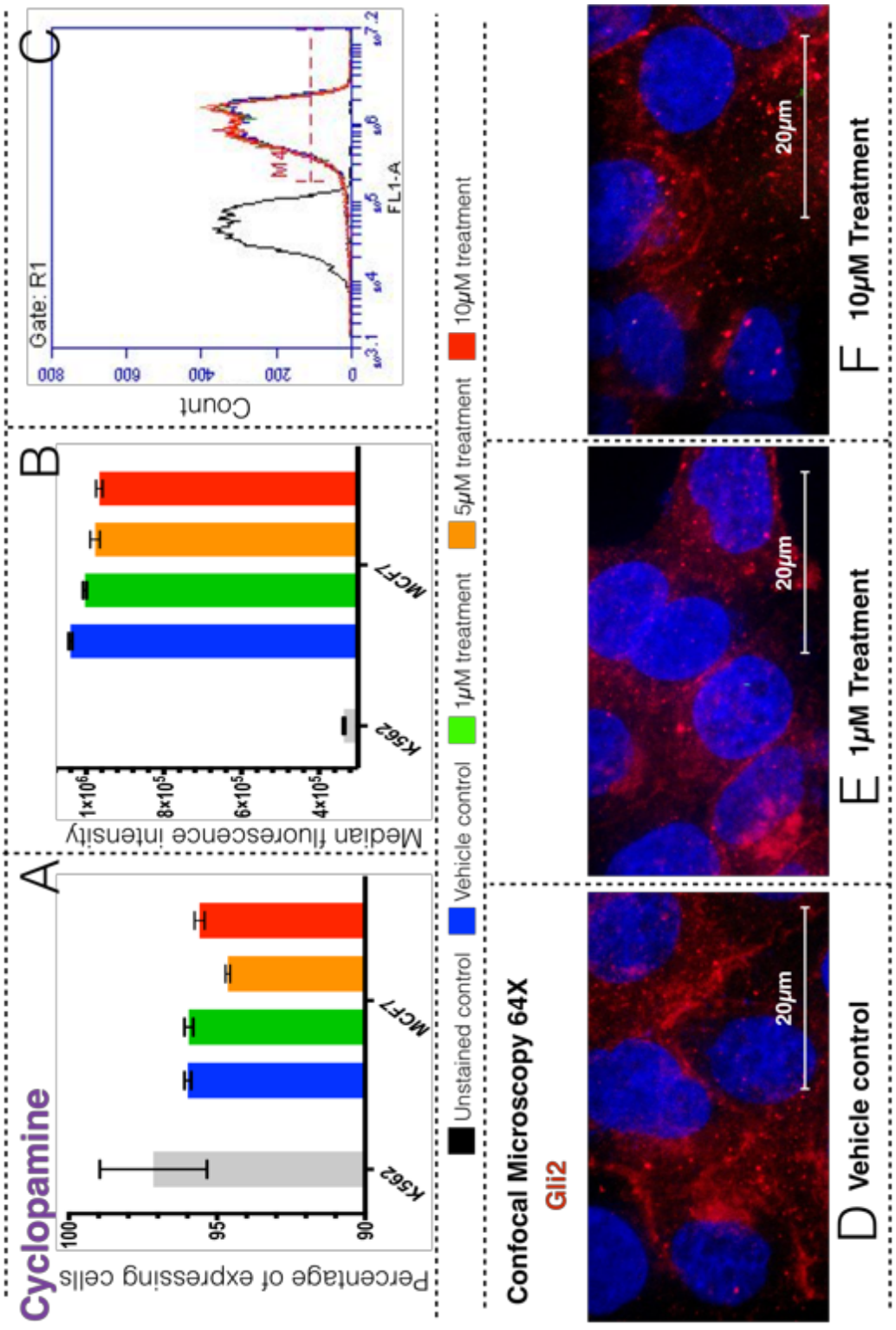

Figure 5-10, Reduction of Gli2 expression following cyclopamine treatment in MCF7.

Flow cytometry analysis of expression of Gli2 protein in MCF7 cells (A) percentage expression (B) MFI and (C) overlay histogram chart. Immunofluorescence Z stacked images of MCF7 cells captured using confocal microscope at 630x magnifications. MCF7 cells were stained with Gli2 (Red) antibody. Vehicle control (D) MCF7 cells following 1μM and 10μM (F) treatment with cyclopamine for 48hours. Cells were visualised by fluorescence labelled secondary antibodies Alexa Fluor® (594). DAPI stain was used to stain cell nuclei (Blue).

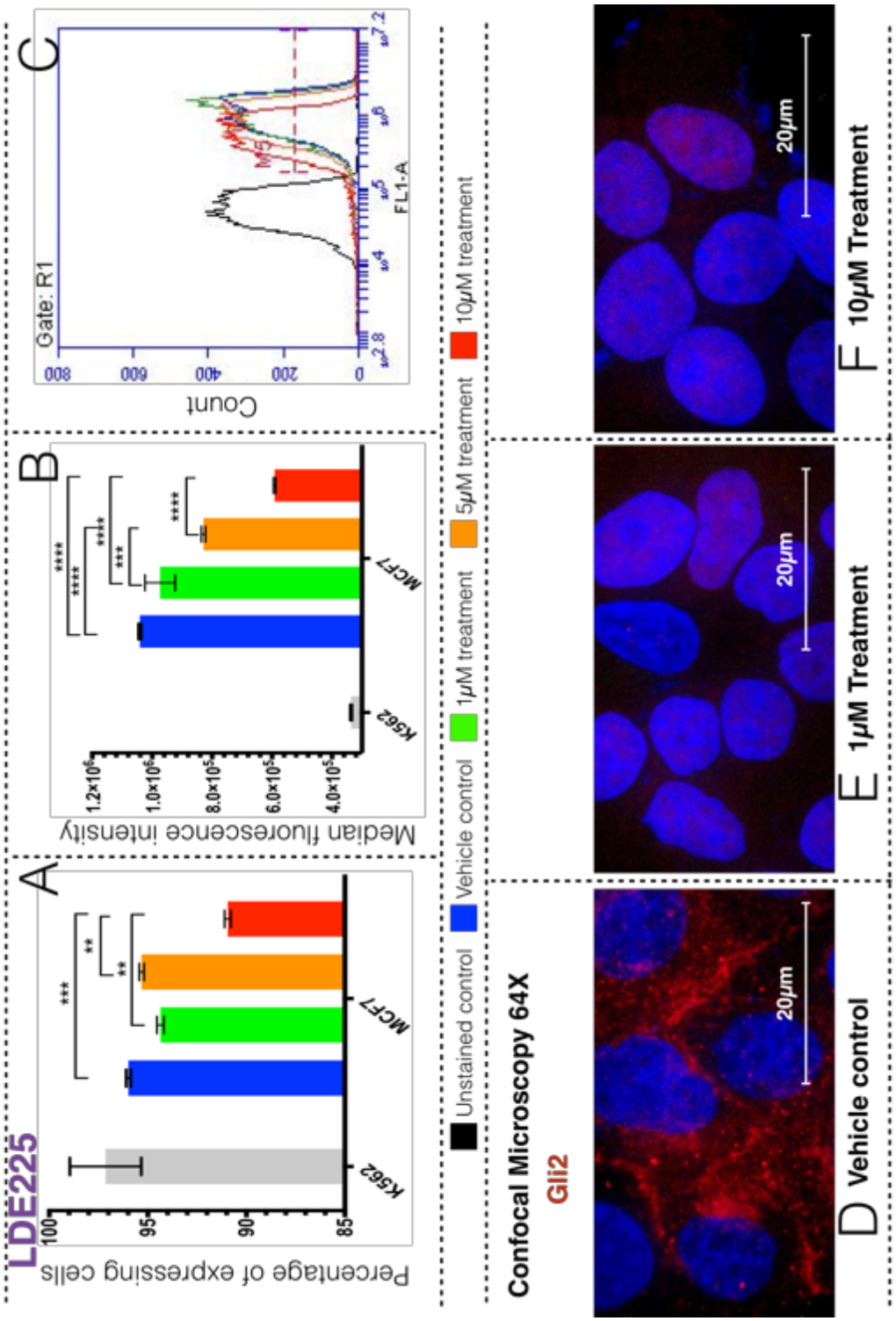

Figure 5-11, Increased nuclear Gli2 and reduction of overall Gli2 expression in MCF7 following treatment with LDE225.

Flow cytometry analysis of expression of Gli2 protein in MCF7 cells (A) percentage expression (B) MFI and (C) overlay histogram chart. Immunofluorescence Z stacked images of MCF7 cells captured using confocal microscope at 630x magnifications. MCF7 cells were stained with Gli2 (Red) antibody. Vehicle control (D) MCF7 cells following 1μM and 10μM (F) treatment with LDE225 for 48hours. Cells were visualised with fluorescence labelled secondary antibodies Alexa Fluor® (594). DAPI stain was used to stain cell nuclei (Blue).

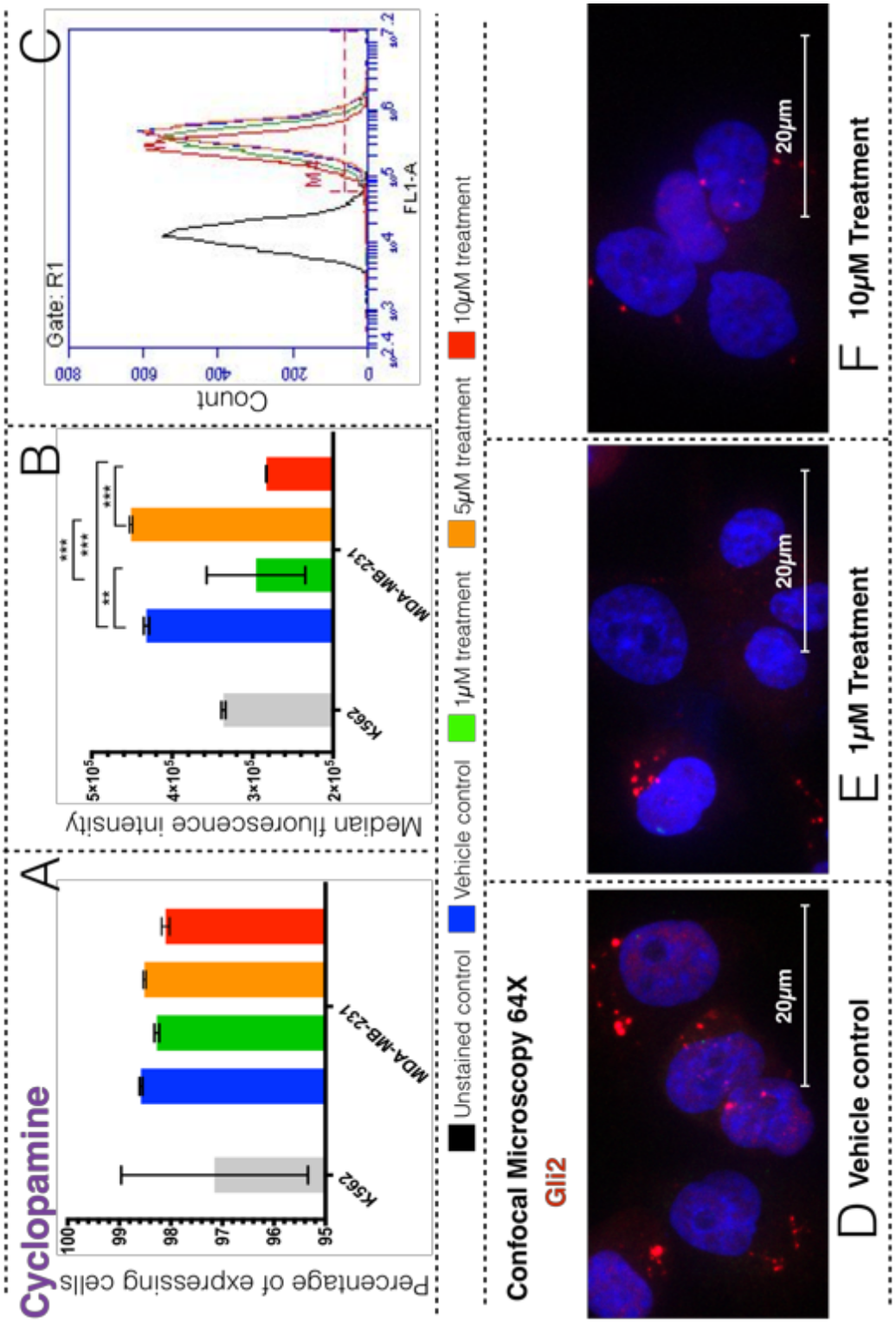

Figure 5-12, Alteration of Gli2 expression and localisation in MDA-MB-231 following cyclopamine treatment.

Flow cytometry analysis of expression of Gli2 protein in MDA-MB-231 cells (A) percentage expression (B) MFI and (C) overlay histogram chart. Immunofluorescence Z stacked images of MDA-MB-231 cells captured using confocal microscope at 630x magnifications. MDA-MB-231 cells were stained with Gli2 (Red) antibody. Vehicle control (D) MDA-MB-231 cells following 1μM and 10μM (F) treatment with cyclopamine for 48hours. Cells were visualised with fluorescence labelled secondary antibodies Alexa Fluor® (594). DAPI stain was used to stain cell nuclei (Blue).

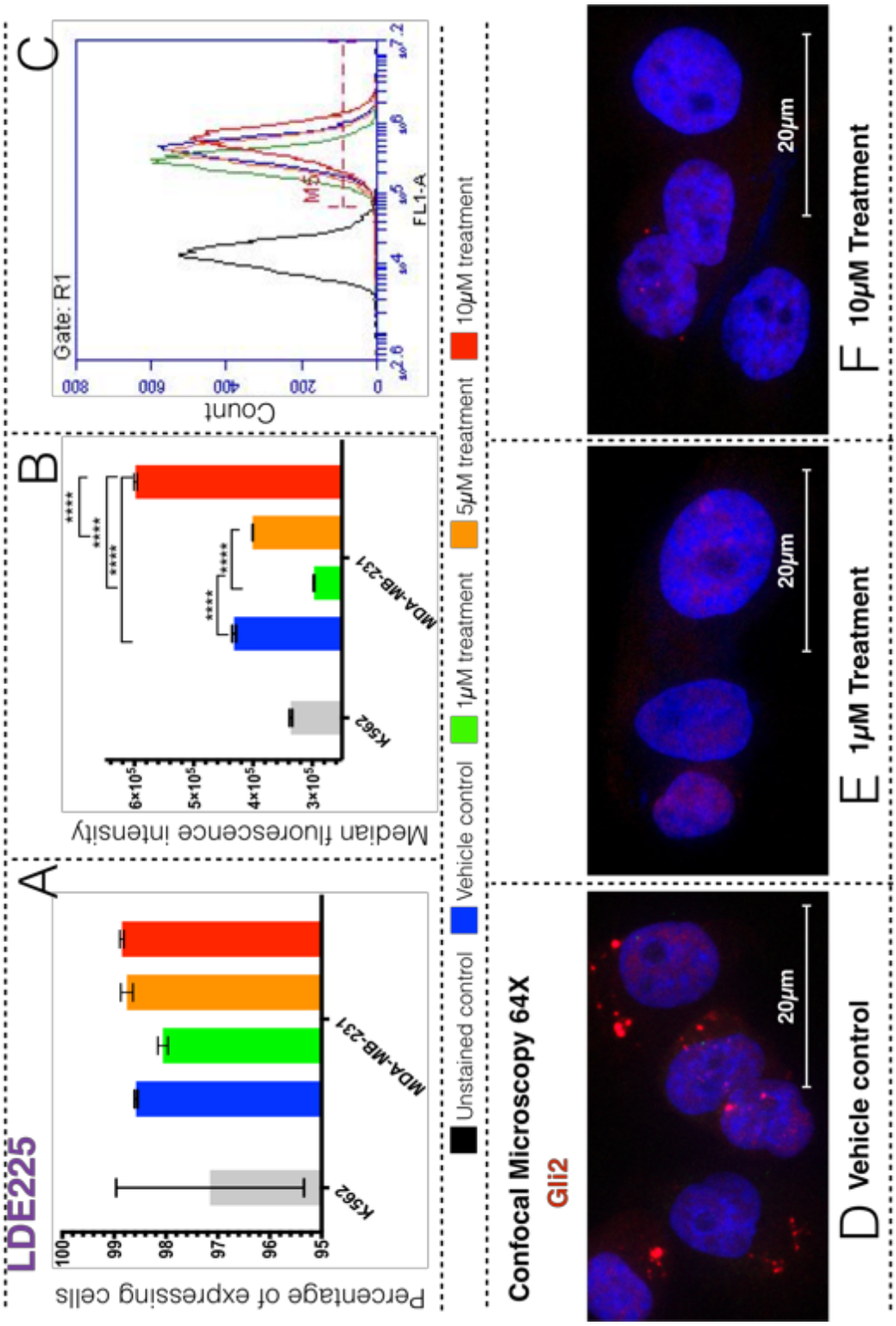

Figure 5-13, Alteration of Gli2 expression and localisation in MDA-MB-231 following treatment with LDE225.

Flow cytometry analysis of expression of Gli2 protein in MDA-MB-231 cells (A) percentage expression (B) MFI and (C) overlay histogram chart. Immunofluorescence Z stacked images of MDA-MB-231 cells captured using confocal microscope at 630x magnifications. MDA-MB-231 cells were stained with Gli2 (Red) and antibody. Vehicle control (D) MDA-MB-231 cells following 1μM and 10μM (F) treatment with LDE225 for 48hours. Cells were visualised with fluorescence labelled secondary antibodies Alexa Fluor® (594). DAPI stain was used to stain cell nuclei (Blue).

Following cyclopamine treatment, the overall expression of Gli3 decreased in MCF7 as seen in Figure 5-14-A and B and ICF images showed increase of Gli3 nuclear accumulation in Figure 5-14-E and F. Gli3 decreased to a lesser degree following LDE225 treatment of MCF7 as shown in Figure 5-15-A and B with less nuclear localisation as observed in Figure 5-15-E and F. Gli3 expression in MDA-MB-231 increased as seen in Figure 5-16-A and B with a dose-dependent increase in nuclear localisation as observed in ICF images in Figure 5-16-E and F. Treatment with LDE225 decreases Gli3 expression in MDA-MB-231 cells as seen by flow cytometry results in Figure 5-17-A and B, concurrent with increased nuclear localisation, as observed in ICF images in Figure 5-17-E and F.

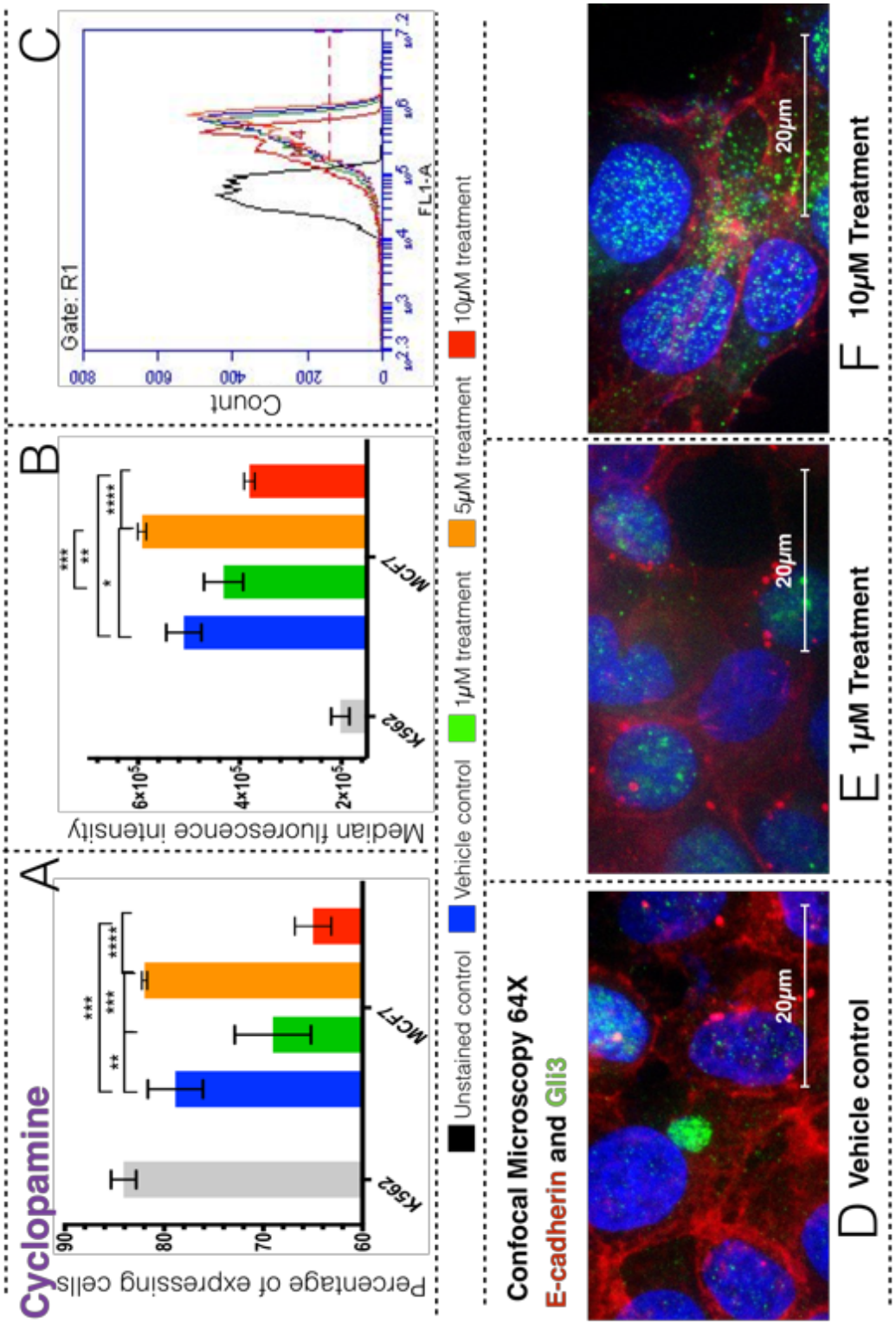

Figure 5-14, Alteration of Gli3 expression following cyclopamine treatment in MCF7.

Flow cytometry analysis of expression of Gli2 protein in MCF7 cells (A) percentage expression (B) MFI and (C) overlay histogram chart. Immunofluorescence Z stacked images of MCF7 cells captured using confocal microscope at 630x magnifications. MCF7 cells were stained with Gli3 (Green) and E-cadherin (Red) antibodies. Vehicle control (D) MCF7 cells following 1μM and 10μM (F) treatment with cyclopamine for 48hours. Cells were visualised with fluorescence labelled secondary antibodies Alexa Fluor® (488 and 594). DAPI stain was used to stain cell nuclei (Blue).

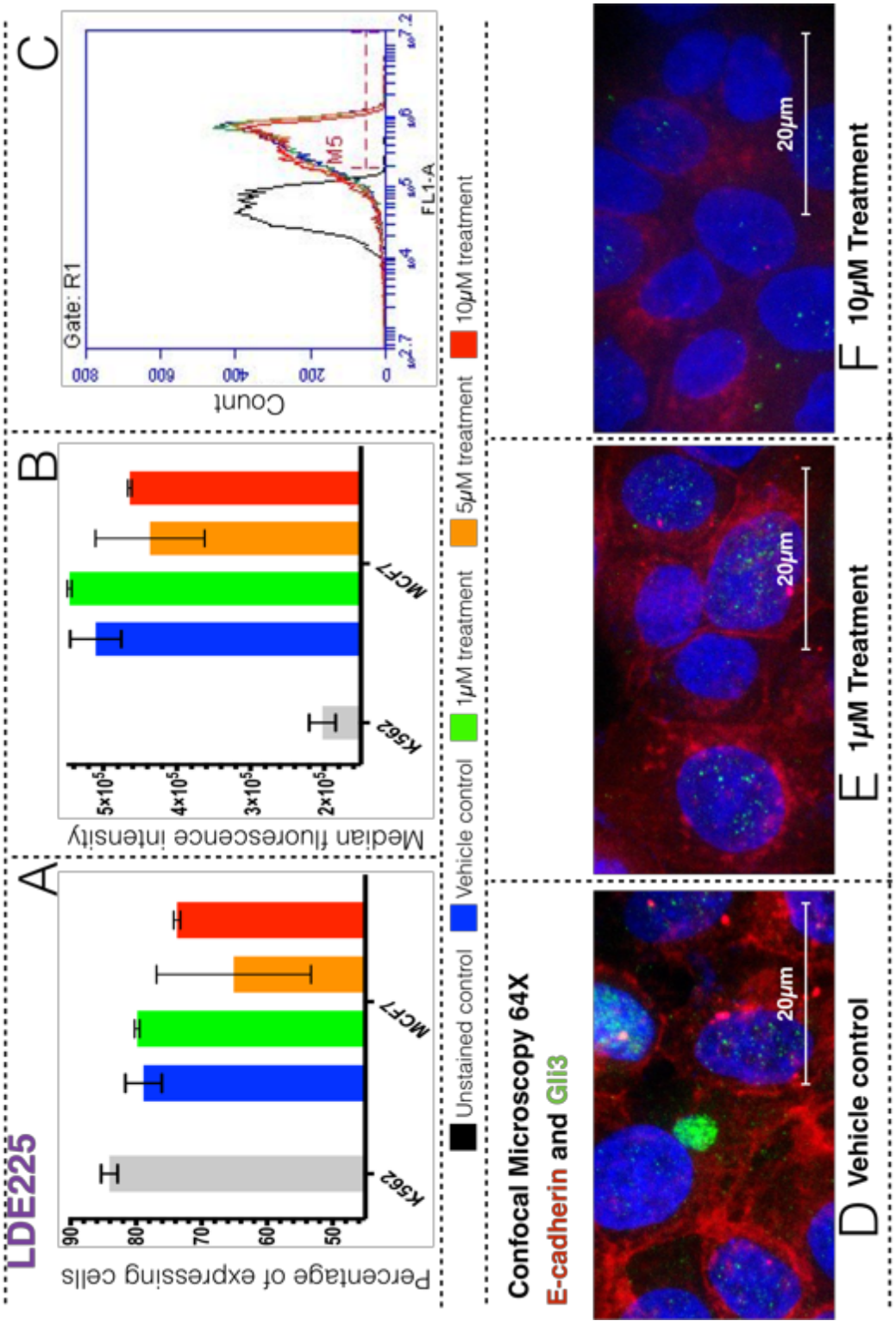

Figure 5-15, Alteration of Gli3 localisation and expression in MCF7 following treatment with LDE225.

Flow cytometry analysis of expression of Gli3 protein in MCF7 cells (A) percentage expression (B) MFI and (C) overlay histogram chart. Immunofluorescence Z stacked images of MCF7 cells captured under confocal microscope at 630x magnifications. MCF7 cells were stained with Gli3 (Green) and E-cadherin (Red) antibodies. Vehicle control (D) MCF7 cells following 1μM and 10μM (F) treatment with LDE225 for 48hours. Cells were visualised by fluorescence labelled secondary antibodies Alexa Fluor® (488 and 594). DAPI stain was used to stain cell nuclei (Blue).

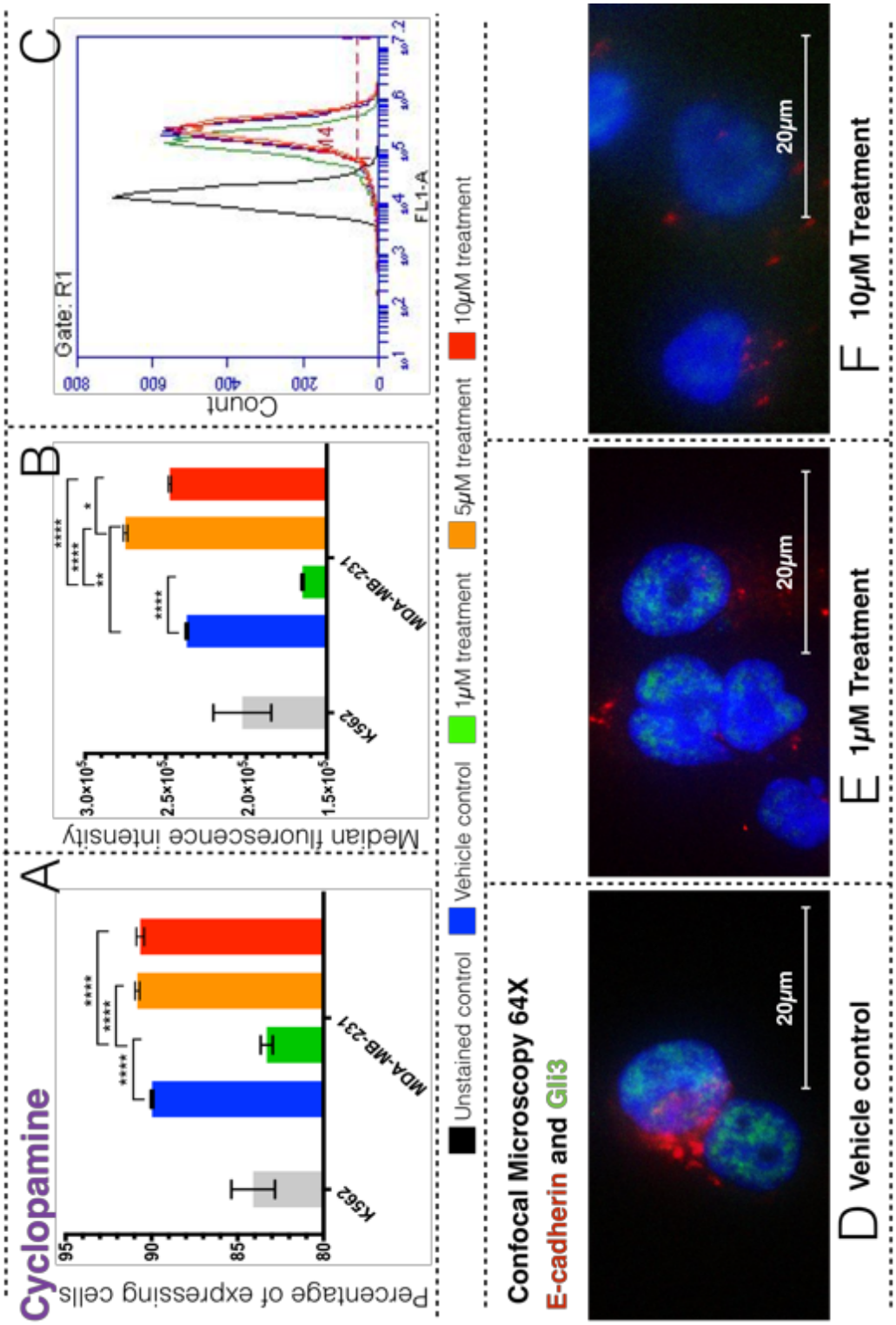

Figure 5-16, Alteration of Gli3 expression and localisation following cyclopamine treatment of MDA-MB-231.

Flow cytometry analysis of expression of Gli3 protein in MDA-MB-231 cells (A) percentage expression (B) MFI and (C) overlay histogram chart. Immunofluorescence Z stacked images of MDA-MB-231 cells captured under confocal microscope at 630x magnifications. MDA-MB-231 cells were stained with Gli3 (Green) and E-cadherin (Red) antibodies. Vehicle control (D) MDA-MB-231 cells following 1μM and 10μM (F) treatment with cyclopamine for 48hours. Cells were visualised with fluorescence labelled secondary antibodies Alexa Fluor® (488 and 594). DAPI stain was used to stain cell nuclei (Blue).

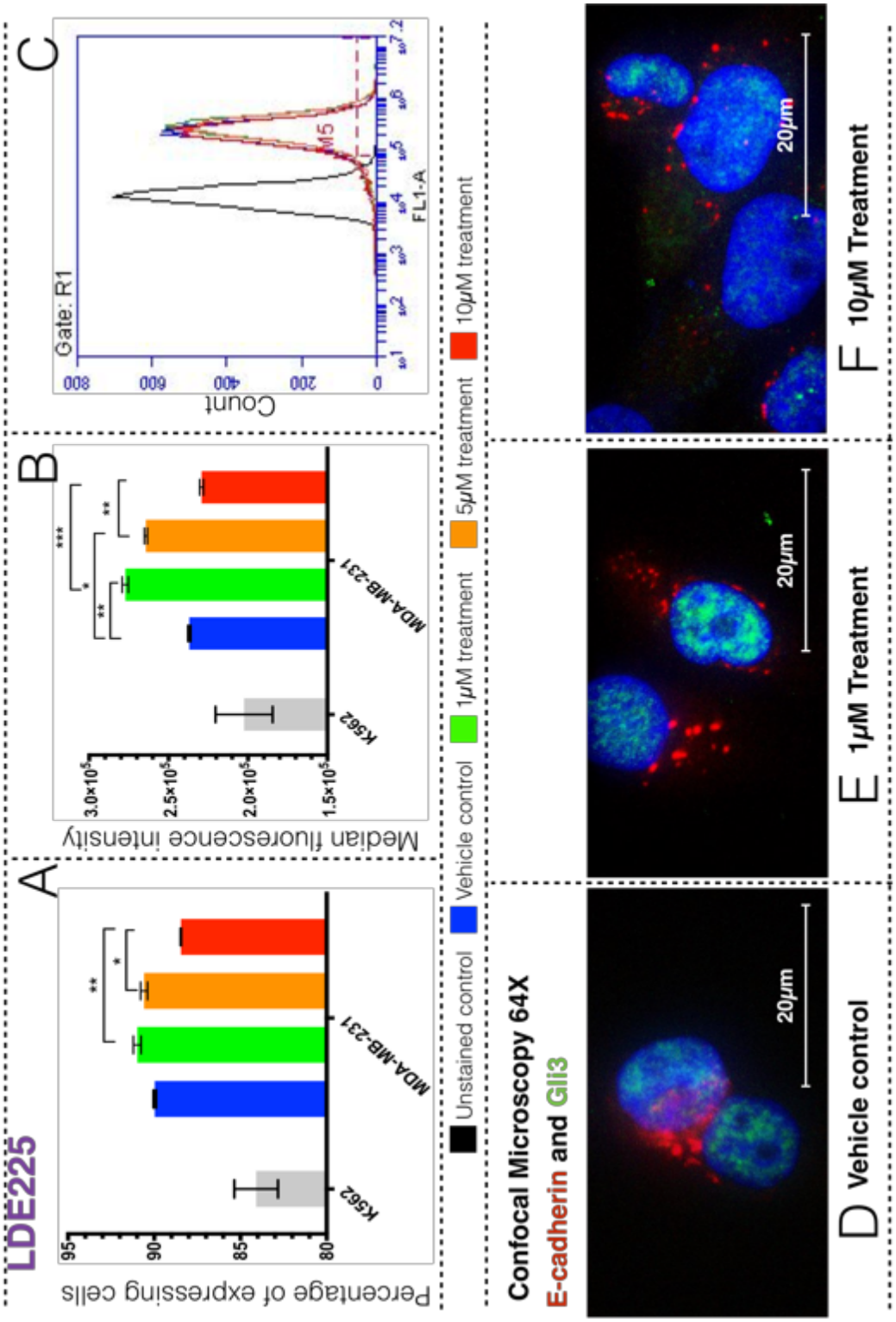

Figure 5-17, Alteration of Gli3 expression and localisation in MDA-MB-231 following treatment with LDE225.

Flow cytometry analysis of expression of Gli3 protein in MDA-MB-231 cells (A) percentage expression (B) MFI and (C) overlay histogram chart. Immunofluorescence Z stacked images of MDA-MB-231 cells captured under confocal microscope at 630x magnifications. MDA-MB-231 cells were stained with Gli3 (Green) and E-cadherin (Red) antibodies. Vehicle control (D) MDA-MB-231 cells following 1μM and 10μM (F) treatment with LDE225 for 48hours. Cells were visualised with fluorescence labelled secondary antibodies Alexa Fluor® (488 and 594). DAPI stain was used to stain cell nuclei (Blue).

5.2.5 Reduction of β-catenin expression in MCF7 and MDA-MB-231 cells following inhibition of Hh signalling

β-catenin protein is involved in the regulation of EMT via Wnt signalling and changes in the expression of this protein are implicated in EMT-associated change in human cancers (Shan *et al.*, 2015). Hence, assessment of nuclear accumulation and changes in expression of β-catenin was assessed following treatment of breast cancer cell lines with either cyclopamine or LDE225 using flow cytometry, whereby, changes in positivity (percentage of positive cells) and MFI (level of expression) were evaluated.

Positivity of β-catenin expression was represented at percentage of positive cells and changes in the level of expression in the population of positive cells were represented in the graph as median fluorescence intensity (MFI). β-catenin positivity decreased in MCF7 cells following cyclopamine or LDE225 treatment and the level of β-catenin expression increased as summarised in Figure 5-31. The positivity of β-catenin decreased by 2% (p-value<0.01), 4% (p-value<0.0001) and 5% (p-value<0.0001) following 1μM, 5μM and 10μM cyclopamine treatment as seen in Figure 5-31. The level of β-catenin expression in MCF7 increased by 20% (p-value<0.01), by 40% (p-value<0.0001) and 30% (p-value<0.0001) as presented in (Figure 5-31-B). Following treatment of MCF7 with 1μM, 5μM and 10μM LDE225, β-catenin positivity decreased by 45% (p-value<0.0001), 45% (p-value<0.0001) and 51% (p-value<0.0001), respectively as seen in Figure 5-31-D. The overlay histograms showed a population of low expressing cells that increased in number in dose-dependent manner following cyclopamine (Figure 5-31-C) or LDE225 treatment (Figure 5-31-F).

The positivity and level of β-catenin expression in MDA-MB-231 cells decreased in a dose-dependent manner following treatment with either cyclopamine or LDE225 as summarised in Figure 5-19. The positivity of β-catenin decreased by 0.5% (p-value<0.01), 0.5% (p-value<0.01) and 1 % (p-value<0.0001) following 1μM, 5μM and 10μM cyclopamine treatment as seen in Figure 5-19-A. The level of β-catenin expression following cyclopamine treatment in MDA-MB-231 cells decreased by 8% (p-value<0.0001) and 20% (p-value<0.0001) as presented in Figure 5-19-B. As shown in Figure 5-19-D, β-catenin positivity decreased by 1% (p-value<0.0001), 1% (p-value<0.0001) and 2% (p-value<0.0001) at 1μM, 5μM 10μM LDE225, respectively.

MFI, as shown in Figure 5-19-E, decreased by 13% (p-value<0.0001), 17% (p-value<0.0001) and 24% (p-value<0.0001) at 1µM, 5µM and 10µM LDE225 treatment, respectively. Overlay histograms showed a population of low to none expressing cells that increase at the highest concentration of both cyclopamine and LDE225 treatment (Figure 5-19-C and F).

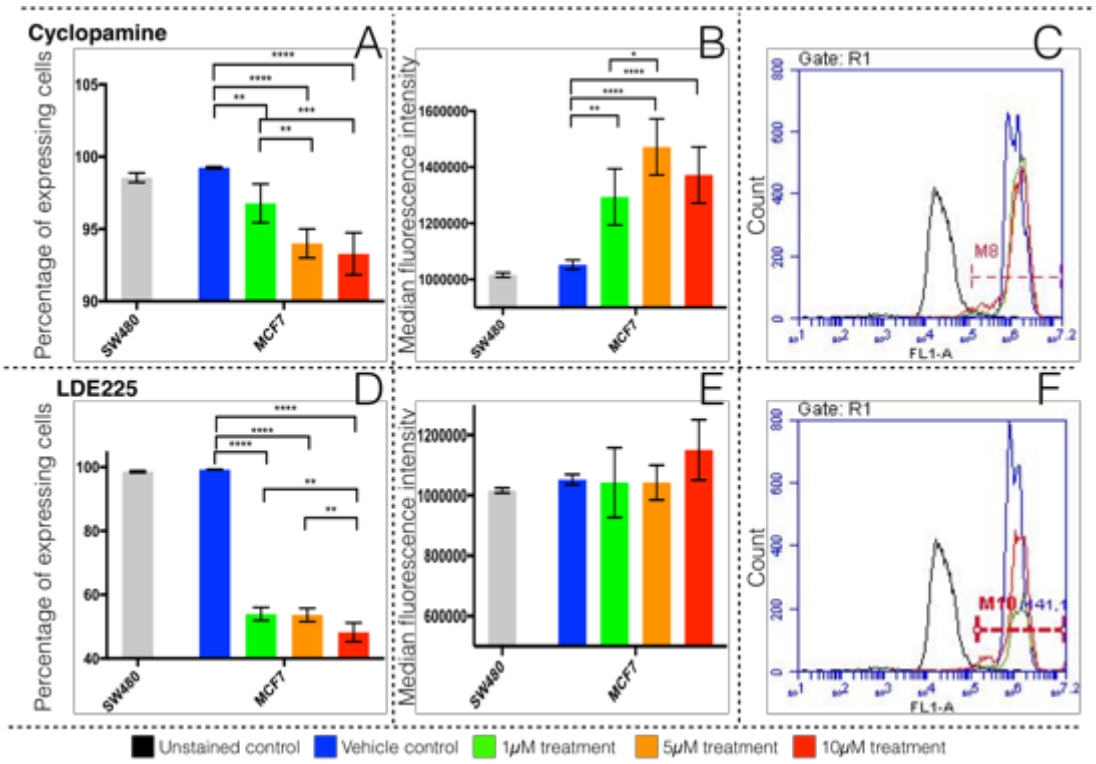

Figure 5-18, Reduction of β-catenin in luminal breast cancer cell line MCF7 following treatment with either cyclopamine or LDE225.

Presentation of percentage of β-catenin protein expression in MCF7 following treatment with either cyclopamine or LDE225 at 1µM, 5µM and 10µM. Percentage of positive cells were estimated using flow cytometry, and SW480 cell line was used as positive control for β-catenin protein expression. Bars present the percentage of β-catenin positive cells and MFI of β-catenin following treatment with cyclopamine (A and B) or LDE225 (D and E). Results displayed as bars of MFI ± S.D. Overlap histograms of the β-catenin protein in MCF7 cells, comparing (unstained cells, vehicle control, 1µM, 5µM, and 10µM) of cyclopamine treatment (C) and LDE225 treatment (F). This figure is representative of n=3 experiments in triplicate. Statistical analysis was conducted, and significant difference between samples was indicated by * p-value<0.05, ** p-value<0.01, *** p-value<0.001 and **** p-value<0.0001.

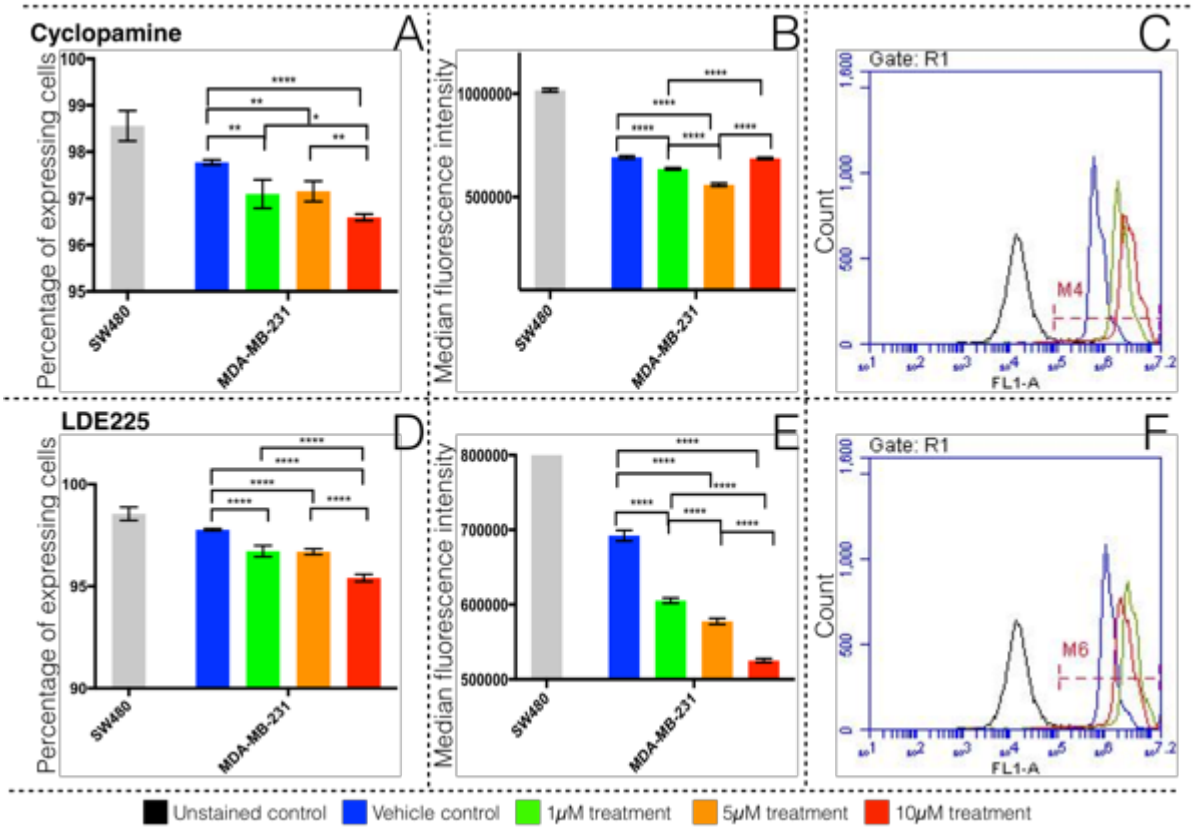

Figure 5-19, Reduction of β-catenin in the triple-negative and basal-like breast cancer cell line MDA-MB-231 following treatment with cyclopamine or LDE225.
Presentation of percentage of β-catenin protein expression in MDA-MB-231 following treatment with either cyclopamine or LDE225 at 1μM, 5μM and 10μM. Percentage of positive cells were estimated using flow cytometry, and SW480 cell line was used as positive control for β-catenin protein expression. Bars present the percentage of β-catenin positive cells and MFI of β-catenin following treatment with cyclopamine (A and B) or LDE225 (D and E). Results displayed as bars of MFI ± S.D. Overlap histograms of the β-catenin protein in MDA-MB-231 cells, comparing (unstained cells, vehicle control, 1μM, 5μM, and 10μM) of cyclopamine treatment (C) and LDE225 treatment (F). This figure is representative of n=3 experiments in triplicate. Statistical analysis was conducted, and significant difference between samples was indicated by * p-value<0.05, ** p-value<0.01, *** p-value<0.001 and **** p-value<0.0001.

5.2.6 Increased E-cadherin in breast cancer cell lines following treatment with cyclopamine or LDE225

The expression level of E-cadherin protein was assessed to evaluate the effect of Hh inhibition on epithelial marker expression in MCF7 and MDA-MB-231 cells. E-cadherin increased in a dose-dependent manner in MCF7 following treatment with either cyclopamine or LDE225 as summarised in Figure 5-33. The positivity of E-cadherin in MCF7 cells increased by 5% (p-value<0.01) and 7% (p-value<0.001) at 1μM and 10μM, respectively as shown in Figure 5-33-A. MFI of E-cadherin in MCF7 cells decreased by 18% (p-value<0.0001) and 6% (p-value 0.05) as seen in Figure 5-33-

B. Using Western blotting, E-cadherin in MCF7 showed a four-fold increase (p-value<0.05) and 5-fold increase (p-value<0.05) in MCF7 following 5μM and 10μM cyclopamine treatment compared to the vehicle control as seen in Figure 5-33-D and Figure 5-33-E. By flow cytometry the positivity of E-cadherin in MCF7 following 1μM, 5μM and 10μM LDE225 treatment increased by 5% (p-value<0.001), 8% (p-value<0.0001) and 9% (p-value<0.0001), respectively as seen in Figure 5-33-F. The level (MFI) of E-cadherin expression in MCF7 following 10μM LDE225 treatment increased by 35% (p-value<0.0001) compared to the vehicle control as presented in Figure 5-20-G. The ratio of E-cadherin expression in MCF7 following 1μM, 5μM and 10μM LDE225 treatment showed 1.8-fold increase (p-value<0.01), 5.2-fold increase (p-value<0.0001) and eight-fold increase (p-value<0.0001) compared to the vehicle control as seen in Figure 5-33-I and Figure 5-33-J. The overlap histogram showed that there was a population of low-to-negative expressing cells observed before and after treatment with all concentrations cyclopamine or LDE225 (Figure 5-33-C and H).

The positivity of E-cadherin in MDA-MB-231 cells increased following treatment with cyclopamine or LDE225 as summarised in Figure 5-21. As seen in Figure 5-21-A, the positivity of E-cadherin in MDA-MB-231 cells increased by 16% (p-value<0.0001) following 10μM cyclopamine treatment. E-cadherin protein showed 1.5% increase and 3.5% increase following 5μM and 10μM cyclopamine treatment in MDA-MB-231 compared to the vehicle control (Figure 5-21). The positivity and MFI of E-cadherin in MDA-MB-231 cells decreased by 6% (p-value<0.0001) following 1μM LDE225 treatment as seen in Figure 5-21-F and Figure 5-21-G. Positivity of E-cadherin showed a 4% increase (p-value<0.0001) in MDA-MB-231 after 10μM treatment with LDE225, as shown in Figure 5-21-I and Figure 5-21-J.

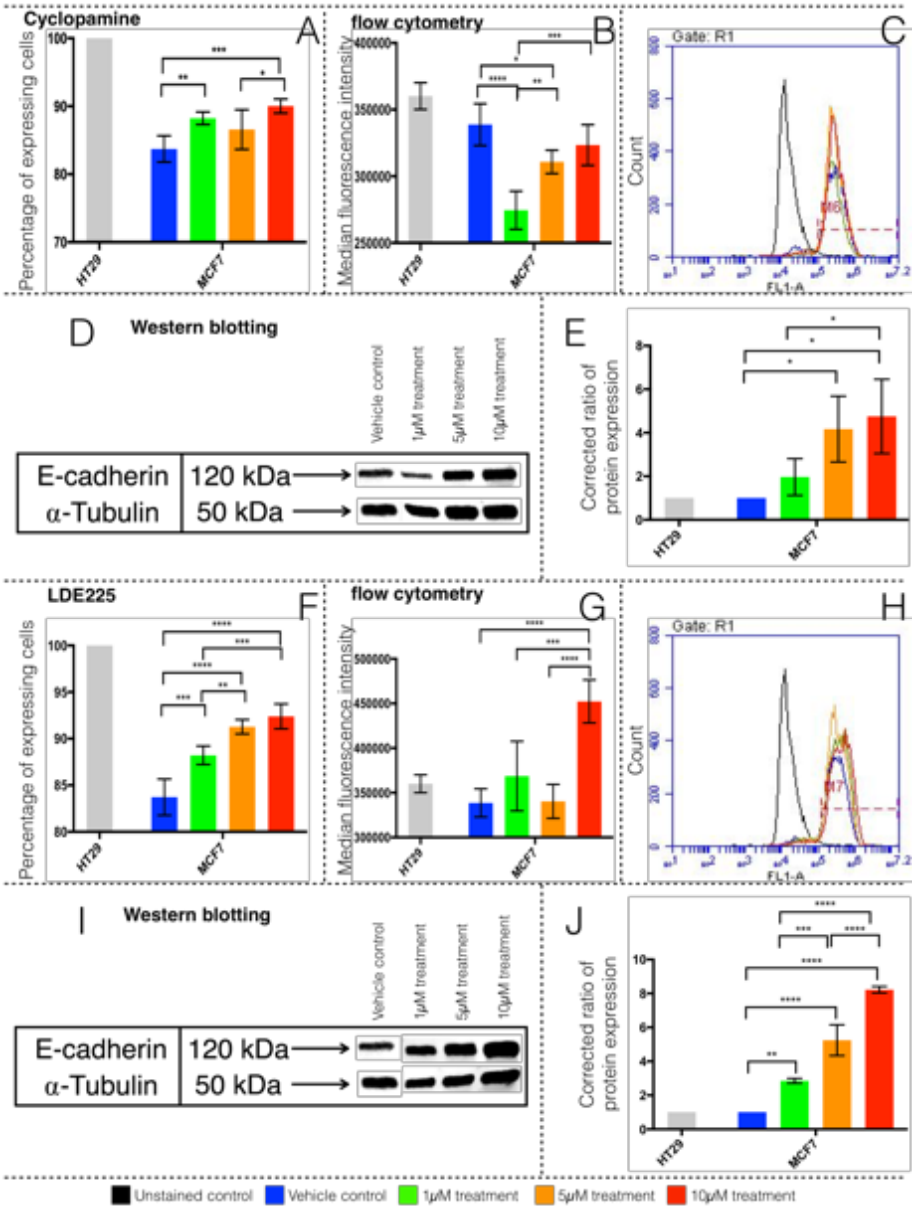

Figure 5-20, E-cadherin expression increased in a dose-dependent manner following treatment with cyclopamine or LDE225 of MCF7 cell line.

Expression of E-cadherin protein in MCF7 following treatment with two types of Hh inhibitors (cyclopamine or LDE225) at 1μM, 5μM and 10μM. Percentage of positive cells were estimated by flow cytometry (A, B, C, F, G, and H). HT29 cell line was used as a positive control for E-cadherin protein expression. The relative expression of E-cadherin protein was estimated by Western blotting and was corrected against loading control α-tubulin. The ratios presented were calculated as relative expression against vehicle control (D, E, I, and J). Bars present the percentage of E-cadherin positive cells following cyclopamine treatment (A) or LDE225 (F). Results displayed as bars of means of percentages of cells ± S.D. Bars present MFI of E-cadherin following cyclopamine treatment (B) or LDE225 treatment (G). Results displayed as bars of MFI ± S.D. Overlap histograms of E-cadherin protein in MCF7 cells, comparing (unstained cells, vehicle control, 1μM, 5μM, and 10μM) of cyclopamine treatment (C) or LDE225 treatment (H). The relative expression of E-cadherin in MCF7 cells following treatment with cyclopamine (E) or LDE225 (J) at three concentrations for 48 hours. Results displayed as bars of averages of corrected ratio of E-cadherin protein ± S.D. E-cadherin protein band at 120 kDa following cyclopamine treatment (D) or LDE225 treatment (I) compared against vehicle control and bands of loading control protein α-tubulin at 50 kDa band sizes. This figure is representative of n=3 experiments in triplicate. Statistical analysis was conducted, and significant differences between samples were indicated by * p-value<0.05, ** p-value<0.01, *** p-value<0.001 and **** p-value<0.0001.

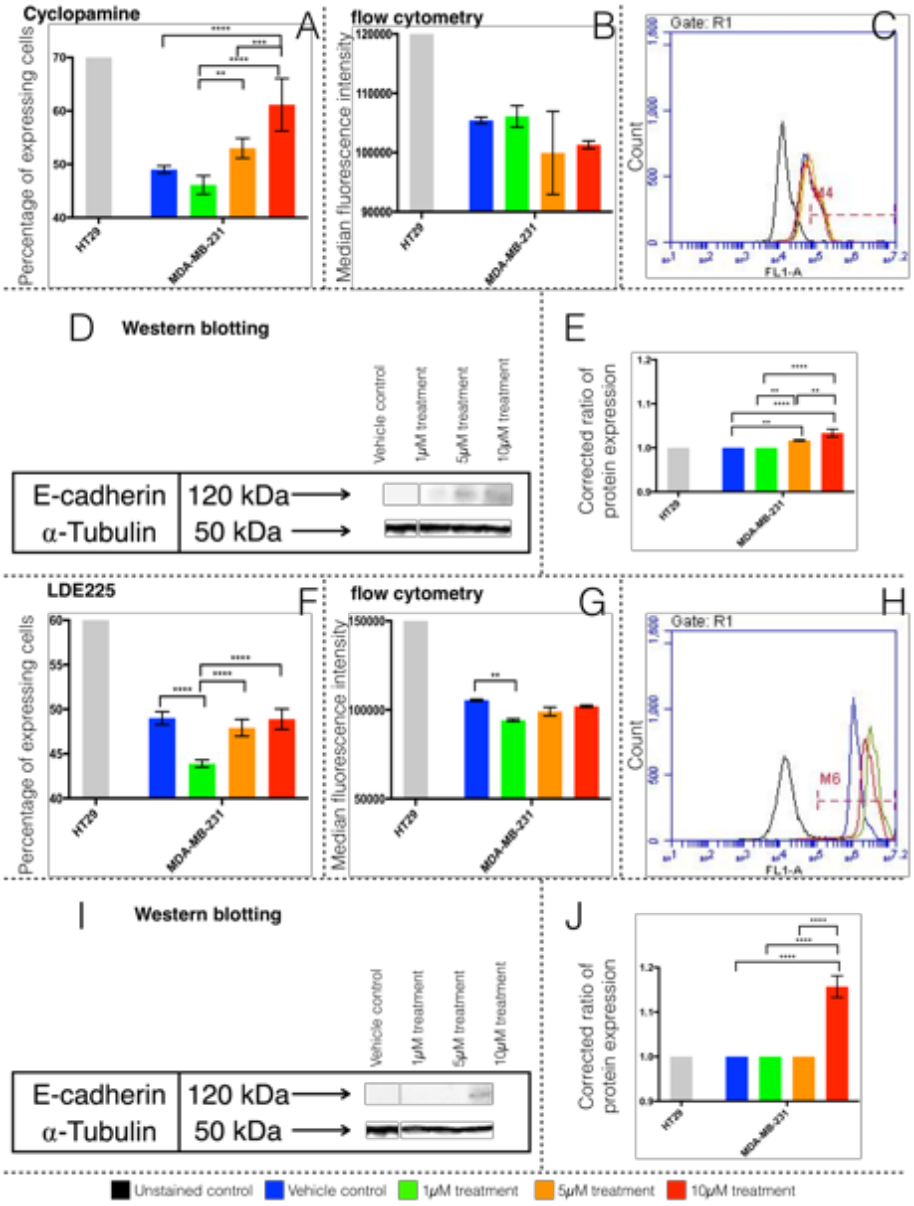

Figure 5-21, E-cadherin expression increased in MDA-MB-231 cells following treatment with cyclopamine or LDE225.

Expression of E-cadherin protein in MDA-MB-231 following treatment with two types of Hh inhibitors (cyclopamine or LDE225) at 1μM, 5μM and 10μM. Percentage of positive cells were estimated by flow cytometry (A, B, C, F, G, and H). HT29 cell line was used as a positive control for E-cadherin protein expression. The relative expression of E-cadherin protein was estimated by Western blotting and was corrected against loading control α-tubulin. The ratios presented were calculated as relative expression against vehicle control (D, E, I, and J). Bars present the percentage of E-cadherin positive cells following cyclopamine treatment (A) or LDE225 (F). Results displayed as bars of means of percentages of cells ± S.D. Bars present MFI of E-cadherin following cyclopamine treatment (B) or LDE225 treatment (G). Results displayed as bars of MFI ± S.D. Overlap histograms of E-cadherin protein in MCF7 cells, comparing (unstained cells, vehicle control, 1μM, 5μM, and 10μM) of cyclopamine treatment (C) or LDE225 treatment (H). The relative expression of E-cadherin in MDA-MB-231 cells following treatment with cyclopamine (E) or LDE225 (J) at three concentrations for 48 hours. Results displayed as bars of averages of corrected ratio of E-cadherin protein ± S.D. E-cadherin protein band at 120 kDa following cyclopamine treatment (D) or LDE225 treatment (I) compared against vehicle control and bands of loading control protein α-tubulin at 50 kDa band sizes. This figure is representative of n=3 experiments in triplicate. Statistical analysis was conducted, and significant differences between samples were indicated by * p-value<0.05, ** p-value<0.01, *** p-value<0.001 and **** p-value<0.0001.

5.2.7 Inhibition of Hh signalling with cyclopamine or LDE225 decreases motility and invasion of breast cancer cells

The number of migrated and invaded cells were counted and presented as average cells/field and compared against the vehicle control. One concentration of treatment (1μM) was selected, to eliminate the bystander reduction of motility of cells due to increased apoptosis (Figure 5-3 and Figure 5-4).

The inhibition of Hh signalling in MCF7 cells with cyclopamine (Figure 5-22-A) or LDE225 (Figure 5-22-B) caused a decrease in the number of migrated cells without reaching statistical significance (Figure 5-22-A and B). There was a 20 % reduction in the average number of cells that invaded the Matrigel® following both treatments. The average number of cells/field that invaded was reduced following cyclopamine (p-value < 0.01) or LDE225 (p-value<0.01) (Figure 5-22-C and D).

Treatment of MDA-MB-231 with either cyclopamine or LDE225 resulted in a significant reduction in cell migration by 8% and 16% respectively (p-value<0.05 and p-value<0.0001 respectively), as shown in Figure 5-23-A and B. The average number of cells that invaded the Matrigel® matrix was reduced in both treatments by 12 and 20% respectively with a significant decrease seen following LDE225 treatment (p-value<0.01) (Figure 5-23-D).

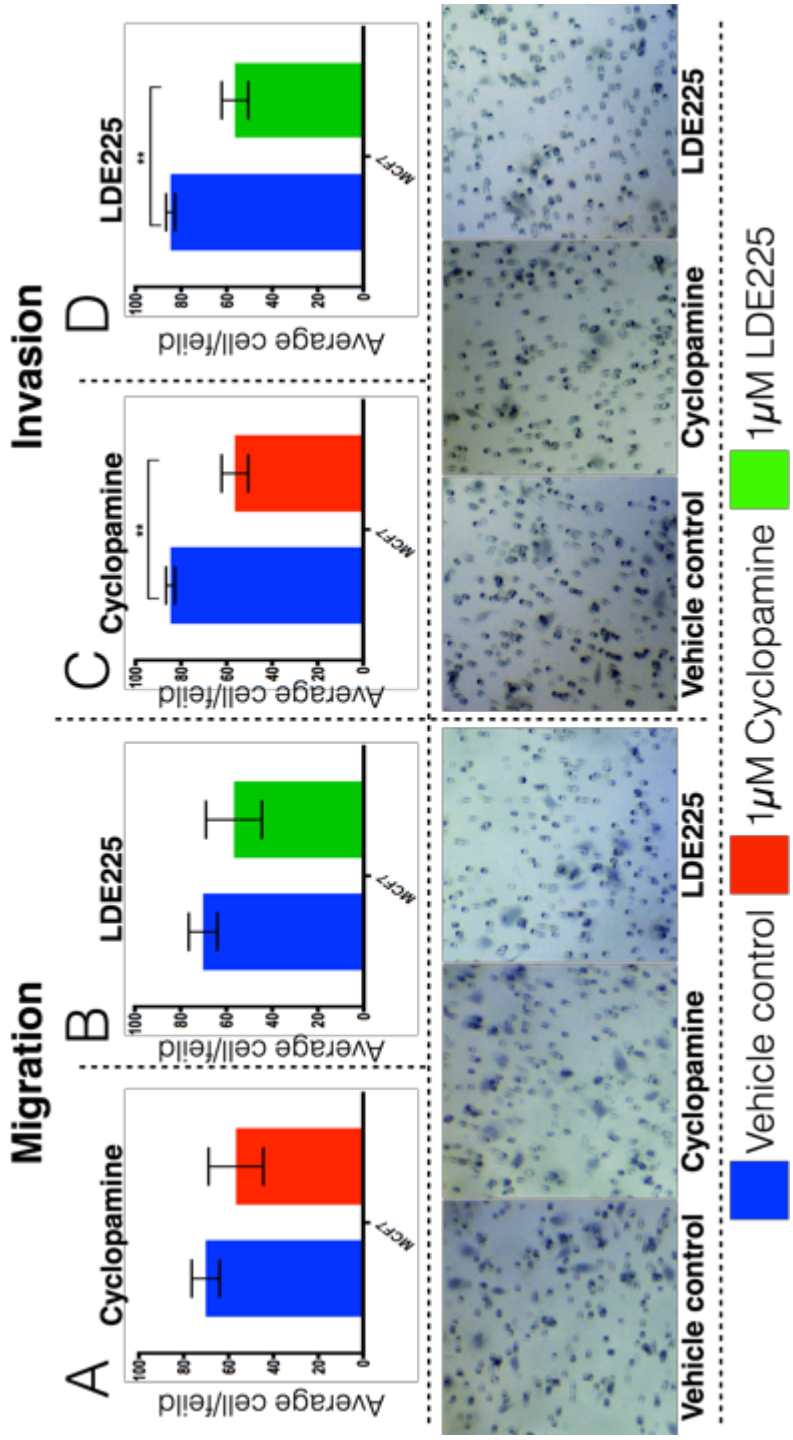

Figure 5-22, Reduction in the cellular motility and invasion of MCF7 cells following treatment with cyclopamine or LDE225.
Average number of cells/field of MCF7. A and B show average of migrated cells following cyclopamine (A) or LDE225 (B) treatment for 24 hours compared to the vehicle control (Blue). C and D representing averages of invading MCF7 cells following treatment with either cyclopamine (C) or LDE225 (D) compared to the vehicle control (Blue). Representatives microscopic images of fields of inserts (vehicle control, cyclopamine, or LDE225 treated cells) visualised by haematoxylin staining (blue cells). Results displayed as bars of mean ± S.D. This figure is representative of n=3 experiments in triplicate. Statistical analysis was conducted, and significant differences between samples were indicated by * p-value<0.05, ***p-value<0.01 and **** p-value<0.0001.

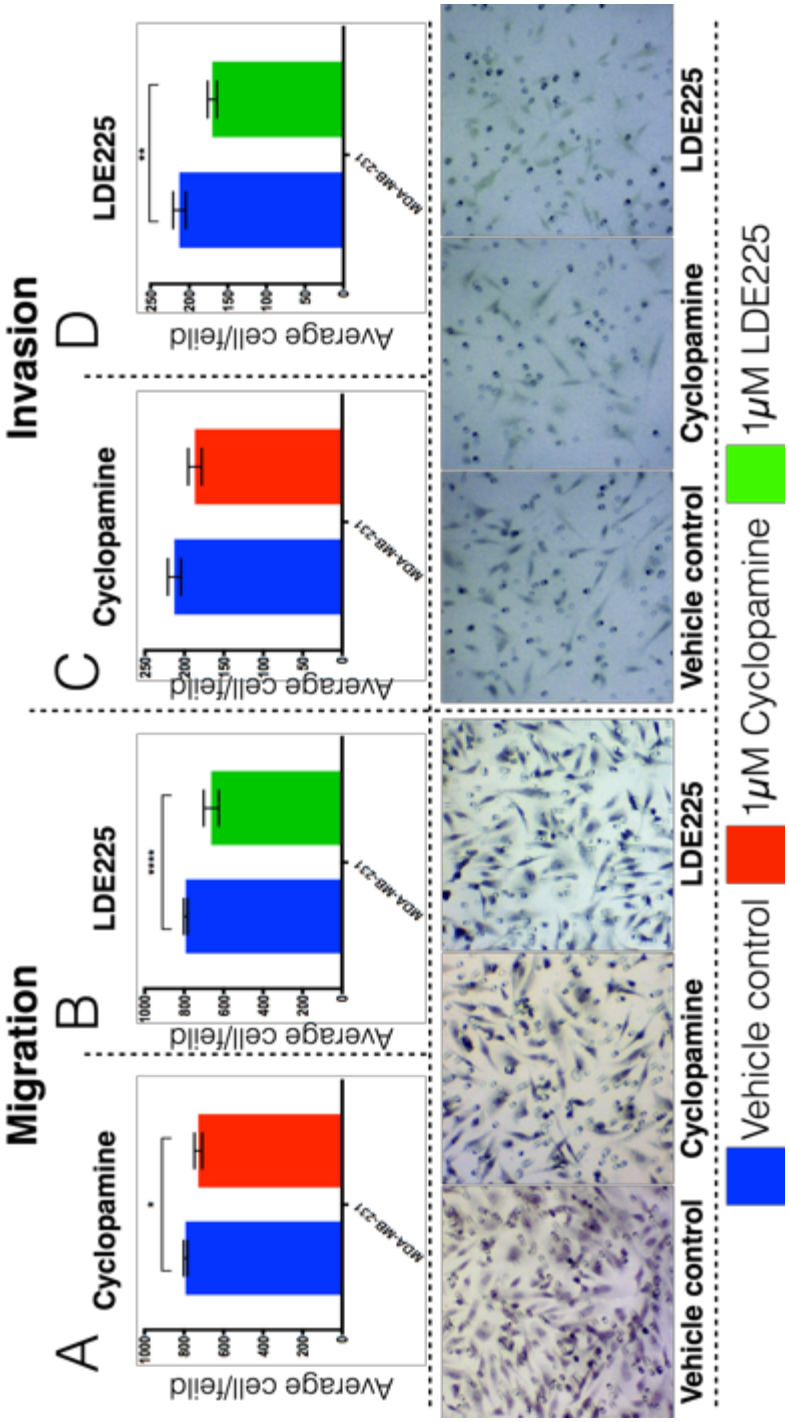

Figure 5-23, Reduction in the cellular motility and invasion of MDA-MB-231 cells following treatment with cyclopamine or LDE225.
Average number of cells/field of MDA-MB-231. A and B show average of migrated cells following cyclopamine (A) or LDE225 (B) treatment for 24 hours compared to the vehicle control (Blue). C and D representing averages of invading MDA-MB-231 cells following treatment with either cyclopamine (C) or LDE225 (D) compared to the vehicle control (Blue). Representatives microscopic images of fields of inserts (vehicle control, cyclopamine, or LDE225 treated cells) visualised by haematoxylin staining (blue cells). Results displayed as bars of mean ± S.D. This figure is representative of n=3 experiments in triplicate. Statistical analysis was conducted, and significant differences between samples were indicated by * p-value<0.05, ***p-value<0.01 and **** p-value<0.0001.

5.2.8 Treatment with cyclopamine or LDE225 reduced β-catenin-related transcription in MCF7 and MDA-MB-231

A TOPFLASH reporter assay for Wnt/β-catenin signalling was used to assess the effect of treatment with either cyclopamine or LDE225 on canonical Wnt signalling by measuring the catenin-related transcription (CRT). Following reporter plasmid transfection, cells were treated for 24hours with either cyclopamine or LDE225 (1μM), and then lysed to measure CRT.

The colorectal cancer cell line SW480 was included as a positive control for the transfection procedure (high TOPFLASH activity). This cell line was transfected previously by Qualtrough *et al.* (2015) and the results obtained here were similar to those observed previously, confirming successful transfection. Furthermore, treatment of SW480 with cyclopamine showed an equivalent inhibition of CRT reporter activity to that reported by Qualtrough *et al.* (2015). It was also noted that treatment with LDE225 resulted in a 50% reduction in CRT in SW480, which was greater than the effect observed with cyclopamine treatment (Figure 5-24-C).

The data showed CRT reduction in MCF7 (Figure 5-24-A) and MDA-MB-231 cells (Figure 5-24-B) with either cyclopamine or LDE225. The reduction of CRT level in MCF7 was significant following cyclopamine (p-value<0.0001). The difference between the CRT level in MCF7 following treatment with either cyclopamine or LDE225 treatments were also significant (p-value<0.001) (Figure 5-24-A). A statistically significant reduction in CRT was observed in MDA-MB-231 following treatment with cyclopamine (p-value<0.05) or LDE225 (p-value<0.0001) compared to the vehicle control (Figure 5-24-B).

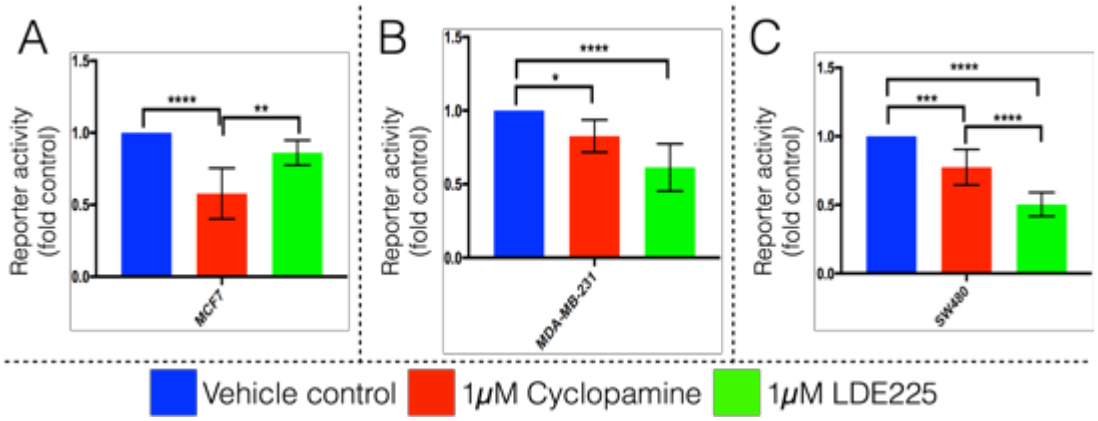

Figure 5-24, CRT of MCF7, MDA-MB-231 and SW480 cells reduced following treatment with cyclopamine of LDE225

The β-CRT reporter levels (fold control) following 24 hours of treatment with 1μM of cyclopamine or 1μM of LDE225 compared to vehicle control for A- MCF7 cells, B- MDA-MB-231 cells, and SW480. Data showed activity of TOPFLASH reporter, corrected against FOPFLASH and normalised to *Renilla* control plasmid (transfection efficiency control). The data represented mean from three separate experiments performed in triplicate and value shown as fold control ±S.D. Statistical analysis was conducted, and significant differences between samples were indicated by * p-value<0.05, ** p-value<0.01, *** p-value<0.001 and **** p-value<0.0001.

5.3 Discussion

5.3.1 Inhibition of Hedgehog (Hh) signalling in MCF7 (luminal) and MDA-MB-231 (triple-negative and basal-like) reduced cell yield and increased cell death

Two cell lines were selected to assess the effect of Hh inhibition by treatment with cyclopamine or LDE225. MCF7 (luminal) and MDA-MB-231 (TNBC and basal-like) are considered representative for their molecular subtypes of breast cancer. MCF7 cells have epithelial morphology with low metastatic ability, while MDA-MB-231 cells have mesenchymal morphology with high metastatic ability (Kenny *et al.*, 2007a; Rizwan *et al.*, 2015).

Several previous studies reported the effect of inhibiting Hh signalling using cyclopamine on breast cancer cell lines, summarised in Table 5-1, as cyclopamine is a naturally-occurring plant alkaloid and the first identified Hh inhibitor (Bryden *et al.*, 1971). High concentrations (higher than 10μM) of cyclopamine may cause off-target effects (Yauch *et al.*, 2008) and non-specific cytotoxicity (Lipinski *et al.*, 2008). Thus, doses over 10μM for both treatments were avoided in experimentations.

Previous work has shown that high concentrations of cyclopamine (20μM) caused significantly reduced proliferation of both MCF7 and MDA-MB-231 (Mukherjee *et al.*, 2006; Zhang *et al.*, 2009). However, Kubo *et al.* (2004) showed that at 10μM, cyclopamine reduced viability but not proliferation of MCF7 and MDA-MB-231. As shown in Figure 5-1-A, treatment with cyclopamine caused a dose-dependent decrease of MCF7 cell yield, however, this decrease did not reach statistical significance potentially due to inter-experimental variation. Whereas, treatment of MDA-MB-231 cells with 5μM and 10μM cyclopamine caused a decrease of cell yield (p-value<0.05, and p-value<0.0001, respectively as shown in Figure 5-2-A. Cyclopamine also decreased the viability of MCF7 and MDA-MB-231 in a dose-dependent manner, as seen in Figure 5-1-B and Figure 5-2-B. In concurrence, Thomas *et al.* (2011) showed that cyclopamine treatment decreased proliferation in breast cancer cell lines.

LDE225 was discovered in 2010 in a high throughput *in vitro* screen (Pan *et al.*, 2010). It is a small molecule inhibitor that antagonises Smoothened (Smo) preventing it from transducing the downstream Hh signal and activating the Gli transcription factors (Jain *et al.*, 2017). This inhibitor was approved by the US Food and Drug

Administration for the treatment of basal-cell carcinoma following a successful Phase II clinical trial (Dummer *et al.*, 2016).

LDE225 treatment causes reduced proliferation of several other cancer types including melanoma (Jalili *et al.*, 2013), non-small cell lung carcinoma (Della Corte *et al.*, 2015) and ovarian cancer (Steg *et al.*, 2012). Since its success in preliminary clinical trials, relatively few studies have used it for inhibiting Hh signalling to investigate its potential therapeutic effect in breast cancer cells. Heller *et al.* (2012) and Matevossian and Resh (2015) reported that LDE225 reduced breast cancer cell line proliferation *in vitro*. Their findings concur with the current results. We showed that inhibition of Hh signalling in MCF7 and MDA-MB-231 by LDE225 resulted in reduction of cell yield and cell viability in a dose-dependent manner as summarised in Figure 5-1 and Figure 5-2. Treatment with LDE225 in animal xenografts also dose-dependently caused inhibition of breast cancer cell proliferation (Han *et al.*, 2015; Di Mauro *et al.*, 2017).

In combination with a reduction in cell yield, we showed that treatment with cyclopamine or LDE225 increased apoptosis in MCF7 and MDA-MB-231 cells as seen in Figure 5-3 and Figure 5-4. Previous studies reported that cyclopamine reduced cell yield by increasing MCF7 and MDA-MB-231 apoptosis (Mukherjee *et al.*, 2006; Zhang *et al.*, 2009; Zhuang *et al.*, 2013). The effect of LDE225 on apoptosis in breast cancer cells has not, however, been previously reported. Nonetheless, LDE225 is known to induce apoptosis in other human cancer cell lines including melanoma (Jalili *et al.*, 2013), gastric cancer (Han *et al.*, 2009), and prostate cancer (Shigemura *et al.*, 2011).

In summary, the inhibition of Hh signalling in breast cancer cell lines showed a dose-dependent decrease in cell yield with a concomitant induction of cell death. The MCF7 cell line proved more sensitive to this growth inhibition than MDA-MB-231. Correspondingly, more cell death was seen in MCF7 cells than in MDA-MB-231 following treatment with either cyclopamine or LDE225. Also, it was notable that most apoptosis seen in MCF7 is early apoptosis whereas most apoptosis seen in MDA-MB-231 cells were late apoptosis. This could be due to the duration of treatment, or a difference in mechanisms of oncogene/tumour suppressor imbalances between the two cell lines.

5.3.2 Gli protein expression levels and localisation were altered following inhibition of Hh signalling by cyclopamine and LDE225

Gli proteins are zinc-finger transcription factors that have activator and repressor forms (Ruiz i Altaba *et al.*, 2007). Gli1 is expressed as an active from while Gli2 and Gli3 have two forms (active and inactive) (Figure 0-8) (Ruiz i Altaba *et al.*, 2007). The level of expression and localisation of the three Gli proteins reflects the status of the Hh signalling pathway (Figure 0-7) (Ruiz i Altaba *et al.*, 2007) and alteration in expression levels and subcellular localisation were documented previously in human cancers (Ruiz i Altaba *et al.*, 2002). Estimation of nuclear localisation of Gli proteins in breast cancer samples indicated the status of Hh signalling and assessing nuclear localisation correlated with several clinicopathological characteristics (ten Haaf *et al.*, 2009; Li *et al.*, 2012). Here we used flow cytometry to assess Gli proteins expression levels and immunocytofluorescence (ICF) for investigation of subcellular localisation changes in response to hedgehog pathway inhibition.

Herein, Gli proteins levels were not compared between cell lines and observation of variation of localisation following treatment was assessed visually using confocal microscopy. Most of previously published work focussed on studying the alteration of Gli1 only. Until the time of submitting this work, regulation of Gli1, Gli2 and Gli3 proteins localisation following Hh inhibition has not been reported and this is the first study to show alteration of level and subcellular localisation of Gli proteins in breast cancer cells after Hh inhibition using either cyclopamine or LDE225.

The data showed that MCF7 and MDA-MB-231 expressed Gli1, Gli2 and Gli3 (Figure 5-5) which was similar to the findings of previous studies (Kubo *et al.*, 2004; Dennler *et al.*, 2007; ten Haaf *et al.*, 2009; Zhang *et al.*, 2009; Ramaswamy *et al.*, 2012; Wang *et al.*, 2014; Song *et al.*, 2016; Kurebayashi *et al.*, 2017). Also, nuclear localisation of Gli1 was higher in MCF7 than MDA-MB-231, which concurs with finding of Wolf *et al.* (2007). They also reported that high expression of Gli1 in MCF7 correlated with higher Gli reporter activity than that seen in MDA-MB-231 which confirmed that the nuclear localisation of Gli1 indicates increased Hh activity in breast cancer (Wolf *et al.*, 2007). Other studies also showed that Gli1 had nuclear and cytoplasmic localisation in MCF7 but cytoplasmic in MDA-MB-231 (Kubo *et al.*, 2004; Kameda *et al.*, 2009).

Alteration of Gli1 localisation following LDE225 treatment in breast cancer cell lines was not reported previously. Decreased expression of *Gli1* was reported in previous work on breast cancer cell lines (Kubo *et al.*, 2004; Zhang *et al.*, 2009;

Thomas *et al.*, 2011). Kubo *et al.* (2004) also showed Gli1 expression in MCF7 cells was reduced following treatment with cyclopamine without changing subcellular localisation. However, current data were captured under higher magnification and co-localisation using Z-stack confocal microscopy imaging which is more suitable and sensitive for assessing alteration of subcellular localisation. In MDA-MB-231 cells, treatment with cyclopamine decreased both nuclear and cytoplasmic localisation of Gli1 (Figure 5-8-A and B). However, LDE225 caused a reduction in nuclear and cytoplasmic localisation of Gli1 in multiple myeloma (Blotta *et al.*, 2012). Treatment of MCF7 and MDA-MB-231 cells with LDE225 caused reduced nuclear Gli1 in a dose-dependent manner greater than that observed following cyclopamine treatment (Figure 5-8). This suggests a more potent effect of LDE225 in reducing of Hh activity in breast cancer cell lines. The reduction in nuclear localisation was visibly pronounced in MCF7 cells especially after treatment with LDE225 at the highest dose (10μM).

In breast cancer, overexpression of *Gli1* was also associated with active proliferation and high mitotic activity in an animal model (Fiaschi *et al.*, 2009). The inhibition of Hh signalling caused a reduction in Gli1 expression in MCF7 and MDA-MB-231 cells (Table 5-5 and Table 5-6) and this reduction was associated with decrease in cell yield after 48hours (Figure 5-3 and Figure 5-4). Kameda *et al.* (2009) and Colavito *et al.* (2014) showed that knocking down of *Gli1* caused a significant reduction in cell proliferation compared to vehicle control. Diao *et al.* (2016) indicated that inhibiting Gli1 by *siRNA* resulted in a significant reduction in cell proliferation. MCF7 and MDA-MB-231 showed reduced cell yield following 48hours treatment with cyclopamine or LDE225 which is consistent with previous findings (Figure 5-3 and Figure 5-4).

Im *et al.* (2013) evaluated Hh related protein expression in breast cancer samples and showed that expression of Gli2 was associated with the worst overall survival. Alteration of Gli2 protein localisation in breast cell lines following Hh inhibition by cyclopamine or LDE225 was not previously reported. Inhibition of Hh signalling by GANT61 (a Gli1 and Gli2 blocker and inhibitor of Gli mediated transcription) in MCF7 resulted in reduction of Gli2 expression, however no analysis of treatment effect on the nuclear localisation was assessed in this study (Kurebayashi *et al.*, 2017). Here, data showed that Gli2 expression was reduced following treatment with either cyclopamine or LDE225 (Figure 5-3).

Song *et al.* (2016) showed that MDA-MB-231 had strong expression of *Gli1* and *Gli2* and that inhibition of Hh signalling by cyclopamine resulted in a reduction of both *Gli1* and *Gli2*. This agrees with our data as we showed that inhibition of Hh signalling in MDA-MB-231 cells by 1μM and 5μM cyclopamine significantly decreased Gli2 expression (Figure 5-12-A and B). The inhibition by cyclopamine also caused increased nuclear localisation of Gli2 in MDA-MB-231 (Figure 5-12-E and F). Following LDE225 treatment, there was increased expression of Gli2 in a dose-dependent manner (Figure 5-12 and Figure 5-13–A and B) with a notable reduction in cytoplasmic localisation (Figure 5-13-E and F).

Gli3 is the suppressor form of the Gli proteins and it is expressed as a full-length inactive form that requires cleavage for activation (Figure 0-8) (Ruiz i Altaba *et al.*, 2007). High expression of Gli3 in colorectal cancer was associated with a poorly-differentiated histological grade (Iwasaki *et al.*, 2013). None of the previous work in breast cancer studied the effect of inhibiting Hh signalling on expression and localisation of Gli3 in breast cancer cell lines. High expression of Gli3 was seen in luminal epithelial cells of the developing mammary gland (Hatsell and Cowin, 2006). This increased expression was associated with decreased activation of Hh signalling that is required during that stage of breast cancer development (Hatsell and Cowin, 2006).

5.3.3 Reduction in catenin related transcription following treatment with cyclopamine or LDE225 in MCF7 and MDA-MB-231 cells

To ascertain whether there is crosstalk between Hh and Wnt signalling, the expression of β-catenin protein was assessed by flow cytometry and ICF following Hh pathway inhibition. CRT was measured using the TOPFLASH reporter assay (Korinek *et al.*, 1997) and compared following treatment with either cyclopamine or LDE225 at 1μM (Figure 5-24). Qualtrough *et al.* (2015) showed that CRT was reduced following inhibiting Hh signalling with cyclopamine in colon cancer cell lines in a dose-dependent manner compared to the vehicle control. Here, SW480 (a colon cancer cell line), used previously by Qualtrough *et al.* (2015), was used as a positive control, and similar reduction of CRT was seen following treatment with 1μM cyclopamine (Figure 5-24-C). In addition, following treatment with 1μM LDE225 CRT was reduced to half the level of the vehicle control, which is greater than the reduction seen following cyclopamine treatment (Figure 5-24-C).

This is the first study to investigate the effect of inhibiting Hh signalling on the Wnt/β-catenin pathway in breast cancer cells. Recently, Arnold *et al.* (2017) showed that there was a correlation between the simultaneous activation of both signalling pathways and a poorer prognosis in TNBC patients.

The expression and subcellular localisation of β-catenin in response to Hh inhibition has not previously been reported in breast cancer. Inhibition of Hh, by cyclopamine or LDE225, led to reduction of β-catenin expression in both cell lines studied here (Table 5-3). This decrease in expression was also accompanied by increased cell membrane localisation and decreased cytoplasmic and nuclear localisation, noted especially in the luminal cell line MCF7 (Table 5-11 and Table 5-12).

Ulloa *et al.* (2007) showed that Gli3 which is synthesised in the absence of Hh signalling can antagonise β-catenin. This offers a potential explanation for the findings presented here, as inhibition of Hh caused an increase in the nuclear localisation of Gli3 in both cell lines (

Table 5-5), and this was associated with a decrease in CRT. Furthermore, Maeda *et al.* (2006) showed that Gli1 transcriptional activity was enhanced by β-catenin, whereas here we showed that a decrease in nuclear localisation of Gli1, following inhibition of Hh signalling, is associated with reduced activity of β-catenin. Therefore, the findings presented here suggest that there is an interaction between these signalling pathways in breast cancer cells, and although further analysis is required, this may have serious relevance for the clinical management of breast cancer.

Table 5-3: Decrease in β-catenin protein in a dose-dependent manner following cyclopamine or LDE225 in MCF7 and MDA-MB-231 cell lines.

Summary of changes in the level of β-catenin expression following the inhibition of Hh signalling by two treatments (cyclopamine or LDE225) at three concentrations (1μM, 5μM, and 10μM). Arrows indicate the change in expression of β-catenin compared to vehicle control.

Treatment	1μM cyclopamine	5μM cyclopamine	10μM cyclopamine	1μM LDE225	5μM LDE225	10μM LDE225
MCF7	↓	↓↓	↓↓↓	↓↓↓	↓↓↓	↓↓↓
MDA-MB-231	↓	↓	↓	↓	↓	↓

Table 5-4: Decrease in cytoplasmic β-catenin in MCF7 cell line following inhibition of Hh pathway by either cyclopamine or LDE225.

Summary of changes in β-catenin cytoplasmic localisation following treatment with cyclopamine or LDE225 at two concentrations of treatment (1μM and 10μM) for 48 hours. Arrows indicate qualitative observation of level of cytoplasmic localisation of β-catenin compared to that seen in vehicle control.

Treatment	1 μM cyclopamine	10 μM cyclopamine	1 μM LDE225	10 μM LDE225
MCF7	↓	↓↓	↓	↓↓
MDA-MB-231	-	-	-	-

Table 5-5: Decrease in the nuclear localisation of β-catenin in MCF7 cells following inhibition of the Hh signalling.

This table summarises the effect of Hh inhibition by cyclopamine and LDE225 on the nuclear localisation of β-catenin protein at two concentrations of the treatment (1 μM and 10 μM) for 48 hours. Arrows indicate the qualitative observation of the level of expression of the marker compared to the vehicle control.

Treatment	1 μM cyclopamine	10 μM cyclopamine	1 μM LDE225	10 μM LDE225
MCF7	↓	↓	↓	↓↓
MDA-MB-231	-	-	-	-

5.3.4 Inhibition of Hh signalling by cyclopamine and LDE225 induced the expression of E-cadherin and reduced motility and invasion in both MCF7 and MDA-MB-231 cells

Cellular changes associated with EMT is a critical component in human cancer metastasis including breast cancer (Sarrio *et al.*, 2008; Wang and Zhou, 2013). In associated with EMT-like changes many of the transcription factors act as repressors for the epithelial adhesion molecule E-cadherin and subsequently promote invasion and metastasis (Hajra *et al.*, 2002; Peinado *et al.*, 2004). Therefore, E-cadherin expression levels were assessed following inhibition of Hh signalling by either cyclopamine or LDE225. The effect of Hh inhibition on motility and invasion of breast cancer cell lines by a single concentration of treatments (1μM) was also measured. The selection of this dose was based on previous findings (Figure 5-3 and Figure 5-4). At 1μM, no significant induction of cell death was seen, which would cause decreased motility and invasion scores due to the presence of fewer cells in the assay.

In human breast cancer samples, Fiaschi *et al.* (2009) showed that cells with high Gli1 expression lacked expression of E-cadherin and increased possibility of metastatic spread. Also, O'Toole *et al.* (2011) used *in vivo* models to show that

increased tumour grade and invasion was associated with an increased activation of Hh signalling in breast cancer cells by manipulating Hh ligand secretion.

E-cadherin protein expression increased in both cell lines assessed in this study following 48 hours treatment with cyclopamine or LDE225 in a dose-dependent manner (Table 5-10).

Membrane localisation of E-cadherin increased in MCF7 cells following inhibition by either cyclopamine or LDE225 while cytoplasmic localisation increased in MDA-MB-231 (Table 5-7 and Table 5-8). Concurring with this finding, Song *et al.* (2016) showed that E-cadherin increased in breast cancer cells following inhibition of Hh signalling using cyclopamine for 72 hours. They concluded that canonical Hh pathway activation is essential for enhancing migration capacity of breast cancer cells by reducing E-cadherin and increasing the production of matrix metalloproteases (Song *et al.*, 2016). In colon cancer, Qualtrough *et al.* (2015) showed that inhibition of Hh signalling by cyclopamine stimulated the expression of E-cadherin in benign and malignant colorectal tumour cell lines.

Table 5-6: Increase in E-cadherin expression following treatment with cyclopamine or LDE225 in MCF7 and MDA-MB-231.
Alteration in E-cadherin expression following inhibition of Hh signalling by cyclopamine or LDE225 at three concentrations (1µM, 5µM, and 10µM). Arrows indicate change in expression of protein compared to vehicle control.

	Treatment	1µM cyclopamine	5µM cyclopamine	10µM cyclopamine	1µM LDE225	5µM LDE225	10µM LDE225
E-cadherin	MCF7	↑	↑↑	↑↑↑	↑	↑	↑↑
	MDA-MB-231	-	↑	↑↑	-	-	↑↑

Table 5-7: Increase in the membrane localisation of E-cadherin in MCF7 cell line following inhibition of the Hh signalling by cyclopamine and LDE225.
Effect of inhibiting Hh signalling by cyclopamine or LDE225 on membrane localisation of E-cadherin at two concentrations (1µM and 10µM) for 48hours. Arrows indicate qualitative observation of level of membrane localisation of E-cadherin compared to vehicle control.

	Treatment	1µM cyclopamine	10µM cyclopamine	1µM LDE225	10µM LDE225
E-cadherin	MCF7	-	↑↑	↑	↑
	MDA-MB-231	-	-	-	-

Table 5-8: Increase in E-cadherin cytoplasmic localisation in both cell lines following inhibition of Hh signalling.
Effect of Hh signalling inhibition by cyclopamine or LDE225 on the cytoplasmic localisation of E-cadherin following treatment with two concentrations (1μM and 10μM) for 48hours. Arrows indicate qualitative observation of level of cytoplasmic E-cadherin compared to vehicle control.

	Treatment	1 μM cyclopamine	10 μM cyclopamine	1 μM LDE225	10 μM LDE225
E-cadherin	MCF7	↑	↑	↑	↑
	MDA-MB-231	↑	↑	↑	↑

The inhibition of Hh signalling in breast cancer cell lines (MCF7 and MDA-MB-231) by cyclopamine or LDE225 caused significant reduction in the motility and invasion of both cell lines (Table 5-9). The MCF7 cell line was less motile than MDA-MB-231, which is expected because MDA-MB-231 is a more aggressive cell line and displays a more mesenchymal phenotype (Rizwan *et al.*, 2015). Furthermore, treatment with either one of the inhibitors resulted in a significant decrease in MCF7 cell invasion through Matrigel™ (Table 5-9). In MDA-MB-231 cells, the reduction of both motility and invasion was more significant following inhibition by LDE225 (Table 5-9) suggesting a differential effect of inhibitors dependent on the breast cancer subtype. Kameda *et al.* (2009) showed that treatment of MDA-MB-231 with 10μM and 30μM cyclopamine reduced invasion in a dose-dependent manner. A similar inhibition of invasion was observed following knocking down *Gli1* in MDA-MB-231 (Kameda *et al.*, 2009; Kwon *et al.*, 2011). Here, the assessment of Gli1 localisation and level of expression showed that decreased expression and nuclear localisation of Gli1 was associated with decrease in motility and invasion of breast cancer cells.

Table 5-9: inhibition of Hh signalling caused decrease in motility and invasion of breast cancer cells.
Effect of inhibiting Hh signalling by 1μM cyclopamine or LDE225 on motility and invasion of MCF7 and MDA-MB-231 cells. Changes in motility and invasion of cells was indicated as arrows compared to vehicle control.

Cell lines	Assay	Treatment	
		1μM cyclopamine	1μM LDE225
MCF7	Motility	↓	↓
	Invasion	↓↓↓	↓↓↓
MDA-MB-231	Motility	↓	↓↓
	Invasion	↓	↓↓↓

5.4 Conclusion

The cell viability, cell yield and apoptosis showed that the inhibition of the Hh signalling using either cyclopamine or LDE225 resulted in reduction of cellular viability and cell yield. This is the first study to show this effect and compared it between two cell lines that represent to two molecular subtypes of breast cancer (luminal and TNBC). Most of the cell death were early apoptosis in MCF7 (luminal) seen following Hh inhibition, whereas, in MDA-MB-231 (Basal and TNBC) most cell death was late cell death.

Assessment of the level of expression and localisation of the Gli proteins was novel in this study and was not investigated previously. Also, comparing the expression level and subcellular localisation following Hh inhibition using either cyclopamine or LDE225 in two cell lines that belong to two molecular subgroup of breast cancer was not conducted previously. The Gli protein expression analysis and changes of localisation of the proteins showed that there was a difference in the mechanism of action of the pathway in the two breast cancer cell lines. Suggesting a key difference in the way the two cell lines respond to each drug and difference in the cell trafficking of the Gli proteins between both cell lines. This can also explain why the changes in viability, cell yield and apoptosis levels varied between the two cell lines.

The Hedgehog (Hh) signalling pathway is potentially involved in tumour invasion and it may be facilitated by stimulating EMT-like changes in the cells.

Evaluation of the effect of Hh inhibition on CRT is also novel for the current study. We were able to show reduction in CRT for the first time *in vitro* as a result of Hh inhibition in breast cancer, thereby, confirming the potential crosstalk between these signalling pathways and highlighting them as a potential regulator of EMT in this disease. The association between decreased CRT and the decrease in expression and nuclear localisation of Gli1 support this conclusion. Also, the increase in nuclear Gli3 indicates that in breast cancer this protein may have an inhibitory effect on β-catenin, which merits further investigation. Inhibition of Hh signalling by cyclopamine or LDE225 treatment caused significant reduction of motility and invasion of MCF7 and MDA-MB-231 cells.

6. Chapter Six: General Discussion

90% of breast cancer-related deaths are caused by distant metastasis (Tsai and Yang, 2013). Identifying pathways involved the regulation of metastasis is crucial for developing targeted treatments. Understanding alteration of these pathways could lead to better selection of patients that would benefit from such treatment. EMT is a regulatory process that is involved in many normal physiological processes and is also involved in cancer metastasis (Wang and Zhou, 2013). This study aimed to investigate the process of EMT in breast cancer and to understand the regulation of this process. This study also aimed to identify a pathway potentially involved in the regulation of EMT in breast cancer and to investigate the effect of inhibiting this pathway.

6.1 Breast cancer cell lines undergo changes associated with EMT when subjected to a stimulus using a cell-density-based model

An *in vitro* cell density-based model was developed to investigate EMT using breast cancer cell lines. This model produces a stimulus that provokes EMT in breast cancer cells by reducing the degree of cell-cell contact. To evaluate the effect of these changes in cell-cell interaction, cellular morphology and the expression of E-cadherin, β-catenin and vimentin were assessed. Using this model, we were able to show that breast cancer cell lines undergo morphological changes associated with EMT. Assessment of E-cadherin, β-catenin and vimentin confirmed that breast cancer cell lines undergo alteration in expression levels, and localisation of proteins indicative of EMT-associated change.

Initially, we hypothesised that the molecular subtype of breast cancer can influence their ability to undergo EMT. Upon investigating a panel of breast cancer cell lines representing the major molecular subtypes of breast cancers, we were able to confirm that all cell lines were able to undergo EMT-associated change. All cell lines showed morphological alteration with associated changes in both the level and localisation of E-cadherin, β-catenin and vimentin proteins. However, the propensity of breast cancer cell lines to undergo EMT was not dictated by the molecular subtype to which they belong to. All breast cancer cell lines were equally able to undergo EMT when subjected density-based stimulus. Also, the confirmation that breast cancer cell lines from different molecular subtypes were able to undergo EMT, has an impact on understanding breast cancer invasion and metastasis *in vivo*.

Changes in β-catenin localisation indicated potential activation of Wnt/β-catenin signalling in breast cancer cell lines. The morphology, and both the expression and localisation of EMT-related proteins showed that in the high-density culture the cells had more epithelial phenotype and in the lower density they showed a more mesenchymal phenotype. In one cell line the opposite was observed. Furthermore, two TNBC cell lines showed significant changes in the medium density with increased epithelial phenotype. Thus, medium density was standardised as the seeding density for all further analysis.

6.2 Gli1, Gli2 and Gli3 expression showed that Hh signalling may be involved in breast cancer metastasis and suggests crosstalk with Wnt/β-catenin signalling

Previous work showed that Hh signalling works in parallel with Wnt/β-catenin during the phases of mammary gland development (reviewed by Flemban and Qualtrough, 2015). Thus, investigation of the co-activation of Wnt and Hh signalling in a cohort of breast cancer samples was carried out in combination with of assessment of tissue distribution and subcellular localisation. Recent work showed that there was co-expression of Wnt/β-catenin and Hh signalling in breast cancer samples (Arnold *et al.*, 2017).

Most previous works focused on studying Gli1 and β-catenin, alone or in combination. What previous studies overlooked was assessing the tissue distribution of these proteins together with their subcellular localisation. Also, in our data, we combined evaluating Hh and Wnt/β-catenin proteins with the estimation of E-cadherin status in both the tumour centre and at the invasive front. Altogether this approach provided new insight into the assessment of EMT in breast cancer.

Analysis showed that Hh signalling was expressed in breast cancer samples and that the expression of Gli proteins was higher at the invasive front where EMT is thought to be active. The analysis confirmed that there was a correlation between Hh and Wnt/β-catenin signalling activation that occurred at the invasive front. Also, activation of Hh signalling in breast cancer correlated with decreased E-cadherin. Previous work confirmed overexpression of specific components compared to normal mammary cells (Mukherjee *et al.*, 2006). Activation of Hh signalling in the tumour may suggests that breast cancer cells develop an autocrine activation loop of Hh signalling instead of depending on paracrine signalling (Theunissen and de Sauvage, 2009).

6.3 Inhibition of Hh signalling with cyclopamine or LDE225 caused an alteration in EMT and reduced CRT

Two cell lines were selected (MCF7 and MDA-MB-231) and treated with cyclopamine or LDE225 to assess the effect on viability, cell yield and cell death. Analysis showed that breast cancer cell lines showed inhibition of proliferation, measured as cell yield, following 48hours treatment. The treatments increased cell death, with reduced viability, in a dose-dependent manner. Treatment with cyclopamine or LDE225 caused an alteration of both the localisation and level of expression of Gli proteins that confirmed a direct effect of the drug on the Hh signalling pathway activity. Also, the effect of Hh inhibition on cell yield and cell death concurred with *in vivo* observations, as we showed that Gli1 expression and nuclear localisation correlated with increased tumour size. This was in agreement with previous findings showing the effect of Hh inhibition *in vivo* and found that treatment with a Hh inhibitor resulted in a reduction of tumour size (Benvenuto *et al.*, 2016).

Hh inhibition reduced both cell motility and invasion through extracellular matrix *in vitro*. This reduced of motility was associated with altered levels and localisation of E-cadherin and β-catenin. Together with the increase in E-cadherin expression these data suggest that inhibition of Hh signalling with cyclopamine or LDE225 resulted in a reduction of EMT in breast cancer and decreased cancer cell motility. This showed that inhibition of Hh signalling using either cyclopamine or LDE225 cause reduction in EMT-associated changes, which could translate to utilising the Hh signalling for metastatic cancer therapy.

To further investigate the potential crosstalk between Hh and Wnt/β-catenin, CRT was measured using the TOPFLASH reporter assay (Korinek *et al.*, 1997). Data showed that inhibition of Hh signalling in breast cancer cell lines resulted in the reduction of CRT which was reflected in the changes in both the expression and localisation of β-catenin. Thus, we were able to confirm the crosstalk between Hh and Wnt signalling pathways.

7. General Conclusion

Our data confirmed that breast cancer cells undergo EMT-like change that is not governed by the molecular subtype of breast cancer cell lines. The *in vitro* density model provides a useful tool for understanding EMT in breast cancer.

Screening for the expression of Gli1, Gli2 and Gli3 in a cohort of patient samples showed that Hh signalling is active in breast cancer. Correlation of increased expression of Gli proteins with the invasive front suggests an association between Hh signalling and EMT. Expression of the components of the Hh pathway in breast cancer human samples and also in cell lines led to the investigation of autocrine signalling *in vitro* using cell lines. *In vitro* data showed that inhibition of Hh signalling has both anti-tumour growth and anti-metastatic effects which could be exploited therapeutically to reduce mortality due to this incurable disease. Following the treatment of two cell lines with cyclopamine or LDE225 both cell yield and viability decreased, while cell death increased, in a dose-dependent manner. Activated Hh signalling observed *in vivo* correlated with increased tumour size, which is a prognostic indicator and can be explained by the *in vitro* data showing that Hh inhibition causes reduced cell yield. However, further investigation is required to understand the mechanism of this correlation. These findings support utilising Gli proteins as prognostic markers to identify patients that could benefit from targeted therapy. This also may reduce clinical trial failure in the future.

Further analysis of tissue distribution and subcellular localisation showed that Hh signalling activation was associated with Wnt/β-catenin and E-cadherin expression. β-catenin expression and localisation and CRT levels showed that Hh inhibition with cyclopamine or LDE225 treatment co-inhibited Wnt/β-catenin signalling. Hh inhibition may be of therapeutic benefit in a percentage of breast cancer patients. These patients once correctly identified and treated using Hh inhibitors could show reduced tumour growth and reduced propensity for metastasis, thereby greatly improving prognosis for this subset of breast cancer patients.

8. Limitations

Due to limitations in time and resources, the assessment of EMT transcription factors including Slug, Snail, and Twist was not conducted after subjecting breast cancer cell lines to EMT-associated change using the seeding density model. Also, these transcription factors were not evaluated after inhibition of Hh signalling using cyclopamine and LDE225. There was a limitation of the number of patient samples used in this study by staining and evaluation of the full patient samples cohort. To improve statistical analysis the sample size should be at least 48 cases for Fisher's exact test and 220 cases for Chi-square test (calculated with GPower 3.0.10). This would allow confirmation of the relationship between Gli1, Gli2, Gli3, β-catenin and E-cadherin expression and the clinicopathological characteristics. Assessing Gli1, Gli2, and Gli3 in a full cohort could provide additional information and strengthen the statistical significance and conclusions drawn. Further confirmation of the effect of Hh inhibition on the outputs of Hh signalling could have been assessed using Gli reporters. Despite these limitations, this study has furthered our knowledge of the role of Hh signalling in breast cancer, its potential influence on patient prognosis, and highlights its therapeutic potential in the globally most common cancer diagnosed in females.

9. Future Direction

- To assess the changes of EMT-related transcription factors such as Slug, Snail and Twist in response to changes in seeding density.
- To investigate the effect of Hh signalling inhibition on the levels of Hh and Wnt-specific target genes together with EMT transcription factors such as Slug, Snail, Twist, Zeb and LEF-1.
- To evaluate the expression of other Hh signalling components including Smo, Patched and Shh in breast cancer samples.
- To investigate the expression of Gli1, Gli2, Gli3, β-catenin and E-cadherin in a larger cohort of breast cancer samples. To improve statistical analysis the sample size should be at least 48 cases for Fisher's exact test and 220 cases for Chi-square test (calculated with GPower 3.0.10) then to analyse for correlation between marker expression and clinical criteria.
- Determine the effect of expression of Gli1, Gli2 and Gli3 expression on both the short-term and long-term survival of patients to assess whether these proteins have prognostic value together with meta-analysis of associated pathological report criteria.
- Analysis of changes in nuclear co-localisation of Gli proteins in breast cancer cell lines using imaging software to provide semi-quantitative data, such as velocity software.
- Use monoclonal antibodies specific for the activator form of Gli proteins and compare to the repressor forms.
- To eliminate the possibility of off-target effect,s using Shh rescue (by Shh add back to the system) and checking the effect of Hh inhibition using treatments on CRT and E-cadherin expression and localisation.
- To assess the effect of Hh signalling inhibition on the cell cycle of breast cancer cell lines.
- To confirm the effect of cyclopamine or LDE225 treatment on outputs of Hh signalling using Gli reporters.
- Cell sorting of treated cell lines could provide analysis of subpopulations of breast cancer cells.

10.References

Aberger, F. and Ruiz, I. A. A. (2014). Context-dependent signal integration by the GLI code: the oncogenic load, pathways, modifiers and implications for cancer therapy. *Semin Cell Dev Biol, 33*, pp. 93-104.

Aberle, H., Bauer, A., Stappert, J., Kispert, A. and Kemler, R. (1997). beta-catenin is a target for the ubiquitin-proteasome pathway. *EMBO J, 16*(13), pp. 3797-3804.

Adams, C. L. and Nelson, W. J. (1998). Cytomechanics of cadherin-mediated cell-cell adhesion. *Curr Opin Cell Biol, 10*(5), pp. 572-577.

Aden, D. P., Fogel, A., Plotkin, S., Damjanov, I. and Knowles, B. B. (1979). Controlled synthesis of HBsAg in a differentiated human liver carcinoma-derived cell line. *Nature, 282*(5739), pp. 615-616.

Agyeman, A., Jha, B. K., Mazumdar, T. and Houghton, J. A. (2014). Mode and specificity of binding of the small molecule GANT61 to GLI determines inhibition of GLI-DNA binding. *Oncotarget, 5*(12), pp. 4492-4503.

Agyeman, A., Mazumdar, T. and Houghton, J. A. (2012). Regulation of DNA damage following termination of Hedgehog (HH) survival signaling at the level of the GLI genes in human colon cancer. *Oncotarget, 3*(8), pp. 854-868.

Akram, M. and Siddiqui, S. A. (2012). Breast cancer management: past, present and evolving. *Indian J Cancer, 49*(3), pp. 277-282.

Aleskandarany, M. A., Negm, O. H., Green, A. R., Ahmed, M. A., Nolan, C. C., Tighe, P. J., Ellis, I. O. and Rakha, E. A. (2014). Epithelial mesenchymal transition in early invasive breast cancer: an immunohistochemical and reverse phase protein array study. *Breast Cancer Res Treat, 145*(2), pp. 339-348.

Alexaki, V. I., Javelaud, D., Van Kempen, L. C., Mohammad, K. S., Dennler, S., Luciani, F., Hoek, K. S., Juarez, P., Goydos, J. S.,

Fournier, P. J., Sibon, C., Bertolotto, C., Verrecchia, F., Saule, S., Delmas, V., Ballotti, R., Larue, L., Saiag, P., Guise, T. A. and Mauviel, A. (2010). GLI2-mediated melanoma invasion and metastasis. *J Natl Cancer Inst, 102*(15), pp. 1148-1159.

Alvarez-Medina, R., Cayuso, J., Okubo, T., Takada, S. and Marti, E. (2008). Wnt canonical pathway restricts graded Shh/Gli patterning activity through the regulation of Gli3 expression. *Development, 135*(2), pp. 237-247.

Antonyak, M. A., Miller, A. M., Jansen, J. M., Boehm, J. E., Balkman, C. E., Wakshlag, J. J., Page, R. L. and Cerione, R. A. (2004). Augmentation of tissue transglutaminase expression and activation by epidermal growth factor inhibit doxorubicin-induced apoptosis in human breast cancer cells. *J Biol Chem, 279*(40), pp. 41461-41467.

Arnedos, M., Bihan, C., Delaloge, S. and Andre, F. (2012). Triple-negative breast cancer: are we making headway at least? *Ther Adv Med Oncol, 4*(4), pp. 195-210.

Arnold, K. M., Pohlig, R. T. and Sims-Mourtada, J. (2017). Co-activation of Hedgehog and Wnt signaling pathways is associated with poor outcomes in triple negative breast cancer. *Oncol Lett, 14*(5), pp. 5285-5292.

Atkins, H., Hayward, J. L., Klugman, D. J. and Wayte, A. B. (1972). Treatment of early breast cancer: a report after ten years of a clinical trial. *Br Med J, 2*(5811), pp. 423-429.

Badve, S., Dabbs, D. J., Schnitt, S. J., Baehner, F. L., Decker, T., Eusebi, V., Fox, S. B., Ichihara, S., Jacquemier, J., Lakhani, S. R., Palacios, J., Rakha, E. A., Richardson, A. L., Schmitt, F. C., Tan, P. H., Tse, G. M., Weigelt, B., Ellis, I. O. and Reis-Filho, J. S. (2011). Basal-like and triple-negative breast cancers: a critical review with an emphasis on the implications for pathologists and oncologists. *Mod Pathol, 24*(2), pp. 157-167.

Bai, C. B. and Joyner, A. L. (2001). Gli1 can rescue the in vivo function of Gli2. *Development, 128*(24), pp. 5161-5172.

Bao, C., Kim, M. C., Chen, J., Song, J., Ko, H. W. and Lee, H. J. (2016). Sulforaphene Interferes with Human Breast Cancer Cell Migration and Invasion through Inhibition of Hedgehog Signaling. *J Agric Food Chem, 64*(27), pp. 5515-5524.

Barker, N., van de Wetering, M. and Clevers, H. (2008). The intestinal stem cell. *Genes Dev, 22*(14), pp. 1856-1864.

Barsky, S. H. and Karlin, N. J. (2006). Mechanisms of disease: breast tumor pathogenesis and the role of the myoepithelial cell. *Nat Clin Pract Oncol, 3*(3), pp. 138-151.

Barton, M. B., Elmore, J. G. and Fletcher, S. W. (1999). Breast symptoms among women enrolled in a health maintenance organization: frequency, evaluation, and outcome. *Ann Intern Med, 130*(8), pp. 651-657.

Batlle, E., Henderson, J. T., Beghtel, H., van den Born, M. M., Sancho, E., Huls, G., Meeldijk, J., Robertson, J., van de Wetering, M., Pawson, T. and Clevers, H. (2002). Beta-catenin and TCF mediate cell positioning in the intestinal epithelium by controlling the expression of EphB/ephrinB. *Cell, 111*(2), pp. 251-263.

Behrens, I., Kamm, W., Dantzig, A. H. and Kissel, T. (2004). Variation of peptide transporter (PepT1 and HPT1) expression in Caco-2 cells as a function of cell origin. *J Pharm Sci, 93*(7), pp. 1743-1754.

Behrens, J., Mareel, M. M., Van Roy, F. M. and Birchmeier, W. (1989). Dissecting tumor cell invasion: epithelial cells acquire invasive properties after the loss of uvomorulin-mediated cell-cell adhesion. *J Cell Biol, 108*(6), pp. 2435-2447.

Benhaj, K., Akcali, K. C. and Ozturk, M. (2006). Redundant expression of canonical Wnt ligands in human breast cancer cell lines. *Oncol Rep, 15*(3), pp. 701-707.

Benton, G., Crooke, E. and George, J. (2009). Laminin-1 induces E-cadherin expression in 3-dimensional cultured breast cancer cells by inhibiting DNA methyltransferase 1 and

reversing promoter methylation status. *FASEB J, 23*(11), pp. 3884-3895.

Benvenuto, M., Masuelli, L., De Smaele, E., Fantini, M., Mattera, R., Cucchi, D., Bonanno, E., Di Stefano, E., Frajese, G. V., Orlandi, A., Screpanti, I., Gulino, A., Modesti, A. and Bei, R. (2016). In vitro and in vivo inhibition of breast cancer cell growth by targeting the Hedgehog/GLI pathway with SMO (GDC-0449) or GLI (GANT-61) inhibitors. *Oncotarget, 7*(8), pp. 9250-9270.

Berman, D. M., Karhadkar, S. S., Hallahan, A. R., Pritchard, J. I., Eberhart, C. G., Watkins, D. N., Chen, J. K., Cooper, M. K., Taipale, J., Olson, J. M. and Beachy, P. A. (2002). Medulloblastoma growth inhibition by hedgehog pathway blockade. *Science, 297*(5586), pp. 1559-1561.

Berman, D. M., Karhadkar, S. S., Maitra, A., Montes De Oca, R., Gerstenblith, M. R., Briggs, K., Parker, A. R., Shimada, Y., Eshleman, J. R., Watkins, D. N. and Beachy, P. A. (2003). Widespread requirement for Hedgehog ligand stimulation in growth of digestive tract tumours. *Nature, 425*(6960), pp. 846-851.

Berx, G., Cleton-Jansen, A. M., Strumane, K., de Leeuw, W. J., Nollet, F., van Roy, F. and Cornelisse, C. (1996). E-cadherin is inactivated in a majority of invasive human lobular breast cancers by truncation mutations throughout its extracellular domain. *Oncogene, 13*(9), pp. 1919-1925.

Bevers, T. B., Anderson, B. O., Bonaccio, E., Buys, S., Daly, M. B., Dempsey, P. J., Farrar, W. B., Fleming, I., Garber, J. E., Harris, R. E., Heerdt, A. S., Helvie, M., Huff, J. G., Khakpour, N., Khan, S. A., Krontiras, H., Lyman, G., Rafferty, E., Shaw, S., Smith, M. L., Tsangaris, T. N., Williams, C., Yankeelov, T. and National Comprehensive Cancer, N. (2009). NCCN clinical practice guidelines in oncology: breast cancer screening and diagnosis. *J Natl Compr Canc Netw, 7*(10), pp. 1060-1096.

Bienz, M. (1999). APC: the plot thickens. *Curr Opin Genet Dev, 9*(5), pp. 595-603.

Binns, W., Thacker, E. J., James, L. F. and Huffman, W. T. (1959). A congenital cyclopiantype malformation in lambs. *J Am Vet Med Assoc, 134*(4), pp. 180-183.

Blick, T., Widodo, E., Hugo, H., Waltham, M., Lenburg, M. E., Neve, R. M. and Thompson, E. W. (2008). Epithelial mesenchymal transition traits in human breast cancer cell lines. *Clin Exp Metastasis, 25*(6), pp. 629-642.

Blotta, S., Jakubikova, J., Calimeri, T., Roccaro, A. M., Amodio, N., Azab, A. K., Foresta, U., Mitsiades, C. S., Rossi, M., Todoerti, K., Molica, S., Morabito, F., Neri, A., Tagliaferri, P., Tassone, P., Anderson, K. C. and Munshi, N. C. (2012). Canonical and noncanonical Hedgehog pathway in the pathogenesis of multiple myeloma. *Blood, 120*(25), pp. 5002-5013.

Boice, J. D., Jr., Preston, D., Davis, F. G. and Monson, R. R. (1991). Frequent chest X-ray fluoroscopy and breast cancer incidence among tuberculosis patients in Massachusetts. *Radiat Res, 125*(2), pp. 214-222.

Bonadonna, G., Brusamolino, E., Valagussa, P., Rossi, A., Brugnatelli, L., Brambilla, C., De Lena, M., Tancini, G., Bajetta, E., Musumeci, R. and Veronesi, U. (1976). Combination chemotherapy as an adjuvant treatment in operable breast cancer. *N Engl J Med, 294*(8), pp. 405-410.

Brambilla, C., De Lena, M., Rossi, A., Valagussa, P. and Bonadonna, G. (1976). Response and survival in advanced breast cancer after two non-cross-resistant combinations. *Br Med J, 1*(6013), pp. 801-804.

Brennan, D., Chen, X., Cheng, L., Mahoney, M. and Riobo, N. A. (2012). Noncanonical Hedgehog signaling. *Vitam Horm, 88*, pp. 55-72.

Brinton, L. A., Hoover, R. and Fraumeni, J. F., Jr. (1983a). Epidemiology of minimal breast cancer. *JAMA, 249*(4), pp. 483-487.

Brinton, L. A., Hoover, R. and Fraumeni, J. F., Jr. (1983b). Reproductive factors in the aetiology of breast cancer. *Br J Cancer, 47*(6), pp. 757-762.

Brinton, L. A., Schairer, C., Hoover, R. N. and Fraumeni, J. F., Jr. (1988). Menstrual factors and risk of breast cancer. *Cancer Invest, 6*(3), pp. 245-254.

Briscoe, J. and Therond, P. (2005). Hedgehog signaling: from the Drosophila cuticle to anti-cancer drugs. *Dev Cell, 8*(2), pp. 143-151.

Brisken, C., Heineman, A., Chavarria, T., Elenbaas, B., Tan, J., Dey, S. K., McMahon, J. A., McMahon, A. P. and Weinberg, R. A. (2000). Essential function of Wnt-4 in mammary gland development downstream of progesterone signaling. *Genes Dev, 14*(6), pp. 650-654.

Bryden, M. M., Evans, H. E. and Keeler, R. F. (1971). Cyclopia in sheep caused by plant teratogens. *J Anat, 110*(Pt 3), pp. 507.

Bryne, M., Boysen, M., Alfsen, C. G., Abeler, V. M., Sudbo, J., Nesland, J. M., Kristensen, G. B., Piffko, J. and Bankfalvi, A. (1998). The invasive front of carcinomas. The most important area for tumour prognosis? *Anticancer Res, 18*(6B), pp. 4757-4764.

Bukholm, I. K., Nesland, J. M., Karesen, R., Jacobsen, U. and Borresen-Dale, A. L. (1998). E-cadherin and alpha-, beta-, and gamma-catenin protein expression in relation to metastasis in human breast carcinoma. *J Pathol, 185*(3), pp. 262-266.

Busch, E. L., McGraw, K. A. and Sandler, R. S. (2014). The potential for markers of epithelial-mesenchymal transition to improve colorectal cancer outcomes: a systematic review. *Cancer Epidemiol Biomarkers Prev, 23*(7), pp. 1164-1175.

Cai, J., Guan, H., Fang, L., Yang, Y., Zhu, X., Yuan, J., Wu, J. and Li, M. (2013). MicroRNA-374a activates Wnt/beta-catenin

signaling to promote breast cancer metastasis. *J Clin Invest, 123*(2), pp. 566-579.

Cai, K., Jiang, L., Wang, J., Zhang, H., Wang, X., Cheng, D. and Dou, J. (2014). Downregulation of beta-catenin decreases the tumorigenicity, but promotes epithelial-mesenchymal transition in breast cancer cells. *J Cancer Res Ther, 10*(4), pp. 1063-1070.

Cailleau, R., Olive, M. and Cruciger, Q. V. (1978). Long-term human breast carcinoma cell lines of metastatic origin: preliminary characterization. *In Vitro, 14*(11), pp. 911-915.

Cailleau, R., Young, R., Olive, M. and Reeves, W. J., Jr. (1974). Breast tumor cell lines from pleural effusions. *J Natl Cancer Inst, 53*(3), pp. 661-674.

Cao, X., Geradts, J., Dewhirst, M. W. and Lo, H. W. (2012). Upregulation of VEGF-A and CD24 gene expression by the tGLI1 transcription factor contributes to the aggressive behavior of breast cancer cells. *Oncogene, 31*(1), pp. 104-115.

Carter, C. L., Allen, C. and Henson, D. E. (1989). Relation of tumor size, lymph node status, and survival in 24,740 breast cancer cases. *Cancer, 63*(1), pp. 181-187.

Casciola-Rosen, L., Rosen, A., Petri, M. and Schlissel, M. (1996). Surface blebs on apoptotic cells are sites of enhanced procoagulant activity: implications for coagulation events and antigenic spread in systemic lupus erythematosus. *Proc Natl Acad Sci U S A, 93*(4), pp. 1624-1629.

Caussinus, E., Colombelli, J. and Affolter, M. (2008). Tip-cell migration controls stalk-cell intercalation during Drosophila tracheal tube elongation. *Curr Biol, 18*(22), pp. 1727-1734.

Chai, F., Zhou, J., Chen, C., Xie, S., Chen, X., Su, P. and Shi, J. (2013). The Hedgehog inhibitor cyclopamine antagonizes chemoresistance of breast cancer cells. *Onco Targets Ther, 6*, pp. 1643-1647.

Chakrabarti, R., Hwang, J., Andres Blanco, M., Wei, Y., Lukacisin, M., Romano, R. A., Smalley, K., Liu, S., Yang, Q., Ibrahim, T.,

Mercatali, L., Amadori, D., Haffty, B. G., Sinha, S. and Kang, Y. (2012). Elf5 inhibits the epithelial-mesenchymal transition in mammary gland development and breast cancer metastasis by transcriptionally repressing Snail2. *Nat Cell Biol, 14*(11), pp. 1212-1222.

Chao, Y. L., Shepard, C. R. and Wells, A. (2010). Breast carcinoma cells re-express E-cadherin during mesenchymal to epithelial reverting transition. *Mol Cancer, 9*, pp. 179.

Charafe-Jauffret, E., Ginestier, C., Monville, F., Finetti, P., Adelaide, J., Cervera, N., Fekairi, S., Xerri, L., Jacquemier, J., Birnbaum, D. and Bertucci, F. (2006). Gene expression profiling of breast cell lines identifies potential new basal markers. *Oncogene, 25*(15), pp. 2273-2284.

Che, J., Zhang, F. Z., Zhao, C. Q., Hu, X. D. and Fan, S. J. (2013). Cyclopamine is a novel Hedgehog signaling inhibitor with significant anti-proliferative, anti-invasive and anti-estrogenic potency in human breast cancer cells. *Oncol Lett, 5*(4), pp. 1417-1421.

Chekhun, S., Bezdenezhnykh, N., Shvets, J. and Lukianova, N. (2013). Expression of biomarkers related to cell adhesion, metastasis and invasion of breast cancer cell lines of different molecular subtype. *Exp Oncol, 35*(3), pp. 174-179.

Chen, A., Beetham, H., Black, M. A., Priya, R., Telford, B. J., Guest, J., Wiggins, G. A., Godwin, T. D., Yap, A. S. and Guilford, P. J. (2014). E-cadherin loss alters cytoskeletal organization and adhesion in non-malignant breast cells but is insufficient to induce an epithelial-mesenchymal transition. *BMC Cancer, 14*, pp. 552.

Chen, M. H., Yip, G. W., Tse, G. M., Moriya, T., Lui, P. C., Zin, M. L., Bay, B. H. and Tan, P. H. (2008). Expression of basal keratins and vimentin in breast cancers of young women correlates with adverse pathologic parameters. *Mod Pathol, 21*(10), pp. 1183-1191.

Chen, Y. T., Stewart, D. B. and Nelson, W. J. (1999). Coupling assembly of the E-cadherin/beta-catenin complex to

efficient endoplasmic reticulum exit and basal-lateral membrane targeting of E-cadherin in polarized MDCK cells. *J Cell Biol, 144*(4), pp. 687-699.

Cheng, J. C., Auersperg, N. and Leung, P. C. (2012). EGF-induced EMT and invasiveness in serous borderline ovarian tumor cells: a possible step in the transition to low-grade serous carcinoma cells? *PLoS One, 7*(3), pp. e34071.

Christofori, G. (2006). New signals from the invasive front. *Nature, 441*(7092), pp. 444-450.

Chu, E. Y., Hens, J., Andl, T., Kairo, A., Yamaguchi, T. P., Brisken, C., Glick, A., Wysolmerski, J. J. and Millar, S. E. (2004). Canonical WNT signaling promotes mammary placode development and is essential for initiation of mammary gland morphogenesis. *Development, 131*(19), pp. 4819-4829.

Chuang, P. T. and McMahon, A. P. (1999). Vertebrate Hedgehog signalling modulated by induction of a Hedgehog-binding protein. *Nature, 397*(6720), pp. 617-621.

Cichon, M. A., Nelson, C. M. and Radisky, D. C. (2015). Regulation of epithelial-mesenchymal transition in breast cancer cells by cell contact and adhesion. *Cancer Inform, 14*(Suppl 3), pp. 1-13.

Clark, A. G. and Vignjevic, D. M. (2015). Modes of cancer cell invasion and the role of the microenvironment. *Curr Opin Cell Biol, 36*, pp. 13-22.

Clevers, H. and Nusse, R. (2012). Wnt/beta-catenin signaling and disease. *Cell, 149*(6), pp. 1192-1205.

Coates, A. S., Keshaviah, A., Thurlimann, B., Mouridsen, H., Mauriac, L., Forbes, J. F., Paridaens, R., Castiglione-Gertsch, M., Gelber, R. D., Colleoni, M., Lang, I., Del Mastro, L., Smith, I., Chirgwin, J., Nogaret, J. M., Pienkowski, T., Wardley, A., Jakobsen, E. H., Price, K. N. and Goldhirsch, A. (2007). Five years of letrozole compared with tamoxifen as initial adjuvant therapy for postmenopausal women with

endocrine-responsive early breast cancer: update of study BIG 1-98. *J Clin Oncol, 25*(5), pp. 486-492.

Colavito, S. A., Zou, M. R., Yan, Q., Nguyen, D. X. and Stern, D. F. (2014). Significance of glioma-associated oncogene homolog 1 (GLI1) expression in claudin-low breast cancer and crosstalk with the nuclear factor kappa-light-chain-enhancer of activated B cells (NFkappaB) pathway. *Breast Cancer Res, 16*(5), pp. 444.

Colditz, G. A., Stampfer, M. J., Willett, W. C., Hennekens, C. H., Rosner, B. and Speizer, F. E. (1990). Prospective study of estrogen replacement therapy and risk of breast cancer in postmenopausal women. *JAMA, 264*(20), pp. 2648-2653.

Cole, M. P., Jones, C. T. and Todd, I. D. (1971). A new anti-oestrogenic agent in late breast cancer. An early clinical appraisal of ICI46474. *Br J Cancer, 25*(2), pp. 270-275.

Coleman, M. P., Quaresma, M., Berrino, F., Lutz, J. M., De Angelis, R., Capocaccia, R., Baili, P., Rachet, B., Gatta, G., Hakulinen, T., Micheli, A., Sant, M., Weir, H. K., Elwood, J. M., Tsukuma, H., Koifman, S., GA, E. S., Francisci, S., Santaquilani, M., Verdecchia, A., Storm, H. H., Young, J. L. and Group, C. W. (2008). Cancer survival in five continents: a worldwide population-based study (CONCORD). *Lancet Oncol, 9*(8), pp. 730-756.

Conacci-Sorrell, M., Simcha, I., Ben-Yedidia, T., Blechman, J., Savagner, P. and Ben-Ze'ev, A. (2003). Autoregulation of E-cadherin expression by cadherin-cadherin interactions: the roles of beta-catenin signaling, Slug, and MAPK. *J Cell Biol, 163*(4), pp. 847-857.

Conway, K., Edmiston, S. N., Cui, L., Drouin, S. S., Pang, J., He, M., Tse, C. K., Geradts, J., Dressler, L., Liu, E. T., Millikan, R. and Newman, B. (2002). Prevalence and spectrum of p53 mutations associated with smoking in breast cancer. *Cancer Res, 62*(7), pp. 1987-1995.

Cooper, A. (1840). *On the anatomy of the breast,* Longman, Orme, Green, Brown, and Longmans.

Cooper, M. K., Porter, J. A., Young, K. E. and Beachy, P. A. (1998). Teratogen-mediated inhibition of target tissue response to Shh signaling. *Science, 280*(5369), pp. 1603-1607.

Corbit, K. C., Aanstad, P., Singla, V., Norman, A. R., Stainier, D. Y. and Reiter, J. F. (2005). Vertebrate Smoothened functions at the primary cilium. *Nature, 437*(7061), pp. 1018-1021.

CRUK. (2017). Available from: http://www.cancerresearchuk.org/health-professional/cancer-statistics/statistics-by-cancer-type/breast-cancer/incidence-invasive [Accessed 17/11/2017 2017].

Cui, W., Wang, L. H., Wen, Y. Y., Song, M., Li, B. L., Chen, X. L., Xu, M., An, S. X., Zhao, J., Lu, Y. Y., Mi, X. Y. and Wang, E. H. (2010). Expression and regulation mechanisms of Sonic Hedgehog in breast cancer. *Cancer Sci, 101*(4), pp. 927-933.

Cuzick, J., Sestak, I., Baum, M., Buzdar, A., Howell, A., Dowsett, M., Forbes, J. F. and investigators, A. L. (2010). Effect of anastrozole and tamoxifen as adjuvant treatment for early-stage breast cancer: 10-year analysis of the ATAC trial. *Lancet Oncol, 11*(12), pp. 1135-1141.

D'Amato, C., Rosa, R., Marciano, R., D'Amato, V., Formisano, L., Nappi, L., Raimondo, L., Di Mauro, C., Servetto, A., Fulciniti, F., Cipolletta, A., Bianco, C., Ciardiello, F., Veneziani, B. M., De Placido, S. and Bianco, R. (2014). Inhibition of Hedgehog signalling by NVP-LDE225 (Erismodegib) interferes with growth and invasion of human renal cell carcinoma cells. *Br J Cancer, 111*(6), pp. 1168-1179.

Daly, C. S., Flemban, A., Shafei, M., Conway, M. E., Qualtrough, D. and Dean, S. J. (2017). Hypoxia modulates the stem cell population and induces EMT in the MCF-10A breast epithelial cell line. *Oncol Rep*.

Daniel, C. W., Robinson, S. and Silberstein, G. B. (1996). The role of TGF-beta in patterning and growth of the mammary ductal tree. *J Mammary Gland Biol Neoplasia, 1*(4), pp. 331-341.

Das, S., Samant, R. S. and Shevde, L. A. (2011). Hedgehog signaling induced by breast cancer cells promotes osteoclastogenesis and osteolysis. *J Biol Chem, 286*(11), pp. 9612-9622.

de Ruijter, T. C., Veeck, J., de Hoon, J. P., van Engeland, M. and Tjan-Heijnen, V. C. (2011). Characteristics of triple-negative breast cancer. *J Cancer Res Clin Oncol, 137*(2), pp. 183-192.

Dean, S. J. and Rhodes, A. (2014). Triple negative breast cancer: the role of metabolic pathways. *Malays J Pathol, 36*(3), pp. 155-162.

Della Corte, C. M., Bellevicine, C., Vicidomini, G., Vitagliano, D., Malapelle, U., Accardo, M., Fabozzi, A., Fiorelli, A., Fasano, M., Papaccio, F., Martinelli, E., Troiani, T., Troncone, G., Santini, M., Bianco, R., Ciardiello, F. and Morgillo, F. (2015). SMO Gene Amplification and Activation of the Hedgehog Pathway as Novel Mechanisms of Resistance to Anti-Epidermal Growth Factor Receptor Drugs in Human Lung Cancer. *Clin Cancer Res, 21*(20), pp. 4686-4697.

Denef, N., Neubuser, D., Perez, L. and Cohen, S. M. (2000). Hedgehog induces opposite changes in turnover and subcellular localization of patched and smoothened. *Cell, 102*(4), pp. 521-531.

Dennler, S., Andre, J., Alexaki, I., Li, A., Magnaldo, T., ten Dijke, P., Wang, X. J., Verrecchia, F. and Mauviel, A. (2007). Induction of sonic hedgehog mediators by transforming growth factor-beta: Smad3-dependent activation of Gli2 and Gli1 expression in vitro and in vivo. *Cancer Res, 67*(14), pp. 6981-6986.

Dent, R., Trudeau, M., Pritchard, K. I., Hanna, W. M., Kahn, H. K., Sawka, C. A., Lickley, L. A., Rawlinson, E., Sun, P. and Narod, S. A. (2007). Triple-negative breast cancer: clinical features and patterns of recurrence. *Clin Cancer Res, 13*(15 Pt 1), pp. 4429-4434.

Derksen, P. W., Liu, X., Saridin, F., van der Gulden, H., Zevenhoven, J., Evers, B., van Beijnum, J. R., Griffioen, A.

W., Vink, J., Krimpenfort, P., Peterse, J. L., Cardiff, R. D., Berns, A. and Jonkers, J. (2006). Somatic inactivation of E-cadherin and p53 in mice leads to metastatic lobular mammary carcinoma through induction of anoikis resistance and angiogenesis. *Cancer Cell, 10*(5), pp. 437-449.

Deugnier, M. A., Moiseyeva, E. P., Thiery, J. P. and Glukhova, M. (1995). Myoepithelial cell differentiation in the developing mammary gland: progressive acquisition of smooth muscle phenotype. *Dev Dyn, 204*(2), pp. 107-117.

Deugnier, M. A., Teuliere, J., Faraldo, M. M., Thiery, J. P. and Glukhova, M. A. (2002). The importance of being a myoepithelial cell. *Breast Cancer Res, 4*(6), pp. 224-230.

Dewis, R. and Gribbin, J. (2009). *Breast Cancer: Diagnosis and Treatment: An Assessment of Need*,Cardiff (UK).

Dey, N., Young, B., Abramovitz, M., Bouzyk, M., Barwick, B., De, P. and Leyland-Jones, B. (2013). Differential activation of Wnt-beta-catenin pathway in triple negative breast cancer increases MMP7 in a PTEN dependent manner. *PLoS One, 8*(10), pp. e77425.

Di Mauro, C., Rosa, R., D'Amato, V., Ciciola, P., Servetto, A., Marciano, R., Orsini, R. C., Formisano, L., De Falco, S., Cicatiello, V., Di Bonito, M., Cantile, M., Collina, F., Chambery, A., Veneziani, B. M., De Placido, S. and Bianco, R. (2017). Hedgehog signalling pathway orchestrates angiogenesis in triple-negative breast cancers. *Br J Cancer, 116*(11), pp. 1425-1435.

Diao, Y., Azatyan, A., Rahman, M. F., Zhao, C., Zhu, J., Dahlman-Wright, K. and Zaphiropoulos, P. G. (2016). Blockade of the Hedgehog pathway downregulates estrogen receptor alpha signaling in breast cancer cells. *Oncotarget, 7*(44), pp. 71580-71593.

Ding, F., Wang, M., Du, Y., Du, S., Zhu, Z. and Yan, Z. (2016). BHX Inhibits the Wnt Signaling Pathway by Suppressing beta-catenin Transcription in the Nucleus. *Sci Rep, 6*, pp. 38331.

Ding, M. and Wang, X. (2017). Antagonism between Hedgehog and Wnt signaling pathways regulates tumorigenicity. *Oncol Lett, 14*(6), pp. 6327-6333.

Ding, Y. L., Zhou, Y., Xiang, L., Ji, Z. P. and Luo, Z. H. (2012). Expression of glioma-associated oncogene homolog 1 is associated with invasion and postoperative liver metastasis in colon cancer. *Int J Med Sci, 9*(5), pp. 334-338.

Dixon, A. R., Ellis, I. O., Elston, C. W. and Blamey, R. W. (1991). A comparison of the clinical metastatic patterns of invasive lobular and ductal carcinomas of the breast. *Br J Cancer, 63*(4), pp. 634-635.

Dixon, J. M., Anderson, T. J., Page, D. L., Lee, D. and Duffy, S. W. (1982). Infiltrating lobular carcinoma of the breast. *Histopathology, 6*(2), pp. 149-161.

Drasin, D. J., Robin, T. P. and Ford, H. L. (2011). Breast cancer epithelial-to-mesenchymal transition: examining the functional consequences of plasticity. *Breast Cancer Res, 13*(6), pp. 226.

Dummer, R., Guminski, A., Gutzmer, R., Dirix, L., Lewis, K. D., Combemale, P., Herd, R. M., Kaatz, M., Loquai, C., Stratigos, A. J., Schulze, H. J., Plummer, R., Gogov, S., Pallaud, C., Yi, T., Mone, M., Chang, A. L., Cornelis, F., Kudchadkar, R., Trefzer, U., Lear, J. T., Sellami, D. and Migden, M. R. (2016). The 12-month analysis from Basal Cell Carcinoma Outcomes with LDE225 Treatment (BOLT): A phase II, randomized, double-blind study of sonidegib in patients with advanced basal cell carcinoma. *J Am Acad Dermatol, 75*(1), pp. 113-125 e115.

Dwedar, F. I., Khalil, G. I., Nayer, S. A. and Farouk, A. (2016). Aberrant Vimentin Methylation Is Characteristic of Breast Cancer. *Advances in Breast Cancer Research, 5*(04), pp. 150.

Early Breast Cancer Trialists' Collaborative, G. (2005). Effects of chemotherapy and hormonal therapy for early breast cancer on recurrence and 15-year survival: an overview of the randomised trials. *Lancet, 365*(9472), pp. 1687-1717.

Easton, D. F., Ford, D. and Bishop, D. T. (1995). Breast and ovarian cancer incidence in BRCA1-mutation carriers. Breast Cancer Linkage Consortium. *Am J Hum Genet, 56*(1), pp. 265-271.

Eblaghie, M. C., Song, S. J., Kim, J. Y., Akita, K., Tickle, C. and Jung, H. S. (2004). Interactions between FGF and Wnt signals and Tbx3 gene expression in mammary gland initiation in mouse embryos. *J Anat, 205*(1), pp. 1-13.

Edge, S. B. and Compton, C. C. (2010). The American Joint Committee on Cancer: the 7th edition of the AJCC cancer staging manual and the future of TNM. *Ann Surg Oncol, 17*(6), pp. 1471-1474.

Efstathiou, J. A., Liu, D., Wheeler, J. M., Kim, H. C., Beck, N. E., Ilyas, M., Karayiannakis, A. J., Mortensen, N. J., Kmiot, W., Playford, R. J., Pignatelli, M. and Bodmer, W. F. (1999). Mutated epithelial cadherin is associated with increased tumorigenicity and loss of adhesion and of responsiveness to the motogenic trefoil factor 2 in colon carcinoma cells. *Proc Natl Acad Sci U S A, 96*(5), pp. 2316-2321.

Eifel, P., Axelson, J. A., Costa, J., Crowley, J., Curran, W. J., Jr., Deshler, A., Fulton, S., Hendricks, C. B., Kemeny, M., Kornblith, A. B., Louis, T. A., Markman, M., Mayer, R. and Roter, D. (2001). National Institutes of Health Consensus Development Conference Statement: adjuvant therapy for breast cancer, November 1-3, 2000. *J Natl Cancer Inst, 93*(13), pp. 979-989.

Eiro, N., Pidal, I., Fernandez-Garcia, B., Junquera, S., Lamelas, M. L., del Casar, J. M., Gonzalez, L. O., Lopez-Muniz, A. and Vizoso, F. J. (2012). Impact of CD68/(CD3+CD20) ratio at the invasive front of primary tumors on distant metastasis development in breast cancer. *PLoS One, 7*(12), pp. e52796.

Elston, C. W. and Ellis, I. O. (1991). Pathological prognostic factors in breast cancer. I. The value of histological grade in

breast cancer: experience from a large study with long-term follow-up. *Histopathology, 19*(5), pp. 403-410.

Evrard, A., Cuq, P., Ciccolini, J., Vian, L. and Cano, J. P. (1999). Increased cytotoxicity and bystander effect of 5-fluorouracil and 5-deoxy-5-fluorouridine in human colorectal cancer cells transfected with thymidine phosphorylase. *Br J Cancer, 80*(11), pp. 1726-1733.

Ewald, A. J., Brenot, A., Duong, M., Chan, B. S. and Werb, Z. (2008). Collective epithelial migration and cell rearrangements drive mammary branching morphogenesis. *Dev Cell, 14*(4), pp. 570-581.

Farmer, P., Bonnefoi, H., Becette, V., Tubiana-Hulin, M., Fumoleau, P., Larsimont, D., Macgrogan, G., Bergh, J., Cameron, D., Goldstein, D., Duss, S., Nicoulaz, A. L., Brisken, C., Fiche, M., Delorenzi, M. and Iggo, R. (2005). Identification of molecular apocrine breast tumours by microarray analysis. *Oncogene, 24*(29), pp. 4660-4671.

Fendrich, V., Waldmann, J., Feldmann, G., Schlosser, K., Konig, A., Ramaswamy, A., Bartsch, D. K. and Karakas, E. (2009). Unique expression pattern of the EMT markers Snail, Twist and E-cadherin in benign and malignant parathyroid neoplasia. *Eur J Endocrinol, 160*(4), pp. 695-703.

Fiaschi, M., Rozell, B., Bergstrom, A. and Toftgard, R. (2009). Development of mammary tumors by conditional expression of GLI1. *Cancer Res, 69*(11), pp. 4810-4817.

Fidler, I. J. and Kripke, M. L. (1977). Metastasis results from preexisting variant cells within a malignant tumor. *Science, 197*(4306), pp. 893-895.

Fisher, B., Redmond, C., Fisher, E. R., Bauer, M., Wolmark, N., Wickerham, D. L., Deutsch, M., Montague, E., Margolese, R. and Foster, R. (1985). Ten-year results of a randomized clinical trial comparing radical mastectomy and total mastectomy with or without radiation. *N Engl J Med, 312*(11), pp. 674-681.

Fisher, B., Redmond, C., Poisson, R., Margolese, R., Wolmark, N., Wickerham, L., Fisher, E., Deutsch, M., Caplan, R., Pilch, Y. and et al. (1989). Eight-year results of a randomized clinical trial comparing total mastectomy and lumpectomy with or without irradiation in the treatment of breast cancer. *N Engl J Med, 320*(13), pp. 822-828.

Flemban, A. and Qualtrough, D. (2015). The Potential Role of Hedgehog Signaling in the Luminal/Basal Phenotype of Breast Epithelia and in Breast Cancer Invasion and Metastasis. *Cancers (Basel), 7*(3), pp. 1863-1884.

Fogh, J., Fogh, J. M. and Orfeo, T. (1977). One hundred and twenty-seven cultured human tumor cell lines producing tumors in nude mice. *J Natl Cancer Inst, 59*(1), pp. 221-226.

Fournier, A. K., Campbell, L. E., Castagnino, P., Liu, W. F., Chung, B. M., Weaver, V. M., Chen, C. S. and Assoian, R. K. (2008). Rac-dependent cyclin D1 gene expression regulated by cadherin- and integrin-mediated adhesion. *J Cell Sci, 121*(Pt 2), pp. 226-233.

Fu, J., Rodova, M., Nanta, R., Meeker, D., Van Veldhuizen, P. J., Srivastava, R. K. and Shankar, S. (2013). NPV-LDE-225 (Erismodegib) inhibits epithelial mesenchymal transition and self-renewal of glioblastoma initiating cells by regulating miR-21, miR-128, and miR-200. *Neuro Oncol, 15*(6), pp. 691-706.

Fu, Y. Z., Yan, Y. Y., He, M., Xiao, Q. H., Yao, W. F., Zhao, L., Wu, H. Z., Yu, Z. J., Zhou, M. Y., Lv, M. T., Zhang, S. S., Chen, J. J. and Wei, M. J. (2016). Salinomycin induces selective cytotoxicity to MCF-7 mammosphere cells through targeting the Hedgehog signaling pathway. *Oncol Rep, 35*(2), pp. 912-922.

Gallet, A. and Therond, P. P. (2005). Temporal modulation of the Hedgehog morphogen gradient by a patched-dependent targeting to lysosomal compartment. *Dev Biol, 277*(1), pp. 51-62.

Gao, M. Q., Kim, B. G., Kang, S., Choi, Y. P., Park, H., Kang, K. S. and Cho, N. H. (2010). Stromal fibroblasts from the interface zone of human breast carcinomas induce an epithelial-mesenchymal transition-like state in breast cancer cells in vitro. *J Cell Sci, 123*(Pt 20), pp. 3507-3514.

Gao, Q., Yuan, Y., Gan, H. Z. and Peng, Q. (2015). Resveratrol inhibits the hedgehog signaling pathway and epithelial-mesenchymal transition and suppresses gastric cancer invasion and metastasis. *Oncol Lett, 9*(5), pp. 2381-2387.

Garg, M. (2013). Epithelial-mesenchymal transition - activating transcription factors - multifunctional regulators in cancer. *World J Stem Cells, 5*(4), pp. 188-195.

Geddes, D. T. (2007). Inside the lactating breast: the latest anatomy research. *J Midwifery Womens Health, 52*(6), pp. 556-563.

Geyer, F. C., Lacroix-Triki, M., Savage, K., Arnedos, M., Lambros, M. B., MacKay, A., Natrajan, R. and Reis-Filho, J. S. (2011). beta-Catenin pathway activation in breast cancer is associated with triple-negative phenotype but not with CTNNB1 mutation. *Mod Pathol, 24*(2), pp. 209-231.

Gilles, C., Polette, M., Mestdagt, M., Nawrocki-Raby, B., Ruggeri, P., Birembaut, P. and Foidart, J. M. (2003). Transactivation of vimentin by beta-catenin in human breast cancer cells. *Cancer Res, 63*(10), pp. 2658-2664.

Giudici, D., Ornati, G., Briatico, G., Buzzetti, F., Lombardi, P. and di Salle, E. (1988). 6-Methylenandrosta-1,4-diene-3,17-dione (FCE 24304): a new irreversible aromatase inhibitor. *J Steroid Biochem, 30*(1-6), pp. 391-394.

Gong, P., Wang, Y., Liu, G., Zhang, J. and Wang, Z. (2013). New insight into Ki67 expression at the invasive front in breast cancer. *PLoS One, 8*(1), pp. e54912.

Gonnissen, A., Isebaert, S. and Haustermans, K. (2015). Targeting the Hedgehog signaling pathway in cancer: beyond Smoothened. *Oncotarget, 6*(16), pp. 13899-13913.

Gonzalez, D. M. and Medici, D. (2014). Signaling mechanisms of the epithelial-mesenchymal transition. *Sci Signal, 7*(344), pp. re8.

Gradishar, W. J., Anderson, B. O., Balassanian, R., Blair, S. L., Burstein, H. J., Cyr, A., Elias, A. D., Farrar, W. B., Forero, A., Giordano, S. H., Goetz, M. P., Goldstein, L. J., Isakoff, S. J., Lyons, J., Marcom, P. K., Mayer, I. A., McCormick, B., Moran, M. S., O'Regan, R. M., Patel, S. A., Pierce, L. J., Reed, E. C., Salerno, K. E., Schwartzberg, L. S., Sitapati, A., Smith, K. L., Smith, M. L., Soliman, H., Somlo, G., Telli, M., Ward, J. H., Shead, D. A. and Kumar, R. (2017). NCCN Guidelines Insights: Breast Cancer, Version 1.2017. *J Natl Compr Canc Netw, 15*(4), pp. 433-451.

Graff, J. R., Gabrielson, E., Fujii, H., Baylin, S. B. and Herman, J. G. (2000). Methylation patterns of the E-cadherin 5' CpG island are unstable and reflect the dynamic, heterogeneous loss of E-cadherin expression during metastatic progression. *J Biol Chem, 275*(4), pp. 2727-2732.

Green, J., Leigh, I. M., Poulsom, R. and Quinn, A. G. (1998). Basal cell carcinoma development is associated with induction of the expression of the transcription factor Gli-1. *Br J Dermatol, 139*(5), pp. 911-915.

Grigore, A. D., Jolly, M. K., Jia, D., Farach-Carson, M. C. and Levine, H. (2016). Tumor Budding: The Name is EMT. Partial EMT. *J Clin Med, 5*(5).

Grosse-Wilde, A., Fouquier d'Herouel, A., McIntosh, E., Ertaylan, G., Skupin, A., Kuestner, R. E., del Sol, A., Walters, K. A. and Huang, S. (2015). Stemness of the hybrid Epithelial/Mesenchymal State in Breast Cancer and Its Association with Poor Survival. *PLoS One, 10*(5), pp. e0126522.

Group, B. I. G. C., Mouridsen, H., Giobbie-Hurder, A., Goldhirsch, A., Thurlimann, B., Paridaens, R., Smith, I., Mauriac, L., Forbes, J., Price, K. N., Regan, M. M., Gelber, R. D. and Coates, A. S. (2009). Letrozole therapy alone or in sequence

with tamoxifen in women with breast cancer. *N Engl J Med, 361*(8), pp. 766-776.

Gudjonsson, T., Ronnov-Jessen, L., Villadsen, R., Rank, F., Bissell, M. J. and Petersen, O. W. (2002). Normal and tumor-derived myoepithelial cells differ in their ability to interact with luminal breast epithelial cells for polarity and basement membrane deposition. *J Cell Sci, 115*(Pt 1), pp. 39-50.

Guo, W., Keckesova, Z., Donaher, J. L., Shibue, T., Tischler, V., Reinhardt, F., Itzkovitz, S., Noske, A., Zurrer-Hardi, U., Bell, G., Tam, W. L., Mani, S. A., van Oudenaarden, A. and Weinberg, R. A. (2012). Slug and Sox9 cooperatively determine the mammary stem cell state. *Cell, 148*(5), pp. 1015-1028.

Gupta, S., Takebe, N. and Lorusso, P. (2010). Targeting the Hedgehog pathway in cancer. *Ther Adv Med Oncol, 2*(4), pp. 237-250.

Gusterson, B. A. and Stein, T. (2012). Human breast development. *Semin Cell Dev Biol, 23*(5), pp. 567-573.

Ha, G. H., Kim, J. L. and Breuer, E. K. (2013). TACC3 is essential for EGF-mediated EMT in cervical cancer. *PLoS One, 8*(8), pp. e70353.

Habib, J. G. and O'Shaughnessy, J. A. (2016). The hedgehog pathway in triple-negative breast cancer. *Cancer Med, 5*(10), pp. 2989-3006.

Hajra, K. M., Chen, D. Y. and Fearon, E. R. (2002). The SLUG zinc-finger protein represses E-cadherin in breast cancer. *Cancer Res, 62*(6), pp. 1613-1618.

Halin, C., Mora, J. R., Sumen, C. and von Andrian, U. H. (2005). In vivo imaging of lymphocyte trafficking. *Annu Rev Cell Dev Biol, 21*, pp. 581-603.

Halsted, W. S. (1907). I. The Results of Radical Operations for the Cure of Carcinoma of the Breast. *Ann Surg, 46*(1), pp. 1-19.

Hamperl, H. (1970). The myothelia (myoepithelial cells). Normal state; regressive changes; hyperplasia; tumors. *Curr Top Pathol, 53*, pp. 161-220.

Han, B., Qu, Y., Jin, Y., Yu, Y., Deng, N., Wawrowsky, K., Zhang, X., Li, N., Bose, S., Wang, Q., Sakkiah, S., Abrol, R., Jensen, T. W., Berman, B. P., Tanaka, H., Johnson, J., Gao, B., Hao, J., Liu, Z., Buttyan, R., Ray, P. S., Hung, M. C., Giuliano, A. E. and Cui, X. (2015). FOXC1 Activates Smoothened-Independent Hedgehog Signaling in Basal-like Breast Cancer. *Cell Rep, 13*(5), pp. 1046-1058.

Han, M. E., Lee, Y. S., Baek, S. Y., Kim, B. S., Kim, J. B. and Oh, S. O. (2009). Hedgehog signaling regulates the survival of gastric cancer cells by regulating the expression of Bcl-2. *Int J Mol Sci, 10*(7), pp. 3033-3043.

Hanahan, D. and Weinberg, R. A. (2011). Hallmarks of cancer: the next generation. *Cell, 144*(5), pp. 646-674.

Hankey, B. F., Curtis, R. E., Naughton, M. D., Boice, J. D., Jr. and Flannery, J. T. (1983). A retrospective cohort analysis of second breast cancer risk for primary breast cancer patients with an assessment of the effect of radiation therapy. *J Natl Cancer Inst, 70*(5), pp. 797-804.

Hanna, A. and Shevde, L. A. (2016). Erratum to: 'Hedgehog signaling: modulation of cancer properties and tumor microenvironment'. *Mol Cancer, 15*(1), pp. 35.

Harvey, E. B., Schairer, C., Brinton, L. A., Hoover, R. N. and Fraumeni, J. F., Jr. (1987). Alcohol consumption and breast cancer. *J Natl Cancer Inst, 78*(4), pp. 657-661.

Hase, K., Shatney, C., Johnson, D., Trollope, M. and Vierra, M. (1993). Prognostic value of tumor "budding" in patients with colorectal cancer. *Dis Colon Rectum, 36*(7), pp. 627-635.

Hassiotou, F. and Geddes, D. (2013). Anatomy of the human mammary gland: Current status of knowledge. *Clin Anat, 26*(1), pp. 29-48.

Hatsell, S. J. and Cowin, P. (2006). Gli3-mediated repression of Hedgehog targets is required for normal mammary development. *Development, 133*(18), pp. 3661-3670.

Haverty, P. M., Lin, E., Tan, J., Yu, Y., Lam, B., Lianoglou, S., Neve, R. M., Martin, S., Settleman, J., Yauch, R. L. and Bourgon, R. (2016). Reproducible pharmacogenomic profiling of cancer cell line panels. *Nature, 533*(7603), pp. 333-337.

Hay, E. D. and Zuk, A. (1995). Transformations between epithelium and mesenchyme: normal, pathological, and experimentally induced. *Am J Kidney Dis, 26*(4), pp. 678-690.

Hazan, R. B., Phillips, G. R., Qiao, R. F., Norton, L. and Aaronson, S. A. (2000). Exogenous expression of N-cadherin in breast cancer cells induces cell migration, invasion, and metastasis. *J Cell Biol, 148*(4), pp. 779-790.

He, Y., Liu, Z., Qiao, C., Xu, M., Yu, J. and Li, G. (2014). Expression and significance of Wnt signaling components and their target genes in breast carcinoma. *Mol Med Rep, 9*(1), pp. 137-143.

Heimann, R., Lan, F., McBride, R. and Hellman, S. (2000). Separating favorable from unfavorable prognostic markers in breast cancer: the role of E-cadherin. *Cancer Res, 60*(2), pp. 298-304.

Heller, E., Hurchla, M. A., Xiang, J., Su, X., Chen, S., Schneider, J., Joeng, K. S., Vidal, M., Goldberg, L., Deng, H., Hornick, M. C., Prior, J. L., Piwnica-Worms, D., Long, F., Cagan, R. and Weilbaecher, K. N. (2012). Hedgehog signaling inhibition blocks growth of resistant tumors through effects on tumor microenvironment. *Cancer Res, 72*(4), pp. 897-907.

Hemalatha, A., Suresh, T. N. and Kumar, M. L. (2013). Expression of vimentin in breast carcinoma, its correlation with Ki67 and other histopathological parameters. *Indian J Cancer, 50*(3), pp. 189-194.

Hennighausen, L. and Robinson, G. W. (2001). Signaling pathways in mammary gland development. *Dev Cell, 1*(4), pp. 467-475.

Hens, J. R. and Wysolmerski, J. J. (2005). Key stages of mammary gland development: molecular mechanisms involved in the formation of the embryonic mammary gland. *Breast Cancer Res, 7*(5), pp. 220-224.

Herrmann, H. and Aebi, U. (2004). Intermediate filaments: molecular structure, assembly mechanism, and integration into functionally distinct intracellular Scaffolds. *Annu Rev Biochem, 73*, pp. 749-789.

Herschkowitz, J. I., Simin, K., Weigman, V. J., Mikaelian, I., Usary, J., Hu, Z., Rasmussen, K. E., Jones, L. P., Assefnia, S., Chandrasekharan, S., Backlund, M. G., Yin, Y., Khramtsov, A. I., Bastein, R., Quackenbush, J., Glazer, R. I., Brown, P. H., Green, J. E., Kopelovich, L., Furth, P. A., Palazzo, J. P., Olopade, O. I., Bernard, P. S., Churchill, G. A., Van Dyke, T. and Perou, C. M. (2007). Identification of conserved gene expression features between murine mammary carcinoma models and human breast tumors. *Genome Biol, 8*(5), pp. R76.

Hong, T., Watanabe, K., Ta, C. H., Villarreal-Ponce, A., Nie, Q. and Dai, X. (2015). An Ovol2-Zeb1 Mutual Inhibitory Circuit Governs Bidirectional and Multi-step Transition between Epithelial and Mesenchymal States. *PLoS Comput Biol, 11*(11), pp. e1004569.

Howard, B. A. and Gusterson, B. A. (2000). Human breast development. *J Mammary Gland Biol Neoplasia, 5*(2), pp. 119-137.

Huangfu, D., Liu, A., Rakeman, A. S., Murcia, N. S., Niswander, L. and Anderson, K. V. (2003). Hedgehog signalling in the mouse requires intraflagellar transport proteins. *Nature, 426*(6962), pp. 83-87.

Huber, M. A., Kraut, N. and Beug, H. (2005). Molecular requirements for epithelial-mesenchymal transition during tumor progression. *Curr Opin Cell Biol, 17*(5), pp. 548-558.

Hui, M., Cazet, A., Nair, R., Watkins, D. N., O'Toole, S. A. and Swarbrick, A. (2013). The Hedgehog signalling pathway in breast development, carcinogenesis and cancer therapy. *Breast Cancer Res, 15*(2), pp. 203.

Hulsken, J., Birchmeier, W. and Behrens, J. (1994). E-cadherin and APC compete for the interaction with beta-catenin and the cytoskeleton. *J Cell Biol, 127*(6 Pt 2), pp. 2061-2069.

Hunt, N. C., Douglas-Jones, A. G., Jasani, B., Morgan, J. M. and Pignatelli, M. (1997). Loss of E-cadherin expression associated with lymph node metastases in small breast carcinomas. *Virchows Arch, 430*(4), pp. 285-289.

Im, S., Choi, H. J., Yoo, C., Jung, J. H., Jeon, Y. W., Suh, Y. J. and Kang, C. S. (2013). Hedgehog related protein expression in breast cancer: gli-2 is associated with poor overall survival. *Korean J Pathol, 47*(2), pp. 116-123.

Imhof, B. A., Vollmers, H. P., Goodman, S. L. and Birchmeier, W. (1983). Cell-cell interaction and polarity of epithelial cells: specific perturbation using a monoclonal antibody. *Cell, 35*(3 Pt 2), pp. 667-675.

Ingham, P. W. and McMahon, A. P. (2001). Hedgehog signaling in animal development: paradigms and principles. *Genes Dev, 15*(23), pp. 3059-3087.

Iorns, E., Drews-Elger, K., Ward, T. M., Dean, S., Clarke, J., Berry, D., El Ashry, D. and Lippman, M. (2012). A new mouse model for the study of human breast cancer metastasis. *PLoS One, 7*(10), pp. e47995.

Iwasaki, H., Nakano, K., Shinkai, K., Kunisawa, Y., Hirahashi, M., Oda, Y., Onishi, H. and Katano, M. (2013). Hedgehog Gli3 activator signal augments tumorigenicity of colorectal cancer via upregulation of adherence-related genes. *Cancer Sci, 104*(3), pp. 328-336.

Jain, S., Song, R. and Xie, J. (2017). Sonidegib: mechanism of action, pharmacology, and clinical utility for advanced basal cell carcinomas. *Onco Targets Ther, 10*, pp. 1645-1653.

Jalili, A., Mertz, K. D., Romanov, J., Wagner, C., Kalthoff, F., Stuetz, A., Pathria, G., Gschaider, M., Stingl, G. and Wagner, S. N. (2013). NVP-LDE225, a potent and selective SMOOTHENED antagonist reduces melanoma growth in vitro and in vivo. *PLoS One, 8*(7), pp. e69064.

Janda, C. Y., Waghray, D., Levin, A. M., Thomas, C. and Garcia, K. C. (2012). Structural basis of Wnt recognition by Frizzled. *Science, 337*(6090), pp. 59-64.

Javed, A. and Lteif, A. (2013). Development of the human breast. *Semin Plast Surg, 27*(1), pp. 5-12.

Jeanes, A., Gottardi, C. J. and Yap, A. S. (2008). Cadherins and cancer: how does cadherin dysfunction promote tumor progression? *Oncogene, 27*(55), pp. 6920-6929.

Jeng, K. S., Sheen, I. S., Jeng, W. J., Lin, C. C., Lin, C. K., Su, J. C., Yu, M. C. and Fang, H. Y. (2013). High expression of patched homolog-1 messenger RNA and glioma-associated oncogene-1 messenger RNA of sonic hedgehog signaling pathway indicates a risk of postresection recurrence of hepatocellular carcinoma. *Ann Surg Oncol, 20*(2), pp. 464-473.

Jenkins, D. (2009). Hedgehog signalling: emerging evidence for non-canonical pathways. *Cell Signal, 21*(7), pp. 1023-1034.

Jiang, Y., Zou, L., Zhang, C., He, S., Cheng, C., Xu, J., Lu, W., Zhang, Y., Zhang, H., Wang, D. and Shen, A. (2009). PPARgamma and Wnt/beta-Catenin pathway in human breast cancer: expression pattern, molecular interaction and clinical/prognostic correlations. *J Cancer Res Clin Oncol, 135*(11), pp. 1551-1559.

Johnson, E., Theisen, C. S., Johnson, K. R. and Wheelock, M. J. (2004). R-cadherin influences cell motility via Rho family GTPases. *J Biol Chem, 279*(30), pp. 31041-31049.

Jolly, M. K., Boareto, M., Huang, B., Jia, D., Lu, M., Ben-Jacob, E., Onuchic, J. N. and Levine, H. (2015). Implications of the Hybrid Epithelial/Mesenchymal Phenotype in Metastasis. *Front Oncol, 5*, pp. 155.

Jolly, M. K., Tripathi, S. C., Jia, D., Mooney, S. M., Celiktas, M., Hanash, S. M., Mani, S. A., Pienta, K. J., Ben-Jacob, E. and Levine, H. (2016). Stability of the hybrid epithelial/mesenchymal phenotype. *Oncotarget, 7*(19), pp. 27067-27084.

Jonsson, G., Staaf, J., Olsson, E., Heidenblad, M., Vallon-Christersson, J., Osoegawa, K., de Jong, P., Oredsson, S., Ringner, M., Hoglund, M. and Borg, A. (2007). High-resolution genomic profiles of breast cancer cell lines assessed by tiling BAC array comparative genomic hybridization. *Genes Chromosomes Cancer, 46*(6), pp. 543-558.

Junxia, W., Ping, G., Yuan, H., Lijun, Z., Jihong, R., Fang, L., Min, L., Xi, W., Ting, H., Ke, D. and Huizhong, Z. (2010). Double strand RNA-guided endogeneous E-cadherin up-regulation induces the apoptosis and inhibits proliferation of breast carcinoma cells in vitro and in vivo. *Cancer Sci, 101*(8), pp. 1790-1796.

Kaemmerer, D., Peter, L., Lupp, A., Schulz, S., Sanger, J., Baum, R. P., Prasad, V. and Hommann, M. (2012). Comparing of IRS and Her2 as immunohistochemical scoring schemes in gastroenteropancreatic neuroendocrine tumors. *Int J Clin Exp Pathol, 5*(3), pp. 187-194.

Kaighn, M. E., Narayan, K. S., Ohnuki, Y., Lechner, J. F. and Jones, L. W. (1979). Establishment and characterization of a human prostatic carcinoma cell line (PC-3). *Invest Urol, 17*(1), pp. 16-23.

Kallergi, G., Papadaki, M. A., Politaki, E., Mavroudis, D., Georgoulias, V. and Agelaki, S. (2011). Epithelial to mesenchymal transition markers expressed in circulating

tumour cells of early and metastatic breast cancer patients. *Breast Cancer Res, 13*(3), pp. R59.

Kalluri, R. and Weinberg, R. A. (2009). The basics of epithelial-mesenchymal transition. *J Clin Invest, 119*(6), pp. 1420-1428.

Kameda, C., Tanaka, H., Yamasaki, A., Nakamura, M., Koga, K., Sato, N., Kubo, M., Kuroki, S., Tanaka, M. and Katano, M. (2009). The Hedgehog pathway is a possible therapeutic target for patients with estrogen receptor-negative breast cancer. *Anticancer Res, 29*(3), pp. 871-879.

Karayiannakis, A. J., Nakopoulou, L., Gakiopoulou, H., Keramopoulos, A., Davaris, P. S. and Pignatelli, M. (2001). Expression patterns of beta-catenin in in situ and invasive breast cancer. *Eur J Surg Oncol, 27*(1), pp. 31-36.

Karhadkar, S. S., Bova, G. S., Abdallah, N., Dhara, S., Gardner, D., Maitra, A., Isaacs, J. T., Berman, D. M. and Beachy, P. A. (2004). Hedgehog signalling in prostate regeneration, neoplasia and metastasis. *Nature, 431*(7009), pp. 707-712.

Kasper, M., Jaks, V., Fiaschi, M. and Toftgard, R. (2009). Hedgehog signalling in breast cancer. *Carcinogenesis, 30*(6), pp. 903-911.

Kaufman, M. W., Marti, J. R., Gallager, H. S. and Hoehn, J. L. (1984). Carcinoma of the breast with pseudosarcomatous metaplasia. *Cancer, 53*(9), pp. 1908-1917.

Kedeshian, P., Sternlicht, M. D., Nguyen, M., Shao, Z. M. and Barsky, S. H. (1998). Humatrix, a novel myoepithelial matrical gel with unique biochemical and biological properties. *Cancer Lett, 123*(2), pp. 215-226.

Keeler, R. F. and Binns, W. (1964). Chemical Compounds of Veratrum Californicum Related to Congenital Ovine Cyclopian Malformations: Extraction of Active Material. *Proc Soc Exp Biol Med, 116*, pp. 123-127.

Kenny, P., Lee, G., Myers, C., Neve, R., Semeiks, J., Spellman, P., Lorenz, K., Lee, E., Barcellos-Hoff, M., Petersen, O., Gray, J. and Bissell, M. (2007a). The morphologies of breast cancer

cell lines in three-dimensional assays correlate with their profiles of gene expression. *Molecular oncology, 1*(1), pp. 84-96.

Kenny, P. A., Lee, G. Y., Myers, C. A., Neve, R. M., Semeiks, J. R., Spellman, P. T., Lorenz, K., Lee, E. H., Barcellos-Hoff, M. H., Petersen, O. W., Gray, J. W. and Bissell, M. J. (2007b). The morphologies of breast cancer cell lines in three-dimensional assays correlate with their profiles of gene expression. *Mol Oncol, 1*(1), pp. 84-96.

Khramtsov, A. I., Khramtsova, G. F., Tretiakova, M., Huo, D., Olopade, O. I. and Goss, K. H. (2010). Wnt/beta-catenin pathway activation is enriched in basal-like breast cancers and predicts poor outcome. *Am J Pathol, 176*(6), pp. 2911-2920.

Kil, W. H., Kim, S. M., Lee, J. E., Park, K. S. and Nam, S. J. (2014). Anticancer effect of silibinin on the xenograft model using MDA-MB-468 breast cancer cells. *Ann Surg Treat Res, 87*(4), pp. 167-173.

Kim, J. H., Shin, H. S., Lee, S. H., Lee, I., Lee, Y. S., Park, J. C., Kim, Y. J., Chung, J. B. and Lee, Y. C. (2010a). Contrasting activity of Hedgehog and Wnt pathways according to gastric cancer cell differentiation: relevance of crosstalk mechanisms. *Cancer Sci, 101*(2), pp. 328-335.

Kim, J. Y., Ko, G. H., Lee, Y. J., Ha, W. S., Choi, S. K., Jung, E. J., Jeong, C. Y., Ju, Y. T., Jeong, S. H. and Hong, S. C. (2012). Prognostic value of sonic hedgehog protein expression in gastric cancer. *Jpn J Clin Oncol, 42*(11), pp. 1054-1059.

Kim, N. G., Koh, E., Chen, X. and Gumbiner, B. M. (2011). E-cadherin mediates contact inhibition of proliferation through Hippo signaling-pathway components. *Proc Natl Acad Sci U S A, 108*(29), pp. 11930-11935.

Kim, S. Y., Dunn, I. F., Firestein, R., Gupta, P., Wardwell, L., Repich, K., Schinzel, A. C., Wittner, B., Silver, S. J., Root, D. E., Boehm, J. S., Ramaswamy, S., Lander, E. S. and Hahn, W. C. (2010b). CK1epsilon is required for breast cancers

dependent on beta-catenin activity. *PLoS One, 5*(2), pp. e8979.

King, T. D., Suto, M. J. and Li, Y. (2012). The Wnt/beta-catenin signaling pathway: a potential therapeutic target in the treatment of triple negative breast cancer. *J Cell Biochem, 113*(1), pp. 13-18.

Kish, T. and Corry, L. (2016). Sonidegib (Odomzo) for the Systemic Treatment of Adults With Recurrent, Locally Advanced Basal Cell Skin Cancer. *P T, 41*(5), pp. 322-325.

Klymkowsky, M. W. and Savagner, P. (2009). Epithelial-mesenchymal transition: a cancer researcher's conceptual friend and foe. *Am J Pathol, 174*(5), pp. 1588-1593.

Kokkinos, M. I., Wafai, R., Wong, M. K., Newgreen, D. F., Thompson, E. W. and Waltham, M. (2007). Vimentin and epithelial-mesenchymal transition in human breast cancer--observations in vitro and in vivo. *Cells Tissues Organs, 185*(1-3), pp. 191-203.

Kopan, R. (2002). Notch: a membrane-bound transcription factor. *J Cell Sci, 115*(Pt 6), pp. 1095-1097.

Korinek, V., Barker, N., Morin, P. J., van Wichen, D., de Weger, R., Kinzler, K. W., Vogelstein, B. and Clevers, H. (1997). Constitutive transcriptional activation by a beta-catenin-Tcf complex in APC-/- colon carcinoma. *Science, 275*(5307), pp. 1784-1787.

Korinek, V., Barker, N., Willert, K., Molenaar, M., Roose, J., Wagenaar, G., Markman, M., Lamers, W., Destree, O. and Clevers, H. (1998). Two members of the Tcf family implicated in Wnt/beta-catenin signaling during embryogenesis in the mouse. *Mol Cell Biol, 18*(3), pp. 1248-1256.

Koscielny, S., Tubiana, M., Le, M. G., Valleron, A. J., Mouriesse, H., Contesso, G. and Sarrazin, D. (1984). Breast cancer: relationship between the size of the primary tumour and the probability of metastatic dissemination. *Br J Cancer, 49*(6), pp. 709-715.

Kowalski, P. J., Rubin, M. A. and Kleer, C. G. (2003). E-cadherin expression in primary carcinomas of the breast and its distant metastases. *Breast Cancer Res, 5*(6), pp. R217-222.

Kratochwil, K. (1986). Tissue combination and organ culture studies in the development of the embryonic mammary gland. *Dev Biol (N Y 1985), 4*, pp. 315-333.

Kubo, M., Nakamura, M., Tasaki, A., Yamanaka, N., Nakashima, H., Nomura, M., Kuroki, S. and Katano, M. (2004). Hedgehog signaling pathway is a new therapeutic target for patients with breast cancer. *Cancer Res, 64*(17), pp. 6071-6074.

Kumar, S., Park, S. H., Cieply, B., Schupp, J., Killiam, E., Zhang, F., Rimm, D. L. and Frisch, S. M. (2011). A pathway for the control of anoikis sensitivity by E-cadherin and epithelial-to-mesenchymal transition. *Mol Cell Biol, 31*(19), pp. 4036-4051.

Kurebayashi, J., Koike, Y., Ohta, Y., Saitoh, W., Yamashita, T., Kanomata, N. and Moriya, T. (2017). Anti-cancer stem cell activity of a hedgehog inhibitor GANT61 in estrogen receptor-positive breast cancer cells. *Cancer Sci, 108*(5), pp. 918-930.

Kwon, Y. J., Hurst, D. R., Steg, A. D., Yuan, K., Vaidya, K. S., Welch, D. R. and Frost, A. R. (2011). Gli1 enhances migration and invasion via up-regulation of MMP-11 and promotes metastasis in ERalpha negative breast cancer cell lines. *Clin Exp Metastasis, 28*(5), pp. 437-449.

Lancet. (1997). Breast cancer and hormone replacement therapy: collaborative reanalysis of data from 51 epidemiological studies of 52,705 women with breast cancer and 108,411 women without breast cancer. Collaborative Group on Hormonal Factors in Breast Cancer. *Lancet, 350*(9084), pp. 1047-1059.

Land, C. E., Boice, J. D., Jr., Shore, R. E., Norman, J. E. and Tokunaga, M. (1980). Breast cancer risk from low-dose exposures to ionizing radiation: results of parallel analysis

of three exposed populations of women. *J Natl Cancer Inst, 65*(2), pp. 353-376.

Lasfargues, E. Y. and Ozzello, L. (1958). Cultivation of human breast carcinomas. *J Natl Cancer Inst, 21*(6), pp. 1131-1147.

Leake, R., Barnes, D., Pinder, S., Ellis, I., Anderson, L., Anderson, T., Adamson, R., Rhodes, T., Miller, K. and Walker, R. (2000). Immunohistochemical detection of steroid receptors in breast cancer: a working protocol. UK Receptor Group, UK NEQAS, The Scottish Breast Cancer Pathology Group, and The Receptor and Biomarker Study Group of the EORTC. *J Clin Pathol, 53*(8), pp. 634-635.

Lee, M. Y., Sun, L. and Veltmaat, J. M. (2013). Hedgehog and Gli signaling in embryonic mammary gland development. *J Mammary Gland Biol Neoplasia, 18*(2), pp. 133-138.

Lee, S. T., Welch, K. D., Panter, K. E., Gardner, D. R., Garrossian, M. and Chang, C. W. (2014). Cyclopamine: from cyclops lambs to cancer treatment. *J Agric Food Chem, 62*(30), pp. 7355-7362.

Leibovitz, A., Stinson, J. C., McCombs, W. B., 3rd, McCoy, C. E., Mazur, K. C. and Mabry, N. D. (1976). Classification of human colorectal adenocarcinoma cell lines. *Cancer Res, 36*(12), pp. 4562-4569.

Lemmon, M. A. and Schlessinger, J. (2010). Cell signaling by receptor tyrosine kinases. *Cell, 141*(7), pp. 1117-1134.

Lewis, M. T. (2001). Hedgehog signaling in mouse mammary gland development and neoplasia. *J Mammary Gland Biol Neoplasia, 6*(1), pp. 53-66.

Lewis, M. T., Ross, S., Strickland, P. A., Sugnet, C. W., Jimenez, E., Scott, M. P. and Daniel, C. W. (1999). Defects in mouse mammary gland development caused by conditional haploinsufficiency of Patched-1. *Development, 126*(22), pp. 5181-5193.

Lewis, M. T. and Veltmaat, J. M. (2004). Next stop, the twilight zone: hedgehog network regulation of mammary gland

development. *J Mammary Gland Biol Neoplasia, 9*(2), pp. 165-181.

Lewis-Tuffin, L. J., Rodriguez, F., Giannini, C., Scheithauer, B., Necela, B. M., Sarkaria, J. N. and Anastasiadis, P. Z. (2010). Misregulated E-cadherin expression associated with an aggressive brain tumor phenotype. *PLoS One, 5*(10), pp. e13665.

Li, J. and Zhou, B. P. (2011). Activation of beta-catenin and Akt pathways by Twist are critical for the maintenance of EMT associated cancer stem cell-like characters. *BMC Cancer, 11*, pp. 49.

Li, Q. and Mattingly, R. R. (2008). Restoration of E-cadherin cell-cell junctions requires both expression of E-cadherin and suppression of ERK MAP kinase activation in Ras-transformed breast epithelial cells. *Neoplasia, 10*(12), pp. 1444-1458.

Li, Y., Yang, W., Yang, Q. and Zhou, S. (2012). Nuclear localization of GLI1 and elevated expression of FOXC2 in breast cancer is associated with the basal-like phenotype. *Histol Histopathol, 27*(4), pp. 475-484.

Liberio, M. S., Sadowski, M. C., Soekmadji, C., Davis, R. A. and Nelson, C. C. (2014). Differential effects of tissue culture coating substrates on prostate cancer cell adherence, morphology and behavior. *PLoS One, 9*(11), pp. e112122.

Liedtke, C. and Kiesel, L. (2012). Breast cancer molecular subtypes--modern therapeutic concepts for targeted therapy of a heterogeneous entity. *Maturitas, 73*(4), pp. 288-294.

Lin, S. Y., Xia, W., Wang, J. C., Kwong, K. Y., Spohn, B., Wen, Y., Pestell, R. G. and Hung, M. C. (2000). Beta-catenin, a novel prognostic marker for breast cancer: its roles in cyclin D1 expression and cancer progression. *Proc Natl Acad Sci U S A, 97*(8), pp. 4262-4266.

Lipinski, R. J., Hutson, P. R., Hannam, P. W., Nydza, R. J., Washington, I. M., Moore, R. W., Girdaukas, G. G.,

Peterson, R. E. and Bushman, W. (2008). Dose- and route-dependent teratogenicity, toxicity, and pharmacokinetic profiles of the hedgehog signaling antagonist cyclopamine in the mouse. *Toxicol Sci, 104*(1), pp. 189-197.

Listerman, I., Gazzaniga, F. S. and Blackburn, E. H. (2014). An investigation of the effects of the core protein telomerase reverse transcriptase on Wnt signaling in breast cancer cells. *Mol Cell Biol, 34*(2), pp. 280-289.

Liu, C. Y., Lin, H. H., Tang, M. J. and Wang, Y. K. (2015). Vimentin contributes to epithelial-mesenchymal transition cancer cell mechanics by mediating cytoskeletal organization and focal adhesion maturation. *Oncotarget, 6*(18), pp. 15966-15983.

Liu, S., Cong, Y., Wang, D., Sun, Y., Deng, L., Liu, Y., Martin-Trevino, R., Shang, L., McDermott, S. P., Landis, M. D., Hong, S., Adams, A., D'Angelo, R., Ginestier, C., Charafe-Jauffret, E., Clouthier, S. G., Birnbaum, D., Wong, S. T., Zhan, M., Chang, J. C. and Wicha, M. S. (2014). Breast cancer stem cells transition between epithelial and mesenchymal states reflective of their normal counterparts. *Stem Cell Reports, 2*(1), pp. 78-91.

Liu, S., Dontu, G., Mantle, I. D., Patel, S., Ahn, N. S., Jackson, K. W., Suri, P. and Wicha, M. S. (2006a). Hedgehog signaling and Bmi-1 regulate self-renewal of normal and malignant human mammary stem cells. *Cancer Res, 66*(12), pp. 6063-6071.

Liu, W. F., Nelson, C. M., Pirone, D. M. and Chen, C. S. (2006b). E-cadherin engagement stimulates proliferation via Rac1. *J Cell Biol, 173*(3), pp. 431-441.

Lo, H. W., Hsu, S. C., Xia, W., Cao, X., Shih, J. Y., Wei, Y., Abbruzzese, J. L., Hortobagyi, G. N. and Hung, M. C. (2007). Epidermal growth factor receptor cooperates with signal transducer and activator of transcription 3 to induce epithelial-mesenchymal transition in cancer cells via up-

regulation of TWIST gene expression. *Cancer Res, 67*(19), pp. 9066-9076.

Lombaerts, M., van Wezel, T., Philippo, K., Dierssen, J. W., Zimmerman, R. M., Oosting, J., van Eijk, R., Eilers, P. H., van de Water, B., Cornelisse, C. J. and Cleton-Jansen, A. M. (2006). E-cadherin transcriptional downregulation by promoter methylation but not mutation is related to epithelial-to-mesenchymal transition in breast cancer cell lines. *Br J Cancer, 94*(5), pp. 661-671.

Lozzio, C. B. and Lozzio, B. B. (1975). Human chronic myelogenous leukemia cell-line with positive Philadelphia chromosome. *Blood, 45*(3), pp. 321-334.

Lundgren, K., Nordenskjold, B. and Landberg, G. (2009). Hypoxia, Snail and incomplete epithelial-mesenchymal transition in breast cancer. *Br J Cancer, 101*(10), pp. 1769-1781.

Ma, H., Li, H. Q. and Zhang, X. (2013). Cyclopamine, a naturally occurring alkaloid, and its analogues may find wide applications in cancer therapy. *Curr Top Med Chem, 13*(17), pp. 2208-2215.

Maeda, M., Johnson, K. R. and Wheelock, M. J. (2005). Cadherin switching: essential for behavioral but not morphological changes during an epithelium-to-mesenchyme transition. *J Cell Sci, 118*(Pt 5), pp. 873-887.

Maeda, O., Kondo, M., Fujita, T., Usami, N., Fukui, T., Shimokata, K., Ando, T., Goto, H. and Sekido, Y. (2006). Enhancement of GLI1-transcriptional activity by beta-catenin in human cancer cells. *Oncol Rep, 16*(1), pp. 91-96.

Mahler-Araujo, B., Savage, K., Parry, S. and Reis-Filho, J. S. (2008). Reduction of E-cadherin expression is associated with non-lobular breast carcinomas of basal-like and triple negative phenotype. *J Clin Pathol, 61*(5), pp. 615-620.

Mailleux, A. A., Spencer-Dene, B., Dillon, C., Ndiaye, D., Savona-Baron, C., Itoh, N., Kato, S., Dickson, C., Thiery, J. P. and Bellusci, S. (2002). Role of FGF10/FGFR2b signaling during

mammary gland development in the mouse embryo. *Development, 129*(1), pp. 53-60.

Malhotra, G. K., Zhao, X., Band, H. and Band, V. (2010). Histological, molecular and functional subtypes of breast cancers. *Cancer Biol Ther, 10*(10), pp. 955-960.

Mamuya, F. A. and Duncan, M. K. (2012). aV integrins and TGF-beta-induced EMT: a circle of regulation. *J Cell Mol Med, 16*(3), pp. 445-455.

Manuel Iglesias, J., Beloqui, I., Garcia-Garcia, F., Leis, O., Vazquez-Martin, A., Eguiara, A., Cufi, S., Pavon, A., Menendez, J. A., Dopazo, J. and Martin, A. G. (2013). Mammosphere formation in breast carcinoma cell lines depends upon expression of E-cadherin. *PLoS One, 8*(10), pp. e77281.

Marigo, V., Davey, R. A., Zuo, Y., Cunningham, J. M. and Tabin, C. J. (1996). Biochemical evidence that patched is the Hedgehog receptor. *Nature, 384*(6605), pp. 176-179.

Mariner, D. J., Davis, M. A. and Reynolds, A. B. (2004). EGFR signaling to p120-catenin through phosphorylation at Y228. *J Cell Sci, 117*(Pt 8), pp. 1339-1350.

Marro, M., Nieva, C., Sanz-Pamplona, R. and Sierra, A. (2014). Molecular monitoring of epithelial-to-mesenchymal transition in breast cancer cells by means of Raman spectroscopy. *Biochim Biophys Acta, 1843*(9), pp. 1785-1795.

Martin, M., Pienkowski, T., Mackey, J., Pawlicki, M., Guastalla, J. P., Weaver, C., Tomiak, E., Al-Tweigeri, T., Chap, L., Juhos, E., Guevin, R., Howell, A., Fornander, T., Hainsworth, J., Coleman, R., Vinholes, J., Modiano, M., Pinter, T., Tang, S. C., Colwell, B., Prady, C., Provencher, L., Walde, D., Rodriguez-Lescure, A., Hugh, J., Loret, C., Rupin, M., Blitz, S., Jacobs, P., Murawsky, M., Riva, A., Vogel, C. and Breast Cancer International Research Group, I. (2005). Adjuvant docetaxel for node-positive breast cancer. *N Engl J Med, 352*(22), pp. 2302-2313.

Martin, M., Ruiz-Borrego, M., Trigo, J. M., Antolin, S., Garcia-Saenz, J. A., Hernando, A., Ocaña, A., Rojo, F., Lopez-Tarruella, S., Corral, J., Ribelles, N., Calvo, L., Moreno, F., Caballero, R. and Carrasco, E. (2015). Abstract OT1-1-06: A phase I study of LDE225 in combination with docetaxel in patients with triple negative (TN) advanced breast cancer (ABC): GEICAM/2012-12 (EDALINE study). *Cancer Research, 75*(9 Supplement), pp. OT1-1-06-OT01-01-06.

Martinez, V. and Azzopardi, J. G. (1979). Invasive lobular carcinoma of the breast: incidence and variants. *Histopathology, 3*(6), pp. 467-488.

Mascotti, K., McCullough, J. and Burger, S. R. (2000). HPC viability measurement: trypan blue versus acridine orange and propidium iodide. *Transfusion, 40*(6), pp. 693-696.

Matevossian, A. and Resh, M. D. (2015). Hedgehog Acyltransferase as a target in estrogen receptor positive, HER2 amplified, and tamoxifen resistant breast cancer cells. *Mol Cancer, 14*, pp. 72.

Mazumdar, T., DeVecchio, J., Agyeman, A., Shi, T. and Houghton, J. A. (2011). The GLI genes as the molecular switch in disrupting Hedgehog signaling in colon cancer. *Oncotarget, 2*(8), pp. 638-645.

McCready, J., Arendt, L. M., Rudnick, J. A. and Kuperwasser, C. (2010). The contribution of dynamic stromal remodeling during mammary development to breast carcinogenesis. *Breast Cancer Res, 12*(3), pp. 205.

McGuire, W. L. and Clark, G. M. (1992). Prognostic factors and treatment decisions in axillary-node-negative breast cancer. *N Engl J Med, 326*(26), pp. 1756-1761.

McMahon, A. P., Ingham, P. W. and Tabin, C. J. (2003). Developmental roles and clinical significance of hedgehog signaling. *Curr Top Dev Biol, 53*, pp. 1-114.

Meisner, A. L., Fekrazad, M. H. and Royce, M. E. (2008). Breast disease: benign and malignant. *Med Clin North Am, 92*(5), pp. 1115-1141, x.

Memmi, E. M., Sanarico, A. G., Giacobbe, A., Peschiaroli, A., Frezza, V., Cicalese, A., Pisati, F., Tosoni, D., Zhou, H., Tonon, G., Antonov, A., Melino, G., Pelicci, P. G. and Bernassola, F. (2015). p63 Sustains self-renewal of mammary cancer stem cells through regulation of Sonic Hedgehog signaling. *Proc Natl Acad Sci U S A, 112*(11), pp. 3499-3504.

Mestdagt, M., Polette, M., Buttice, G., Noel, A., Ueda, A., Foidart, J. M. and Gilles, C. (2006). Transactivation of MCP-1/CCL2 by beta-catenin/TCF-4 in human breast cancer cells. *Int J Cancer, 118*(1), pp. 35-42.

Micalizzi, D. S., Farabaugh, S. M. and Ford, H. L. (2010). Epithelial-mesenchymal transition in cancer: parallels between normal development and tumor progression. *J Mammary Gland Biol Neoplasia, 15*(2), pp. 117-134.

Michno, K., Boras-Granic, K., Mill, P., Hui, C. C. and Hamel, P. A. (2003). Shh expression is required for embryonic hair follicle but not mammary gland development. *Dev Biol, 264*(1), pp. 153-165.

Mickey, D. D., Stone, K. R., Wunderli, H., Mickey, G. H., Vollmer, R. T. and Paulson, D. F. (1977). Heterotransplantation of a human prostatic adenocarcinoma cell line in nude mice. *Cancer Res, 37*(11), pp. 4049-4058.

Miele, L., Miao, H. and Nickoloff, B. J. (2006). NOTCH signaling as a novel cancer therapeutic target. *Curr Cancer Drug Targets, 6*(4), pp. 313-323.

Millet, A. V. and Dirbas, F. M. (2002). Clinical management of breast pain: a review. *Obstet Gynecol Surv, 57*(7), pp. 451-461.

Moll, R., Mitze, M., Frixen, U. H. and Birchmeier, W. (1993). Differential loss of E-cadherin expression in infiltrating ductal and lobular breast carcinomas. *Am J Pathol, 143*(6), pp. 1731-1742.

Moraes, R. C., Zhang, X., Harrington, N., Fung, J. Y., Wu, M. F., Hilsenbeck, S. G., Allred, D. C. and Lewis, M. T. (2007).

Constitutive activation of smoothened (SMO) in mammary glands of transgenic mice leads to increased proliferation, altered differentiation and ductal dysplasia. *Development, 134*(6), pp. 1231-1242.

Morin, P. J., Sparks, A. B., Korinek, V., Barker, N., Clevers, H., Vogelstein, B. and Kinzler, K. W. (1997). Activation of beta-catenin-Tcf signaling in colon cancer by mutations in beta-catenin or APC. *Science, 275*(5307), pp. 1787-1790.

Morrow, C. M., Mruk, D., Cheng, C. Y. and Hess, R. A. (2010). Claudin and occludin expression and function in the seminiferous epithelium. *Philos Trans R Soc Lond B Biol Sci, 365*(1546), pp. 1679-1696.

Moussaif, M. and Sze, J. Y. (2009). Intraflagellar transport/Hedgehog-related signaling components couple sensory cilium morphology and serotonin biosynthesis in Caenorhabditis elegans. *J Neurosci, 29*(13), pp. 4065-4075.

Mukherjee, S., Frolova, N., Sadlonova, A., Novak, Z., Steg, A., Page, G. P., Welch, D. R., Lobo-Ruppert, S. M., Ruppert, J. M., Johnson, M. R. and Frost, A. R. (2006). Hedgehog signaling and response to cyclopamine differ in epithelial and stromal cells in benign breast and breast cancer. *Cancer Biol Ther, 5*(6), pp. 674-683.

Murone, M., Luoh, S. M., Stone, D., Li, W., Gurney, A., Armanini, M., Grey, C., Rosenthal, A. and de Sauvage, F. J. (2000). Gli regulation by the opposing activities of fused and suppressor of fused. *Nat Cell Biol, 2*(5), pp. 310-312.

Nagafuchi, A. and Takeichi, M. (1989). Transmembrane control of cadherin-mediated cell adhesion: a 94 kDa protein functionally associated with a specific region of the cytoplasmic domain of E-cadherin. *Cell Regul, 1*(1), pp. 37-44.

Nakopoulou, L., Mylona, E., Papadaki, I., Kavantzas, N., Giannopoulou, I., Markaki, S. and Keramopoulos, A. (2006). Study of phospho-beta-catenin subcellular distribution in

invasive breast carcinomas in relation to their phenotype and the clinical outcome. *Mod Pathol, 19*(4), pp. 556-563.

NCCP. (2002). Policies and managerial guidelines for national cancer control programs. *Rev Panam Salud Publica, 12*(5), pp. 366-370.

Nelson, C. M., Khauv, D., Bissell, M. J. and Radisky, D. C. (2008). Change in cell shape is required for matrix metalloproteinase-induced epithelial-mesenchymal transition of mammary epithelial cells. *Journal of cellular biochemistry, 105*(1), pp. 25-33.

Neve, R. M., Chin, K., Fridlyand, J., Yeh, J., Baehner, F. L., Fevr, T., Clark, L., Bayani, N., Coppe, J. P., Tong, F., Speed, T., Spellman, P. T., DeVries, S., Lapuk, A., Wang, N. J., Kuo, W. L., Stilwell, J. L., Pinkel, D., Albertson, D. G., Waldman, F. M., McCormick, F., Dickson, R. B., Johnson, M. D., Lippman, M., Ethier, S., Gazdar, A. and Gray, J. W. (2006). A collection of breast cancer cell lines for the study of functionally distinct cancer subtypes. *Cancer Cell, 10*(6), pp. 515-527.

Nieman, M. T., Prudoff, R. S., Johnson, K. R. and Wheelock, M. J. (1999). N-cadherin promotes motility in human breast cancer cells regardless of their E-cadherin expression. *J Cell Biol, 147*(3), pp. 631-644.

Nozawa, Y. I., Lin, C. and Chuang, P. T. (2013). Hedgehog signaling from the primary cilium to the nucleus: an emerging picture of ciliary localization, trafficking and transduction. *Curr Opin Genet Dev, 23*(4), pp. 429-437.

Nusse, R. and Clevers, H. (2017). Wnt/beta-Catenin Signaling, Disease, and Emerging Therapeutic Modalities. *Cell, 169*(6), pp. 985-999.

Nusslein-Volhard, C. and Wieschaus, E. (1980). Mutations affecting segment number and polarity in Drosophila. *Nature, 287*(5785), pp. 795-801.

O'Shaughnessy, J. (2005). Extending survival with chemotherapy in metastatic breast cancer. *Oncologist, 10 Suppl 3*, pp. 20-29.

O'Toole, S. A., Machalek, D. A., Shearer, R. F., Millar, E. K., Nair, R., Schofield, P., McLeod, D., Cooper, C. L., McNeil, C. M., McFarland, A., Nguyen, A., Ormandy, C. J., Qiu, M. R., Rabinovich, B., Martelotto, L. G., Vu, D., Hannigan, G. E., Musgrove, E. A., Christ, D., Sutherland, R. L., Watkins, D. N. and Swarbrick, A. (2011). Hedgehog overexpression is associated with stromal interactions and predicts for poor outcome in breast cancer. *Cancer Res, 71*(11), pp. 4002-4014.

Ogunwobi, O. O., Wang, T., Zhang, L. and Liu, C. (2012). Cyclooxygenase-2 and Akt mediate multiple growth-factor-induced epithelial-mesenchymal transition in human hepatocellular carcinoma. *J Gastroenterol Hepatol, 27*(3), pp. 566-578.

Oka, H., Shiozaki, H., Kobayashi, K., Inoue, M., Tahara, H., Kobayashi, T., Takatsuka, Y., Matsuyoshi, N., Hirano, S., Takeichi, M. and et al. (1993). Expression of E-cadherin cell adhesion molecules in human breast cancer tissues and its relationship to metastasis. *Cancer Res, 53*(7), pp. 1696-1701.

Oloumi, A., McPhee, T. and Dedhar, S. (2004). Regulation of E-cadherin expression and beta-catenin/Tcf transcriptional activity by the integrin-linked kinase. *Biochim Biophys Acta, 1691*(1), pp. 1-15.

Onder, T. T., Gupta, P. B., Mani, S. A., Yang, J., Lander, E. S. and Weinberg, R. A. (2008). Loss of E-cadherin promotes metastasis via multiple downstream transcriptional pathways. *Cancer Res, 68*(10), pp. 3645-3654.

Orlando, L., Colleoni, M., Fedele, P., Cusmai, A., Rizzo, P., D'Amico, M., Chetri, M. C. and Cinieri, S. (2007). Management of advanced breast cancer. *Ann Oncol, 18 Suppl 6*, pp. vi74-76.

Overgaard, M. (1999). Overview of randomized trials in high risk breast cancer patients treated with adjuvant systemic

therapy with or without postmastectomy irradiation. *Semin Radiat Oncol, 9*(3), pp. 292-299.

Overgaard, M., Hansen, P. S., Overgaard, J., Rose, C., Andersson, M., Bach, F., Kjaer, M., Gadeberg, C. C., Mouridsen, H. T., Jensen, M. B. and Zedeler, K. (1997). Postoperative radiotherapy in high-risk premenopausal women with breast cancer who receive adjuvant chemotherapy. Danish Breast Cancer Cooperative Group 82b Trial. *N Engl J Med, 337*(14), pp. 949-955.

Paik, S., Shak, S., Tang, G., Kim, C., Baker, J., Cronin, M., Baehner, F. L., Walker, M. G., Watson, D., Park, T., Hiller, W., Fisher, E. R., Wickerham, D. L., Bryant, J. and Wolmark, N. (2004). A multigene assay to predict recurrence of tamoxifen-treated, node-negative breast cancer. *N Engl J Med, 351*(27), pp. 2817-2826.

Pan, S., Wu, X., Jiang, J., Gao, W., Wan, Y., Cheng, D., Han, D., Liu, J., Englund, N. P., Wang, Y., Peukert, S., Miller-Moslin, K., Yuan, J., Guo, R., Matsumoto, M., Vattay, A., Jiang, Y., Tsao, J., Sun, F., Pferdekamper, A. C., Dodd, S., Tuntland, T., Maniara, W., Kelleher, J. F., 3rd, Yao, Y. M., Warmuth, M., Williams, J. and Dorsch, M. (2010). Discovery of NVP-LDE225, a Potent and Selective Smoothened Antagonist. *ACS Med Chem Lett, 1*(3), pp. 130-134.

Pan, Y., Bai, C. B., Joyner, A. L. and Wang, B. (2006). Sonic hedgehog signaling regulates Gli2 transcriptional activity by suppressing its processing and degradation. *Mol Cell Biol, 26*(9), pp. 3365-3377.

Paredes, J., Correia, A. L., Ribeiro, A. S., Milanezi, F., Cameselle-Teijeiro, J. and Schmitt, F. C. (2008). Breast carcinomas that co-express E- and P-cadherin are associated with p120-catenin cytoplasmic localisation and poor patient survival. *J Clin Pathol, 61*(7), pp. 856-862.

Pasca di Magliano, M. and Hebrok, M. (2003). Hedgehog signalling in cancer formation and maintenance. *Nat Rev Cancer, 3*(12), pp. 903-911.

Pastushenko, I., Brisebarre, A., Sifrim, A., Fioramonti, M., Revenco, T., Boumahdi, S., Van Keymeulen, A., Brown, D., Moers, V., Lemaire, S., De Clercq, S., Minguijon, E., Balsat, C., Sokolow, Y., Dubois, C., De Cock, F., Scozzaro, S., Sopena, F., Lanas, A., D'Haene, N., Salmon, I., Marine, J. C., Voet, T., Sotiropoulou, P. A. and Blanpain, C. (2018). Identification of the tumour transition states occurring during EMT. *Nature, 556*(7702), pp. 463-468.

Patsialou, A., Wyckoff, J., Wang, Y., Goswami, S., Stanley, E. R. and Condeelis, J. S. (2009). Invasion of human breast cancer cells in vivo requires both paracrine and autocrine loops involving the colony-stimulating factor-1 receptor. *Cancer Res, 69*(24), pp. 9498-9506.

Pearson, G. W. and Hunter, T. (2007). Real-time imaging reveals that noninvasive mammary epithelial acini can contain motile cells. *J Cell Biol, 179*(7), pp. 1555-1567.

Peddi, P. F., Ellis, M. J. and Ma, C. (2012). Molecular basis of triple negative breast cancer and implications for therapy. *Int J Breast Cancer, 2012*, pp. 217185.

Peinado, H., Portillo, F. and Cano, A. (2004). Transcriptional regulation of cadherins during development and carcinogenesis. *Int J Dev Biol, 48*(5-6), pp. 365-375.

Perou, C. M., Sorlie, T., Eisen, M. B., van de Rijn, M., Jeffrey, S. S., Rees, C. A., Pollack, J. R., Ross, D. T., Johnsen, H., Akslen, L. A., Fluge, O., Pergamenschikov, A., Williams, C., Zhu, S. X., Lonning, P. E., Borresen-Dale, A. L., Brown, P. O. and Botstein, D. (2000). Molecular portraits of human breast tumours. *Nature, 406*(6797), pp. 747-752.

Peyrieras, N., Hyafil, F., Louvard, D., Ploegh, H. L. and Jacob, F. (1983). Uvomorulin: a nonintegral membrane protein of early mouse embryo. *Proc Natl Acad Sci U S A, 80*(20), pp. 6274-6277.

Pfahler, G. E. (1932). Summary of Results that can be Obtained by Irradiation in Cancer. *Bull N Y Acad Med, 8*(12), pp. 702-716.

Phillips, S. and Kuperwasser, C. (2014). SLUG: Critical regulator of epithelial cell identity in breast development and cancer. *Cell Adh Migr, 8*(6), pp. 578-587.

Phillips, S., Prat, A., Sedic, M., Proia, T., Wronski, A., Mazumdar, S., Skibinski, A., Shirley, S. H., Perou, C. M., Gill, G., Gupta, P. B. and Kuperwasser, C. (2014). Cell-state transitions regulated by SLUG are critical for tissue regeneration and tumor initiation. *Stem Cell Reports, 2*(5), pp. 633-647.

Pizem, J., Popovic, M. and Cor, A. (2011). Expression of Gli1 and PARP1 in medulloblastoma: an immunohistochemical study of 65 cases. *J Neurooncol, 103*(3), pp. 459-467.

Polyak, K. and Weinberg, R. A. (2009). Transitions between epithelial and mesenchymal states: acquisition of malignant and stem cell traits. *Nat Rev Cancer, 9*(4), pp. 265-273.

Porfiri, E., Rubinfeld, B., Albert, I., Hovanes, K., Waterman, M. and Polakis, P. (1997). Induction of a beta-catenin-LEF-1 complex by wnt-1 and transforming mutants of beta-catenin. *Oncogene, 15*(23), pp. 2833-2839.

Prat, A., Parker, J. S., Karginova, O., Fan, C., Livasy, C., Herschkowitz, J. I., He, X. and Perou, C. M. (2010). Phenotypic and molecular characterization of the claudin-low intrinsic subtype of breast cancer. *Breast Cancer Res, 12*(5), pp. R68.

Press, M. F., Finn, R. S., Cameron, D., Di Leo, A., Geyer, C. E., Villalobos, I. E., Santiago, A., Guzman, R., Gasparyan, A., Ma, Y., Danenberg, K., Martin, A. M., Williams, L., Oliva, C., Stein, S., Gagnon, R., Arbushites, M. and Koehler, M. T. (2008). HER-2 gene amplification, HER-2 and epidermal growth factor receptor mRNA and protein expression, and lapatinib efficacy in women with metastatic breast cancer. *Clin Cancer Res, 14*(23), pp. 7861-7870.

Price, M. A. (2006). CKI, there's more than one: casein kinase I family members in Wnt and Hedgehog signaling. *Genes Dev, 20*(4), pp. 399-410.

Proia, T. A., Keller, P. J., Gupta, P. B., Klebba, I., Jones, A. D., Sedic, M., Gilmore, H., Tung, N., Naber, S. P., Schnitt, S., Lander, E. S. and Kuperwasser, C. (2011). Genetic predisposition directs breast cancer phenotype by dictating progenitor cell fate. *Cell Stem Cell, 8*(2), pp. 149-163.

Pronobis, M. I., Rusan, N. M. and Peifer, M. (2015). A novel GSK3-regulated APC:Axin interaction regulates Wnt signaling by driving a catalytic cycle of efficient betacatenin destruction. *Elife, 4*, pp. e08022.

Pruthi, S. (2001). Detection and evaluation of a palpable breast mass. *Mayo Clin Proc, 76*(6), pp. 641-647; quiz 647-648.

Qu, Y., Han, B., Yu, Y., Yao, W., Bose, S., Karlan, B. Y., Giuliano, A. E. and Cui, X. (2015). Evaluation of MCF10A as a Reliable Model for Normal Human Mammary Epithelial Cells. *PLoS One, 10*(7), pp. e0131285.

Qualtrough, D., Buda, A., Gaffield, W., Williams, A. C. and Paraskeva, C. (2004). Hedgehog signalling in colorectal tumour cells: induction of apoptosis with cyclopamine treatment. *Int J Cancer, 110*(6), pp. 831-837.

Qualtrough, D., Kaidi, A., Chell, S., Jabbour, H. N., Williams, A. C. and Paraskeva, C. (2007). Prostaglandin F(2alpha) stimulates motility and invasion in colorectal tumor cells. *Int J Cancer, 121*(4), pp. 734-740.

Qualtrough, D., Rees, P., Speight, B., Williams, A. C. and Paraskeva, C. (2015). The Hedgehog Inhibitor Cyclopamine Reduces beta-Catenin-Tcf Transcriptional Activity, Induces E-Cadherin Expression, and Reduces Invasion in Colorectal Cancer Cells. *Cancers (Basel), 7*(3), pp. 1885-1899.

Qureshi, H. S., Linden, M. D., Divine, G. and Raju, U. B. (2006). E-cadherin status in breast cancer correlates with histologic type but does not correlate with established prognostic parameters. *Am J Clin Pathol, 125*(3), pp. 377-385.

Ragaz, J., Jackson, S. M., Le, N., Plenderleith, I. H., Spinelli, J. J., Basco, V. E., Wilson, K. S., Knowling, M. A., Coppin, C. M., Paradis, M., Coldman, A. J. and Olivotto, I. A. (1997).

Adjuvant radiotherapy and chemotherapy in node-positive premenopausal women with breast cancer. *N Engl J Med, 337*(14), pp. 956-962.

Rakha, E. A., Abd El Rehim, D., Pinder, S. E., Lewis, S. A. and Ellis, I. O. (2005). E-cadherin expression in invasive non-lobular carcinoma of the breast and its prognostic significance. *Histopathology, 46*(6), pp. 685-693.

Rakha, E. A. and Chan, S. (2011). Metastatic triple-negative breast cancer. *Clin Oncol (R Coll Radiol), 23*(9), pp. 587-600.

Rakha, E. A., Elsheikh, S. E., Aleskandarany, M. A., Habashi, H. O., Green, A. R., Powe, D. G., El-Sayed, M. E., Benhasouna, A., Brunet, J. S., Akslen, L. A., Evans, A. J., Blamey, R., Reis-Filho, J. S., Foulkes, W. D. and Ellis, I. O. (2009). Triple-negative breast cancer: distinguishing between basal and nonbasal subtypes. *Clin Cancer Res, 15*(7), pp. 2302-2310.

Rakha, E. A., Pinder, S. E., Bartlett, J. M., Ibrahim, M., Starczynski, J., Carder, P. J., Provenzano, E., Hanby, A., Hales, S., Lee, A. H., Ellis, I. O. and National Coordinating Committee for Breast, P. (2015). Updated UK Recommendations for HER2 assessment in breast cancer. *J Clin Pathol, 68*(2), pp. 93-99.

Rakha, E. A., Reis-Filho, J. S., Baehner, F., Dabbs, D. J., Decker, T., Eusebi, V., Fox, S. B., Ichihara, S., Jacquemier, J., Lakhani, S. R., Palacios, J., Richardson, A. L., Schnitt, S. J., Schmitt, F. C., Tan, P. H., Tse, G. M., Badve, S. and Ellis, I. O. (2010a). Breast cancer prognostic classification in the molecular era: the role of histological grade. *Breast Cancer Res, 12*(4), pp. 207.

Rakha, E. A., Reis-Filho, J. S. and Ellis, I. O. (2008). Basal-like breast cancer: a critical review. *J Clin Oncol, 26*(15), pp. 2568-2581.

Rakha, E. A., Reis-Filho, J. S. and Ellis, I. O. (2010b). Combinatorial biomarker expression in breast cancer. *Breast Cancer Res Treat, 120*(2), pp. 293-308.

Ramaswamy, B., Lu, Y., Teng, K. Y., Nuovo, G., Li, X., Shapiro, C. L. and Majumder, S. (2012). Hedgehog signaling is a novel

therapeutic target in tamoxifen-resistant breast cancer aberrantly activated by PI3K/AKT pathway. *Cancer Res, 72*(19), pp. 5048-5059.

Ramaswamy, S., Ross, K. N., Lander, E. S. and Golub, T. R. (2003). A molecular signature of metastasis in primary solid tumors. *Nat Genet, 33*(1), pp. 49-54.

Ramsbottom, S. A. and Pownall, M. E. (2016). Regulation of Hedgehog Signalling Inside and Outside the Cell. *J Dev Biol, 4*(3), pp. 23.

Ravindranath, A., Yuen, H. F., Chan, K. K., Grills, C., Fennell, D. A., Lappin, T. R. and El-Tanani, M. (2011). Wnt-beta-catenin-Tcf-4 signalling-modulated invasiveness is dependent on osteopontin expression in breast cancer. *Br J Cancer, 105*(4), pp. 542-551.

Reddy, P., Liu, L., Ren, C., Lindgren, P., Boman, K., Shen, Y., Lundin, E., Ottander, U., Rytinki, M. and Liu, K. (2005). Formation of E-cadherin-mediated cell-cell adhesion activates AKT and mitogen activated protein kinase via phosphatidylinositol 3 kinase and ligand-independent activation of epidermal growth factor receptor in ovarian cancer cells. *Mol Endocrinol, 19*(10), pp. 2564-2578.

Redig, A. J. and McAllister, S. S. (2013). Breast cancer as a systemic disease: a view of metastasis. *J Intern Med, 274*(2), pp. 113-126.

Regl, G., Neill, G. W., Eichberger, T., Kasper, M., Ikram, M. S., Koller, J., Hintner, H., Quinn, A. G., Frischauf, A. M. and Aberger, F. (2002). Human GLI2 and GLI1 are part of a positive feedback mechanism in Basal Cell Carcinoma. *Oncogene, 21*(36), pp. 5529-5539.

Reifenberger, J., Wolter, M., Weber, R. G., Megahed, M., Ruzicka, T., Lichter, P. and Reifenberger, G. (1998). Missense mutations in SMOH in sporadic basal cell carcinomas of the skin and primitive neuroectodermal tumors of the central nervous system. *Cancer Res, 58*(9), pp. 1798-1803.

Remmele, W. and Stegner, H. E. (1987). [Recommendation for uniform definition of an immunoreactive score (IRS) for immunohistochemical estrogen receptor detection (ER-ICA) in breast cancer tissue]. *Pathologe, 8*(3), pp. 138-140.

Ribeiro, A. S., Sousa, B., Carreto, L., Mendes, N., Nobre, A. R., Ricardo, S., Albergaria, A., Cameselle-Teijeiro, J. F., Gerhard, R., Soderberg, O., Seruca, R., Santos, M. A., Schmitt, F. and Paredes, J. (2013). P-cadherin functional role is dependent on E-cadherin cellular context: a proof of concept using the breast cancer model. *J Pathol, 229*(5), pp. 705-718.

Ricardo, S., Vieira, A. F., Gerhard, R., Leitao, D., Pinto, R., Cameselle-Teijeiro, J. F., Milanezi, F., Schmitt, F. and Paredes, J. (2011). Breast cancer stem cell markers CD44, CD24 and ALDH1: expression distribution within intrinsic molecular subtype. *J Clin Pathol, 64*(11), pp. 937-946.

Rijsewijk, F., Schuermann, M., Wagenaar, E., Parren, P., Weigel, D. and Nusse, R. (1987). The Drosophila homolog of the mouse mammary oncogene int-1 is identical to the segment polarity gene wingless. *Cell, 50*(4), pp. 649-657.

Rimkus, T. K., Carpenter, R. L., Qasem, S., Chan, M. and Lo, H. W. (2016). Targeting the Sonic Hedgehog Signaling Pathway: Review of Smoothened and GLI Inhibitors. *Cancers (Basel), 8*(2).

Rizwan, A., Cheng, M., Bhujwalla, Z. M., Krishnamachary, B., Jiang, L. and Glunde, K. (2015). Breast cancer cell adhesome and degradome interact to drive metastasis. *NPJ Breast Cancer, 1*, pp. 15017.

Robinson, G. W., Karpf, A. B. and Kratochwil, K. (1999). Regulation of mammary gland development by tissue interaction. *J Mammary Gland Biol Neoplasia, 4*(1), pp. 9-19.

Roose, J., Huls, G., van Beest, M., Moerer, P., van der Horn, K., Goldschmeding, R., Logtenberg, T. and Clevers, H. (1999). Synergy between tumor suppressor APC and the beta-

catenin-Tcf4 target Tcf1. *Science, 285*(5435), pp. 1923-1926.

Rorth, P. (2009). Collective cell migration. *Annu Rev Cell Dev Biol, 25*, pp. 407-429.

Rosa, M., Han, H. S., Ismail-Khan, R., Allam-Nandyala, P. and Bui, M. M. (2015). Beta-catenin expression patterns in matched pre- and post-neoadjuvant chemotherapy-resistant breast cancer. *Ann Clin Lab Sci, 45*(1), pp. 10-16.

Rosen, P. P., Groshen, S., Kinne, D. W. and Hellman, S. (1989a). Contralateral breast carcinoma: an assessment of risk and prognosis in stage I (T1N0M0) and stage II (T1N1M0) patients with 20-year follow-up. *Surgery, 106*(5), pp. 904-910.

Rosen, P. P., Groshen, S., Saigo, P. E., Kinne, D. W. and Hellman, S. (1989b). Pathological prognostic factors in stage I (T1N0M0) and stage II (T1N1M0) breast carcinoma: a study of 644 patients with median follow-up of 18 years. *J Clin Oncol, 7*(9), pp. 1239-1251.

Rouzier, R., Perou, C. M., Symmans, W. F., Ibrahim, N., Cristofanilli, M., Anderson, K., Hess, K. R., Stec, J., Ayers, M., Wagner, P., Morandi, P., Fan, C., Rabiul, I., Ross, J. S., Hortobagyi, G. N. and Pusztai, L. (2005). Breast cancer molecular subtypes respond differently to preoperative chemotherapy. *Clin Cancer Res, 11*(16), pp. 5678-5685.

Rubin, L. L. and de Sauvage, F. J. (2006). Targeting the Hedgehog pathway in cancer. *Nat Rev Drug Discov, 5*(12), pp. 1026-1033.

Ruiz i Altaba, A. (1998). Combinatorial Gli gene function in floor plate and neuronal inductions by Sonic hedgehog. *Development, 125*(12), pp. 2203-2212.

Ruiz i Altaba, A., Mas, C. and Stecca, B. (2007). The Gli code: an information nexus regulating cell fate, stemness and cancer. *Trends Cell Biol, 17*(9), pp. 438-447.

Ruiz i Altaba, A., Sanchez, P. and Dahmane, N. (2002). Gli and hedgehog in cancer: tumours, embryos and stem cells. *Nat Rev Cancer, 2*(5), pp. 361-372.

Saegusa, M., Hashimura, M., Kuwata, T. and Okayasu, I. (2009). Requirement of the Akt/beta-catenin pathway for uterine carcinosarcoma genesis, modulating E-cadherin expression through the transactivation of slug. *Am J Pathol, 174*(6), pp. 2107-2115.

Saitoh, M. (2018). Involvement of partial EMT in cancer progression. *J Biochem*.

Sakakura, T., Kusano, I., Kusakabe, M., Inaguma, Y. and Nishizuka, Y. (1987). Biology of mammary fat pad in fetal mouse: capacity to support development of various fetal epithelia in vivo. *Development, 100*(3), pp. 421-430.

Sakuma, K., Aoki, M. and Kannagi, R. (2012). Transcription factors c-Myc and CDX2 mediate E-selectin ligand expression in colon cancer cells undergoing EGF/bFGF-induced epithelial-mesenchymal transition. *Proc Natl Acad Sci U S A, 109*(20), pp. 7776-7781.

Sanchez, P., Hernandez, A. M., Stecca, B., Kahler, A. J., DeGueme, A. M., Barrett, A., Beyna, M., Datta, M. W., Datta, S. and Ruiz i Altaba, A. (2004). Inhibition of prostate cancer proliferation by interference with SONIC HEDGEHOG-GLI1 signaling. *Proc Natl Acad Sci U S A, 101*(34), pp. 12561-12566.

Sarrio, D., Rodriguez-Pinilla, S. M., Hardisson, D., Cano, A., Moreno-Bueno, G. and Palacios, J. (2008). Epithelial-mesenchymal transition in breast cancer relates to the basal-like phenotype. *Cancer Res, 68*(4), pp. 989-997.

Savagner, P. (2010). The epithelial-mesenchymal transition (EMT) phenomenon. *Ann Oncol, 21 Suppl 7*, pp. vii89-92.

Schatzkin, A., Jones, D. Y., Hoover, R. N., Taylor, P. R., Brinton, L. A., Ziegler, R. G., Harvey, E. B., Carter, C. L., Licitra, L. M., Dufour, M. C. and et al. (1987). Alcohol consumption and breast cancer in the epidemiologic follow-up study of the

first National Health and Nutrition Examination Survey. *N Engl J Med, 316*(19), pp. 1169-1173.

Scherer, W. F., Syverton, J. T. and Gey, G. O. (1953). Studies on the propagation in vitro of poliomyelitis viruses. IV. Viral multiplication in a stable strain of human malignant epithelial cells (strain HeLa) derived from an epidermoid carcinoma of the cervix. *J Exp Med, 97*(5), pp. 695-710.

Schlange, T., Matsuda, Y., Lienhard, S., Huber, A. and Hynes, N. E. (2007). Autocrine WNT signaling contributes to breast cancer cell proliferation via the canonical WNT pathway and EGFR transactivation. *Breast Cancer Res, 9*(5), pp. R63.

Schlosshauer, P. W., Brown, S. A., Eisinger, K., Yan, Q., Guglielminetti, E. R., Parsons, R., Ellenson, L. H. and Kitajewski, J. (2000). APC truncation and increased beta-catenin levels in a human breast cancer cell line. *Carcinogenesis, 21*(7), pp. 1453-1456.

Schmid, S., Bieber, M., Zhang, F., Zhang, M., He, B., Jablons, D. and Teng, N. N. (2011). Wnt and hedgehog gene pathway expression in serous ovarian cancer. *Int J Gynecol Cancer, 21*(6), pp. 975-980.

Schneider, U., Schwenk, H. U. and Bornkamm, G. (1977). Characterization of EBV-genome negative "null" and "T" cell lines derived from children with acute lymphoblastic leukemia and leukemic transformed non-Hodgkin lymphoma. *Int J Cancer, 19*(5), pp. 621-626.

Schnidar, H., Eberl, M., Klingler, S., Mangelberger, D., Kasper, M., Hauser-Kronberger, C., Regl, G., Kroismayr, R., Moriggl, R., Sibilia, M. and Aberger, F. (2009). Epidermal growth factor receptor signaling synergizes with Hedgehog/GLI in oncogenic transformation via activation of the MEK/ERK/JUN pathway. *Cancer Res, 69*(4), pp. 1284-1292.

Seal, M. D. and Chia, S. K. (2010). What is the difference between triple-negative and basal breast cancers? *Cancer J, 16*(1), pp. 12-16.

Selli, C., Erac, Y. and Tosun, M. (2016). Effects of cell seeding density on real-time monitoring of anti-proliferative effects of transient gene silencing. *J Biol Res (Thessalon), 23*, pp. 20.

Shan, S., Lv, Q., Zhao, Y., Liu, C., Sun, Y., Xi, K., Xiao, J. and Li, C. (2015). Wnt/beta-catenin pathway is required for epithelial to mesenchymal transition in CXCL12 over expressed breast cancer cells. *Int J Clin Exp Pathol, 8*(10), pp. 12357-12367.

Shigemura, K., Huang, W. C., Li, X., Zhau, H. E., Zhu, G., Gotoh, A., Fujisawa, M., Xie, J., Marshall, F. F. and Chung, L. W. (2011). Active sonic hedgehog signaling between androgen independent human prostate cancer cells and normal/benign but not cancer-associated prostate stromal cells. *Prostate, 71*(16), pp. 1711-1722.

Shirure, V. S., Liu, T., Delgadillo, L. F., Cuckler, C. M., Tees, D. F., Benencia, F., Goetz, D. J. and Burdick, M. M. (2015). CD44 variant isoforms expressed by breast cancer cells are functional E-selectin ligands under flow conditions. *Am J Physiol Cell Physiol, 308*(1), pp. C68-78.

Siitonen, S. M., Kononen, J. T., Helin, H. J., Rantala, I. S., Holli, K. A. and Isola, J. J. (1996). Reduced E-cadherin expression is associated with invasiveness and unfavorable prognosis in breast cancer. *Am J Clin Pathol, 105*(4), pp. 394-402.

Silberstein, G. B., Flanders, K. C., Roberts, A. B. and Daniel, C. W. (1992). Regulation of mammary morphogenesis: evidence for extracellular matrix-mediated inhibition of ductal budding by transforming growth factor-beta 1. *Dev Biol, 152*(2), pp. 354-362.

Sims, A. H., Howell, A., Howell, S. J. and Clarke, R. B. (2007). Origins of breast cancer subtypes and therapeutic implications. *Nat Clin Pract Oncol, 4*(9), pp. 516-525.

Singh, B. N., Doyle, M. J., Weaver, C. V., Koyano-Nakagawa, N. and Garry, D. J. (2012). Hedgehog and Wnt coordinate

signaling in myogenic progenitors and regulate limb regeneration. *Dev Biol, 371*(1), pp. 23-34.

Singletary, S. E. (2003). Rating the risk factors for breast cancer. *Ann Surg, 237*(4), pp. 474-482.

Skvara, H., Kalthoff, F., Meingassner, J. G., Wolff-Winiski, B., Aschauer, H., Kelleher, J. F., Wu, X., Pan, S., Mickel, L., Schuster, C., Stary, G., Jalili, A., David, O. J., Emotte, C., Antunes, A. M., Rose, K., Decker, J., Carlson, I., Gardner, H., Stuetz, A., Bertolino, A. P., Stingl, G. and De Rie, M. A. (2011). Topical treatment of Basal cell carcinomas in nevoid Basal cell carcinoma syndrome with a smoothened inhibitor. *J Invest Dermatol, 131*(8), pp. 1735-1744.

Slamon, D. J., Clark, G. M., Wong, S. G., Levin, W. J., Ullrich, A. and McGuire, W. L. (1987). Human breast cancer: correlation of relapse and survival with amplification of the HER-2/neu oncogene. *Science, 235*(4785), pp. 177-182.

Slamon, D. J., Leyland-Jones, B., Shak, S., Fuchs, H., Paton, V., Bajamonde, A., Fleming, T., Eiermann, W., Wolter, J., Pegram, M., Baselga, J. and Norton, L. (2001). Use of chemotherapy plus a monoclonal antibody against HER2 for metastatic breast cancer that overexpresses HER2. *N Engl J Med, 344*(11), pp. 783-792.

Sodergren, S. C., Copson, E., White, A., Efficace, F., Sprangers, M., Fitzsimmons, D., Bottomley, A. and Johnson, C. D. (2016). Systematic Review of the Side Effects Associated With Anti-HER2-Targeted Therapies Used in the Treatment of Breast Cancer, on Behalf of the EORTC Quality of Life Group. *Target Oncol, 11*(3), pp. 277-292.

Sommers, C. L., Thompson, E. W., Torri, J. A., Kemler, R., Gelmann, E. P. and Byers, S. W. (1991). Cell adhesion molecule uvomorulin expression in human breast cancer cell lines: relationship to morphology and invasive capacities. *Cell Growth Differ, 2*(8), pp. 365-372.

Song, L., Wang, W., Liu, D., Zhao, Y., He, J., Wang, X., Dai, Z., Zhang, H. and Li, X. (2016). Targeting of sonic hedgehog-Gli

signaling: A potential therapeutic target for patients with breast cancer. *Oncol Lett, 12*(2), pp. 1027-1033.

Sorkin, A. and Duex, J. E. (2010). Quantitative analysis of endocytosis and turnover of epidermal growth factor (EGF) and EGF receptor. *Curr Protoc Cell Biol, Chapter 15*, pp. Unit 15 14.

Sorlie, T., Perou, C. M., Tibshirani, R., Aas, T., Geisler, S., Johnsen, H., Hastie, T., Eisen, M. B., van de Rijn, M., Jeffrey, S. S., Thorsen, T., Quist, H., Matese, J. C., Brown, P. O., Botstein, D., Lonning, P. E. and Borresen-Dale, A. L. (2001). Gene expression patterns of breast carcinomas distinguish tumor subclasses with clinical implications. *Proc Natl Acad Sci U S A, 98*(19), pp. 10869-10874.

Sorlie, T., Tibshirani, R., Parker, J., Hastie, T., Marron, J. S., Nobel, A., Deng, S., Johnsen, H., Pesich, R., Geisler, S., Demeter, J., Perou, C. M., Lonning, P. E., Brown, P. O., Borresen-Dale, A. L. and Botstein, D. (2003). Repeated observation of breast tumor subtypes in independent gene expression data sets. *Proc Natl Acad Sci U S A, 100*(14), pp. 8418-8423.

Sotiriou, C. and Pusztai, L. (2009). Gene-expression signatures in breast cancer. *N Engl J Med, 360*(8), pp. 790-800.

Soule, H. D., Maloney, T. M., Wolman, S. R., Peterson, W. D., Jr., Brenz, R., McGrath, C. M., Russo, J., Pauley, R. J., Jones, R. F. and Brooks, S. C. (1990). Isolation and characterization of a spontaneously immortalized human breast epithelial cell line, MCF-10. *Cancer Res, 50*(18), pp. 6075-6086.

Soule, H. D., Vazguez, J., Long, A., Albert, S. and Brennan, M. (1973). A human cell line from a pleural effusion derived from a breast carcinoma. *J Natl Cancer Inst, 51*(5), pp. 1409-1416.

Souzaki, M., Kubo, M., Kai, M., Kameda, C., Tanaka, H., Taguchi, T., Tanaka, M., Onishi, H. and Katano, M. (2011). Hedgehog signaling pathway mediates the progression of non-invasive breast cancer to invasive breast cancer. *Cancer Sci, 102*(2), pp. 373-381.

Souzaki, R., Tajiri, T., Souzaki, M., Kinoshita, Y., Tanaka, S., Kohashi, K., Oda, Y., Katano, M. and Taguchi, T. (2010). Hedgehog signaling pathway in neuroblastoma differentiation. *J Pediatr Surg, 45*(12), pp. 2299-2304.

Stamataki, D., Ulloa, F., Tsoni, S. V., Mynett, A. and Briscoe, J. (2005). A gradient of Gli activity mediates graded Sonic Hedgehog signaling in the neural tube. *Genes Dev, 19*(5), pp. 626-641.

Stecca, B. and Ruiz, I. A. A. (2010). Context-dependent regulation of the GLI code in cancer by HEDGEHOG and non-HEDGEHOG signals. *J Mol Cell Biol, 2*(2), pp. 84-95.

Steg, A. D., Katre, A. A., Bevis, K. S., Ziebarth, A., Dobbin, Z. C., Shah, M. M., Alvarez, R. D. and Landen, C. N. (2012). Smoothened antagonists reverse taxane resistance in ovarian cancer. *Mol Cancer Ther, 11*(7), pp. 1587-1597.

Steinberg, K. K., Thacker, S. B., Smith, S. J., Stroup, D. F., Zack, M. M., Flanders, W. D. and Berkelman, R. L. (1991). A meta-analysis of the effect of estrogen replacement therapy on the risk of breast cancer. *JAMA, 265*(15), pp. 1985-1990.

Sternlicht, M. D. (2006). Key stages in mammary gland development: the cues that regulate ductal branching morphogenesis. *Breast Cancer Res, 8*(1), pp. 201.

Strober, W. (2001). Trypan blue exclusion test of cell viability. *Curr Protoc Immunol, Appendix 3*, pp. Appendix 3B.

Sultan, A. S., Xie, J., LeBaron, M. J., Ealley, E. L., Nevalainen, M. T. and Rui, H. (2005). Stat5 promotes homotypic adhesion and inhibits invasive characteristics of human breast cancer cells. *Oncogene, 24*(5), pp. 746-760.

Sun, Q., Cibas, E. S., Huang, H., Hodgson, L. and Overholtzer, M. (2014a). Induction of entosis by epithelial cadherin expression. *Cell Res, 24*(11), pp. 1288-1298.

Sun, Y., Wang, Y., Fan, C., Gao, P., Wang, X., Wei, G. and Wei, J. (2014b). Estrogen promotes stemness and invasiveness of ER-positive breast cancer cells through Gli1 activation. *Mol Cancer, 13*, pp. 137.

Sundfeldt, K. (2003). Cell-cell adhesion in the normal ovary and ovarian tumors of epithelial origin; an exception to the rule. *Mol Cell Endocrinol, 202*(1-2), pp. 89-96.

Suzuki, K. and Takahashi, K. (2006). Induction of E-cadherin endocytosis by loss of protein phosphatase 2A expression in human breast cancers. *Biochem Biophys Res Commun, 349*(1), pp. 255-260.

Szczepny, A., Rogers, S., Jayasekara, W. S. N., Park, K., McCloy, R. A., Cochrane, C. R., Ganju, V., Cooper, W. A., Sage, J., Peacock, C. D., Cain, J. E., Burgess, A. and Watkins, D. N. (2017). The role of canonical and non-canonical Hedgehog signaling in tumor progression in a mouse model of small cell lung cancer. *Oncogene, 36*(39), pp. 5544-5550.

Takeichi, M. (1991). Cadherin cell adhesion receptors as a morphogenetic regulator. *Science, 251*(5000), pp. 1451-1455.

Tanaka, H., Nakamura, M., Kameda, C., Kubo, M., Sato, N., Kuroki, S., Tanaka, M. and Katano, M. (2009). The Hedgehog signaling pathway plays an essential role in maintaining the CD44+CD24-/low subpopulation and the side population of breast cancer cells. *Anticancer Res, 29*(6), pp. 2147-2157.

Tanaka, K., Tokunaga, E., Inoue, Y., Yamashita, N., Saeki, H., Okano, S., Kitao, H., Oki, E., Oda, Y. and Maehara, Y. (2016). Impact of Expression of Vimentin and Axl in Breast Cancer. *Clin Breast Cancer, 16*(6), pp. 520-526 e522.

Tang, Y., Wang, Y., Kiani, M. F. and Wang, B. (2016). Classification, Treatment Strategy, and Associated Drug Resistance in Breast Cancer. *Clin Breast Cancer, 16*(5), pp. 335-343.

Tao, Y., Mao, J., Zhang, Q. and Li, L. (2011). Overexpression of Hedgehog signaling molecules and its involvement in triple-negative breast cancer. *Oncol Lett, 2*(5), pp. 995-1001.

Tarin, D., Thompson, E. W. and Newgreen, D. F. (2005). The fallacy of epithelial mesenchymal transition in neoplasia. *Cancer Res, 65*(14), pp. 5996-6000; discussion 6000-5991.

ten Haaf, A., Bektas, N., von Serenyi, S., Losen, I., Arweiler, E. C., Hartmann, A., Knuchel, R. and Dahl, E. (2009). Expression of the glioma-associated oncogene homolog (GLI) 1 in human breast cancer is associated with unfavourable overall survival. *BMC Cancer, 9*, pp. 298.

Thayer, S. P., di Magliano, M. P., Heiser, P. W., Nielsen, C. M., Roberts, D. J., Lauwers, G. Y., Qi, Y. P., Gysin, S., Fernandez-del Castillo, C., Yajnik, V., Antoniu, B., McMahon, M., Warshaw, A. L. and Hebrok, M. (2003). Hedgehog is an early and late mediator of pancreatic cancer tumorigenesis. *Nature, 425*(6960), pp. 851-856.

Theunissen, J. W. and de Sauvage, F. J. (2009). Paracrine Hedgehog signaling in cancer. *Cancer Res, 69*(15), pp. 6007-6010.

Thiery, J. P. (2002). Epithelial-mesenchymal transitions in tumour progression. *Nat Rev Cancer, 2*(6), pp. 442-454.

Thiery, J. P., Acloque, H., Huang, R. Y. and Nieto, M. A. (2009). Epithelial-mesenchymal transitions in development and disease. *Cell, 139*(5), pp. 871-890.

Thiyagarajan, S., Bhatia, N., Reagan-Shaw, S., Cozma, D., Thomas-Tikhonenko, A., Ahmad, N. and Spiegelman, V. S. (2007). Role of GLI2 transcription factor in growth and tumorigenicity of prostate cells. *Cancer Res, 67*(22), pp. 10642-10646.

Thomas, Z. I., Gibson, W., Sexton, J. Z., Aird, K. M., Ingram, S. M., Aldrich, A., Lyerly, H. K., Devi, G. R. and Williams, K. P. (2011). Targeting GLI1 expression in human inflammatory breast cancer cells enhances apoptosis and attenuates migration. *Br J Cancer, 104*(10), pp. 1575-1586.

Tian, X., Liu, Z., Niu, B., Zhang, J., Tan, T. K., Lee, S. R., Zhao, Y., Harris, D. C. and Zheng, G. (2011). E-cadherin/beta-catenin

complex and the epithelial barrier. *J Biomed Biotechnol, 2011*, pp. 567305.

Tobon, H. and Salazar, H. (1974). Ultrastructure of the human mammary gland. I. Development of the fetal gland throughout gestation. *J Clin Endocrinol Metab, 39*(3), pp. 443-456.

Tojo, M., Kiyosawa, H., Iwatsuki, K., Nakamura, K. and Kaneko, F. (2003). Expression of the GLI2 oncogene and its isoforms in human basal cell carcinoma. *Br J Dermatol, 148*(5), pp. 892-897.

Tran, H. D., Luitel, K., Kim, M., Zhang, K., Longmore, G. D. and Tran, D. D. (2014). Transient SNAIL1 expression is necessary for metastatic competence in breast cancer. *Cancer Res, 74*(21), pp. 6330-6340.

Tretli, S. (1989). Height and weight in relation to breast cancer morbidity and mortality. A prospective study of 570,000 women in Norway. *Int J Cancer, 44*(1), pp. 23-30.

Trimboli, A. J., Fukino, K., de Bruin, A., Wei, G., Shen, L., Tanner, S. M., Creasap, N., Rosol, T. J., Robinson, M. L., Eng, C., Ostrowski, M. C. and Leone, G. (2008). Direct evidence for epithelial-mesenchymal transitions in breast cancer. *Cancer Res, 68*(3), pp. 937-945.

Tsai, J. H. and Yang, J. (2013). Epithelial-mesenchymal plasticity in carcinoma metastasis. *Genes Dev, 27*(20), pp. 2192-2206.

Ulloa, F., Itasaki, N. and Briscoe, J. (2007). Inhibitory Gli3 activity negatively regulates Wnt/beta-catenin signaling. *Curr Biol, 17*(6), pp. 545-550.

van 't Veer, L. J., Dai, H., van de Vijver, M. J., He, Y. D., Hart, A. A., Mao, M., Peterse, H. L., van der Kooy, K., Marton, M. J., Witteveen, A. T., Schreiber, G. J., Kerkhoven, R. M., Roberts, C., Linsley, P. S., Bernards, R. and Friend, S. H. (2002). Gene expression profiling predicts clinical outcome of breast cancer. *Nature, 415*(6871), pp. 530-536.

van Amerongen, R., Bowman, A. N. and Nusse, R. (2012). Developmental stage and time dictate the fate of

Wnt/beta-catenin-responsive stem cells in the mammary gland. *Cell Stem Cell, 11*(3), pp. 387-400.

van Dam, P. A., Van Goethem, M. L., Kersschot, E., Vervliet, J., Van den Veyver, I. B., De Schepper, A. and Buytaert, P. (1988). Palpable solid breast masses: retrospective single- and multimodality evaluation of 201 lesions. *Radiology, 166*(2), pp. 435-439.

van de Vijver, M. J., He, Y. D., van't Veer, L. J., Dai, H., Hart, A. A., Voskuil, D. W., Schreiber, G. J., Peterse, J. L., Roberts, C., Marton, M. J., Parrish, M., Atsma, D., Witteveen, A., Glas, A., Delahaye, L., van der Velde, T., Bartelink, H., Rodenhuis, S., Rutgers, E. T., Friend, S. H. and Bernards, R. (2002). A gene-expression signature as a predictor of survival in breast cancer. *N Engl J Med, 347*(25), pp. 1999-2009.

van Genderen, C., Okamura, R. M., Farinas, I., Quo, R. G., Parslow, T. G., Bruhn, L. and Grosschedl, R. (1994). Development of several organs that require inductive epithelial-mesenchymal interactions is impaired in LEF-1-deficient mice. *Genes Dev, 8*(22), pp. 2691-2703.

Van Keymeulen, A., Fioramonti, M., Centonze, A., Bouvencourt, G., Achouri, Y. and Blanpain, C. (2017). Lineage-Restricted Mammary Stem Cells Sustain the Development, Homeostasis, and Regeneration of the Estrogen Receptor Positive Lineage. *Cell Rep, 20*(7), pp. 1525-1532.

Van Keymeulen, A., Rocha, A. S., Ousset, M., Beck, B., Bouvencourt, G., Rock, J., Sharma, N., Dekoninck, S. and Blanpain, C. (2011). Distinct stem cells contribute to mammary gland development and maintenance. *Nature, 479*(7372), pp. 189-193.

van Roy, F. and Berx, G. (2008). The cell-cell adhesion molecule E-cadherin. *Cell Mol Life Sci, 65*(23), pp. 3756-3788.

Varnat, F., Zacchetti, G. and Ruiz i Altaba, A. (2010). Hedgehog pathway activity is required for the lethality and intestinal phenotypes of mice with hyperactive Wnt signaling. *Mech Dev, 127*(1-2), pp. 73-81.

Veltmaat, J. M., Van Veelen, W., Thiery, J. P. and Bellusci, S. (2004). Identification of the mammary line in mouse by Wnt10b expression. *Dev Dyn, 229*(2), pp. 349-356.

Vergara, D., Simeone, P., Franck, J., Trerotola, M., Giudetti, A., Capobianco, L., Tinelli, A., Bellomo, C., Fournier, I., Gaballo, A., Alberti, S., Salzet, M. and Maffia, M. (2016). Translating epithelial mesenchymal transition markers into the clinic: Novel insights from proteomics. *EuPA Open Proteomics, 10*, pp. 31-41.

Volante, M., Brizzi, M. P., Faggiano, A., La Rosa, S., Rapa, I., Ferrero, A., Mansueto, G., Righi, L., Garancini, S., Capella, C., De Rosa, G., Dogliotti, L., Colao, A. and Papotti, M. (2007). Somatostatin receptor type 2A immunohistochemistry in neuroendocrine tumors: a proposal of scoring system correlated with somatostatin receptor scintigraphy. *Mod Pathol, 20*(11), pp. 1172-1182.

von Schlippe, M., Marshall, J. F., Perry, P., Stone, M., Zhu, A. J. and Hart, I. R. (2000). Functional interaction between E-cadherin and alphav-containing integrins in carcinoma cells. *Journal of cell science, 113 (Pt 3)*, pp. 425-437.

Vora, H. H., Patel, N. A., Rajvik, K. N., Mehta, S. V., Brahmbhatt, B. V., Shah, M. J., Shukla, S. N. and Shah, P. M. (2009). Cytokeratin and vimentin expression in breast cancer. *Int J Biol Markers, 24*(1), pp. 38-46.

Vorherr, H. (1974). *The Breast: Morphology, Physiology, and Lactation,* Academic Press.

Vutskits, G. V., Salmon, P., Mayor, L., Vutskits, L., Cudre-Mauroux, C., Soriano, J., Montesano, R., Maillet, P. and Sappino, A. P. (2006). A role for atm in E-cadherin-mediated contact inhibition in epithelial cells. *Breast Cancer Res Treat, 99*(2), pp. 143-153.

Wang, F., Xu, L., Guo, C., Ke, A., Hu, G., Xu, X., Mo, W., Yang, L., Huang, Y., He, S. and Wang, X. (2011a). Identification of RegIV as a novel GLI1 target gene in human pancreatic cancer. *PLoS One, 6*(4), pp. e18434.

Wang, L., Cheng, H., Liu, Y., Wang, L., Yu, W., Zhang, G., Chen, B., Yu, Z. and Hu, S. (2011b). Prognostic value of nuclear beta-catenin overexpression at invasive front in colorectal cancer for synchronous liver metastasis. *Ann Surg Oncol, 18*(6), pp. 1553-1559.

Wang, X., Zhang, J., Fan, M., Zhou, Q., Deng, H., Aisharif, M. J. and Chen, X. (2009). The expression of E-cadherin at the invasive tumor front of oral squamous cell carcinoma: immunohistochemical and RT-PCR analysis with clinicopathological correlation. *Oral Surg Oral Med Oral Pathol Oral Radiol Endod, 107*(4), pp. 547-554.

Wang, X., Zhang, N., Huo, Q., Sun, M., Dong, L., Zhang, Y., Xu, G. and Yang, Q. (2014). Huaier aqueous extract inhibits stem-like characteristics of MCF7 breast cancer cells via inactivation of hedgehog pathway. *Tumour Biol, 35*(11), pp. 10805-10813.

Wang, Y., Ande, S. R. and Mishra, S. (2012). Overexpression of phospho mutant forms of transglutaminase 2 downregulates epidermal growth factor receptor. *Biochem Biophys Res Commun, 417*(1), pp. 251-255.

Wang, Y., Klijn, J. G., Zhang, Y., Sieuwerts, A. M., Look, M. P., Yang, F., Talantov, D., Timmermans, M., Meijer-van Gelder, M. E., Yu, J., Jatkoe, T., Berns, E. M., Atkins, D. and Foekens, J. A. (2005). Gene-expression profiles to predict distant metastasis of lymph-node-negative primary breast cancer. *Lancet, 365*(9460), pp. 671-679.

Wang, Y. and Zhou, B. P. (2011). Epithelial-mesenchymal transition in breast cancer progression and metastasis. *Chin J Cancer, 30*(9), pp. 603-611.

Wang, Y. and Zhou, B. P. (2013). Epithelial-mesenchymal Transition---A Hallmark of Breast Cancer Metastasis. *Cancer Hallm, 1*(1), pp. 38-49.

Wang, Z., Zhang, H., Hou, J., Niu, J., Ma, Z., Zhao, H. and Liu, C. (2015). Clinical implications of beta-catenin protein

expression in breast cancer. *Int J Clin Exp Pathol, 8*(11), pp. 14989-14994.

Warburton, M. J., Ormerod, E. J., Monaghan, P., Ferns, S. and Rudland, P. S. (1981). Characterization of a myoepithelial cell line derived from a neonatal rat mammary gland. *J Cell Biol, 91*(3 Pt 1), pp. 827-836.

Watkins, D. N., Berman, D. M., Burkholder, S. G., Wang, B., Beachy, P. A. and Baylin, S. B. (2003). Hedgehog signalling within airway epithelial progenitors and in small-cell lung cancer. *Nature, 422*(6929), pp. 313-317.

Watson, C. J. and Khaled, W. T. (2008). Mammary development in the embryo and adult: a journey of morphogenesis and commitment. *Development, 135*(6), pp. 995-1003.

Watt, F. M. (1988). Effect of seeding density on stability of the differentiated phenotype of pig articular chondrocytes in culture. *J Cell Sci, 89 (Pt 3)*, pp. 373-378.

Weigelt, B., Geyer, F. C. and Reis-Filho, J. S. (2010). Histological types of breast cancer: how special are they? *Mol Oncol, 4*(3), pp. 192-208.

Weigelt, B., Peterse, J. L. and van 't Veer, L. J. (2005). Breast cancer metastasis: markers and models. *Nat Rev Cancer, 5*(8), pp. 591-602.

Weiss, L., Holmes, J. C. and Ward, P. M. (1983). Do metastases arise from pre-existing subpopulations of cancer cells? *Br J Cancer, 47*(1), pp. 81-89.

Wellings, S. R. and Jensen, H. M. (1973). On the origin and progression of ductal carcinoma in the human breast. *J Natl Cancer Inst, 50*(5), pp. 1111-1118.

Wellings, S. R., Jensen, H. M. and Marcum, R. G. (1975). An atlas of subgross pathology of the human breast with special reference to possible precancerous lesions. *J Natl Cancer Inst, 55*(2), pp. 231-273.

Westermark, B., Ponten, J. and Hugosson, R. (1973). Determinants for the establishment of permanent tissue

culture lines from human gliomas. *Acta Pathol Microbiol Scand A, 81*(6), pp. 791-805.

Wheelock, M. J., Soler, A. P. and Knudsen, K. A. (2001). Cadherin junctions in mammary tumors. *J Mammary Gland Biol Neoplasia, 6*(3), pp. 275-285.

WHO (2008) The global burden of disease : 2004 update. in *Geneva : World Health Organization*. pp. 146. Avialable from: http://www.who.int/iris/handle/10665/43942

Wicking, C., Evans, T., Henk, B., Hayward, N., Simms, L. A., Chenevix-Trench, G., Pietsch, T. and Wainwright, B. (1998). No evidence for the H133Y mutation in SONIC HEDGEHOG in a collection of common tumour types. *Oncogene, 16*(8), pp. 1091-1093.

Wodarz, A. and Nusse, R. (1998). Mechanisms of Wnt signaling in development. *Annu Rev Cell Dev Biol, 14*, pp. 59-88.

Wolf, I., Bose, S., Desmond, J. C., Lin, B. T., Williamson, E. A., Karlan, B. Y. and Koeffler, H. P. (2007). Unmasking of epigenetically silenced genes reveals DNA promoter methylation and reduced expression of PTCH in breast cancer. *Breast Cancer Res Treat, 105*(2), pp. 139-155.

Woodward, W. A., Strom, E. A., Tucker, S. L., McNeese, M. D., Perkins, G. H., Schechter, N. R., Singletary, S. E., Theriault, R. L., Hortobagyi, G. N., Hunt, K. K. and Buchholz, T. A. (2003). Changes in the 2003 American Joint Committee on Cancer staging for breast cancer dramatically affect stage-specific survival. *J Clin Oncol, 21*(17), pp. 3244-3248.

Wu, Y., Ginther, C., Kim, J., Mosher, N., Chung, S., Slamon, D. and Vadgama, J. V. (2012). Expression of Wnt3 activates Wnt/beta-catenin pathway and promotes EMT-like phenotype in trastuzumab-resistant HER2-overexpressing breast cancer cells. *Mol Cancer Res, 10*(12), pp. 1597-1606.

Xie, G., Ji, A., Yuan, Q., Jin, Z., Yuan, Y., Ren, C., Guo, Z., Yao, Q., Yang, K., Lin, X. and Chen, L. (2014). Tumour-initiating capacity is independent of epithelial-mesenchymal

transition status in breast cancer cell lines. *Br J Cancer, 110*(10), pp. 2514-2523.

Xie, J., Murone, M., Luoh, S. M., Ryan, A., Gu, Q., Zhang, C., Bonifas, J. M., Lam, C. W., Hynes, M., Goddard, A., Rosenthal, A., Epstein, E. H., Jr. and de Sauvage, F. J. (1998). Activating Smoothened mutations in sporadic basal-cell carcinoma. *Nature, 391*(6662), pp. 90-92.

Xu, J., Huang, G., Zhang, Z., Zhao, J., Zhang, M., Wang, Y., Liu, Z. and Lu, J. (2015). Up-Regulation of Glioma-Associated Oncogene Homolog 1 Expression by Serum Starvation Promotes Cell Survival in ER-Positive Breast Cancer Cells. *Cell Physiol Biochem, 36*(5), pp. 1862-1876.

Xu, L., Chen, Y. G. and Massague, J. (2000). The nuclear import function of Smad2 is masked by SARA and unmasked by TGFbeta-dependent phosphorylation. *Nat Cell Biol, 2*(8), pp. 559-562.

Xu, L., Kwon, Y. J., Frolova, N., Steg, A. D., Yuan, K., Johnson, M. R., Grizzle, W. E., Desmond, R. A. and Frost, A. R. (2010). Gli1 promotes cell survival and is predictive of a poor outcome in ERalpha-negative breast cancer. *Breast Cancer Res Treat, 123*(1), pp. 59-71.

Xuan, Y. and Lin, Z. (2009). Expression of Indian Hedgehog signaling molecules in breast cancer. *J Cancer Res Clin Oncol, 135*(2), pp. 235-240.

Yamashita, N., Tokunaga, E., Kitao, H., Hisamatsu, Y., Taketani, K., Akiyoshi, S., Okada, S., Aishima, S., Morita, M. and Maehara, Y. (2013). Vimentin as a poor prognostic factor for triple-negative breast cancer. *J Cancer Res Clin Oncol, 139*(5), pp. 739-746.

Yan, D., Avtanski, D., Saxena, N. K. and Sharma, D. (2012). Leptin-induced epithelial-mesenchymal transition in breast cancer cells requires beta-catenin activation via Akt/GSK3- and MTA1/Wnt1 protein-dependent pathways. *J Biol Chem, 287*(11), pp. 8598-8612.

Yang, J., Li, T., Gao, C., Lv, X., Liu, K., Song, H., Xing, Y. and Xi, T. (2014). FOXO1 3'UTR functions as a ceRNA in repressing the metastases of breast cancer cells via regulating miRNA activity. *FEBS Lett, 588*(17), pp. 3218-3224.

Yang, J., Mani, S. A., Donaher, J. L., Ramaswamy, S., Itzykson, R. A., Come, C., Savagner, P., Gitelman, I., Richardson, A. and Weinberg, R. A. (2004). Twist, a master regulator of morphogenesis, plays an essential role in tumor metastasis. *Cell, 117*(7), pp. 927-939.

Yang, J. and Weinberg, R. A. (2008). Epithelial-mesenchymal transition: at the crossroads of development and tumor metastasis. *Dev Cell, 14*(6), pp. 818-829.

Yang, M. H., Wu, M. Z., Chiou, S. H., Chen, P. M., Chang, S. Y., Liu, C. J., Teng, S. C. and Wu, K. J. (2008a). Direct regulation of TWIST by HIF-1alpha promotes metastasis. *Nat Cell Biol, 10*(3), pp. 295-305.

Yang, S. H., Andl, T., Grachtchouk, V., Wang, A., Liu, J., Syu, L. J., Ferris, J., Wang, T. S., Glick, A. B., Millar, S. E. and Dlugosz, A. A. (2008b). Pathological responses to oncogenic Hedgehog signaling in skin are dependent on canonical Wnt/beta3-catenin signaling. *Nat Genet, 40*(9), pp. 1130-1135.

Yassin, M. A., Leknes, K. N., Pedersen, T. O., Xing, Z., Sun, Y., Lie, S. A., Finne-Wistrand, A. and Mustafa, K. (2015). Cell seeding density is a critical determinant for copolymer scaffolds-induced bone regeneration. *J Biomed Mater Res A, 103*(11), pp. 3649-3658.

Yauch, R. L., Gould, S. E., Scales, S. J., Tang, T., Tian, H., Ahn, C. P., Marshall, D., Fu, L., Januario, T., Kallop, D., Nannini-Pepe, M., Kotkow, K., Marsters, J. C., Rubin, L. L. and de Sauvage, F. J. (2008). A paracrine requirement for hedgehog signalling in cancer. *Nature, 455*(7211), pp. 406-410.

Yen, C.-F., Wang, H.-S., Lee, C.-L. and Liao, S.-K. (2014). Roles of integrin-linked kinase in cell signaling and its perspectives

as a therapeutic target. *Gynecology and Minimally Invasive Therapy, 3*(3), pp. 67-72.

Yoshida, C. and Takeichi, M. (1982). Teratocarcinoma cell adhesion: identification of a cell-surface protein involved in calcium-dependent cell aggregation. *Cell, 28*(2), pp. 217-224.

Yoshimoto, A. N., Bernardazzi, C., Carneiro, A. J., Elia, C. C., Martinusso, C. A., Ventura, G. M., Castelo-Branco, M. T. and de Souza, H. S. (2012). Hedgehog pathway signaling regulates human colon carcinoma HT-29 epithelial cell line apoptosis and cytokine secretion. *PLoS One, 7*(9), pp. e45332.

Yue, D., Li, H., Che, J., Zhang, Y., Tseng, H. H., Jin, J. Q., Luh, T. M., Giroux-Leprieur, E., Mo, M., Zheng, Q., Shi, H., Zhang, H., Hao, X., Wang, C., Jablons, D. M. and He, B. (2014). Hedgehog/Gli promotes epithelial-mesenchymal transition in lung squamous cell carcinomas. *J Exp Clin Cancer Res, 33*, pp. 34.

Yuki, K., Yoshida, Y., Inagaki, R., Hiai, H. and Noda, M. (2014). E-cadherin-downregulation and RECK-upregulation are coupled in the non-malignant epithelial cell line MCF10A but not in multiple carcinoma-derived cell lines. *Sci Rep, 4*, pp. 4568.

Zanetti, A., Affatato, R., Centritto, F., Fratelli, M., Kurosaki, M., Barzago, M. M., Bolis, M., Terao, M., Garattini, E. and Paroni, G. (2015). All-trans-retinoic Acid Modulates the Plasticity and Inhibits the Motility of Breast Cancer Cells: ROLE OF NOTCH1 AND TRANSFORMING GROWTH FACTOR (TGFbeta). *J Biol Chem, 290*(29), pp. 17690-17709.

Zeisberg, M. and Neilson, E. G. (2009). Biomarkers for epithelial-mesenchymal transitions. *J Clin Invest, 119*(6), pp. 1429-1437.

Zhang, A., Chen, G., Meng, L., Wang, Q., Hu, W., Xi, L., Gao, Q., Wang, S., Zhou, J., Xu, G., Meng, L. and Ma, D. (2008). Antisense-Snail transfer inhibits tumor metastasis by

inducing E-cadherin expression. *Anticancer Res, 28*(2A), pp. 621-628.

Zhang, D. W., Li, H. Y., Lau, W. Y., Cao, L. Q., Li, Y., Jiang, X. F., Yang, X. W. and Xue, P. (2014). Gli2 silencing enhances TRAIL-induced apoptosis and reduces tumor growth in human hepatoma cells in vivo. *Cancer Biol Ther, 15*(12), pp. 1667-1676.

Zhang, X., Emerald, B. S., Mukhina, S., Mohankumar, K. M., Kraemer, A., Yap, A. S., Gluckman, P. D., Lee, K. O. and Lobie, P. E. (2006). HOXA1 is required for E-cadherin-dependent anchorage-independent survival of human mammary carcinoma cells. *J Biol Chem, 281*(10), pp. 6471-6481.

Zhang, X., Harrington, N., Moraes, R. C., Wu, M. F., Hilsenbeck, S. G. and Lewis, M. T. (2009). Cyclopamine inhibition of human breast cancer cell growth independent of Smoothened (Smo). *Breast Cancer Res Treat, 115*(3), pp. 505-521.

Zhang, Y., Yan, W. and Chen, X. (2011). Mutant p53 disrupts MCF-10A cell polarity in three-dimensional culture via epithelial-to-mesenchymal transitions. *J Biol Chem, 286*(18), pp. 16218-16228.

Zhao, P., Guo, S., Tu, Z., Di, L., Zha, X., Zhou, H. and Zhang, X. (2016). Grhl3 induces human epithelial tumor cell migration and invasion via downregulation of E-cadherin. *Acta Biochim Biophys Sin (Shanghai), 48*(3), pp. 266-274.

Zhu, H., Zhang, G., Wang, Y., Xu, N., He, S., Zhang, W., Chen, M., Liu, M., Quan, L., Bai, J. and Xu, N. (2010). Inhibition of ErbB2 by Herceptin reduces survivin expression via the ErbB2-beta-catenin/TCF4-survivin pathway in ErbB2-overexpressed breast cancer cells. *Cancer Sci, 101*(5), pp. 1156-1162.

Zhuang, Z., Lininger, R. A., Man, Y. G., Albuquerque, A., Merino, M. J. and Tavassoli, F. A. (1997). Identical clonality of both

components of mammary carcinosarcoma with differential loss of heterozygosity. *Mod Pathol, 10*(4), pp. 354-362.

Zhuang, Z., Wang, K., Cheng, X., Qu, X., Jiang, B., Li, Z., Luo, J., Shao, Z. and Duan, T. (2013). LKB1 inhibits breast cancer partially through repressing the Hedgehog signaling pathway. *PLoS One, 8*(7), pp. e67431.

Zlobec, I. and Lugli, A. (2009). Invasive front of colorectal cancer: dynamic interface of pro-/anti-tumor factors. *World J Gastroenterol, 15*(47), pp. 5898-5906.

11. Appendices

11.1 Summary of the morphological changes associated with decrease in seeding densities

The scores in Table 3-2 were then presented as bar charts of changes at different densities. It was noted that cellular spreading increased in all cell lines with decrease in densities (Figure 11-1). Also, the spreading of all the basal-cell lines (BT20, MDA-MB-231 and MCF10A) were more significant than that seen in all the luminal breast cancer cell lines. The two basal-cell lines (BT20 and MDA-MB-231) showed high cellular spreading even in dense cultures. All the other cell lines (MCF7, MDA-MB-361, and MDA-MB-453) showed less cellular spreading in the highest density.

Both luminal breast cancer cell line (MCF7 and MDA-MB-361) and the TNBC cell line (MDA-MB-453) showed strong cell-cell contact morphology at the highest density (Figure 11-2). The basal-like/normal-like breast cancer cell line (MCF10A) showed tight cellular contact as seen in the luminal cell lines that correlated with density. The basal breast cancer cell lines (BT20 and MDA-MB-231) showed non-linear association in response to decrease in density. Both cell lines showed increase in cell-cell contact at the medium density then, lost at the lower density. This pattern was specific to these cell lines only and was the reason the medium density was selected for further analysis.

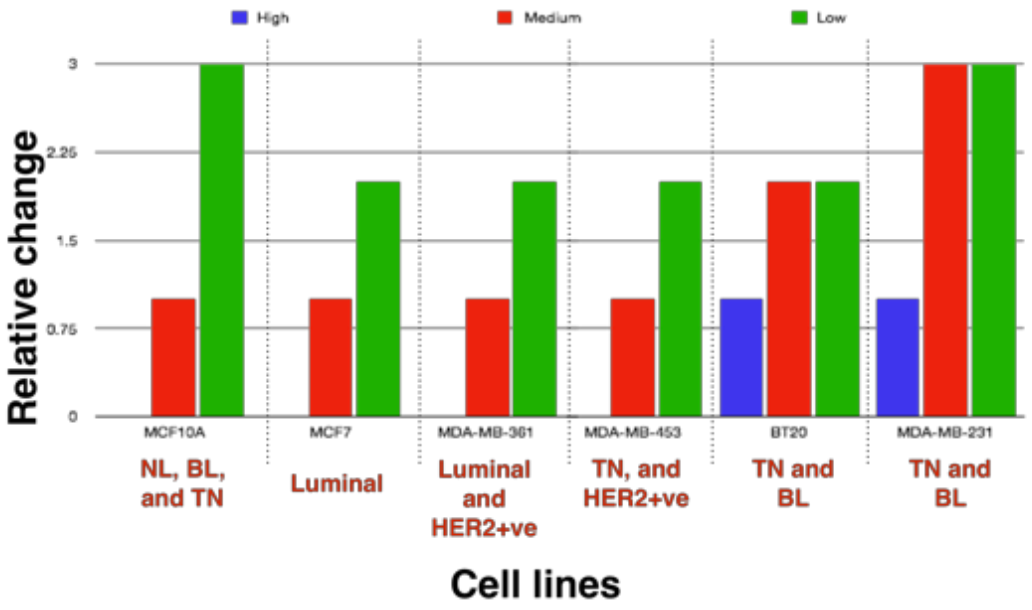

Figure 11-1, Bar charts of qualitative score of the increase in morphological spreading seen at the three densities of breast cancer cell lines

Bar chart presenting the qualitative scores of the increase in morphological spreading associated with decrease in seeding density. In general, all the breast cancer cell lines showed increase in cellular spreading with decrease in seeding density. Highlighted below in red are the subclassification of the breast cancer cell lines including; Luminal, HER2^{+ve} (human EGF receptor two positive), TN (triple-negative), NL, (normal-like), and Basal-like (BL) (basal-like).

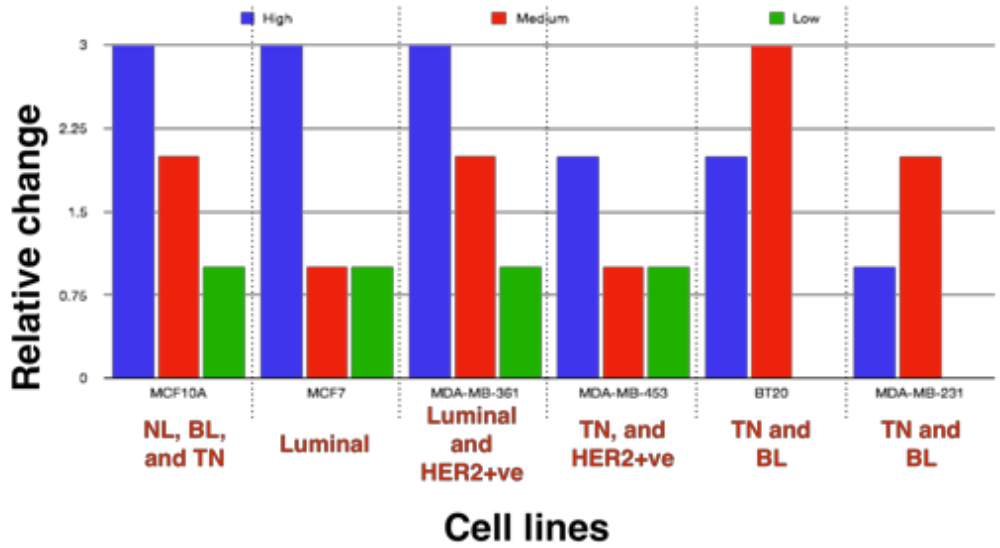

Figure 11-2, Bar charts of the cell-cell contact morphological changes seen at three seeding densities of breast cancer cell lines

Bars charts presenting the qualitative scores summarising the cell-cell contact morphological changes associated with decreasing the seeding density. All the cell lines, except BT20 and MDA-MB-231, showed gradual decrease in cell-cell contact with decreasing density. The basal-cell lines (BT20 and MDA-MB-231) showed a specific pattern in increase in contact at the medium density. Highlighted below in red are the subclassification of the breast cancer cell lines including; Luminal, HER2^{+ve} (human EGF receptor2 positive), TN (triple-negative), NL, (normal-like), and BL (basal-like).

Four cell lines showed an increase in spindle cells morphology inversely associated with seeding density including two luminal cell lines (MCF7 and MDA-MB-361), the normal-like breast cancer cell line (MCF10A) and the TNBC cell line (MDA-MB-453) (Figure 11-3). Also, both basal breast cancer cell lines (BT20 and MDA-MB-231) showed a decrease in the spindle morphology at the medium density which then increased of spindle morphology at the high and low density.

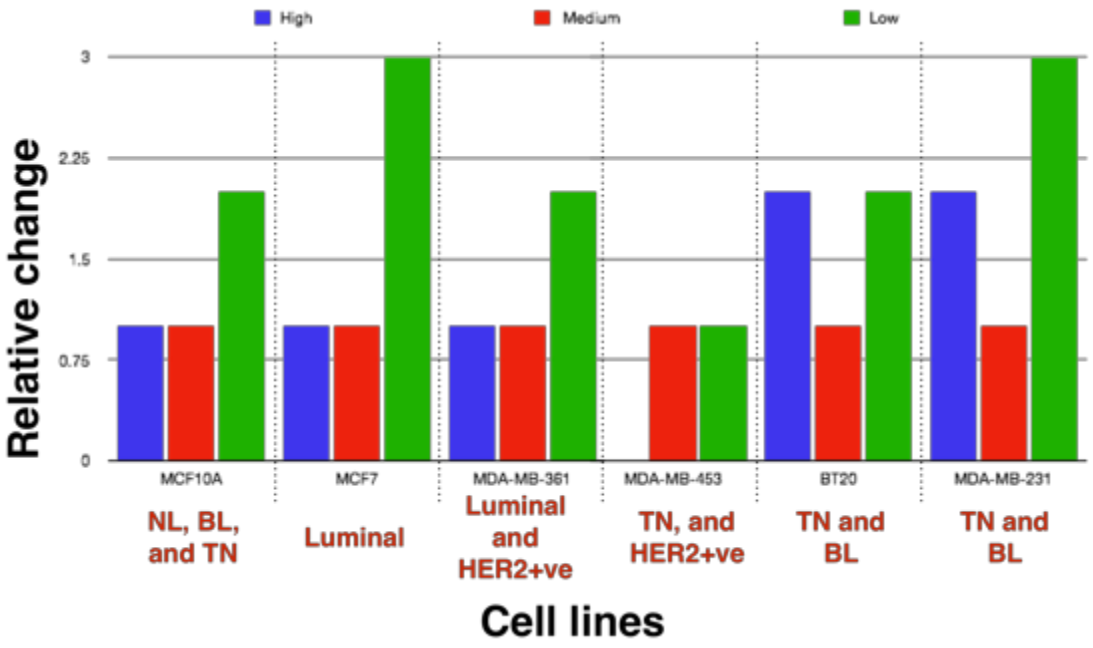

Figure 11-3, Bar charts of the change in spindle cells morphology seen at three seeding densities of breast cancer cell lines

Bars represent the qualitative scores for the spindle morphology seen at three densities of breast cancer cell lines. The luminal cell lines (MCF7 and MDA-MB-361) and the triple-negative cell line (MDA-MB-453) showed increase in spindle morphology with decreasing density. Both of the basal breast cancer cell lines (BT20 and MDA-MB-231) showed a dip in the spindle morphology at the medium density. Highlighted below in red are the subclassification of the breast cancer cell lines including; Luminal, $HER2^{+ve}$ (human EGF receptor2 positive), TN (triple-negative), NL, (normal-like), and BL (basal-like).

Taken together, it can be seen that all the cell lines showed increase in the mesenchymal morphological features with decrease in seeding density. All cell lines showed increase in spindle morphology and cellular spreading with decrease in cell-cell contact, which are all morphological features of mesenchymal morphological change. The luminal cell lines (MCF7 and MDA-MB-361) and the TNBC cell line (MDA-MB-453) showed less significant morphological mesenchymal change compared to that observed in all the basal breast cancer cell lines (BT20, MDA-MB-231 and MCF10A).

It was also noted that there was a specific morphological pattern captured in the medium density of some of the cell lines. As seen at the medium density of the basal-like breast cancer cell lines (BT20 and MDA-MB-231) there was morphological increase in the cell-cell contact at the medium density. Also, there was decrease in the spindle shape at the medium density of both cell lines in the medium density. These observations together supported the importance of including the medium density in further analysis.

11.2 Confirmation of subtype of breast cancer samples showed that all selected cases followed the classification specified in the pathology report

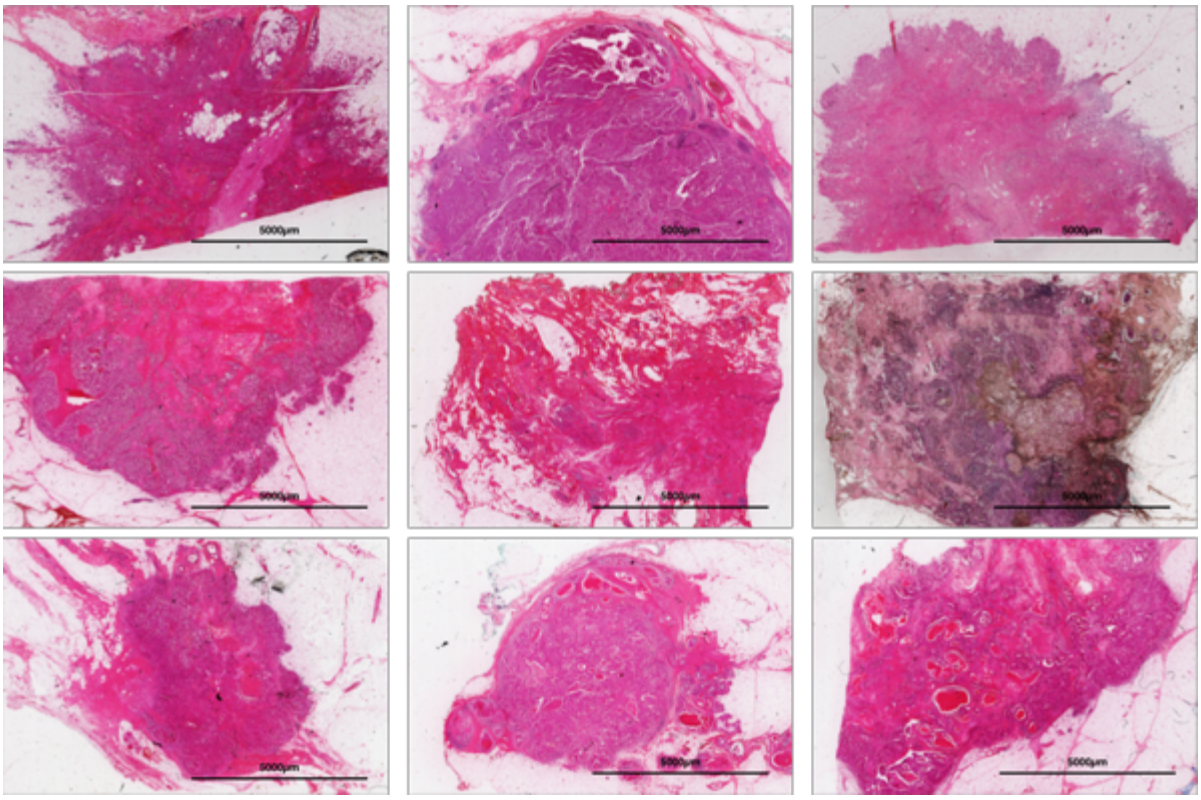

Figure 11-4, Verification of tumour identification in samples
Representative images of nine slides that showed verification of presence of tumour in sections. Sections were stained with H&E and images were captured using GT Vision (*GT Vision, UK*). Scale bar is added in the bottom right corner of the images.

Table 11-1: Summary table of number of cases stained and investigated for β-catenin, E-cadherin, Gli1, Gli2 and Gli3 used and the corresponding clinicopathological parameters

Numbers of sections in each of the clinicopathological parameters (A) Size, (B) Stage and (C) Grade and the total number of cases stained by either β-catenin, E-cadherin, Gli1, Gli2 or Gli3.

Clinical criteria		Count				
		β-catenin	E-cadherin	Gli1	Gli2	Gli3
Size	2cm ≥	14	11	25	12	10
	2cm<	23	12	23	17	13
Stage	T1	13	14	23	14	11
	T2	17	7	19	11	9
	T3	2	0	3	1	1
	T4	0	0	0	0	0
	TX	5	0	3	3	2
Grade	1	1	1	1	1	1
	2	18	12	23	11	9
	3	18	10	24	17	13
Total		37	23	48	29	23

TX= stage not determined in the clinical reports

Table 11-2: Numbers of sections included in the investigation and the corresponding histological subtype

Summary of numbers of cases stained with each antibody (β-catenin, E-cadherin, Gli1, Gli2 and Gli3) and the histological subtype identified in the pathology report. DCIS= ductal carcinoma *in situ*, IDC= invasive ductal carcinoma, LCIS=lobular carcinoma *in situ*, ILC= invasive lobular carcinoma, NST= none specific type.

Histological subtype	Count				
	β-catenin	E-cadherin	Gli1	Gli2	Gli3
DCIS	1	1	2	1	0
DCIS/IDC	15	8	12	11	7
IDC	12	7	18	9	8
LCIS	0	0	0	0	0
LCIS/ILC	1	0	2	0	1
ILC	1	1	4	1	0
Mixed	2	1	3	0	1
Metastatic	1	1	2	2	0
NST	4	4	5	5	6
Total	37	23	48	29	23

Table 11-3: Number of sections and the lymph node and metastasis status as identified in the pathology reports

Summary table that shows the number of sections stained by either β-catenin, E-cadherin, Gli1, Gli2 or Gli3 and the lymph node and metastasis status as reported in the pathology report.

		Count				
		β-catenin	E-cadherin	Gli1	Gli2	Gli3
Lymph node involvement	Positive	16	5	17	12	9
	Negative	18	14	27	13	13
	Possible	2	3	3	3	1
Metastasis	Yes	1	1	2	2	0
	No	35	21	45	26	23
	Possible	0	0	0	0	0
	Total	36 (UI=1)	23	47 (UI=1)	28 (UI=1)	23

UI= undefined in the clinical reports

Table 11-4: Numbers of sections stained for investigation and the molecular subgroup they represent according to the pathology report and after confirmation

Summary of the percentages (A), intensity of the immune staining (B) and IRS score (C) for E-cadherin in human cohort. The tables summarise the numbers and percentages of cases observed in each category of the scale in tumour

A		Count				
		β-catenin	E-cadherin	Gli1	Gli2	Gli3
ER Status	Negative	23	14	34	23	14
	Positive	14	9	14	6	9
PR status	Negative	29	17	39	25	18
	Positive	8	6	9	4	5
HER2 status	Positive	15	9	14	12	8
	Negative	22	14	34	17	15
Molecular subgroup	Luminal A	10	8	11	5	7
	Luminal B	4	1	3	1	2
	HER2	11	8	11	11	6
	TN	12	6	23	12	8
	Total	37	23	48	29	23

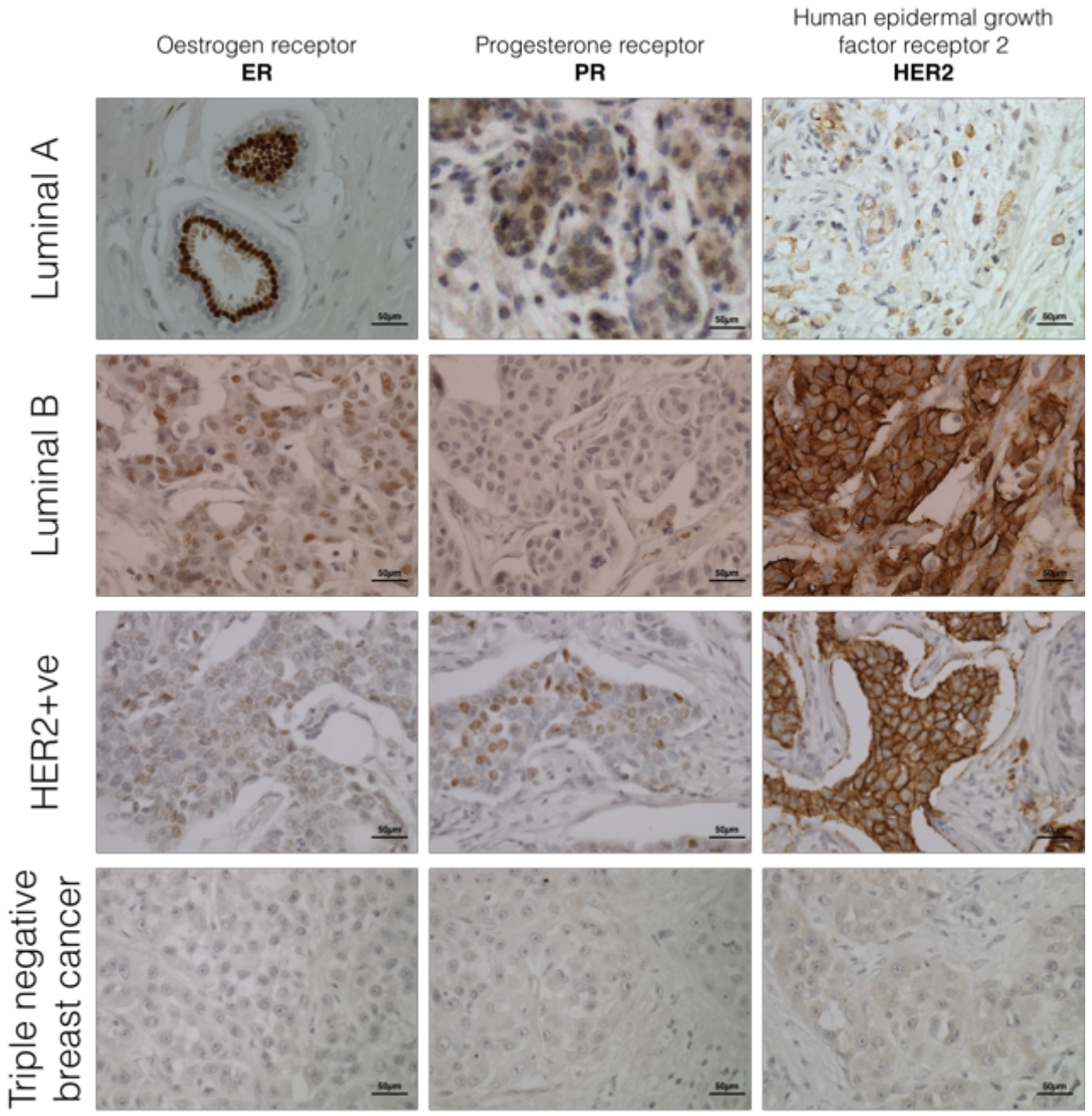

Figure 11-5, Representative immunohistochemistry images for the molecular classification defined by expression of prognostic markers (ER, PR and HER2)
Samples were stained for the prognostic markers ER, PR) and HER2 (human EGF receptor 2) in order to verify their molecular subgroup. Images were captured at 400x magnification and scale bars were added to the bottom right corner.

11.3 Associations between histological subtypes, molecular subgroups and clinicopathological parameters

Statistical analysis was conducted on the total numbers of cases (n=48). There was no difference in age at diagnosis between the histological subtypes (p=-0.136, one-way ANOVA) or molecular subgroups (p=0.574). There was no difference in tumour

size between the histological subtype (p=0.107) or the molecular subgroup (p=0.489). A single case in the cohort was classified as grade 1.

The expression of the ER prognostic marker was negatively correlated with size (-0.340, p=0.02), stage (-0.279, p=0.057), and grade (-0.560, p=0.000) (Table 11-5 and Figure 11-6). PR showed negative correlation with size (-0.247, p=0.09), stage (-0.314, p=0.003), and grade (-0.451, p=0.002) (Table 11-5 and Figure 11-6). The molecular subgroup correlated with size (0.228, p=0.094), stage (0.245, p=0.074), and grade (0.484, p=0.000) (Table 11-5 and Figure 11-6). Statistical analysis showed that the lymph node involvement correlated with stage (0.401, p=0.005) and grade (0.331, p=0.02) (Table 11-6 and Figure 11-7).

Table 11-5: Statistical correlation between expression of prognostic markers and the molecular subgroup (ER, PR and HER2) with clinicopathological parameters (size, stage, grade and histological subtype)

Statistical correlation was analysed using the Kendall's Tau B test. highlighted are the comparisons that showed correlations and highly significant correlations were indicated in bold.

		ER status	PR status	HER2 status	Molecular subgroup
Size	Correlation coefficient	**-0.340***	-0.247	-0.027	0.228
	Sig. (2-tailed)	0.02	0.09	0.854	0.094
	N	48	48	48	48
Stage	Correlation Coefficient	-0.279	**-0.314***	-0.017	0.245
	Sig. (2-tailed)	0.057	0.033	0.91	0.074
	N	45	45	45	45
Grade	Correlation Coefficient	**-0.560****	**-0.451****	-0.101	**0.484****
	Sig. (2-tailed)	0	0.002	0.484	0
	N	48	48	48	48
Histological subtype	Correlation Coefficient	0.12	0.229	0.212	-0.045
	Sig. (2-tailed)	0.359	0.08	0.105	0.713
	N	48	48	48	48

The Kendall's TauB correlation coefficient (between -1 and +1). The statistical significance of the correlation is indicated as follows: *P= <0.05, **P= <0.01.

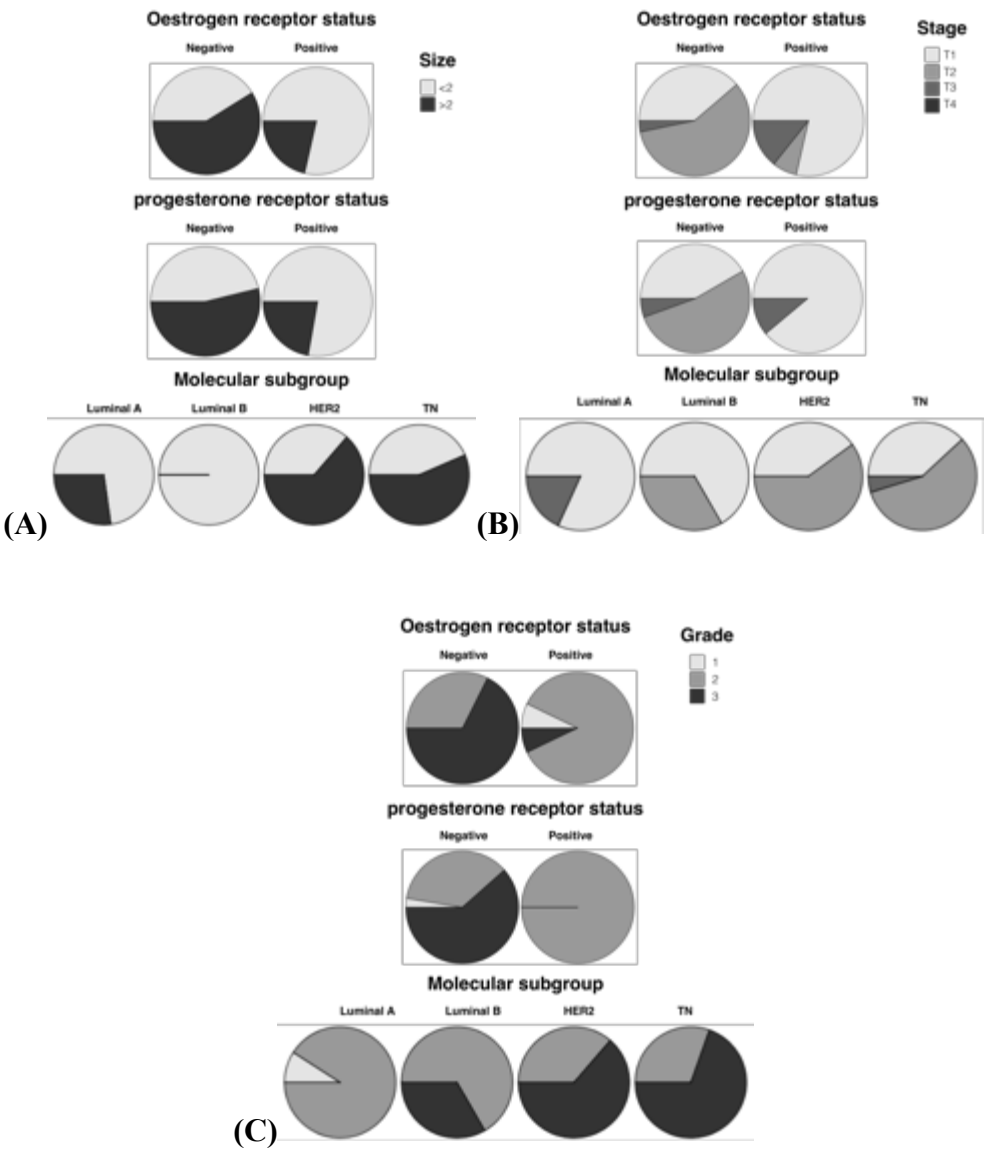

Figure 11-6, Summary of statistical analysis for tumour size (A), stage (B) and grade (C)

Kendall's Tau B test was used to assess the correlations. Figure showing correlation of hormone negative and TN breast cancer cases with increase tumour size, stage, and grade. HER2= Human EGF receptor 2, TN= triple-negative.

Table 11-6: Statistical correlation of lymph node involvement and metastasis with clinicopathological parameters (size, stage, grade, histological subtype, prognostic markers expression and molecular subgroup)

Statistical correlation was analysed using the Kendall's Tau B test. highlighted are the comparisons that showed correlations and highly significant correlations were indicated in bold.

		Lymph node involvement	Metastasis
Size	Correlation coefficient	0.203	-0.198
	Sig. (2-tailed)	0.157	0.18
	N	47	47
Stage	Correlation Coefficient	**0.401****	-0.14
	Sig. (2-tailed)	0.005	0.341
	N	45	45
Grade	Correlation Coefficient	**0.331***	-0.211
	Sig. (2-tailed)	0.02	0.148
	N	47	47
Histological subtype	Correlation Coefficient	-0.159	0.254
	Sig. (2-tailed)	0.22	0.055
	N	47	47
ER status	Correlation Coefficient	-0.122	-0.137
	Sig. (2-tailed)	0.394	0.352
	N	47	47
PR status	Correlation Coefficient	-0.182	-0.103
	Sig. (2-tailed)	0.204	0.487
	N	47	47
HER2 status	Correlation Coefficient	-0.129	-0.105
	Sig. (2-tailed)	0.369	0.475
	N	47	47
Molecular subgroup	Correlation Coefficient	0.057	0.059
	Sig. (2-tailed)	0.674	0.67
	N	47	47

The Kendall's TauB correlation coefficient (between -1 and +1). The statistical significance of the correlation is indicated as follows: *P= <0.05, **P= <0.01.

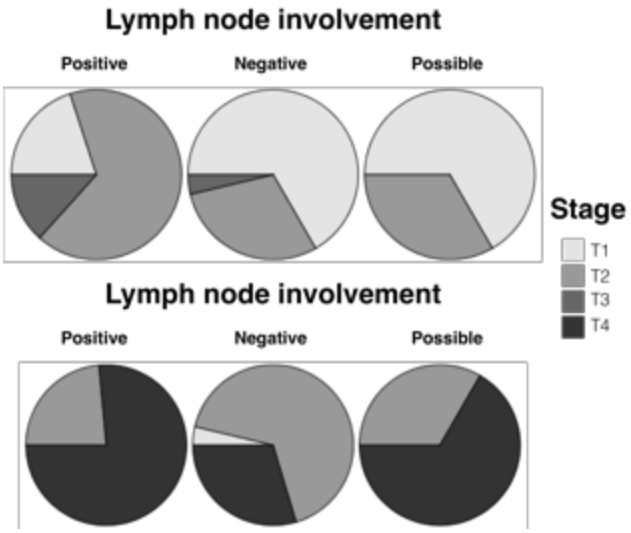

Figure 11-7, Correlation between lymph node involvement of investigated breast cancer cases and the stage of tumour
Kendall's Tau B test was used to assess the correlation between lymph node involvement and the stage of tumour. Figure shows correlation between lymph node involvement and high stage of tumour.

11.3.1 Comparing Gli3 expression in tumour centres and invasive fronts

The percentage of Gli3 positive expressing cells showed an increase at the invasive front compared to the tumour centre, however, this difference did not reach significance (Figure 11-8-A and Table 11-7-A). The intensity of staining showed a significant increase at the invasive front compared to tumour centre (*p*-value= 0.075) (Figure 11-8-B and Table 11-7-B). Gli3 IRS showed that the IRS class at the invasive front was higher than that in the tumour centre, however this difference did not reach statistical significance (*p*-value= 0.124) (Figure 11-8-C and Table 11-7-C).

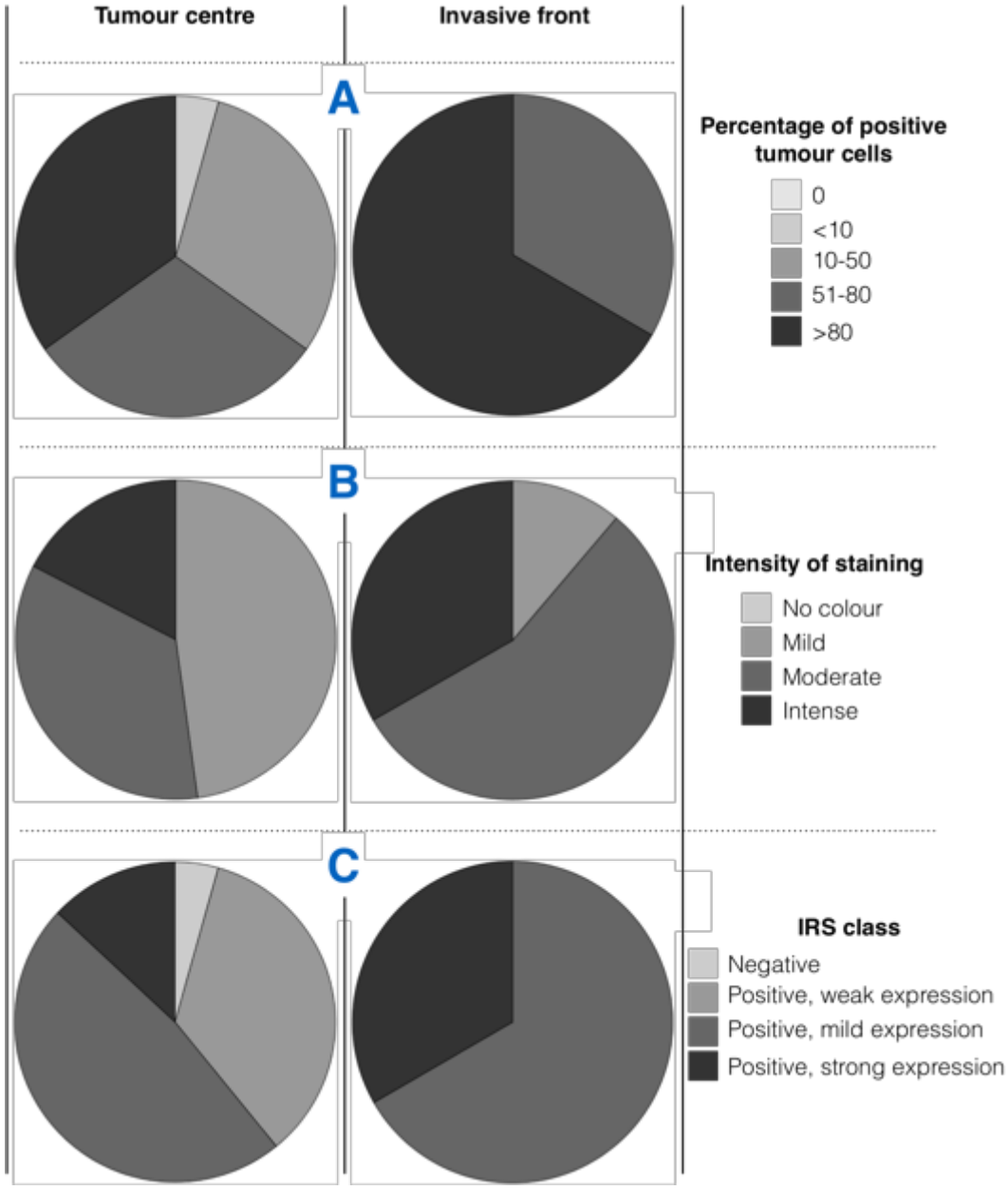

Figure 11-8, Gli3 expression was higher at invasive fronts in breast cancer cohort
Figure showing comparison of Gli2 in tumour centres (to the left) compared to the invasive front (to the right). (A) comparison of percentage of positive cells. (B) comparison of intensity of staining. (C) comparison of IRS class.

Table 11-7: Gli3 staining intensity showed increase at invasive front compared to tumour centre

Tumour centre and invasive front frequency tables (A) for percentage of positive tumour cells, (B) intensity of staining, and (C) IRS class. The numbers are indicated for each score and the percentages were calculated from the total number of samples. Pearson Chi-square test was used to estimate the difference between tumour centre and invasive front.

	A	Tumour centre	Invasive front
		No. (%)	No. (%)
Percentage of positive tumour cells	0	0	0
	<10	1 (4.3)	0
	10-50	7 (30.4)	0
	51-80	7 (30.4)	6 (33.3)
	>80	8 (34.8)	12 (66.7)
	Total	23 (100)	18 (100)
	Missing	0	5 (21.7)
	Total	23 (100)	23 (100)
p-value		0.154	

	B	Tumour centre	Invasive front
		No. (%)	No. (%)
Intensity of staining	No colour	0	0
	Mild	11 (47.8)	2 (11.1)
	Moderate	8 (34.8)	10 (55.6)
	Intense	4 (17.4)	6 (33.3)
	Total	23 (100)	18 (100)
	Missing	0	5 (21.7)
	Total	23 (100)	23 (100)
p-value		0.075	

	C	Tumour centre	Invasive front
		No. (%)	No. (%)
IRS class	Negative	1 (4.3)	0
	Positive, weak expression	8 (34.8)	0
	Positive, mild expression	11 (47.8)	12 (66.7)
	Positive, strong expression	3 (13)	6 (33.3)
	Total	23 (100)	18 (100)
	Missing	0	5 (21.7)
	Total	23 (100)	23 (100)
p-value		0.124	

11.3.2 Gli1 expression correlated with increased tumour size and hormone receptor negative breast cancer

The percentage of Gli1 positive tumour cells in the tumour centre was correlated with an increasing of tumour size (0.288, *p*-value= 0.065) (Figure 11-9). The percentage of Gli1 positive tumour cells also increased with an increased in size.

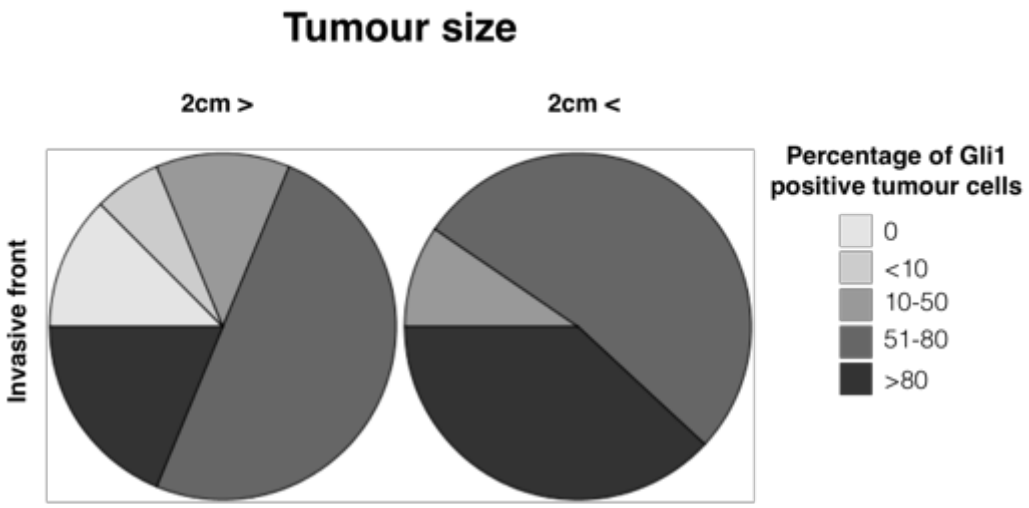

Percentage of positive cells	Tumour size	
	2cm >	2cm <
	No. (%)	No. (%)
0	2 (5.4)	0
<10	1 (2.7)	0
10-50	2 (5.4)	2 (5.4)
51-80	8 (21.6)	11 (29.7)
>80	3 (8.1)	8 (21.6)
Tau B	0.288	
p-value	0.065	
Total	37	

Figure 11-9, Increased percentage of Gli1 positive tumour cells correlated with an increase in tumour size

Figure showing comparison of percentage of tumour positive cells in correlation with tumour size (2cm ≥ or 2cm <). Table showing numbers of cases that correspond to two groups of tumour size (2cm ≥ or 2cm<) and the corresponding percentage of positive tumour cells (0, <10, 10-50, 51-80 or >80). The correlation was calculated using the Kendall's Tau B test.

Nuclear localisation of Gli1 in the tumour centre and at the invasive front showed correlation with increasing clinical tumour stage (0.223, *p*-value = 0.098) (Figure 11-10). Increase in tumour stage correlated with more Gli1 nuclear localisation at invasive fronts.

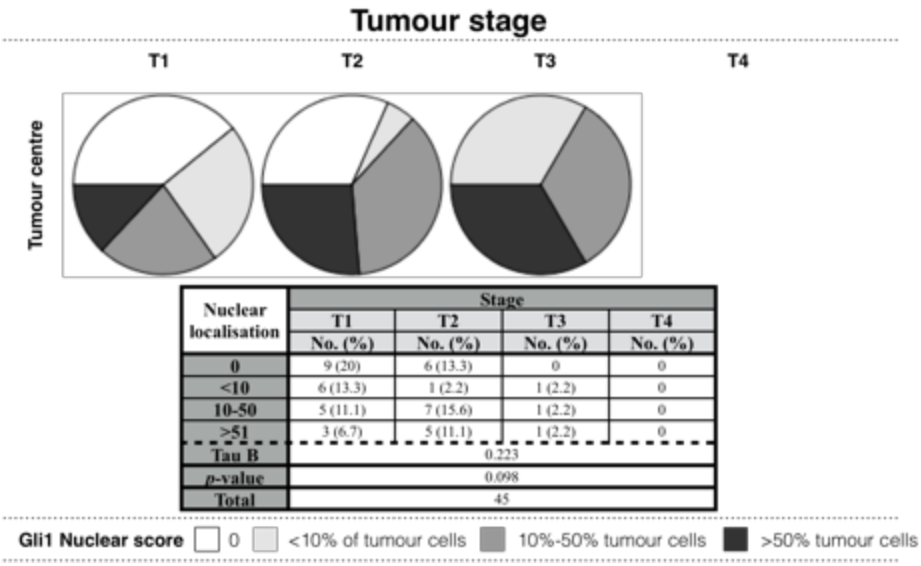

Nuclear localisation	Stage			
	T1	T2	T3	T4
	No. (%)	No. (%)	No. (%)	No. (%)
0	9 (20)	6 (13.3)	0	0
<10	6 (13.3)	1 (2.2)	1 (2.2)	0
10-50	5 (11.1)	7 (15.6)	1 (2.2)	0
>51	3 (6.7)	5 (11.1)	1 (2.2)	0
Tau B	0.223			
p-value	0.098			
Total	45			

Figure 11-10, Increased of nuclear localisation of Gli1 in the tumour centre correlated with tumour stage

Figure showing correlation between increased in Gli1 nuclear localisation and increased in tumour stage in tumour centre. Table below the figures shows the numbers of cases, the corresponding tumour stage (T1, T2, T3 and T4) and the nuclear localisation of Gli1 (presented as 0, <10, 10-50, and >51). The correlation was calculated using the Kendall's Tau B test.

The percentage of Gli1 positive tumour cells in the tumour centre were correlated with the molecular subgroups of breast cancer (0.222, *p*-value = 0.078) (Figure 11-11-A). The percentage of Gli1 positivity was higher in TNBC (0.238, *p*-value = 077). The nuclear localisation of Gli1 in the tumour centre showed correlation with subgroup (0.195, *p*-value = 0.091) (Figure 11-11-B). Increased nuclear localisation of Gli1 was higher in TNBC (0.225, *p*-value = 0.093) and Luminal B breast cancer subtype (0.28, *p*-value = 073).

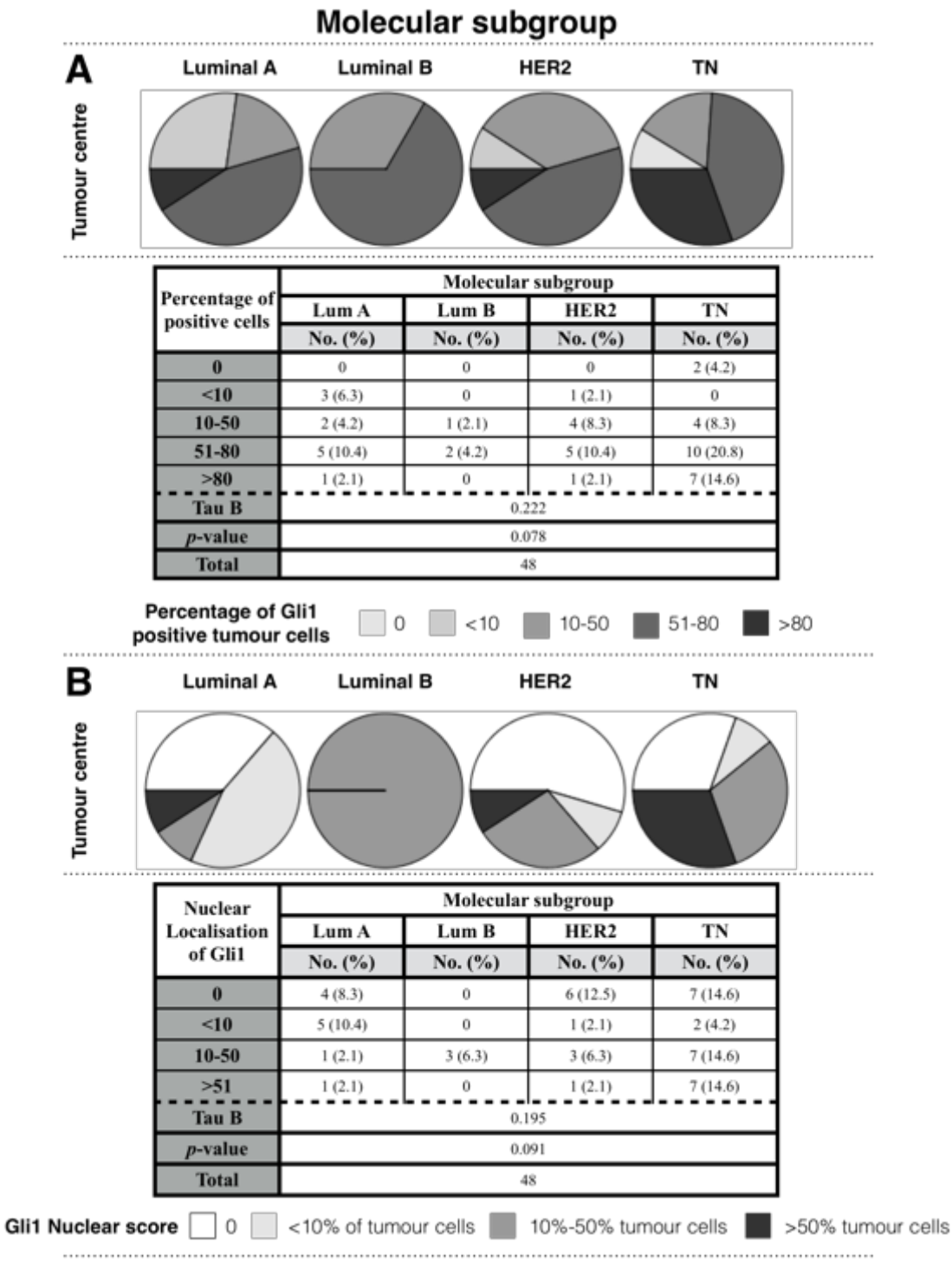

Percentage of positive cells	Molecular subgroup			
	Lum A	Lum B	HER2	TN
	No. (%)	No. (%)	No. (%)	No. (%)
0	0	0	0	2 (4.2)
<10	3 (6.3)	0	1 (2.1)	0
10-50	2 (4.2)	1 (2.1)	4 (8.3)	4 (8.3)
51-80	5 (10.4)	2 (4.2)	5 (10.4)	10 (20.8)
>80	1 (2.1)	0	1 (2.1)	7 (14.6)
Tau B	0.222			
p-value	0.078			
Total	48			

Nuclear Localisation of Gli1	Molecular subgroup			
	Lum A	Lum B	HER2	TN
	No. (%)	No. (%)	No. (%)	No. (%)
0	4 (8.3)	0	6 (12.5)	7 (14.6)
<10	5 (10.4)	0	1 (2.1)	2 (4.2)
10-50	1 (2.1)	3 (6.3)	3 (6.3)	7 (14.6)
>51	1 (2.1)	0	1 (2.1)	7 (14.6)
Tau B	0.195			
p-value	0.091			
Total	48			

Figure 11-11, The percentage of Gli1 positive tumour cells and nuclear localisation in tumour centre correlated with TNBC

Figure showing an increase of the percentage of Gli1 positive tumour cells and nuclear localisation of Gli1 in tumour centre of TNBC. Tables below the pie charts shows the numbers of cases, the molecular subgroup (LumA, LumB, HER2, and TN) and the percentage of positive tumour cells for Gli1 (presented as 0, <10, 10-50 and >51). The correlation was calculated using the Kendall's Tau B test. LumA = Luminal A, LumB = Luminal B, HER2 = Human EGF receptor 2, TNBC = Triple-negative breast cancer.

11.3.3 Gli2 expression correlated with lower stage, lower grade and negative lymph node involvement

Gli2 staining intensity was also higher in lower grade tumours, with low statistical significance (-0.309, *p*-value = 0.077) (Figure 11-12-A). The intensity of Gli2 staining at the invasive front increased in lower grade tumours (-0.266, *p*-value = 0.098) (Figure 11-12-B). Gli2 IRS class in the tumour centre also increased in lower grade tumours (-0.287) with low significance (*p*-value = 0.071) (Figure 11-13). In addition, increased Gli2 nuclear localisation was observed within lower grade tumours (-0.282, *p*-value = 0.08) (Figure 11-14).

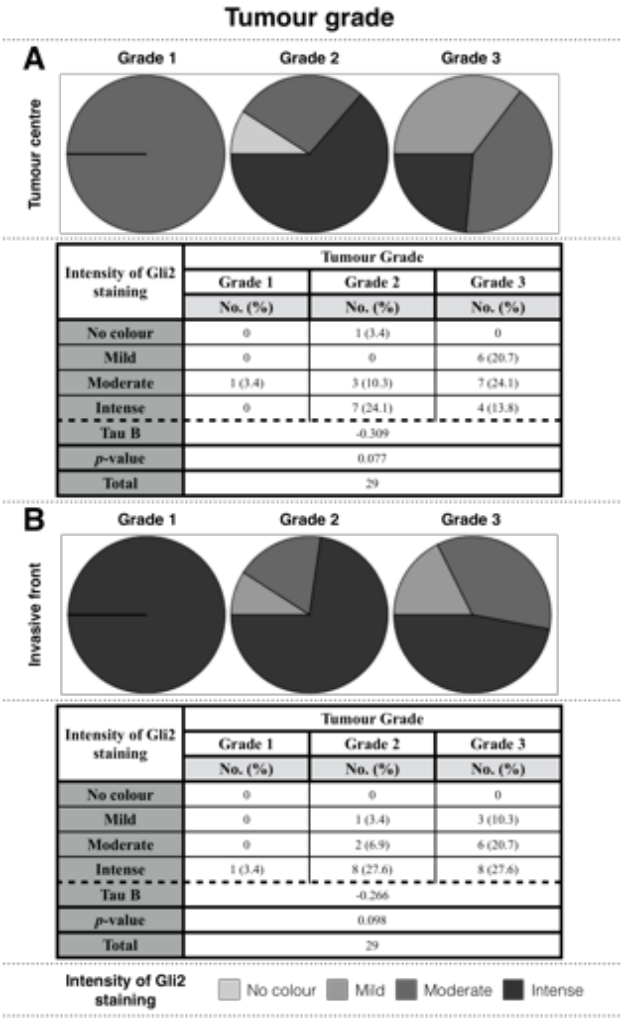

Intensity of Gli2 staining	Tumour Grade		
	Grade 1	Grade 2	Grade 3
	No. (%)	No. (%)	No. (%)
No colour	0	1 (3.4)	0
Mild	0	0	6 (20.7)
Moderate	1 (3.4)	3 (10.3)	7 (24.1)
Intense	0	7 (24.1)	4 (13.8)
Tau B	-0.309		
p-value	0.077		
Total	29		

Intensity of Gli2 staining	Tumour Grade		
	Grade 1	Grade 2	Grade 3
	No. (%)	No. (%)	No. (%)
No colour	0	0	0
Mild	0	1 (3.4)	3 (10.3)
Moderate	0	2 (6.9)	6 (20.7)
Intense	1 (3.4)	8 (27.6)	8 (27.6)
Tau B	-0.266		
p-value	0.098		
Total	29		

Figure 11-12, Intensity of Gli2 staining in the tumour centre and at the invasive front correlated negatively with tumour grade
Figure showing increase of Gli2 staining intensity in tumour centre and at invasive front correlated with lower tumour grade. Table below shows the numbers of cases, tumour grade (grade1, grade2, and grade 3) and the intensity of Gli3 staining in tumour centre and at invasive front. The correlation was calculated using the Kendall's Tau B test.

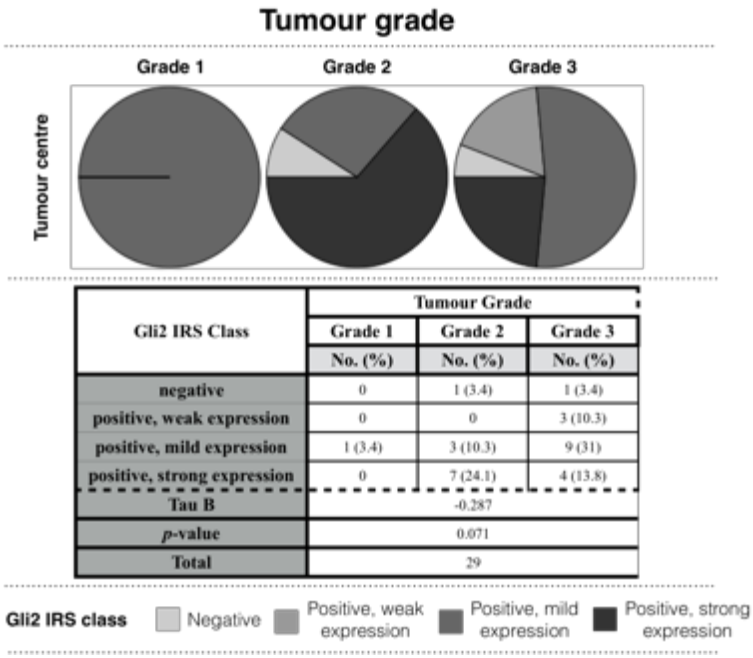

Gli2 IRS Class	Tumour Grade		
	Grade 1	Grade 2	Grade 3
	No. (%)	No. (%)	No. (%)
negative	0	1 (3.4)	1 (3.4)
positive, weak expression	0	0	3 (10.3)
positive, mild expression	1 (3.4)	3 (10.3)	9 (31)
positive, strong expression	0	7 (24.1)	4 (13.8)
Tau B	-0.287		
p-value	0.071		
Total	29		

Figure 11-13, Gli2 IRS class in the tumour centre correlated with lower tumour grade

Figure showing increase of Gli2 IRS class in tumour centre correlated with lower tumour grade. Table shows the numbers of cases, tumour grade (grade1, grade2, and grade3) and the IRS class of Gli2 staining. The correlation was calculated using the Kendall's Tau B test.

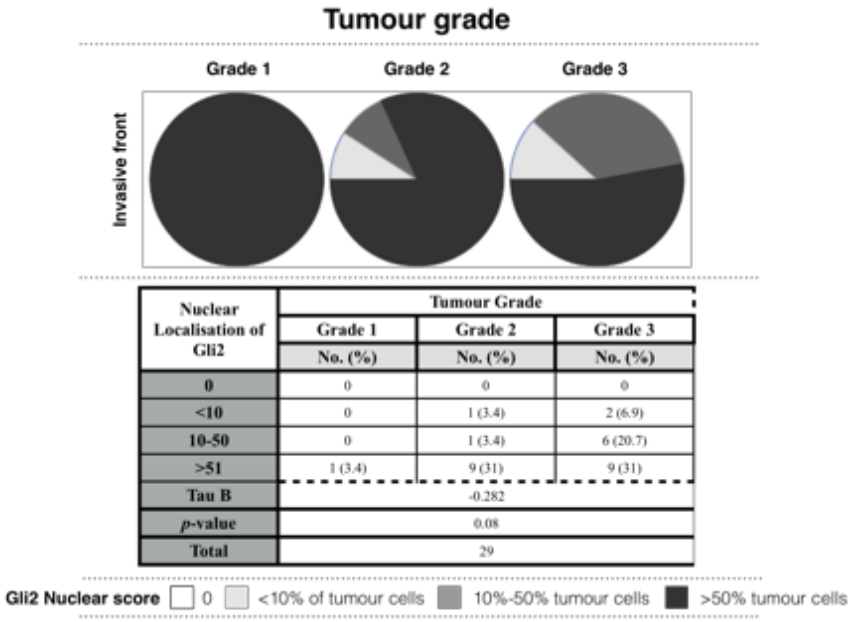

Nuclear Localisation of Gli2	Tumour Grade		
	Grade 1	Grade 2	Grade 3
	No. (%)	No. (%)	No. (%)
0	0	0	0
<10	0	1 (3.4)	2 (6.9)
10-50	0	1 (3.4)	6 (20.7)
>51	1 (3.4)	9 (31)	9 (31)
Tau B	-0.282		
p-value	0.08		
Total	29		

Figure 11-14, Increased nuclear localisation of Gli2 at the invasive front correlated with lower tumour grade

Figure showing increase of nuclear localisation of Gli2 at invasive front correlated with lower tumour grade. Table shows the numbers of cases, tumour grade (grade1, grade2 and grade3) and nuclear localisation of Gli2 (presented as 0, <10, 10-50, and >51). The correlation was calculated using the Kendall's Tau B test.

Lymph node involvement correlated negatively with the percentage of Gli2 positive expressing cells at the invasive front (-0.296, *p*-value = 0.06) (Figure 11-15). Higher Gli2 staining intensity was observed in tumours with negative lymph node involvement (-0.295, *p*-value = 0.077) (Figure 11-16). Increased nuclear localisation of Gli2 at the invasive front correlated with negative lymph node involvement (-0.32, *p*-value = 0.067) (Figure 11-17).

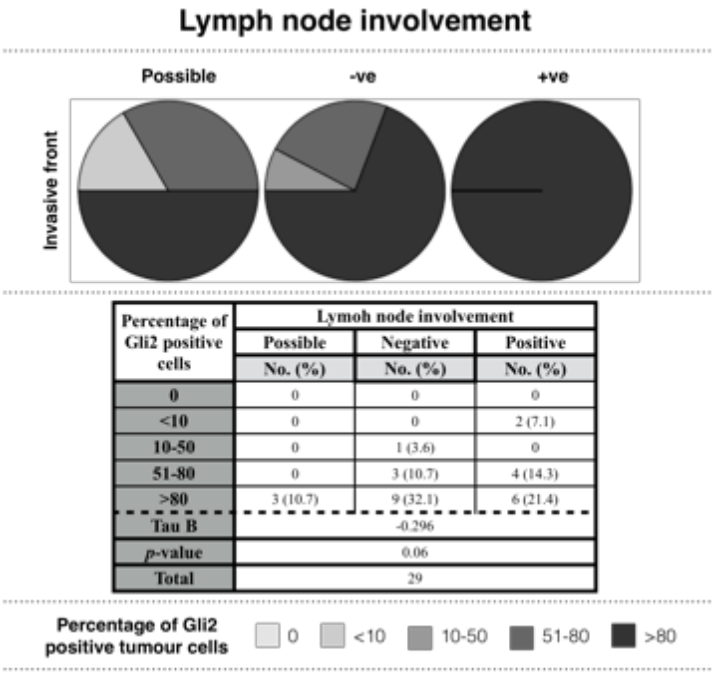

Percentage of Gli2 positive cells	Lymoh node involvement		
	Possible	Negative	Positive
	No. (%)	No. (%)	No. (%)
0	0	0	0
<10	0	0	2 (7.1)
10-50	0	1 (3.6)	0
51-80	0	3 (10.7)	4 (14.3)
>80	3 (10.7)	9 (32.1)	6 (21.4)
Tau B	-0.296		
p-value	0.06		
Total	29		

Figure 11-15, The percentage of Gli2 positive tumour cells at the invasive front correlated with negative lymph node involvement

Figure showing increase of percentage of Gli2 positive tumour cells at invasive front correlated with negative lymph node. Table below shows the numbers of cases, lymph node involvement (possible, negative or positive) and the percentage of Gli2 positive tumour cells at invasive front. The correlation was calculated using the Kendall's Tau B test.

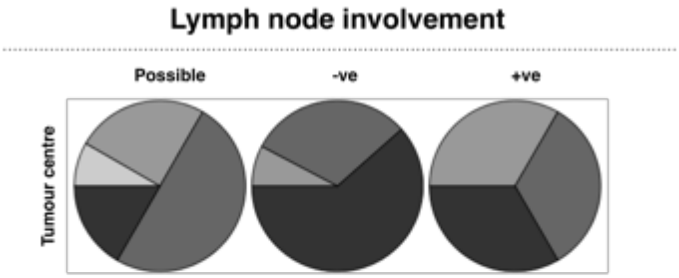

Intensity of Gli2 staining	Lymoh node involvement		
	Possible	Negative	Positive
	No. (%)	No. (%)	No. (%)
No colour	0	0	1 (3.6)
Mild	1 (3.6)	1 (3.6)	3 (10.7)
Moderate	1 (3.6)	4 (14.3)	6 (21.4)
Intense	1 (3.6)	8 (28.6)	2 (7.1)
Tau B	-0.295		
p-value	0.077		
Total	29		

Figure 11-16, Increased intensity of Gli2 staining correlated with negative lymph node involvement

Figure showing increase of intensity of Gli2 staining correlated with negative lymph node involvement. Table below shows the numbers of cases, lymph node involvement (possible, negative and positive), and the intensity of Gli2 staining (no colour, mild, moderate and intense) in tumour centre. The correlation was calculated using the Kendall's Tau B test.

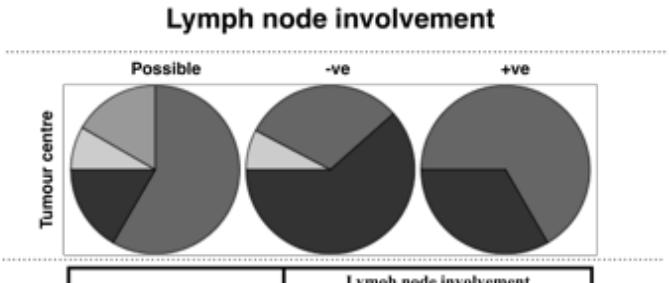

Gli2 IRS Class	Lymoh node involvement		
	Possible	Negative	Positive
	No. (%)	No. (%)	No. (%)
negative	0	1 (3.6)	1 (3.6)
positive, weak expression	0	0	2 (7.1)
positive, mild expression	2 (7.1)	4 (14.3)	7 (25)
positive, strong expression	1 (3.6)	8 (28.6)	2 (7.1)
Tau B	-0.321		
p-value	0.03		
Total	29		

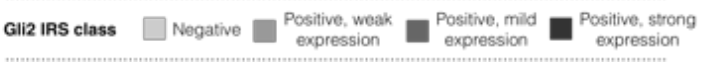

Figure 11-17, Higher Gli2 IRS class in the tumour centre correlated with lymph node negativity

Figure showing higher Gli2 IRS class in tumour centre correlated with negative lymph node involvement. Table shows the numbers of cases, lymph node involvement (possible, negative and positive) and Gli2 IRS class (negative, positive with weak expression, positive with mild expression and positive with strong expression) in tumour centre. The correlation was calculated using the Kendall's Tau B test.

11.3.4 Increased Gli3 correlated with younger mean age at diagnosis and hormone receptor-positive breast cancer

The percentage of Gli3 positive expressing cells in the tumour centre and at the invasive front correlated with a lower mean age at diagnosis (-0.302, *p*-value = 0.069). The percentage of Gli3 positivity in the tumour centre negatively correlated with molecular subgroup (-0.329, *p*-value = 0.074) (Figure 11-18). A lower percentage of Gli3 positive tumour cells was observed with TNBC (-0.331, *p*-value = 0.096).

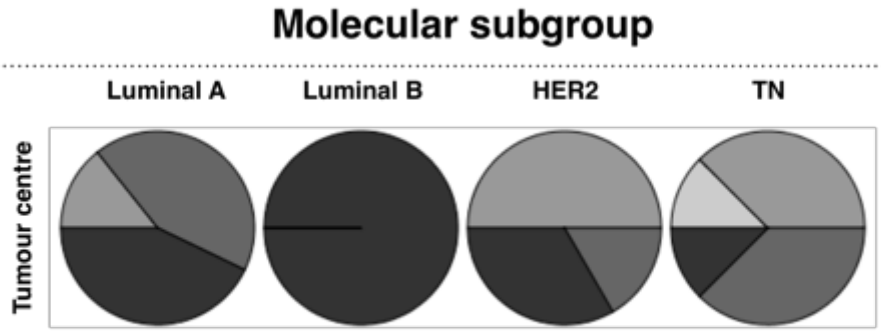

Percentage of positive cells	Molecular subgroup			
	Lum A	Lum B	HER2	TN
	No. (%)	No. (%)	No. (%)	No. (%)
0	0	0	0	0
<10	0	0	0	1 (4.3)
10-50	1 (4.30	0	3	3 (13)
51-80	3 (13)	0	1 (4.3)	3 (13)
>80	3 (13)	2 (8.7)	2 (8.7)	1 (4.3)
Tau B	-0.329			
p-value	0.074			
Total	23			

Figure 11-18, The percentage of Gli3 positive tumour cells correlated with hormone-positive breast cancer
Figure showing an increase in the percentage of Gli3 positive tumour cells in correlation with hormone-positive breast cancer. Table shows the numbers of cases, the molecular subgroup (LumA, LumB, HER2+ve, and TNBC) and the percentage of Gli3 positive tumour cells (presenter as 0, <10, 10-50, 51-80, and >80). The correlation was calculated using the Kendall's Tau B test. LumA = Luminal A, LumB = Luminal B, HER2 = Human EGF receptor 2, TNBC = Triple-negative breast cancer.

11.3.5 Gli1 and Gli2 were co-expressed in breast cancer samples

Table 11-8 summarises that the numbers and clinical criteria of the samples that were stained for all three Gli proteins. Gli1 and Gli2 were co-expressed in breast cancer

samples. The intensity of Gli1 staining in the tumour centre correlated with that of Gli2 in the tumour centre (0.596, *p*-value = 0.064) (Figure 11-19).

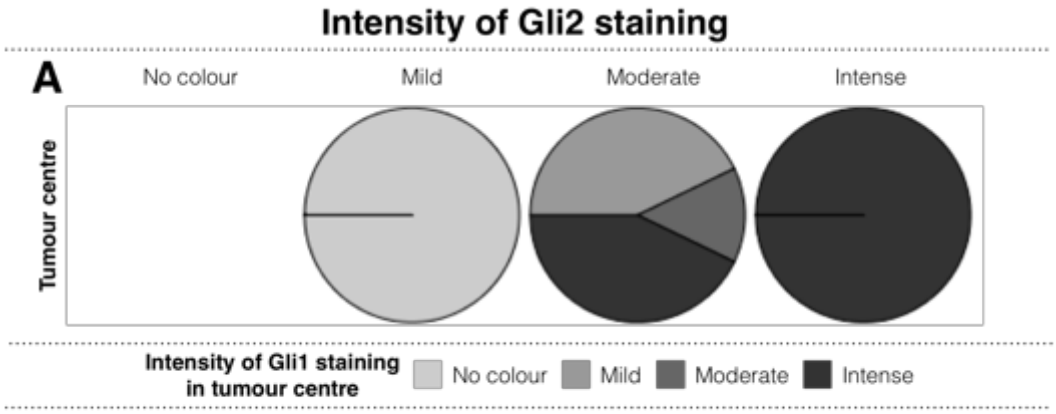

Figure 11-19, Correlation between Gli1 and Gli2 staining intensity in the tumour centre and at the invasive front
Figure showing correlation between Gli1 and Gli2 staining intensity in tumour centre and at invasive front. This correlation confirms a mutual increase of Gli1 and Gli2 intensity at the invasive front and in the tumour centre.

The increase in Gli2 staining in the tumour centre and at the invasive front was in parallel with increased Gli1 nuclear localisation at the invasive front (Figure 11-20). Increased Gli1 nuclear localisation at the invasive front was concomitant with an increase in proportion and intensity of Gli2 staining at the invasive front with high correlation coefficient at the invasive front (0.74, *p*-value = 0.063 and 0.745, *p*-value = 0.083).

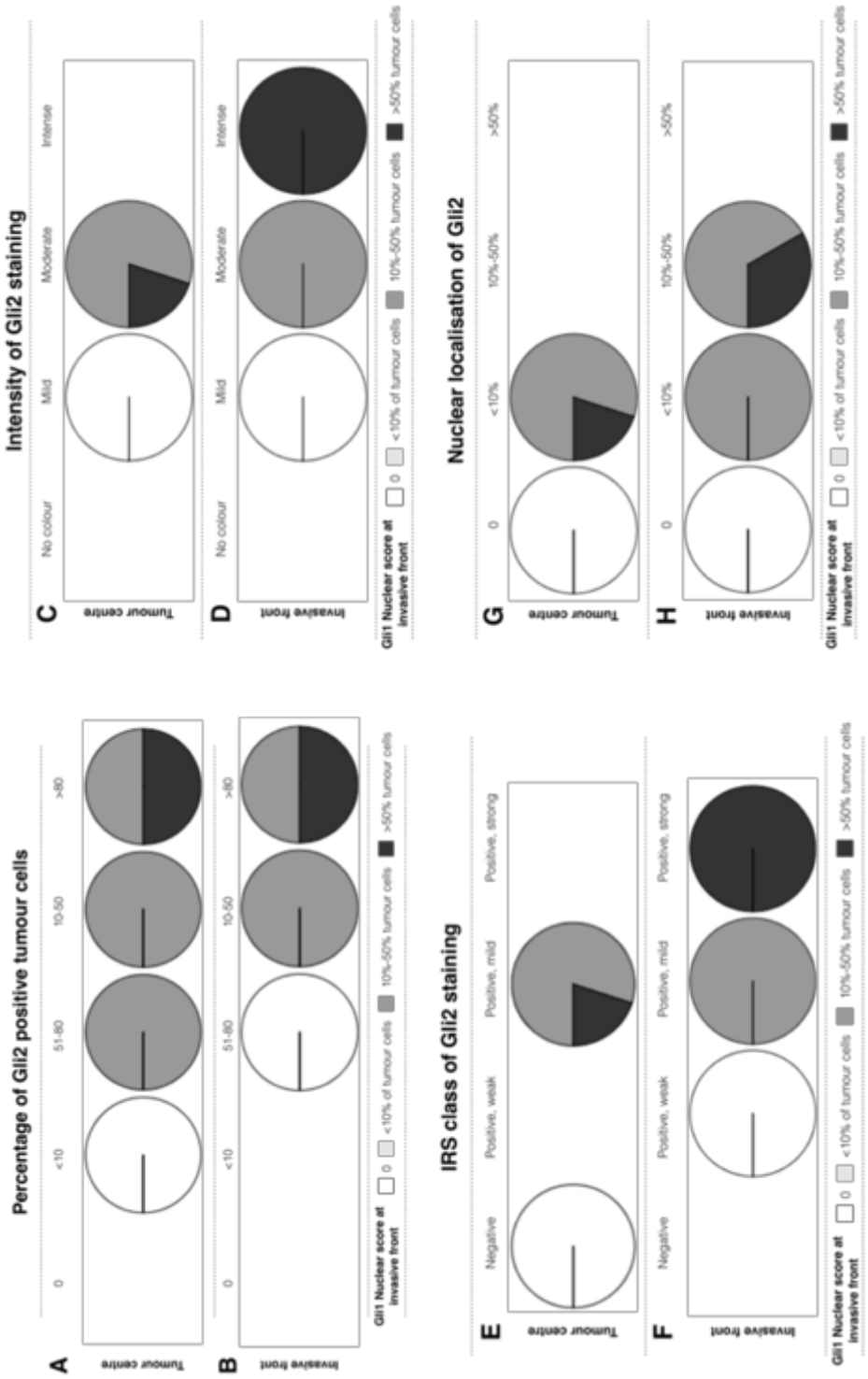

Figure 11-20, Nuclear localisation of Gli1 at the invasive front is correlated with Gli2 staining

Figure showing an increase in Gli1 nuclear localisation in correlation with an increase of Gli2 staining in the tumour centre and at the invasive front. (A and B) shows correlation between the percentage of Gli2 positive tumour cells and an increase in nuclear localisation of Gli1 at the invasive front. (C and D) showed correlation between Gli2 staining intensity and the increase in Gli1 localisation at the invasive front. (E and F) showed correlation between IRS class of Gli2 staining and the increase in nuclear localisation of Gli1 at the invasive front. (G and H) shows the correlation between increased nuclear localisation of Gli2 with increased localisation of Gli1 at the invasive front.

11.3.6 Expression of Gli occurs concomitantly with the expression of β-catenin in breast cancer samples, a marker EMT

β-catenin expression increased at the invasive front significantly (11.3.7). The increase in intensity and IRS class of Gli1 staining was positively correlated with increased in staining intensity and IRS class of β-catenin in serial sections(0.655, *p*-value = 0.094 and 0.745, *p*-value = 0.083, respectively) (Figure 11-21-A and Figure 11-21-B). The nuclear localisation of Gli1 increased concomitantly with β-catenin staining intensity (Figure 11-22-A) (0.745, *p*-value = 0.083) and IRS class (0.745, *p*-value = 0.083) (Figure 11-22-B).

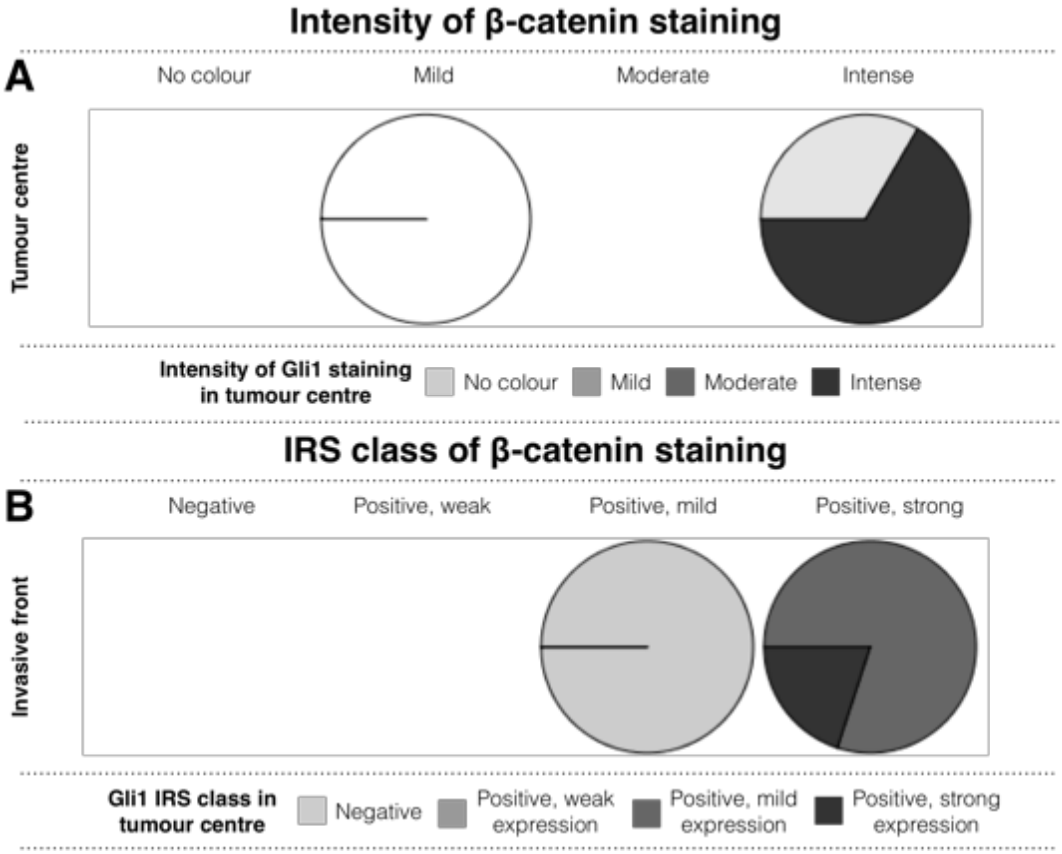

Figure 11-21, Co-expression of Gli1 and β-catenin in breast cancer samples in tumour centre and at invasive front
Figure showing an increase of Gli1 expression in parallel with β-catenin increased expression in the tumour centre and at the invasive front.

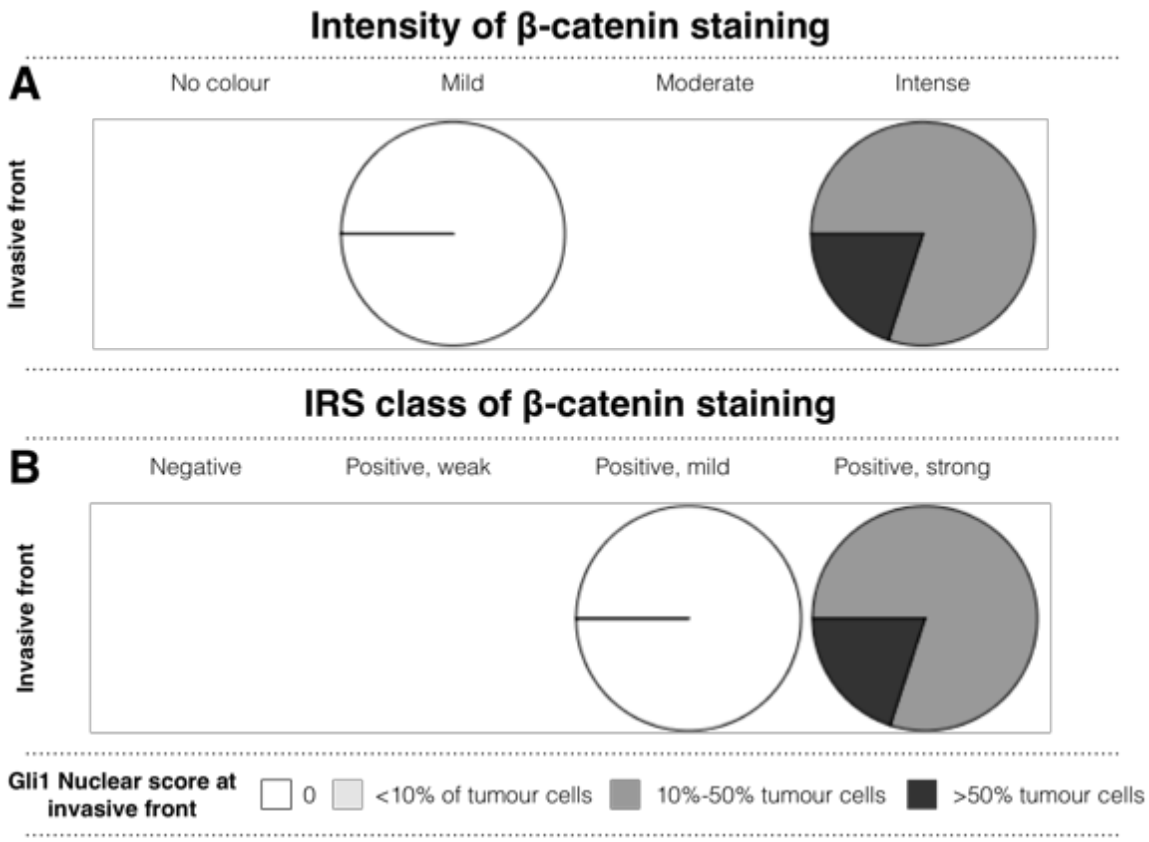

Figure 11-22, Correlation between nuclear localisation of Gli1 and β-catenin staining intensity and IRS class at invasive front
Figure showing increased nuclear localisation of Gli1 in association with an increase of β-catenin staining intensity (A) and IRS class (B) at the invasive front.

The percentage of Gli2 positivity decreased as the percentage of β-catenin tumour expressing cells increased in the tumour centre (-0.606, *p*-value = 0.085) (Figure 11-23). The staining intensity of Gli2 increased in the tumour centre and at the invasive front with increased intensity of β-catenin at the invasive front (0.739, *p*-value = 0.061 and 0.655, *p*-value = 0.094, respectively) (Figure 11-24-A and Figure 11-24-B). The IRS class of Gli2 in the tumour centre and at the invasive front correlated with IRS class of β-catenin at the invasive front (0.739, *p*-value = 0.061 and 0.655, *p*-value = 0.094, respectively) (Figure 11-25-A and Figure 11-25-B). The increase in IRS class of β-catenin at the invasive front was associated with increased IRS class of Gli2 in the tumour centre and at the invasive front.

The nuclear localisation of Gli2 in the tumour centre and the invasive front were associated with increased of β-catenin staining at the invasive front (Figure 11-26). Increased nuclear localisation of Gli2 in the tumour centre was observed to increase

with β-catenin intensity (0.739, *p*-value =0.061) (Figure 11-26-A) and IRS class (0.0739, *p*-value = 0.061) (Figure 11-26-B) at the invasive front. Gli2 nuclear localisation at the invasive front correlated also with intensity (0.655, *p*-value = 0.094) (Figure 11-26-C) and IRS class (0.0655, *p*-value = 0.094) (Figure 11-26-D) of β-catenin staining at the invasive front.

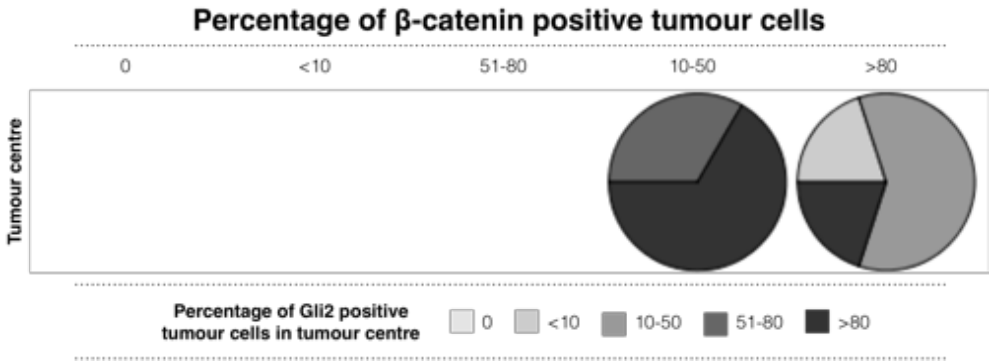

Figure 11-23, Gli2 expression is negatively correlated with β-catenin expression in tumour centre
Figure showing a decreased percentage of Gli2 expressing cells in association with an increased percentage of β-catenin tumour expressing cells.

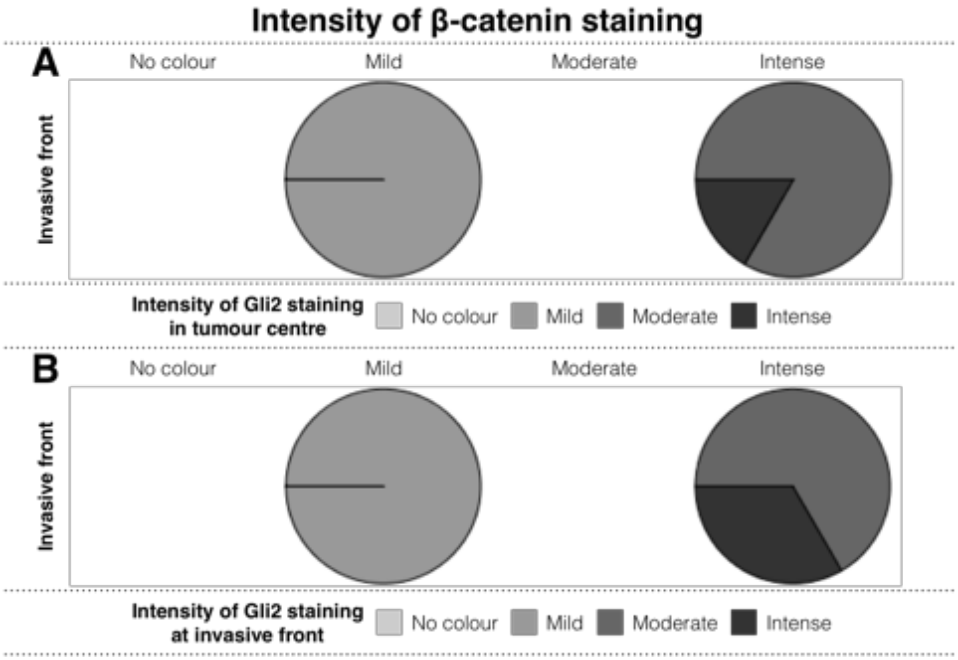

Figure 11-24, Increased Gli2 staining intensity in the tumour centre and invasive front in association with increased β-catenin staining intensity at the invasive front
Figure showing that increased intensity of Gli2 in the tumour centre and at the invasive front correlated with increased staining intensity of β-catenin at the invasive front.

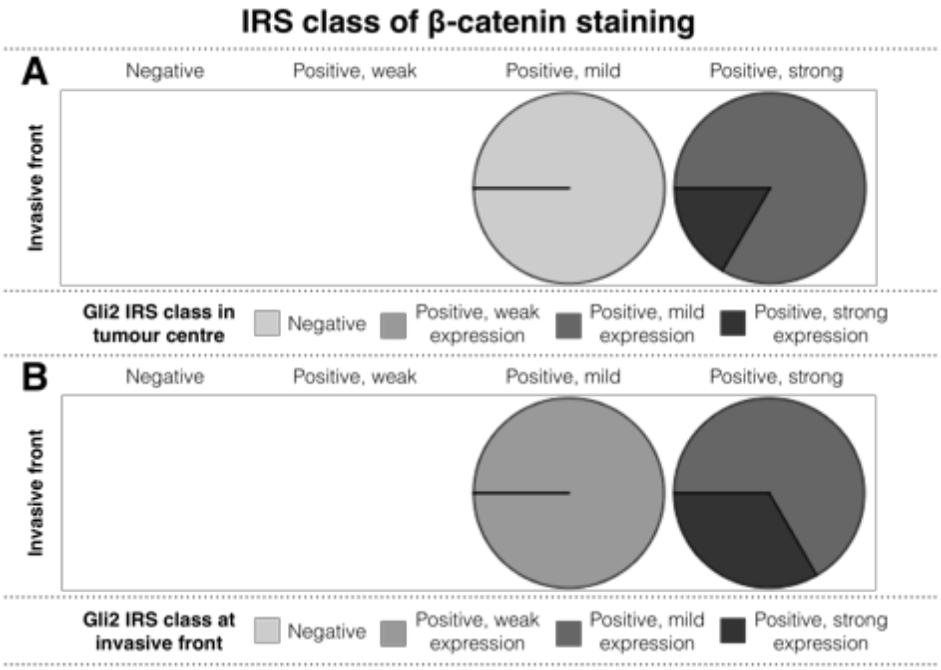

Figure 11-25, IRS class of Gli2 in the tumour centre and at the invasive front correlated with IRS class of β-catenin at the invasive front

Figure showing increase Gli2 IRS class in the tumour centre and at the invasive front in parallel with an increase of β-catenin at the invasive front.

Figure 11-26, Gli2 nuclear localisation in the tumour centre and at the invasive front were associated with increased β-catenin at the invasive front
Figure showing that the nuclear localisation of Gli2 in the tumour centre (A and B) and at the invasive front (C and D) correlated with β-catenin staining intensity (A and C) and IRS class (B and D).

Gli3 staining intensity (Figure 11-27-A) and IRS class (Figure 11-27-B) in the tumour centre correlated negatively with the percentage of β-catenin expressing tumour cells at the invasive front. Gli3 staining intensity was lower in the tumour centre of samples that had high expression of β-catenin at the invasive front (-0.653, *p*-value =

0.094). IRS class of Gli3 staining also showed a decrease with in samples that had a high percentage of positive tumour cells at the invasive front (-0.653, *p*-value = 0.094). Percentage of Gli3 positivity in the tumour centre decreased with increase nuclear localisation of β-catenin in the tumour centre (-0.601, *p*-value = 0.08) (Figure 11-28).

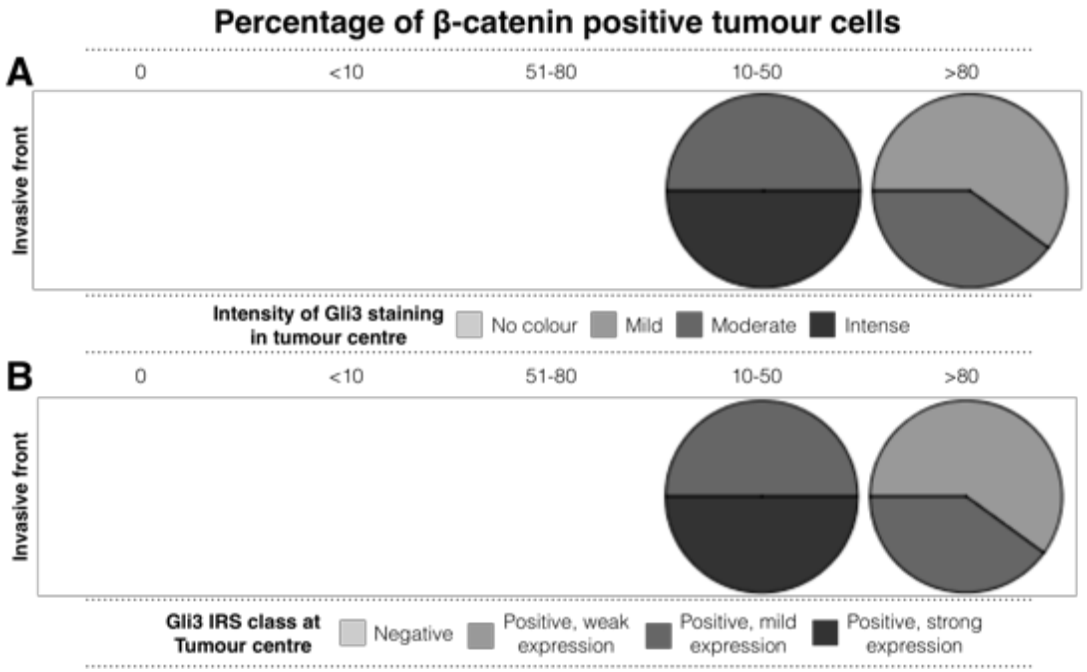

Figure 11-27, Gli3 staining intensity and IRS class in tumour centre correlate negatively with the percentage of β-catenin staining at the invasive front
Figure showing a decrease of Gli3 staining intensity and IRS class in tumour centre correlated with an increase of percentage of β-catenin positive tumour cells.

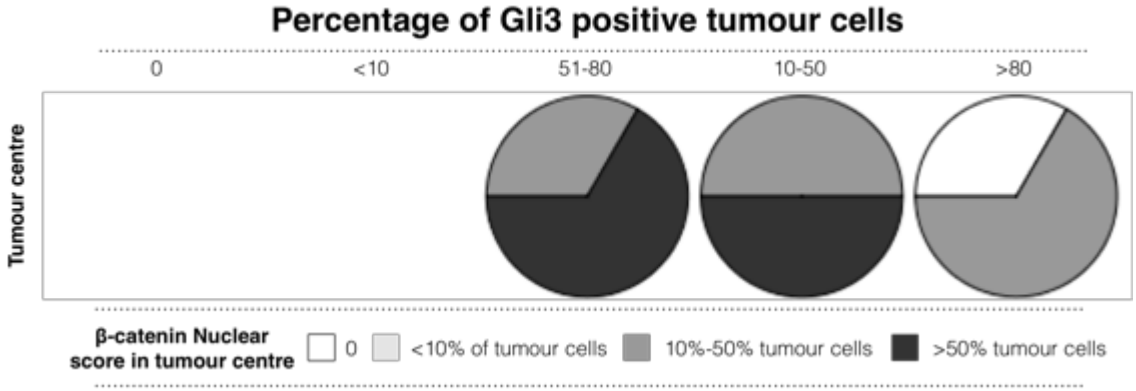

Figure 11-28, Decreased percentage of Gli3 positive tumour cells in the tumour centre correlate with increased β-catenin nuclear score in the tumour centre
Figure showing that increased nuclear localisation of β-catenin in the tumour centre correlated with lower percentage of Gli3 positive tumour cells in the tumour centre.

Table 11-8: Numbers and clinical criteria of breast cancer samples used for cross comparing Gli1, Gli2, Gli3, β-catenin and E-cadherin

Tables showing the number of breast cancer samples that were stained by Gli1, Gli2, Gli3, β-catenin and E-cadherin. The table also summarise the clinical parameters and the numbers of cases that correspond to each parameter. DCIS = Ductal carcinoma *in situ*, IDC = Invasive ductal carcinoma, NST = None specific type, HER2 = Human EGF receptor 2, ER, PR = progesterone receptor.

	Number	%
Tumour size		
2cm ≥	1	11.1
2cm <	8	88.9
Stage		
T1	4	44.4
T2	5	55.6
Grade		
Grade 1	1	11.1
Grade 2	2	22.2
Grade 3	6	66.7
Histological Subtype		
DCIS/IDC	4	44.4
IDC	4	44.4
NST	1	11.1
ER status		
Negative	7	77.8
Positive	2	22.2
PR status		
Negative	8	88.9
Positive	1	11.1
HER2 status		
Positive	4	44.4
Negative	5	55.6
Molecular subgroup		
Luminal A	2	22.2
HER2	4	44.4
Triple-negative	3	33.3
Lymph node involvement		
Positive	3	33.3
Negative	5	55.6
Possible	1	11.1

Table 11-9: Table showing the correlation of Gli1 expression with Age, tumour size, stage, grade, histological subtype, molecular subgroup and prognostic receptor status

Tables showing the correlation between the pathological parameters (age, tumour size, stage, grade, histological subtype, molecular subgroup, prognostic receptor status) with the (percentage of positivity, intensity of immune reaction, IRS class and nuclear score) of Gli1 in tumour centres and at the invasive fronts. DCIS = Ductal carcinoma *in situ*, IDC = Invasive ductal carcinoma, NST = None specific type, HER2 = Human EGF receptor 2, ER, PR = progesterone receptor. Highlighted in bold are the parameters that showed significance and close to significant correlation values.

		Tumour centre			Invasive front			Nuclear score	
		%	Intensity	IRS Class	%	Intensity	IRS Class	Tumour centre	Invasive front
Age	Correlation Coefficient	0.043	-0.09	-0.007	0.14	0.064	0.126	0.168	0.066
	Sig. (2-tailed)	0.698	0.417	0.948	0.282	0.622	0.33	0.13	0.608
	N	48	48	48	37	37	37	48	37
Tumour size	Correlation Coefficient	0.187	0.22	0.192	0.288	0.229	**.311***	**.295***	**.367***
	Sig. (2-tailed)	0.164	0.1	0.152	0.065	0.146	**0.046**	**0.027**	**0.018**
	N	48	48	48	37	37	**37**	**48**	**37**
Tumour stage	Correlation Coefficient	0.093	0.135	0.168	0.212	0.08	0.231	0.223	**.317***
	Sig. (2-tailed)	0.498	0.318	0.212	0.187	0.617	0.146	0.098	**0.043**
	N	45	45	45	34	34	34	45	**34**
Tumour grade	Correlation Coefficient	0.027	-0.063	0.027	0.055	-0.061	-0.043	0.048	0.042
	Sig. (2-tailed)	0.837	0.638	0.84	0.727	0.7	0.781	0.717	0.785
	N	48	48	48	37	37	37	48	37
Histological subtype	Correlation Coefficient	-0.067	0.004	0.014	0.114	0.064	-0.037	0.005	0.042
	Sig. (2-tailed)	0.582	0.977	0.908	0.419	0.65	0.791	0.969	0.762
	N	48	48	48	37	37	37	48	37
ER status	Correlation Coefficient	-0.162	0.234	0.078	0.024	0.194	0.104	-0.081	-0.092
	Sig. (2-tailed)	0.228	0.081	0.562	0.877	0.218	0.506	0.546	0.55
	N	48	48	48	37	37	37	48	37
PR status	Correlation Coefficient	-0.111	0.158	0.026	-0.035	0.15	0.014	-0.074	-0.084
	Sig. (2-tailed)	0.407	0.24	0.847	0.822	0.339	0.929	0.582	0.587
	N	48	48	48	37	37	37	48	37
HER2 status	Correlation Coefficient	0.114	-0.024	0.002	0.014	-0.159	-0.125	0.09	0.103
	Sig. (2-tailed)	0.399	0.859	0.991	0.928	0.313	0.422	0.5	0.506
	N	48	48	48	37	37	37	48	37
Molecular subgroup	Correlation Coefficient	0.222	-0.186	0.006	0.025	-0.172	-0.045	0.195	0.108
	Sig. (2-tailed)	0.078	0.137	0.96	0.862	0.244	0.756	0.119	0.455
	N	48	48	48	37	37	37	48	37
Lymph node involvement	Correlation Coefficient	-0.073	0.044	0.023	0.033	0.07	-0.071	0.073	-0.169
	Sig. (2-tailed)	0.582	0.741	0.861	0.828	0.649	0.645	0.582	0.265
	N	47	47	47	36	36	36	47	36

		Tumour centre			Invasive front			Nuclear score	
		%	Intensity	IRS Class.	%	Intensity	IRS Class.	Tumour centre	Invasive front
DUCTAL	Correlation Coefficient	0.192	0.014	0.04	-0.044	-0.028	0.067	0.034	-0.174
	Sig. (2-tailed)	0.153	0.918	0.767	0.781	0.861	0.669	0.802	0.261
	N	48	48	48	37	37	37	48	37
LOBULAR	Correlation Coefficient	-0.004	-0.103	-0.1	0.038	-0.066	-0.007	0.111	**.311***
	Sig. (2-tailed)	0.974	0.443	0.455	0.808	0.677	0.962	0.407	**0.044**
	N	48	48	48	37	37	37	48	**37**
DCIS	Correlation Coefficient	-0.097	0.024	-0.011	-0.182	-0.086	-0.009	-0.049	0.046
	Sig. (2-tailed)	0.469	0.859	0.934	0.246	0.584	0.955	0.714	0.765
	N	48	48	48	37	37	37	48	37
IDC	Correlation Coefficient	0.263	0.004	0.067	-0.032	-0.073	0.013	0.055	-0.227
	Sig. (2-tailed)	0.05	0.973	0.617	0.837	0.641	0.933	0.681	0.142
	N	48	48	48	37	37	37	48	37
LCIS	Correlation Coefficient	-0.118	-0.091	-0.13	0.126	-0.152	-0.101	0.036	0.109
	Sig. (2-tailed)	0.38	0.499	0.333	0.419	0.335	0.516	0.788	0.479
	N	48	48	48	37	37	37	48	37
ILC	Correlation Coefficient	-0.004	-0.103	-0.1	0.038	-0.066	-0.007	0.111	**.311***
	Sig. (2-tailed)	0.974	0.443	0.455	0.808	0.677	0.962	0.407	**0.044**
	N	48	48	48	37	37	37	48	**37**
LUMA	Correlation Coefficient	-0.16	0.157	-0.038	-0.035	0.043	-0.086	-0.17	-0.044
	Sig. (2-tailed)	0.235	0.242	0.778	0.822	0.785	0.58	0.206	0.778
	N	48	48	48	37	37	37	48	37
LUMB	Correlation Coefficient	-0.027	0.168	0.211	0.086	0.246	0.28	0.143	-0.086
	Sig. (2-tailed)	0.839	0.212	0.115	0.584	0.117	0.073	0.287	0.577
	N	48	48	48	37	37	37	48	37
HER2	Correlation Coefficient	-0.107	-0.071	-0.123	-0.073	0.013	-0.046	-0.18	-0.057
	Sig. (2-tailed)	0.426	0.598	0.357	0.643	0.935	0.766	0.179	0.712
	N	48	48	48	37	37	37	48	37
TNBC	Correlation Coefficient	0.238	-0.154	0.033	0.039	-0.177	-0.051	0.225	0.127
	Sig. (2-tailed)	0.077	0.252	0.805	0.803	0.26	0.743	0.093	0.413
	N	48	48	48	37	37	37	48	37

Table 11-10: Table showing the correlation of Gli2 expression with Age, tumour size, stage, grade, histological subtype, molecular subgroup and prognostic receptor status

Tables showing the correlation between the pathological parameters (age, tumour size, stage, grade, histological subtype, molecular subgroup, prognostic receptor status) with the (percentage of positivity, intensity of immune reaction, IRS class and nuclear score) of Gli2 in tumour centres and at the invasive fronts. DCIS = Ductal carcinoma *in situ*, IDC = Invasive ductal carcinoma, NST = None specific type, HER2 = Human EGF receptor 2, ER, PR = progesterone receptor. Highlighted in bold are the parameters that showed significance and close to significant correlation values.

		Tumour centre			Invasive front			Nuclear score	
		%	Intensity	IRS Class	%	Intensity	IRS Class	Tumour centre	Invasive front
Age	Correlation Coefficient	-0.132	0.044	0.003	0.003	-0.032	-0.042	-0.006	0.058
	Sig. (2-tailed)	0.37	0.763	0.984	0.982	0.83	0.78	0.968	0.702
	N	29	29	29	29	29	29	29	29
Tumour size	Correlation Coefficient	**-.348***	-0.138	-0.239	-0.201	-0.146	-0.183	-0.165	-0.077
	Sig. (2-tailed)	**0.05**	0.437	0.18	0.268	0.421	0.313	0.356	0.673
	N	**29**	29	29	29	29	29	29	29
Tumour stage	Correlation Coefficient	**-.480****	-0.136	-0.216	-0.232	-0.145	-0.178	-0.184	-0.292
	Sig. (2-tailed)	**0.009**	0.462	0.251	0.219	0.44	0.344	0.324	0.125
	N	**26**	26	26	26	26	26	26	26
Tumour grade	Correlation Coefficient	-0.269	-0.309	-0.287	0.009	-0.266	-0.25	**-.383***	-0.282
	Sig. (2-tailed)	0.124	0.077	0.102	0.958	0.136	0.162	**0.03**	0.118
	N	29	29	29	29	29	29	**29**	29
Histological subtype	Correlation Coefficient	0.31	0.154	0.241	**.330***	0.164	0.21	0.132	0.162
	Sig. (2-tailed)	0.057	0.344	0.14	**0.048**	0.323	0.206	0.422	0.334
	N	29	29	29	**29**	29	29	29	29
ER status	Correlation Coefficient	0.119	0.213	0.187	-0.105	0.122	0.112	0.247	0.199
	Sig. (2-tailed)	0.503	0.229	0.295	0.564	0.501	0.539	0.167	0.275
	N	29	29	29	29	29	29	29	29
PR status	Correlation Coefficient	0.067	0.167	0.146	-0.082	-0.013	-0.026	0.193	0.096
	Sig. (2-tailed)	0.707	0.346	0.412	0.651	0.943	0.885	0.279	0.598
	N	29	29	29	29	29	29	29	29
HER2 status	Correlation Coefficient	0.093	**.401***	0.329	0.154	0.191	0.174	**.368***	0.27
	Sig. (2-tailed)	0.598	**0.024**	0.065	0.399	0.291	0.337	**0.039**	0.14
	N	29	**29**	29	29	29	29	**29**	29
Molecular subgroup	Correlation Coefficient	-0.069	0.04	0.007	0.14	-0.043	-0.047	-0.011	-0.083
	Sig. (2-tailed)	0.678	0.813	0.965	0.412	0.8	0.782	0.948	0.629
	N	29	29	29	29	29	29	29	29
Lymph node involvement	Correlation Coefficient	**.419***	0.295	0.321	0.296	0.193	0.252	0.207	0.32
	Sig. (2-tailed)	**0.016**	0.091	0.068	0.097	0.276	0.156	0.238	0.074
	N	**28**	28	28	28	28	28	28	28

		Tumour centre			Invasive front			Nuclear score	
		%	Intensity	IRS Class.	%	Intensity	IRS Class.	Tumour centre	Invasive front
DUCTAL	Correlation Coefficient	**-.416***	-0.023	-0.151	**-.423***	-0.171	-0.222	-0.033	-0.149
	Sig. (2-tailed)	**0.019**	0.897	0.398	**0.02**	0.346	0.221	0.855	0.416
	N	**29**	29	29	**29**	29	29	29	29
LOBULAR	Correlation Coefficient	.	.	.	.	.	.	.	.
	Sig. (2-tailed)	.	.	.	.	.	.	.	.
	N	29	29	29	29	29	29	29	29
DCIS	Correlation Coefficient	-0.17	-0.167	-0.226	-0.278	-0.137	-0.174	-0.114	-0.145
	Sig. (2-tailed)	0.338	0.346	0.204	0.126	0.451	0.337	0.523	0.429
	N	29	29	29	29	29	29	29	29
IDC	Correlation Coefficient	-0.33	0.071	-0.045	**-.460***	-0.223	-0.273	0.068	-0.195
	Sig. (2-tailed)	0.063	0.688	0.799	**0.012**	0.218	0.132	0.705	0.286
	N	29	29	29	**29**	29	29	29	29
LCIS	Correlation Coefficient	.	.	.	.	.	.	.	.
	Sig. (2-tailed)	.	.	.	.	.	.	.	.
	N	29	29	29	29	29	29	29	29
ILC	Correlation Coefficient	0.172	0.203	0.207	0.129	0.148	0.149	0.217	0.13
	Sig. (2-tailed)	0.333	0.252	0.245	0.477	0.416	0.414	0.225	0.476
	N	29	29	29	29	29	29	29	29
LUMA	Correlation Coefficient	0.144	0.251	0.234	-0.013	0.208	0.203	0.281	0.314
	Sig. (2-tailed)	0.417	0.158	0.19	0.945	0.251	0.263	0.116	0.085
	N	29	29	29	29	29	29	29	29
LUMB	Correlation Coefficient	-0.034	-0.045	-0.069	-0.207	-0.16	-0.173	-0.034	-0.208
	Sig. (2-tailed)	0.846	0.799	0.698	0.255	0.378	0.34	0.848	0.255
	N	29	29	29	29	29	29	29	29
HER2	Correlation Coefficient	-0.082	**-.390***	-0.308	-0.078	-0.134	-0.112	**-.361***	-0.196
	Sig. (2-tailed)	0.644	**0.028**	0.084	0.669	0.459	0.539	**0.044**	0.284
	N	29	**29**	29	29	29	29	**29**	29
TNBC	Correlation Coefficient	-0.017	0.209	0.149	0.163	0.032	0.018	0.152	0.029
	Sig. (2-tailed)	0.924	0.239	0.402	0.37	0.86	0.92	0.394	0.874
	N	29	29	29	29	29	29	29	29

Table 11-11: Table showing the correlation of Gli3 expression with Age, tumour size, stage, grade, histological subtype, molecular subgroup and prognostic receptor status

Tables showing the correlation between the pathological parameters (age, tumour size, stage, grade, histological subtype, molecular subgroup, prognostic receptor status) with the (percentage of positivity, intensity of immune reaction, IRS class and nuclear score) of Gli3 in tumour centres and at the invasive fronts. DCIS = Ductal carcinoma *in situ*, IDC = Invasive ductal carcinoma, NST = None specific type, HER2 = Human EGF receptor 2, ER, PR = progesterone receptor. Highlighted in bold are the parameters that showed significance and close to significant correlation values.

		Tumour centre			Invasive front			Nuclear score	
		%	Intensity	IRS Class	%	Intensity	IRS Class	Tumour centre	Invasive front
Age	Correlation Coefficient	-0.302	0.167	0.005	**-.495***	0.067	0.057	-0.08	-0.079
	Sig. (2-tailed)	0.069	0.325	0.977	**0.015**	0.731	0.779	0.629	0.699
	N	23	23	23	**18**	18	18	23	16
Tumour size	Correlation Coefficient	-0.162	0.219	0.075	-0.081	-0.095	-0.161	0.039	-0.084
	Sig. (2-tailed)	0.415	0.28	0.711	0.74	0.684	0.506	0.842	0.729
	N	23	23	23	18	18	18	23	16
Tumour stage	Correlation Coefficient	0	0.174	0.201	0	0	0	-0.09	-0.188
	Sig. (2-tailed)	1	0.406	0.331	1	1	1	0.658	0.438
	N	21	21	21	17	17	17	21	15
Tumour grade	Correlation Coefficient	-0.069	0.119	0.053	0.038	0.034	-0.038	0.006	0.038
	Sig. (2-tailed)	0.724	0.55	0.791	0.873	0.883	0.873	0.974	0.87
	N	23	23	23	18	18	18	23	16
Histological subtype	Correlation Coefficient	0.269	0	0.118	0.089	**.502***	**.512***	**.391***	**.671****
	Sig. (2-tailed)	0.143	1	0.525	0.693	**0.021**	**0.023**	**0.032**	**0.003**
	N	23	23	23	18	**18**	**18**	**23**	**16**
ER status	Correlation Coefficient	**.402***	-0.007	0.207	0.081	0.095	0.161	0.093	0.068
	Sig. (2-tailed)	**0.043**	0.973	0.305	0.74	0.684	0.506	0.637	0.778
	N	**23**	23	23	18	18	18	23	16
PR status	Correlation Coefficient	**.468***	0.074	0.204	0.316	0.062	0	0.284	0.19
	Sig. (2-tailed)	**0.019**	0.715	0.312	0.192	0.79	1	0.151	0.431
	N	**23**	23	23	18	18	18	23	16
HER2 status	Correlation Coefficient	-0.121	-0.299	-0.304	-0.322	-0.048	0.081	-0.061	0.204
	Sig. (2-tailed)	0.541	0.14	0.132	0.184	0.839	0.74	0.756	0.398
	N	23	23	23	18	18	18	23	16
Molecular subgroup	Correlation Coefficient	-0.329	-0.091	-0.226	-0.12	-0.212	-0.272	-0.202	-0.112
	Sig. (2-tailed)	0.074	0.628	0.226	0.592	0.325	0.223	0.27	0.615
	N	23	23	23	18	18	18	23	16
Lymph node involvement	Correlation Coefficient	-0.025	-0.159	-0.184	-0.025	-0.235	-0.19	0.044	-0.104
	Sig. (2-tailed)	0.898	0.425	0.353	0.915	0.304	0.424	0.819	0.659
	N	23	23	23	18	18	18	23	16

		Tumour centre			Invasive front			Nuclear score	
		%	Intensity	IRS Class.	%	Intensity	IRS Class.	Tumour centre	Invasive front
DUCTAL	Correlation Coefficient	-0.209	-0.078	-0.17	0	**-.688****	**-.750****	**-.403***	**-.585***
	Sig. (2-tailed)	0.292	0.699	0.4	1	**0.003**	**0.002**	**0.042**	**0.015**
	N	23	23	23	18	**18**	**18**	**23**	**16**
LOBULAR	Correlation Coefficient	0	0.117	0.099	-0.343	0.303	0.343	-0.096	-0.028
	Sig. (2-tailed)	1	0.566	0.623	0.157	0.194	0.157	0.629	0.908
	N	23	23	23	18	18	18	23	16
DCIS	Correlation Coefficient	-0.279	0.118	-0.007	-0.088	-0.207	-0.175	-0.219	**-.567***
	Sig. (2-tailed)	0.16	0.561	0.971	0.718	0.376	0.47	0.268	**0.019**
	N	23	23	23	18	18	18	23	**16**
IDC	Correlation Coefficient	-0.209	-0.078	-0.17	0	**-.688****	**-.750****	**-.403***	**-.585***
	Sig. (2-tailed)	0.292	0.699	0.4	1	**0.003**	**0.002**	**0.042**	**0.015**
	N	23	23	23	18	**18**	**18**	**23**	**16**
LCIS	Correlation Coefficient	0	0.117	0.099	-0.343	0.303	0.343	-0.096	-0.028
	Sig. (2-tailed)	1	0.566	0.623	0.157	0.194	0.157	0.629	0.908
	N	23	23	23	18	18	18	23	16
ILC	Correlation Coefficient	0	0.117	0.099	-0.343	0.303	0.343	-0.096	-0.028
	Sig. (2-tailed)	1	0.566	0.623	0.157	0.194	0.157	0.629	0.908
	N	23	23	23	18	18	18	23	16
LUMA	Correlation Coefficient	0.217	-0.059	0.029	-0.088	0.207	0.351	0.184	0.247
	Sig. (2-tailed)	0.276	0.771	0.885	0.718	0.376	0.148	0.353	0.305
	N	23	23	23	18	18	18	23	16
LUMB	Correlation Coefficient	0.342	0.084	0.31	0.25	-0.147	-0.25	-0.138	-0.245
	Sig. (2-tailed)	0.085	0.678	0.123	0.303	0.528	0.303	0.484	0.31
	N	23	23	23	18	18	18	23	16
HER2	Correlation Coefficient	-0.088	0.271	0.13	0.175	0.155	0.088	0.155	-0.044
	Sig. (2-tailed)	0.658	0.183	0.518	0.47	0.506	0.718	0.432	0.856
	N	23	23	23	18	18	18	23	16
TNBC	Correlation Coefficient	-0.331	-0.242	-0.332	-0.25	-0.246	-0.25	-0.239	-0.031
	Sig. (2-tailed)	0.096	0.233	0.099	0.303	0.293	0.303	0.227	0.897
	N	23	23	23	18	18	18	23	16

Table 11-12: Table showing the correlation between Gli and Gli2

Tables showing the correlation between with the (percentage of positivity, intensity of immune reaction, IRS class and nuclear score) of Gli1 and Gli2 in tumour centres and at the invasive fronts.

				Gli2							
				Tumour centre			Invasive front			Nuclear score	
				%	Intensity	IRS Class	%	Intensity	IRS Class	Tumour centre	Invasive front
Gli1	Tumour centre	%	Correlation Coefficient	-0.138	-0.432	-0.432	-0.073	-0.227	-0.271	-0.332	-0.253
			Sig. (2-tailed)	0.648	0.175	0.175	0.814	0.469	0.389	0.293	0.451
			N	9	9	9	9	9	9	9	8
		Intensity	Correlation Coefficient	0.5	0.596	0.596	0.491	0.393	0.602	0.301	0.476
			Sig. (2-tailed)	0.102	0.064	0.064	0.118	0.217	0.059	0.346	0.161
			N	9	9	9	9	9	9	9	8
		IRS Class	Correlation Coefficient	**.715***	0.497	0.497	**.755***	0.55	**.762***	0.215	0.582
			Sig. (2-tailed)	**0.019**	0.123	0.123	**0.016**	0.084	**0.017**	0.501	0.087
			N	**9**	9	9	**9**	9	**9**	9	8
	Invasive front	%	Correlation Coefficient	0.167	-0.405	-0.405	0.273	0	0	-0.405	0
			Sig. (2-tailed)	0.671	0.343	0.343	0.503	1	1	0.343	1
			N	6	6	6	6	6	6	6	6
		Intensity	Correlation Coefficient	0.418	0.674	0.674	0.545	0.804	0.804	0.674	**.818***
			Sig. (2-tailed)	0.289	0.114	0.114	0.181	0.051	0.051	0.114	**0.045**
			N	6	6	6	6	6	6	6	**6**
		IRS Class	Correlation Coefficient	0.74	0.745	0.745	0.804	**1.000***	**1.000***	0.745	0.704
			Sig. (2-tailed)	0.063	0.083	0.083	0.051	**.**	**.**	0.083	0.087
			N	6	6	6	6	**0**	**6**	6	6
	Nuclear score	Tumour centre	Correlation Coefficient	0.379	0	0	0.546	0	0.232	-0.249	0.253
			Sig. (2-tailed)	0.209	1	1	0.078	1	0.46	0.43	0.451
			N	9	9	9	9	9	9	9	8
		Invasive front	Correlation Coefficient	0.74	0.745	0.745	0.804	**1.000***	**1.000***	0.745	0.704
			Sig. (2-tailed)	0.063	0.083	0.083	0.051	**.**	**.**	0.083	0.087
			N	6	6	6	6	**6**	**6**	6	6

Table 11-13: Table showing the correlation of Gli1 and Gli3

Tables showing the correlation between with the (percentage of positivity, intensity of immune reaction, IRS class and nuclear score) of Gli1 and Gli3 in tumour centres and at the invasive fronts.

				Gli3							
				Tumour centre			Invasive front			Nuclear score	
				%	Intensity	IRS Class	%	Intensity	IRS Class	Tumour centre	Invasive front
Gli1	Tumour centre	%	Correlation Coefficient	-0.182	-0.455	-0.455	-0.408	0.102	.	-0.291	0
			Sig. (2-tailed)	0.557	0.148	0.148	0.29	0.791	.	0.347	1
			N	9	9	9	7	7	7	9	6
		Intensity	Correlation Coefficient	-0.038	0.354	0.354	0.297	0	.	0.377	0.087
			Sig. (2-tailed)	0.904	0.267	0.267	0.432	1	.	0.229	0.827
			N	9	9	9	7	7	7	9	6
		IRS Class	Correlation Coefficient	-0.34	-0.118	-0.118	-0.198	-0.198	.	0.189	-0.087
			Sig. (2-tailed)	0.279	0.711	0.711	0.6	0.6	.	0.547	0.827
			N	9	9	9	7	7	7	9	6
	Invasive front	%	Correlation Coefficient	-0.364	**-.905***	**-.905***	-0.405	.	.	-0.545	0
			Sig. (2-tailed)	0.372	**0.034**	**0.034**	0.343	.	.	0.181	1
			N	6	**6**	**6**	6	6	6	6	5
		Intensity	Correlation Coefficient	0	0.201	0.201	0.135	.	.	0.545	0.617
			Sig. (2-tailed)	1	0.637	0.637	0.752	.	.	0.181	0.197
			N	6	6	6	6	6	6	6	5
		IRS Class	Correlation Coefficient	-0.402	0	0	0	.	.	0.302	0
			Sig. (2-tailed)	0.328	1	1	1	.	.	0.463	1
			N	6	6	6	6	6	6	6	5
	Nuclear score	Tumour centre	Correlation Coefficient	-0.546	-0.379	-0.379	-0.297	0.198	.	0.109	0.261
			Sig. (2-tailed)	0.078	0.228	0.228	0.432	0.6	.	0.724	0.511
			N	9	9	9	7	7	7	9	6
		Invasive front	Correlation Coefficient	-0.402	0	0	0	.	.	0.302	0
			Sig. (2-tailed)	0.328	1	1	1	.	.	0.463	1
			N	6	6	6	6	6	6	6	5

Table 11-14: Table showing the correlation of Gli1 and β-catenin

Tables showing the correlation between with the (percentage of positivity, intensity of immune reaction, IRS class and nuclear score) of Gli1 and β-catenin in tumour centres and at the invasive fronts.

				β-catenin							
				Tumour centre			Invasive front			Nuclear score	
				%	Intensity	IRS Class	%	Intensity	IRS Class	Tumour centre	Invasive front
Gli1	Tumour centre	%	Correlation Coefficient	0.215	.	.	0.537	-0.396	-0.396	-0.048	-0.519
			Sig. (2-tailed)	0.536	.	.	0.155	0.295	0.295	0.886	0.153
			N	8	8	8	7	7	7	8	7
		Intensity	Correlation Coefficient	-0.296	.	.	-0.507	0.655	0.655	0.316	0.571
			Sig. (2-tailed)	0.414	.	.	0.195	0.094	0.094	0.365	0.128
			N	8	8	8	7	7	7	8	7
		IRS Class	Correlation Coefficient	-0.165	.	.	0.077	0.594	0.594	0.391	0.194
			Sig. (2-tailed)	0.638	.	.	0.839	0.116	0.116	0.247	0.592
			N	8	8	8	7	7	7	8	7
	Invasive front	%	Correlation Coefficient	0.107	.	.	0.539	-0.405	-0.405	-0.201	-0.64
			Sig. (2-tailed)	0.803	.	.	0.206	0.343	0.343	0.637	0.134
			N	6	6	6	6	6	6	6	6
		Intensity	Correlation Coefficient	0.213	.	.	0.135	0.674	0.674	0.201	0.64
			Sig. (2-tailed)	0.617	.	.	0.752	0.114	0.114	0.637	0.134
			N	6	6	6	6	6	6	6	6
		IRS Class	Correlation Coefficient	0	.	.	0	0.745	0.745	0.556	0.589
			Sig. (2-tailed)	1	.	.	1	0.083	0.083	0.197	0.171
			N	6	6	6	6	6	6	6	6
	Nuclear score	Tumour centre	Correlation Coefficient	0.054	.	.	0.447	0.481	0.481	0.622	0.378
			Sig. (2-tailed)	0.877	.	.	0.232	0.199	0.199	0.063	0.294
			N	8	8	8	7	7	7	8	7
		Invasive front	Correlation Coefficient	0	.	.	0	0.745	0.745	0.556	0.589
			Sig. (2-tailed)	1	.	.	1	0.083	0.083	0.197	0.171
			N	6	6	6	6	6	6	6	6

Table 11-15: Table showing the correlation of Gli1 and E-cadherin

Tables showing the correlation between with the (percentage of positivity, intensity of immune reaction, IRS class and nuclear score) of Gli1 and E-cadherin in tumour centres and at the invasive fronts.

				E-cadherin							
				Tumour centre			Invasive front			Nuclear score	
				%	Intensity	IRS Class	%	Intensity	IRS Class	Tumour centre	Invasive front
Gli1	Tumour centre	%	Correlation Coefficient	0.405	-0.215	-0.054	-0.096	-0.473	-0.473	0.405	-0.215
			Sig. (2-tailed)	0.228	0.536	0.877	0.775	0.174	0.174	0.228	0.536
			N	8	8	8	8	8	8	8	8
		Intensity	Correlation Coefficient	-0.278	-0.118	-0.118	0.211	0.434	0.434	-0.278	-0.118
			Sig. (2-tailed)	0.426	0.744	0.744	0.546	0.232	0.232	0.426	0.744
			N	8	8	8	8	8	8	8	8
		IRS Class	Correlation Coefficient	0.556	-0.474	-0.059	0.211	-0.173	-0.173	0.556	-0.474
			Sig. (2-tailed)	0.111	0.191	0.87	0.546	0.633	0.633	0.111	0.191
			N	8	8	8	8	8	8	8	8
	Invasive front	%	Correlation Coefficient	0.625	-0.53	.	0.267	0	0	0.625	-0.53
			Sig. (2-tailed)	0.167	0.264	.	0.557	1	1	0.167	0.264
			N	5	5	5	5	5	5	5	5
		Intensity	Correlation Coefficient	0	0.612	.	0.617	0.408	0.408	0	0.612
			Sig. (2-tailed)	1	0.221	.	0.197	0.414	0.414	1	0.221
			N	5	5	5	5	5	5	5	5
		IRS Class	Correlation Coefficient	0.53	-0.25	.	0.756	0.25	0.25	0.53	-0.25
			Sig. (2-tailed)	0.264	0.617	.	0.114	0.617	0.617	0.264	0.617
			N	5	5	5	5	5	5	5	5
	Nuclear score	Tumour centre	Correlation Coefficient	0	-0.431	**-.700***	-0.383	-0.315	-0.315	0	-0.431
			Sig. (2-tailed)	1	0.216	**0.044**	0.253	0.365	0.365	1	0.216
			N	8	8	**8**	8	8	8	8	8
		Invasive front	Correlation Coefficient	0.53	-0.25	.	0.756	0.25	0.25	0.53	-0.25
			Sig. (2-tailed)	0.264	0.617	.	0.114	0.617	0.617	0.264	0.617
			N	5	5	5	5	5	5	5	5

Table 11-16: Table showing the correlation of Gli2 and Gli3

Tables showing the correlation between with the (percentage of positivity, intensity of immune reaction, IRS class and nuclear score) of Gli2 and Gli3 in tumour centres and at the invasive fronts.

				Gli3							
				Tumour centre			Invasive front			Nuclear score	
				%	Intensity	IRS Class	%	Intensity	IRS Class	Tumour centre	Invasive front
Gli2	Tumour centre	%	Correlation Coefficient	-0.364	-0.038	-0.038	-0.481	-0.096	.	0.109	-0.167
			Sig. (2-tailed)	0.24	0.904	0.904	0.199	0.797	.	0.724	0.672
			N	9	9	9	7	7	7	9	6
		Intensity	Correlation Coefficient	0.203	0.632	0.632	-0.167	-0.167	.	0.608	.
			Sig. (2-tailed)	0.535	0.056	0.056	0.683	0.683	.	0.063	.
			N	9	9	9	7	7	7	9	6
		IRS Class	Correlation Coefficient	0.203	0.632	0.632	-0.167	-0.167	.	0.608	.
			Sig. (2-tailed)	0.535	0.056	0.056	0.683	0.683	.	0.063	.
			N	9	9	9	7	7	7	9	6
	Invasive front	%	Correlation Coefficient	-0.308	0	0	-0.546	0.109	.	0.308	0.204
			Sig. (2-tailed)	0.333	1	1	0.163	0.78	.	0.333	0.623
			N	9	9	9	7	7	7	9	6
		Intensity	Correlation Coefficient	0.04	0.167	0.167	0.109	-0.546	.	0.04	-0.408
			Sig. (2-tailed)	0.901	0.611	0.611	0.78	0.163	.	0.901	0.325
			N	9	9	9	7	7	7	9	6
		IRS Class	Correlation Coefficient	-0.164	0.085	0.085	0.109	-0.546	.	0.123	-0.408
			Sig. (2-tailed)	0.613	0.795	0.795	0.78	0.163	.	0.704	0.325
			N	9	9	9	7	7	7	9	6
	Nuclear score	Tumour centre	Correlation Coefficient	0.395	0.639	0.639	-0.167	-0.167	.	0.439	.
			Sig. (2-tailed)	0.223	0.052	0.052	0.683	0.683	.	0.176	.
			N	9	9	9	7	7	7	9	6
		Invasive front	Correlation Coefficient	-0.054	0	0	-0.327	-0.327	.	0.212	0.204
			Sig. (2-tailed)	0.875	1	1	0.403	0.403	.	0.539	0.623
			N	8	8	8	7	7	7	8	6

Table 11-17: Table showing the correlation of Gli2 and β-catenin

Tables showing the correlation between with the (percentage of positivity, intensity of immune reaction, IRS class and nuclear score) of Gli2 and β-catenin in tumour centres and at the invasive fronts.

				β-catenin							
				Tumour centre			Invasive front			Nuclear score	
				%	Intensity	IRS Class	%	Intensity	IRS Class	Tumour centre	Invasive front
Gli2	Tumour centre	%	Correlation Coefficient	-0.606	.	.	-0.307	0.594	0.594	0.196	-0.065
			Sig. (2-tailed)	0.085	.	.	0.417	0.116	0.116	0.563	0.858
			N	8	8	8	7	7	7	8	7
		Intensity	Correlation Coefficient	-0.501	.	.	-0.572	0.739	0.739	0	0.161
			Sig. (2-tailed)	0.172	.	.	0.147	0.061	0.061	1	0.67
			N	8	8	8	7	7	7	8	7
		IRS Class	Correlation Coefficient	-0.501	.	.	-0.572	0.739	0.739	0	0.161
			Sig. (2-tailed)	0.172	.	.	0.147	0.061	0.061	1	0.67
			N	8	8	8	7	7	7	8	7
	Invasive front	%	Correlation Coefficient	-0.507	.	.	-0.163	0.632	0.632	0.3	-0.069
			Sig. (2-tailed)	0.156	.	.	0.676	0.105	0.105	0.382	0.854
			N	8	8	8	7	7	7	8	0
		Intensity	Correlation Coefficient	-0.059	.	.	-0.338	0.655	0.655	-0.105	0.286
			Sig. (2-tailed)	0.87	.	.	0.388	0.094	0.094	0.763	0.447
			N	8	8	8	7	7	7	8	7
		IRS Class	Correlation Coefficient	-0.25	.	.	-0.338	0.655	0.655	0.223	0.286
			Sig. (2-tailed)	0.491	.	.	0.388	0.094	0.094	0.524	0.447
			N	8	8	8	7	7	7	8	7
	Nuclear score	Tumour centre	Correlation Coefficient	-0.25	.	.	-0.572	0.739	0.739	-0.334	0.161
			Sig. (2-tailed)	0.491	.	.	0.147	0.061	0.061	0.34	0.67
			N	8	8	8	7	7	7	8	7
		Invasive front	Correlation Coefficient	-0.231	.	.	0	0.655	0.655	-0.231	0.071
			Sig. (2-tailed)	0.554	.	.	1	0.094	0.094	0.554	0.849
			N	7	7	7	7	7	7	7	7

Table 11-18: Table showing the correlation of Gli2 and E-cadherin

Tables showing the correlation between with the (percentage of positivity, intensity of immune reaction, IRS class and nuclear score) of Gli2 and E-cadherin in tumour centres and at the invasive fronts.

				E-cadherin							
				Tumour centre			Invasive front			Nuclear score	
				%	Intensity	IRS Class	%	Intensity	IRS Class	Tumour centre	Invasive front
Gli2	Tumour centre	%	Correlation Coefficient	0.106	-0.563	0	0.35	0.412	0.412	0.106	-0.563
			Sig. (2-tailed)	0.759	0.115	1	0.307	0.248	0.248	0.759	0.115
			N	8	8	8	8	8	8	8	8
		Intensity	Correlation Coefficient	0.275	-0.293	0.488	0.347	0.143	0.143	0.275	-0.293
			Sig. (2-tailed)	0.45	0.439	0.197	0.339	0.705	0.705	0.45	0.439
			N	8	8	8	8	8	8	8	8
		IRS Class	Correlation Coefficient	0.275	-0.293	0.488	0.347	0.143	0.143	0.275	-0.293
			Sig. (2-tailed)	0.45	0.439	0.197	0.339	0.705	0.705	0.45	0.439
			N	8	8	8	8	8	8	8	8
	Invasive front	%	Correlation Coefficient	0.056	-0.652	-0.237	0.105	0.173	0.173	0.056	-0.652
			Sig. (2-tailed)	0.874	0.072	0.514	0.763	0.633	0.633	0.874	0.072
			N	8	8	8	8	8	8	8	8
		Intensity	Correlation Coefficient	**.728***	0.258	**.775***	**.918***	0.378	0.378	**.728***	0.258
			Sig. (2-tailed)	**0.046**	0.495	**0.04**	**0.011**	0.317	0.317	**0.046**	0.495
			N	**8**	8	**8**	**8**	8	8	**8**	8
		IRS Class	Correlation Coefficient	0.564	-0.067	0.467	**0.711**	0.293	0.293	0.564	-0.067
			Sig. (2-tailed)	0.121	0.86	0.217	**0.05**	0.439	0.439	0.121	0.86
			N	8	8	8	**8**	8	8	8	8
	Nuclear score	Tumour centre	Correlation Coefficient	0.42	0.149	**.745***	0.53	0.218	0.218	0.42	0.149
			Sig. (2-tailed)	0.248	0.693	**0.049**	0.144	0.564	0.564	0.248	0.693
			N	8	8	**8**	8	8	8	8	8
		Invasive front	Correlation Coefficient	0.169	0.4	0.4	0.653	0.645	0.645	0.169	0.4
			Sig. (2-tailed)	0.666	0.327	0.327	0.094	0.114	0.114	0.666	0.327
			N	7	7	7	7	7	7	7	7

Table 11-19: Table showing the correlation of Gli3 and β-catenin

Tables showing the correlation between with the (percentage of positivity, intensity of immune reaction, IRS class and nuclear score) of Gli2 and β-catenin in tumour centres and at the invasive fronts.

				β-catenin							
				Tumour centre			Invasive front			Nuclear score	
				%	Intensity	IRS Class	%	Intensity	IRS Class	Tumour centre	Invasive front
Gli3	Tumour centre	%	Correlation Coefficient	0.282	.	.	-0.079	-0.102	-0.102	-0.601	0
			Sig. (2-tailed)	0.43	.	.	0.838	0.791	0.791	0.08	1
			N	8	8	8	7	7	7	8	7
		Intensity	Correlation Coefficient	-0.237	.	.	-0.653	0.422	0.422	-0.105	0.276
			Sig. (2-tailed)	0.514	.	.	0.094	0.28	0.28	0.763	0.461
			N	8	8	8	7	7	7	8	7
		IRS Class	Correlation Coefficient	-0.237	.	.	-0.653	0.422	0.422	-0.105	0.276
			Sig. (2-tailed)	0.514	.	.	0.094	0.28	0.28	0.763	0.461
			N	8	8	8	7	7	7	8	7
	Invasive front	%	Correlation Coefficient	0.632	.	.	-0.2	-0.2	-0.2	0.447	0.632
			Sig. (2-tailed)	0.157	.	.	0.655	0.655	0.655	0.317	0.157
			N	6	6	6	6	6	6	6	6
		Intensity	Correlation Coefficient	.	.	.	.	.	.	.	.
			Sig. (2-tailed)	.	.	.	.	.	.	.	.
			N	6	6	6	6	6	6	6	6
		IRS Class	Correlation Coefficient	.	.	.	.	.	.	.	.
			Sig. (2-tailed)	.	.	.	.	.	.	.	.
			N	6	6	6	6	6	6	6	6
	Nuclear score	Tumour centre	Correlation Coefficient	-0.059	.	.	-0.163	0.632	0.632	0.105	0.414
			Sig. (2-tailed)	0.87	.	.	0.676	0.105	0.105	0.763	0.269
			N	8	8	8	7	7	7	8	7
		Invasive front	Correlation Coefficient	0.617	.	.	0.756	.	.	-0.617	0
			Sig. (2-tailed)	0.197	.	.	0.114	.	.	0.197	1
			N	5	5	5	5	5	5	5	5

Table 11-20: Table showing the correlation of Gli3 and E-cadherin

Tables showing the correlation between with the (percentage of positivity, intensity of immune reaction, IRS class and nuclear score) of Gli2 and E-cadherin in tumour centres and at the invasive fronts.

				E-cadherin							
				Tumour centre			Invasive front			Nuclear score	
				%	Intensity	IRS Class	%	Intensity	IRS Class	Tumour centre	Invasive front
Gli3	Tumour centre	%	Correlation Coefficient	0.111	0.355	0.355	0.053	-0.087	-0.087	0.111	0.355
			Sig. (2-tailed)	0.75	0.327	0.327	0.88	0.811	0.811	0.75	0.327
			N	8	8	8	8	8	8	8	8
		Intensity	Correlation Coefficient	-0.056	-0.059	0.237	-0.105	-0.173	-0.173	-0.056	-0.059
			Sig. (2-tailed)	0.874	0.87	0.514	0.763	0.633	0.633	0.874	0.87
			N	8	8	8	8	8	8	8	8
		IRS Class	Correlation Coefficient	-0.056	-0.059	0.237	-0.105	-0.173	-0.173	-0.056	-0.059
			Sig. (2-tailed)	0.874	0.87	0.514	0.763	0.633	0.633	0.874	0.87
			N	8	8	8	8	8	8	8	8
	Invasive front	%	Correlation Coefficient	0.135	0.316	0.2	0.135	-0.2	-0.2	0.135	0.316
			Sig. (2-tailed)	0.752	0.48	0.655	0.752	0.655	0.655	0.752	0.48
			N	6	6	6	6	6	6	6	6
		Intensity	Correlation Coefficient	-0.405	-0.632	**-1.000***	-0.539	-0.2	-0.2	-0.405	-0.632
			Sig. (2-tailed)	0.343	0.157	**.**	0.206	0.655	0.655	0.343	0.157
			N	6	6	**6**	6	6	6	6	6
		IRS Class	Correlation Coefficient	.	.	.	.	.	.	.	.
			Sig. (2-tailed)	.	.	.	.	.	.	.	.
			N	6	6	6	6	6	6	6	6
	Nuclear score	Tumour centre	Correlation Coefficient	-0.111	-0.237	-0.237	-0.421	-0.434	-0.434	-0.111	-0.237
			Sig. (2-tailed)	0.75	0.514	0.514	0.227	0.232	0.232	0.75	0.514
			N	8	8	8	8	8	8	8	8
		Invasive front	Correlation Coefficient	-0.261	0	-0.645	-0.348	-0.129	-0.129	-0.261	0
			Sig. (2-tailed)	0.511	1	0.12	0.381	0.756	0.756	0.511	1
			N	6	6	6	6	6	6	6	6

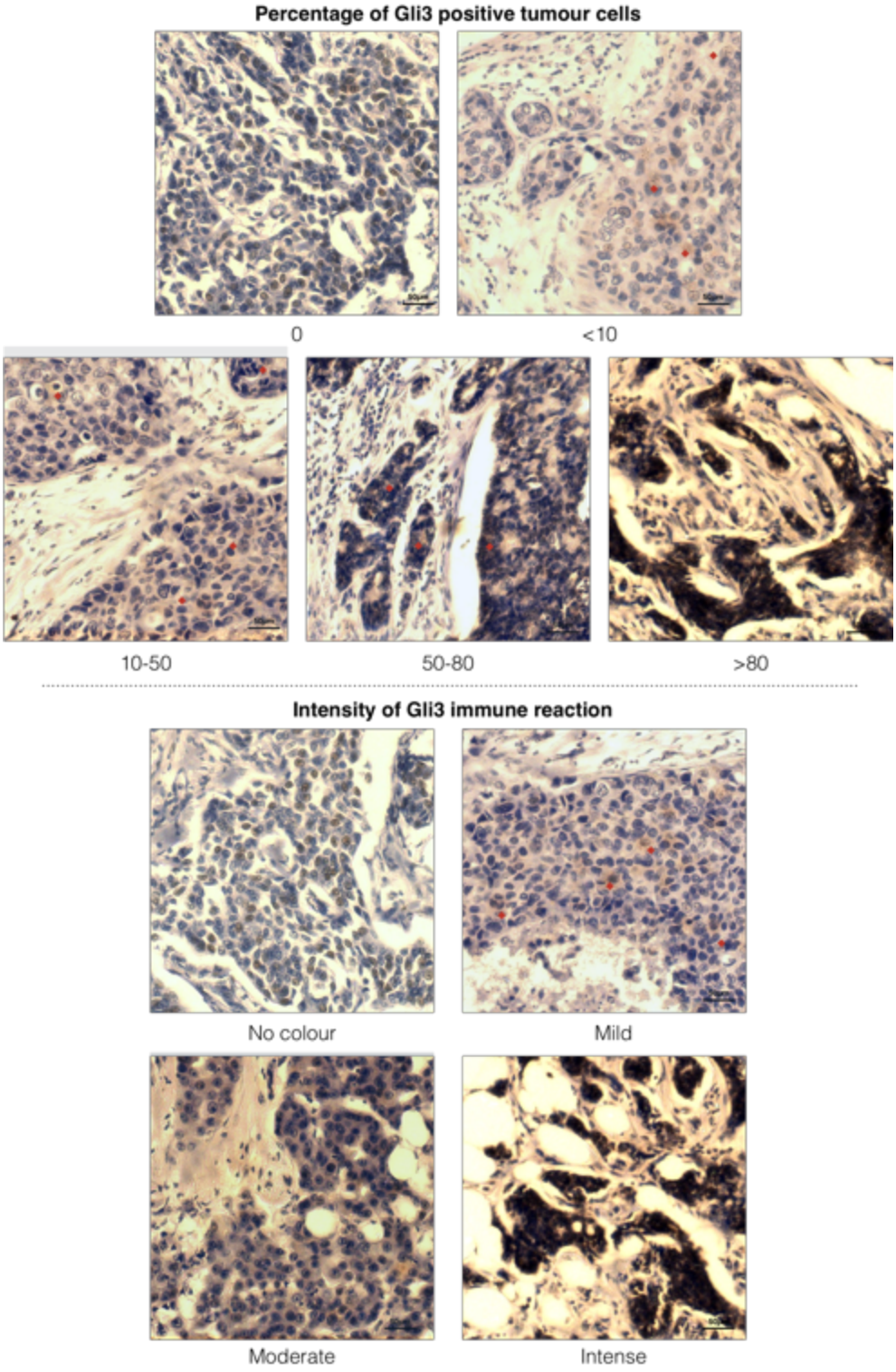

Figure 11-29, Representation of percentage of Gli3 positive tumour cells and the intensity of immune reaction in breast cancer sections

Representative sections stained for Gli3 by IHC. Images were captured by Leica microscope in 400x magnification. (A) the percentage of Gli3 positive tumour cells. (B) the intensity of the staining. Scale bars were added to the bottom right corner of each image. (♦) was used to indicate area of positivity in images.

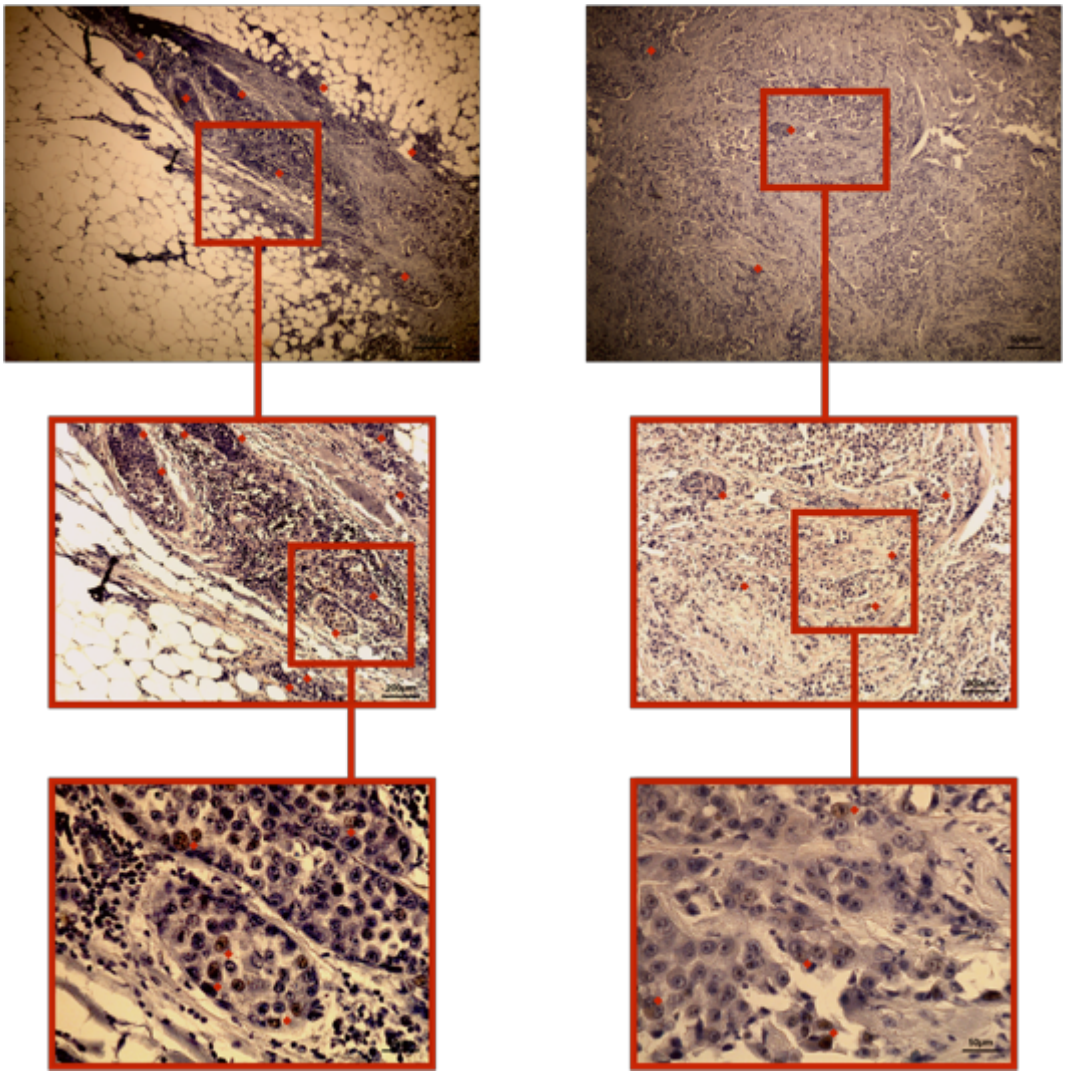

Figure 11-30, Gli3 expression was higher in invasive fronts of breast cancer samples
Representative IHC images of the same breast cancer sample showing higher Gli2 in the invasive front (B) compared to the tumour centre (A). Images were captured using three different magnifications (100X, 200X and 400X) by the Leica microscope. (♦) was used to indicate area of positivity in images.

11.3.7 β-catenin and E-cadherin expression is higher in invasive front compared to tumour centre

Expression of β-catenin and E-cadherin were compared in tumour centres and invasive fronts of breast cancer cases. The percentage of positive cells and intensity of staining of β-catenin was assessed according to the scores presented in Figure 11-31. Out of 37 cases stained with β-catenin, invasive front was not identifiable in two (5.4%) of cases (Table 11-21-A).

Out of 37 cases, 23 (62.2%) showed β-catenin positivity in more than 80% of tumour cells in the tumour centres compared to 29 (66.6%) invasive fronts (Table 11-21-A and Figure 11-32-A). 28 (75.7%) tumour centres showed intense β-catenin staining compared to 34 (82.9%) invasive fronts (Table 11-21-B and Figure 11-32-B). 26 (70.3%) cases had the highest IRS scores for β-catenin staining in tumour centres compared to 28 (80%) in the invasive front (Table 11-21-C and -Figure 11-32-C). This was confirmed by looking at breast cancer cases as seen in the representative images (Figure 11-33). The percentage of positive expressing cells and IRS classes of β-catenin were correlated in tumour centre and invasive front (0.477** and 0.293, respectively).

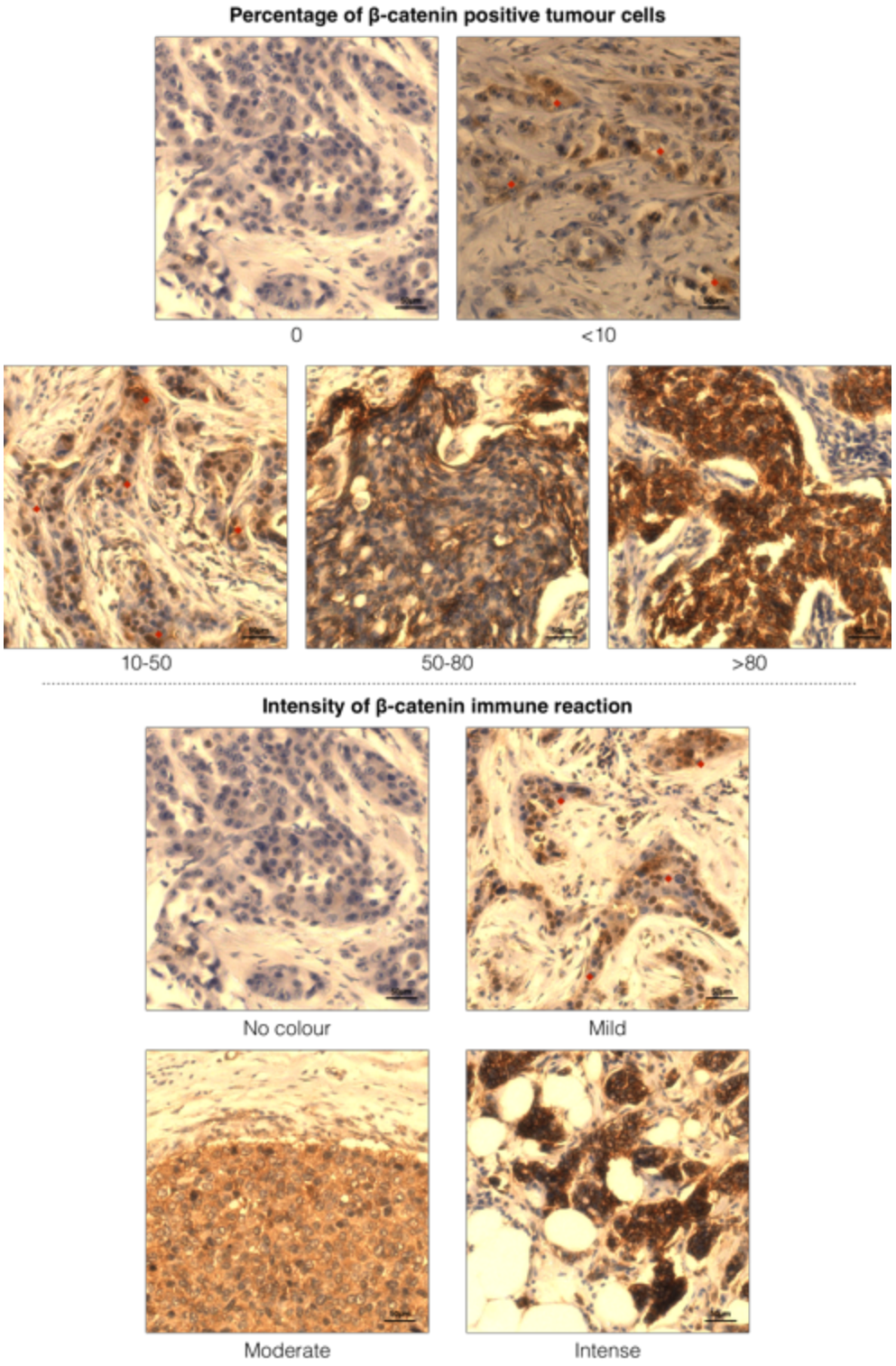

Figure 11-31, Representation of percentage of β-catenin positive tumour cells and the intensity of immune reaction in breast cancer sections

Representative sections stained for β-catenin by IHC. Images were captured by Leica microscope in 400x magnification. (A) the percentage of β-catenin positive tumour cells. (B) the intensity of the staining. Scale bars were added to the bottom right corner of each image. (♦) was used to indicate area of positivity in images.

Table 11-21: Frequency tables for percentage of positive cells, intensity of staining, and IRS class of the sections included in the analysis of β-catenin in breast cancer cohort

Tumour centre and invasive front frequency tables (A) for percentage of positive tumour cells, (B) intensity of staining, and (C) IRS class. The numbers are indicated for each score and the percentages were calculated from the total number of samples. Kendell's tau B test was used to assess the correlations with in each parameter in the tumour centre and invasive front.

	A	Tumour centre	Invasive front
		No. (%)	No. (%)
Percentage of positive tumour cells	0	0	0
	<10	1 (2.7)	0
	10-50	2 (5.4)	2 (5.7)
	51-80	11 (29.7)	9 (25.7)
	>80	23 (62.2)	24 (66.6)
	Total	37 (100)	35 (100)
	Missing	0	2 (5.4)
	Total	37 (100)	37 (100)
TauB		0.477*	

	B	Tumour Centre	Invasive front
		No. (%)	No. (%)
Intensity of staining	No colour	0	0
	Mild reaction	1 (2.7)	1 (2.9)
	Moderate reaction	8 (21.6)	5 (14.3)
	Intense reaction	28 (75.7)	29 (82.9)
	Total	37 (100	35 (100)
	Missing	0	2 (5.4)
	Total	37 (100)	37 (100)
TauB		-	

	C	Tumour Centre	Invasive front
		No. (%)	No. (%)
IRS class	Negative	0	0
	Positive, weak expression	1 (2.7)	0
	Positive, mild expression	10 (27)	7 (20)
	Positive, strong expression	26 (70.3)	28 (80)
	Total	37 (100)	35 (100)
	Missing	0	2 (5.4)
	Total	37 (100)	37 (100)
TauB		0.293	

The Kendall's TauB correlation coefficient (between -1 and +1). The statistical significance of the correlation is indicated as follows: *P= <0.05, **P= <0.01.

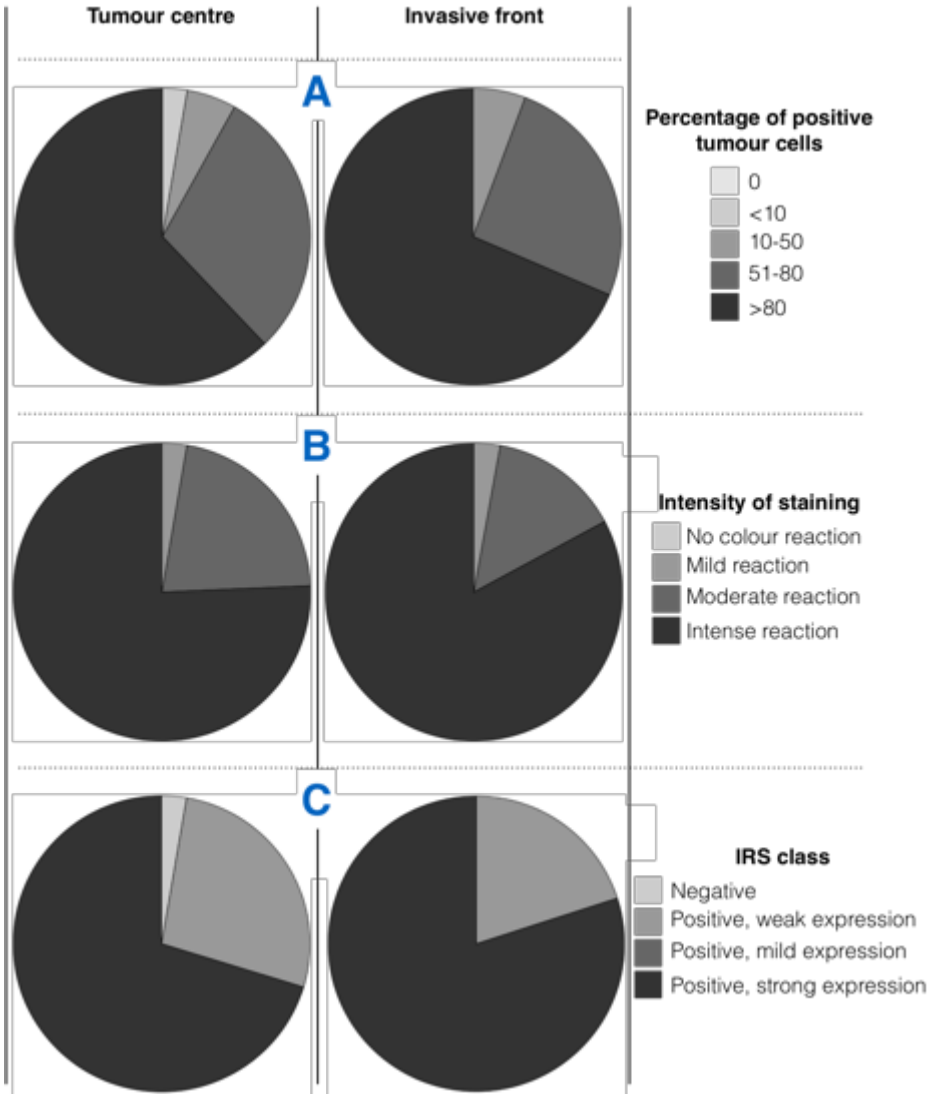

Figure 11-32, β-catenin expression was higher in invasive fronts in breast cancer cohort

Figure showing comparison of β-catenin in tumour centres (to the left) compared to the invasive front (to the right). (A) comparison of percentage of positive cells. (B) comparison of intensity of staining. (C) comparison of IRS class.

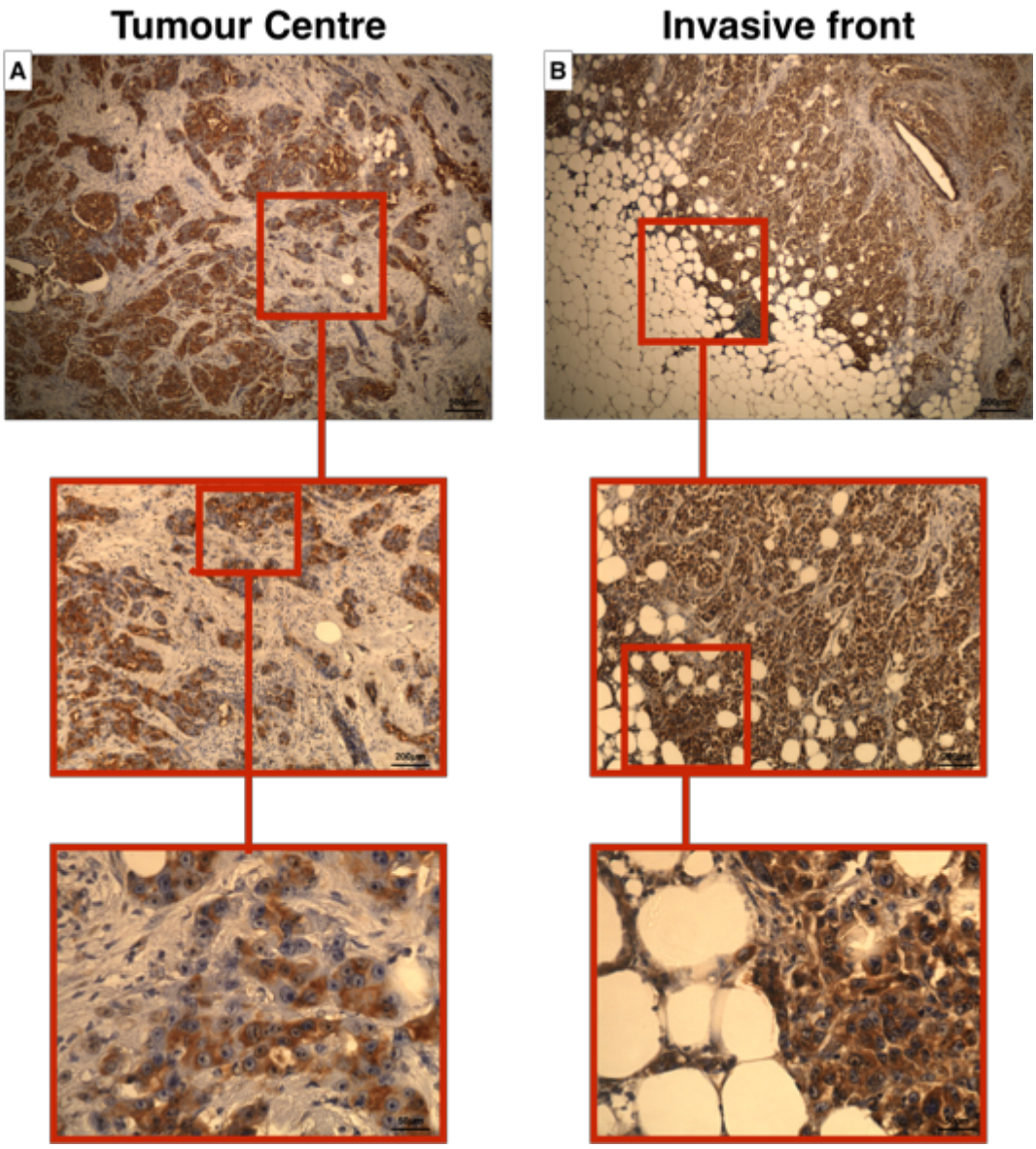

Figure 11-33, β-catenin expression was higher in invasive fronts of breast cancer samples

Representative IHC images of the same breast cancer sample showing higher β-catenin in the invasive front (B) compared to the tumour centre (A). Images were captured using three different magnifications (100X, 200X and 400X) by the Leica microscope.

Two cases (5.4%) showed negative nuclear staining of β-catenin in tumour centres compared to none of the cases in the invasive front (Table 11-22). In tumour centre, β-catenin nuclear positivity was higher than 50% in 13 (35.1%) cases compared to 15 (42.9%) cases in the invasive front (Figure 11-34). The nuclear localisation of β-catenin in tumour cells was correlated in tumour centres and invasive fronts (0.463**).

Table 11-22: Frequency tables of β-catenin nuclear localisation in breast cancer cases showing increased nuclear expression of β-catenin in tumour invasive front

Tables showing nuclear expression of β-catenin in cells in tumour centre and invasive front. The numbers are indicated for each score and the percentages were calculated from the total number of samples. Kendell's tau B test was used to assess the correlations with in each parameter in the tumour centre and invasive front.

A	Nuclear expression of β-catenin	
	Tumour Centre	Invasive Front
	No. (%)	No. (%)
No nuclear expression	2 (5.4)	0
<10% of tumour cells	9 (24.3)	5 (14.3)
10% - 50% of tumour cells	13 (35.1)	15 (42.9)
≥51% of tumour cells	13 (35.1)	15 (42.9)
Total included	37 (100)	35 (100)
Missing	0	2 (5.4)
Total	37 (100)	37(100)
TauB	0.463**	

The Kendall's TauB correlation coefficient (between -1 and +1). The statistical significance of the correlation is indicated as follows: *P= <0.05, **P= <0.01.

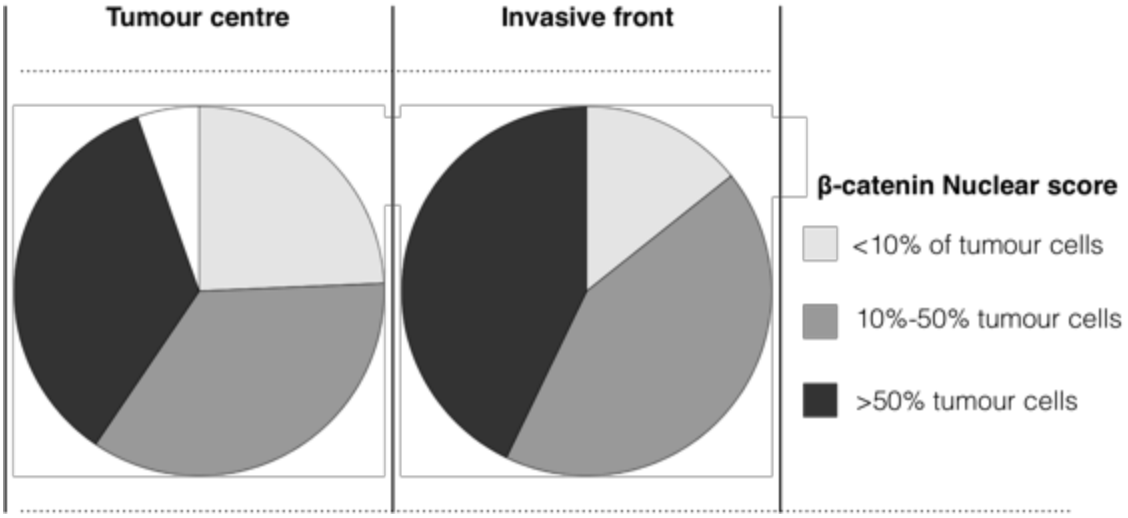

Figure 11-34, β-catenin expression was higher in invasive fronts in breast cancer cohort

Figure showing comparison of β-catenin in tumour centres (to the left) compared to the invasive front (to the right).

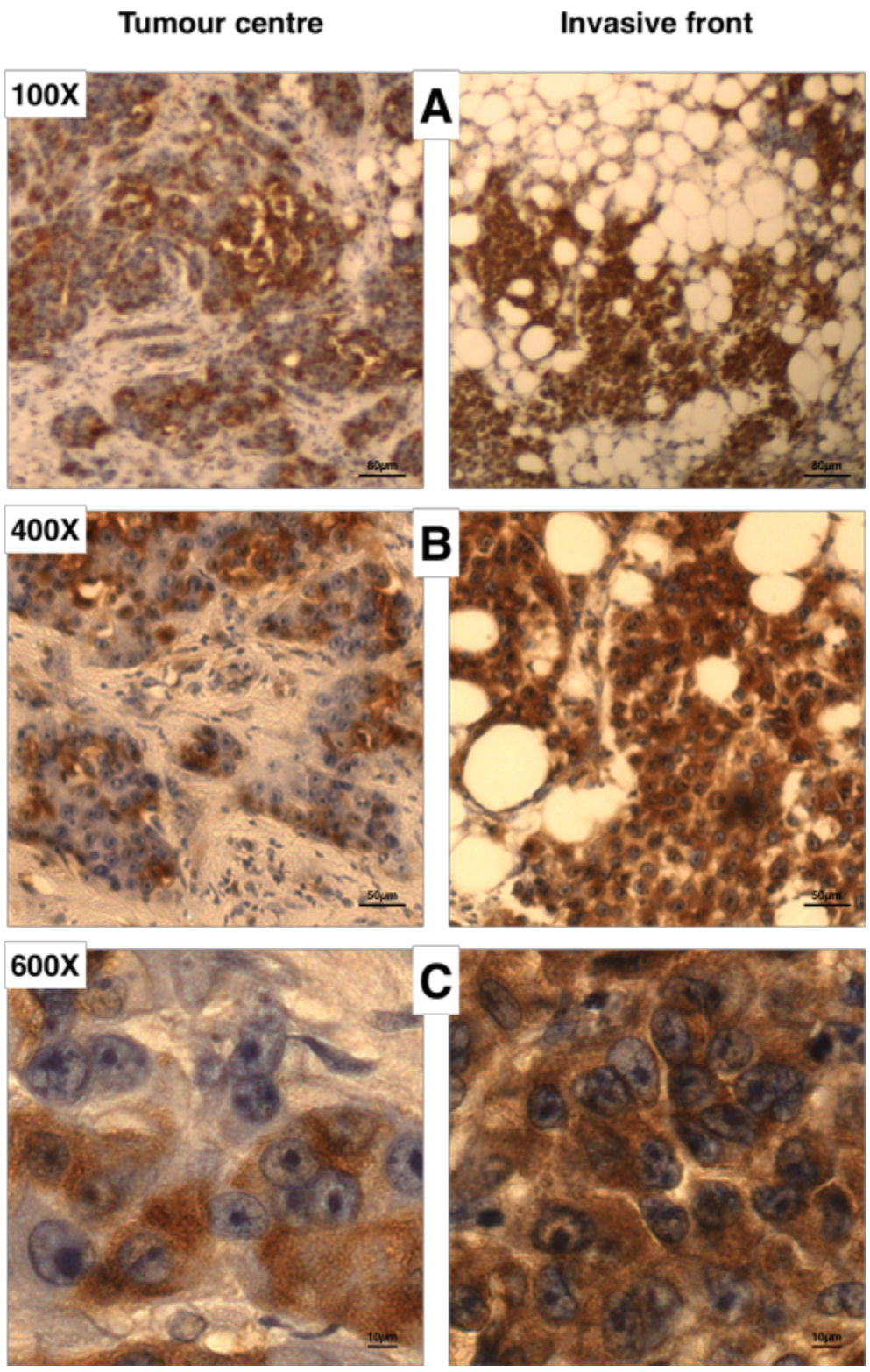

Figure 11-35, Nuclear expression of β-catenin in tumour cells is higher in invasive front of breast cancer

Representative IHC images of the same breast cancer sample showing increased nuclear localisation of β-catenin in tumour cells in the invasive front (to right) compared to the tumour centre (to left). Images were captured using three different magnifications (100X, 400X and 600X) by the Leica microscope.

The percentage of positive cells and intensity of E-cadherin staining were assessed according to the scores presented in Figure 11-36. Invasive fronts were identifiable in all cases stained for E-cadherin (23) (Table 11-23-A).

Out of 23 cases, 14 (60.9%) cases showed E-cadherin positivity in more than 80% of tumour cells in the tumour centres compared to 16 (69.6%) invasive fronts (Table 11-23-A and Figure 11-37-A). 14 (60.9%) tumour centres showed intense E-cadherin staining compared to 19 (82.6%) invasive fronts (Table 0-1-B and Figure 11-37-B). 13 (56.5%) cases had the highest IRS scores of E-cadherin in tumour centres compared to 19 (82.6%) in the invasive front (Table 0-1-C and Figure 11-37-C). This was confirmed by looking at breast cancer cases as seen in the representative images (Figure 11-38). The percentage of positive expressing cells, staining intensity and IRS classes were correlated in tumour centre and invasive front (0.466*, 0.406* and 0.513*, respectively).

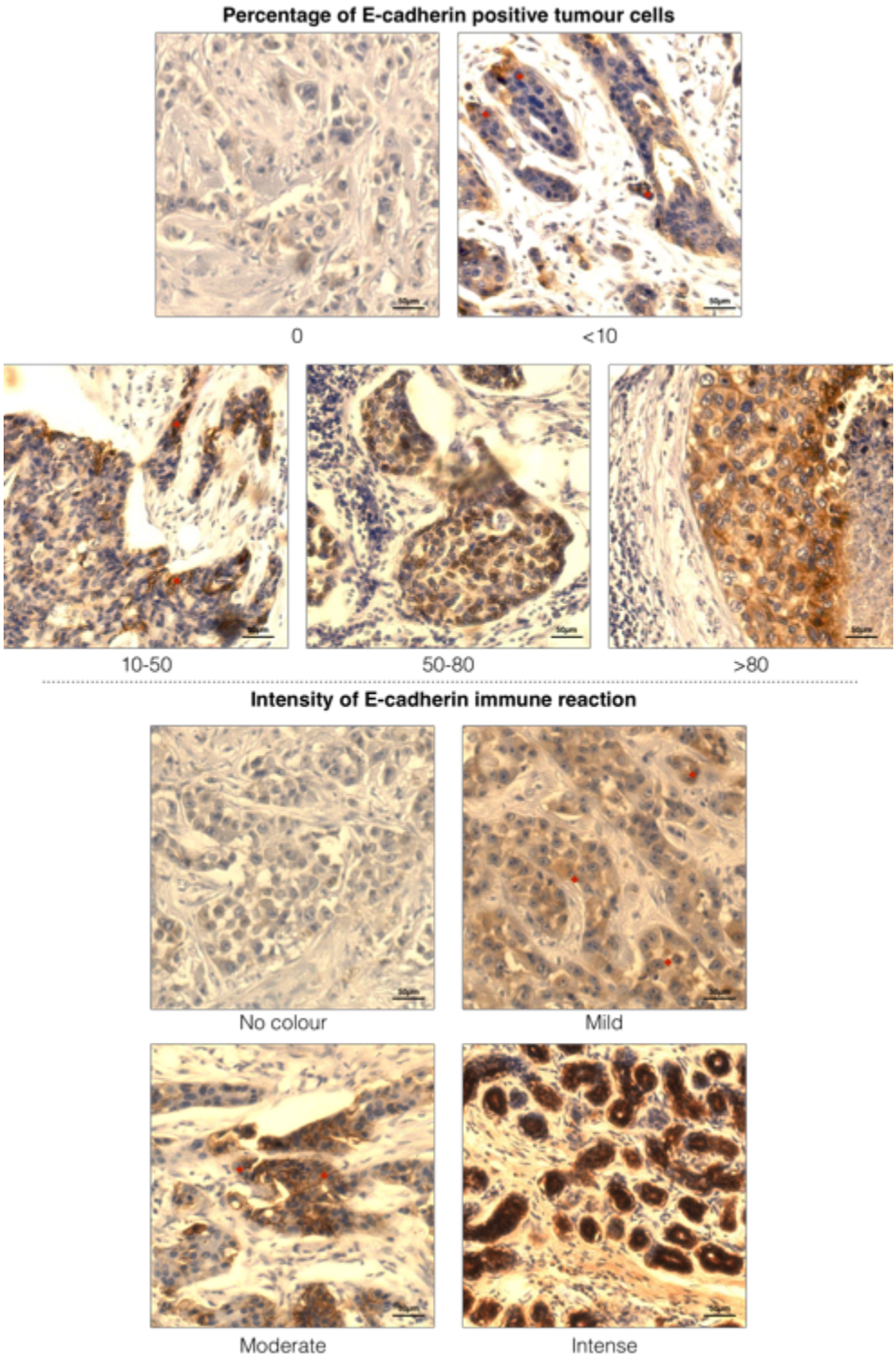

Figure 11-36, Representation of percentage of E-cadherin positive tumour cells and the intensity of immune reaction in breast cancer sections

Representative sections stained for E-cadherin by IHC. Images were captured by Leica microscope in 400x magnification. (A) the percentage of E-cadherin positive tumour cells. (B) the intensity of the staining. Scale bars were added to the bottom right corner of each image. (♦) was used to indicate area of positivity in images.

Table 11-23: Frequency tables for percentage of positive cells, intensity of staining, and IRS class of the sections included in the analysis of E-cadherin in breast cancer cohort

Tumour centre and invasive front frequency tables (A) for percentage of positive tumour cells, (B) intensity of staining, and (C) IRS class. The numbers are indicated for each score and the percentages were calculated from the total number of samples. Kendell's tau B test was used to assess the correlations with in each parameter in the tumour centre and invasive front.

	A	Tumour centre	Invasive front
		No. (%)	No. (%)
Percentage of positive tumour cells	0	0	0
	<10	0	1 (4.3)
	10-50	3 (13)	1 (4.3)
	51-80	6 (26.1)	5 (21.7)
	>80	14 (60.9)	16 (69.6)
	Total	23 (100)	23 (100)
TauB		0.466*	

	B	Tumour Centre	Invasive front
		No. (%)	No. (%)
Intensity of staining	No colour	0	0
	Mild reaction	1 (4.3)	2 (8.7)
	Moderate reaction	8 (34.8)	2 (8.7)
	Intense reaction	14 (60.9)	19 (82.6)
	Total	23 (100)	23 (100)
TauB		0.406*	

	C	Tumour Centre	Invasive front
		No. (%)	No. (%)
IRS class	Negative	0	1 (4.3)
	Positive, weak expression	0	0
	Positive, mild expression	10 (43.5)	3 (13)
	Positive, strong expression	13 (56.5)	19 (82.6)
	Total	23 (100)	23 (100)
TauB		0.513*	

The Kendall's TauB correlation coefficient (between -1 and +1). The statistical significance of the correlation is indicated as follows: *P= <0.05, **P= <0.01.

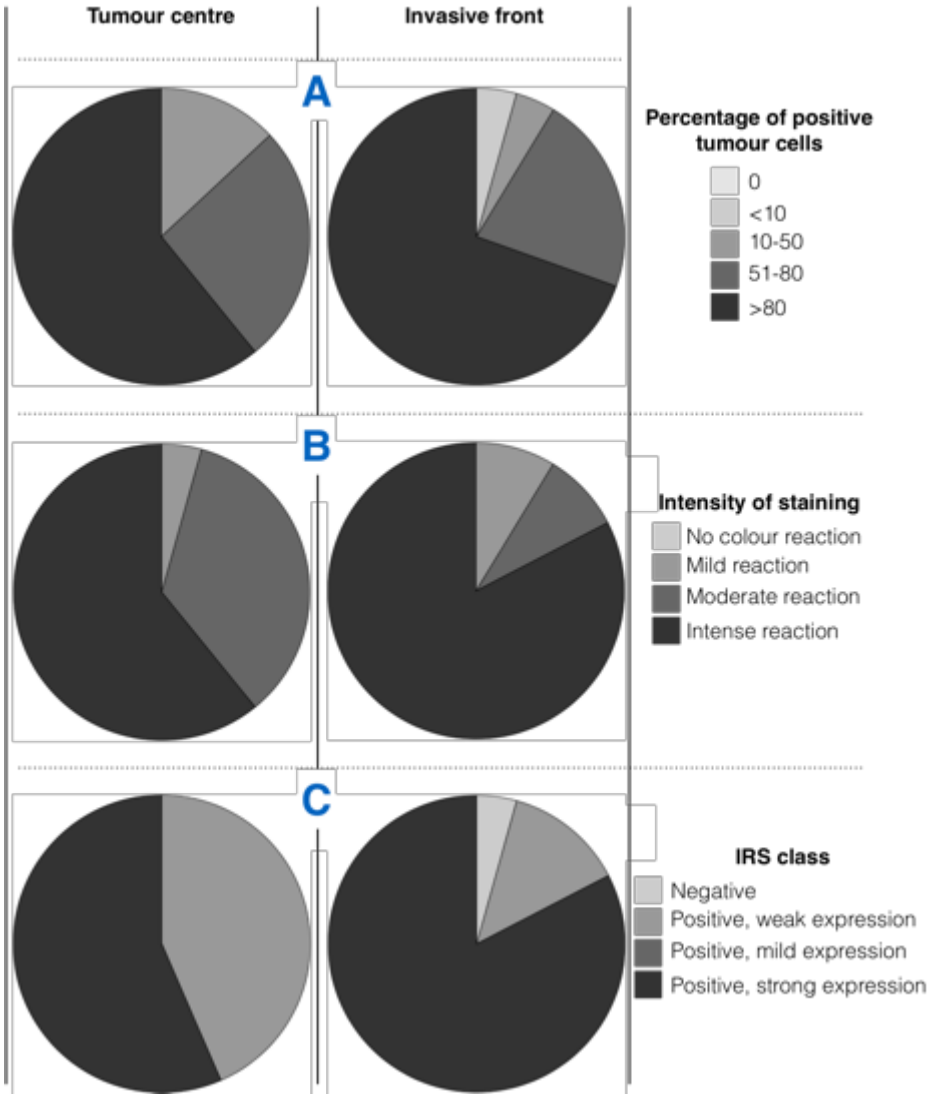

Figure 11-37, E-cadherin expression was higher in invasive fronts in breast cancer cohort

Figure showing comparison of E-cadherin in tumour centres (to the left) compared to the invasive front (to the right). (A) comparison of percentage of positive cells. (B) comparison of intensity of staining. (C) comparison of IRS class.

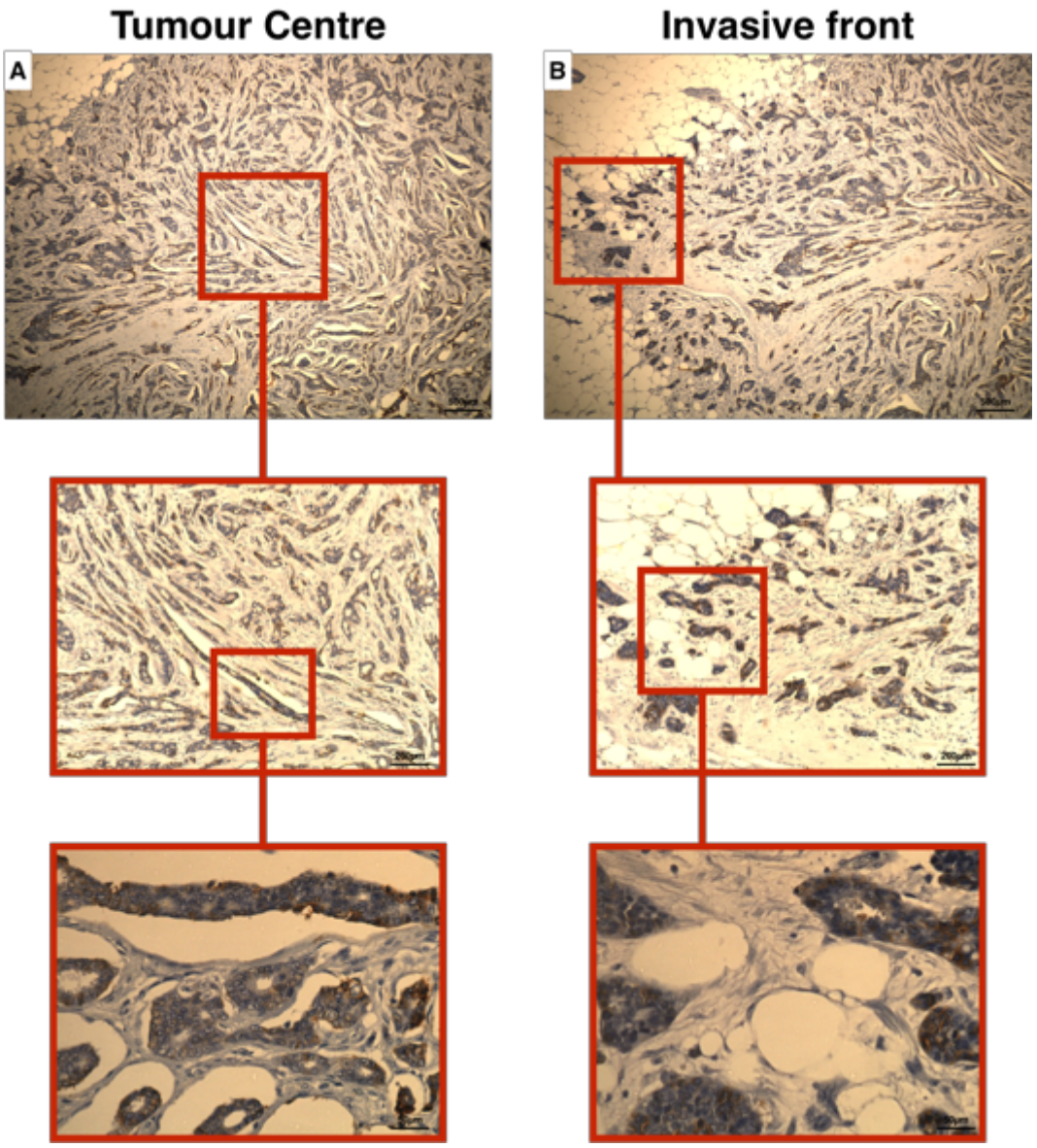

Figure 11-38, E-cadherin expression was higher in invasive fronts of breast cancer samples
Representative IHC images of the same breast cancer sample showing higher E-cadherin in the invasive front (B) compared to the tumour centre (A). Images were captured using three different magnifications (100X, 200X and 400X) by the Leica microscope.

11.3.8 Alteration in localisation and level of Gli1 in breast cancer cells following treatment with cyclopamine or LDE225

Alteration of Gli1 and β-catenin localisation in the cell lines was evaluated to determine whether localisation changed following treatment with cyclopamine or LDE225. The morphology of MCF7 and MDA-MB-231 was observed under a phase

contrast microscope in both cell lines and did not change following treatment with 1μM and 10μM cyclopamine or LDE225.

Gli1 protein was highly visible in cytoplasm and nucleus of MCF7 cells with β-catenin showing localisation in regions area of cell-cell contact. Following 1μM and 10μM cyclopamine treatment, Gli1 was visibly reduced with less nuclear localisation in MCF7 cells. β-catenin localisation in MCF7 cells was not visibly changed following 1μM and 10μM cyclopamine. Nuclear localisation of Gli1 protein reduced following 1μM and 10μM of LDE225 treatment in MCF7. The cytoplasmic localisation was notably reduced following the highest concentration of LDE225.

β-catenin protein was visible in the cytoplasm and in areas of cell-cell contact of MDA-MB-231 in both the vehicle control and following 1μM and 10μM treatment with cyclopamine or LDE225. There was an increase in cell-cell contact localisation of β-catenin at the highest concentration of either treatment. Gli1 protein was highly expressed in the cytoplasm and nucleus of MDA-MB-231. The Gli1 protein visibly decreased in the cytoplasm and nucleus of cells following either treatment.

11.3.9 Hedgehog inhibition regulates the expression of Gli1 in both MCF7 and MDA-MB-231

Gli1 is the active form of Gli, upon activation of Hh pathway, this protein translocates to the nucleus where it acts as a transcription factor (Ruiz i Altaba *et al.*, 2007) (Figure 0-7). Therefore positivity (the percentage of Gli1 positive cells) and (level of expression (MFI)) were evaluated following pathway inhibition with either cyclopamine or LDE225 using flow cytometry and compared against the vehicle control.

In MCF7 cells, Gli1 positivity showed a 10% increase compared to the vehicle control following 1μM, 5μM and 10μM cyclopamine treatment (p-value<0.0001). MFI (level of Gli1 expression) showed a 40% increase in level compared to that of the vehicle control following cyclopamine treatment at all concentrations (p-value<0.0001). Gli1 positivity following LDE225 treatment increased by 12% (p-value<0.0001) and 8% (p-value<0.0001) at 1μM and 5μM, respectively, while decreasing at 10μM treatment by 5% (p-value<0.0001). The level of Gli1 expression (MFI) in MCF7 increased following LDE225 treatment at 1μM by 40% (p-value<0.0001) and at 5μM by 30% (p-value<0.0001) .

Treatment of MDA-MB-231 with 1µM cyclopamine or LDE225 increased Gli1 positivity by 5% (p-value<0.0001) and 2%, respectively. Gli1 positivity in MDA-MB-231 increased by 2% (p-value<0.01) at 5µM and 10µM treatment with cyclopamine. The positivity of Gli1 decreased by 3% (p-value<0.05). Gli1 level of expression (MFI) increased following cyclopamine treatment at 1µM, 5µM and 10µM by 78% (p-value<0.0001), 17% (p-value<0.0001) and 8% (p-value<0.001). MFI (level of Gli1 expression) of MDA-MB-231 increased following 1µM and 5µM LDE225 treatment by 17% (p-value<0.01), 13% (p-value<0.05).

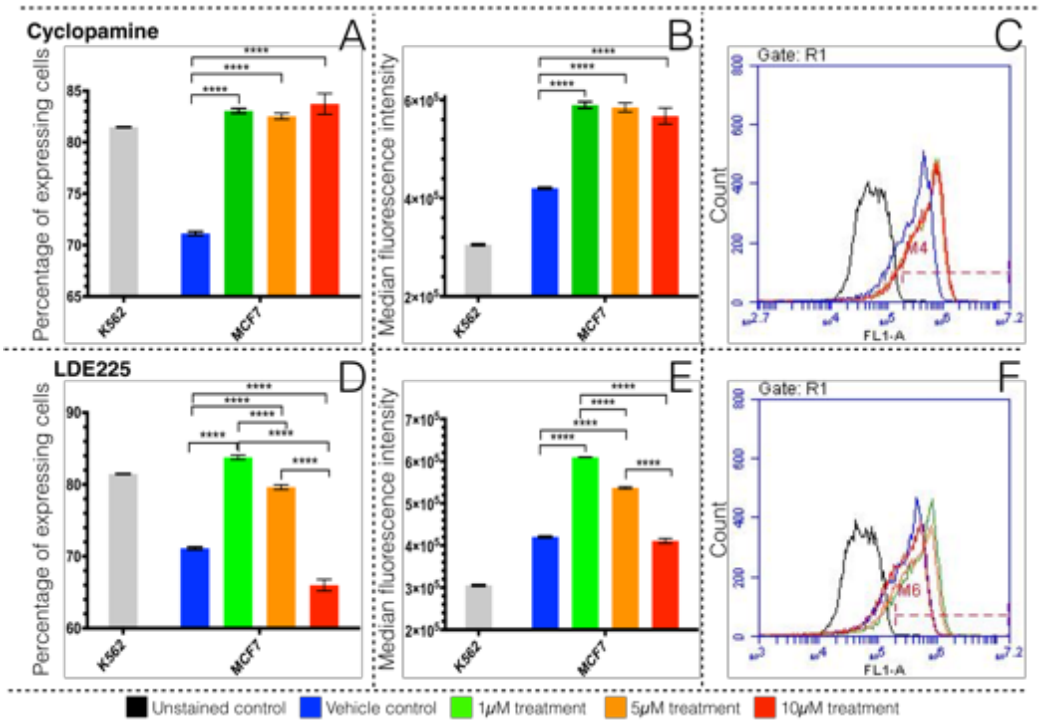

Figure 11-39, Increase of Gli1 positivity (percentage positive cells) of MCF7 following cyclopamine or LDE225 treatment.
Presentation of percentage of Gli1 protein expression in MCF7 following treatment with either cyclopamine or LDE225 at 1µM, 5µM and 10µM. Percentage of positive cells were estimated using flow cytometry, and K562 cell line was used as positive control for Gli1 protein expression. Bars present the percentage of Gli1 positive cells and MFI of Gli1 following treatment with cyclopamine (A and B) or LDE225 (D and E). Results displayed as bars of MFI ± S.D. Overlap histograms of the Gli1 protein in MCF7 cells, comparing (unstained cells, vehicle control, 1µM, 5µM, and 10µM) of cyclopamine (C) or LDE225 treatment (F). This figure is representative of n=3 experiments in triplicate. Statistical analysis was conducted, and significant difference between samples was indicated by **** p-value<0.0001.

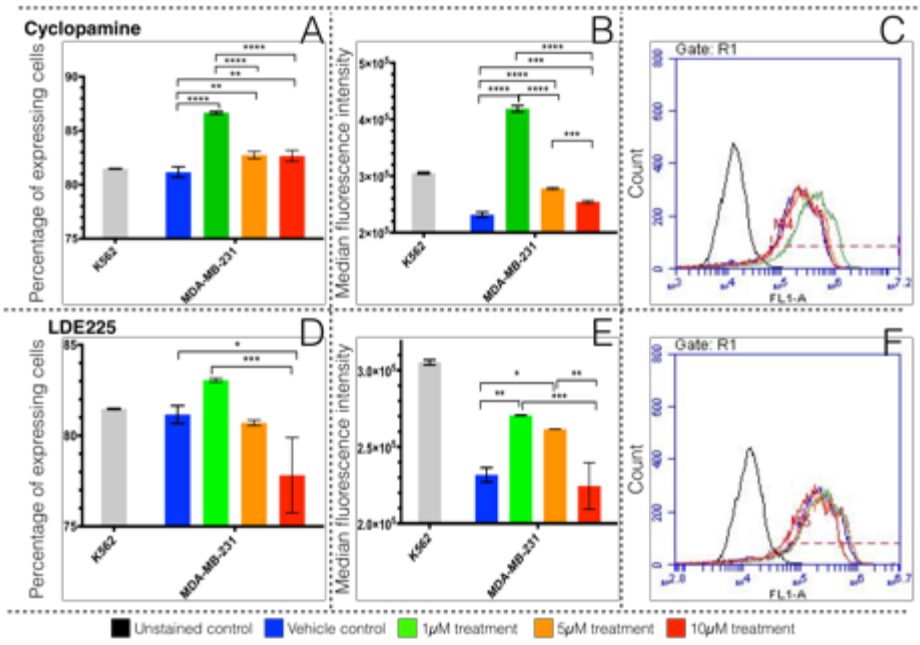

Figure 11-40, Increase of Gli1 positivity in MDA-MB-231 cells following cyclopamine or LDE225 treatment.
Presentation of percentage of Gli1 protein expression in MDA-MB-231 following treatment with either cyclopamine or LDE225 at 1μM, 5μM and 10μM. Percentage of positive cells were estimated using flow cytometry, and K562 cell line was used as positive control for Gli1 protein expression. Bars present the percentage of Gli1 positive cells and MFI of Gli1 following treatment with cyclopamine (A and B) or LDE225 (D and E). Results displayed as bars of MFI ± S.D. Overlap histograms of the Gli1 protein in MDA-MB-231 cells, comparing (unstained cells, vehicle control, 1μM, 5μM, and 10μM) of cyclopamine (C) or LDE225 treatment (F). This figure is representative of n=3 experiments in triplicate. Statistical analysis was conducted, and significant difference between samples was indicated by * p-value<0.05, ** p-value<0.01, *** p-value<0.001 and **** p-value<0.0001.

11.3.10 Alteration of Gli2 expression following treatment with cyclopamine or LDE225.

Positivity of Gli2 (percentage of positive cells) and level of expression (MFI) were evaluated using flow cytometry. Those parameters were evaluated in the cells following pathway inhibition with either cyclopamine or LDE225 and compared against the vehicle control. Gli2 has been shown to have two forms with opposing actions (activator and repressor) depending on post-transcriptional modification (Figure 0-8) (Ruiz i Altaba *et al.*, 2007).

Gli2 positivity (percentage of positive cells) and MFI (level of Gli2 expression) in MCF7 cells decreased following cyclopamine or LDE225. The positivity of Gli2 decreased following 10μM cyclopamine treatment by 5% (p-value<0.001). Level of Gli2 expression in MCF7 cells decreased by 17% (p-value<0.0001) at 1μM and decreased by 40% (p-value<0.0001) at 5μM of LDE225 treatment. The overlay

histogram of MCF7 cells after cyclopamine treatment showed that there were two populations of positive cells, one showing a higher expression level (MFI) than the other. The overlay histogram of vehicle control, 1μM and 5μM LDE225 showed that there were two populations of positively expressing cells, one having a higher level of expression than the other.

Gli2 positivity in MDA-MB-231 decreased by less than 2% following 1μM and 5μM cyclopamine and following 10μM cyclopamine treatment which did not reach statistical significance in all comparisons. MFI (level of Gli2 expression) showed a sharp decrease following 1μM and 10μM cyclopamine treatment (*p*-value0.01 and *p*-value<0.001 respectively) summarised in **Error! Reference source not found.**-B. MFI increased following 5μM treatment in MDA-MB-231 cells to reach a level similar to that in the vehicle control. MFI showed a dropped to half the level of vehicle control following 1μM LDE225 treatment (*p*-value<0.0001). MFI increased following 5μM to reach a level similar to the vehicle control (*p*-value<0.0001). Following 10μM treatment by LDE225, MFI of MDA-MB-231 cells doubled compared to the level seen in vehicle control (*p*-value<0.0001).

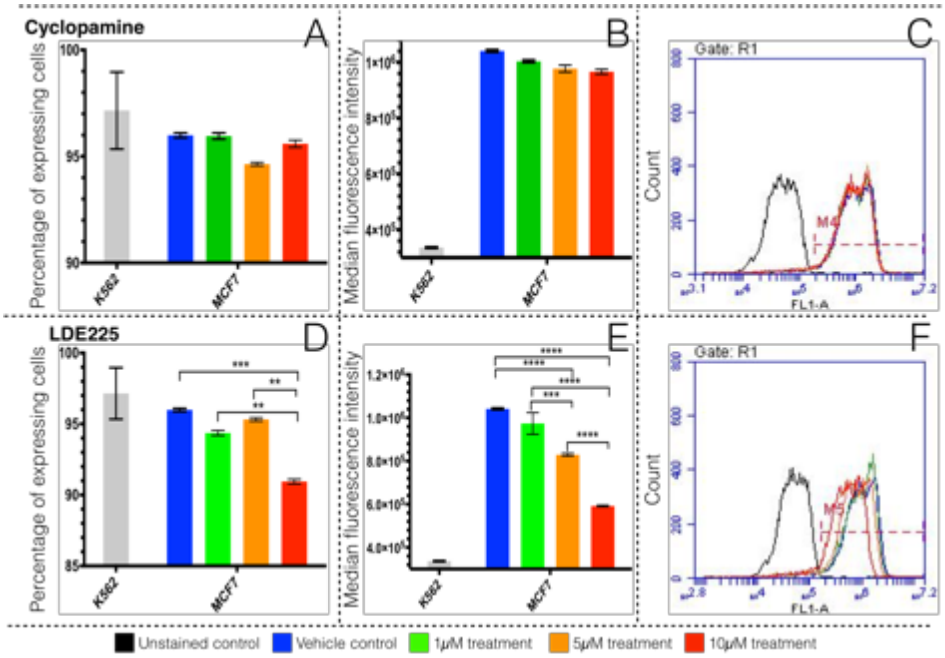

Figure 11-41, Reduction of Gli2 in a dose-dependent manner following treatment with cyclopamine or LDE225

Presentation of percentage of Gli2 protein expression in MCF7 following treatment with either cyclopamine or LDE225 at 1μM, 5μM and 10μM. Percentage of positive cells was estimated using flow cytometry, and K562 cell line was used as a positive control for Gli2 protein expression. Bars present the percentage of Gli2 positive cells and MFI of Gli2 following treatment with cyclopamine (A and B) or LDE225 (D and E). Results displayed as bars of MFI ± S.D. Overlap histograms of the Gli2 protein in MCF7 cells, comparing (unstained cells, vehicle control, 1μM, 5μM, and 10μM) of cyclopamine treatment (C) and LDE225 treatment (F). This figure is representative of n=3 experiments in triplicate. Statistical analysis was conducted, and significant difference between samples was indicated by ** *p*-value<0.01, *** *p*-value<0.001 and **** *p*-value<0.0001.

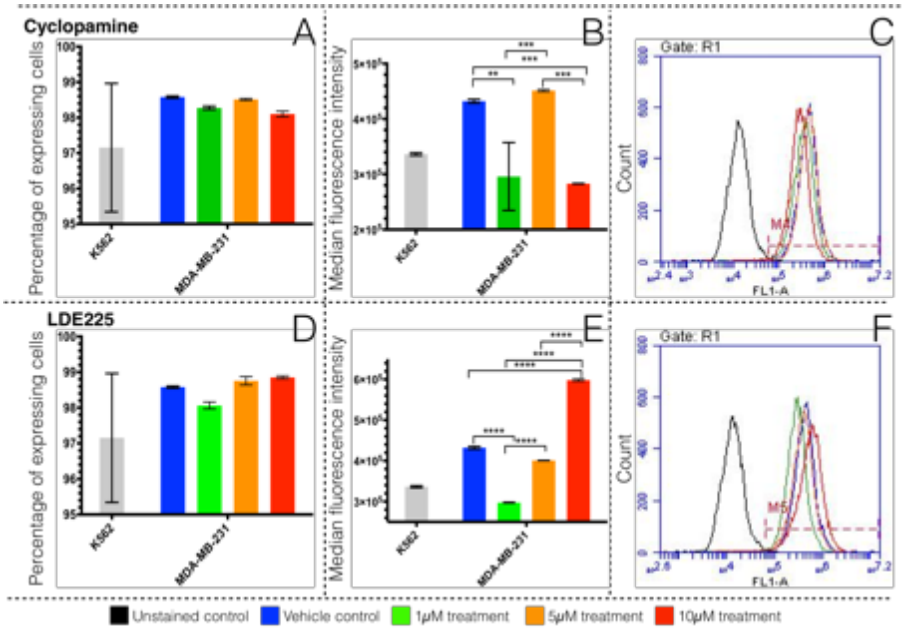

Figure 11-42, Alteration in Gli2 level of expression in MDA-MB-231 cells following treatment with cyclopamine or LDE225.
Presentation of percentage of Gli2 protein expression in MDA-MB-231 following treatment with either cyclopamine or LDE225 at 1μM, 5μM and 10μM. Percentage of positive cells were estimated using flow cytometry, and K562 cell line was used as positive control for Gli2 protein expression. Bars present the percentage of Gli2 positive cells and MFI of Gli2 following treatment with cyclopamine (A and B) or LDE225 (D and E). Results displayed as bars of MFI ± S.D. Overlap histograms of the Gli2 protein in MDA-MB-231 cells, comparing (unstained cells, vehicle control, 1μM, 5μM, and 10μM) of cyclopamine (C) or LDE225 treatment (F). This figure is representative of n=3 experiments in triplicate. Statistical analysis was conducted, and significant difference between samples was indicated by ** p-value<0.01, *** p-value<0.001 and **** p-value<0.0001.

11.3.11 Alteration of Gli3 expression following cyclopamine or LDE225 treatment of breast cancer cell lines

Gli3 is the repressor form of the Gli proteins (Figure 0-8) (Ruiz i Altaba *et al.*, 2007), therefore, assessing changes in Gli3 expression was essential for determining the effect of inhibiting the Hh signalling pathway using cyclopamine or LDE225. The expression of Gli3 was evaluated in the cells using flow cytometry to estimate the percentage of positive cells (positivity) and MFI (level of expression).

Gli3 positivity of MCF7 decreased significantly following 1μM and 10μM cyclopamine by 13% (p-value<0.01) and by 16% (p-value<0.0001). The level of Gli3 expression (MFI) decreased by 12% (p-value<0.01) at 1μM and by 20% (p-value<0.001) 5μM treatment with cyclopamine. The histograms of 5μM and 10μM cyclopamine or LDE225 treatments showed that there was a separate population of low Gli3 expressing cells that was not distinct in vehicle or 1μM treatment.

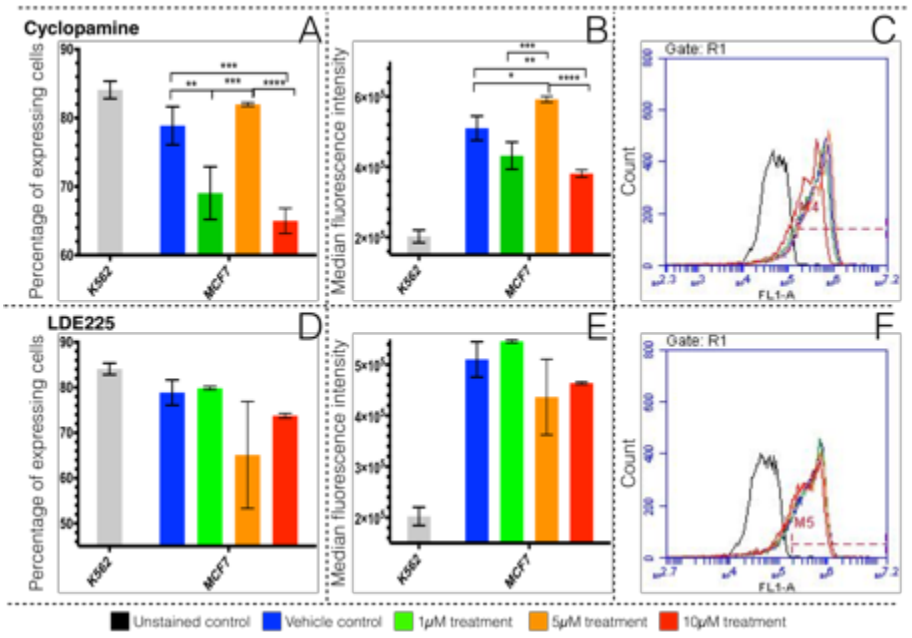

Figure 11-43, Dose-dependent decrease of Gli3 in MCF7 cells following either cyclopamine or LDE225 treatment.
Presentation of percentage of Gli3 protein expression in MCF7 following treatment with either cyclopamine or LDE225 at 1μM, 5μM and 10μM. Percentage of positive cells were estimated using flow cytometry, and K562 cell line was used as positive control for Gli3 protein expression. Bars present the percentage of Gli3 positive cells and MFI of Gli3 following treatment with cyclopamine (A and B) or LDE225 (D and E). Results displayed as bars of MFI ± S.D. Overlap histograms of the Gli3 protein in MCF7 cells, comparing (unstained cells, vehicle control, 1μM, 5μM, and 10μM) of cyclopamine treatment (C) and LDE225 treatment (F). This figure is representative of n=3 experiments in triplicate. Statistical analysis was conducted, and significant difference between samples was indicated by * *p*-value<0.05, ** *p*-value<0.01, and **** *p*-value<0.0001.

In MDA-MB-231, Gli3 positivity dropped following 1μM treatment with cyclopamine by 6% (*p*-value<0.0001). Gli3 positivity was higher than the vehicle control following 5μM and 10μM cyclopamine treatment without statistical significance. MFI (level of Gli3 expression) in MDA-MB-231 cells decreased by 30% following 1μM cyclopamine (*p*-value<0.0001). MFI of Gli3 in MDA-MB-231 following 5μM and 10μM treatment was greater than the vehicle control with statistical significance between the vehicle control and 5μM treatment (*p*-value 0.001). Gli3 positivity increased following 1μM and 5μM treatment with LDE225 in MDA-MB-231 cells by 1% without reaching statistical significance. The positivity of Gli3 decreased following treatment with LDE225 at the highest concentration compared to vehicle control, but without significance. MFI increased following 1μM and 5μM LDE225 treatment in MDA-MB-231 cells by 17% (*p*-value<0.01) and 13% (*p*-value<0.05), respectively compared to the vehicle control.

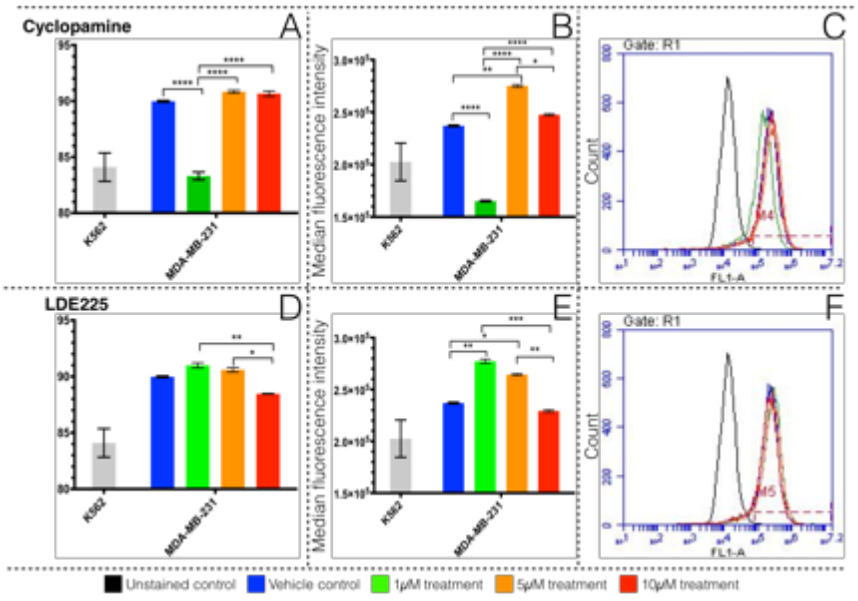

Figure 11-44, Alteration of Gli3 positivity and MFI of MDA-MB-231 cells following treatment with either cyclopamine or LDE225.
Percentage of positive cells were estimated using flow cytometry, and K562 cell line was used as positive control for Gli3 protein expression. Bars present the percentage of Gli3 positive cells and MFI of Gli3 following treatment with cyclopamine (A and B) or LDE225 (D and E). Results displayed as bars of MFI ± S.D. Overlap histograms of the Gli3 protein in MDA-MB-231 cells, comparing (unstained cells, vehicle control, 1μM, 5μM, and 10μM) of cyclopamine (C) or LDE225 treatment (F). This figure is representative of n=3 experiments in triplicate. Statistical analysis was conducted, and significant difference between samples was indicated by * p-value<0.05, ** p-value<0.01, *** p-value<0.001 and **** p-value<0.0001.

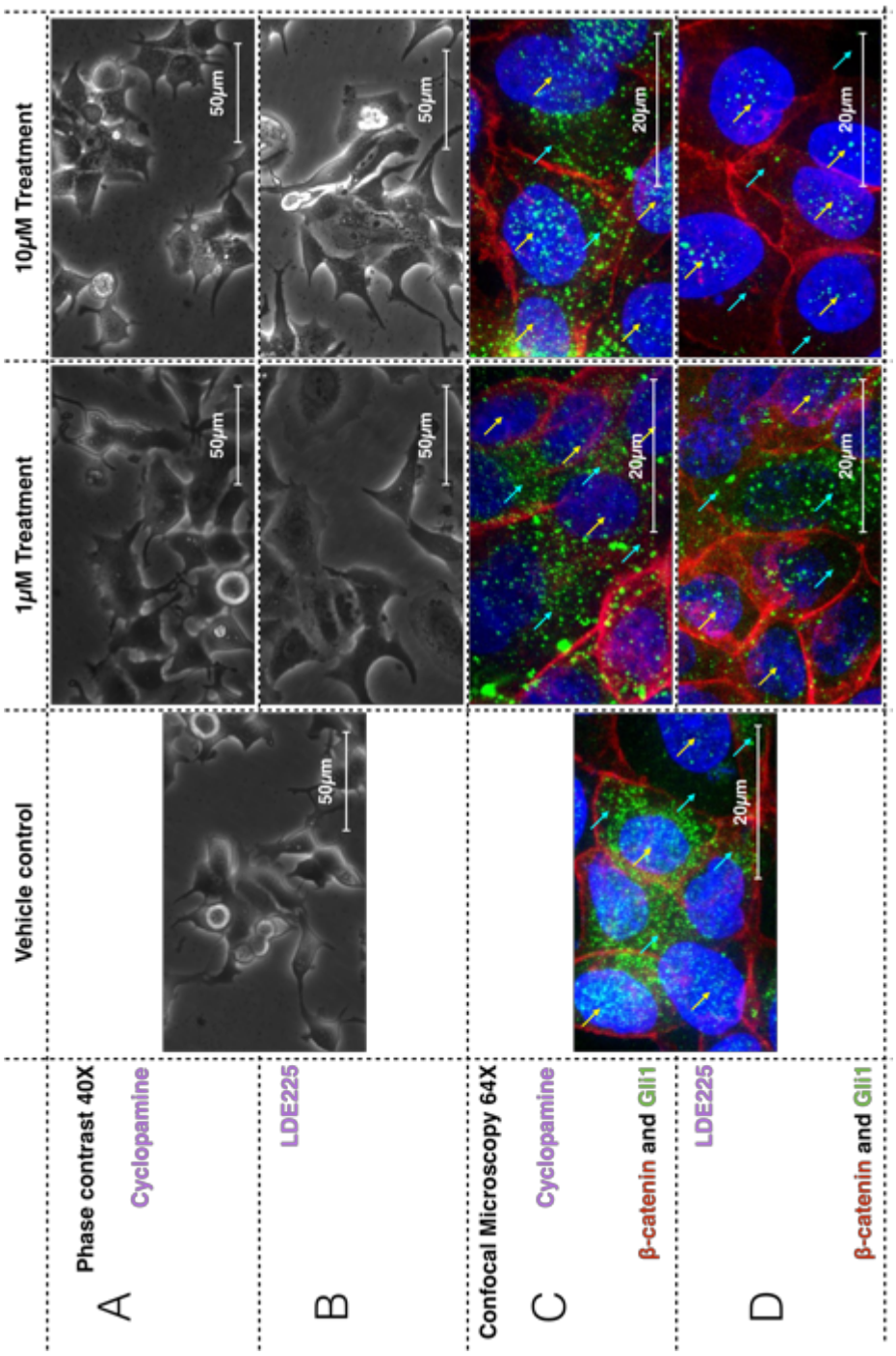

Figure 11-45, Morphology of MCF7 cells and visual alteration of Gli1 and β-catenin localisation following treatment with cyclopamine or LDE225.
Visual presentation of MCF7 following treatment for 48 hours with either cyclopamine or LDE225 at 1μM or 10μM compared to vehicle control. Phase contrast images of MCF7 cells captured under 400x magnification using black and white camera of a Leica phase contrast microscope (A and B). Immunofluorescence Z stacked images of MCF7 cells captured under confocal microscope at 630x magnification. MCF7 cells were double stained for β-catenin (Red) and Gli1 (green) and visualised by fluorescence labelled secondary antibodies Alexa Fluor® (488 and 594). DAPI was used to stain nucleus of cells (Blue). Yellow arrows were used to highlight localisation of the protein in nucleus of cells and light blue arrows were used to highlight cytoplasmic localisation of protein. Visual localisation of β-catenin and Gli1 proteins in MCF7 cells treated with cyclopamine (C) or LDE225 (D). This figure is a representative of three biological repeats with similar observations.

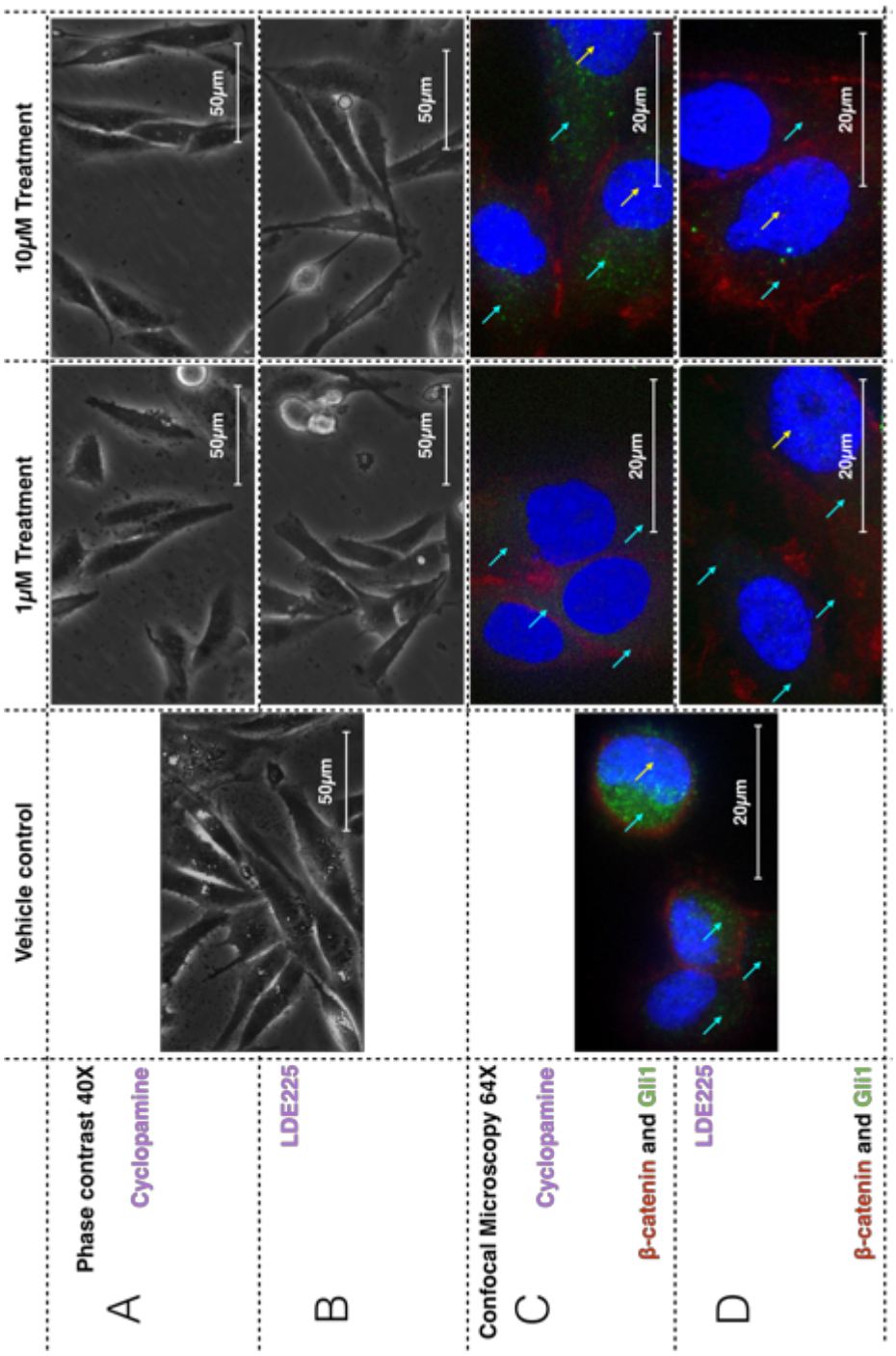

Figure 11-46, Morphology of MDA-MB-231 cells and visual alteration of Gli1 and β-catenin localisation following treatment with cyclopamine or LDE225.

Visual presentation of MDA-MB-231 following treatment for 48 hours with either cyclopamine or LDE225 at 1μM or 10μM compared to vehicle control. Phase contrast images of MDA-MB-231 cells captured under 400x magnification using black and white camera of a Leica phase contrast microscope (A and B). Immunofluorescence Z stacked images of MDA-MB-231 cells captured under confocal microscope at 630x magnification. MDA-MB-231 cells were double stained for β-catenin (Red) and Gli1 (green) and visualised by fluorescence labelled secondary antibodies Alexa Fluor® (488 and 594). DAPI was used to stain nucleus of cells (Blue). Yellow arrows were used to highlight localisation of the protein in nucleus of cells and light blue arrows were used to highlight cytoplasmic localisation of protein. Visual localisation of β-catenin and Gli1 proteins in MDA-MB-231 cells treated with cyclopamine (C) or LDE225 (D). This figure is a representative of three biological repeats with similar observations.

11.3.12 Alteration of nuclear localisation of Gli2 and Gli3 in MCF7 and MDA-MB-231 following treatment with Hh inhibitors

Gli2 and Gli3 were visually observed under a confocal microscope (following immunocytochemistry) to determine whether Hh inhibition with 1μM or 10μM of either cyclopamine or LDE225 affects the localisation of both proteins. Gli2 protein was cytoplasmic in MCF7 and no clear nuclear localisation of the protein was noted in the vehicle control. No changes in the level nor the localisation of Gli2 were observed in MCF7 following cyclopamine treatment with 1μM or 10μM in MCF7 were observed. The cytoplasmic localisation of Gli2 was visibly reduced in cells at 1μM and 10μM of LDE225 whereas conversely, the nuclear localisation increased.

The localisation of β-catenin in MCF7 cells was cytoplasmic and at area of cell-cell contact. It was observed that the level of expression of β-catenin protein was visibly reduced following treatment with cyclopamine or LDE225 in MCF7 cells. Gli3 protein was both cytoplasmic and in the nucleus of MCF7 cells. Following inhibition with cyclopamine, the cytoplasmic Gli3 reduced with a concomitant increase in nuclear localisation, especially at 10μM cyclopamine or LDE225. Gli3 was reduced in MCF7 cells following inhibition with LDE225 and the nuclear localisation increased at the highest dose compared to the vehicle control. Cytoplasmic Gli3 in MCF7 cells was reduced following LDE225 in parallel with increased nuclear localisation in a dose-dependent manner.

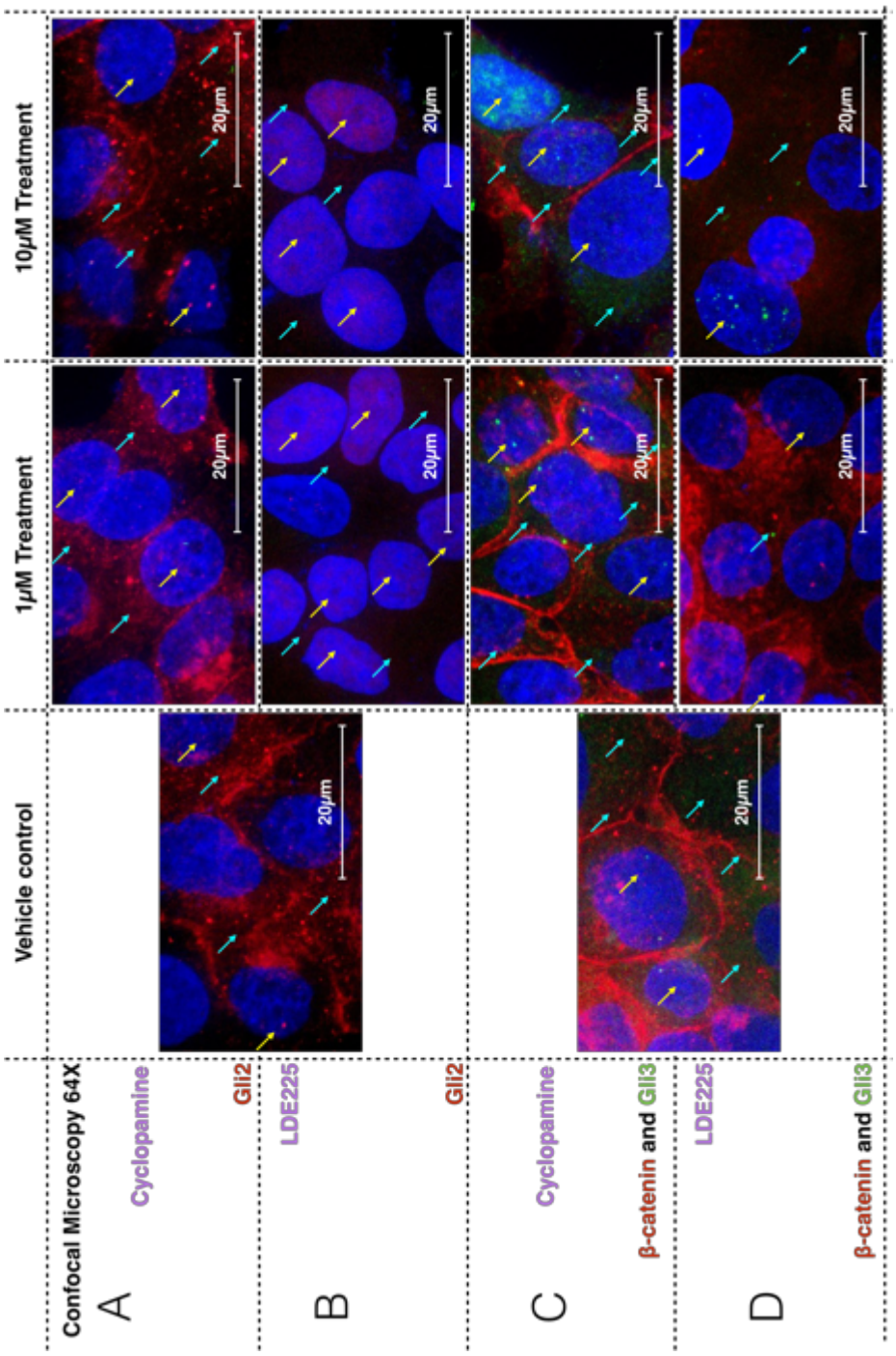

Figure 11-47, Alteration of Gli2, Gli3 and β-catenin localisation in MCF7 cells following treatment with cyclopamine or LDE225.
Immunofluorescence Z stacked images of MCF7 cells captured under confocal microscope at 630x magnification. MCF7 cells were double stained for Gli2 or β-catenin (Red) and Gli3 (green) and visualised by fluorescence labelled secondary antibodies Alexa Fluor® (488 and 594). DAPI was used to stain nucleus of cells (Blue). Yellow arrows were used to highlight localisation of the protein in nucleus of cells. Light blue arrows were used to highlight cytoplasmic localisation of protein. Visual localisation of Gli2 in MCF7 cells treated with cyclopamine (A) or LDE225 (B). Localisation of β-catenin (Red) and Gli3 (Green) in MCF7 cells following treatment with cyclopamine (C) or LDE225 (D) at 1 and 10μM compared to the vehicle control. This figure is a representative of three biological repeats with similar observations.

Gli2 localisation in MDA-MB-231 cells was both nuclear and cytoplasmic. Gli2 was visibly reduced in the cytoplasm and nucleus of MDA-MB-231 cells following cyclopamine treatment with no clear difference in localisation of protein at both 1μM and 10μM. Following LDE225 treatment of MDA-MB-231 cells, cytoplasmic localisation of Gli2was notably reduced. The localisation of β-catenin in MDA-MB-231 cells was at the border of cells in the vehicle control. The expression of β-catenin in MDA-MB-231 cells increased with concentration of cyclopamine and showed cell-cell contact localisation.

The expression of Gli3 in MDA-MB-231 cells was cytoplasmic without visible nuclear localisation. The nuclear localisation of Gli3 increased following cyclopamine treatment, and no difference was observed following treatment at both concentrations. Gli3 cytoplasmic localisation was reduced following treatment without clear difference between treatments at both concentrations of cyclopamine. Cytoplasmic localisation of Gli3 was reduced following LDE225 treatment in MDA-MB-231 with a notable reduction in nuclear protein following treatment at 10 μM.

In MCF7 cells, the expression of E-cadherin was strong with notable cytoplasmic and membrane localisation in the vehicle control. E-cadherin expression in MDA-MB-231 cells was cytoplasmic showing punctate deposits of protein without clear membrane localisation in the vehicle control. Following cyclopamine treatment of MCF7, membrane localisation of E-cadherin increased without visible changes in the level of protein. E-cadherin localisation was not visually changed in MDA-MB-231 following cyclopamine treatment. In MCF7 cells, localisation of E-cadherin was not visually altered following LDE225 treatment. In the MDA-MB-231 cell line, E-cadherin protein level increased without cell-cell contact localisation.

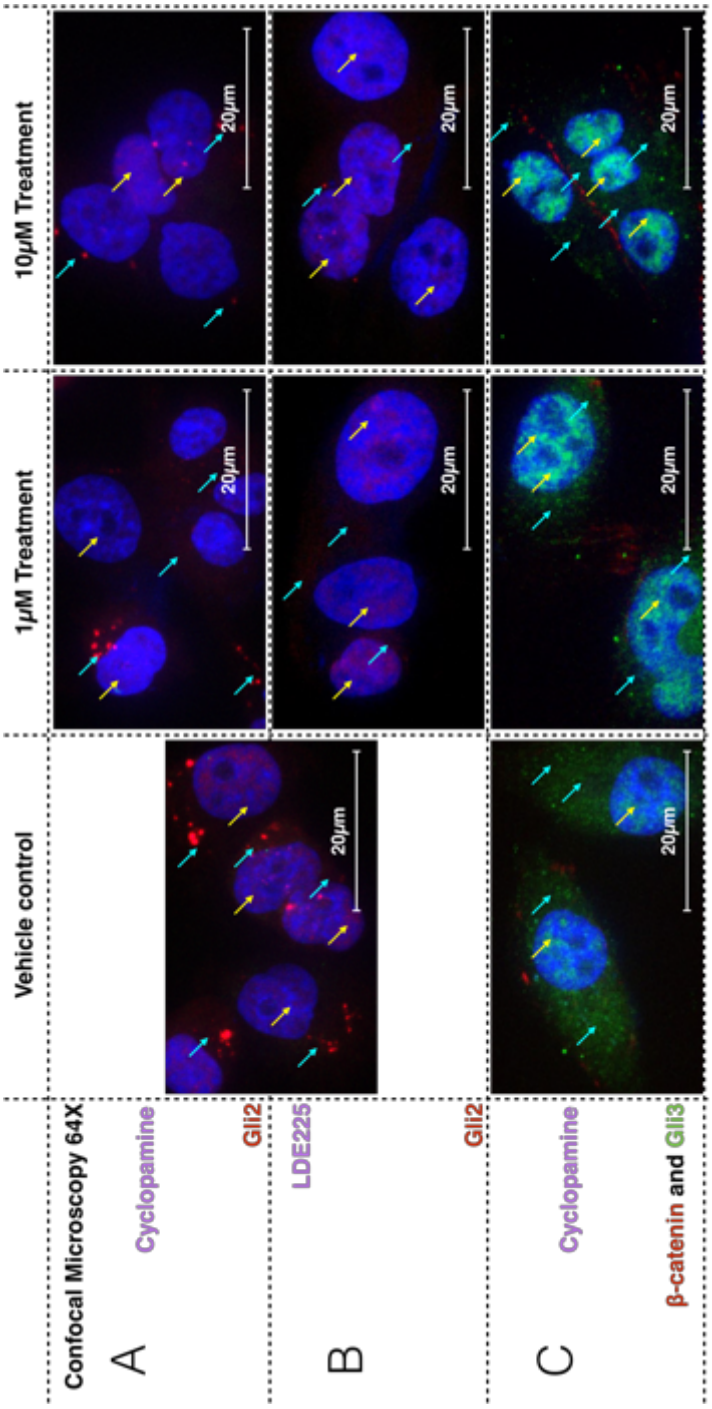

Figure 11-48, Changes in localisation of Gli2, Gli3 and β-catenin proteins in MDA-MB-231 cells following treatment with cyclopamine or LDE225.

Immunofluorescence Z stacked images of MDA-MB-231 cells captured under confocal microscope at 630x magnification. MDA-MB-231 cells were double stained for Gli2 or β-catenin (Red) and Gli3 (green) and visualised by fluorescence labelled secondary antibodies Alexa Fluor® (488 and 594). DAPI was used to stain nucleus of cells (Blue). Yellow arrows were used to highlight localisation of the protein in nucleus of cells. Light blue arrows were used to highlight cytoplasmic localisation of protein. Visual localisation of Gli2 in MDA-MB-231 cells treated with cyclopamine (A) or LDE225 (B). Localisation of β-catenin (Red) and Gli3 (Green) in MDA-MB-231 cells following treatment with cyclopamine (C) or LDE225 (D) at 1 and 10μM compared to the vehicle control. This figure is a representative of three biological repeats with similar observations.

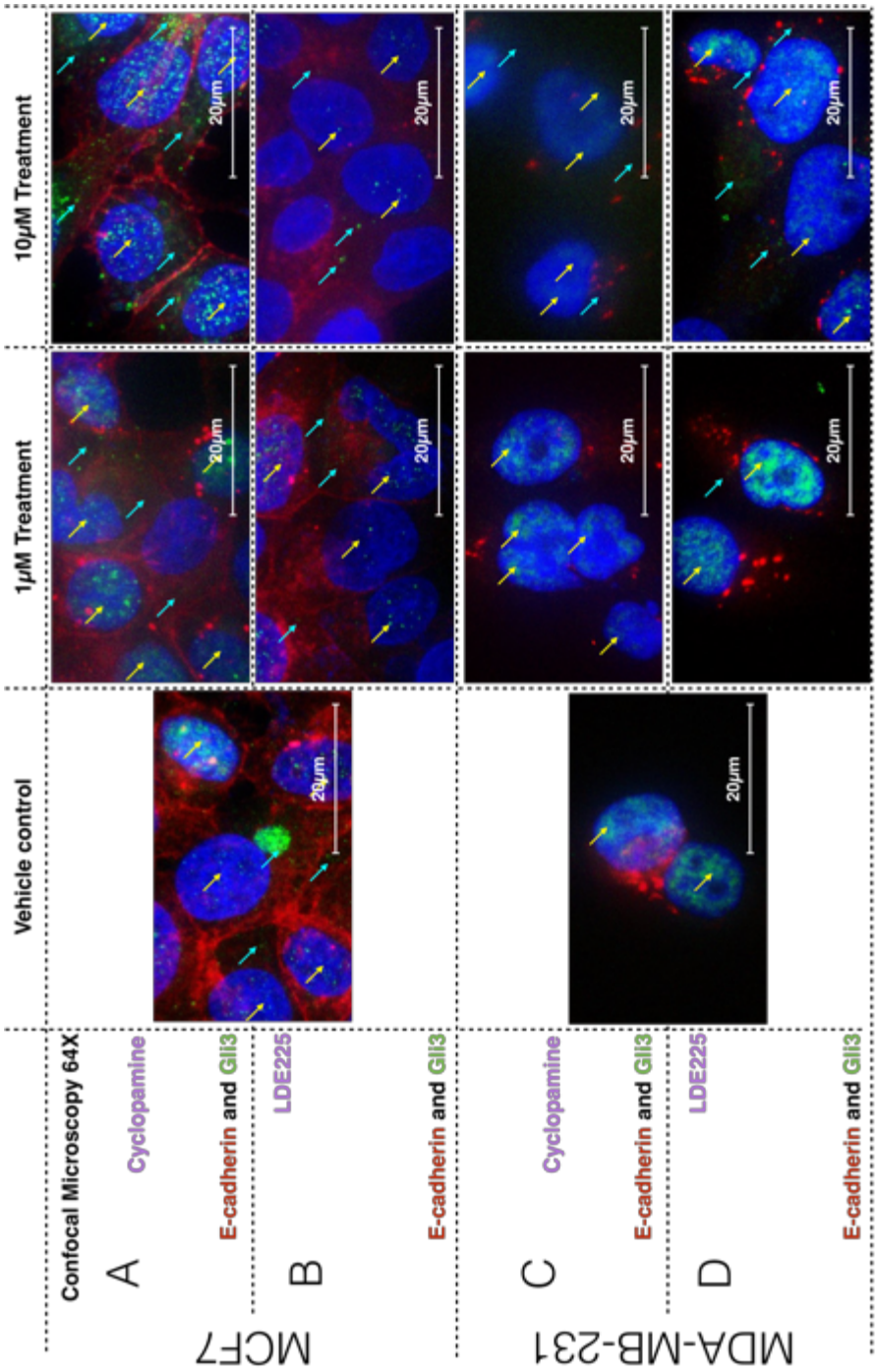

Figure 11-49, Alteration of Gli3 and E-cadherin localisation in MCF7 and MDA-MB-231 cells following treatment with cyclopamine or LDE225.
Immunofluorescence Z stacked images of MCF7 (A and B) and MDA-MB-231 (C and D) captured under confocal microscope at 630x magnifications. MCF7 and MDA-MB-231 cells were double stained for E-cadherin (Red) and Gli3 (green) and visualised by fluorescence labelled secondary antibodies Alexa Fluor® (488 and 594). DAPI was used to stain nucleus of cells (Blue). Yellow arrows were used to highlight localisation of protein in nucleus of cells. Light blue arrows were used to highlight cytoplasmic localisation of protein. Visual localisation of Gli3 (Green) and E-cadherin (Red) in MCF7 and cells treated with cyclopamine (A) or LDE225 (B) at 1 and 10μM compared to the vehicle control. localisation of E-catenin (Red) and Gli3 (Green) in MDA-MB-231 cells following treatment with cyclopamine (C) or LDE225 (D) at 1 and 10μM compared to the vehicle control. This figure is a representative of three biological repeats with similar observations.

The alteration in level of expression of Gli1, Gli2 and Gli3 in MCF7 and MDA-MB-231 cell lines following treatment with cyclopamine or LDE225 were summarised in Table 11-24, the nuclear and cytoplasmic localisation of the proteins as seen by confocal microscopy are also summarised in Table 11-25 and Table 11-26.

Table 11-24: Gli1 expression increased in MCF7 and MDA-MB-231 concurrent with decreased Gli2 and Gli3 expression as seen by flow cytometry following treatment with Hh inhibitors.
This table summarises changes in Gli proteins expression following treatment with cyclopamine or LDE225 at 1μM, 5μM and 10μM. Arrows indicate the change of expression compared to the vehicle control.

		1 μM cyclopamine	5 μM cyclopamine	10 μM cyclopamine	1 μM LDE225	5 μM LDE225	10 μM LDE225
Gli1	MCF7	↑↑↑	↑↑↑	↑↑↑	↑↑	↑↑	↑
	MDA-MB-231	↑↑	↑	↑	↑	-	↓
Gli2	MCF7	-	↓	-	↓	-	↓↓
	MDA-MB-231	↓	-	↓↓	↓↓	↓	↑
Gli3	MCF7	↓↓	-	↓↓	-	-	↓
	MDA-MB-231	↓↓	↑	-	↑	-	-

Table 11-25: Decreased nuclear Gli1 with increased nuclear Gli3 following treatment with cyclopamine or LDE225.
This table summarises the effect of inhibiting Hh signalling on nuclear localisation of Gli1, Gli2, and Gli3 after treatment with cyclopamine or LDE225 at 1μM and 10μM for 48hours as seen by confocal microscopy. Arrows indicate qualitative observation of expression compared to the vehicle control.

	Treatment	1 μM cyclopamine	10 μM cyclopamine	1 μM LDE225	10 μM LDE225
Gli1	MCF7	↓	↓	↓	↓↓↓
	MDA-MB-231	↓	↓	↓↓	↓↓
Gli2	MCF7	↑	↑	↑↑	↑↑
	MDA-MB-231	↓↓	↓	-	-
Gli3	MCF7	↑	↑↑	-	↑
	MDA-MB-231	↑↑↑	↑↑↑	↑↑↑	↑

Table 11-26: Decrease of cytoplasmic localisation of Gli1, Gli2 and Gli3 in MCF7 and MDA-MB-231 cells following inhibition of Hh signalling.

This table summarises the effect of cyclopamine or LDE225 treatment on cytoplasmic localisation of Gli1, Gli2 and Gli3 at 1µM and 10µM as seen by confocal microscopy. Arrows indicate observation of expression compared to the vehicle control.

	Treatment	1 µM cyclopamine	10 µM cyclopamine	1 µM LDE225	10 µM LDE225
Gli1	MCF7	↓	↓	↓	↓↓↓
	MDA-MB-231	↓	↓	↓↓↓	↓↓↓
Gli2	MCF7	-	-	↓↓	↓↓
	MDA-MB-231	↓↓↓	↓↓↓	↓↓	↓↓
Gli3	MCF7	-	-	↓	↓↓
	MDA-MB-231	↓	↓↓	↓↓	↓↓

12. Research outputs

12.1 Publications

- Flemban, A. and Qualtrough, D. (2015). The Potential Role of Hedgehog Signalling in the Luminal/Basal Phenotype of Breast Epithelia and in Breast Cancer Invasion and Metastasis. Cancers (Basel), 7(3), pp. 1863-1884.
- Daly, C. S., Flemban, A., Shafei, M., Conway, M. E., Qualtrough, D. and Dean, S. J. (2017). Hypoxia modulates the stem cell population and induces EMT in the MCF-10A breast epithelial cell line. Oncol Rep.

12.2 Presentation

12.2.1 poster presentation

1) Investigation of the Process of Epithelial Mesenchymal Transition in Triple Negative and Basal Like Breast Cancer. In CRIB Annual Meeting 10th January 2014

2) The investigation of epithelial mesenchymal transition in triple negative and basal like breast cancer. In CRIB Annual Meeting 16th January 2015

3) Investigation of new tissue biomarkers for triple negative breast cancer. In the postgraduate conference. 27th June 2014.

4) The investigation of Epithelial Mesenchymal Transition in Triple Negative Breast Cancer and Basal Like Breast Cancer. In the Centre for Research in Biosciences (CRIB) Annual Meeting. At 16th of January 2015

5) The investigation of epithelial mesenchymal transition in triple negative and basal like breast cancer. In the postgraduate conference. 26th June 2015.

6) The investigation of epithelial mesenchymal transition in triple negative and basal like breast cancer. In the Saudi Cultural Bureau Conference in London 31st – 1st February 2015.

7) The investigation of the regulation of the process of epithelial mesenchymal transition in triple negative and basal like breast cancer. In the BACR/CRUL joint meeting, Evolution and intratumural heterogeneity. 11th June 2015. London.

8) The Investigation of the Regulation of the process of Epithelial Mesenchymal Transition in Triple Negative and Basal like Breast Cancer. In the NCRI Cancer Conference at 1st-4th of November 2015

9) The effect of cyclopamine on hedgehog signalling pathway in breast cancer cells. At the UK Breast Cancer Research Symposium. At 22nd and 23rd of July 2016

10) The Role of Hedgehog Signalling Pathway in the Regulation of Epithelial Mesenchymal Transition (EMT) in Breast Cancer. In The Centre for Research in Bioscience (CRIB) Annual Meeting. At the 13th of January 2017.

12.2.2 Oral Presentation

1) Sub classification of Breast Cancer Cell Lines According to their Response to Stimuli to Epithelial Mesenchymal Transition (EMT) and Expression of a set of EMT markers. At the Centre for Research in Biosciences (CRIB) Annual Meeting. At the 13th of January 2017